BULETINUL INSTITUTULUI POLITEHNIC DIN IASI

Publicat de

UNIVERSITATEA TEHNICĂ "GH. ASACHI", IAŞI

Tomul LIII (LVII)

Fasc. 4

Secţia
ŞTIINŢA ŞI INGINERIA MATERIALELOR

2007

BULETINUL INSTITUTULUI POLITEHNIC DIN IAŞI
BULLETIN OF THE POLYTECHNIC INSTITUTE OF JASSY
Tomul LIII (LVII) 2007

MATERIALS SCIENCE AND ENGINEERING

CONTENTS

BULETINUL INSTITUTULUI POLITEHNIC DIN IAŞI
BULLETIN OF THE POLYTECHNIC INSTITUTE OF JASSY
Tomul LIII (LVII) 2007

ŞTIINŢA ŞI INGINERIA MATERIALELOR

CUPRINS

BULETINUL INSTITUTULUI POLITEHNIC DIN IAŞI
Tomul LIII (LVII), Fasc. 4, 2007
Secţia
ŞTIINŢA ŞI INGINERIA MATERIALELOR

STUDIES CONCERNING THE INFLUENCE OF THE COOLING RATE IN THE DEVELOPMENT OF TWO – PHASE STRUCTURES OF BRASSES

BY

CRISTINA ALBU-IACOB

Abstract: The paper shows the experimental results of some specific heat treatmen. schedule applied on CuZn40. with different cooling rates. For this alloy we made experiments at S.C. Mecanica "Ceahlau" S.A., Piatra Neamt. The examples presented shows big influence of cooling rate in the structure of the high zinc brasses. and the consequences in the hardness of these cooper base alloys. The experiments shows the importance of a correc. heat treatment schedule and a precise temperature control, obtained only with an automatic equipment for the heat treatment process.

Keywords: heat treatment, high zinc brasses, cooling rate, temperature control

1. Introduction

In high-zinc Cu-Zn alloys the desired structure consists of a mixture of two phases of comparable quantity. The morphology and amount of each are varied by control of the high temperature used and the cooling rate from that temperature. The referred microstructure can be quite complex, and the required treatment differs considerably for different systems, so that a systematic treatment of the principles involved is difficult.

In the Cu-Zn system, alloys containing about 40% Zn serve as the basis for many commercial alloys. The Cu-Zn phase diagram (figure 1) shows that the alloys of interest are in the region of α and β phase stability. The β phase is body-centered cubic, with the copper and zinc atoms located at random on the lattice sites.

On cooling to temperatures below the dashed line (about 450°C), the copper and zinc atoms take specific relative positions on the sites, forming an ordered structure, or a superlattice. This phase is denoted β' in figure 1. If the composition is exactly 50 at. % Zn, then the ordered structure is based on a body-centered cubic cell with zinc atoms at the center and copper atoms on the corners (or vice versa).

The formation of an ordered structure from a disordered matrix of the same basic lattice involves the localized exchange of atom positions (via the vacancy mechanism) to the desired structure.

An ordered region grows by atoms at the β/β' interface, taking on the arrangement of the ordered β' region. When two interfaces from neighboring regions meet, the arrangement of atoms may be out of sequence (out of phase). Such an interface is called an antiphase boundary, and the enclosed regions are called domains. The properties of the β' ordered structure depend on the degree of perfection

(correctness of relative atom location) within the domains and on the domain size, both of which depend on the temperature and time involved in forming β' from β.

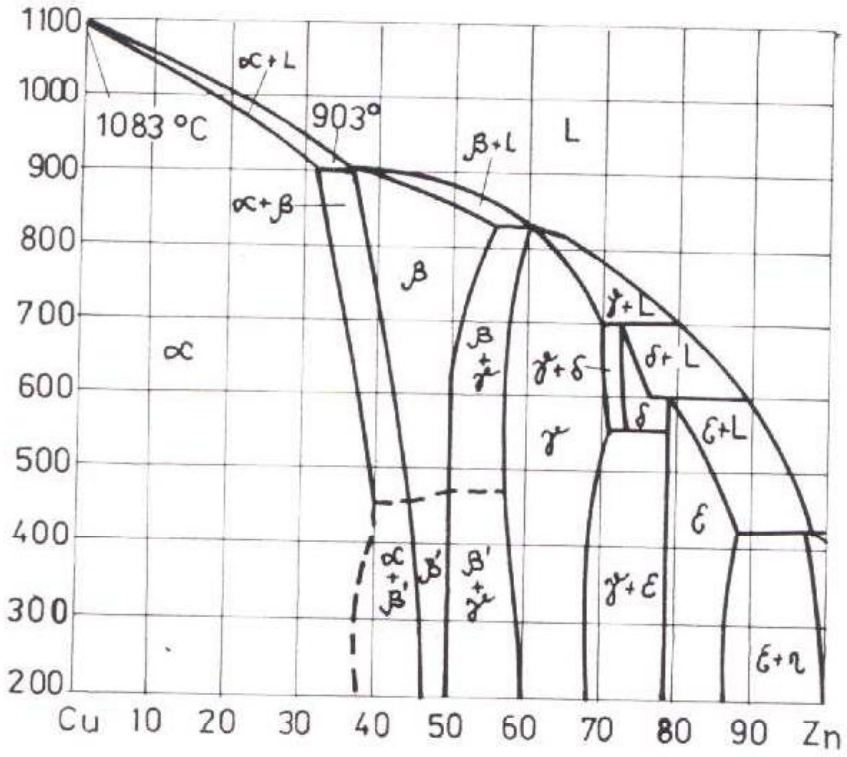

Fig.1. The Cu-Zn equilibrium diagram

These alloys in the β' form are not suitable for commercial use, because this structure is brittle. However, alloys in which the β' phase coexists with the ductile α phase are useful. The Cu-40Zn alloy can be heat treated at high temperature so that it is all β. The structure developed at lower temperatures depends on the heat treatment, because this controls precipitation and formation of the α phase.

2. Experimental results

We made experiments using CuZn40 and we applied different heat treatment schedules. The purpose was to show the importance of the precise temperature control in the cooling process. For this alloy we made experiments at S.C. Mecanica "Ceahlau" S.A., Piatra Neamt. The chemical attack for obtaining of these microstructures has been performed with a compound containing ferric chloride (10 g), concentrated chloride hydride (30 cm^3) and distilled water (120 cm^3). If the alloy is cooled slowly from 800 °C, the phase diagram (figure 1) shows that at 25 °C the alloy should consist of approximately equal amounts of α and β'. Figure 2 shows a typical microstructure of annealed Cu-40Zn presented in figure 3 (curve 1). This structure was obtained with a cooling rate of 2 °C/min. The white regions are the β' and the dark and gray regions are α (optical micrograph 100 x).

In figure 3 it is presented the way that the amount of β' influences hardness

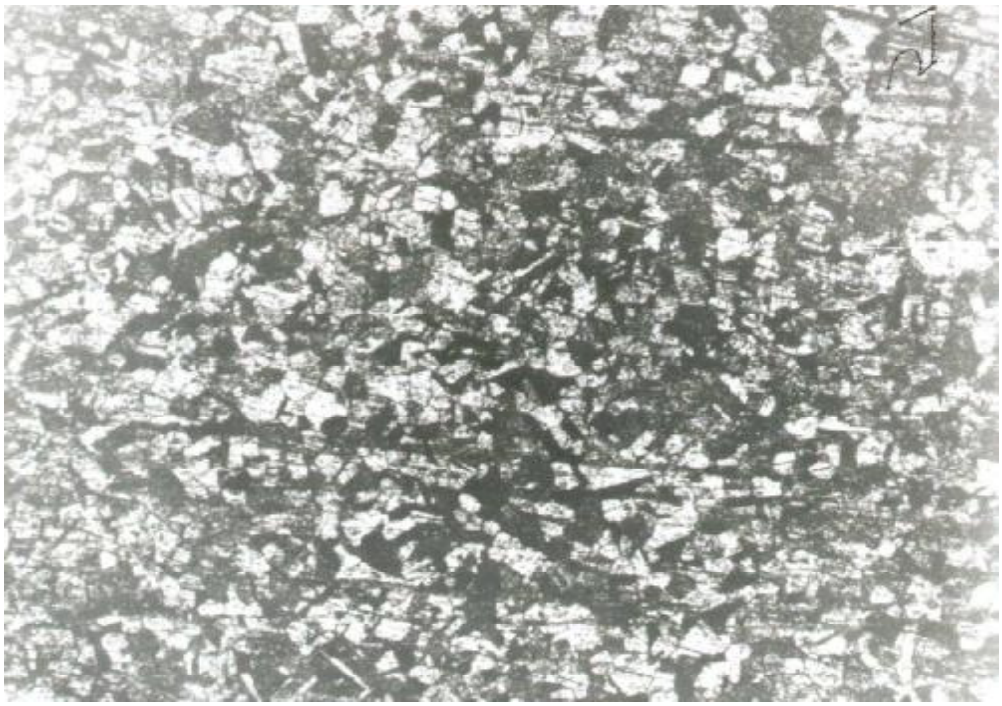

Fig. 2. The microstructure of Cu-40Zn slowly cooled

In figure 3 it is presented the way that the amount of β' influences hardness

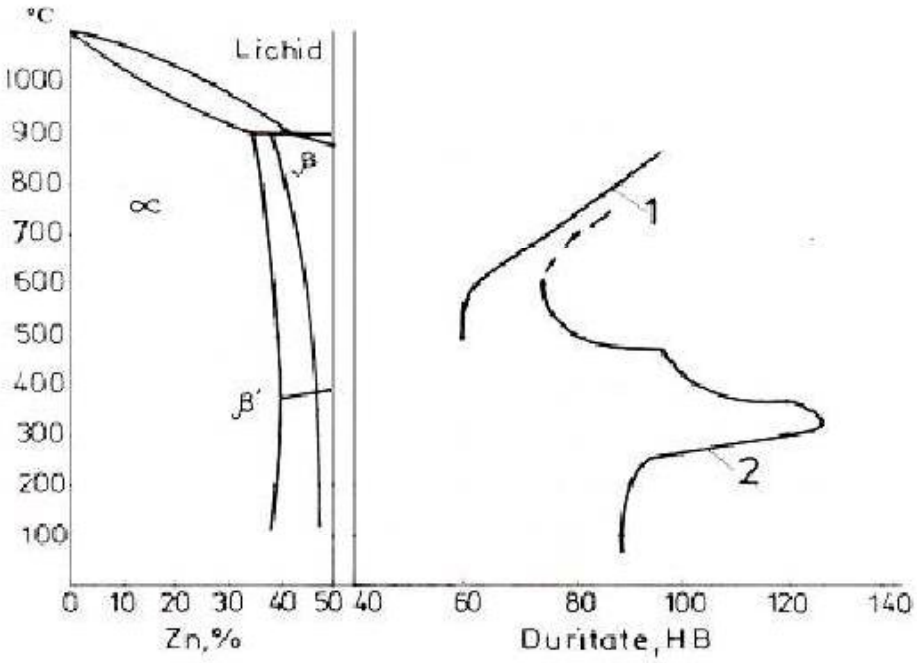

Fig.3. The influence of the heat treatment schedule on the hardness of Cu-40Zn; 1 - annealed at 700°C, slowly cooled , heated 30 min at temperature indicated, water quenched, 2 - heated 30 min at 800°C rapidly cooled, heated 30 min at temperature indicated, water quenched.

The alloy was cooled slowly from 700 °C, where it was mostly β, to 25 °C, then reheated to temperature for 30 min, followed by rapid cooling. On heating at 800 °C (curve 2), the structure is all β, and on rapid cooling little α forms. Figure 4 shows a typical microstructure of Cu-40Zn with a rapidly cooling (curve 2, figure 3).

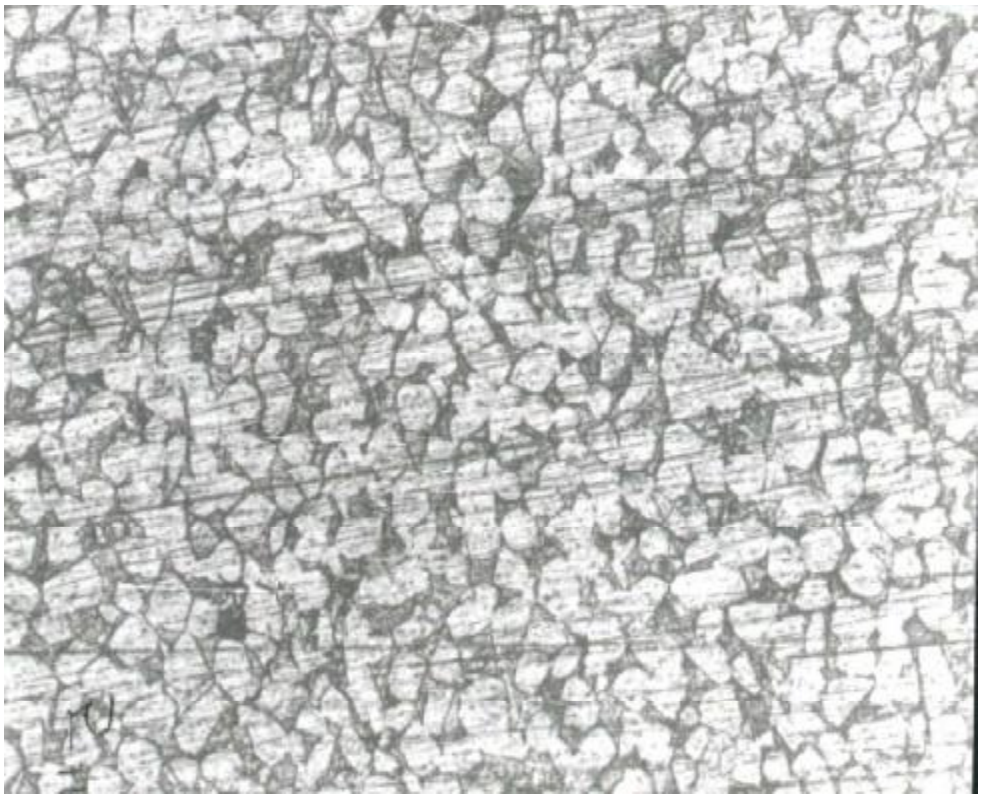

Fig.4. The microstructure of Cu-40Zn rapidly cooled

However, the β orders to β`, giving a hardness around 90 HB. Reheating for 30 min in the lower temperature range (25 to 500 °C) is not sufficient to affect significantly the originally slowly cooled structure, and the hardness remains constant. In this temperature range, the structure consists of approximately equal amounts of α and β'. However, as the temperature increases from 500 °C, 30 min is sufficient time to allow the equilibrium amounts and α and β to form. Thus, as the temperature increases, increasing amounts of β and decreasing amounts of α are present at temperature, giving increasing amounts of β'on cooling rapidly to 25 °C, and hence a rise in hardness.

If the Cu-40Zn alloy is cooled rapidly to 25 °C after sufficient holding (for example, 30 min) above about 750 °C, a structure of essentially all β` is obtained. Often some α is observed to have formed in the β grain boundaries, and the morphology will vary somewhat depending on the exact cooling rate.

On reheating β'in the intermediate temperature range, the morphology of the α formed will vary depending on the exact heat treatment. Also, reheating will influence the change in the ordered structure. Both changes affect properties, and the hardness can be increased considerably by judicious treatment. In figure 3 are shown hardness

data for a Cu-40Zn alloy after reheating for 30 min following an initial treatment of quenching from 800 °C. The maximum hardness obtained by treatment around 300 °C (125 HB at 320°C).

Received April 20, 2007 *Technichal colledge of transport, Piatra Neamț*

REFERENCES

1. Albu-Iacob, C., **Contribuții privind îmbunătățirea constructiv/funcțională a instalațiilor de tratament termic al aliajelor de cupru, Teza de doctorat**, UTI, 2002
2. Mendenhall, J.H., **Understanding Copper Alloys,** Wiley, 1998
3. Sheppard, T., **Materials Science Technology,** v 4, (iulie 1999), p 636
4. Sontea, S., Vladoi, M., Zaharia, N., **Metale și aliaje de cupru de turnatorie,** Scrisul Romanesc, Craiova 1981
5. ***, **Heat Treating of Copper Alloys,** Heat Treatment, v 4, ASM International

STUDII PRIVIND INFLUENȚA VITEZEI DE RĂCIRE ASUPRA FORMĂRII STRUCTURILOR BIFAZICE ALE ALAMELOR

Rezumat: Lucrarea arata rezultatele experimentale obtinute in urma unor tratamente termice specifice aplicate alamei binare cu 40 % zinc, cu structura bifazica. Pentru acest aliaj am facut experimente la S.C. Mecanica "Ceahlau" S.A. Piatra Neamt. Exemplele prezentate arata influenta mare a vitezei de racire in structura obtinuta in alamele bifazice cu continut ridicat de zinc si deci influenta acesteia asupra duritatii respectivelor aliaje. Experimentele arata in acelasi timp importanta stabilirii unei corecte scheme de tratament termic si un control strans al temperaturii, obtinut practic cu un echipament automatizat pentru conducerea procesului.

BULETINUL INSTITUTULUI POLITEHNIC DIN IAŞI
Tomul L(III (LVII), Fasc. 4, 2007
Secţia
ŞTIINŢA ŞI INGINERIA MATERIALELOR

ON POSSIBILITY OF CU ELASTIC MODULI EVALUATION BYX-RAY DIFFRACTOMETRY DATA

BY

T.I.BABJUCK, S.G.AVDEJEV and I.V.SHEVCHUK

Abstract: By using of lattice f.c.c. model wi.h the central interaction in a first coordination sphere by known x-ray diffractometry data were evaluated Cu C_{ij} elastic moduli in harmonic approximation. With accounting of conductivity electrons and zero oscillations influence on deviations from Cauchy correlations the resul.s of calculations were appeared in reasonable correlation with existing experimental data.

Keywords: diffraction spec.ra, characteristic temperature, elastic moduli.

1. Introduction and the settlement of problem

It is known, that from the intensities and x-ray interferentions shift thermal dependencies data may be obtained some information about dynamics of crystalline lattice: coefficients of thermal expansion $\alpha(T)$, the values of x-ray characteristic temperatures $\Theta(T)$ and their thermal dependencies $\Theta_p(T)$.

In work [1] was showed, that Θ_p is the characteristic of f-MΘ^2_p connection rigidity, at least at central interactions in first two coordination spheres. In one's turn, the $\Theta_p(T)$ dependence, actually, is reflecting decreasing of crystalline elastic moduli C_{ijkl} with growth of temperature and may be used for determination of Gruneisen parameters and force constants f,g,h, figurating in expansion of lattice potential by displacements ranges [2,3]. Further, using the f.c.c lattice model with central interaction of nearest neighboures, one can evaluate the values of ant their thermal dependencies, if f,g,h are known [4]. Despite the circumstance, that such models leads to fulfilment of Cauchy's ratios $C_{ijkl} - C_{jikl}$ ($i \neq j$), they are elastically stable and in contrast to continual were characterized with dispersion of oscillations [4,5].

From this point of view may be interesting the using of the single parameter f, obtained from x-ray diffractometry data, to calculate values of Cu C_{ijkl} at T=0.The range of calculation reliability may be increased by taking to account further the influence of electrons of conductivity [6] and zero oscillations [7].In this work such calculation of C_{ijkl} is provided for Cu.The choice of Cu is caused by a reason, that for copper x-ray diffractometry Θ_p and $\Theta_p(T)$ data are most spreaded and correlating.

2. Results of calculation and discussion

According to [5] for f.c.c. lattice in harmonic approximation, elastic moduli in Foight signature ($C_{ijkl} \rightarrow C_{\mu\nu}$) correspondingly are equal to:

$$C_{11} = 2f/a;\ C_{12} = f/a;\ C_{44} = f/a \quad (1) \qquad (1)$$

where a the lattice parameter, f link rigidity parameter, determined as f=0,15(k / ħ)²mθ²$_\rho$ (0) [3] (in standard signature).

At temperature T=0 parameter f, according to [3], may be determined as:

$$f \quad 0{,}1397\left(\frac{k}{\hbar}\right)^2 m\theta_{\rho}^2 \qquad (2)$$

For determination of harmonic values for $\tilde{f}$ and $C\mu\tilde{V}$ parameters one must use $\tilde{a}(\theta)$ and $\tilde{\theta}\rho(\theta)$, quantities, which are conditioned by the way of linear extrapolation of experimental dependencies $a(T)$ and $\theta\rho(T)$ from a region of high temperatures $T>\theta\rho$ to T=0 K [4]. Such extrapolation is more rightful for $\theta\rho(T)$, than for $\theta_D(T)$, because a thermal dependence of the first of them actually is not influenced with low-thermal anomalies, conditioned by the difference of the real frequency spectral distribution function $g(\omega)$ from Debye parabola [3]. As showed in [2]

$$\theta\rho(T) - \theta\rho(0) (1- 2\gamma\beta(T-T0)) \qquad (3)$$

where β - the volumetrical thermal expansion coefficient

The necessary x-ray diffractometry data, obtained by calculations of C after (1) are adduced in table 1

Table 1.

metal	$\theta\rho$ K	γr	$\beta\cdot10^6$ K^{-1}	$\theta\rho(0)$	a (0)$\cdot10^{10}$m	$f\cdot10^1$ dyn/cm^2
Cu	298	1.96	54,42	317	3,5940	2,763
$C\mu v\cdot10^{-12}$ dyn/cm^2						
C_{11}		C_{12}		C_{44}		
1,538		0,769		0,769		

Because for metals the Cauchy ratio is not accomplished, one may have a reason to take into account non-central interactions, using the known De-Launey model [6], according to which for metals of cubic symmetry

$$C_{12}-C_{44}=K_{el} \qquad (4)$$

where K_{el} - the pressing module of electron gase of conductivity. The value of K_{el} may be calculated by determination of Fermy energy μ_0 of collectivized electrons at T=0 K

$$K_{el}=2/3\mu_0/V, \text{ where } \mu_0\frac{h}{2m}\left(\frac{3Nn_a}{8\pi V}\right)^{\frac{2}{3}} \qquad (5)$$

From other side, even at T=0 K and central interactions the transgression of Cauchy relation is conditioned by the existence of zero oscillations, which in addition are unharmonic. This circumstance may be taking into account by using [4] (correlation 15.27)

$$C_{12}-C_{44} \quad \frac{9U(T)\gamma^2}{NV_z} \qquad (6)$$

where N Avogadro number; V- the volume of elementary cell; U(T) the energy of lattice oscillation, which is equal to zero energy U(0)=9/8NkΘ$_D$ at T=0 in Debye approximation. Cause at T=0 the substitution has appears as a good approximation, the parameter in (5) one way take equal to ordinary Gruneisen parameter, given in table 1.

One may see from (4) and (6), that the influence of conductivity electrons and zero oscillations on declinations from Cauchy ratios requires the accounting of their summary deposition. The procedure of specification of adduced in table 1 values $C_{\mu 0}$ for Cu is described below.

Using known numerical values of V_a, n_e, and m*, one can obtain μ_0=7,1eV, K_{el} = $0{,}769 \cdot 10^{12}$ dyn/cm². Further, taking to account (4) and (6), we have obtain:

$$C_{12} - C_{44} \quad 0.24 \cdot 10^{12}\ dyn/cm^2 \qquad (7)$$

Using data of table 1 and follow (6) one may find: C_{12}=$1{,}013 \cdot 10^{12}$ dyn/cm², C_{44}=$0{,}769 \cdot 10^{12}$ dyn/cm².

The self-coordination of results for such specified calculation of $C_{\mu}{}^{V}$ may be easy verified by determining of Young and shift moduli E and G. Numerical values of elastic moduli , calculated with using of $C_{\mu}{}^{V}$, Cu, are given in table 2.

It is clear, that specified in a such way elastic moduli values for Cu must be compared with harmonic values $C_{\mu}{}^{V}(T)$ from a region of high temperatures at T= 0 K. A such comparison is reflected in a table 2, where $C_{\mu}{}^{V}$ and elastic moduli Cu are taken from [7].

Table 2.

Determination	$C_{\mu 0}$, GPa			Elastic moduli		
	C11	C12	C44	Ex., GPa	Gx., GPa	K, GPa
Calculation	153.8	101,3	76.9	123,4	50,7	118,8
Exper. extrapolation for T=0	176,2	124,9	81,7	137,4	51,4	142,0

From a table one may see, that although the evaluation of $C_{\mu 0}$ is made with using of simplified theoretical models, their results, nevertheless, are in reasonable correlation with experimental data for Cu and the maximal declination makes up about 10 %.

Let us note in conclusion, that the using of 0p as a measure of rigidity of (f--M0²p) connection , in combination with physical reasoning, described in [1], may be useful also in applied context. It is clear, that described above process of $C_{\mu 0}$ evaluation by x-ray diffractometry data can not be regard as the universal method. Nevertheless, for such objects as alpha-solid solutions on a base of Cu, Ag et al metals with known electron concentration, such previous evaluations of $C_{\mu 0}$, with no doubt may appeared useful.

3. Conclusions

1 There was showed the possibility of Cu elastic moduli evaluation by known x-ray diffractometry data with using of lattice f.c.c. model with central interaction.

2 There are obtained values of elastic moduli with accounting of electrons of conductivity and zero oscillations influence on deviations from Cauchy ratios, were appeared in reasonable correlation with experimental data

Received April 11, 2007 *Vinnytsya National Tecinical University*

REFERENCES

1. Михальченко В.П., Лотоцкий В.Б. *Об использовании рентгеновской характеристической температуры дебая для оценки межатомной связи в кристаллической решетке*, **Физика металлов и металловедение**, 1971. Т. 32. – № 6. – с. 1300–1305.
2. Михальченко В.П., Купта Г.П. *Определение постоянной Грюнайзена 12% хромистого феррита рентгенографическим методом*. **Украинский физический журнал**, – 1963. Т.8, – № 7, – с. 779 – 785.
3. Михальченко В.П. *Об оценке ангармонических коэффициентов третьего и четвертого порядков по экспериментальным данным температурной зависимости интенсивности рентгеновских интерференций*, **Украинский физический журнал**. 1965. Т. 10 – № 4 – с. 436 – 442.
4. Ludwinq W., **Springer Tract in Modern Physics**. ed. by E. Hohler. Berlin, Heidelberg. New-York. 1967 – V. 43.
5. ***, **Рассеяние тепловых нейтронов,** Под ред. И.Иноземаффа, М. Атомиздат, 1970.
6. De-Launey, *On specific Heat of Solids*, **Solid State Phys.**, 1956, V. 2., p. 219.
7. Лейбфрид Г., **Микроскопическая теория механических и тепловых свойств кристаллов**, М., Л.: 1963.
8. Францевич И.Н., Воронов Ф.Ф, Бакута С.А., **Упругие постоянные и модули упругости металлов и неметаллов**, Киев, Наукова думка, 1982, с. 286.

POSIBILITĂŢI DE EVALUARE A MODULULUI ELASTIC A Cu CU AJUTORUL DIFRACTOMETRIEI CU RAZE X

Rezumat: Prin folosirea unei model de reţea ele şi considerând interacţiunea cu aceasta a radiaţiei X în prima sferă de coordinaţie s-a evaluat prin difractometrie cu raze X modulul de elasticitate, utilizând o aproximare armonică. Ţinând cont de electronii de conducţie şi neglijând influenţa oscilaţiilor asupra devierii de la corelaţiile Cauchy, rezultatele calculelor prezintă erori mici faţă de datele experimentale.

BULETINUL INSTITUTULUI POLITEHNIC DIN IAŞI
Tomul LIII (LVII), Fasc. 4, 2007
Secţia
ŞTIINŢA ŞI INGINERIA MATERIALELOR

THE CHEMICAL CRYSTALLINE PHOSPHATATION OF STEEL SEMI PRODUCTS FOR COLD EXTRUSION

BY

COSTICĂ BEJINARIU, IOAN RUSU, VIOREL MOLDOVEANU and ŞTEFAN TOMA

Abstract: The paper presents the phosphatation technology for indirect cold extrusion of steel semi products. On present the technological flow sheet for phosphatation, the necessary elements for analysis of phosphate layer, the chemical composition and the work parameters for: chemical alkaline degreasing, chemical acid pickling and chemical crystalline phosphatation. On present too the design of the phosphatation installation for laboratory and the execution of installation.

Keywords: chemical crystalline phosphatation, steel, cold extrusion.

1. Introduction

It is well known the fact that the process of cold extrusion creates displacements of material with specific high pressures and in a short period of time.

By the fact that the material of the semi product frictions the surface of the tool while the distortion takes place, it is natural to appear effects of the phenomena characterized by the destruction of the surfaces in the process, overstressing the tools and the equipment and corrosion of the deformed material because of welding in points or surfaces of the material with the surface of the tool

It was necessary the elaboration of a method that creates an intermediate layer between the material to be deformed and the tool. This layer has to be wired with the material to be deformed and to present certain porosity in order to allow the immersion of a lubricant

The method is based on the interaction between phosphoric acid (diluted solution that often contains additions of phosphate of Zn, Mn, Fe) with the superficial layer of the semi product, with the reaction:

$$Fe \quad 2\,H_3PO_4 \quad Fe(H_2PO_4)_3 \quad H_2,$$

that is simultaneous with the reaction:

$$3\,Me(H_2PO_4)_2 \Leftrightarrow Me_3(PO_4)_2 \quad 4\,H_3PO_4$$

in which Me = Zn, Mn, Fe.

The phosphate layer is porous and covers, in fact, only 0,1 ÷ 0,5 % of the metal surface. The retention of the lubricant is, in this way, 13 times more pronounced in comparison with the one of the unphosphated metal surface

By phosphatation, the technologist must prescribe a depth of phosphated layer of $1 \div 15\ \mu m$ or, expressed differently, of $30 \div 40\ mg/dm^2$.

2. The technology of phosphatation

The technological flow sheet for phosphatation of the semi products from OLC 15, destined to cold extrusion, for the stage of laboratory tests, is established and presented in Figure 1.

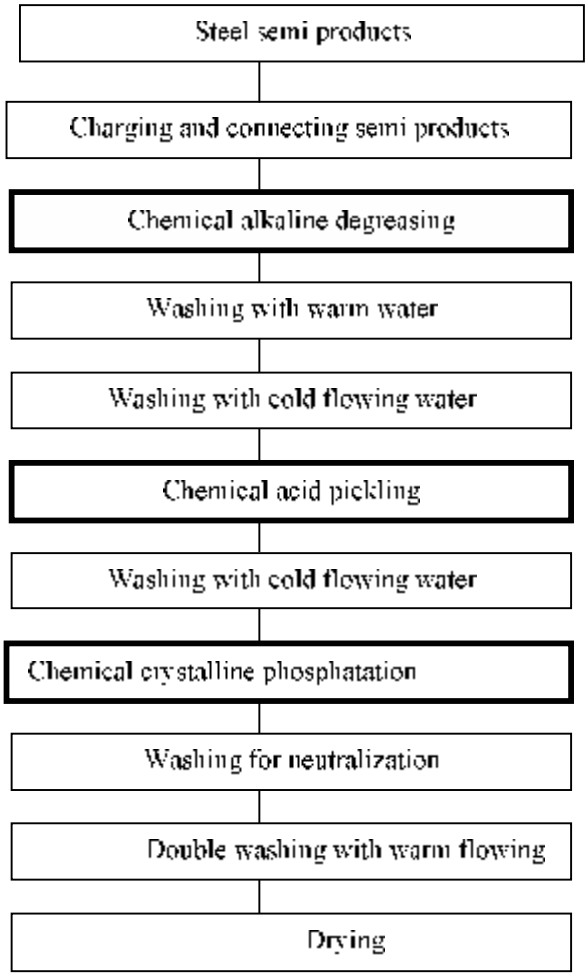

Figure 1. Technological flow sheet for phosphatation of the semi products from OLC 15, destined to cold extrusion

After the crystalline phosphatation, on the surface of the semi products forms a layer of trizinc-phospate tetrahydrate $Zn_3(PO_4)_2 \cdot 4H_2O$ known as *hopeit*, which, melting a 900 °C, behaves very well at temperatures of 200÷300 °C, touched in the process of cold extrusion (as a thermo effect of the deformation).

The analysis of the obtained phosphate layer is made by checking the following parameters:

- Presence of the phosphate layer;
- Aspect of the phosphate layer;
- Structure of the phosphate layer;
- Thickness of the phosphate layer;
- Adherence of the phosphate layer;
- The degree of impregnation with oil of the phosphate layer;
- Corrosion endurance of the phosphate layer.

The chemical composition and the parameters of the work regimen used for chemical alkaline degreasing of the steel pieces in the static tub in the process of immersion are presented in *Table 1*.

Table 1. Chemical alkaline degreasing.

Cr. no.	Name of the components	Concentration, [g/l]
1	Sodium hydroxide, NaOH	40
2	Sodium carbonate, Na_2CO_3	30
3	Trisodium phosphate, $Na_3PO_4 \cdot 10\ H_2O$	30
4	Sodium silicate, $Na_2SiO_3 \cdot 9\ H_2O$	5
5	Detergent (tensioactive)	3÷10
Cr. no.	**Name of the parameters**	**Value**
1	Temperature, [°C]	80÷90
2	Acidity [pH]	11÷12
3	Time for degreasing, [min]	10

The chemical composition and the parameters of the work regime used in chemical acid pickling of the steel pieces in the static in the static tub in the process of immersion are presented in *Table 2*.

Table 2. Chemical acid pickling.

Cr. no.	Name of the components	Concentration, [g/l]
1	Hydrochloric acid, HCl (ρ = 1,19)	150
2	Hexamethyltetramine, $C_6H_{12}N_4$	0,45
3	Sodium sulphate, $Na_2SO_4 \cdot 10\ H_2O$	0,15
Cr. no.	**Name of the parameters**	**Value**
1	Temperature, [°C]	20÷25
2	Time for pickling, [min]	Max.30

The chemical composition and the parameters of the work regime used in chemical crystalline phosphatation of the steel pieces in the static in the static tub in the process of immersion are presented in *Table 3*.

Table 3. Chemical crystalline phosphatation

Cur. no.	Name of the components	Concentration, [g/l]
1	Phosphoric acid, H_3PO_4 (ρ = 1,7)	5,940
2	Azotic acid, HNO_3 (ρ = 1,4)	1,840
3	Zinc, Zn	1,980
4	Sodium hydroxide, NaOH	0,375
5	Sodium nitrite, $NaNO_2$	0,225
6	**Sodium tripoliphosphate,** $Na_5P_3O_{10}$	0,025
Cur. no.	**Name of the parameters**	**Value**
1	Temperature, [°C]	70÷90
2	Acidity [pH]	2÷3
3	Time for phosphatation, [min]	20÷30

Based of the technological flow sheet for phosphatation of the semiproducts of OLC 15 destined for cold extrusion (figure 1), it has been elaborated the phosphatation installation presented in figure 2.

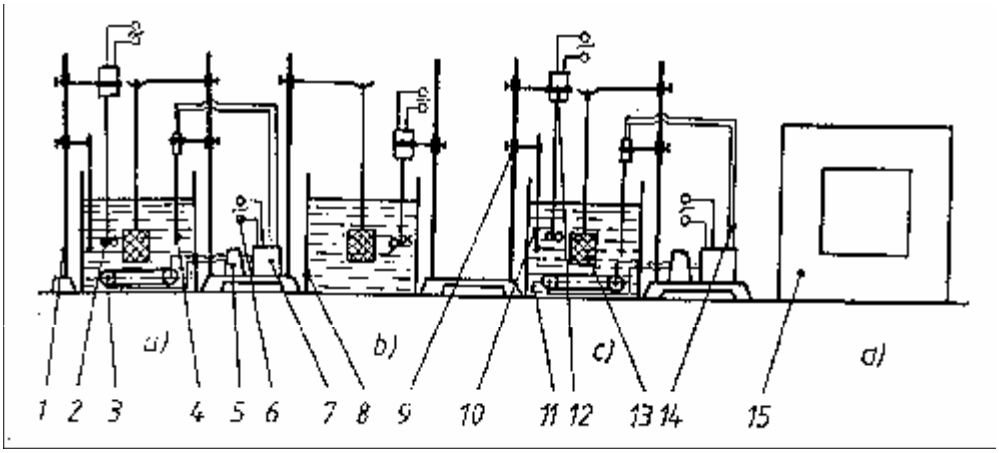

Figure 2. The phosphatation installation for cold extrusion of steel. a) degreasing; b)pickling; c)chemical crystalline phosphatation; d)drying; 1 stillage; 2 stirrer; 3 electrical resistance; 4 thermocouple, 5- relay; 6 plug, 7 temperature regulator, 8 tub made of stainless steel; 9 clip; 10 thermometer; 11 chemical solution; 12 stir motor; 13 basket for tubes, 14 conductor; 15 stove.

In figure 3 is presented the general view of the installation of chemical crystalline phosphatation for the stage of laboratory tests.

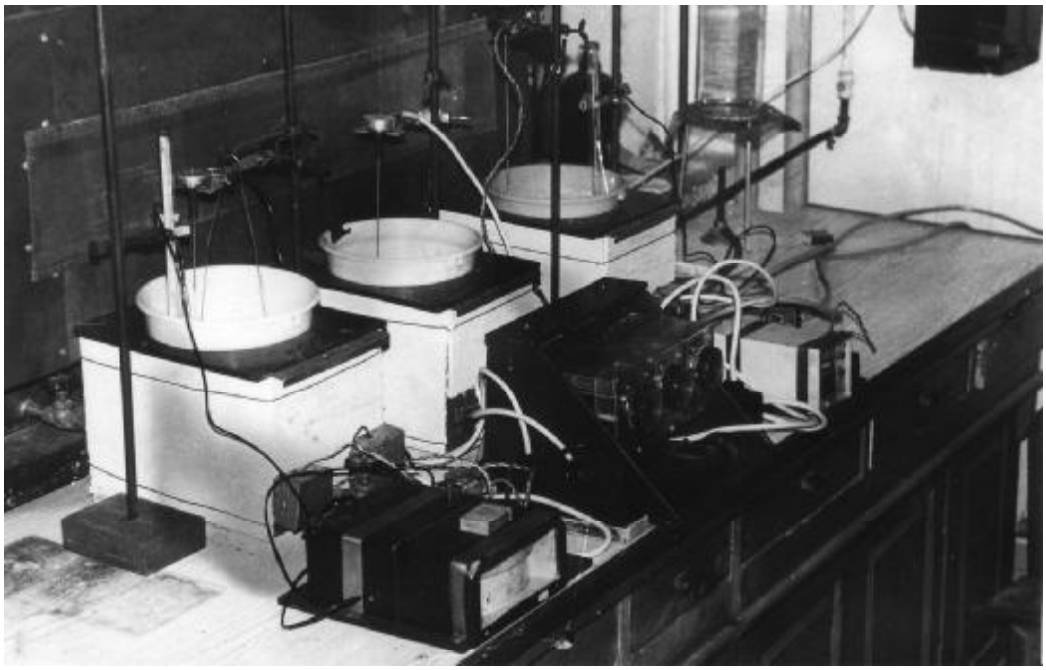

Figure 3.General view of the phosphatation installation.

Warming the degreasing and crystalline phosphatation solutions is made in tubs of stainless steel by protected electrical resistance

The work temperature is maintained with the help of the electronically thermo regulator type 1RT-96 with the domain of temperatures 0÷400 °C and thermocouple Fe-Const. type T.F.A., Swiss.

The time of work is established by timers with the domain of measurement 0÷6 h and sounding warning NTRE 2837-86.

Stirring the baths is made by stirrers driven by electrical engines type SIEMENS 1AF 2210 0A, 220V.

Drying the tubes after the chemical crystalline phosphatation is made in a stove with electrical warming and the domain of temperatures 100÷150 °C

The phosphate layer justifies the use at extrusion only if it contains the adequate lubricant. In this way, it is used a lubricant based on bisulphide of molybdenum.This is stable until the temperature of 450 °C which is superior to the one in the process of extrusion (200÷250 °C), because of the thermal effect of the plastic deformation

3. Conclusions

-The trizinc tetrahidrate phosphate layer Zn3(PO4)2 4H2O, is porous and covers 0,1-0,5 of semi product surface that conduce to a lubricant retention by 13 times more than no phosphate metallic surface.

-The passing time of semi products from chemical acid pickling bath to phosphate bath must be as short as possible.

-The installation permits the phosphatation in laboratory conditions. For industrial scale are additional necessary washing and neutralization baths

Received April 29, 2007 *The "Gh.Asachi" Technical University Iaşi*

REFERENCES

1. Bejinariu C., **Extrudarea indirectă la rece a oţelurilor**, Editura Tehnopress Iaşi, 2004, ISBN 973-702-002-2

FOSFATAREA CHIMICĂ CRISTALINĂ A SEMIFABRICATELOR DIN OŢEL PENTRU EXTRUDARE LA RECE

Rezumat: Lucrarea prezintă tehnologia fosfatării în vederea extrudării indirecte la rece a semifabricatelor din oţel. Se prezintă fluxul tehnologic pentru fosfatarea chimică cristalină, compoziţia chimică şi parametrii regimului de lucru pentru degresare chimică alcalină, decapare chimică acidă şi fosfatare chimică cristalină. De asemenea, concepţia instalaţiei de fosfatare de laborator şi instalaţia realizată.

BULETINUL INSTITUTULUI POLITEHNIC DIN IAŞI
Tomul L(III (LVII), Fasc. 4, 2007
Secţia
ŞTIINŢA ŞI INGINERIA MATERIALELOR

ASPECTS REGARDING THE MEASURING AND ENVIRONMENT OF THE ATOMIC FORCE MICROSCOPE

BY

MARIUS DAN BENŢA

Abstract: In contact AFM electrostatic and/or surface tension forces from the adsorbed gas layer pull the scanning tip toward the surface. It can damage samples and distort image data. Therefore, contact mode imaging is heavily influenced by frictional and adhesive forces compared to non-contact or tapping mode. Non-contact imaging generally provides low resolution and can also be hampered by the contaminant layer which can interfere with oscillation. Tapping Mode AFM was developed as a method to achieve high resolution without inducing destructive frictional forces both in air and fluid. With the Tapping Mode technique, the very soft and fragile samples can be imaged successfully. Also, incorporated with Phase Imaging, The tapping mode AFM can be used to analyze the components of the membrane.

Keywords: exterior scanning; nanotechnology; cantilever; microscopy

1. Introduction

AFM stands for Atomic Force Microscopy or Atomic Force Microscope and is often called the "Eye of Nanotechnology". AFM, also referred to as SPM or Scanning Probe Microscopy, is a high-resolution imaging technique that can resolve features as small as an atomic lattice in the real space. It allows researchers to observe and manipulate molecular and atomic level features.[5].

The predecessor of AFM is STM, Scanning Tunneling Microscopy or the Scanning Tunneling Microscope, was invented in 1981 be G. Binnig and H. Rohrer who shared the 1986 Nobel Price in Physics for their invention. An excellent technique, STM is limited to imaging conducting surfaces.[5].

AFM has much broader potential and application because it can be used for imaging any conducting or non-conducting surface. The number of applications for AFM has exploded since it was invented in 1986 and now encompass many fields of nanoscience and nanotechnology. It provides the ability to view and understand events as they occur at the molecular level which will increase our understanding of how systems work and lead to new discoveries in many fields. These include life science, materials science, electrochemistry, polymer, science, biophysics, nanotechnology, and biotechnology. [5].

The AFM can be operated in two principal modes: a. - with feedback control; b. - without feedback control. [9].

The AFM consists of a microscale cantilever with a sharptip (probe) at its end that is used to scan the specimen surface. The cantilever is typically silicon or silicon nitride with a tip radius of curvature on the order of nanometers. When the tip is brought into proximity of a sample surface, forces between the tip and the sample lead to a deflection

of the cantilever according to Hooke's law. Hook's law gives F = -kz, where F is the force, k is the stiffness of the lever, and z is the distance the lever is bent.[10].

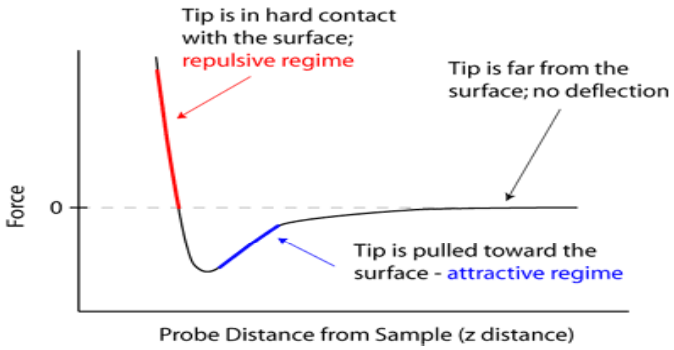

Fig.1 measuring forces

2. Measurement environment considerations:

Table 1: Given the wide variety of applications that use particles, it makes sense that there are many different ways to analyze and characterize particles. The following is a partial list of the material classes of particles in different environmental media, as analyzed by an AFM:

Imaging in air:	-dry powders, -evaporated suspensions, -bio – particles, -carbon nanotubes, -TEM samples, -SEM samples,
Imaging in liquid:	-bio particles in buffer, -inorganic particles 3,2 hard surface materials,
Imaging embedded particles:	-soft polymer and bio-materials, -membranes and defects,

There are two primary considerations for selecting instrumentation: a) single particle versus ensemble, and b) the environment the measurement is made in – air, liquid, vacuum. Table 1 shows a comparison of the most common material classifications and environmental media for particle analysis. In general, morphological information, such as shape and aspect ratio, as well as surface information, such as texture and roughness parameters, cannot be obtained using ensemble techniques.

Imaging in air - A substantial advantage of using an AFM for Nanoparticle characterization is that the scanning may be done in ambient conditions. Thus, most applications for characterizing Nanoparticles are performed in air

Imaging in liquid - AFM is an essential tool to identify topographical features of particles submerged in liquid. The range of applications include soft polymers, bio-particles (cells, membranes, viruses) and a variety of inorganic particles.

Imaging of embedded particles - Nanoparticles that are imbedded in surfaces can be visualized using physical measurement techniques such as vibrating phase and LFM27. Certainly, if particles largely extend out of the surface, then traditional methods for topographic imaging will work.

3. Imaging environment

Table 2: application environment

	air	fluid	vacuum	Special gas
AFM				
TEM				
OPTICAL				
SEM				

4. Measuring domain analysis

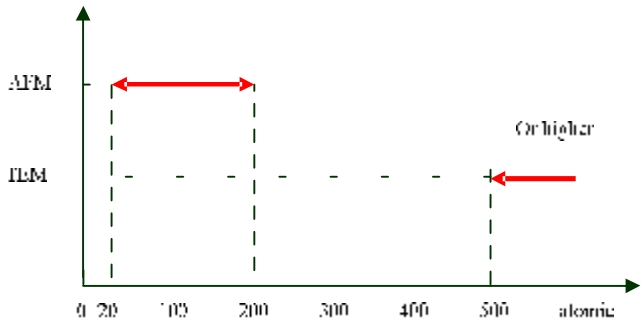

Fig. 3 measuring domain for AFM and TEM

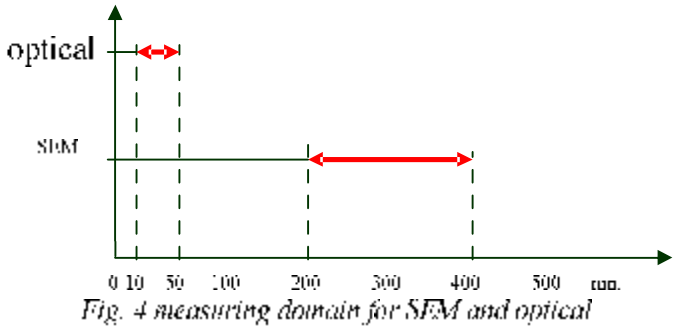

Fig. 4 measuring domain for SEM and optical

5. Advantages and disadvantages

The AFM has several advantages over the scanning electron microscope (SEM). Unlike the electron microscope which provides a two-dimensional projection or a two-dimensional image of a sample, the AFM provides a true three-dimensional surface profile.[12]

Additionally, samples viewed by AFM do not require and special treatments (such as metal/carbon coatings) that would irreversibly change or damage the sample. While an electron microscope needs an expensive vacuum environment for proper operation, most AFM modes can work perfectly well in ambient air or even a liquid environment. This makes it possible to study biological macromolecules and even living organisms. In principle, AFM can provide higher resolution than SEM. It has been shown to give true atomic resolution in ultra-high vacuum (UHV). UHV AFM is comparable in resolution to Scanning Tunneling Microscopy and Transmission Electron Microscopy.[3].

A disadvantage of AFM compared with the scanning electron microscope (SEM) is the image size. The SEM can image an area on the order of millimeters by millimeters with a depth of field on the order of millimeters. The AFM can only image a maximum height on the order of micrometres and a maximum scanning area of around 150 by 150 micrometres. Another inconvenience is that at high resolution, the quality of an image is limited by the radius of curvature of the probe tip, and an incorrect choice of tip for the required resolution can lead to image artifacts. Traditionally the AFM could not scan images as fast as an SEM, requiring several minutes for a typical scan, while an SEM is capable of scanning at near real-time (although at relatively low quality) after the chamber is evacuated. The relatively slow rate of scanning during

6. Conclusions

In general, AFM individual particle size characterization is both cost and time effective, see Figure below. AFM resolution is greater or comparable to traditional techniques. The main advantage of AFM for particle characterization is unambiguous morphology determination along with direct measurements of volume and 3D display.[13]

The AFM can be operated in two principal modes: a. - with feedback control; b. - without feedback control.[12]

When the tip is brought into proximity of a sample surface, forces between the tip and the sample lead to a deflection of the cantilever according to Hooke's law. [7]

Received April 11, 2007 *Transilvania University of Brasov*

REFERENCES

1. R. Wiesendanger, **Scanning Probe Microscopy and Spectroscopy**, Cambridge University Press, Cambridge 1994;

2. D. Sarid. **Scanning Force Microscopy**, Oxford Series in Optical and Imaging Sciences, Oxford University Press, New York 1991,

3. W. Cross SPM – Scanning Probe Microscopy Website;
4. F. Giessibl, *Advances in Atomic Force Microscopy*, **Reviews of Modern Physics** 949-983 2003;
5. P. M. Hoffmann, A. Oral, R.A. Grimble, H. O Ozer, S. Jeffery, J.B. Pethica, Proc. Royal Soc. 2001;
6. Albrecht, T.R., Akamine, S., Carver, T.E., and Quate, C.F. (1990) *Microfabrication of cantilever styli for the atomic force microscope*. **J. Vac. Sci. Technol.** A 8(4), 3386-3396
7. Binnig, G., Quate, C.F., and Gerber, Ch. (1986) *Atomic force microscope* **Phys. Rev. Lett.** 56(9), 930-933
8. Meyer, G. and Amer, N.M. (1988) *Novel optical approach to atomic force microscopy*, **Appl. Phys. Lett.** 53(12), 1045-1047
10. Binnig, G., Quate, C.F., and Gerber, Ch. (1986) *Atomic force microscope* **Phys. Rev. Lett.** 56(9), 930-933
11. Putman, C.A.J., De Grooth, B.G., Van Hulst, N.F., and Greve, J. (1992) *A detailed analysis of the optical beam deflection technique for use in atomic force microscopy* **J. App. Phys.** 72(1), 6-12
12. S. Dror. **Scanning force microscopy: with applications to electric, magnetic and atomic forces**, Oxford University Press, 1994
13. www. agilent/find/afm

ASPECTE PRIVIND MĂSURAREA ŞI MEDIUL DE LUCRU AL MICROSCOPULUI DE FORŢĂ ATOMICĂ

Rezumat: În contact cu câmpul electrostatic şi/sau tensiunile superficiale din MFA forţele ce apar în stratul superficial de gaz absorbit forţează deplasarea scanării spre suprafaţă. Acest fapt conduce la deteriorarea epruvetelor şi distorsionarea imaginii obţinute.

BULETINUL INSTITUTULUI POLITEHNIC DIN IAŞI
Tomul LIII (LVII), Fasc. 4, 2007
Secţia
ŞTIINŢA ŞI INGINERIA MATERIALELOR

DYNAMICS OF THE HYDRAULIC DRIVE CONTROL SYSTEM WITH VARIABLE-DISPLACEMENT PUMP

BY

YU. BURENNIKOV, L. KOZLOV and S. REPINSKIY

Abstract: A basic circuit for designing automatic regulator of the variable-displacement pump is proposed. It is based on a combined control method that provides the pump flow rate stabilization as well as constant-power operation of the pump. A mathematical model of the proposed system is presented. It is determined how the control system design parameters influence dynamic characteristics and stability of the variables that describe control system state. The combination of design parameters providing stable operation has been determined as well as the required quality parameters throughout the whole range of the hydraulic drive functioning both for flow rate and pressure regulator operation.

Keywords: automatic pump regulator, hydraulic drive, dynamic characteristics, variable displacement pump, mathematical model, oscillation, transient process quality parameters, flow rate regulator, control system, stability, regulation time.

1. The study of the dynamics of the hydraulic drive control system

Variable-displacement pumps often come to be the most significant components of hydraulic drives for technological mobile machines. At the same time hydraulic components manufacturers in response to the hydraulic drive development trends strive to increase hydrodrive efficiency and to use the potential of hydroautomatics for remote control. This makes it necessary to improve variable-displacement pump control by using automatic regulators. All these trends and requirements lead to higher efficiency and to increased versatility of the pumps [1-4].
While designing automatic regulators for variable-displacement pumps first of all it is necessary to determine the influence of different regulator and variable-displacement pump parameters on the dynamic characteristics and stability of the system. This can be done by means of mathematic modelling. Our main purpose is to choose the parameters of the variable-displacement pump control system on the basis of its dynamics and stability research.

The authors have developed a basic circuit for designing automatic regulator of the variable-displacement pump that is based on a combined control principle that provides pump flow rate stabilization as well as constant-power mode of pump operation (Fig. 1). Such regulator satisfies all the requirements to pump regulators of the new generation [1-3].

The circuit includes axial-piston variable-displacement pump 1, variable throttles 7, flow rate regulator 8 with spool 9 and spring 10 that is connected to hydraulic lines 3 and 16 and controls the flow from hydraulic line 3 to control piston 4. Swash plate 2 of the pump is under the influence of pistons 4, 5 and spring 6. At the

output of the control piston 4 there is throttle 15. Pressure regulator 11 with spool 12 and springs 13, 14 limits maximum pressure in the pressure line and provides constant-power mode of pump operation.

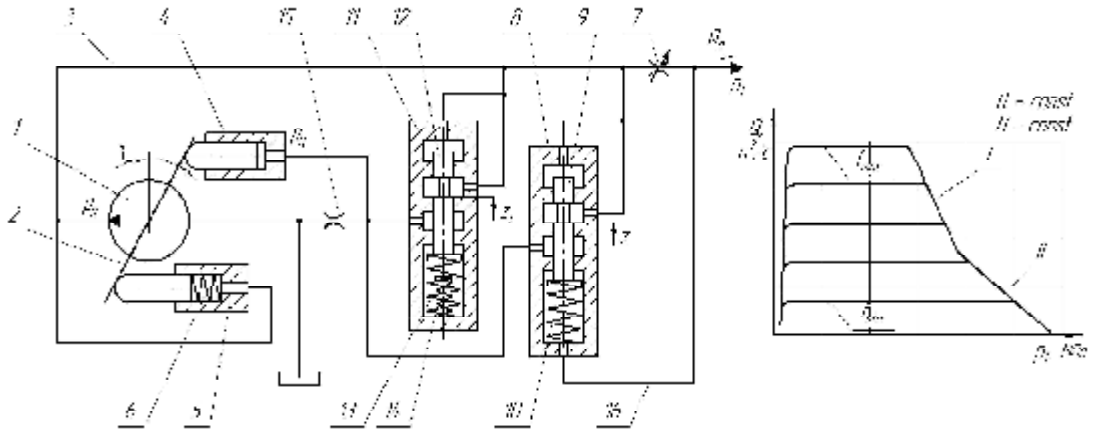

Fig. 1 Basic circuit of the variable-displacement pump control system

In a steady-state operation mode control system works in the following way. Pressures p_{II}, p_1 and spring 10 force acting on spool 9 determine its position so that pressure p_{II} in piston 4 balances the torque on swash plate 2 which is created by pressure p_{II} in piston 5 together with spring 6. Spring 10 is selected so that it can maintain constant pressure differential on throttle 7. When pressure p_{II} increases considerably, pressure regulator 11 with spool 12, springs 13, 14 operates so that pressure fluid flows to control piston 4 moving the swash plate to provide constant-power mode of pump operation.

Static characteristics of the pump with the proposed control system are described as a relationship shown in fig. 1, where f_{max}, f_{min} are maximal and minimal areas of the opening of the throttle 7 working port. Two springs 13 and 14 provide two regions on the static characteristic that approximate total characteristic to a hyperbolic curve describing constant-power mode of pump operation. Region I is provided by spring 13 operation and region II – by simultaneous operation of springs 13, 14.

According to the basic circuit, mathematical model of the variable-displacement pump control system includes equations of forces and torques acting on the control elements of the system, and flow continuity equations for corresponding lines. Equations of the mathematical model were set up under the following assumptions: hydraulic lines are of small length and so the influence of hydraulic losses and wave processes on the drive dynamics was considered to be negligible; working fluid temperature is constant; chambers compliance and compression of the working fluid were taken into account as average values for the given intervals of pressure variations; flow rate coefficients for the throttling and spool elements are constant; control system operation modes are cavitation-free; hydrodynamic forces acting on regulator spools were neglected as well as their masses. The adopted assumptions being taken into account, equations of the mathematical model of the pump control system will be written:

$$\frac{\pi d_p^2}{4} \cdot d_R \cdot k \cdot n \cdot \operatorname{tg}\gamma \quad \mu \cdot f_{op}\sqrt{\frac{2(p_H \quad p_1)}{\rho}} \cdot sign(p_H - p_1) +$$

$$+ \mu \cdot f(z)\sqrt{\frac{2(p_H \quad p_M)}{\rho}} \cdot sign(p_H - p_M) + \tag{1}$$

$$+ \mu \cdot f_1(z_1)\sqrt{\frac{2(p_H - p_M)}{\rho}} \cdot sign(p_H \quad p_M) + \beta_1 \cdot W_H \frac{dp_H}{dt}$$

$$I\frac{d^2\gamma}{dt^2} \quad p_H \cdot F_1 \cdot \ell \quad p_M \cdot F_2 \cdot \ell + M_C \quad b_\gamma \frac{d\gamma}{dt} \tag{2}$$

$$b_P \frac{dz}{dt} \quad p_H \cdot f_P \quad p_1 \cdot f_P \quad c_P(z_P + z) - T_P \cdot sign\frac{dz}{dt} \tag{3}$$

$$b_{P1}\frac{dz_1}{dt} \quad p_H \cdot f_{P1} - c_{P1}(z_{P1} + z_1) - T_{P1} \cdot sign\frac{dz_1}{dt} \tag{4}$$

$$\mu \cdot f(z)\sqrt{\frac{2(p_H - p_M)}{\rho}} \cdot sign(p_H \quad p_M) +$$

$$+ \mu \cdot f_1(z_1)\sqrt{\frac{2(p_H - p_M)}{\rho}} \cdot sign(p_H - p_M) \quad \mu \cdot f_0\sqrt{\frac{2p_M}{\rho}} + \beta_2 \cdot W_M \frac{dp_M}{dt} \tag{5}$$

where p_H is pump output pressure; γ – pump swash plate turning angle; p_H pressure of the swash plate control piston; p_1 – load pressure of the actuator; F_1 – area of control piston 4; F_2 – area of control piston 5; I – moment of inertia of pump swash plate; b_γ – kinematic viscosity coefficient of the pump swash plate; d_p – pump piston diameter; d_R – diameter of pistons locations in the pump rotor; k – the number of pump pistons; n – speed of pump shaft rotation; ℓ – arm of the control cylinders action on the pump swash plate; M_C anti-torque moment of the pump swash plate that was calculated from the following formular in N·m [4];

$$M_C \quad 26{,}4 \quad 3{,}2\left(\frac{p_H \quad 9\cdot10^6}{7\cdot10^6}\right) \quad 9{,}9\left(\frac{Q_n - 0{,}67\cdot10^{-3}}{0{,}5\cdot10^{-2}}\right) \quad 2{,}2\left(\frac{p_H \quad 9\cdot10^6}{7\cdot10^6}\right)\times\left(\frac{Q_n - 0{,}67\cdot10^{-3}}{0{,}5\cdot10^{-2}}\right);$$

Q_n – flow rate of the working fluid that flows to the actuator; z – displacement of the spool 9 of the flow rate regulator 8; z_1 – displacement of the spool 12 of the pressure regulator 11; $f_P \quad \frac{\pi \cdot d_P^2}{4}$ – end face area of the flow regulator spool 9; d_P – end face diameter of the flow regulator spool 9; $f_{P1} \quad \frac{\pi \cdot d_{P1}^2}{4}$ – end face area of the pressure regulator spool 12; d_{P1} end face diameter of the pressure regulator spool 12; c_P – spring 10 rate of the flow rate regulator 8; c_{P1} total rate of springs 13, 14 of the pressure regulator 11; z_P, z_{P1} initial compression value of the springs of flow rate regulator 8 and pressure regulator 11 correspondingly; $f(z), f_1(z_1)$ opening areas of the working ports of flow rate regulator 8 and pressure regulator 11; b_P, b_{P1} – kinematic viscosity coefficients for the flow rate and pressure regulators correspondingly; T_P, T_{P1} dry friction forces of the spools of flow rate and pressure

regulators correspondingly; ρ – pressure fluid density; μ flow rate coefficient of throttling elements; f_{0p} – opening area of the variable throttle 7 work port; f_0 work port opening area of the throttle 15 in the discharge line of the pump swash plate control piston; W_H pressure fluid volume in pressure line section adjacent to the pump; $W_Ц$ – pressure fluid volume in the pump swash plate control piston and hydraulic line section adjacent to it; β_1, β_2 – generalized coefficients of the pressure fluid compression by the W_H and $W_Ц$ volumes correspondingly.

The values of work port opening areas of the flow rate and pressure regulator spools are approximated by the expression

$$f(z) \quad 0{,}1\cdot10^{-6}\ \text{m}^2 \ \text{if} \ 0 < z < z_{\text{min}},$$
$$f(z) \quad k_Z \cdot z \ \text{if} \ z_{\text{min}} < z < z_{\text{max}};$$

$$f_1(z_1) \quad 0{,}1\cdot10^{-6}\ \text{m}^2 \ \text{if} \ 0 < z_1 < z_{1\text{min}},$$
$$f_1(z_1) \quad k_{Z1} \cdot z_1 \ \text{if} \ z_{1\text{min}} < z_1 < z_{1\text{max}};$$

where $z_{\text{min}}, z_{1\text{min}}$ are spool displacement values when throttling slots of the flow rate and pressure regulators are opened; $z_{\text{max}}, z_{1\text{max}}$ spool displacement values, when throttling slots of the flow rate and pressure regulators are closed; k_Z, k_{Z1} – opening area coefficients of the work ports of the flow rate regulator 8 and pressure regulator 11 correspondingly.

Equation set that describes behavior of the variable-displacement pump control system was investigated using MATLAB Simulink software package. Using mathematical model a transient process was obtained that has made it possible to find dynamic characteristics of the variables describing control system state. Pump output pressure p_H, pump swash plate turning angle γ, fluid pressure $p_{Ц}$ of the pump swash plate control piston, displacement z of the flow regulator spool and displacement z_1 of the pressure regulator spool were considered as variables that describe state of the variable-displacement pump control system.

As a result of processing the data obtained by means of mathematical model the influence of the main regulator design parameters on the transient process quality parameters was determined: regulation time, oscillations, overcontrol and the stability of control system state variables.

Regulation time t_p in the hydraulic drive was determined according to the moment of variable value entering the ±5% range relatively to the steady-state value of the corresponding variable.

Overcontrol of the hydraulic drive was found from the formular:

$$\sigma \quad \frac{A_{\text{max}}}{A}\cdot 100\%,$$

where A_{max} is maximal value of the variable, that describes hydraulic drive condition; A – steady-state value of the variable.

Fig. 2 shows the relationships of such transient process quality parameters as regulation time t_p, oscillation k and overcontrol σ of the one control system state variable-pump output pressure p_H versus main parameters of the regulator.

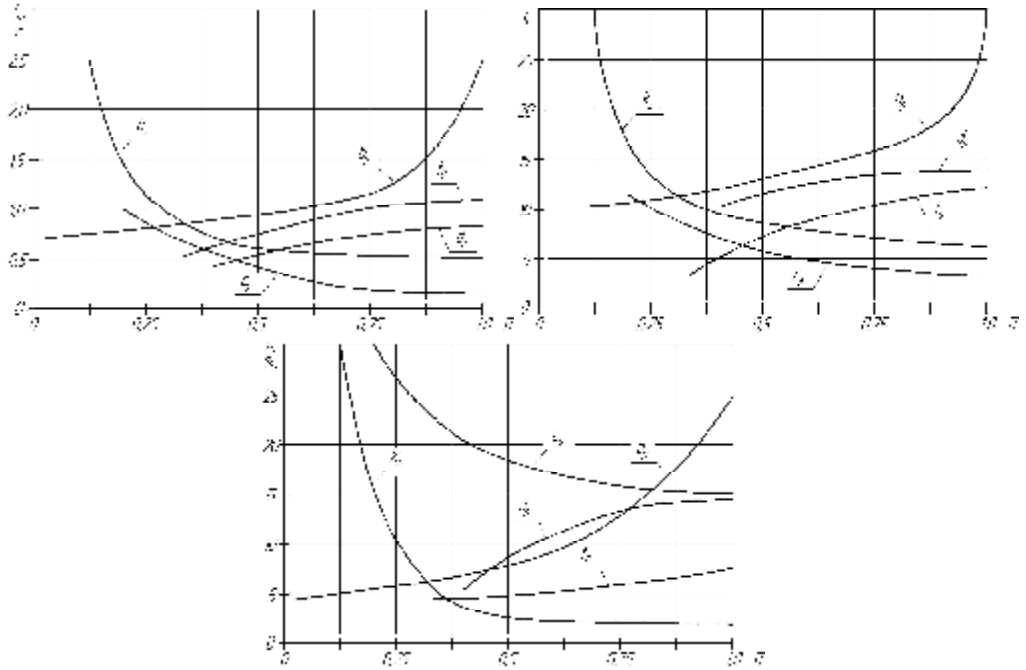

Fig. 2 Influence of the main regulator parameters on the regulation time, oscillation and overcontrol.

In Fig. 2 along the abscissa axis the values of non-dimensional parameters are plotted: $\Pi = \Pi_i / \Pi_{i\max}$, where Π_i – actual current parameter values, $\Pi_{i\max}$ – maximal parameter values. Parameter maximal values were equal to the upper limits of the parameters change range: $d_p = (4{,}0...10{,}0)\cdot10^{-3}$ m; $c_p = (0{,}8...4{,}0)\cdot10^{4}$ N/m; $k_2 = (0{,}5...4{,}0)\cdot10^{-3}$ m; $b_p = 5...200$ N·c/m; $f_0 = (0{,}5...1{,}5)\cdot10^{-6}$ m^2. Such regulator parameters as k_2, b_p and c_p have the strongest influence on the transient process quality. The presented results can be used for designing variable-displacement pump control system with pre-defined dynamic characteristics. To satisfy high requirements to the speed of response, it is recommended to increase spring rate c_p and coefficient k_2 of the work port opening area of the flow rate regulator spool; to reduce kinematic viscosity coefficient b_p and diameter d_p of the flow rate regulator spool as well as to reduce opening areas f_0 of the throttle work port in the discharge line of pump swash plate control piston.

The operation stability of the hydraulic drive with variable-displacement pump was determined according to the type of transient process under changing pressure p_1 at the actuator input and opening area f_{sp} of the variable throttle which define the load and the speed of the actuator motion. Such transient process was considered to be stable under which oscillation amplitude of the variables, describing the state of the hydraulic drive control system, was increasing continuously.

Fig. 3 shows the influence of such flow rate regulator parameters as d_p, b_p, k_2 and f_0 in $p_1 - f_{sp}$ coordinates. When plotting stability regions, shading was directed towards stable region.

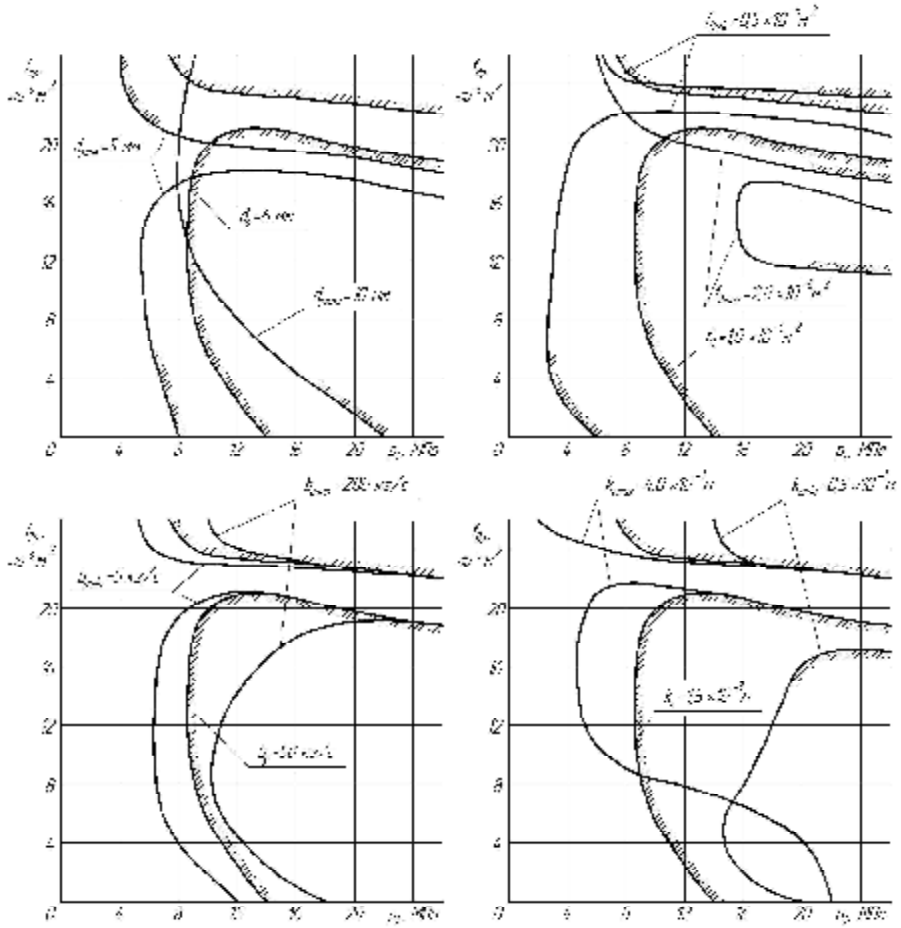

Fig. 3 The influence of the variable pump control system parameters on the location of the system stability limits (for flow regulator operation)

f_{z1} value has the most evident influence on stability. If the openings area f_{z1} of the work part of the throttle at the output of the pump swashplate control piston is reduced, stable operation region is extended considerably. The value of b_{y1} also has strong influence on stability. The reduction of b_{y1} value from 5 to 50 N·c/m provides extended stability range of the hydraulic drive operation. The extended stability region can also be achieved by reducing diameter d_{y1} of the flow regulator spool in the range from 5 to 6×10^{-3} m and increasing opening area coefficient k_{z1} of the work port of the flow regulator spool to $4{,}0\times10^{-3}$ m

The obtained relationships have made it possible to define the set of flow regulator parameters for stable operation of the variable-displacement pump in the entire range of the actuator flow and pressure values. In particular, under the combination of flow regulator parameters that change in the intervals d_{y1} = 5…6 mm; f_{z1} = (0,5…1,0)×10^{-6} m^2; b_{y1} = 5…20 N·c/m; k_{z1} = (1,5…4,0)×10^{-3} m, control system of the variable-displacement pump with automatic regulator is stable in the entire range of the hydraulic drive operation.

Fig. 4 shows the influence on stability of such pressure regulator parameters as d_{y2}, b_{y2}, k_{z2} and f_{z2} in the $p_H - Q_H$ coordinates The value of f_{z2} has the most evident

influence on the hydraulic drive control system under pressure regulator operation as well as under flow rate regulator operation. However the nature of this influence is different. As opening area f_t of the work port of the throttle at the discharche of the pump swash plate control piston changes in the interval from 1,0 to $1,5\times10^{-6}$ m^2, stability region under pressure regulator operation is extended considerably. As for flow rate regulator operation, stability region is extended when the value of f_t is reduced to $0,5\times10^{-6}$ m^2. Due to the different nature f_0 influence on the stability of pressure and flow rate regulators, it was found that in the interval of f_t changing from 0,8 to $1,2\times10^{-6}$ m^2 the sufficiently wide range of hydrodrive stable operation is provided both for flow rate and pressure regulators operation.

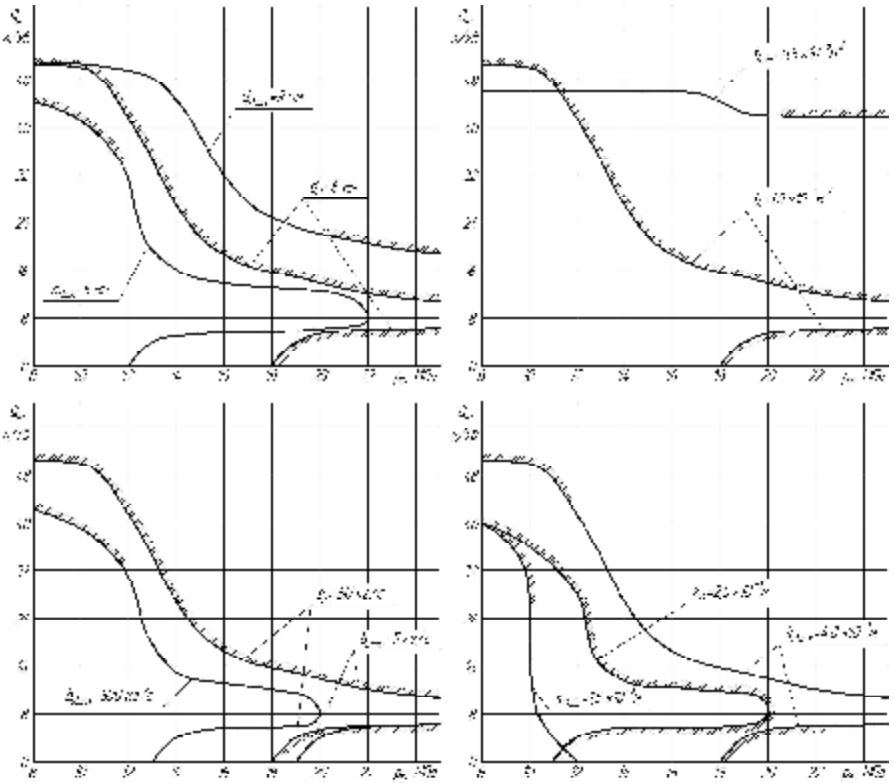

Fig. 4 The influence of the variable pump control system parameters on the location of the system stability limits (for pressure regulator operation)

The kinematic viscosity coefficient b_{p1} of the pressure regulator spool also has a strong influence on stability. To provide stable operation of the hydraulic drive control system it is necessary that b_{p1}>50 N·s/m. Stability region can also be extended by reducing the diameter d_{p1} of pressure regulator spool in the interval from 5 to 6×10^{-3} m and also reducing the opening area coefficient $k_{\Omega 1}$ of the pressure regulator work part to $1,5\times10^{-3}$ m.

The obtained relationship have made is possible to find such combination of the pressure regulator parameters for stable operation of the variable-displacement pump control system in the whole range of the changing flow delivered to the actuator and pump output pressure. In particular, under the combination of pressure regulator

parameters changing in the interval d_{p1}= 5…6 mm; f_0= (1,0…1,5)×10^{-6} m^2; b_{p1}= 50…500 N·c/m; k_{z1}= (0,5…2,5)×10^{-3} m variable-displacement pump control system with automatic regulator is stable in the entire range of the hydraulic drive operation.

Conclusion

Mathematical model of the variable-displacement pump control system with automatic regulator has been developed. The automatic regulator provides both pump flow rate stabilization and constant-power mode of pump operation. Resulting from research and analysis of transient process quality parameters and of the stability of the proposed variable-displacement pump control system, the combination of such regulator design parameters has been found that provides the pre-defined dynamic characteristics and stable operation of the variable-displacement pump control system in the entire operation range both for flow rate regulator and pressure regulator operation: d_p= 5…6 mm; d_{p1}= 5…6 mm; f_0= (0,8…1,2)×10^{-6} m^2; b_p= 20…50 N·c/m; b_{p1}= 50…500 N·c/m; k_z= (1,5…4,0)×10^{-3} m; k_{z1}= (0,5…2,5)×10^{-3} m

Received April 5, 2007

Vinnytsia National Technical University, Vinnytsia, Ukraine

REFERENCES

1. Буренніков Ю.А., Козлов Л.Г., Рєпінський С.В. *Удосконалення схем регуляторів подачі насосів гідросистем, чутливих до навантаження, та їх статичні характеристики* // **Вісник ВПІ** – 2004. – №5. – С. 88-92.

2. Ju. Burennikov, L. Kozlov, S. Repinskiy, G. Kozlova *Modelling of the variable-displacement pump control system using MATLAB Simulink software package* // **Tehnomus XIII**: Tehnologii şi produse noi în construcţia de maşini: a XIII-a Conferinţă Ştiinţifică cu participare internaţională Universitatea „Ştefan cel Mare" Suceava. Facultatea de Inginerie Mecanică – Suceava: Editura Universităţii din Suceava. 2005 – P. 516-520.

3. Буренніков Ю.А., Козлов Л.Г., Рєпінський С.В. *Моделювання системи керування насосом змінної продуктивності за допомогою програмного пакета MATLAB Simulink* // **Інформаційні технології та комп'ютерна інженерія**. 2006. №1(5). С. 89-93.

4. Козлов Л.Г. **Вдосконалення систем керування гідроприводів з LS-регулюванням**. – Дис. канд. техн. наук: 05.02.03. – Вінниця, 2000.

DINAMICA SISTEMULUI DE CONTROL AL DIRECŢIEI CU POMPĂ VARIABILĂ

Rezumat: Lucrarea propune un nou concept de regulator automat cu pompă cu dispunere variabilă. Aceasta se bazează pe un control combinat ce determină stabilizarea debitului pompei, dar şi o putere utilă constantă a pompei. Se propune un model matematic prin care se analizează cîţi parametrii de proiectare influenţează caracteristicile dinamice şi stabilitatea variabilelor ce descriu starea sistemului de control.

BULETINUL INSTITUTULUI POLITEHNIC DIN IAŞI
Tomul L(III (LVII), Fasc. 4, 2007
Secţia
ŞTIINŢA ŞI INGINERIA MATERIALELOR

VERSATIL TITANIUM ALLOY FOR BIOMEDICAL APPLICATION TO SPINAL IMPLANTS

BY

A. BUZAIANU[1], DOINA RADUCANU[2], ROXANA TRUSCA[1], E. VASILE[1], V. D. COJOCARU[2], I. RUSU[3], C. MUNTEANU[3], M. LOZNEANU[3] and O. CARP[4]

Abstract: Titanium alloys are prized for their excellent strength/weight ratio and relatively high temperature capability in the aerospace industry, for airframe and engine components. Titanium alloys have an excellent corrosion resistance and are also useful in the chemical industry and for biomedical implants. The most popular alpha+beta alloys are Ti-6A-4V, with a general purpose alloy. The special properties of these alloys made them more and more used in medicine lately. Because the interactions between cells and tissues with biomaterials at the tissue implant interface are almost exclusively surface phenomena, surface properties of implant alloys are of great importance. Nitriding under low discharge conditions may constitute interesting techniques, allowing the formation of surface layers on parts with sophisticated shapes. They may also permit to modulate surface topography in a way to improve the features of titanium alloys for various applications in medicine..

Keywords: Ti-6Al-4V alloy, biomedical application, titanium nitriding, spinal implants, SEM investigation.

1. Introduction

It is well known that titanium alloys have some attractive properties enabling them to be used in industries such as aerospace, marine and medicine while their poor tribological properties often are an obstacle in mechanical engineering applications. Ti-6Al-4V alloy is used as an implant material but, at the present, due to the toxicity of vanadium, its use is restricted and it became necessary to increase its surfaces' biocompatibility. These latter properties can be improved by applying nitriding surface treatments. Conventionally nitriding is conducted at high temperatures. The higher is the surface temperature of a sample the more efficient is the process of titanium nitriding and consequently the TiN phase formation. However the surface temperature during nitriding appeared to play a key role for the future properties of a processing material and in some cases it cannot be increased up to high values. A high-temperature plasma nitriding reduces the fatigue strength of titanium alloys. Literature reveals that a range of surface engineering techniques have been applied to titanium alloy substrates, including conventional thermo-chemical processes such as nitriding. Thermo-chemical processes have enjoyed only limited success, because of the long treatment times, high temperatures and unevenness of the surface microstructure. In addition, problems associated with poor ductility and significant reductions in the fatigue limit have also been reported in literature. That is why techniques allowing nitriding at relatively low temperatures have been developed over the last years. One of the temperature treatments, referred to as intensified plasma processing, enables surface treatment at a relatively low temperature of 673-772 K, [1].

Surgical implants are used in spinal surgery to correct scoliosis or a lateral curvature of the spine. One leading manufacturer of such surgical implants, who designs, machines and finishes implants and screws usually has three lines of implants: plates and screws for spines that are degenerating or have undergone trauma; hooks and rods and "cages" to replace damaged vertebrae. The nitriding coats of their implants force a direct and long-term stable osteointegration at the contact areas of the bone tissue with biocompatible materials. Variable plasma nitriding systems are exclusively reserved for medical applications. Some of the implant design variants are presented in Figure1.The histological data have shown that the times and modalities of osteointegration have been not altered by the PVD nitriding treated surfaces.

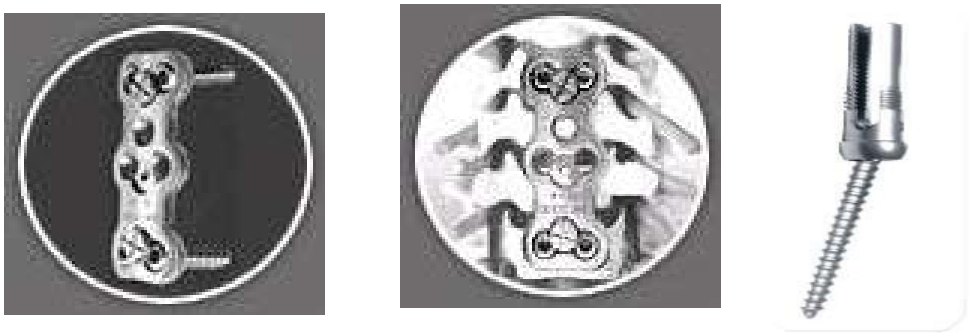

Fig.1. Cervical plating (left-CESCO tip) and Polyaxial screw of a spinal implant meant to repair articular cartilage.

Titanium nitride coatings have already been adopted in the biomedical field and many studies show their high biocompatibility. The objective of this investigation was to evaluate the nitriding process at various atmospheres and to determine how temperature affects the nitriding of Ti-6Al-4V alloys in dynamic nitrogen atmosphere. Also studied were the thermo- chemical treatments aiming to improve the surface properties of Ti-alloys, the influence of nitridation treatments at 800 and 1100K, the oxidation resistance of Ti-6Al-4V and the conditions for the formation of nitrided layers.

2. Materials and methods

The coating is applied with the PVD (Physical Vapor Deposition) process by a vacuum chamber, titanium nitride vapors condense on the surface, thus forming an extremely hard film, only a few microns thick. The prosthesis from the same commercial Ti-6Al-4V were ground flat and mechanically polished to a 0.5 alumina finish and nitrided in a conventional plasma nitriding equipment. Deposition material such as titanium is vaporized by means of an electric arc. Voltages in the range of 500 to 600V and currents from 300 to 400mA were adjusted to maintain the cathode temperature between 673 and 943K. These now highly charged titanium ions were mixed with nitrogen gas forming plasma. The positively charged titanium plasma is attracted to the negatively charged part to be coated. Ion by ion, titanium bonds to the part, growing a thin hard film on its surface. Mixtures of nitrogen and hydrogen (ratios in vol, N/H = 3/2) under a total pressure of 1 to 1.5 kPa were used. After nitriding the samples were cooled in the treatment chamber in a nitrogen atmosphere.

Nitridation may increase resistance to oxidation, but the influence of nitriding treatments depends on the composition of the material. For Ti-6Al-4V, the nitride layer prevented oxygen dissolution into the alloy during the earliest stages of oxidation, thus reducing the contribution of this process to the total mass. Certain results confirm the good biocompatibility of TiN + Ti2N AlphaTi(N) surface layers and this alloy's potential in bone surgery applications [2]. The widely used Ti-6Al-4V alloy is also the most common forging alloy. The chemical analyses of the samples correspond to ASTM F136 standard requirements and are shown in Table 1. The samples of commercial Ti-6Al-4V alloys are within the parameters of their respective standards

Table 1. The chemical composition of the samples [wt %].

Material	Ti %	Al %	V %	C %	Fe %	H %	N %	O %
ASTM F136	Bal	5,5 – 6,5	3,5 – 4,5	0,08	0,25	0,012	0,05	0,13
Ti-6Al-4V cast alloy	Bal	6,07	4,30	0,01	0,15	0,0024	0,009	0,13

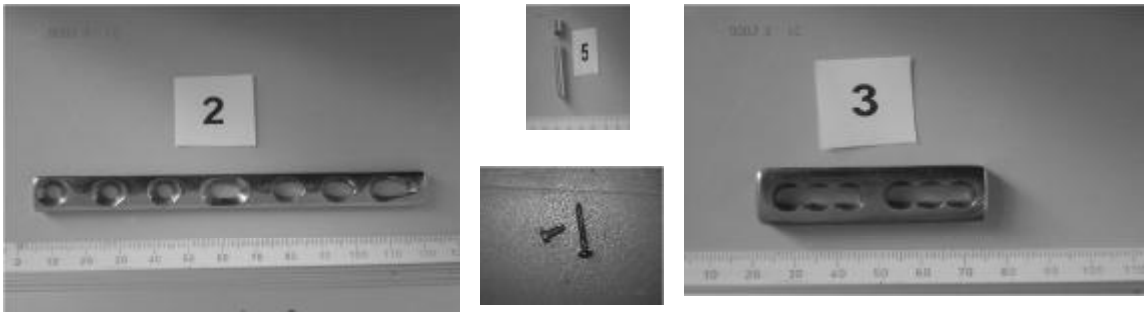

Fig. 2. Cervical plating systems of spinal implant (Inter body fusions for reconstructive spinal surgery) in experimental program.

In order to validate the titanium alloy composition and the prosthesis structural integrity, a representative series of tests - including cross-sectioning and microscopic inspection - was performed on representative prosthetic products. Tests also included inspections of porosity and inclusions (oxide particles). This ensured that the implant articular surface was homogeneous, without porosity or oxide particles that could cause increased wear or reduced fatigue strength. Scanning electron microscope energy dispersive X-ray analyses (EDX spectrometer) were available for the qualitative chemical analysis of the implant. A Hitachi S-2600 scanning electron microscope (SEM) was used to examine and analyze the particulate debris. The samples were prepared for microscopy by polishing them to smooth finish. Rockwell hardness was performed on samples that were hand polished according to microscopy samples. The remaining experiments were conducted on samples that were mounted in resin which underwent a much more rigorous polishing process. These samples were then etched with Kroll's reagent (100 ml H_2O + 5ml HNO_3 3ml HF), etching being

useful for Ti-Al-V alloys to better show their microstructure when observed under optical microscope.

3. Results and discussion

The influence of the main processing parameters such as temperature and time on the microstructure and the formation of new phases during the processes of nitriding are discussed. Based on investigations presented in the literature also analyzed are the effects of nitriding on the micro hardness and the corrosion resistance of titanium alloys. The improved mechanical properties, which arise from these thermo chemical treatments, are discussed in relation to the nitriding process applying at alloys used for implants. During the electrochemical process of corrosion in the body, titanium alloy can free vanadium ions, which may reduce the biocompatibility of the alloy and jeopardize the fate of implants.

The vanadium ions obstruct the function of cells in the vicinity of implants, as well as of cells at remote locations after the corrosion by-products are transported to distant locations inside the body. The stable coherent titanium oxide (TiO_2) forms a film and, in presence of TiN (electrical and thermal insulation), the electrochemical reactions that lead to corrosion are reduced or prevented. The oxidized metallic surface and ionic vanadium migration are stopped by "passivated"- surface implants.

In fact, implants of Ti-6Al-4V alloys exhibit a better corrosion resistance after surface nitriding. Microstructures can influence mechanical properties of titanium alloys. Fine microstructures enhance the strength and ductility of the titanium alloy and retard crack nucleation. Coarse microstructures are more resistant to creep and fatigue crack growth [2]. The transformed Beta sample with a fine microstructure was less hard than either the as-forged sample or the alpha + beta sample. The beta transformed sample had the lowest averages for the hardness testing of the three samples.

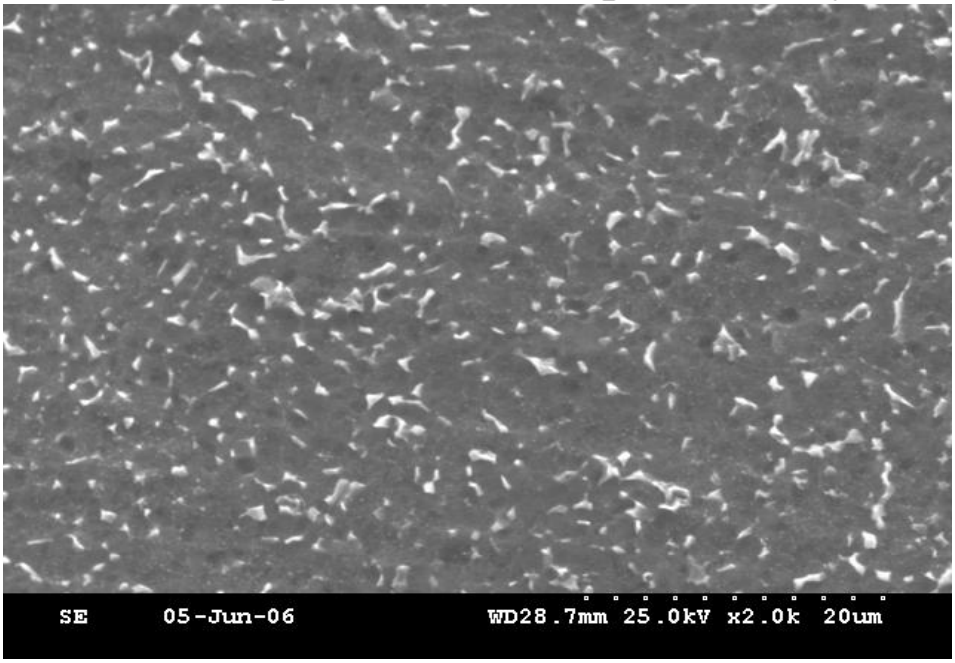

Fig. 3. SEM image Ti-6Al-4V alloy sample treated and aged.

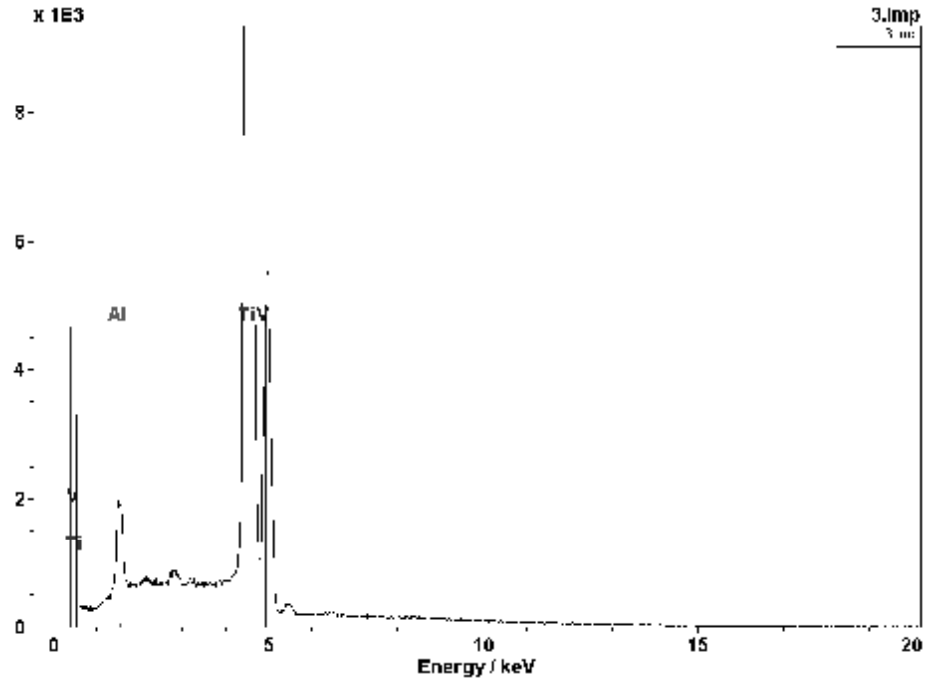

Fig.4. EDX spectrum analyses of Ti-6Al-4V.

The major event in phase chemistry and microstructure development of titanium alloys is the transformation from the low temperature hcp "alpha-phase" to the high temperature bcc "beta-phase". Certain alloying elements, particularly transition metal such as V, stabilize the cubic beta-phase and decrease the alpha-beta transformation temperature. These transition metals are "beta stabilizers". Simple metals, such as Al and interstitial solutes [O, N] are alpha-stabilizers and increase the temperature of the alpha-beta transformation [3]. Structured Ti-6Al-4V alloy adapted variable surface morphology. One can observe in Figure 3 that α-phase (globular alpha) has a larger volume fraction in the as-forged sample than the β-phase. The SEM micrograph for alloy showed that the grain size for α + β specimen is about 20-30μm, which is approximately the same as for the β-transformed sample. A precipitation hardening of titanium alloys is brought about by inter-metallic phases ω-phases in betha phases . The precipitation of the ω-phases can be brought about by ageing in the temperature range of 670-870K. (isothermal ω-phases). As related to Ti-6Al-4V, the vanadium content can locally reach a level of 20-25% (Figure 4). This content must be regarded as critical because of the toxicity of vanadium. Fortunately, the ω-phases are sub microscopically small. The vanadium particles were analyzed by energy dispersive x-ray analysis and dispersive spectroscopy (EDS). This determined the relative chemical content of individual particles. Representative particles from each specimen were photographed at various magnifications to document particle morphology.

The relative amount of alpha and beta phases at temperature 770K, can be roughly indicated from the psuedobinary phase diagram. After an air quench, the original beta phase transforms to the Widmanstätten alpha + beta. This is illustrated in the above micrography. Thus the quenched alpha + beta alloy contains two micro constituents (primary alpha and Widmanstätten alpha beta and two phases (alpha beta). The alpha phase is present in two morphologies: primary alpha and alpha

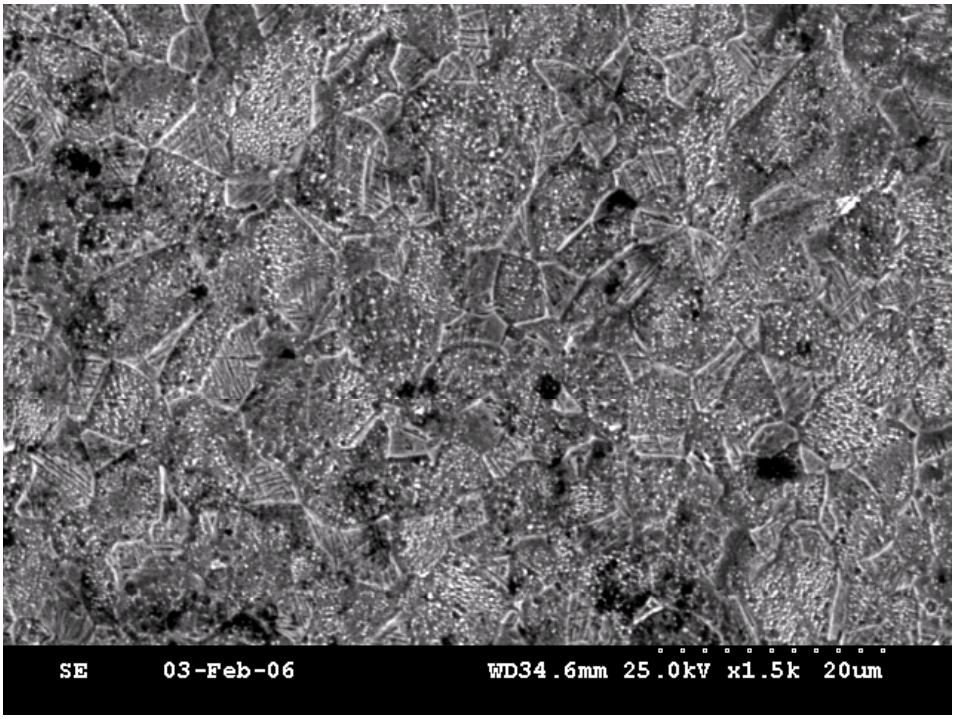

Fig.5. Ti-6Al-4V- the SEM micrograph for alloy showed the grain size for α β specimen (X150⁰)

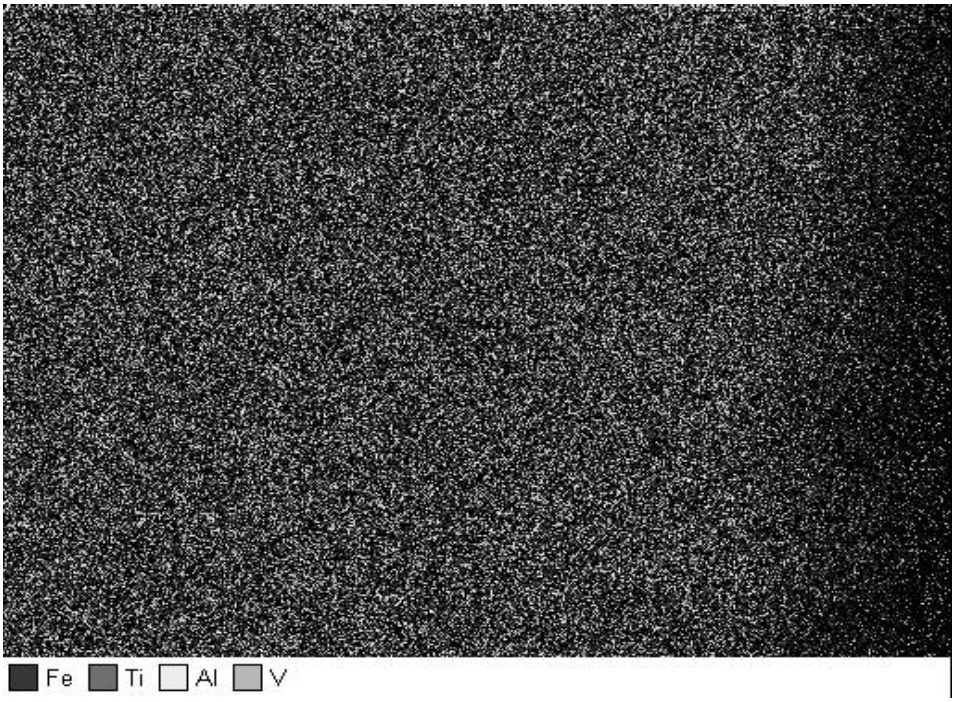

Fig.6. Analyses of Ti-6Al-4V energy dispersive spectroscopy (EDS) of the Fe-Ti-Al-V in alloy.

needles in the Widmanstätten morphology. The primary alpha develops during the anneal, and has no orientation relationship with the beta phase. The Widmanstätten alpha forms during the quench by precipitation in the beta, forming as platelets with the basal planes of the hexagonal alpha. Such hot forged alloys have a different microstructure with improved creep resistance. After the heat nitriding treatment the alloy samples presented a homogeneous layer on its surface and a change in the

surface color. The nitride formation is substantially slowed on account of the reduction in the partial pressure of nitrogen to 1Pa, because of the reduction in the boundary nitrogen concentration at the gas-metal interface; eliminating the barrier effect from the nitride film activates the diffusion of the nitrogen into the titanium, which favors the formation of deep hardened layers.

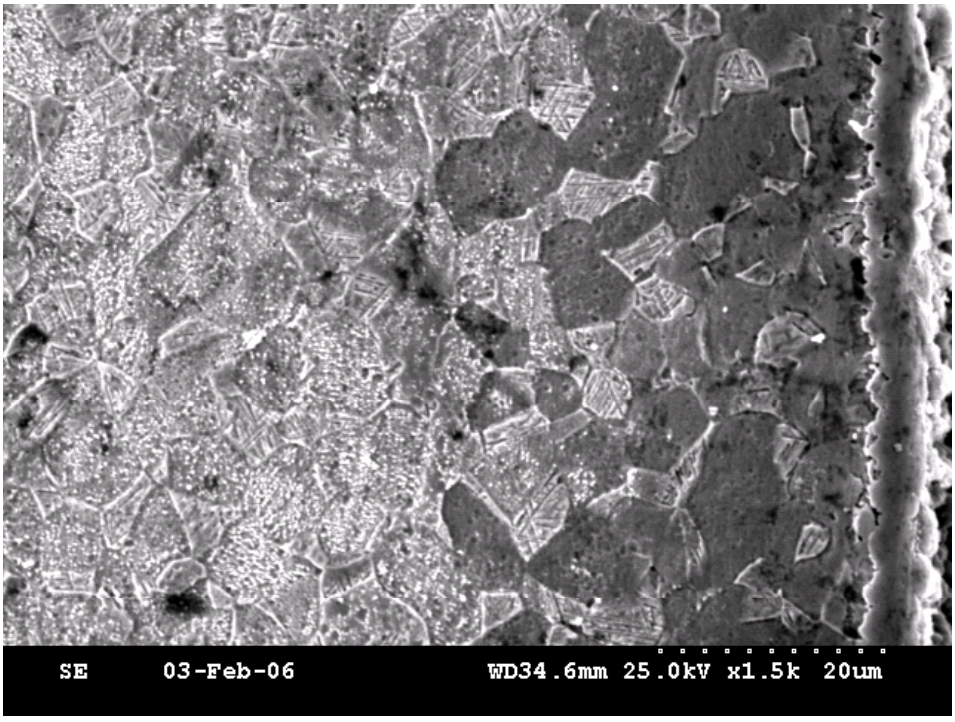

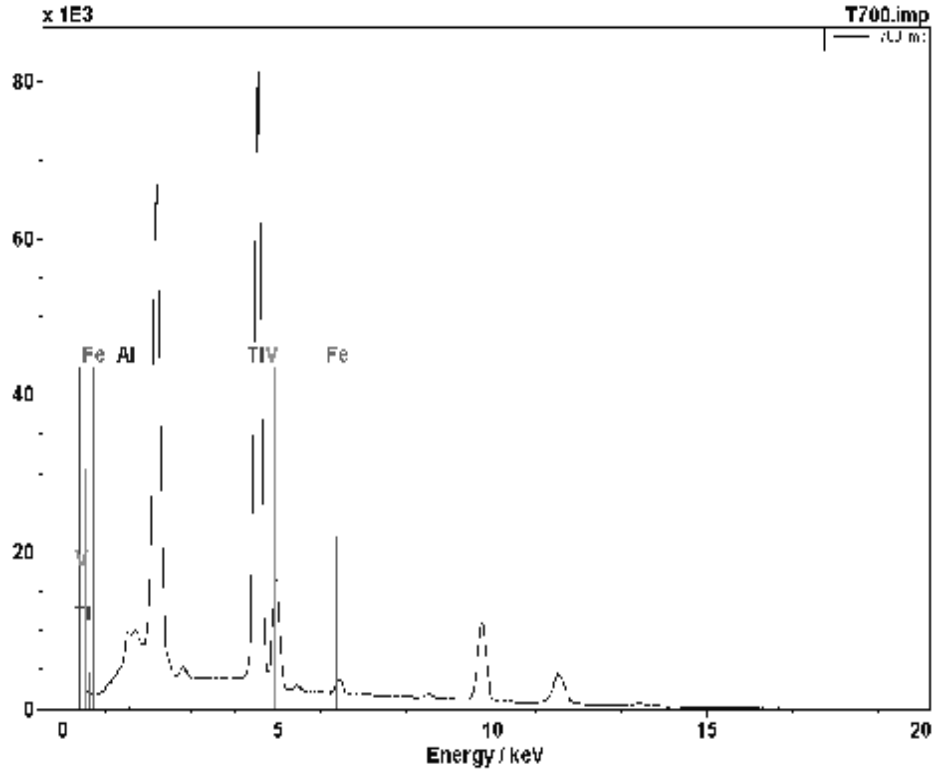

Fig.6. SEM images and their respective EDX spectrum for the Ti6Al4V nitriding treated at 950K.

These processes affect the diffusion-layer morphology. During titanium-alloy nitriding in nitrogen atmospheric pressure, a diffusion layer is formed starting at about 1070K. The effect of nitriding on the near-surface composition of (α + β)Ti6Al4V is a very complex function of the process parameters. Below 773K it is possible for ε-Ti2N and δ-δTiN to coexist [2]. In Ti6Al4V raising the isothermal hold temperature from 1070K to 1120K increases the diffusion-layer thickness from 20 to 50μm in a 6 h treatment [4]. The nitrogen-enriched layer becomes harder and less plastic, and the surface micro hardness which is completely due to the hardness of the nitride TiN (as obtained in experiment 530 to 600 $HV_{0.05}$).

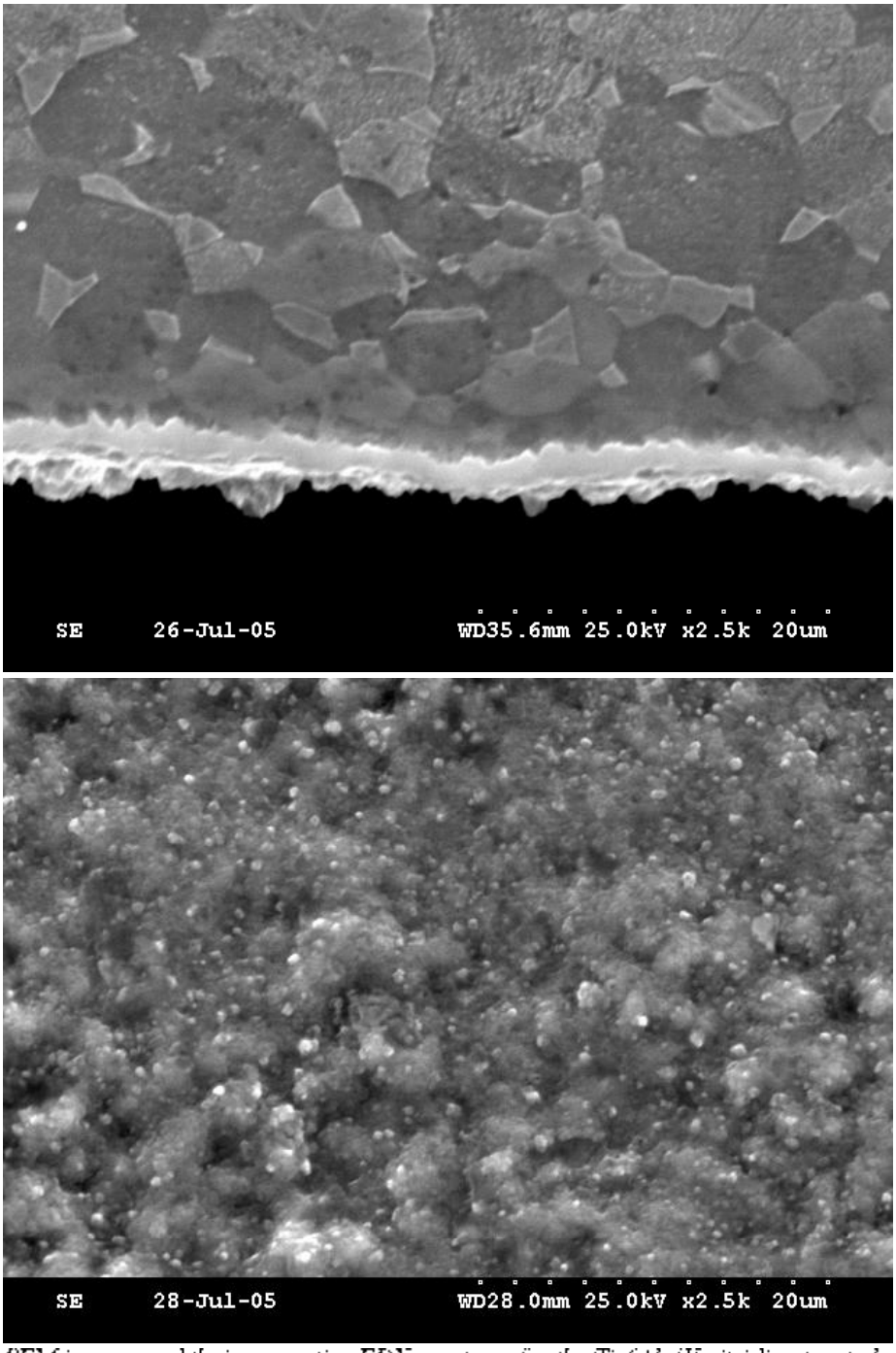

Fig. 7. The SEM images and their respective EDX spectrum for the Ti-6Al-4V nitriding treated at 1050K.

As the temperature is raised, the diffusion is activated and the nitride formation and gas saturation are accelerated, determining an ongoing growth of the diffusion layer.

4. Conclusions

1. Because the interactions between cells and tissues with biomaterials at the tissue implant interface are almost exclusively surface phenomena, surface properties of implants are of great importance. As a result, surface atoms of prosthesis will attempt to reduce their free energy by rearranging and bonding to any available reactive molecules to reach a more favorable energy state.
2. Tests on Ti-6Al-4V alloys implants have indicated that wear is dramatically influenced by titanium nitride (TiN). It also makes possible to improve the quality of prosthesis superficies, preventing the vanadium ions' dislocation
3. A gold-colored superficies titanium nitride coating is used to identify areas for the surgeon's manipulation. We believe it will be a relevant contribution that may bring significant improvements of health and aesthetic value in the implant field.

Acknowledgements

The authors thank the Romanian Ministry of Education and Research for having financially supported this research project within the National CEEX Programmer.

Received April 16, 2007

[1] *S.C. METAV-R&D S.A Bucharest, Romania.*
[2] *University Politechnic of Bucharest, Romania*
[3] *Technical University "Gh. Asachi", Iasi, Romania.*
[4] *Departments of Neurological Surgery - Emergency Hospital, Constanta, Romania.*

REFERENCES

1. S.L.R da Silva, L.O.Kerber,L.Amaral, C.A. dos Santos. *X-ray diffraction measurements of plasma-nitrided Ti-6Al-4V,* **Surface and Coatings Technology** 116-119 (1999) 342-346 Elsvier.
2. R.G. Vardiman, R.A.Kant, *The improvement of fatigue life in Ti-6Al-4V by ion implantation.* **J.Appl. Physics** 1982;53;690-4.
3. M.Peters. C.Leyens. **Titan und Titanlegierungen.** Wiley-VCH Verlag GmbH. Weinheim (2002) 432.
4. C.D Peterson, B.M.Hillberry, D.A.Heck *Component of total knee prostheses using Ti-6Al-4V, titanium nitride coated Ti-6Al-4V, and cobalt-chromium-molybdenum femoral components.* **J. Biomed Mater Res** 1988;22-887-90

ALIAJ DE TITAN PENTRU APLICATII BIOMEDICALE CU UTILIZARE LA OBTINEREA IMPLANTURILOR SPINALE

Rezumat: Unul dintre cele mai utilizate aliaje de titan, adaptabil si cu multiple aplicatii este:Ti-6Al-4V. Proprietatile speciale, in special mecanice pe care le detine, il face apt de a fi utilizat pentru fabricarea implanturilor. Existenta ionilor de vanadiu, ce s-a dovedit ca prezinta un anumit grad de toxicitate pentru tesuturi, a condus la ideea tratarii prin nitrurare a suprafetelor implanturilor realizate, in scopul blocarii migrarii ionilor de vanadiu in organism.

BULETINUL INSTITUTULUI POLITEHNIC DIN IAŞI
Tomul LIII (LVII), Fasc. 4, 2007
Secţia
ŞTIINŢA ŞI INGINERIA MATERIALELOR

EXPERIMENTAL MODEL FOR EVALUATION OF BENDING BODY INTENSITY AND CORRELATION OF THE SEMIPLANETARY ROLLING PROCESS FACTOR

BY

NICOLAE CANANAU, GHEORGHE GURAU and PETRICA ALEXANDRU

Abstract: The application of a semiplanetary rolling leads at unsymmetrical state of stress for the body thickness, and the effect is the appearance of a bending moment. Thus the rolled body is curved. The intensity of bending is function by the thickness reduction and the geometrical factors: initial thickness, the ratio wid.h/thickness. In the work is presented the results of researchers concerning the effect of process factors on the intensity of bending of the worked body by semiplanetary rolling.

Keywords: semi-planetary rolling, strain, stress.

1. Introduction

Semi-planetary rolling is an interesting deformation process. The rolling process is performed in a rolling stand mill consisting by a planetary cylinder and a massive cylinder (figure 1) what determines a non-uniform strain repartition into the thickness of rolled body [1]. The penetration of the satellite cylinder is much greater then the penetration of the massive cylinder [2].

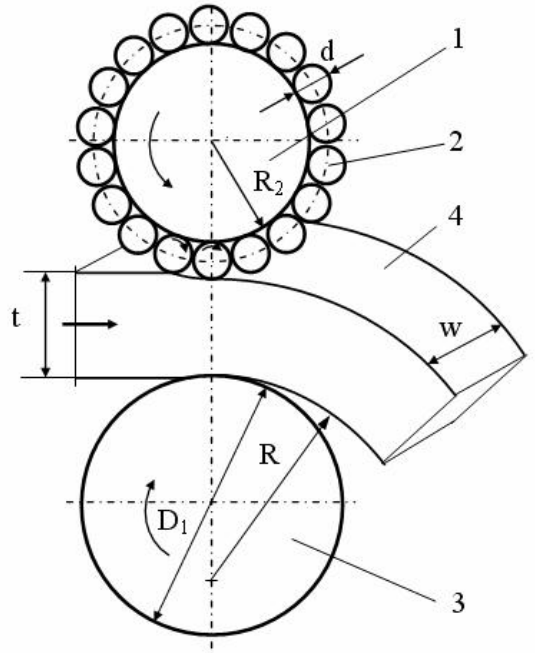

Fig. 1. Scheme of semi-planetary rolling: 1-planetary cylinder, 2-satellyte cylinder, 3-massive cylinder, 4-semi-product.

The non-uniformity of the strain induces a compression stress field with the intensity of the stress greater in the proximity of the planetary cylinder and smaller in the proximity of the massive cylinder because the diameter of the satellite cylinder is much smaller then the diameter of the massive cylinder.

Consequently, into the deformation zone is developed a bending moment as result of the variation of the stress intensity. This bending moment induces the curving of the deformed body or the unbending of the curved body.

An example of the semi-planetary rolling application may be the unbending of the continuous cast slab in the on-line regime. Also, through the semi-planetary rolling may be worked curved pieces.

The obtaining of the adequate quality of the rolled product the correct leading of the rolling process is necessary.

The factors of the semi-planetary rolling process are the reduction of the thickness, geometrical ratio b/h of the body, the radius R of the rolled product or the ratio R/h (we denote b the width h the thickness).

The paper objective is the establishing of the link among the relative thickness reduction and curvature radius for different values of the geometrical ratios of body. The establishing of this correlation is necessary to evaluate the practical possibilities of application of this procedure at the unbending process of continuous cast slabs

2. Experimental conditions

The experimental researches have been effectuated at a semi-planetary rolling stand mill (fig.2) composed by a massive cylinder (diameter of 80mm) and a planetary ensemble, composed by 18 satellite cylinders (diameter of 12mm) and a support cylinder (diameter of 56mm). Length of the active surface is 50mm.

In the aim of the simulation of semi-planetary rolling process the samples have been worked of lead

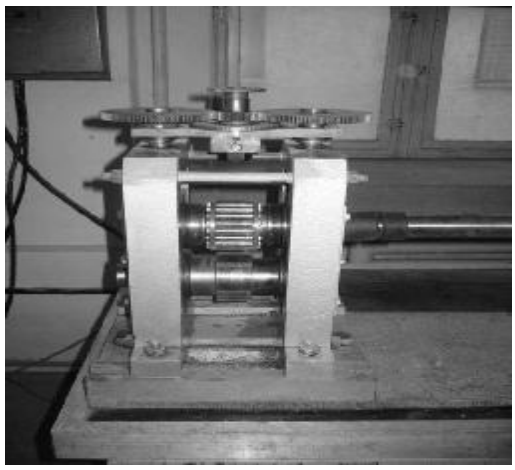

Fig. 2. Semiplanetary rolling stand mill (laboratory model).

The dimensions of the samples are rendered in table 1. They were programmed for various values of the initial thickness and width, i.e. various values of the geometrical ratio b/h.

Table 1. Dimensions of the lead samples

Length	Width	Thickness
100	10	6, 9, 13, 16
	20	6, 9, 13, 16
	30	6, 9, 13, 16

The experimental process consists in the measuring of the sample dimensions, programming the value of the thickness reduction, semi-planetary rolling and measuring of the effective value of thickness and radius of the rolled samples.

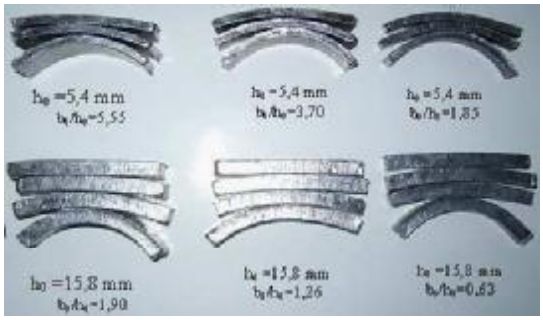

Fig. 3. Semiplanetary rolled samples

3. Results and interpretation

In figure 3 are showed some examples of semi-planetary rolled samples. The results of the experimental researches are systematized graphic in the figures 4, 5.

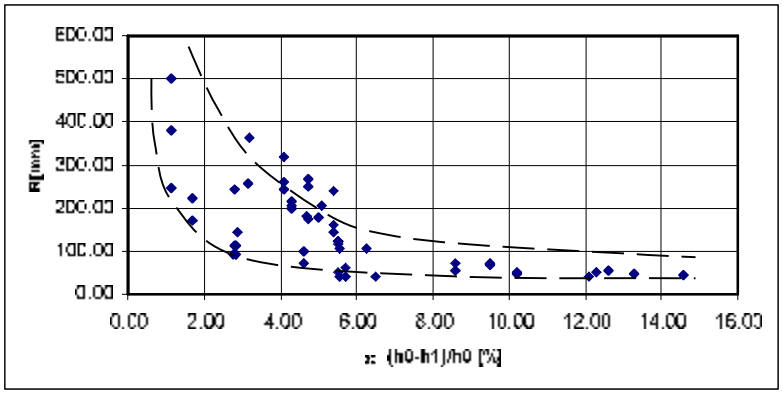

Fig. 4. Variation of curvature radius with relative thickness reduction

In figure 4 is showed the variation of the curvature radius of semi-planetary rolled samples, in absolute values, in the all cases of their geometrical factors, in function of the relative reduction of thickness.

In figure 5 is showed the variation of the ratio - curvature radius/initial thickness of semi-planetary rolled samples, in the all cases of their geometrical factors, in function of the relative reduction of thickness.

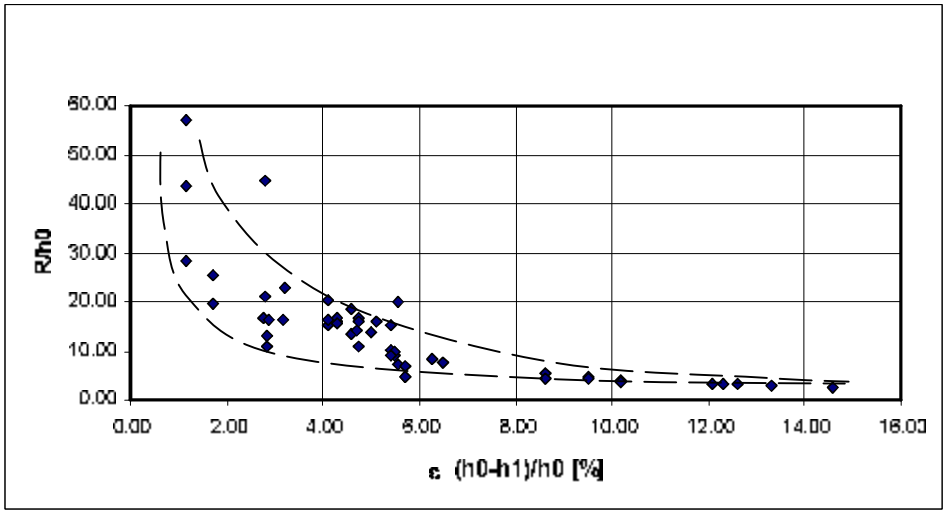

Fig. 5. Variation of R/h_0 ratio with relative thickness reduction

It observes a smaller dispersion of experimental data for ratio R/h_0 (figure 5), than values R (figure 4)

Consequently, the ratio R/h allows a better evaluation of the deformation degree (relative reduction of the thickness) what is necessary at the unbending of a continuous cast slab with a date curvature radius and date thickness

4. Correlation of the results

The influence of the reduction of thickness on the curvature radius is certitude The increasing of the thickness reduction determines the adequate increasing of the curvature radius. For establishing a truthful correlation we made the refining of experimental data using a specializing soft (DATAFIT).

As result of the solving of experimental data the regress equation has been established

$$\frac{R}{h_i} \quad 41{,}89 \cdot \varepsilon^{-0{,}846} \cdot 1{,}05^{\frac{b_0}{h_0}} \qquad (1)$$

The comparative representation of the experimental results and regression surface, conform the equation (1) as showed in figure 6

The influence of the b/h ratio on the R/h ratio for different values of the relative thickness reduction is presented in figure 7. Is evident the b/h ratio has grater influence for reduced values of deformation degree on the values of R/h ratio

Is evident the b/h ratio has grater influence for reduced values of deformation degree on the values of R/h ratio.

The variation of the R/h ratio with relative reduction of thickness (ε), is presented in figure 8. This graphic may be used at the evaluation of the deformation degree necessary for unbending of cast slabs.

Thus, for known R/h ratio and b/h ratio, in function of the geometry of continuous casting machine and geometry of crystallizer we can establish the value of the relative thickness reduction

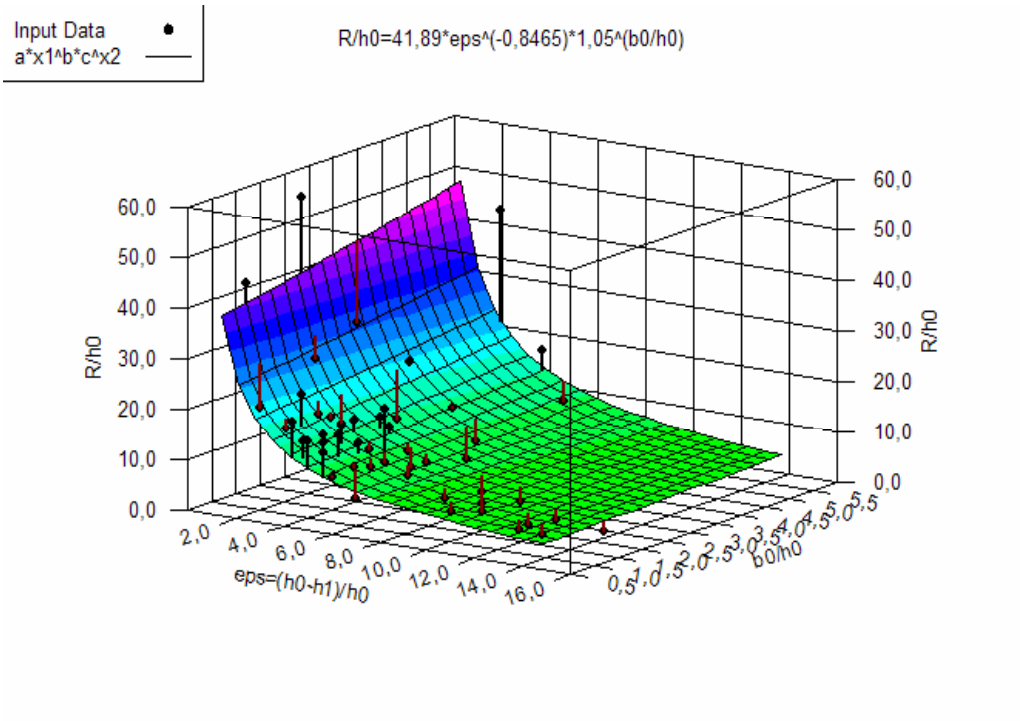

Fig. 6. The regression surface and the experimental value of the ratio R/h_0 in function of the relative reduction.

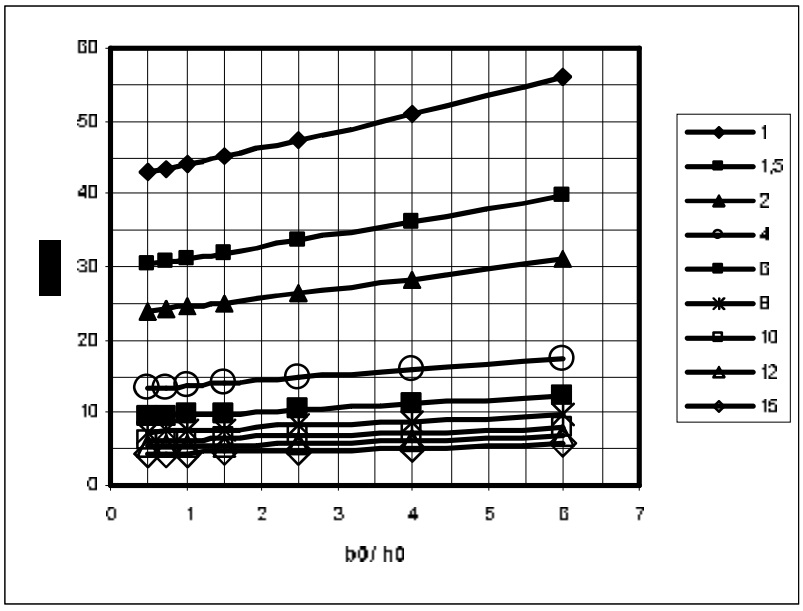

Fig. 7. The influence of the b/h ratio on the R/h ratio for different values of the relative thickness reduction

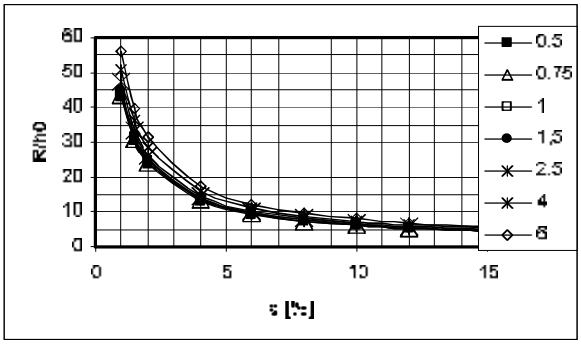

Fig. 8. The variation of the R/h ratio with relative reduction of thickness (ε), for the various value of ratio b/h.

5. Conclusions

The experimental researches demonstrated:

1. Semiplanetary rolling is a deformation method what induces a non uniform deformation in the thickness of rolled body. This phenomenon determines the curving or unbending of rolled body.
2. In case of semiproduct with certain value of geometric ratio b/h, in aim of obtaining a certain curvature radius by semiplanetary rolling the establishing an adequate value of relative reduction is necessary.
3. Unbending a continuous cast slab may be realized by semiplanetary rolling selecting the adequate value of relative reduction correlated with geometrical ratio b/h and R/h ratio (R being the radius of curve thread).
4. The researches demonstrated at the geometrical ratio b/h greater of two in the body section is developed a plane deformation state. In this case the base factor for programming of semiplanetary rolling process is the thickness reduction.

Consequently the semiplanetary rolled may be applied at the exit of continuous cast slab of curve thread of casting machine in the aim of unbending with out tensile stresses. This fact will have as effect the elimination of cracks on the superior surface of continuous cast slab. Finally it will assure the quality of metallurgic products and decreasing of production costs.

Received April 21, 2007 *Dunarea de Jos University of Galati*

REFERENCES

1. Wiesenfeld, D., 1999. *Thread and form rolling - planetary (rotary) versus flat die machines*, **Steel Time Intern.**, Sept. 1999.
2. Anon, 1995, *Thin Hot Strip Using Planetary Mil*, **Steel Time Intern.**, Sept. 1995, 33-35.
3. Cănănău, N., Ivănescu, A., 2001, *Study on the Relation between the Quality of Continuous Cast Slabs and the Surface Discontinuities of the Steel Thick Sheet*, **"International Conference on Advances in Materials and Processing Technologies"**, September 18-21. Leganes. Madrid. Spain. vol. 2, p.949-954.
4. Cănănău, N., Gurău, G., 2005, *Semi-planetary rolling process and experimental simulation* **Buletinul Institutului Politehnic Iasi**, tom L1, Fasc.2, p.59-65.
5. Moussy, F., Franciosi, P., 1990, **Physique et mechanique de la mise en forme des metaux**, Presses de CNRS, IRSID, Paris.

6. Gelin, J., Oudin, J., Ravalard, Y., 1984, *Influence de quelques parametres metallurgiques sur la rupture ductile des aciers a bas de moyen carbone*, **Mem. Et. Sci. Rev. Metall** 81
7. Cănănău, N., **Cercetari privind comportarea sub tensiune a unor oteluri turnate continuu, la temperaturi de 850 - 1200 ^{0}C**. Contract de cercetare, Universitatea din Galaţi, 2002

MODEL EXPERIMENTAL DE EVALUARE A INTENSITĂŢII DE ÎNCOVOIERE A UNUI CORP ŞI CORELAREA ACESTUIA CU FACTORII PROCESULUI DE LAMINARE SEMIPLANETARĂ

Rezumat: Aplicarea laminării semiplanetare conduce la o stare asimetrică de tensiuni pe grosimea corpului, efectul fiind cel de apariţie a unui moment de încovoiere. În consecinţă corpul laminat este curb. Intensitatea încovoierii este funcţie de grosimea reducerii şi de factorii geometrici. În lucrare sunt prezentate rezultatele cercetărilor privind efectul factorilor de proces asupra intensităţii de încovoiere.

BULETINUL INSTITUTULUI POLITEHNIC DIN IAŞI
Tomul L(III (LVII), Fasc. 4, 2007
Secţia
ŞTIINŢA ŞI INGINERIA MATERIALELOR

CHANGES OF FINE STRUCTURE AND MICROSTRUCTURE INDUCED BY SEMI-PLANETARY ROLLING

BY

NICOLAE CANANAU, CONSTANTIN GHEORGHIES, GHEORGHE GURAU and CARMELA GURAU

Abstract: The strain intensity in the proximity of planetary cylinder, in the case of semi-planetary rolling is greater than in the proximity of the massive cylinder. This fact leads at the variation of the microstructure and fine structure characteristics: the mosaic block dimension, second order stresses, dislocations density, micro-hardness into the thickness of rolled body. In the paper it presents the research results for identify and evaluate the structure modifications at the semi-planetary rolling.

Keywords: fine structure, x-ray, semiplanetary rolling

1. Introduction

Plastic deformation strongly affects the microstructure and mechanical properties of the material. Thus plastic deformation leads to the variation of the dimension of mosaic blocks, dislocation density, value of second order stress, at the fine structure level and, consequently, change of the mechanical properties (for example micro-hardness).

The microstructure evolution and the changes of the mechanical properties induced by plastic deformation depend not only on the deformation process but also on the properties of the material, in particular on its crystalline structure, stacking fault energy and the value of the self-diffusion coefficient [1]

The semi-planetary rolling model is presented in figure 1 and it leads to an asymmetrical stress and strain state on the thickness of the semi-product [2].

The strain developed in the proximity of the superior planetary cylinder has greater intensity then the strains developed in the proximity of massive cylinder.

As effect, after semi-planetary rolling the body, with initial rectilinear form, becomes curve body. Also, as a reversible process, the curved body may take a final rectilinear form.

An important application of semi-planetary rolling, which may become a solution for quality assurance of the metallurgical products, may be the unbending of the continuous cast slabs of different metallic materials that have in certain temperature range a fragility domain. Thus is the case of the construction steels with great mechanical resistance, micro and low alloyed steels with fine microstructure.

At the same time in the unbending zone, into the proximity of interior surface of slab section, a plane tensile stress state is developed. Coupled, these two causes, respectively, the reduced plasticity of steel and the bi-axial tensile stress state may lead at the appearance of the superficial fissures and the discontinuity defect.

The semi-planetary rolling applied at unbending zone, to the exit of slab from curve thread of the continuous casting machine, for example placing a semiplanetary rolling mill into the drawing mill, induces an unbending moment in the condition of the compression stress state [3, 4].

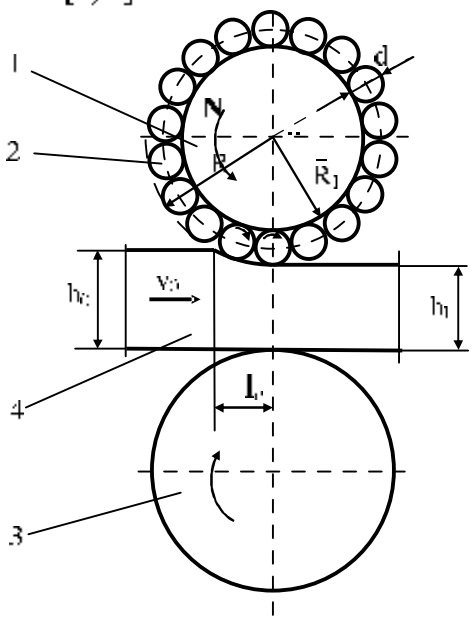

Fig.1. Scheme of semi-planetary rolling process: 1-planetary cylinder, 2-satellite cylinder, 3-massive inferior cylinder, 4-rolled body

The semiplanetary rolling is characterized by the variation of strain intensity in the thickness of the body, grater in the proximity of the planetary cylinder, smaller in the proximity of the massive cylinder and minimum values at the half of thickness This fact will lead at the changes of the crystalline lattice and variation of microstructure and of the properties of deformed material.

2. Research conditions

In the aim of the observing of the influence of the deformation on the structure and properties of deformed material we made a metallographic study, analyze by diffraction of the X-radiation and the measurement of the micro hardness [5 - 7].

The samples were prepared form aluminium and their shape was rectangular prism having dimension of 10×12×100 mm.

The deformation has been performed on a original semiplanetary rolling mill which is composed of a planetary cylinder with appearance surface of 80mm, composed by a support cylinder and 18 satellite cylinders with active surface dimensions of Ø12×50mm, and the massive cylinder surface of Ø80×50mm. The revolution of the planetary cylinder is 200 rpm and of massive cylinder is 2 rpm.

Analysis of fine structure modifications induced of the semiplanetary rolling has been performed on a diffractometer type DRON 3. This apparatus has following work parameter: copper anti-cathode (λ=1.541 Å), U= 34 kV, I=30 mA, and monocromathor in the diffracted beam

The micro-hardness was measured with an adequate apparatus type PMT-3 and for micro-structural analysis an optical microscope equipped with a digital system for quantitative analysis.

3. Experimental results

In the figure 2 the microstructures of the initial (non-deformed) and deformed aluminum samples are presented, respectively. Because the deformation degree is relatively small, the semiplanetary rolling does not produce a visible modification of the crystalline grains. The dimension of crystalline grains increases in the proximity of the planetary cylinder and near the massive cylinder this structural parameter is not modified.

According to the X-ray diffraction analysis the aluminum sample was cross scanned with the advance step of 2 mm, resulting 6 measuring points. In figure 3 is shown the irradiation scheme of the samples.

In order to analysis of fine structure of aluminum samples the diffraction lines (111) and (311) are considered. First diffraction line is used at the evaluation of the dimension of mosaic blocks in the $\langle 111 \rangle$ crystallographic direction.

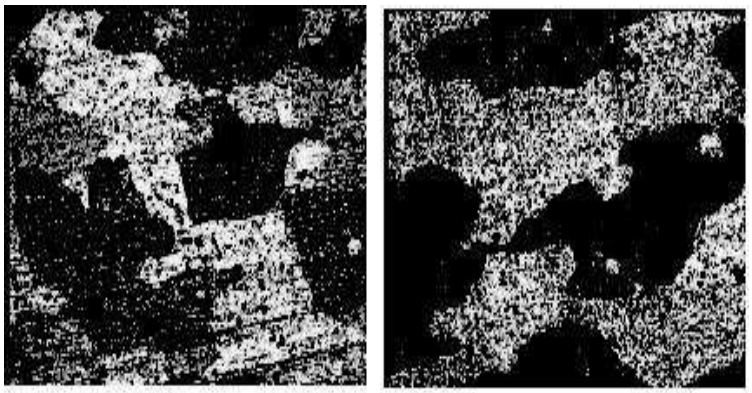

Fig. 2. Microstructure of aluminum samples before (a) and after (b) deformation

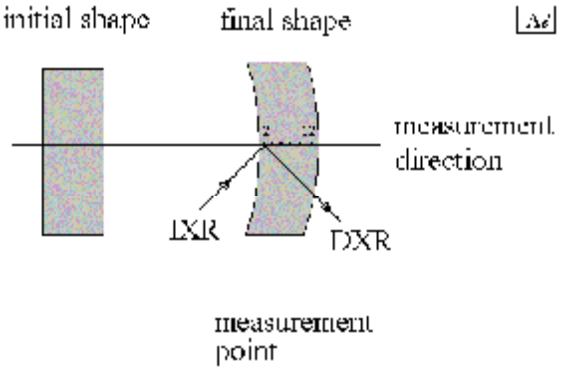

Fig. 3. Irradiation and X-ray scanning scheme of deformed sample

The evaluation of the second order internal stress and the dislocation density levels is done from the analysis of the second diffraction line.

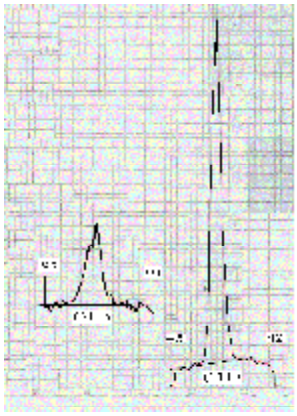

Fig. 4. Aspects of the diffraction lines (111) and (311) for deformed aluminum sample

The (111) diffraction line appears into angular range, $2\theta \in (42^{\circ}, 45^{\circ})$ and the (311) diffraction line is in angular domain, $2\theta \in (94^{\circ}, 97^{\circ})$. In figure 4 the shape of above mentioned diffraction lines is displayed.

In figure 5 the variation of the (111) diffraction line width, $B_{(111)}$, that is inverse proportional with the mosaic blocks dimensions, $D_{(111)}$, is carried out. Between the two sizes there is the relation:

$$D_{(111)} \approx \frac{1}{B_{(111)}} \qquad (1)$$

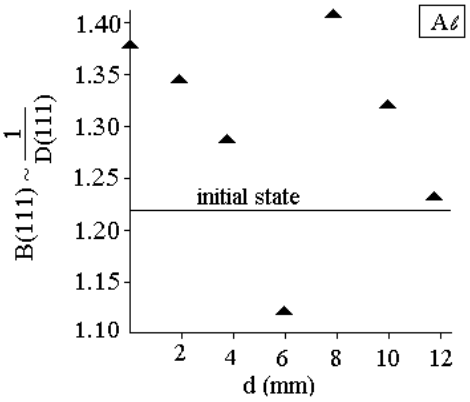

Fig. 5. Cross distribution of the width of diffraction line on cross section

The analysis shows that the deformation determines the increasing of the mosaic block dimensions.

The mosaic block dimensions have an important variation. In the marginal layer, at the proximity of the contact surface with the planetary cylinder the dimension of the mosaic block decreases. The value of the mosaic block dimension follows the variation of deformation intensity. At the middle of the thickness an abrupt jump of the mosaic block dimensions is observed.

This fact may be determined by the extension of the mosaic blocks at the very small plastic deformation. In the part of the massive cylinder the value of mosaic blocks dimension it maintains at the contact surface and decreases to the interior layers. This aspect is explained by the action of the dead zone into the marginal layer at the contact surface with the massive cylinder. It denotes because of the small value of the b/h ratio the deformation in the width direction of sample is great enough for determine smaller deformation intensity in direction of the thickness

In figure 6 it presents the distributions of the widths of diffraction lines (311). The width of diffraction line is direct proportional to the level of the second order internal stress, according to the relation:

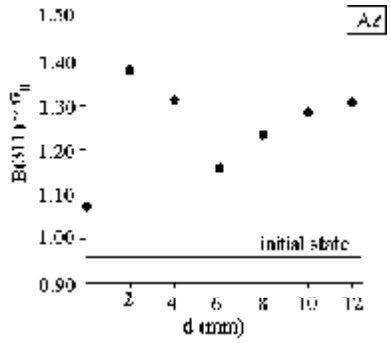

Fig. 6. Cross distribution of the second order internal stress

The second order stress registers a minim value at the middle of the deformed body. At the contact surface with the planetary cylinder the second order stress has a lower value

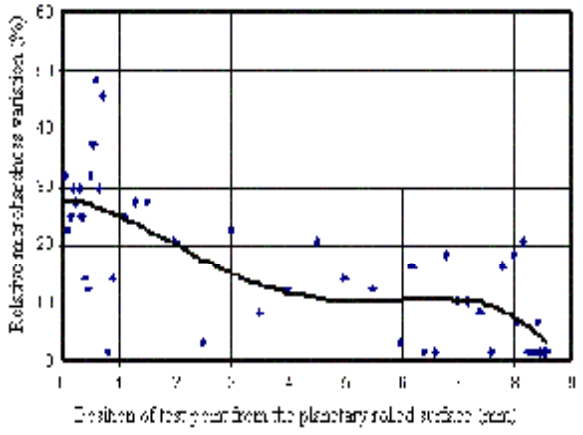

Fig. 7 Cross distribution of micro hardness

This fact can be explained by the effect of mechanical relaxation induced by the deformation in width direction, because the ratio b/h is small, relatively. Consequently, the second order stresses really correspond to the repartition of the strain intensity in the thickness of sample. Therefore the repartition of the second order stresses is the most factors for study of influence of asymmetrical deformation of the fine structure of metallic material. The variation of micro-hardness is showed in figure 7 and its can be connected with distribution of second order stresses

4. Conclusions

Semiplanetary rolling is an interesting deformation process for the obtaining of the curve pieces or for unbending of the curved parts. Because the diameter of the satellite cylinder is much smaller of the diameter of massive cylinder the strain intensity is variable in the section of the body. This is greater at the proximity of planetary cylinder, smaller at the proximity of massive cylinder. Between the strain intensity and the modification of micro and fine structure is a correlation. The experimental researches proved this correlation. The dimension of the crystalline grain is very small influenced.

The dimension of the mosaic blocks follows the variation of the strain intensity for the value of the ratio b/h great, relatively. Thus, in the proximity of the planetary cylinder this factor has great value, registers a minimum at the middle of the thickness The best parameter of the fine structure what very good corresponds at the variation of the principal deformation factor of the semiplanetary rolling process, respectively, local strain intensity is the second order internal stress. Thus, in case of the deformed body with the geometrical ratio b/h small, because the deformation to the width direction is enough great, in the proximity of the planetary cylinder appears a relaxation of the second order stresses. The second order stress has a minimum value at the middle of the thickness and increases slowly to the massive cylinder proximity. In case of the geometrical ratio greater of 2 the deformation in the width direction is negligible and the second order stress has the maximum value at the proximity of the planetary cylinder where the strain intensity has maximum value

The micro-hardness increases with 25% almost in the proximity of the planetary cylinder and littler, 5% approximately, at the proximity of the massive cylinder.

Received April 21, 2007 *Dunarea de Jos University of Galati*

REFERENCES

1. Kurzydowski K. J. et al. *Effect of severe plastic deformation on the microstructure and mechanical properties of Al and Cu*. **REV. ADV. SCI** 8 (2004)
2. Cănănău N., Ivănescu A., Cănănău D., *Study on the Deformation Process at the Semi-planetary Rolling*, **ACTA MECHANICA SLOVACA**, Kosice, nr.3 (2001).
3. Cănănău N., Potecasu O., Gurău G., Preda A., *Experiemntal researches on the thickness reduction influence to the bending slab billet in the semiplanetary rolling process*, **The Conference, UGAL MAT-2005**, 91-95, oct. (2005).
4. Cănănău N., Gurău G., *Researches concerning the semiplenetary rolling process*, **The 12th International Congres „METALURGY AND MATERIALS"**, Istanbul Turkey, sept. (2005).
5. Heidelbach F., et al. *Orientation and misorientation characteristics of annealed, rolled and recrystallized copper*. **MAT. SCI. ENG** A215, 39-49, (1996).
6. Kocks U. F., Tomé C., Wenk H.-R., **Texture and Anisotropy. Preferred Orientations in Polycrystals and Their Effect on Materials Properties.** Cambridge University Press, 1998.
7. Gheorghieș, C. **Controlul structurii fine a materialelor cu radiații X.** Editura tehnică. București. 1990.

MODIFICĂRI ALE STRUCTURII FINE PRIN LAMINAREA SEMIPLANETARĂ

Rezumat: Mărimea tensiunii în apropierea cilindrului planetar, în cazul deformării semiplanetare, este mai mare decât în vecinătatea unui cilindru masiv. Acest fap. conduce la modificarea microstructurii și caracteristicilor fine: dimensiunea blocurilor mozaic, tensiuni de ordinul doi, densitatea de dislocații, microduritatea în stratul superficial deformat. Lucrarea prezintă rezultatele cercetărilor în vederea identificării și evaluării modificărilor microstructurale la laminarea semiplanetară.

BULETINUL INSTITUTULUI POLITEHNIC DIN IAŞI
Tomul LIII (LVII), Fasc. 4, 2007
Secţia
ŞTIINŢA ŞI INGINERIA MATERIALELOR

CONSIDERATION CONCERNING THE MANUFACTURING OF HEAVY ALLOYS WITH NANOMETRIC STRUCTURE BY POWDER METALLURGY TECHNIQUES

BY

IRINA CARCEANU*, ANGELA POPA*, C. MACOVEI*, GEORGETA COSMELEAŢĂ** and I. ROCEANU***

Abstract: The aims of the paper consists in the development of complex multifunction materials with nanometric structure for special use (civil – heavy duty electrical contacts, and/or military – hard core of small and medium calibre ammunition) with the aid of integrated and flexible technologies for industrial applications. The paper presents briefly some aspects regarding the present stage in production of homogeneous mixtures of W-Ni-Cu powders system for manufacturing the materials made of heavy alloys type.

Keywords: mechanical alloying; heavy alloys; heavy duty electrical contacts.

1. Introduction

Hard alloys based on tungsten (AGW) are this category of metallic materials that have as main compound the tungsten, alloyed with one or many transition metals, like Ni, Cu, Fe, Co etc. Tungsten base hard alloys, composite type have a characteristic embeding structure, biphasic, where the major phase is formed by spheroidal tungsten grains, crystallized in cubic system with centered volume (ccv), embeded in a more ductile matrix, formed by a solid solution sof alloying metal or metals (as a rule from iron group) saturated in tungsten, crystallized in cubic system with centered sides (ccs). This type of alloys have an unique configuration of remarkable properties consisting of: high density, superior mechanical resistance, high ductility, good corrosion resistance, high capacity of radiation absorption, good processing properties, remarkable toughness.

Mechanical alloying is a versatile method of some advanced materials producing by the solid state powder processing and has already received numerous industrial applications.

At a qualitative level, the phenomena occurring during mechanical alloying have been understood and consist, essentially in a continuos process of deformation, fracturing, local heating, solid state welding and re-fracturing of powder particles under the effect of the transferred energy from the milling balls [1]. Submicron or nanocrystalline powders, amorphous phases or intermetallic compounds may be thus obtained at room temperature. Mechanical alloying has a wide range of materials such as: alloys (Al-Fe, Al-Ni, W-Cu, W-Ni-Cu, W-Ni-Fe); intermetallics (Si-Cu, Ti-C, Ti-Si, Ti-Br); magnetics (Fe-Si, Fe-Be-N, Ba-Fe-O); hard materials (W-C, V-C, Ti-

C, Si-N, Fe-C) and many others[2] are suitable to be processed nowadays by mechanical alloying.

In recent years the group of tungsten based materials known as heavy alloys by virtue of their high density (16 to 18,5 x 10^3 kg m^{-3}) have found an increasing number of applications in mass balancing and inertial gyroscopes and vibration dampeners, and also in, radioactive shielding and heavy duty electrical contacts. Processing such materials by mechanical alloying is very attractive, but through investigation is still required to keep under controlthe resulting material characteristics, mainly its microstructure (very fine structure, high dispersion grade, amorphous phases etc.). [3]

2. Experimental conditions

Experiments concerning the obtaining of composite powders using mechanical alloying were performed by: • experimental materials systems choose; • powder characterization in accordance with actual international standards; • gravimetric dosage of component powders; • filling in planetary mill with W-Ni-Cu powders and balls followed by milling during 192 h period; • dosing the W-Ni-Cu powders mixture after the mechanical alloying, by homogenization of this mixture during 35 h; • binding the obtaining powder mixture, with was obtained with pressing binder; • pressing; • debinding-presintering; • sintering; • characterizing the products resulted; • mechanical processing.

As raw materials is has been used pure W, Ni, and Cu powders with the following weight ratio: W:Ni:Cu = 95:3.5:1.5. The characteristics were determined according to International Standards: ISO 3923/1 Apparent density; ISO 4490 Flowing rate. The particle size was measured with a Fisher apparatus (powder permeability to water). A mixture of tungsten, nickel and copper powders were ground in an attritor, without protective atmosphere or lubricant

Copper powder used for the experiment had an average particle size of 6 μm and a morphology of irregular shape. Tungsten powder was of a spheroidal particle shape with an average size of 1 μm. In Figures 1-2 is showed the morphological aspect of W and Ni particles; it could be notice micronics particles of irregular shapes with surface roughness (tungsten particles), respective particle with spherical shape with a powerful tendency of agglomeration (nickel particles).

Table.1. Raw powders characteristics for the starting materials

Material	Flowing rate $^{s}/_{50g}$	Apparent density $^{g}/_{cm}3$	Particle size FSSS (μm)
W	not flowing	3,40 ± 0,01	1,62 ± 0,01
Ni	not flowing	2 46 ± 0,01	4.86 ± 0,01
Cu	not flowing	1,34 + 0,01	5.81 + 0,01

For milling it has been used an attritor with the following parameters • milling speed = 100 rot/min; • milling time = 192 hours; • ball / powder weight ratio = 3:1; • filling grade = 25 %.

The copper powder used for the realisation of homogenised mixed powder, was reduced preliminary in Siemens Plania, in hydrogen atmosphere at the 270^0C temperature.

Figure 3 shows the scanning electron microscopy (SEM) morphologies of reduced copper powder particles before mechanical alloying processing; it could be noticed the micronic particles of irregular shapes (dendritic structure).

The mechanically alloyed powder was taken out of the container periodically to follow the progress of alloying every 20 hours. The grinding total time is 192 hours. After 30 hours milling we can observe the sticking of the powder to steel balls and tank of attritor. After a longer time the powder started to agglomerate.

The powders were mechanically alloyed together with the copper reduced powder, then they were homogenized during 35 h, in a taper closed having a 75 mm diameter and 95 mm length, fixed on a rotating device, the rotation n= 60 rot/ min.

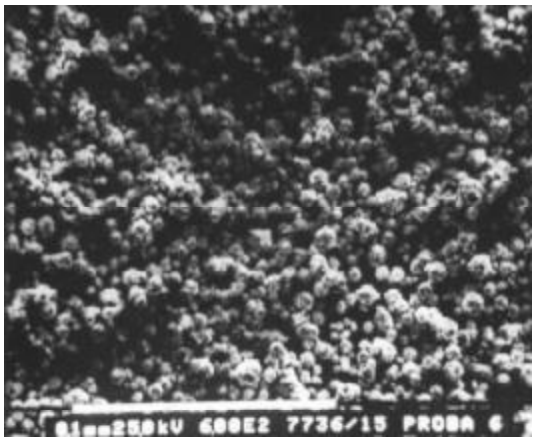

Fig. 1. Morphologic aspect of Ni powder 2480X

Fig.2. Morphologic aspect of W powder 2480X

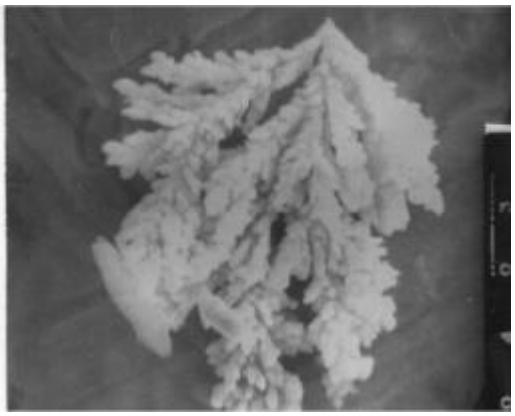

Fig.3. Morphologic aspect of reduced copper powder-particles of dendritic shapes 3000X

The characteristics of powder mixtures wich are mechanically alloyed are presented in Table 2.

Table.2. The characteristics of processed powders

Powder type	Main diameter FSSS (μm)	Flow rate s/50 g	Free descharged apparent density g/cm^3
W-Ni-Cu	**0,20 ±0,01**	**No flow**	**4,88 ±0,01**

We could be observed that increasing milling time lead to increasing apparent density and decreasing particle size; increasing of apparent density could be explained by particle shape changes during milling, so, by increasing milling time, the sharp edge of the particles becomes rounded. It means that particles packing amount increase and, also mechanical interlocking are reduced /4/. There are presented also conglomerates with irregular shapes formed by welding of many particles; as a result, after 192 hours grinding, the shape of particles submitted to mechanical alloying was not yet stabilized.

The figure 4 emphasises the aspect of W-Ni-Cu composite powders having fine grains, a homogenous distribution and uniform repartition of components.

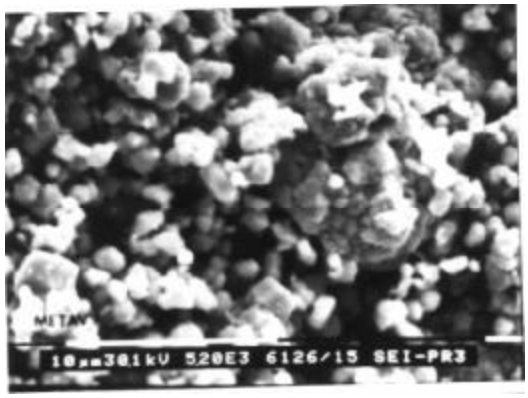

Fig.4. System of W-Ni-Cu particles 4780X

The powder mixtures were, then, binded to paraffin (2%), sieved in a semidry state by a sieve with 0,1 mm mesh size and dried, finally obtainig a mixture "ready to be pressed".

The pressing was perfomed bilaterally on a steel die with a circular section , showing following characteristics: ϕ_{ext}=47 mm, ϕ_{int}=14,3 mm; S=(ϕ_{ext}^2-ϕ_{int}^2) =15, 73 cm^2, for a specific pressure, were debinded in the Siemens Plania Furnance, in a hydrogene atmosphere, by using as packing agent - allumina, wich was calcined in advance at 1450 ^{0}C, during 5 h, in order to provide heat resistance (endurance).

The parameters of the debinding presintering process were: • H_2 atmosphere; • heating rate up to 500^{0}C: 0,8 ^{0}C/min; • heting rate between 500-800^{0}C:3,5 ^{0}C/min; • presintering temperature: 800^{0}C; • 30 min exposure time to presintering temperature; • total duration of the debinding – presintering cycle: 8h 30 min

The sintering operation was realized in heating evacuated induction furnace, with intermediate frequency currents, of Balzers type, the sintering operation parameters are: • sintering temperature: 1250^{0}C; • 60 minute exposure time to sintering temperature; • total duration of the cycle: 8 hours.

The produced sintered material was characterised by the physical mechanical and structural properties all along the stage. In Table no 3 are emphasized the physical and mechanical characteristics of the sintered markers from mechanically alloyed powder mixtures as compares with the materials offered by recognized producers in the field the reference material type ***Electroputere Craiova ROMANIA***.

The sintered grades were prepared for metallographic examination with the aim to:

- determine the presence, time and repartition of pores;
- determine the microstructure

Table.3. Physical and mechanical characteristics of sintered markers

Material type	Density (g/cm^3)	Brinell Hardness HB	Electric resistivity (Ω m 10^{-8})	Stretch resistance (N/mm^2)
Sintered markers 1250^{0}C	16.99	220	2.80	790

The samples for analyse were realised by gradually emphasizing the phases by Murakami attack. In Figures 5-6 it is presented the microstructure of W-Ni-Cu sintered material at 1250^0 C/1h, as attacked, at 2000X and respectively 10000X magnification.

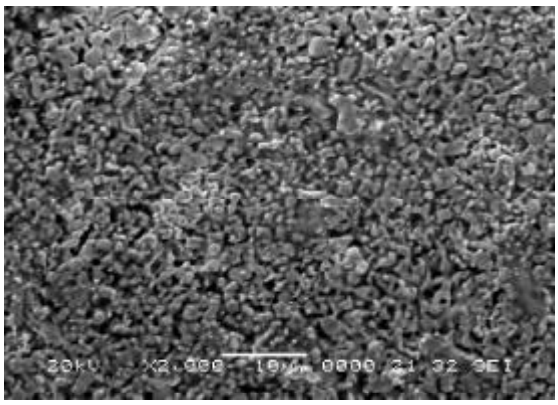

Fig.5. Microstructure of W Ni-Cu sintered material at 1250^0 C/1h, 2000X

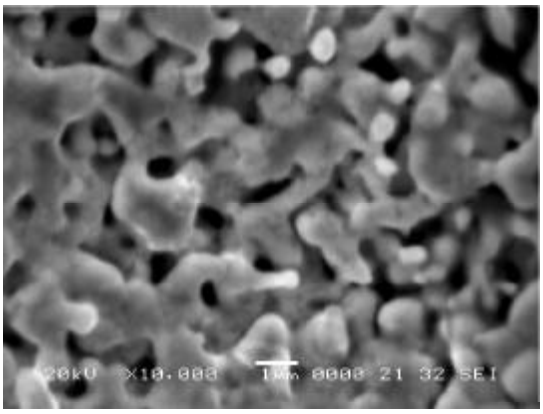

Fig.6. View of W-Ni-Cu sintered material at 1250° C/1h, 10000X

One can remark a homogenous and uniform structure of the W-Ni-Cu sintered material as well as the lack of porosity which has as a result the obtaining of a particular density of material, very close to the theoretical density. The microstructural analyse emphasized the uniform repartition of the two phases present in the material: the Ni-Cu metallic binder phase and the tungsten (W) phase.

The experimental results from Table 3 and Figure 6 give us reasons to consider the tehnological flow-sheet we have investigated in this paper (including mechanical alloying) as a valuable route for manufacturing a series of products which are representative for the W-Ni-Cu system. In Figure 7 is showed the representative product from W-Ni-Cu system high power electric contacts which fit out the Diesel Engines and in Figure 8 is presented small and medium ammunition projectile.

Fig.7. High power electric contacts which fit out the Diesel Engines

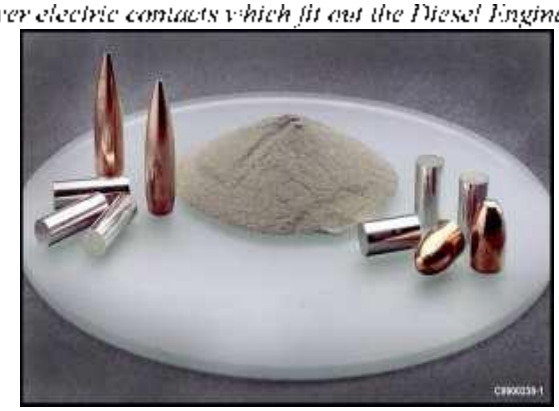

Fig. 8. Small and medium ammunition projectile

3. Conclusions

The experiments lead to the following conclusions:

• During the milling process, powder particles are trapped between the milling balls and the plastically deformed, thus rupturing the layers of surface contaminants on individual particles and exposing a clean metal surface;

• By the mechanical alloying tehnique was obtained powder composed of W-Ni-Cu with a very fine granulation, a uniform repartition;

• The more homogeneous of the materials provided by the mechanical alloying process appears to have had a significant effect on the densification of the particular powders, perhaps by allowing both of the liquid-phase-driven sintering mechanisms to proceed more effectively;

• The emphasized technological flow will allow the manufacturing of products which are representative to the W-Ni-Cu system – high power electric contacts which fit out the Diesel Engines with superior physical and mechanical properties, which comply with the users requirements.

Received April 19, 2007

**Metallurgical Research Institute of Bucharest*
***University POLITEHNICA of Bucharest*
****Defence University " Carol I " of Bucharest*

REFERENCES

1. H. Froes, C. Suryanarayana, *Metal Powder Report*, 1994, no. 49, pp. 14-18.
2. Ian Kerr, Glenn Creston, *Metal Powder Report*, 1993, no. 48, pp. 36-38.
3. S. Lee, T. H. Kim, T. G. KanY. **Powder Metallurgy World Congress**, 1994, vol. II, pp. 1501-1504.
4. Irina Carceanu, Cristian Coman, **Journal of Advanced Materials**, 2002, vol. 34, no. 3, pp. 56-58.

CONSIDERATII PRIVIND REALIZAREA ALIAJELOR GRELE CU STRUCTURA NANOMETRICA PRIN TEHNICI SPECIFICE METALURGIEI PULBERILOR

Rezumat: Scopul lucrari constă in realizarea si dezvoltarea unor materiale complexe multifunctionale cu structura nanometrica pentru aplicatii speciale (domeniul civil – contacte electrice de mare putere, si/sau din domeniul militar – munitie pentru sisteme de armament de calibru mic si mijlociu) utilizând tehnologii integrate pentru aplicatii industriale. Lucrarea prezinta cateva aspecte privind stadiul actual al producerii de amestecuri omogene de pulberi din sistemul W-Ni-Cu pentru realizarea materialelor din grupa aliajelor grele, repere multifunctionale cu caracteristici controlate din materiale complexe cu structura nanometrica pentru aplicatii speciale din domeniul civil si/sau militar.

BULETINUL INSTITUTULUI POLITEHNIC DIN IAŞI
Tomul LIII (LVII), Fasc. 4, 2007
Secţia
ŞTIINŢA ŞI INGINERIA MATERIALELOR

DEPENDENCE BETWEEN DEFORMATION SPEEDS AND HIGH ALLOY STEEL PLASTIC DEFORMATION STRENGTH

BY

DORIN CATANA

Abstract: In this paper is presented for the tool steel Rp_5 the evolution of the strength at deformation depending on two parameters: the temperature and the deformation speed ϕ. For the determination of equation what makes the connection between the strength at deformation and parameters it was used results of the experimental trials effected for different of temperatures but at the constant speed. Knowing the strength at deformation may be chosen the deformation process with that is deformed the tool steel Rp_5.

Keywords: plastic deformation.

1. Introduction

In this moment the weight of the production of the cutting tools is obtained an in totally through cutting processing, next following process is that to obtain from laminated semi-product. Due to the technical which were in progress for the past decades in the area of material science of as well as of regularize the technologies of obtain the sintered dusts, last in the lapse the production of the sintered components tools had a spectacular growth. With all the technological production support in domain of cutting tools, this area has in this moment a series of drawbacks

A negative appearance meted in cutting tools is that of the big consumption of expensive high alloy steels that are practically convert in chips. Besides one antecedent presented it must added, the fact as the large amount of chips removal in the manufacture time of the cutting tools and from the other side is the big consume of the manual labour, aspect which corroborates with the first, conduct to increase the price of the tools. Because most cutting tools are made from molten semi-product, the large microstructure is present in cutting tools that are made and determines a behaviour bed

Because of the material microstructure has influence on mechanical and technological property, of these depending the exploitation property of cutting tools, it began to search solutions for bettering, this in the sense her finish, because such material microstructure determine to superior mechanic and technological properties.

The casting structure of tools isn't proper to manufacture of cutting, the molten ingots are processing through plastic deformation with the scope to finish of the structure and obtain of laminate semi-products that shall be used to the remaking of the cutting tools.

Therefore the plastic deformation parameters must monitoring carefully in the sight eliminates on how much possible these drawbacks The utilize method of

operation by the plastic deformation are: forging of accuracy, extrusion and isotherm forging. The parts obtained through forging of accuracy in comparison with that are made by normal punching have the finite functional surfaces. This advantage is obtained combining the hot press with calibration. Beside the dimensional accuracy, the surface quality of parts obtained by accuracy forging is very good.

Another technological process which begin to often use in the plastic deformation of the tool steels is extrusion. Besides the decrease of the consumption of material, extrusion offers significant decreases of the cost through the elimination of chip removal processes for the punching parts, due to the high accuracy obtained.

Isotherm press is another method with raised efficiency. It is known that the formation of the part to outlines and definitive surfaces means the salving of labour and material

When is necessary a raised resistant in company with a good tenacity, the material structures obtained through forging are still unsurpassed. In the case of the part with simple geometry, for obtains the shape approach of the definitive, the part must forging in many stages, with reheating before each stage. An application of the isotherm punching is represented by the isotherm forging that is a slow and uniform process of the material setting in shape. Because the material opposes with a slack resistant, the total force that the press machine must to develop is lower, frequently of 10 as far as 30 of either than is necessary in normal punching.

For the another side many cutting tools aren`t inadequate, because the thermic treatment was incomplete, reasons therefore the parts of tool has hardness enforced of technology, what means a normal wear and the low tenacity, but another zones are a low hardness than is desirable. Some of the appearances presented hereinbefore determine either a quick wear or tearing of the cutting parts, this makes as to the tool become out premature from ordinariness. From one presented, is detached the conclusion as the with all the technological progress registered, the production of cutting tools must still to solve a series of which his problems drives to the lift quality.

2. Theoretical considerations

As a result to experimental tests effectuated to warm it can establish the evolution of the deformation strength depending on temperature for the steel mark Rp5. These determinations they accomplished only that with different speeds of deformation. For each deformation speed it established the deformation equation that permits to determine the deformation strength equation depending on temperature.

These equations have next form:

$$R_d = a \cdot e^{bt} , \qquad (1)$$

where:

R_d – the deformation strength;

a, b – the equation coefficients;

t – the deformation temperature.

In order to whole the image of the evolution of the deformation strength must as this for a large interval of the deformation speeds as part of area of the hot plastic deformation. With the help of the equations determined it can establish form of the equation that permits to determine the deformation strength depending on two

parameters that are temperature and the deformation speed. Taking count of the equation form's (1), the result is that form of equation of two variables shall be of course an exponential equation. The equation shall have next form:

$$R_d = a \cdot e^{b \cdot t + c \cdot v}, \quad (2)$$

where: R_d the deformation strength; t the deformation temperature; v the relative deformation speed; a, b, c – the equation coefficients.

With the help of equation value coefficients that was established to constant relative deformation speed it may possible to calculate the (2) equation coefficients. Following the calculus, the equation of the deformation strength depending on temperature and relative deformation speed has next form:

$$R_d = 89{,}72 \cdot e^{-0{,}00663 \cdot t - 0{,}0075 \cdot v}. \quad (3)$$

Utilizing the program PROGR$_d$ written in the Visual Basic language it was determined the deformation strength for different values of the temperature and speed (see the figure 1). The temperature interval for which was calculating the deformation strength is contained between 900 and 1200° C, and relative deformation speed has the values contained between 60 and 180 s (what corresponds to a deformation speeds of 1,2-3,6 m/s. This means that is possible to utilize equipments from the mechanic press or hummer category.

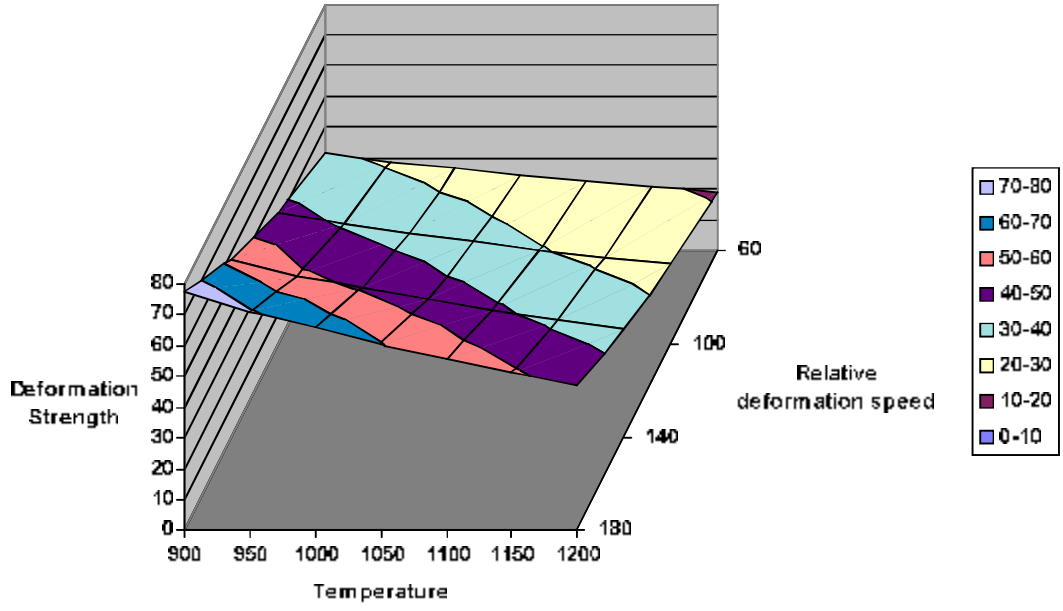

Figure 1 Deformation strength in function of deformation speed and temperature

3. Conclusions

The realization through plastic deformation of the cutting tools begins to more and more used-up.

The development of this technological process was possible for the next advantages:

- it is done saving until 60 % high steel alloy;
- it is eliminated the operations of chip removal;

- upper cutting tools microstructure in comparison with microstructure realizing by the traditional technologies;
- the hardness of the cutting tools increases;
- mechanical resistant of the cutting tools is enlarged.

The determination of the deformation strength for a large range of the relative deformation speeds as well as for a sufficient interval of temperatures permits an easy choice of deformation parameters.

The optimization of the deformation process shall drive besides material saving, to a homogeneous and fine microstructure which shall cause increase of the mechanic and technological cutting tools properties, for the next cutting tools generation.

Received April 11, 2007 *Transilvania University of Brasov*

REFERENCES

1. Adrian M., Badea S. **Bazele proceselor de deformare plastică**. Editura Tehnică. Bucureşti. 1983
2. Catana D. **Contributii la obtinerea sculelor aschietoare prin deformare plastica**. Teza de doctorat. Universitatea Transilvania din Brasov 1996
2. Drăgan I., ş. a. **Tehnologia deformărilor plastice**. Editura Didactică şi Pedagogică, Bucureşti, 1979
3. Ştefiu C., Oprean C-tin. **Măsurări geometrice în construcţia de maşini**. Editura Ştiinţifică şi Enciclopedică, Bucureşti, 1988

DEPENDENTA DINTRE VITEZA DE DEFORMARE SI REZISTENTA LA DEFORMARE A OTELURILOR INALT ALIATE

Rezumat: Lucrarea prezinta pentru otelul rapid Rp_5 evolutia rezistentei la deformare in functie de doi parametri (temperature si viteza de deformare). Pentru a determina ecuatia care face legatura intre rezistenta la deformare si cei doi parametri: au fost utilizate rezultatele experimentale obtinute pentru diferite temperaturi dar la viteza constanta. Cunoasterea vitezei de deformare este importanta, pentru ca ne permite sa alegem procesul de deformare cu care va fi prelucrat otelul rapid marca Rp_5 in vederea obtinerii unor scule aschietoare cu proprietati mai bune decat cele obtinute folosind prelucrarile prin aschiere.

BULETINUL INSTITUTULUI POLITEHNIC DIN IAŞI
Tomul LIII (LVII), Fasc. 4, 2007
Secţia
ŞTIINŢA ŞI INGINERIA MATERIALELOR

DETERMINATION OF COHESIVE ENERGY DENSITY OF POLYURETHANE MEMBRANES BY SWELLING MEASUREMENTS

BY

GABRIELA CIOBANU, GABRIELA CARJA, MARIA HARJA and LĂCRĂMIOARA ISTRATI

Abstract: Polyurethane (PU) membranes are prepared through the phase inversion method, where a multicomponent casting solution is immersed in a coagulant bath. The obtained membranes have an asymmetric structure and various porosity and thickness. Swelling studies of several industrial solvents are investigated through polyurethane membranes. Experimental determination of cohesive energy density value for the prepared membranes is done by measuring the swelling coefficients in water and several alcohols. In addition, the solubility parameters of the membranes are also calculated. The cohesive energy density and solubility parameter of the thicker membranes show higher values than those of the thinner membranes. All the membranes show a tendency to swell with ethanol.

Keywords: polyurethane membranes, swelling measurements, cohesive energy density

1. Introduction

Development of integrally skinned asymmetric membranes by Loeb and Sourirajan in 1960 was a major breakthrough in membranes technology [1]. Integrally skinned asymmetric membranes can be prepared through the phase inversion method, where a multicomponent casting solution is immersed in a coagulant bath. An asymmetric membrane having a very thin dense and selective skin layer (typically less than 0.1 μm), supported by a much thicker (100 – 200 μm) highly permeable non-selective layer (which provides structural support), can be prepared by a dry / wet phase inversion process. The skin layer of these asymmetric membranes becomes defect-free by introduction an evaporation step [2-4].

Today most membranes are fabricated by phase inversion process. The membranes are used extensively in reverse osmosis for the removal of salt from water. Over the past 30 years, many other polymers have been fabricated into asymmetric membranes for a variety of specific separation and purification applications [5-8].
Filter membranes are categorized as symmetric, asymmetric, porous or non-porous, depending on their filtration behaviour, materials used and manufacturing processes.

Normally, they are manufactured from polymers, composite materials between two polymers, or between polymer and ceramic [9-12]. These membranes have been used in gas and liquid processes.

The goal of work is the determination of cohesive energy density for polyurethane membranes; this allows further providing useful information about its solubility in the system. The cohesive energy density of a polymer is the closest approximation of its solubility prediction provided than some specific interactions between the polymer and solvent are not present. The value of cohesive energy density

also depends on the chemical structure and different constituent groups present in the polymer. Experimental determination of cohesive energy density value for a number of polymers has been done by measuring the swelling coefficients in series of solvents (water and several alcohols) [13,14].

2. Experimental

Materials: Polyurethane (PU) membranes are prepared by using the method and materials described elsewhere [15]. The PU membranes are prepared by casting a PU solution containing a calculated amount of PU polymer on a glass plate and allowing the solvent to evaporate under caloric radiation. Some pure membranes are prepared and are denoted as: *MP-1* (300 μm thickness, 4.0 μm pore diameter in active layer and 8.0 μm pore diameter in substructure) and *MP-2* (200 μm thickness, 2.0 μm pore diameter in active layer and 20.5 μm pore diameter in substructure).

Deionized water, methanol (Aldrich Chemicals, 99.9 %) and ethanol (Aldrich Chemicals) were employed in swelling experiments.

Method: Swelling of pure liquids in the membranes is investigated on 1.5 x 5 cm^2 membrane strips at room temperature (20 + 2 ^{0}C). To desorb the water from the polymer, the membrane was treated at 150 ^{0}C under vacuum before measuring the swelling.

A piece of membrane after drying to constant weight (w_d) was immersed in the pure liquid (water or alcohol) for at least 1 hour. When the sorption equilibrium was reached, the piece was weighed rapidly after blotting free surface liquid.

The swelling coefficient (*SC*) is calculated using the following relationship:

$$SC = \frac{w_s - w_d}{w_d} \cdot \frac{1}{d} \qquad (1)$$

where w_d is weight of dry membrane (g), w_s is weight of solvent swollen membrane (g) and d is density of solvent taken (g/cm^3).

The values of swelling coefficients (*SC*) for polyurethane membranes in different solvents are given in Table 1. Solubility parameters (δ_s) of different solvents were noted from the literature [16,17]

Table 1. Results of swelling measurements of polyurethane membranes.

Solvent	δ_s (cal/ cm^3)$^{1/2}$	*SC* cm^3/g	
		MP-1	MP-2
water	23.50	3.5227	2.9379
methanol	14.28	3.8403	3.3109
ethanol	12.92	3.8626	3.3289

3. Results and discussion

Polymer – solute compatibility is analyzed by using the Hildebrand solubility parameter [16-18]. According to the regular solution theory [17], the change in

enthalpy of mixing for a polymer solution per unit volume, when only dispersion forces are involved, is calculated as:

$$\Delta H = \phi_s \cdot \phi_p \cdot (\delta_s - \delta_p)^2 \quad (2)$$

where ϕ_s and ϕ_p are the volume fraction of solvent and polymer, respectively, and δ_s and δ_p are the Hildebrand solubility parameters of the solvent and polymer, respectively. Polymer – solvent compatibility increases as the values of δ_s and δ_p approach each other. The Hildebrand solubility parameter for a pure component is defined by:

$$\delta = (\Delta E / V)^{1/2} \quad (3)$$

where $\Delta E / V$ is the energy of vaporization per unit volume, also termed the cohesive energy density. From equation (2), Gee [13] concluded that the maximum swelling of polymer will occur when $\delta_s \approx \delta_p$. Hence a plot between the swelling coefficient (SC) and δ_s values of the solvent gives a Gaussian curve whose maxima will correspond to δ_p. It was also shown that:

$$SC = SC_{max} \cdot e^{-(\delta_s - \delta_p)^2 \cdot \phi_s} \quad (4)$$

Thus, by plotting $[(1/\phi_s) \cdot \ln(SC_{max}/SC)]^{1/2}$ versus δ_s, a straight line is obtained whose intersection point with the abscissa will give δ_p.

The values for SC versus δ_s, and for $[(1/\phi_s) \cdot \ln(SC_{max}/SC)]^{1/2}$ versus δ_s respectively, have been plotted for polyurethane membranes and the values of δ_p obtained are quite the same. The solubility parameter (δ_p) values obtained by plots and the cohesive energy density ($\Delta E / V$) values calculated by equation (3) for polyurethane membranes are shows in Table 2.

Table 2. Solubility parameter (δ_p) and cohesive energy density ($\Delta E / V$) for polyurethane membranes.

Membrane	δ_p $(cal/cm^3)^{1/2}$	$\Delta E / V$ cal/cm^3
MP-1	13.75	189.0625
MP-2	13.25	175.5625

From the date on degree of swelling (Table 1), all membranes showed a tendency to swell with ethanol, while swelling only a little with water. This is due to the fact that the distance between the solubility parameter of membrane and that of water is too far for water to swell the membrane. The cohesive energy density and solubility parameter (Table 2) of the thicker membranes show higher values than those of the thinner membranes.

4. Conclusions

Swelling studies of several industrial solvents are investigated through polyurethane membranes obtained through the phase inversion method. Experimental

determination of cohesive energy density value for the prepared membranes is done by measuring the swelling coefficients in water and several alcohols. The solubility parameters of the membranes are also calculated. The cohesive energy density and solubility parameter of the thicker membranes show higher values than those of the thinner membranes. All the membranes show a tendency to swell with ethanol.

Received March 20, 2007 *The "Gh.Asachi" Technical University Iaşi*

REFERENCES

1. Loeb, S. and Sourirajan, S. – *Membrane formation by phase inversion method*, **Advan. Chem. Ser., 38**, 1963, **117-132**
2. Pinnau, I. and Koros, W.J. – *Structures and gas separation properties of asymmetric polysulfone membranes made by dry, wet, and dry - wet phase inversion*, **J. Appl. Polym. Sci., 43**, 1991, **1491-1499**
3. Kesting, R.E. – *Synthetic polymeric membranes*, New York: McGraw-Hill Book Company, 1971, **116-157**
4. Sarbolouki, M.N. – *Preparation of Skinned Membranes Without Evaporation Step*, **J. Polym. Sci. Pt. C; Polymer Letters, 11**, 1973, **753-756**
5. Reuvers, A.J., van den Berg, J.W.A. and Smolders, C.A. – *Formation of membranes by means of immersion precipitation. I. A model to describe mass transfer during immersion precipitation*, **J. Membr. Sci., 34**, 1987, **45-65**
6. Zeman, L. and Fraser, T. – *Formation of air - cast cellulose acetate membranes. I: Study of macrovoid formation*, **J. Membr. Sci., 84 (1-2)**, 1993, **93-106**
7. Castellari, C. and Ouani, S. – *Preparation of reverse osmosis membranes*, **J. Membr. Sci., 9**, 1981, **29-41**
8. Cheng, L.P., Soh, Y.S., Dwan, A.H. and Gryte, C.C. – *Preparation of membranes by the immersion precipitation process*, **J. Polym. Sci., Part B: Polym. Phys., 32**, 1994, **1413-1421**
9. Nunes, S.P., Ruffmann, B., Rikowski, E., Vetter, S. and Richau, K. – *Inorganic modification of proton conductive polymer membranes for direct methanol fuel cells*, **J. Membr. Sci., 203**, 2002, **215-225**
10. Bottino, A., Capannelli, G., D'Asti, V. and Piaggio, P. – *Preparation and properties of novel organic - inorganic porous membranes*, **Sep. Purif. Technol., 22**, 2001, **269-275**
11. Nunes, S.P., Peinemann, K.V., Ohlrogge, K., Alpers, A., Keller, M. and Pires, A.T.N. – *Membranes of poly(ether imide) and nanodispersed silica*, **J. Membr. Sci., 157**, 1999, **219-226**
12. Chen, X., Ping, Z.H. and Long, Y.C. – *Separation properties of alcohol - water mixture through silicalite - filled silicone rubber membranes by pervaporation*, **J. Appl. Polym. Sci., 67 (4)**, 1998, **629-636**
13. Allen, G., Gee, G. and Wilson, G. – *Intermolecular forces and chain flexibilities in polymers: I. Internal pressures and cohesive energy densities of simple liquids*, **Polymer, 1**, 1960, **456-466**
14. Bajpai, U.D.N. and Bajpai, A.K. – *Determination of cohesive energy density of polyacryl - amide by swelling measurement*, **J. Appl. Polym. Sci., 43**, 1991, **2279-2281**
15. Ciobanu, G. and Bezdadea, M. – *SAPO - 5 zeolite - filled polyurethane membranes. I. Preparation and morphological characterisation*, **Revista de Chimie**, Bucureşti, **55 (3)**, 2004, **140-143**
16. Brandrup, D.J. and Immergut, E.H. – *Polymer Hand - book*, Wiley, New York, 1975, **52-99**
17. Hildebrand, J. and Scott, R. – *The Solubility of Non - Electrolytes*, 3rd ed. Van Nostrand Reinhold, New York, 1949, **74-86**
18. Scatchard, G. – *Selected values of chemical thermodynamic properties*, **Chem. Rev., 8**, 1931, **321-334**.

DETERMINAREA DENSITĂŢII ENERGIEI DE COEZIUNE A MEMBRANELOR POLIURETANICE PRIN MĂSURAREA GRADULUI DE UMFLARE

Rezumat: În lucrarea de faţă se prezintă posibilitatea determinării densităţii energiei de coeziune pentru membrane poliuretanice obţinute prin tehnica inversiei de fază. Prin metoda de turnare s-au obţinut membrane asimetrice poroase, cu diverse porozităţi şi grosimi. Studiile de umflare a membranelor în diverşi solvenţi (apă şi alcooli inferiori) au urmărit în final stabilirea densităţii energiei de coeziune şi a parametrului de solubilitate pentru membranele studiate. Densitatea energiei de coeziune şi parametrul de solubilitate pentru membranele cu grosimi şi pori mari au valori mai ridicate comparativ cu cele ale membranelor cu grosimi şi pori mai mici. Rezultatele indică faptul că membranele prezintă o tendinţă evidentă de a se umfla în alcool etilic.

BULETINUL INSTITUTULUI POLITEHNIC DIN IAŞI
Tomul L(III (LVII), Fasc. 4, 2007
Secţia
ŞTIINŢA ŞI INGINERIA MATERIALELOR

MICROSTRUCTURAL CHANGES OF BEARING STEELS 100Cr6 AND 100CrMn6 INDUCED BY THERMOMECHANICAL TREATMENTS

BY

RADU COMANECI

Abstract: For most commercial products in the steel industry, their external shapes are the result of hot-deformation, whilst the necessary mechanical properties are obtained from the alloy design and by heat treatment after hot deformation. A combination of plastic deformation and phase transformations in the same treatment cycle is an effective method for the improvement of mechanical properties of steels. In particular, the thermomechanical treatment (TMT) applied in different ways on bearing steel not only induces the increase of required properties, but also can determine – for some variants of the treatment - the improvement of both contact fatigue life and dimension stability. This one is the result of some structural phase changes such as the decrease of residual austenite amount, the finishing of martensite or the changes concerning the carbide dimensions and morphology. In this context, the paper aims both to estimate the effects of the TMT on the bearing steels microstructure and to confirm the results of diffractographic investigation on TMT structure.

Keywords: thermomechanical treatment, bearing steel, martensite tetragonality.

1. Introduction

The classic technological process of bearing rings consists in hot deformation/ free cooling-air/ globulisation annealing/ machining operations/ austenization/ quenching, oil/ low tempering/ final grinding. After classic technological process, we find a structure with a large amount of residual austenite (16.90% Ares for 100Cr6 and 14.8% for 100CrMn6 respectively). The structure which is obtained after globulisation annealing contents coagulated carbides and the martensite obtained after the quenching has a well-known acicular morphology and a coarse appearance.

The high-temperature thermomechanical treatment (HT-TMT) consisting in hot deformation of the austenite and subsequent quenching to martensite – in regulated conditions of hot-deformation - leads to the simultaneous improvement of strength and plasticity in high-strength martensitic state [1]. In particular, for some steels, such as bearing steel, if the HT-TMT is succeeded by a high tempering and a secondary quenching after that (we called this Hereditary Thermomechanical Treatment H-TMT), it is possible to obtain some favorable structural phase changes such as the decrease of residual austenite (Ares) amount, the finishing of martensite (M) and another carbide (K) dimensions and morphology [2, 3]

This finding is consistent with the results of other investigation (such as the determination of martensite tetragonality) and it is explained in terms of decrease of carbon content in the austenite before quenching [3] The hot deformation is a stimulating process for the fine and more dispersing carbide separation after the high tempering in comparison with classic annealing. Became important to get the

evolution of tetragonality of martensite to estimate the really changes take place during HT/H-TMT processes.

2. Theoretical approach

The tetragonality oh the martensite *c/a* can be estimated by the interpretation of diffractographic images. It depends on carbon amount, so the problem remains the determination of tetragonal phase carbon. It's been established that this is possible if we assume that both austenite and martensite have the same quantity of carbon. In the conditions of no diffusive α-transformation, the mentioned hypothesis is correct
From the relation of interplanar distance:

$$\frac{1}{d_{hkl}} \quad \sqrt{\frac{h^2+k^2}{a^2}+\frac{l^2}{c^2}} \tag{1}$$

the two dimension of tetragonal cell, are expressed in terms of carbon amount ($\%C_M$):

$$a \quad a_o(1+k_1\cdot\%C_M) \tag{2}$$

$$c \quad c_o(1+k_2\cdot\%C_M) \tag{3}$$

where $a_o = c_o = 2{,}866$Å (for austenite), $k_1 = -0{,}00454$ and $k_2 = 0{,}04054$. So:

$$\frac{1}{d_{hkl}^2} \quad \frac{h^2+k^2}{a_o^2(1+k_1\cdot\%C_M)^2}+\frac{l^2}{c_o^2(1+k_2\cdot\%C_M)^2} \tag{4}$$

Because of the very small k_1, k_2 and $\%C_M$ values, we assume that:

$$(1+k_{1,2}\cdot\%C_M)^2 \sim 1+2k_{1,2}\cdot\%C_M; \quad \frac{1}{1+2k_{1,2}\cdot\%C_M} \sim 1 \quad 2k_{1,2}\cdot\%C_M \tag{5}$$

and equation (4) became:

$$\frac{1}{d_{hkl}^2} \quad \frac{(h^2+k^2)(1-2k_1\cdot\%C_M)}{a_o^2}+\frac{l^2(1-2k_2\cdot\%C_M)}{c_o^2}$$
$$\frac{(h^2+k^2)(1-2k_1\cdot\%C_M)+l^2(1-2k_2\cdot\%C_M)}{2{,}866^2} \tag{6}$$

Assuming that the peak is the results of combined diffraction on plane (hkl) and (h'k'l'), the Bragg relation became:

$$d_{hkl} \quad \frac{\lambda}{2\sin\left(\frac{2\theta_{hkl}}{2}\right)}, \; d_{h'k'l'} \quad \frac{\lambda}{2\sin\left(\frac{2\theta_{h'k'l'}}{2}\right)} \tag{7}$$

$$\frac{d_{hkl}^2}{d_{h'k'l'}^2} \quad \frac{\sin^2\left(\frac{2\theta_{h'k'l'}}{2}\right)}{\sin^2\left(\frac{2\theta_{hkl}}{2}\right)} \quad \frac{(h^2+k^2)(1 \quad 2k_1\cdot\%C_M)+l^2(1-2k_2\cdot\%C_M)}{(h'^2+k'^2)(1 \quad 2k_1\cdot\%C_M)+l'^2(1 \quad 2k_2\cdot\%C_M)} \tag{8}$$

From equation (9), we get $\%C_M$:

$$\%C_M \quad \frac{1}{2}\cdot\frac{\sin^2\left(\frac{2\theta_{hkl}}{2}\right)\cdot(h'^2+k'^2+l'^2) \quad \sin^2\left(\frac{2\theta_{h'k'l'}}{2}\right)\cdot(h^2+k^2+l^2)}{k_1\left[(h'^2+k'^2)-(h^2+k^2)\right]+k_2(l'^2-l^2)} \tag{9}$$

Finally, we determine the martensite tetragonality by using equation (10) or (11), derived from equations (2) and (3):

$$c/a = 1 + 0{,}045 \cdot \%C_M \quad (10)$$

$$a = 2{,}866(1 - 0{,}00454 \cdot \%C_M), \quad c = 2{,}866(1 + 0{,}04054 \cdot \%C_M) \Rightarrow c/a \quad (11)$$

3. Experimental results

Therefore we applied on bearing steels 100Cr6 and 100CrMn6 two TMT variants, (see Table 1):

a) - austenization/ hot deformation/ quenching from deformation temperature/ low tempering (**HT-TMT**);

b) - austenization/ hot deformation/ quenching from deformation temperature/ high tempering/ reaustenization/ quenching/ low tempering (**H-TMT**).

Table 1. The TMT-variants parameters of experimental researches

Operation	TMT parameters	Nominal parameter values
Austenization	$T_A = 850 - 1100°C$, 10min	T_d = 850; 950; 1050 °C ε = 20; 40; 60%
Hot deformation	T_d = 850-1100°C, ε_{real} = 60%	
Quenching	From T_d, oil 60-80°C	
High tempering	T_{temp} = 690°C, τ_{temp} = 4 ÷ 8h	τ_{temp} = 4, 8h
Reaustenization	T'_A=850°C, 8min	-
Secondary quenching	From T'_A, oil 60-80°C	
Low tempering	$T_{temp} = 160 - 200°C$, 3h	T_{temp} = 160; 200°C

The experimental data analysis by diffraction procedures shows the followings:

A. The first thermomechanical treatment variant (HT-TMT) induces in all hot deformation regimes an increased quantity of residual austenite, up to 35 - 40% - diffractografic examination, figure 1 and 2.

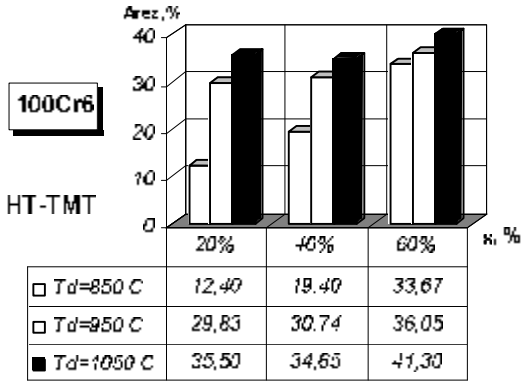

Figure 1. The retained austenite amount of 100Cr6 steel after HT-TM;

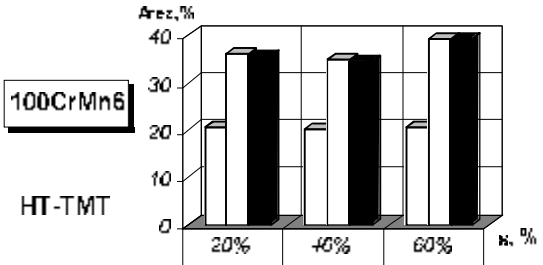

	20%	40%	60%
□ Td=850 C	20,69	20,16	20,73
□ Td=950 C	36,05	34,92	39,18
■ Td=1050 C	35,57	34,30	39,15

Figure 2. The retained austenite amount of 100CrMn6 steel after HT-TTM

That means that the hot-deformation determines a brake action on the α-phase transformation both the temperature and deformation are increasing.

B. The second thermomechanical treatment variant (H-TMT) induces in all hot deformation regimes an decreased quantity of residual austenite, from min. 2.45% to max. 8.3% - diffractographic examination, figure 3 and 4

In all situations, the optimum low tempering temperature range is 150-170°C.

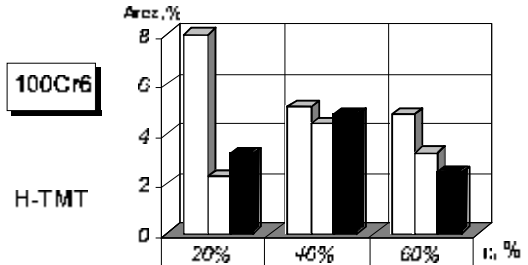

	20%	40%	60%
□ Td=850 C	6,30	5,11	4,77
□ Td=950 C	2,33	4,40	3,25
■ Td=1050 C	3,20	4,80	2,45

Figure 3. The retained austenite amount of 100Cr6 steel after H-TTM

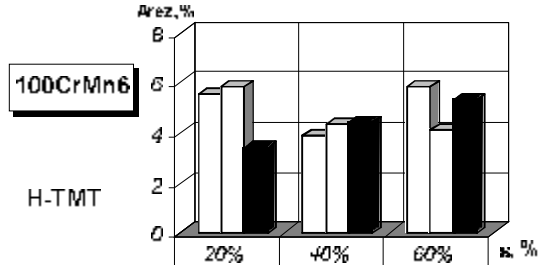

	20%	40%	60%
□ Td=850 C	5,56	3,86	5,81
□ Td=950 C	5,86	4,34	4,09
■ Td=1050 C	3,40	4,40	5,30

Figure 4. The retained austenite amount of 100CrMn6 steel after HT-TTM

In the second thermomechanical treatment (TI-TMT) variant, after high tempering up to 680-690°C (8h) there is stimulated the carbide precipitation mechanism and the carbon content in the matrix is decreasing. That reveals that tetragonality parameter normally decreases, figure 5-8. After reaustenisation, the quasi absence oh the carbon inside of the matrix determines the speeding up the subsequent martensite transformation, with an expected decrease of residual austenite amount under about 5% (with a single exception, for $\varepsilon = 20\%$ at $T_d = 850°C$, when is registered about 8%).

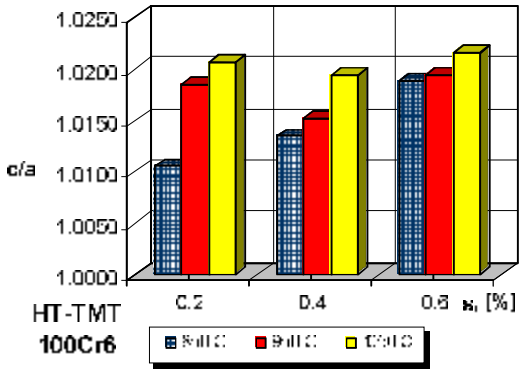

Figure 5. The tetragonality c/a of 100Cr6 steel after HT-TTM

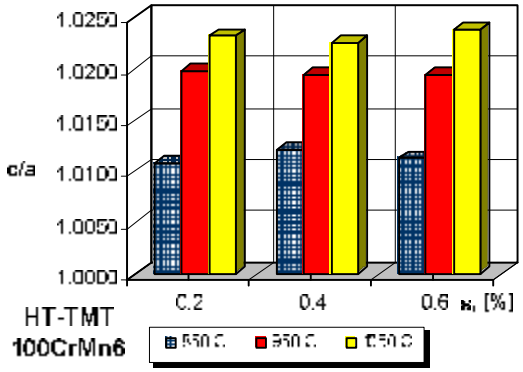

Figure 6. The tetragonality c/a of 100CrMn6 steel after HT-TTM

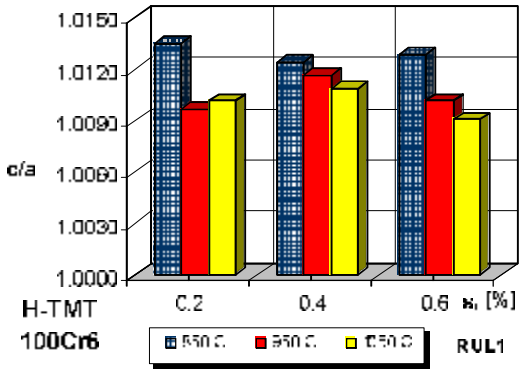

Figure 7. The tetragonality c/a of 100Cr6 steel after H-TTM

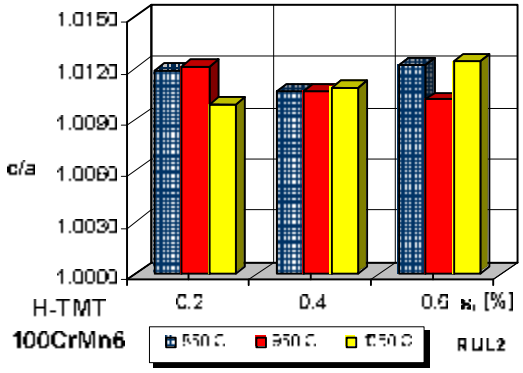

Figure 8. The tetragonality c/a of 100CrMn6 steel after H-TTM

4. Conclusions

The thermomechanical treatment applied in II-TMT variant stimulates the carbide precipitation during the high tempering after the quenching from the deformation temperature. Thus, the carbon content in the matrix decrease and a favourable structure for subsequent martensite transformation appears. After reaustenization, this one determines an accelerated martensite transformation

The II-TMT technology determines by the final quenching a good level of residual austenite, under 5-6%, which creates a set of premises for the increasing of ball bearing behavior during the exploitation. Considering the importance and the significant weight of ball bearings in techniques, these results could have major consequences. The mentioned structural changes was confirmed by the evolution of martensite tetragonality.

Received April 12, 2007 *The "Gh.Asachi" Technical University Iaşi*

REFERENCES

1. Bernshtein, M.L. **The thermomechanical treatment of the steels**, Metallurghia, Moskva, 1983
2. M. L. Bernshtein, E. I. Demina and K. E. Safonova, *Thermomechanical treatment of ball-bearing steel*, **Material Science and Heat Treatment**. Springer New York, ISSN0026-0673, pp. 13-18. New York, 2004.
3. Comaneci, R., Galusca, D.G., Comanici A. *Studies concerning the effects of high temperature thermomechanical treatment (HT-TMT) on structure and hardness of Romanian ball-bearing steel Rul1 (100Cr6)*, **METAL 98**, vol. 3, ISBN 80-8612214-X, Ostrava, Czech Republic, 1998.
4. Comaneci, R. **Studies and researches concerning the thermomechanical treatment applications in machine-building industry**, Ph.D. Thesis, "Gh. Asachi" Technical University of Iasi, Romania, 1999.

MODIFICARI STRUCTURALE ALE OTELURILOR DE RULMENTI 100Cr6 SI 100CrMn6 INDUSE PRIN TRATAMENT TERMOMECANIC

Rezumat: Combinarea deformării plastice cu transformările de fază în acelaşi ciclu de tratament termic reprezintă o metodă de îmbunătăţire a proprietăţilor mecanice ale oţelurilor. În particular, aplicarea TTM în diferite variante pe oţelurile de rulmenţi determină nu numai îmbunătăţirea proprietăţilor, dar şi creşterea rezistenţei la oboseală şi a stabilităţii dimensionale. Acestea sunt rezultatul modificărilor structurale cum ar fi scăderea conţinutului de austenită reziduală, finisarea martensitei sau modificarea dimensiunilor sau a morfologiei carburilor. În acest context, lucrarea vine să confirme prin analiză difractografică modificările structurale induse prin tratament termomecanic.

BULETINUL INSTITUTULUI POLITEHNIC DIN IAŞI
Tomul LIII (LVII), Fasc. 4, 2007
Secţia
ŞTIINŢA ŞI INGINERIA MATERIALELOR

FINITE ELEMENT AND EXPERIMENTAL INVESTIGATION OF EQUAL CHANNEL ANGULAR PRESSING OF ALUMINUM AND AA5083 ALUMINUM ALLOY

BY

RADU COMANECI and LUCIAN ZAHARIA

Abstract: Bulk nanostructured materials represent the application of nanotechnology in the engineering material area. Severe Plastic Deformation (SPD) is an efficient and low cost top-down method for producing ultrafine or nanostructured bulk materials. Among various techniques, Equal Channel Angular Pressing (ECAP) is one of the most affordable processes because of its prominent feature to fabricate workpiece repeatedly without changing the geometry. The aim of this paper is to present experimental and finite element investigations on load requirements for Al99.5 and AA5083 aluminum alloy subjected to ECAP. In order to validate the numerical proposed simulation, the results were compared with experimental data.

Keywords: finite element, equal channel angular pressing, aluminum, severe plastic deformation

1. Introduction

The ultra-fined materials have been widely investigated due to its mechanical properties such as high specific strength and ductility. Various forming techniques have been developed to obtain such mechanical properties. Among them, equal channel angular pressing (ECAP) is an effective technique to improve the material strength by imposing severe plastic strain into the workpiece.

Due of its prominent feature to fabricate the workpiece repeatedly without changing the geometry of the workpiece, many studies of the ECAP process have been conducted experimentally and numerically so far to investigate the effect of process parameters on material behavior and strain distribution. [1, 2]

Equal channel angular pressing (ECAP) is process capable of imparting a severe plastic deformation in a metal workpiece. Such deformation is achieved by simple shear during an extrusion into a die, without changing the specimen cross section. The ECAP purpose is obtaining the ultra-fine grained bulk materials. For practical application, die geometry, material properties and process conditions influence the magnitude of plastic deformation imposed and its homogeneity. These factors play a fundamental role in resulting microstructure and mechanical properties of processed material.

As the mechanical properties of the severely deformed material are linked to the deformation history, understanding the phenomena associated with strain and deformation load development in the ECAP process is very important. For this purpose, the results of modeling ECAP using the finite element method are presented for various geometric conditions.

In this study FEM analysis made possible a better understanding of process and of its related operative parameters, both for tools both for material behaviour.
The investigation aim was to obtain the level deformation load on workpiece, hence two and three dimensional FEM analysis on two different aluminum alloys and different tools geometry were carried out. FEM results were compared with workpieces really processed by one pass ECAP.

2. Experimental

Commercially available rectangular bars 10x10mm of an Al99.5 and AA5083 aluminum alloy (4.5Mg, 0.7Mn) were considered for this study. Samples of 60mm length were cut from the bars and subjected to homogenization for AA 5083 alloy (500°C for 24h) and annealing for Al99.5 (180°C for 3h).

The system for processing the samples is based on a deformation tool (die) is made up of two asymmetrical half dies machined from two blocks of H11 tool steel heat treated with nominal hardness of 58HRC, Figure 1.

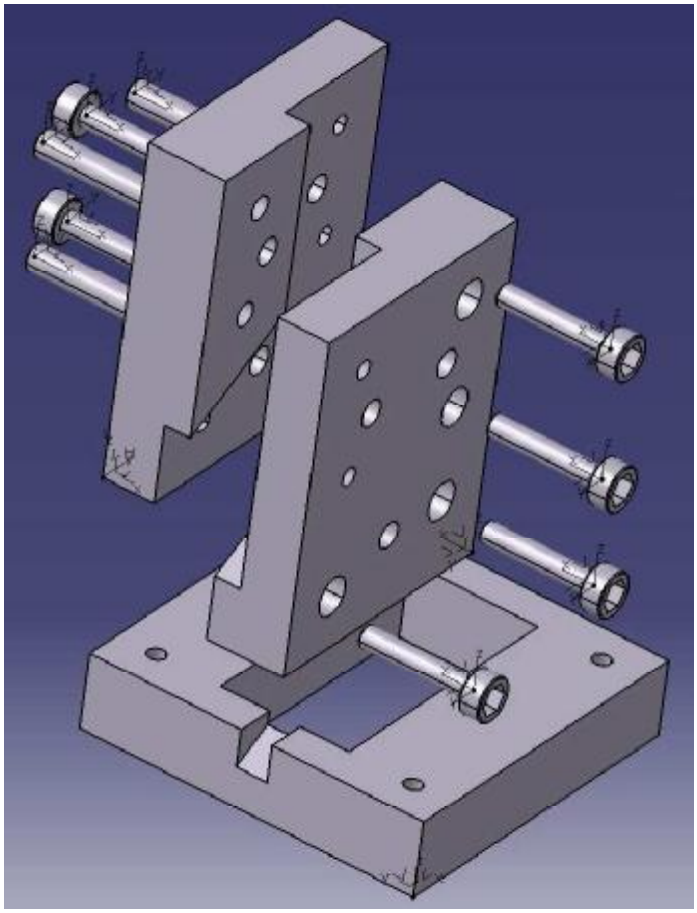

Figure 1. The ECAP die (2φ = 120°)

Channels having rectangular dimension of 10mm were machined with $2\varphi = 120°$ angle intersection of channels and $\psi = 21°$ outer channel arc angle, corresponding to 4mm outer radius (R = 4mm), Figure 2

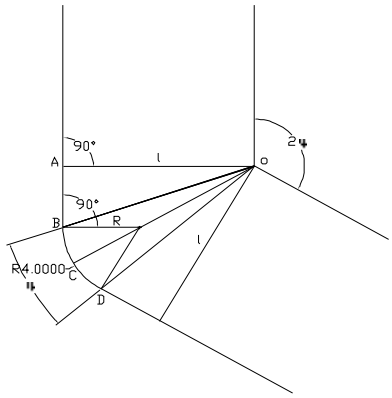

Figure 2. The die geometry

Practical experience shows that a calibrated length of 15mm after the corner followed by an enlargement of the exit channel may reduce friction and lower the pressure load.

The two half dies were centered with 3 bolts and assembled and held together with 6 screws ϕ12mm, Figure 1. An inferior plate piece supplementary stress constrains the two half dies. ECAP tests were carried out at room temperature. The samples were coated with a lubricant based on zinc sthearat. Plunger speed was 8.75mm/s.

3. Prediction of deformation load

Both Al99.5 and AA5083 aluminum alloy are one pass extrusion simulated at room temperature. The friction between the ECAP die and the samples is assumed by the shear friction model:

$$\tau = m \cdot K \tag{1}$$

where m is the friction factor (0.12) and K is the shear strength of the material.

The workpiece material was considered as plastic body and the die as rigid body respectively. The billet is discretized into 4836 tetrahedral elements

Three design scenarios are analyzed:

A - there are two arc transitions at both sides of the extrusion channels (R, r ≠ 0; in particular R = 4mm and r = 2mm) – 120_4_2, Figure 3.

B - there is only one arc (outer) transition at one side of the channels (R ≠ 0, r = 0; in particular R = 4mm) – 120_4_0, Figure 4.

C - there is no arc transition, so the channels are intersected at a sharp corner (R = 0, r = 0) – 120_0_0, Figure 5.

The total strain ε of the workpiece in one pass through the die is given by Eq. (2), [3]:

$$\varepsilon = \frac{1}{\sqrt{3}} \left[2ctg\left(\frac{\varphi}{2} + \frac{\psi}{2}\right) + \psi \cos ec\left(\frac{\varphi}{2} + \frac{\psi}{2}\right) \right] \tag{2}$$

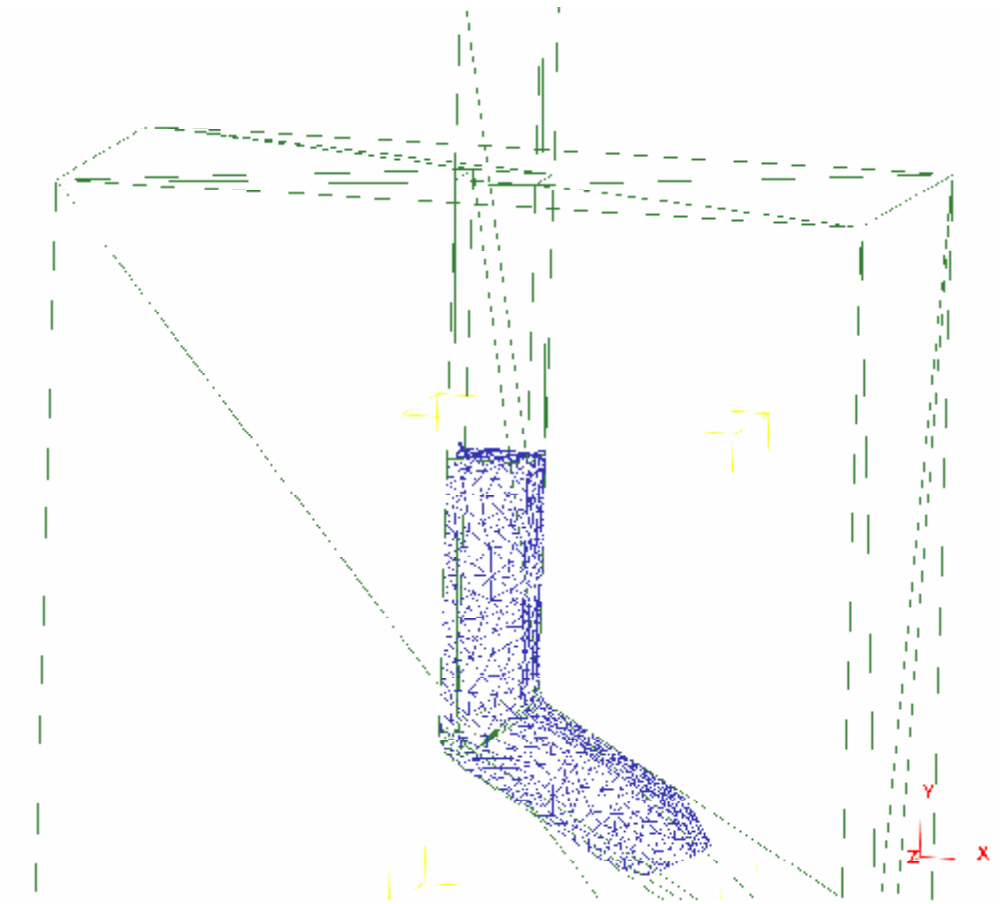

Figure 3. 3D Assembly of ECAP 120_4_2

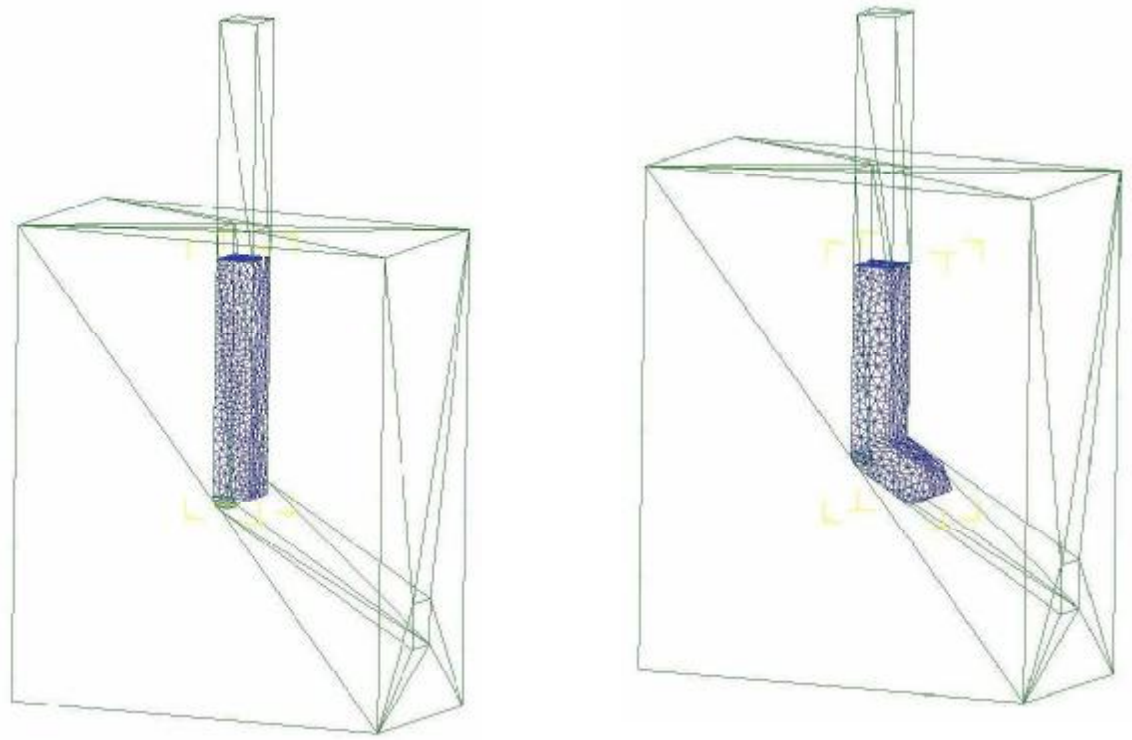

Figure 4. 3D Assembly of ECAP 120_4_0

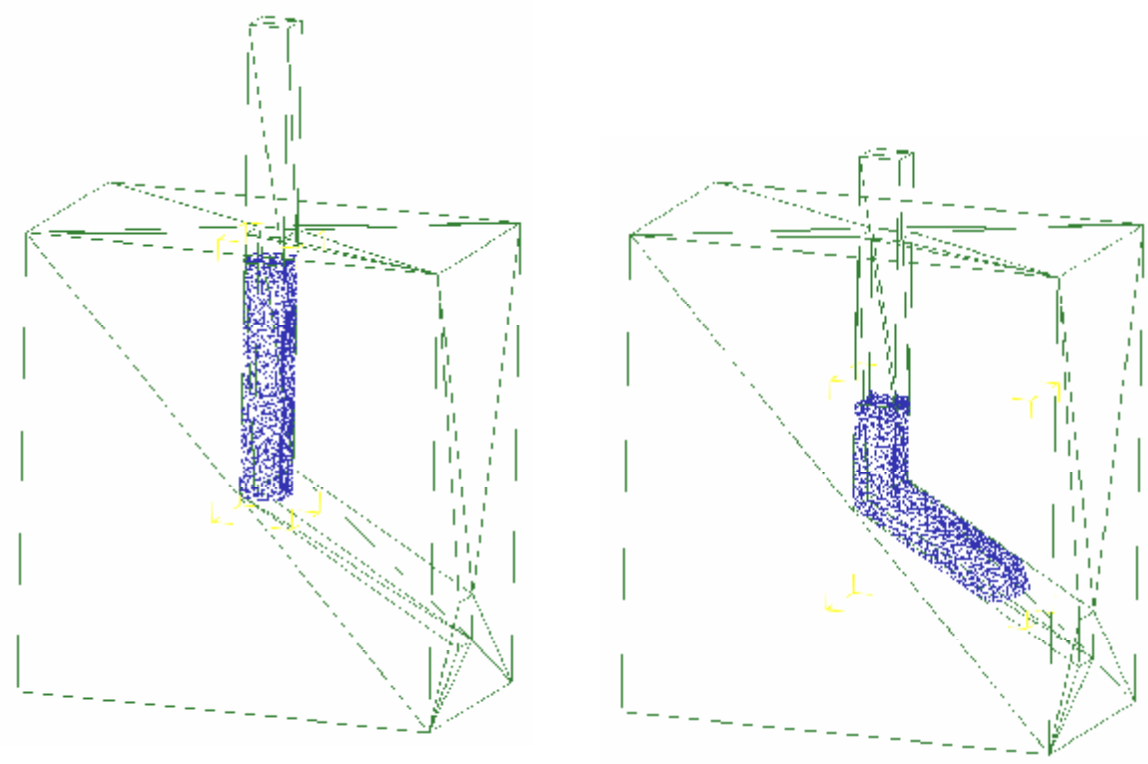

Figure 5. 3D Assembly of ECAP 120 0 0

4. Experimental results

The study of deformation load for three design cases can give both the necessary level of the forces in the severe plastic deformation process and important information for die design. For eventually decreasing of load level it could be necessary to change the die geometry, or friction condition, or technological parameters (deformation temperature and/or plunger speed). It is true that the deformation load is no so critical for small billets like our samples, but for large wokpieces, become clearly that the deformation load needs to be considered

Figure 6 – 11 shows the predicted loads for Al99.5 and AA5083 subjected to severe plastic deformation by $ECAP_{120}$.

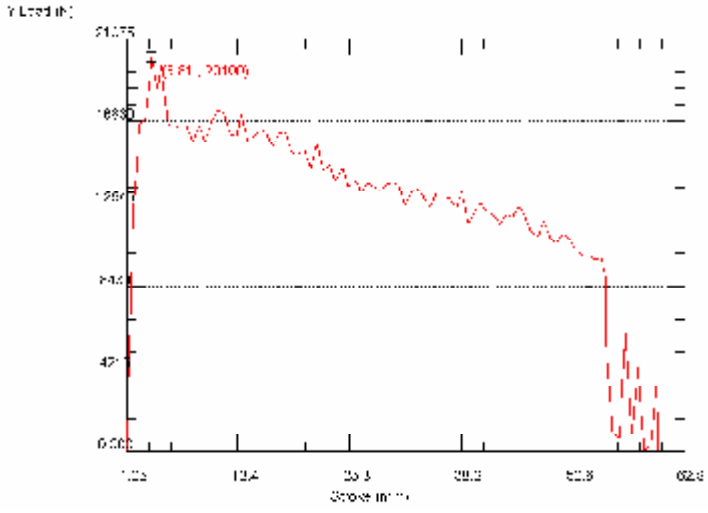

Figure 6. Load prediction for Al99.5 ECAP 120 0 0

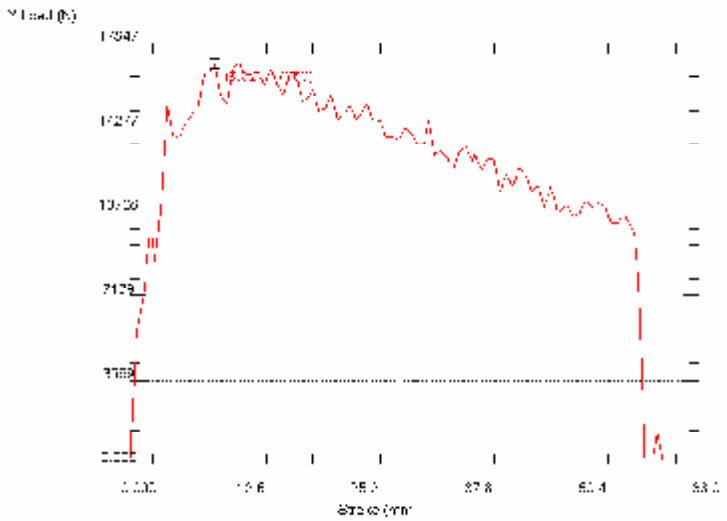

Figure 7. Load prediction for Al99.5 ECAP 120_4_0

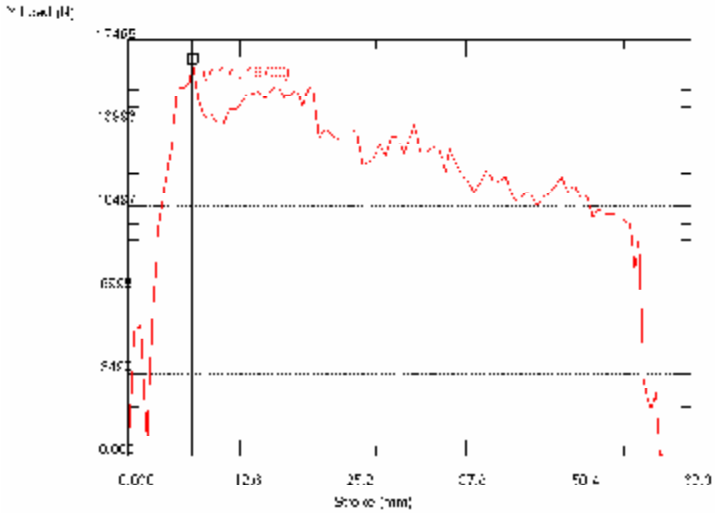

Figure 8. Load prediction for Al99.5 ECAP 120_4_2

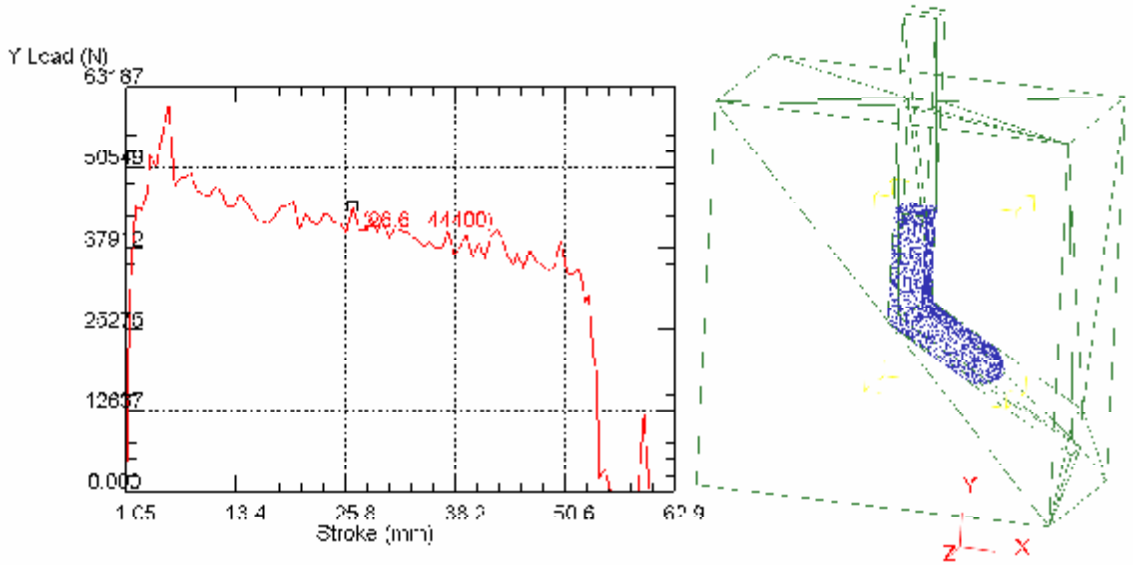

Figure 9. Load prediction for AA5083 ECAP 120_0_0

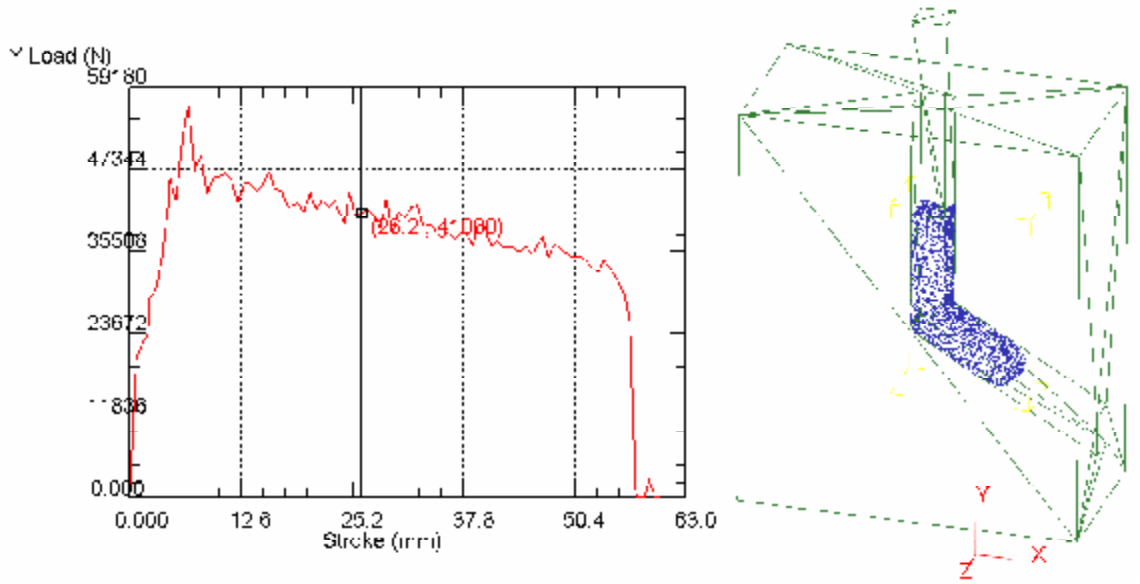

Figure 10. Load prediction for AA5083 ECAP 120 4 0

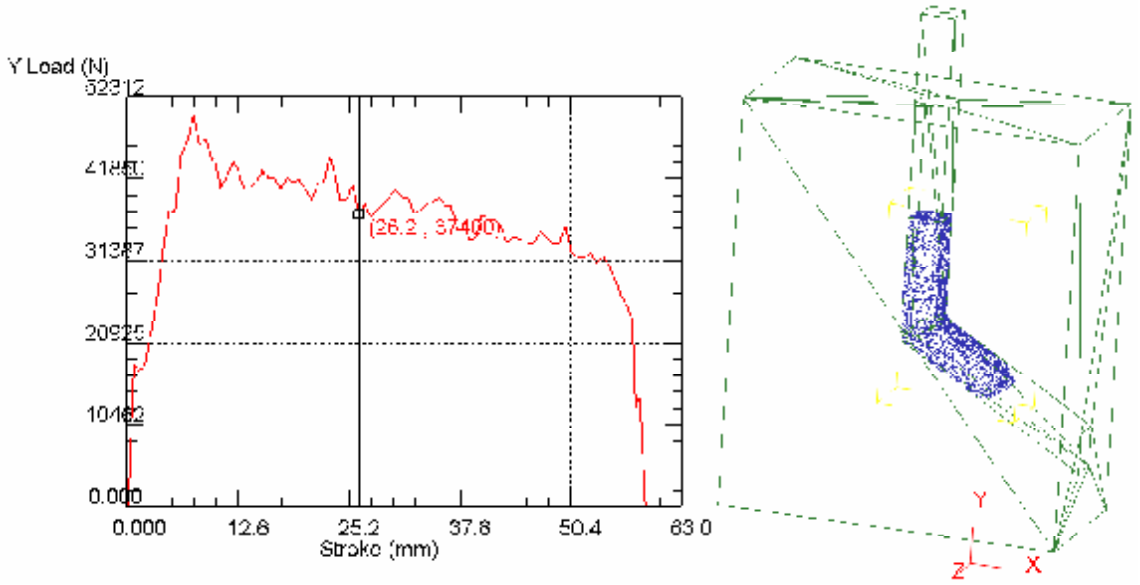

Figure 11. Load prediction for AA5083 ECAP 120 4 2

There are both some similarities and differences between predicted and registered loads in $ECAP_{120}$ process. The both predicted and reported deformation loads registers a pronounced increase in the first phase of the process. This situation is well emphasized especially in the cases of the dies without fillet radii for both Al99.5 and AA5083 alloy.

The registered load vs. plunger stroke, Figure 12, shows a little different slope of force increasing in the first stage. The situation correspond the time range where the die channel fills with material. The first sector of the loading curve consisting of a rise up to peak is no so rapidly like the predicted one. That probably because of the expulsion phase of the previously pressed sample. The level of predicted and reported loads is similarly both for Al99.5 and for AA5083 alloy.

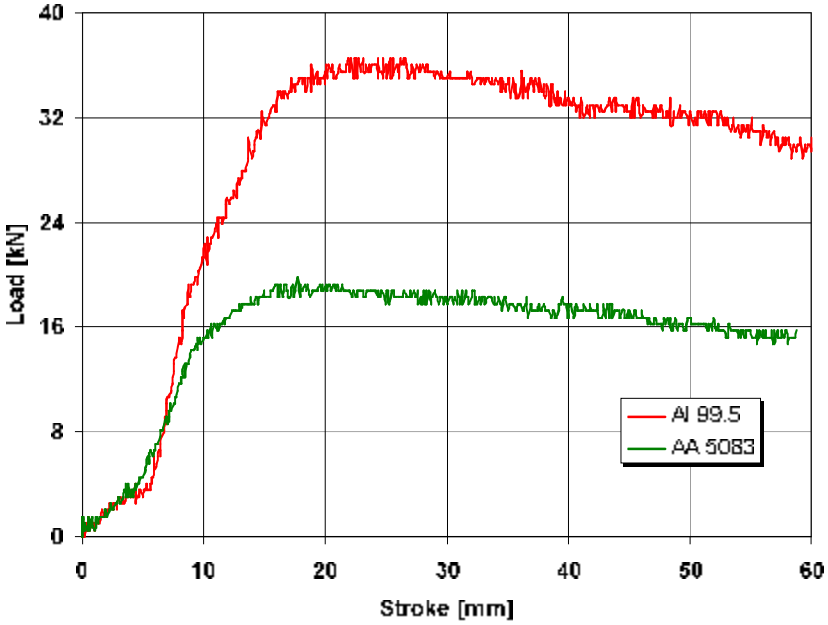

Figure 12. Deformation load of Al99.5 and AA5083 during $ECAP_{120}$ (120 4 2)

5. Conclusions

In this study, numerical simulation of an ECAP with Al99.5 and AA5083 alloy rectangular specimens was carried out by applying three-dimensional finite element analysis. It was found that the deformation load requirements are clearly sensitive to the die geometry. Experimental data validates present finite element investigation. The deformation behavior study through FE simulation in ECAP process provides basic and useful information for optimizing die design and process determination.

Received April 17, 2007 *The "Gh.Asachi" Technical University Iaşi*

REFERENCES

1. M. W. Fu, M. S. Yong, Q. Pei, and H. H. Hng, *Deformation Behavior Study of Multi-Pass ECAE Process for Fabrication of Ultrafine or Nanostructured Bulk Materials*, **Materials and Manufacturing Processes**, 21, 501–506, 2006.
2. J.H. Lee, I.H. Son, Y.T. Im, *Finite element investigation of equal channel angular extrusion process*, **Materials Transactions**, The Japan Institute of Metals 45 (2004) 2165-2171
3. M. Vedani, P. Bassani, M. Cabibbo, V. Latini and E. Evangelista, *Experimental Aspects Related to Equal Channel Angular Pressing of a Commercial AA6082 Alloy*, **Metallurgical Sci. and Tech.**, vol21, no 2, 3-9, 2003.

CERCETARI EXPERIMENTALE SI ANALIZA CU ELEMENT FINIT PRIVIND DEFORMAREA ALUMINIULUI SI A ALIAJULUI AA5083 IN CANALE UNGHIULARE EGALE

Rezumat: Materialele nanostructurale industriale reprezinta o aplicatie importanta a nanotehnologiei in domeniul materialelor. Deformarea plastica severa este o metoda ieftina si eficienta de producere a materialelor cu structura ultrafina/nanometrica. Printre metodele de obtinere, presarea in canale unghiulare egale (ECAP) este varianta cea mai abordabila intrucat procesul este repetitiv, fara modificarea geometriei piesei. Scopul lucrarii este de a prezenta cercetari prin MEF si unele rezultate experimentale privind estimarea fortelor necesare in procesul de deformare plastica severa a Al99.5 si a aliajului AA5083 prin procedeul ECAP.

BULETINUL INSTITUTULUI POLITEHNIC DIN IAŞI
Tomul LIII (LVII), Fasc. 4, 2007
Secţia
ŞTIINŢA ŞI INGINERIA MATERIALELOR

MATHEMATICAL MODEL FOR ADVANCED DESOXYDATION IN VACUUM OF METALS

BY

ION CONSTANTIN, DRAGOS TALOI, LIANA MARIA VLĂDUŢIU and LILIANA TALOI

Abstract: The paper presents a new mathematical model for advanced desoxydation in vacuum of liquid metals. The model has two components: a thermodinamical one, that allows to determine the oxygen content in the metallic bath at its interface with the gaseous phase, and a diffusive component that allows a theoretical determination of the final average content of oxygen in different technological conditions of temperature, depth of the metallic bath, time, initial concentration of the oxygen and the vacuum degree. The presented model has been applied to the copper desoxydation in vacuum.

Keywords: desoxydation, kinetic model, thermodinamics, oxygen diffusivity, liquid copper.

1. Introduction

Electro physical and mechanical properties of metals are at a large extent dependent of the purity degree, of the impurities nature and of the material state (if cast, deformed or annealed). In many situations, as a result of refining processes, either oxidating or electrolytic, the metals can contain oxygen that negatively affects especially their plasticity and ductility. For instance, in the case of copper, after the thermal and electrolytic refining, it contains about 500...800 ppm, and to obtain conductors of thin sections and high electrical conductibility, the admitted oxygen content is bellow 20...30 ppm. That is why, in some instances, supplementary desoxydation operations - with different reducing agents or in vacuum – are necessary. Considering the thermodynamic and kinetic properties of liquid systems Me – O, authors developed a mathematical model allowing to determine one of the parameters as a function of the other parameters of the process. The model has two components : a thermodynamic component for the oxygen concentration at the interface with the gaseous phase determination and a kinetic component to determine either the length of time necessary for desoxydation or the residual concentration of oxygen as functions of temperature, the metallic bath depth, the vacuum degree and the initial concentration of oxygen.

2. Thermodynamic model for the surface concentration calculus at the vacuum desoxydation

During in vacuum desoxydation, at the metallic bath – gaseous phase interface occurs a physical process of interphasic distribution of oxygen, possible to be represented by the transformation :

$$[O]_{\text{in Me}} \rightarrow \tfrac{1}{2}\{O_2\}_{\text{gaseous phase}} \qquad (1)$$

Reaction (1) can be decomposed into the algebraic sum of the following two elementary:

$$[O]_{in\ Me} \rightarrow \tfrac{1}{2}\{O_2\}\ (p_{O_2} \quad 1\ atm) \tag{2}$$

$$\tfrac{1}{2}\{O_2\}\ (p_{O_2} \quad 1\ atm) \rightarrow \tfrac{1}{2}\{O_2\}_{gaseous\ phase} \tag{3}$$

As a result, the variation of the partial molar free energy of the reaction (1) can be written as the algebraic sum of the partial molar free energies variations for the transformations (2) and (3):

$$\overline{\Delta G}_1 \quad \overline{\Delta G}_2 + \overline{\Delta G}_3 \tag{4}$$

where :

$\overline{\Delta G}_1 \quad RT \ln a_O$ is the variation of the partial molar free energy for the reaction (1) ;

a_O - oxygen activity at the interface metallic bath gaseous phase ;

$\overline{\Delta G}_2$ is the variation of the partial molar free energy for the reaction (2) of oxygen dissolution in the metal Me in normal conditions, usually known for the most metals ;

$\overline{\Delta G}_3 \quad RT \ln p_{O_2}^{1/2}$ is the variation of the partial molar free energy for the reaction (3).

p_{O_2} - is the partial pressure of oxygen in gaseous phase, in atm. In advanced vacuum conditions, this pressure can be considered as being equal to the remnant total pressure of the gaseous phase.

From reaction (4) we can obtain the oxygen activity in liquid metal at different temperatures and different partial pressures of oxygen in gaseous phase. Considering the very low concentration of oxygen in liquid metals submitted to desoxydation, the solution metal – oxygen obeys the Henry's law and therefore, the oxygen activity can be expressed as a function of the limit coefficient of activity (γ_O^0) and its atomic fraction (X_O) by the equation:

$$a_O \quad \gamma_O^0 X_O \tag{5}$$

From the activity limit coefficient γ_O^0 as temperature function equation coupled with the relation (5), we can determine the equilibrium atomic fraction of oxygen in metal.

Viewing the purity of metals submitted to desoxydation, the metallic bath can be considered during the desoxydation process as being a binary solution of metal and oxygen and therefore, it results:

$$X_O \quad \frac{\frac{C_O}{M_O}}{\frac{C_O}{M_O} + \frac{C_{Cu}}{M_{Me}}} \tag{6}$$

where:

C_O and C_{Me} are the concentrations of oxygen and metal, respectively, in weight percents ;

M_O and M_{Me} are the atomic mass of oxygen and, respectively, metal

Since the oxygen concentration (C_O) is far lower than that of the metal, (C_{Me}) from the equation (9) the equilibrium concentration of oxygen at the interface with the gaseous phase (C_S) can be obtained:

$$C_S \quad C_O \sim \frac{100M_O}{M_{Me}} X_O \tag{7}$$

3. Kinetic model of metals desoxydation in vacuum

Vacuum desoxydation is kinetically conditioned by the oxygen diffusion from the metallic bath at the interface with the gaseous phase. From this considering, we developed a kinetic model of metals desoxydation in the following hypotheses :

- the temperature is constant and uniform all the metallic bath out and for all the length of the process ;
- the oxygen concentration at the beginning of the desoxydation process is uniform in all the metallic bath volume (C_0);
- at the interface metallic bath gaseous phase the interaction (1) occurs with high enough rates so that it is not determinant for the global kinetics of the process;
- at the interface metallic bath gaseous phase, an equilibrium concentration (C_S) is instantaneously reached and, for a certain temperature, maintained constant for all the length of the process;
- the metallic bath is in a relatively stationary regime, meaning the vertical component of possible convective currents can be neglected .

With these hypotheses, the desoxydation process can be kinetically conditioned by the oxygen diffusion from the metallic bath at its interface with the gaseous phase. This diffusion can be represented by the Fick's second law equation :

$$\frac{\partial C_O}{\partial t} \quad D_{O\ Me} \frac{\partial^2 C_O}{\partial y^2} \quad \text{for} \quad 0 \le y \le h \tag{8}$$

where:

C_O is the oxygen concentration in the moment t at the distance y from the interface metallic bath gaseous phase ;

h – thickness of the metallic bath ;

$D_{O\ Me}$ - oxygen diffusivity in the liquid metal ; the value is known from experimental measurements

The initial and limit conditions of the diffusion equation in the imposed situation will be:

$$\text{I.C.} \quad C_O \quad C_0 \quad \text{at} \quad t = 0 \ \text{and} \ 0 \le y \le h;$$

$$\text{L.C} \quad C_O \quad C_S \quad \text{at} \quad t > 0 \ \text{and} \ y = 0;$$

$$\frac{\partial C_O}{\partial y} \quad 0 \quad \text{at} \quad t > 0 \ \text{and} \ y = h$$

For these conditions, the diffusion equation admits the solution [1]:

$$\frac{C_O \quad C_S}{C_0 \quad C_S} \quad 1 - \frac{4}{\pi} \sum_{n=0}^{\infty} \frac{1}{2n+1} e^{-D_{O\ Me}(2n+1)^2 \pi^2 t / 4h^2} \sin \frac{(2n+1)\pi y}{2h} \tag{9}$$

Because the oxygen concentration will be variable on the height of the metallic bath as a result of its diffusion from the bulk volume to the interface with the gaseous phase, it is convenient to define an average concentration (C_m) for all the height of the bath, according to the equation [2] :

$$C_m = \frac{1}{h}\int_0^h C_O dy \qquad (10)$$

from this resulting [3]:

$$F = \frac{C_m - C_0}{C_S - C_0} = 1 - \frac{8}{\pi^2}\sum_{n=0}^{\infty}\frac{1}{(2n+1)^2}\exp\left[-(2n+1)^2\pi^2 D_{O-Cu}t/4h^2\right] \qquad (11)$$

where $F = \frac{C_m - C_0}{C_S - C_0}$ represents the saturation fraction of oxygen .

By mathematical solution of the equation (10), knowing the temperature and the vacuum degree, the following can be determinate:

- the necessary time for desoxydation : for an imposed final average concentration of oxygen, the saturation fraction of oxygen can be determinate and from the equation **(11)** the ratio $x = D_{O-Cu}t/4h^2$ results. From the expression of this ratio, the time necessary for the process development can be calculated;
- the final average concentration of oxygen in the metallic bath after an imposed length of time of desoxydation : one can determine the value of the x ratio and from the equation **(11)** the saturation fraction can be calculated. From this fraction, the residual average concentration of oxygen is easily calculated.

4. Applications of the model of copper desoxydation

To exemplify the model, we suppose a process of copper desoxydation in vacuum, in the following conditions : temperature 1,100 – 1,300 ^{0}C, vacuum degree 0.01…0.1 mm Hg, initial concentration of oxygen in copper 0.05 % , depth of metallic bath h = 10 mm, time of desoxydation 1…4 hours. It is to determine the final average concentration of oxygen in the copper bath.

To determine the oxygen concentration at the interface metallic bath – gaseous phase and the diffusion coefficient of oxygen in copper, we used the following experimental data [4,5,6]:

$$\overline{\Delta G}_2 = -20860 + 1{,}66T\ , cal/at.g\ oxigen;$$

$$\ln\gamma_O^O = \frac{10500}{T} + 5{,}55$$

$$D_{O/Cu} = 8{,}16\cdot 10^{-1}\exp(-6500/T)$$

Results of calculations in the mentioned conditions are synthesised in the figures 1-4.

5. Conclusions

From the obtained results, the following conclusions can be drawn:

- Oxygen concentration at the interface metallic bath – gaseous phase is practically independent of temperature and significantly variable with the degree of vacuum. Saturation fraction of oxygen, as well as the ratio $\frac{D_{O-Cu}t}{4h^2}$ do not vary with temperature ;

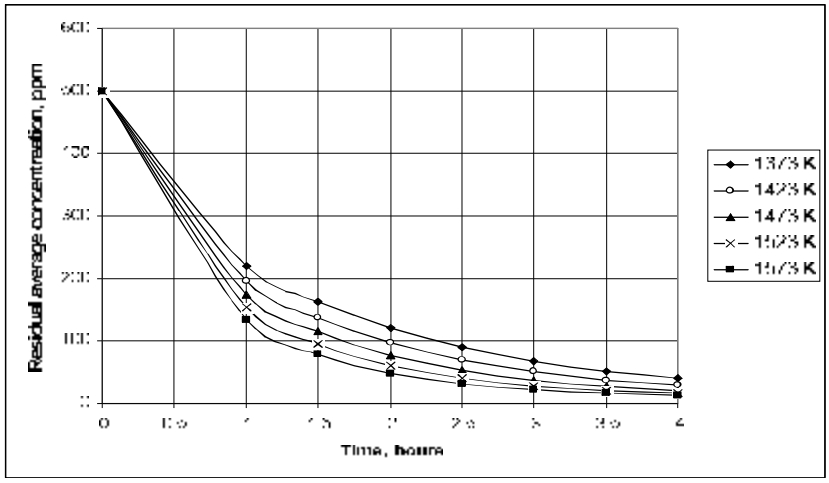

Fig.1. Residual average concentration of oxygen versus temp at different temperatures and pressure 0,01 mmHg.

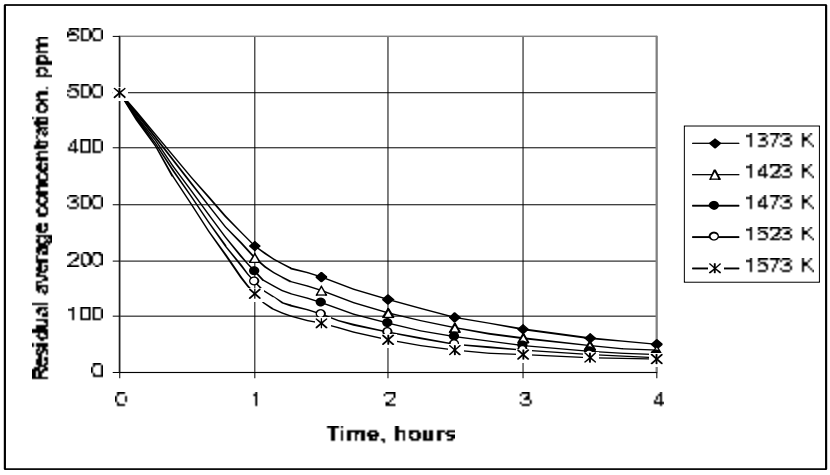

Fig.2. Residual average concentration of oxygen versus temp at different temperatures and pressure 0,05 mmHg.

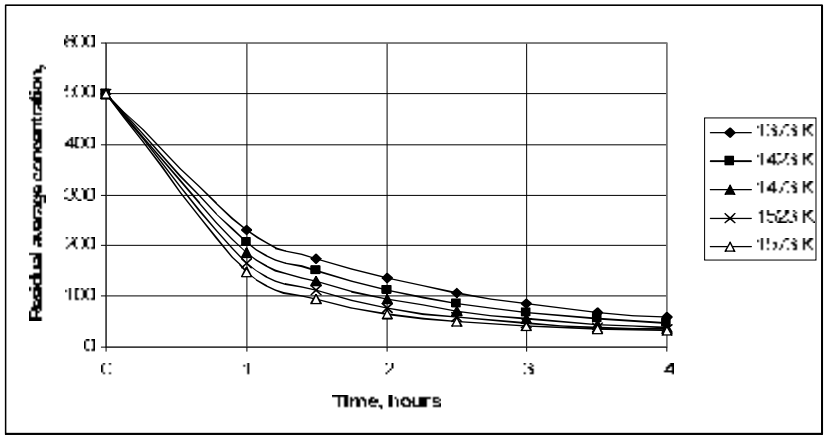

Fig.3. Residual average concentration of oxygen versus temp at different temperatures and pressure 0.1 mmHg.

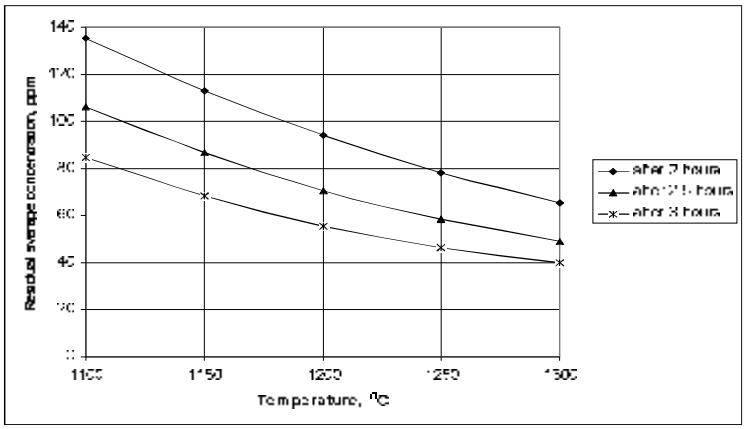

Fig.4. Residual average concentration of oxygen versus temp at different temperatures and pressure 0,1 mmHg.

- Time of desoxydation is almost linearly lowering with temperature increase and considerably reduces with the increasing vacuum degree;
- The obtained results prove that the model developed for the process of copper desoxydation illustrate very well the oxygen behaviour during the process and can be utilised in practice to determine the necessary length of time for desoxydation as a function of temperature and of the vacuum degree, in order to obtain a technologically imposed average concentration of oxygen.

Received April 16, 2007 *University POLITEHNICA of Bucharest*

REFERENCES

1. J. Crank, **The Matematics of Diffusion**, Clarendon Press, Oxford, 1956;
2. I.Constantin, D. Taloi, Liana Vlăduţiu, **Procese de difuzie şi transfer de masă**, Editura didactică şi pedagogică, Bucureşti, 2005;
3. J. Szekely, N.J. Themelis, **Rate Phenomena in Process Metallurgy**, Wiley Interscience, NY 1971
4. I. Constantin, Teza de doctorat " **Contribuţii la studiul cinetic şi termodinamic al sistemelor Cu – X – O;**", Universitatea Politehnica Bucureşti. 1987.
5. I. Constantin D. Taloi, Liana Vlăduţiu. Liliana Taloi, *Diffusivity of Oxigen in Liquid Copper*, International Conference on Materials Science and Engineeing, **BRAMAT**. Braşov. 24-26.02.05. ISBN 973-635-454-7;
6. I. Constantin, D. Taloi, Liana Maria Vladutiu, Florentina Pereteanu, *Diffusivity of Oxygen in Copper from Electrochemical Measurements*. **Junior Euromat** 2006, Lausanne, Switzerland 4-8 september 2006.

MODEL MATEMATIC DE DEZOXIDARE AVANSATĂ ÎN VID A METALELOR

Rezumat: Lucrarea prezintă un model matematic de dezoxidare avansată în vid a metalelor în stare lichidă. Modelul elaborat are două componente: o componentă termodinamică, care permite determinarea concentraţiei oxigenului în baia metalică la interfaţa cu faza gazoasă şi o componentă difuzivă, care permite determinarea teoretică a concentraţiei medii finale a oxigenului în diferite condiţii de temperatură, adâncime a băii metalice, timp, concentraţie iniţială a oxigenului şi grad de vidare. Modelul elaborat a fost aplicat la dezoxidarea cuprului în vid.

BULETINUL INSTITUTULUI POLITEHNIC DIN IAŞI
Tomul LIII (LVII), Fasc. 4, 2007
Secţia
ŞTIINŢA ŞI INGINERIA MATERIALELOR

RESEARCH ON THE FACTORS THAT HAVE AN INFLUENCE UPON THE STRUCTURES AND PROPERTIES OF THE A_5 STEEL STRIPS INTENDED FOR DEEP-DRAWING

BY

ELENA DRUGESCU, OCTAVIAN POTECAŞU, FLORENTINA POTECAŞU and PETRICA ALEXANDRU

Abstract: The paper presents the results of the research on the influence of cold working by rolling upon the properties of the A_5 steel strips intended for deep-drawing. The cold deformation degree and the thermic treatment recristallization were considered to be more important, among the technological factors that influence the structure and the properties of the current research. The experiments lead to the conclusion that, in the case of bell-type furnaces, better results are obtained for a range of relative deformation degree by 35-40% so that the mechanical and technological are corresponsive and characteristic structures present uniformity and smooth grain size.

Keywords: cold deformation, mechanical characteristics, anisotropy coefficient

1. Introduction

At present the steels A5 for drawing plates (ZES) manufactured by S.C.SIDEX S.A, at present are much more accurately made and this calls for revised cold deformation by rolling and thermal treatments procedures without affecting the quality of the final products.

An attempt is made in the paper to show how the cold plastic deformation and recristallization thermal treatment affect both the mechanical properties and the structure of the steel plates. A number of five coils from the same charge were used. Based on the experimental results a proposal has been advanced to modify the cold and hot deformation technologies while using the existing equipment. The quality technical conditions for the strips ZES-CAR BODIES are in compliance with the standard STAS 10318/80 as follows:

Table 1. The composition of the strip ZES-CAR BODIES

	C_{max} [%]	Mn [%]	Si [%]	S_{max} [%]	P_{max} [%]	Cr_{max} [%]	Ni [%]	Cu_{max} [%]	Al [%]
I	0,08	0,40	0,1	0,03	0,025	0,03	0,1	0,1	-
II	0,08	0,20-0,40	-	0 015	0,020	-	-	-	0,03-0,08

The chemical composition of the liquid steel, grade A5 is given in the table 2 (I- according to STAS-10318, II- according to the technological instructions provided by SIDEX).

The mechanical and technological fractures depending on the strip thickness according to table 2.

Table 2. Mechanical and technological fractures depending on the strip thickness

Thickness [mm]	Yield Point [N/mm^2]	Ultimate Strength [N/mm^2]	Breaking Elongation A_5[%]	Erichsen Index [mm]
0.8	max.220	270-340	min.36	min. 10,65
1.5	max.220	270-340	min.36	min. 11.8

Mean size of ferrite grains should have 6-9 points. Ferrite grain non-uniformity of the same sample should be within the limits of there adjourning points at the most. Roughness should be within 1.2 1.8μm

2. Experimental results

The experiments were carried out in two stages, in laboratory and industry.

In the first stage, cold working plate samples were provided by cold rolling mill factory was used. The A5 steel chemical composition is given in the table 3.

Table 3. A5 steel chemical composition

C [%]	Mn [%]	Si [%]	S [%]	P [%]	Al [%]
0,04	0,25	0,10	0,09	0 012	0,05

Samples were taken from the cold rolled strip of different degrees of deformation 2,2%, 6.5%, 15,2%; 32,5%; 50% and 65 %.

In the second stage was used an experimental charge and the reductions of thickness, applied in TANDEM rolling mill of the five experimental coils are given in the table 4.

Table 4.The reductions applied in TANDEM rolling mill of the five experimental coils

Coil number	Thickness of strip [mm]	Thickness of cold rolled strip [mm]	Degree of deformation [%]
1	2,36	1,50	36,0
2	2,42	1,50	38,0
3	2,60	1,50	42 0
4	2,85	1,50	48 0
5	2,97	1,50	49 0

The thermal treatment was applied into both stages in the cold rolling-mill factory of SIDEX, according to the diagram is presented in figure 1.

For each degree of deformation, a number of minimum 5 samples were provided for the three directions: 0°, 45° and 90° with respect to the rolling direction.

After the manufacturing cycle (cold rolling, recristallization, annealing, dressing and adjustment) had finished, samples were taken from the middle part of the steel coil and test bars (specimens) were made under the same conditions

The samples were thermal treated for recristallization in a bell - type furnace at S.C. SIDEX

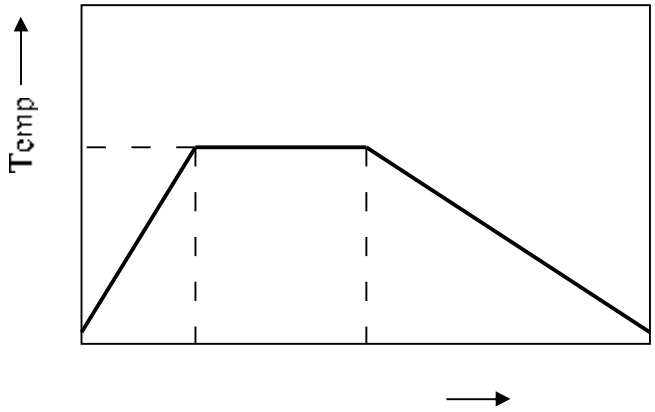

Fig.1. *Thermal treatment diagram for the experimental ZES CAR BODIES strip coils*

The degree of deformation significantly affects the structure and the mechanical and technological properties of the A5 steel strip as well as their distribution in the corresponding directions with respect to the rolling direction (0°, 45° and 90°).

The mechanical characteristics are mainly affected by the reduction cold deformation while high reduction cold deformation affects elongation only.

A degree of deformation of 32.5% provided the best results in terms of properties and their distribution on the plate plane (fig.2)

The correlation between the structured features, as indicated by the optical microscope, and the mechanical and technological properties is neither directly obvious nor of the same intensity in all the cases investigated. Starting from these conclusions the authors made further experiments at industrial level using a number of 5 coils from the same charge. The charge chemical composition is given in table 5.

Table 5. The chemical composition by charge for the five coils used in industrial experiment.

C [%]	Mn [%]	Si [%]	S [%]	P [%]	Al [%]
0,04	0,31	0,03	0,018	0,015	0,048

The results of the mechanical, ultimate -strength, lower yielding limit, breaking elongation tests and the anisotropy coefficient are shown as histograms in Fig.3.

The mechanical characteristics of the coils used in the industrial experiments were well within the required limits as provided by the standard in force for the drawing class A5. The best results were obtained with the cold rolled coil of 38%

degree of deformation; mean breaking elongation $A5_m$=40%; mean anisotropy coefficient r_m=1.7 (Fig.3) and I_r=12.1. The microstructures show a relatively uniform granulation in the cross and longitudinal sections, with fine and globular separations of the tertiary cementite in the ferrite matrix (fig. 4).

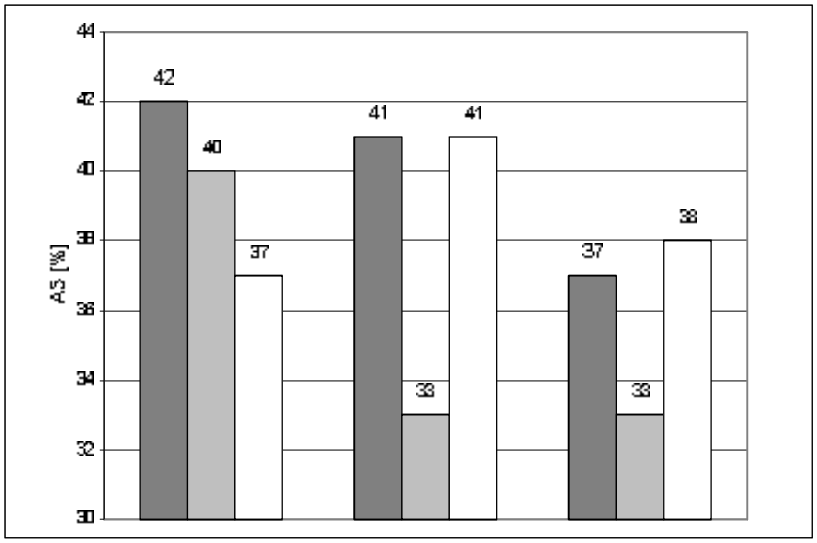

2a.

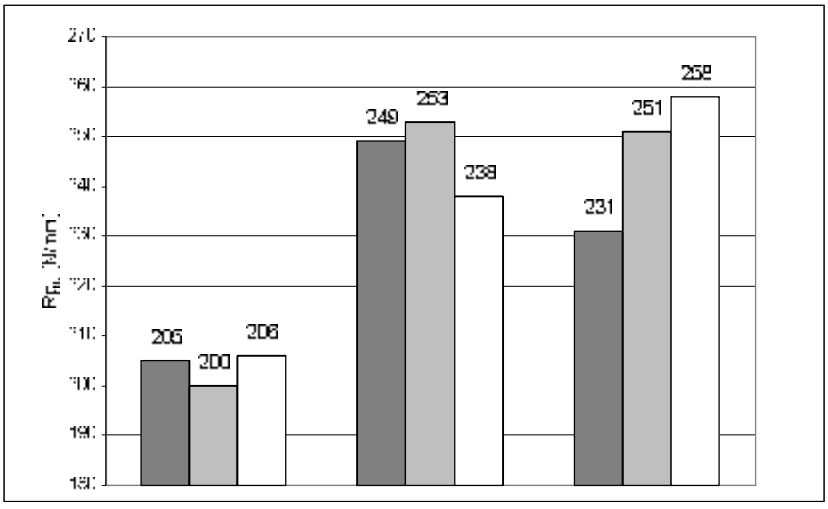

2b

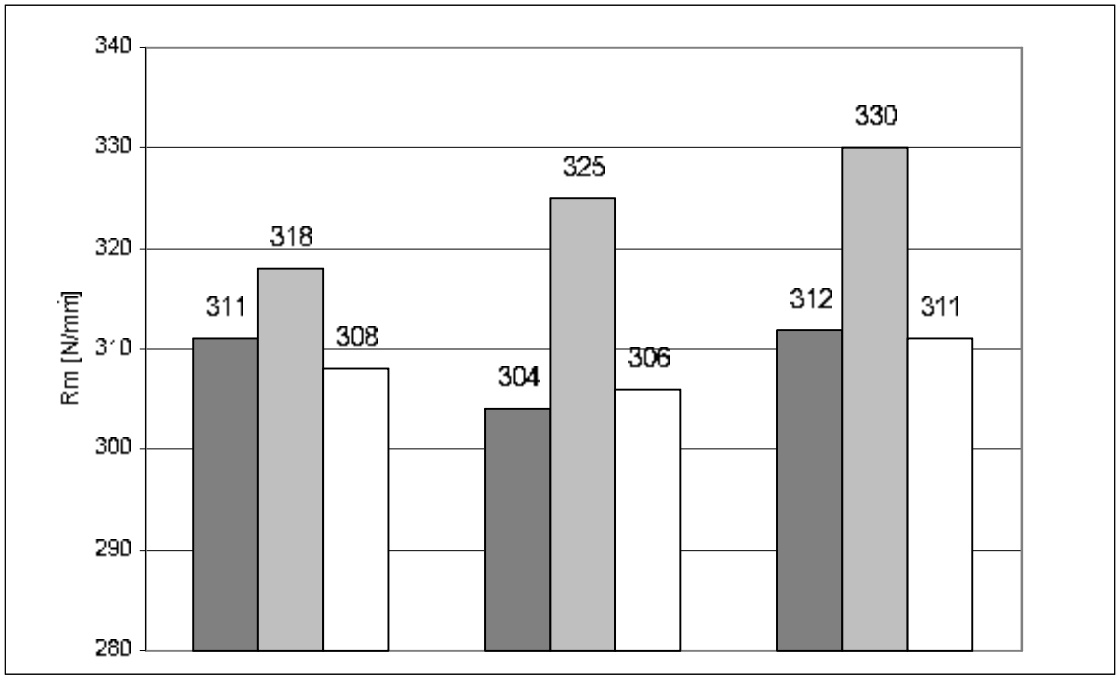

2c.

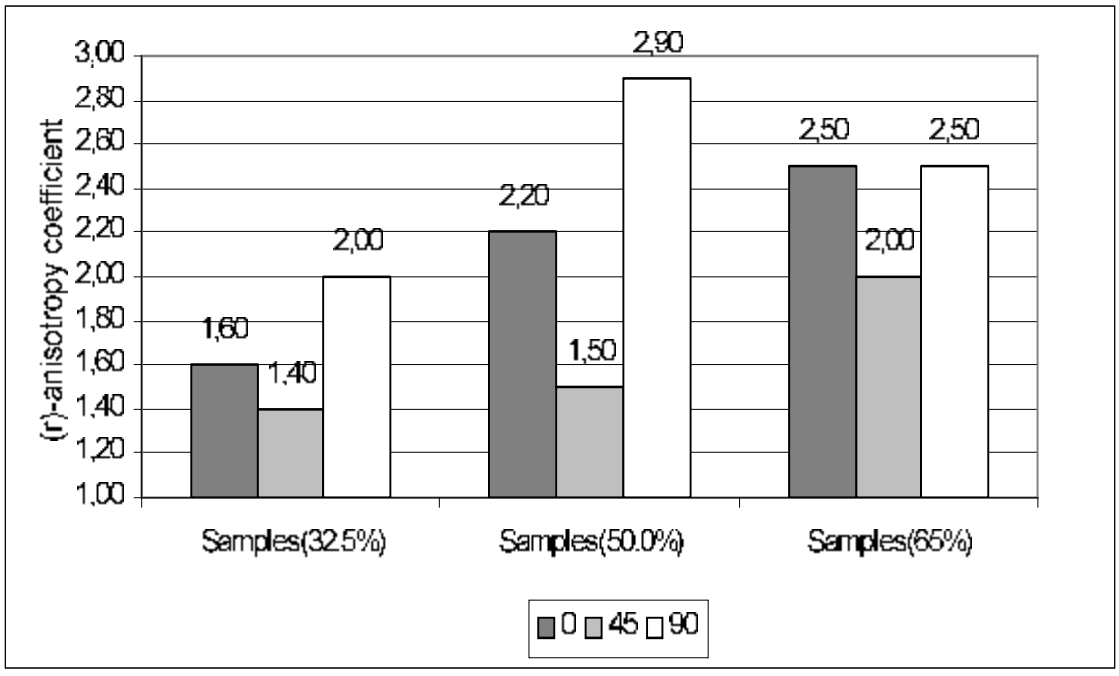

2d.

Fig 2. Histograms of the evalues taken by the mechanical characteristics (2a, 2b, 2c) and the anisotropy coefficients (2d) for cold deformation samples by rolling over the three sampling directions - 0^0, 45^0 and 90^0 by rolling directions.

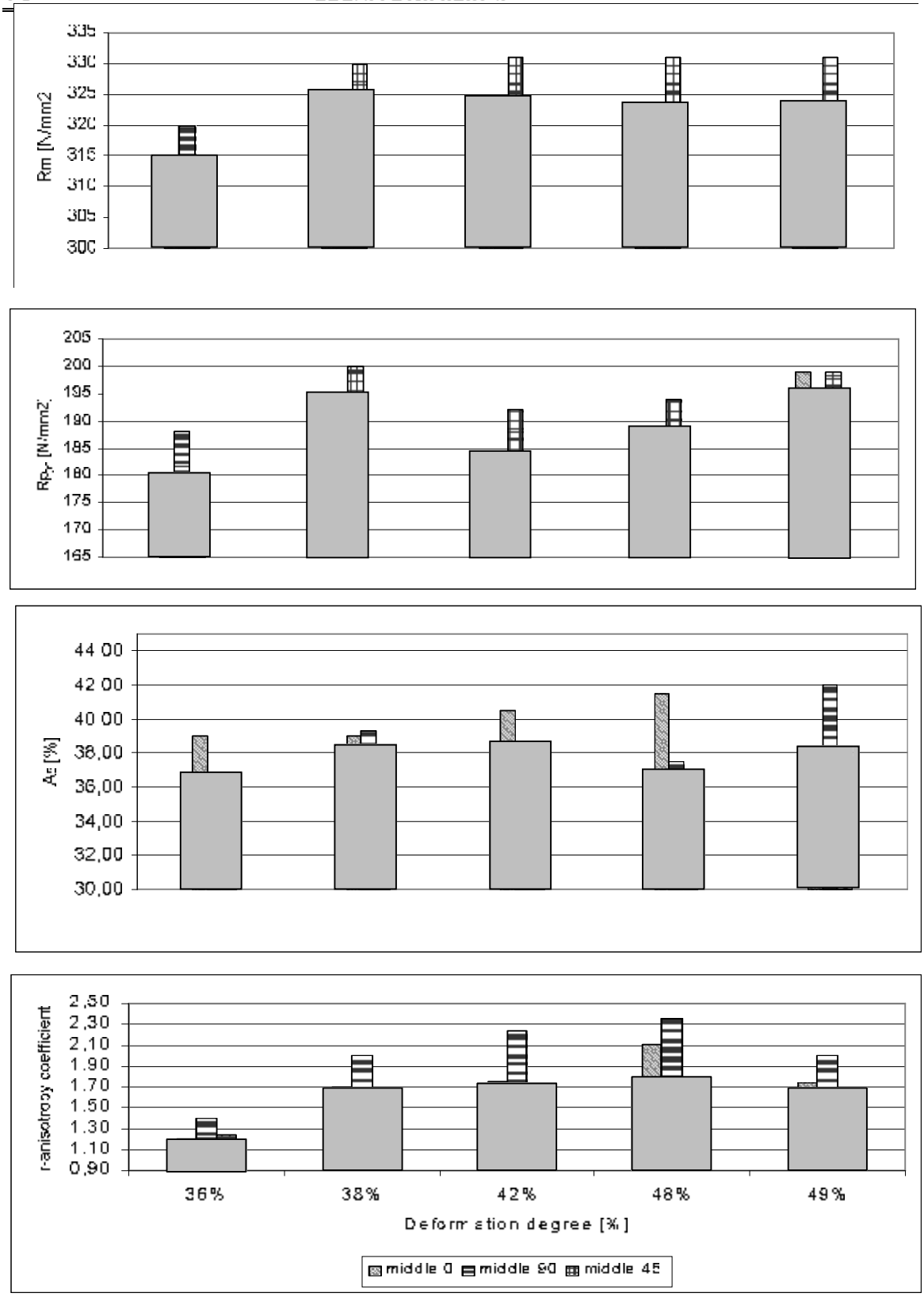

Fig. 3. Histograms showing the values of the mechanical characteristics and anisotropy coefficient from middle of coil in longitudinal (0), transverse (90) and diagonally (45) direction and the mean values calculated with formula: $x_m = \frac{x_0 + x_{90} + 2 \cdot x_{45}}{4}$ .. mean value

Significant differences were found between the values of the mechanical properties in the initial, middle and end areas with each coil and also within these areas there were differences between the three directions (parallel, perpendicular and 45° inclined to the rolling direction)

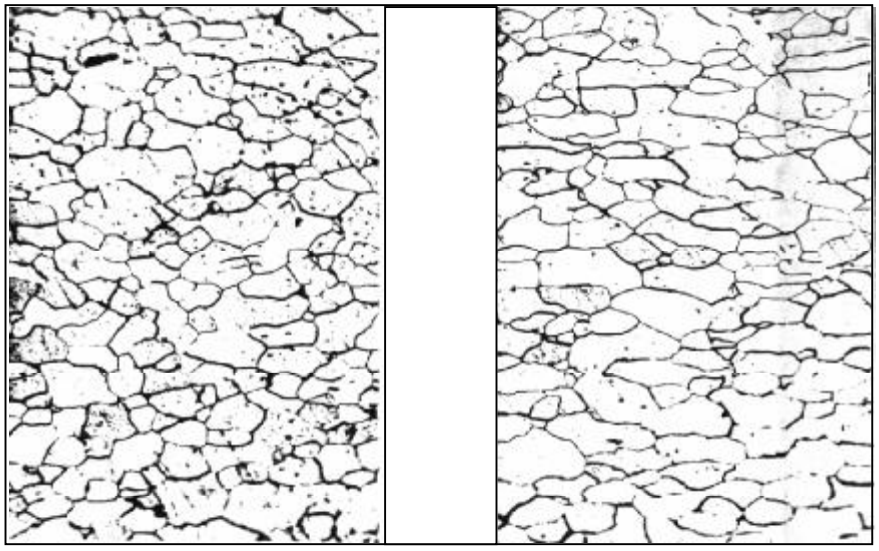

a b

Fig. 4. The microstructure of the steel coil strip A5 obtained by rolling cold deformation with 38% relative degree reduction of thickness: a) cross section; b) longitudinal section. (magnification 250x).

The testing conducted on the sampled specimens according to the 45° direction show that the steel plate features less favorable drawing behavior, having min. values of the breaking elongation and anisotropy coefficient, while the yielding limit and the ultimate strength take max. values as compared with the same characteristics determined in cross and longitudinal sections.

As for as the coils are concerned, it can be seen that the evolution of their characteristics cannot be repeated along the strip length; thus for each coil specific values of the initial, middle and end crease are obtained

3. Conclusions

The industrial experiment also shows that A5 drawing strip of lower reduction when cold rolled can be obtained (about 35-40%); the advantages are:
-improved strip quality due to a lower anisotropy of the mechanical characteristics (A_5, $Rp_{0.2}$, R_m) and the anisotropy coefficient in the plate plane;
-smaller number of cylinders of the cold rolling due to the lower deformation force applied to a less hard strip (lower quenching);
-lower risks of accidental strip breaking during rolling;
-lower power consumption for cold rolling;
-lower power consumption for the whole (cold and hot) deformation process.

Received April 19, 2007 *Dunarea de Jos University of Galati*

REFERENCES

1. **Engl**, B., Potte –Schmidt, K., "*Korneigenschaften und ihr Einfluss auf dasunterbesonderer Berucksichtingung von kaltgewalzten Feinblechstahles*; **Stahl und Eisen** nr.7,1994.
2. Drugescu, F., Potecasu, O., "*Cercetari privind influenta laminarii si a tratamentului termic de recristalizare asupra structurii benzilor din otel A5*" - vol XV **Tehnologii mecanice si utilaje tehnologice**, pag. 88-94, Universitatea "Lucian Blaga" din Sibiu. 1995
3. Potecasu, O., Dugescu, F.," *Influenta tratamentului termic de cristalizare asupra proprietatilor benzilor din otel A5*", volumul 1.3. **Proceedings of the Scientific Communications Meeting of "Aurel Vlaicu" University**, pag. 170-175, 1995

CERCETAREA FACTORILOR CE INFLUENȚEAZĂ STRUCTURA ȘI PROPRIETĂȚILE TABLELOR DIN OȚEL A5 FOLOSITE LA LAMINARE INTENSĂ

Rezumat: lucrarea prezintă rezultatele cercetărilor asupra influenței deformării la rece prin laminare asupra proprietăților tablelor din oțel A5. Gradul de deformare la rece și tratamentul termic de recristalizare au fost considerate ca fiind cele mai importante printre factorii tehnologiei ce influențează structura și proprietățile.

BULETINUL INSTITUTULUI POLITEHNIC DIN IAŞI
Tomul LIII (LVII), Fasc. 4, 2007
Secţia
ŞTIINŢA ŞI INGINERIA MATERIALELOR

SYNTHESIS AND CHARACTERIZATION OF ORGANIC PHASE GOLD NANOPARTICLES OBTAINED THROUGTH CHLOROAURATE IONS REDUCTION WITH SODIUM CITRATE

BY

FILCENCO- OLTEANU ANTONETA, RADULESCU ROZALIA, AURELIAN FLORIAN, PANTURU EUGENIA and GRIGORAS LUCI

Abstract: The reproducible making of gold nanoparticles of well-defined size and good monodispersion is still a challenge for researchers. This paper presents a method to produce stable gold nanoparticles by the reduction of hydrogen tetrachloroaurate ions in the organic phase, with sodium citrate. The characteristics of colloidal gold solutions reduced with sodium citrate were determined by UV-visible mass spectrometry. The particle size and size distribution were determined by electronic transmission microscopy (TEM) and the obtained results exhibit their nanometric dimensions.

Keywords: gold, nanoparticles, organic phase, sodium citrate

1. Introduction

Nanomaterials have a great importance in industrial applications due to their electronic, magnetic, optical [1] and catalyst [2] properties. Another important feature of nanoparticles is their large spectrum (range), an important characteristic in catalytic processes. Nanoparticle applications are found in communications, data storage [4,5], solar energy conversion [6]. It is well known that certain physical and mechanical properties of materials modify with the reduction of their particle size. Unfortunately, only a few synthesis methods of nanostructured powders are applicable at industrial scale

Materials performance depend on their properties. Properties, in their turn, depend on the atomic structure, composition, microstructure, defects and interfaces, which are controlled by the synthesis kynetics and thermodynamics.

The synthesis of powders and their subsequent processing have a great influence over the final properties of the resulted materials. The selection of suitable processing methods determines, to a great extent, the results obtained for the final products.

At present, the obtaining of nanopowders for different practical applications uses nonconventional processing methods, capable to offer better homogenity, increased purity, low sintherizing temperatures and a fine microstructure, with as small as possible grains.

Gold nanoparticles have raised the researchers' attention due to their numerous applications in catalytic processes [7] and in the DNA sequence determination [8].

Specialized literature presents a series of synthesis methods of different shapes [9] and size [10] gold nanoparticles which, by large, can be classified into two

sections, function of their growth environment, i.e. polar (aqueous) or non-polar (organic) environment.

Generally, the gold hydrosols synthesis methods in aqueous phase suppose [1] the chloric-gold ions reduction with different reducing agents, such as: the citric acid [11], the sodium borohydride [12], the gold ion reduction by irradiation [13,14] and the sono-chemical reduction [15]

The synthesis of gold nanoparticles in nonpolar environments are based on the research performed by Burst &co. [16] who have managed to transfer the chloroaurate ions from the aqueous phase into the organic phase by using the tetraoctil ammonium bromide. After the phase transfer, the gold ions have been reduced and covered with alcanethiols[16]-alkylamines[17], thus obtaining stable monodispersed gold nanoparticles.

This paper presents the synthesis and characteristics of gold nanoparticles obtained in the organic phase with the use of sodium citrate. The gold nanoparticles characteristics were determined by in UV - visible spectoscopy (UV-Vis) and by electronic transmission microscopy (TEM).

2. Materials and methods

2.1. Materials and devices

Experiments were performed by using: the tetra-octilammonia, toluene, MERCK produced de-ionised water, Aldrich tetrachloroauric acid (HAuCl4). Stirring was performed with a magnetic device.

2.2. Gold nanoparticles synthesis in the organic phase with sodium citrate

The aqueous solution of 0.01M tetrachloroauric acid was mixed with a 0.05M tetraoctil ammonium bromide solution in toluene for 10 minutes, to a 1:2.5 volume ratio at which the solution becomes orange. In order to obtain the desired size gold nanoparticles, a 10-2M (1) and respectively 5x10-3M (2) sodium citrate solution was added by dripping under strong agitation, to a volume ratio between the mixed solution and the sodium citrate of 4:1. Stirring was maintained for 30 minutes at the environment temperature, the mixture being then transferred into a separating funnel. The reduction of gold metallic ions and the formation of nanoparticles has been evidenced by the modification of the solution colour, from orange to ruby red. After the phases separation, the organic ruby red phase which contains gold nanoparticles has been first washed with 2% hydrochloric acid for neutralization and several times with distilled water. After washing and phases separation, the organic phase has been kept into a dark colour glass bottle.

2.3. UV-Vis spectroscopic studies

The optical properties of gold colloidal solutions (1) and (2) have been characterized through UV-Vis spectrometry, by using a CECIL spectrophotometer within a wave length between 400 and 700 nm.

2.4. Electronic transmission microscopic measurements

The electronic transmission microscopy analysis (TEM) was made by using a CM12 Philips electronic microscope, with a 2Å resolution. The sample were prepared by

placing a drop of gold colloidal solution on copper grid that has been covered with a very thin amorphous carbon layer. The examination has been made by electronic transmission microscopy in light fascicle (TEM-BF) and electron diffraction (SAED).

3. Results and discussion

The nanoparticle transfer mechanism from the aqueous solution into the organic solvent involves their hydrophobization. The aqueous solution containing the tetrachloroauric ions is mixed with the organic solvent which contains the coverage molecules (the tetraoctil ammonium bromide). Upon the mixture of the two phases, the coverage molecules will „wrap" the gold metallic nanoparticles, making them hydrophobic and thus facilitating their transfer into the organic solvent. The nanoparticle transfer from an aqueous environment into an organic one can be observed also by the change in the colour (from pale yellow to orange).

Figure 1 presents the UV-Vis spectra of gold colloidal solutions in the first experiment (10-2M) and in the second experiment (5x10-3M) respectively. Curve 3 corresponds to the Oct4N+AuCl4- complex resulted from the mixture of the tetracloroauric acid with the tetraoctil ammonium bromide solution in toluene

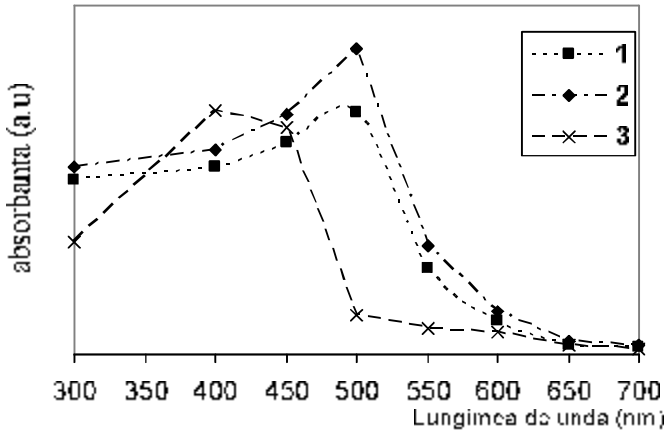

Figure 1. UV-Vis Spectrum of 10-2M (curve 1), 5x10-3M (curve 2) gold colloidal solutions and of Oct4N AuCl4- complex (curve 3)

A strong absorbtion can be noticed in case of curve 3, around the 347nm value of the Oct4N AuCl4- complex resulted from the mixture of the tetracloroauric acid with the tetraoctil ammonium bromide solution in toluene. The absorbtion band is characteristic for the AuCl4 6-transfer band between the metal and the ligand.

The reduction of the Oct4N AuCl4- complex with sodium citrate leads to the formation of gold nanoparticles covered with the citrate ions, as illustrated by spectra 1 and 2 which reached their maximum around 530 nm. One can also notice that the absorbtion spectrum for curve 1 is flatter, which indicates a certain degree of aggregation of the obtained nanoparticles, in contrast to the sharper absorbtion spectrum registered for curve 2.

In spite of the fact that the samples exhibit a certain degree of aggregation, the colloidal gold solutions obtained in the organic phase with the aid of sodium citrate are

stable for about 2 months, if preserved in a dark, constat temperature environment. A certain nanoparticle agglomeration is evident with time.

The electronic transmission microscopy enables to obtain qualitative data on the nanoparticle dimensions and on their distribution by size, as well as information on their microstructural and microcompositional morphology. The electronic transmission microscopy results (TEM) for the two samples are presented in Figures 2 and 3.

Figure 2 A presents the image obtained by electronic transmission microscopy of gold nano-particles obtained by the reduction of 0.011M tetrachloroauric acid with 10-2 M sodium citrate (1). A uniform gold nanoparticle distribution may be noticed. Figure B presents the distribution curve of nanoparticles dimensions. The continuous line overlapping the histogram is a Gaussian curve which gives information on the mean particle size, found to be in the range of 5-7 nm

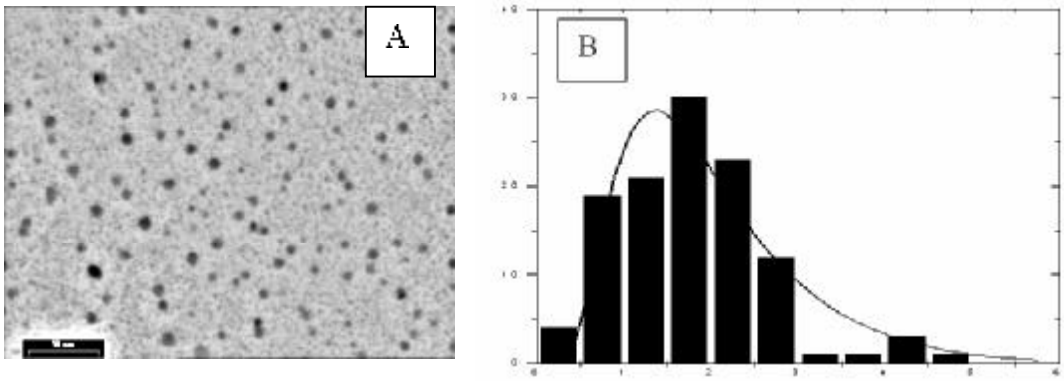

Figure 2. TEM image for A nano-particles obtained in the organic phase through 10-2 M sodium citrate reduction; B- Histogram of gold nanoparticle size distribution for the same sample.

Figure 3 A shows the image obtained through electronic transmission microscopy of gold nanoparticles obtained in the organic phase, using sodium citrate 5x10-3 M (2) solution as a reducing agent. An uneven distribution of gold nanoparticles is noticed; Figure B presents the nano-particle size distibution curve. The continuous line is a Gaussian fit to the histogram and gives information on the mean particles size, found to be in the range of 1-3 nm.

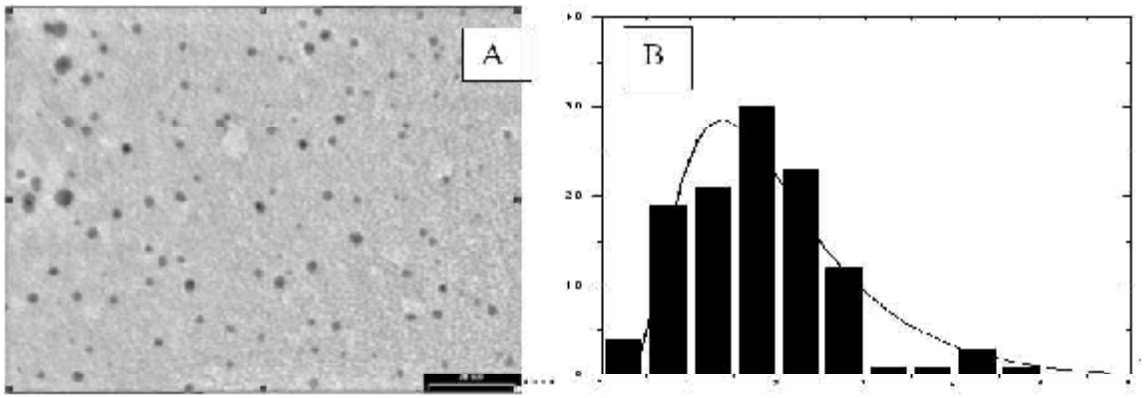

Figure 3 TEM image for A nano-particles obtained in the organic phase by using a 5x10-3 M sodium citrate solution as a reducing agent; B - Histogram of gold nano-particle size distribution for the same sample.

The size of the obtained gold nanoparticles increases with the concentration of the sodium citrate solution. The results obtained through electronic transmission microscopy for these samples are consonant with those obtaine through UV spectroscopy.

4. Conclusions

This paper presented the organic phase synthesis of gold nanoparticles through the reduction of chloroauric ions with sodium citrate. In order to vary the nanoparticles dimensions, experiments were conducted with sodium citrate solutions of different concentrations: 10-2M (1) and 5x10-3M (2). Following TEM investigations, the obtained nanoparticle sizes increased with the concentration of the reducing agent, all the other conditions remaining unchanged. Gold nanoparticle applications are found in solar energy conversion.

Acknowledgements

The authors thank the Romanian Ministry of Education and Research for having financially supported this research project within the National CEEX Programme.

Received April 18, 2007

Research and Development National Institute for Metals and Radioactive Resources Bucharest

REFERENCES

1 Wyatt P. McConnell, James P. Novak, Louis C. Brousseau, III, Ryan R. Fuierer, Robert C. Tenent, and Daniel L. Feldheim, *J.Phys.Chem* B 104 8925-8930(2000)
2 M. Králik and A. Biffis, *J.Mol.Catal.*A 177,113-138(2001)
3 R.F.Marzke, *Cata. Rev.-Sci.Eng.*,1979,19,43.
4 Schmid,G **Clusters and Colloids: From Theory to Application**, VCH; Weinheim,1994
5 Ditlbacher,H.; Krenn J.R.; Lamprecht B.;Leitner A ; Aussenegg, **F.R. Opt. Lett.2000**, 25, 563.
6 Graetzel, M. **Electrochemistry in Colloids and Dispersions**; Raymond A. Mackay, John Texter;VCH;Weinheim,1992.
7. Baschong, W. and Wrigley, N. G., *J. Electron. Microsc. Tech.*, 1990, 14, 313
8. Elghanian, R., Storhoff, J. J., Mucic, R. C., Letsinger, R. L., and Mirkin, C. A., *Science*, 1997, 277, 1078.
9(a) Hayat M A 1991 *Colloidal gold* (San Diego, CA: Academic Press); (b) Bradley J S 1994 *Clusters and colloids* (Weinheim: VCH) pp 459–544
10. (a) Jana N. R., Gearheart C. and Murphy C. 2001 *J. Phys. Chem.* B105 4065; (b) Dujardin S., Mann, S., Hsin L. B. and Wang C. R. C. 2001 *Chem. Commun.* 1264; (c) Malikova N., Pastoriza- Santos I., Schierhorn M., Kotov N. A. and Liz-Marzan L. M. 2002 *Langmuir* 18 3694; (d) Jin R., Cao Y., Mirkin C. A., Kelly K. L., Schatz G. C. and Zheng J. G. 2001 *Science* 294 1901
11.Turkevich, J., Garton, G. and Stevenson, P. C., *J. Colloid Sci.*, 1954, 9, 26.
12.Handley, D. A., *Colloidal Gold: Principles, Methods and Applications* (ed. Hayat, M. A.), Academic Press, San Diego, 1989, vol. 1, chap. 2.
13. Henglein, A., *Langmuir*, 1999, 15, 6738.
14. Clachard, L., Remita, H., Khatouri, J., Keita, B., Nadjo, L., and Belloni, J., *New. J. Chem.*, 1998, 1257.
15. Mizukoshi, Y., Fujimoto, T., Nagata, Y., Oshima, R. and Maeda, Y., *J. Phys. Chem.*, 2000, **B104**, 6028.

16. (a) Brust M, Walker M, Bethell D, Schiffrin D J and Whyman R 1994 *J. Chem. Soc., Chem. Commun.* 801; (b) Fink J, Kiely C J, Bethell D and Schiffrin D J 1998 *Chem. Mater.* 10 922
17. Leff D V, Brandt L and Heath J R 1996 *Langmuir* 12 4723

SINTEZA SI CARACTERIZAREA NANOPARTICULELOR DE AUR OBTINUTE IN FAZA ORGANICA PRIN REDUCEREA IONILOR CLOROAURICI CU AJUTORUL CITRATULUI DE SODIU

Rezumat: Obtinerea reproductibila a nanoparticulelor de aur de dimensiuni bine definite si cu o buna monodispersie, reprezinta o provocare pentru cercetatori. Lucrarea prezinta obtinerea nanoparticulelor de aur stabile, prin reducerea ionilor cloroaurici in faza organica, cu ajutorul citratului de sodiu. Caracterizarea solutiilor de aur coloidal reduse cu ajutorul citratului de sodiu s-a realizat prin spectroscopie UV– vizibil. Dimensiunea si distributia dimensiunilor particulelor s-a determinat prin microscopie TEM. rezultatele obtinute demonstrand ca acestea sunt in domeniul nano.

BULETINUL INSTITUTULUI POLITEHNIC DIN IAŞI
Tomul LIII (LVII), Fasc. 4, 2007
Secţia
ŞTIINŢA ŞI INGINERIA MATERIALELOR

CASTING PATTERN DESTINED TO CORELATE THE EXPANDED PARAMETERS PROCESS WITH QUALITY DEMANDS FOR THE GATING SYSTEM AND FULL MOULD CASTING

BY

LUCIA FIRESCU*, IOAN MĂRGINEAN**, CONSTANTIN BRATU** and MARIA ROMAN*

Abstract The article presents a specific casting pattern imagining correlating the expanded parameters process with quality demands for pattern used to obtain the metal castings by lost foam casting. Using this pattern assure both the decrease of the necessary cost to obtain the pattern and, respectively, of the metal castings and ecological conditions to the production process.

Keywords: casting pattern, gating systems, expanded parameters, lost foam casting

1. Introduction

The most used material for lost foam is polystyrene. The polystyrene patterns are obtain by expanding the gasified granules, which allows to obtain very complex shapes, with minimum energy consumptions and in a very short time, so there are lower costs comparing to the conventionally materials patterns (wood, metal etc.). The technology applied to realize the polystyrene pattern and the gate system has the same technology phases. The process parameters which assure those patterns obtain are the same but with different values, because the quality conditions for casting patterns are different to those for gate system. So, for casting pattern are chooses the process parameters adequate to the medium wall thickness and to the surface roughness (smoothen degree) of the metal casting and, in the case of the gate system are using the parameters adequate with the dimensions resulted by its dimensioning calculations. Usually, in order to obtain a superior surfaces quality involve more technological severity and, implicit, bigger producing costs. Because the gate system is a technological addition in the castings producing process, it is not justify effectuating this expenditure. The presented considerations leads to the necessity of realize a pattern which allows the expended process parameters correlation with quality demands for polystyrene casting pattern and gate system, in the context of the foundry patterns reducing fabrication costs and, consequently, of the castings. The casting process present a reduce volume of the atmospheric emissions and a low pollution degree.

2. Pattern geometrical configuration

Started to the fact that the demanded industrial castings has gross weight between hundred grams (less than 1 kg) and hundred kilograms (tons) and that exist a

correlation between casting weight and the section dimension of the gate system, the pattern was imagined like an unitary body, formed of many different diameters cylinders, positioned coaxial and superpose. The cylinders size was establish by gate system dimensioning calculation on the base of the filling casting mould lows (continuity and hydraulically flow laws) and to the metal or alloy directional solidification, in order to obtain superior quality castings. Superpose coaxial cylinders diameters satisfy the technological necessities of the castings with wall thickness between 15÷80 mm and weight between $1 \div 10^3$ kg / cast piece. The smaller cylinder diameter correspond to the technological necessities of the small castings, with weight from less 1 kg to 10 kg, presented the guarantee that the metal / alloy casting in the gate system will not solidify before the casting, so there will not be technological problems and castings defects. The bigger cylinder diameter correspond to the technological necessities of the big castings (with weight from 100 kg to tons), bigger values for the gate system are used in the industrial practice only exceptionally. In figure 1 it is schematic presented the pattern for determination of the optimal expended parameters to obtain lost foam patterns for casting and gate system used to the metal casting.

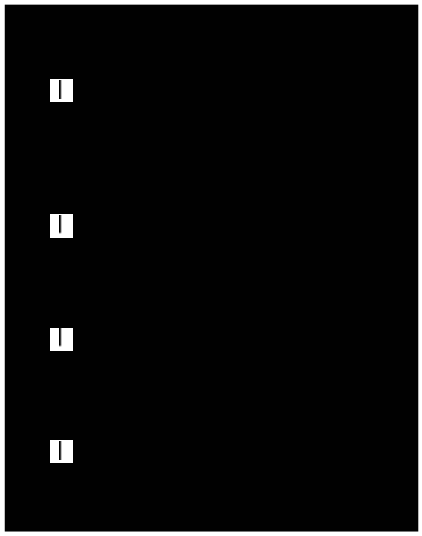

Figure 1. Pattern geometrical configuration

3. Pattern realization and aplication

Polystyrene granules are steam preexpanded, obtaining preexpanded granules. Lost foam is obtained by die expanded of the preexpanded polystyrene granules. In function of demands for the casting it is establish the expanding parameters (steam pressure and expanding running time). The analysis of the obtain patterns quality is done on the basis of the quality demands for the casting and the gate system type-dimensional characteristics which are named in the cast technology of the piece. The 2, 3 and 4 figures present stages of the pattern realization.

Figure 2. Unexpanded polystyrene granules

Figure 3. Expanded polystyrene granules

Figure 4. Patterns realized with optimal exponded parameters

If at the visual control the patterns are corresponding, they are analyzed piece by piece. In the figure 5 it is presented a pattern verified by vertical axis sectioning.

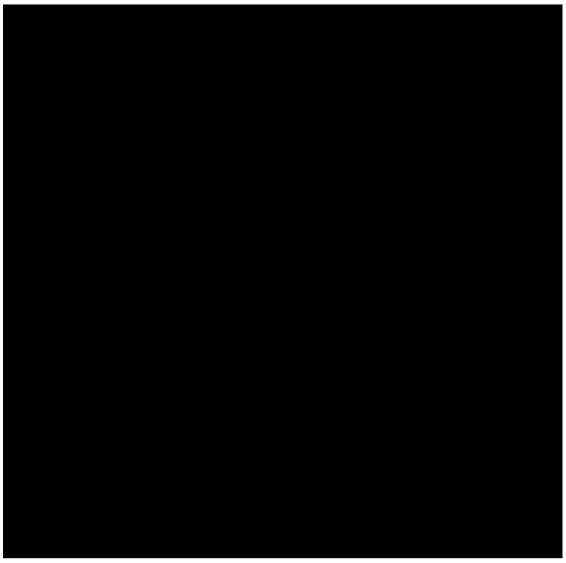

Figure 5. Pattern quality verifying

It is identify the cylinder of the analyzed pattern which is corresponding to the type-dimensional casting class and then it is verify if its surface correspond to the casting surface quality demands (roughness and surface defects). If its surface does not correspond to the casting surface quality demands, it is considering that the expanding parameters are not the optimal one and it is necessary to obtain another pattern, with another parameters expanding set. If the analyzed cylinder is corresponding both to the type-dimensional casting class and to the surface quality demands, it is considering that the expanding parameters are the optimal one.

After that, it is identify, for the same pattern, the cylinder which has the closer diameter to the gate system dimension. If it is identify, for the analyzed pattern, the cylinder which corresponding to the imposed conditions by cast technology, than it is considering that the applied expanded parameters to obtain lost foam patterns for casting and gate system are the optimal one. Figure 6 shows the result of using the pattern.

Figure 6. Casting – gate system assembly obtain by using the pattern

4. Conclusions

Using the presented pattern allow the expanding parameters programming and control so that we obtain cast pattern with corresponding physical-mechanical and technological characteristics both metallic materials and type-dimensions for the castings, and the lost foam destination: casting or gate system.

Among the pattern using advantages, we mention:

- the determination of the optimal expanded parameters for obtain polystyrene lost foam patterns, in the desired quality class;
- providing some technological information about starting material using to the expanding polystyrene.

Received April 14, 2007

**INCDMNR-IMNR, Pantelimon, Jud. Ilfov*
***CIMS-POLITEHNICA University, Bucharest*

REFERENCES

1. Marginean I., *Cercetări privind mărirea compactităţii si îmbunătăţirea calităţii pieselor turnate*, Teza de doctorat, Bucuresti, 1995;
2. Marginean I., Ibraim I., *Modele gazificabile din polistiren si tehnologia formelor de turnare fără liant*, OIDICM, Bucuresti, 1997.

MODEL DE TURNARE PENTRU CORELAREA PARAMETRILOR DE EXPANDARE CU CERINŢELE DE CALITATE PENTRU TURNAREA CU MODELE GAZEIFICABILE

Rezumat: Articolul prezintă un model conceput pentru corelarea parametrilor procesului de expandare cu cerinţele de calitate pentru modelele utilizate în procedeul de obţinere a pieselor metalice prin turnare cu modele gazeificabile. Utilizarea modelului asigură atât scăderea cheltuielilor necesare obţinerii modelelor şi, implicit, ale pieselor turnate cât şi condiţii ecologice de desfăşurare a procesului de producţie.

BULETINUL INSTITUTULUI POLITEHNIC DIN IAŞI
Tomul LIII (LVII), Fasc. 4, 2007
Secţia
ŞTIINŢA ŞI INGINERIA MATERIALELOR

ABOUT THE DESIGN OF ADD FILLER MATERIALS WITHOUT NICKEL CONTENT FOR CAST IRON WELDING – PART I

BY

DIANA ANTONIA GHEORGHIU, DORIN LUCA, COSTICĂ BEJINARU and STEFAN TOMA

Abstract: Reducing or even eliminating nickel into the cast iron electrodes is still a major challenge for those who are interested into cast iron welding. The present work demonstrates that an important role plays the carbon presentation form into the electrode coat upon the qualities of the weld. The carbon presentation effect is estimated through the adherence of the deposed material – designed electrodes on the base material, a grey cast iron grade.

Keywords: base material, electrode wire, electrode coat, graphite, carbon compound, interface.

Each of the commercial existing consumable for cast iron welding can be included into one of the six groups that are unanimous accepted. The best performances are accomplished with the materials from the third group, the nickel base add – material. The chemical composition of those consumables requires a nickel percentage that ranges between 45 to 98 weight content. Nickel is an expensive, strategic element. Reducing nickel consumption is a great interest for welding cast iron costs and for other interesting nickel utilities. In this case, steel electrodes, with carbon steel core wire becomes an interesting option.

1. Theoretical considerations

Cast irons are difficult to weld. White cast iron is generally considered unweldable, while ductile cast iron or some malleable grades are almost always easier to weld than a gray cast iron.

All the types have in common an important susceptibility to cracking. This tendency is due to the high carbon content: during heating for welding the carbon diffuse into the heated base metal and into the weld pool. When cooling takes place, carbides and martensite, both brittle and susceptible to cracking structures are formed, because the high cooling rate. The fragile structures develop into the weld and into the heat affected zone

Cracking tendency can be controlled through an adequate technology: preheating base material, small heat amount, short weld, etc.

When nickel base consumables are used crack tendency is reduced. Nickel does not form carbides and has a low solubility for carbon. So, as the weld metal solidifies, carbon is rejected from the solution as free carbon, graphite. The weld has, thanks to the nickel contempt, a good ductility and a good shrinkage coefficient. But in the heat - affected zone (HAZ) the effect of the welding cycle is the same. Special techniques as a low preheat must be used even with this type of materials

The most critical zone of the cast iron welds is the partial melted region. It is the hardest, most fragile region of the weld. At the interface melted and then solidified metal and only heated base material, a great number of discontinuities are formed. The nature of the discontinuities, pores or/and graphite flakes is not well established /1/.

To achieve a quantitative evaluation of the discontinuities amount and their influence upon the weld quality a specific trial sample and device, has been accomplished /2/. The device estimates the adherence force for the deposed material to the base material. Higher the discontinuities amount, smaller the adherence of the add material. Preliminary tests, with commercial available electrodes, proved that the discontinuities in the partial melted zone occur even for the special designed electrodes, even if the adherence force is better than that of the other electrodes. Also, the tests revealed that the coat of the electrode plays an important role in weld quality. The coat effect is widely accepted as an important one, but not quantified.

The final weld quality represents the result of the interaction between filler wire, electrode coat and base material.

The discontinuity amount has a complex dependence. It depends partially on the electrode coat formula, welding regime and electrode wire type. The purpose of the present work is to emphasize some aspects regarding the coat formula influence for a given wire composition with no nickel.

The main functions of an electrode coat are:

- protecting the molten electrode tip and the weld pool from the atmosphere;
- providing the alloying elements, if necessary;
- ensuring the alloying elements transfer through arc, in the cast iron case especially carbon, silicon and manganese.

For the present work, the effect of the carbon as alloy element into the coat was monitorized. Carbon powders have been introduced into the designed coats in two different forms, graphite and a carbon compound.

2. Base material and materials for the designed electrodes

As base material gray cast iron grade Fc250 has been selected. It has a poor weldability and a major tendency to form discontinuities at the interface. Base material structure as cast and an interface microstructure are presented in figure 1.

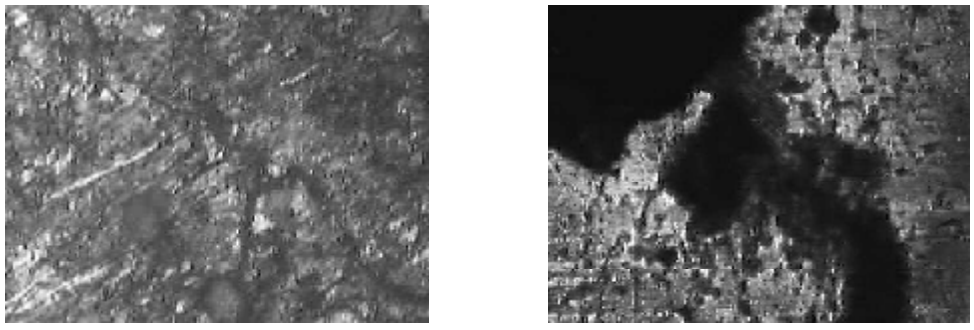

Fig. 1. Cast iron structure: a. as cast, 100:1; b. interface aspect,300:1, nital etches.

As electrode core has been used a S10 wire, a common material for general purpose electrodes. The chemical composition of the wire is available in Table 1.

Table 1. The chemical composition of the S10 wire

	C	Mn	Si	Ni	Cr	S, max	P, max	Fe
S10	0,1	0,5	0,03	0,25	0,18	0,03	0,03	Bal

The wires have 2mm diameter, 300 mm length, an average mass of 10,5grams and linear density of 0,035g/mm. The alloying elements, including carbon, were mixed into a flux formula. The amount of each flux component and its main designation are grouped into Table 2.

Table 2. Flux components into the designed electrodes

Compound	Formula	Function	Amount, %
Calcium carbonate	$CaCO_3$	Shield gas	35
Dolomite	$CaMg(CO_3)_2$	Shield gas	30
Rutile	TiO_2	Slag former	5
Silica	SiO_2	Slag former	5
Fluorspar	CaF_2	Arc stabilizer	10
Feldspar		Arc stabilizer	5
Sodium silicate		Binder	10

The literature regarding cast iron welding as well as electrode producers emphasize the need of graphitizing elements into the coat, even for nickel base one. In the experiments carbon and silicon were used as graphitizing elements. Including silicon into the coat as graphitizing impose a specified amount of manganese, as support for silicon transfer through the arc /3/. From the specified amount of each component into the coat, only a given percentage will be deposited on the base metal. The element quantities in the designed coat have considered the transfer coefficient for every element. Powder mixtures made of ferrosilicon, ferromanganese and a carbon carrying powder (graphite or carbon compound) were prepared.

3. Experimental work

The S10 wires were mechanically cleaned and air blasted just before the prepared coat is deposed on it.

Powders with carbon (graphite or carbon compound), ferrosilicon and ferromanganese in appropriate percentage for each experimental formula were mixed together with an appropriate amount of flux mixture. The mixtures were calculated to ensure imposed values for carbon equivalent, with respect to the chemical composition of the wire. The imposed values for carbon equivalent are 5; 7,5; 10. The carbon equivalent for the electrode was accomplished for both carbon forms

4. Results

With the designed electrodes three to five samples have been welded. The welding process parameters were: no preheat, welding current 100A, welding time 10 seconds, then a constant heat input. The adhesion force for the new electrodes has been compared to the adhesion force that has been measured to the nickel electrode. In figure 2 are presented the results.

As shown in figure 2, the adhesion force for one of the tested electrodes is greater than that of the commercial CARBOWELD nickel electrode

It is an encouraging fact that stimulates further investigations regarding modalities to improve cast iron weld quality through coat formula. It must be noticed that the results can be adapted for flux core arc welding.

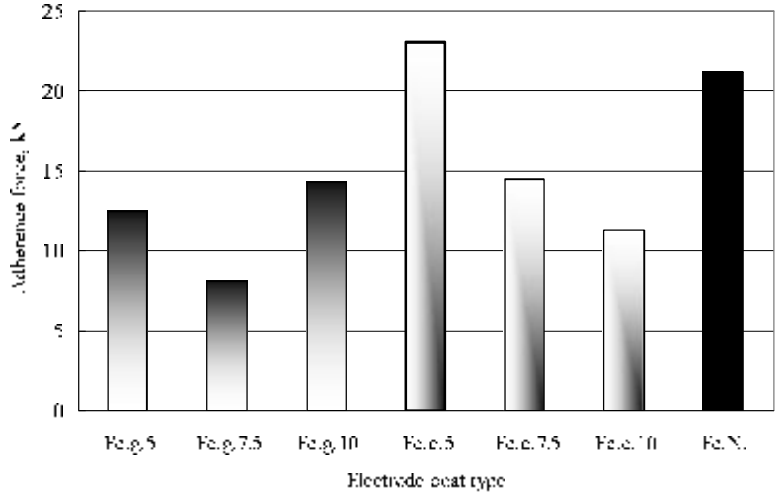

Fig. 2. Experimental measured adhesion force: Fe.g.5 – carbon graphite, CE=5; Fe.g.7,5 - carbon graphite, CE=10; Fe.g.10 - carbon graphite, CE=10; Fe.c 5 - carbon compound, CE=5, Fe.c 7,5 - carbon compound, CE=7,5; Fe.c.10 - carbon compound, CE=10; Fe.N - nickel electrode.

5 Conclusions

- For carbon as graphite powder the adhesion force is higher for a greater carbon equivalent value;
- the use of carbon as a compound assures the higher adherence when the lowest carbon equivalent value is applied.

The results are promising both economic and technical. A low C.E. that is a small amount of alloying elements and a good, even better adhesion than that of the nickel electrodes are a good departure for further investigations. More carbon compounds and mixtures must be tested as well as some other mechanical properties.

Received April 20, 2007 *The "Gh.Asachi" Technical University Iaşi*

REFERENCES

1. Ciszewski. G. *Bindung zwischen Auftragschicht und Grundwerkstoff beim Kaltschweißen von Gußeisen Theorie der Grafitsperrschicht. Schweißen und Schneiden.* nr. 38, 1986. p. 132…135.
2. Diana Gheorghiu, C. Bejinaru - *Device and sample for determinating the adhesion of the clad welds*, **Buletinul Institutului Politehnic Iaşi**, *Tom L (LIV) fasc. 1-2*, p. 107…112, 2004
3. Bär. F., Boamă Clara, Centea. O., Ivancenco, A., Marcu V., Micloşi, V., Popoviyi, V., Raţiu, M., Sălăgean, T., Stoianovici, P., **Sudarea metalelor,** Editura Tehnică. Bucureşti, 1965

PROIECTAREA UNOR MATERIALE DE ADAOS FARA NICHEL PENTRU SUDAREA FONTELOR –I

Rezumat: Reducerea sau eliminarea nichelului în electrozi destinaţi sudării fonturilor este în continuare o problemă importantă pentru cei interesaţi în sudarea fonturilor. Lucrarea de faţă demonstrează că asupra calităţii or suturii un rol important îl are modul de prezentare al carbonului în învelişul de electrod. Efectul jucat de carbon prin modul de prezentare este evaluat prin măsurarea aderenţei metalului depus – electrozi noi proiectaţi la materialul de bază, o marcă de fontă cenuşie.

BULETINUL INSTITUTULUI POLITEHNIC DIN IAŞI
Tomul LIII (LVII), Fasc. 4, 2007
Secţia
ŞTIINŢA ŞI INGINERIA MATERIALELOR

ABOUT THE DESIGN OF ADD FILLER MATERIALS WITHOUT NICKEL CONTENT FOR CAST IRON WELDING – PART II

BY

DIANA ANTONIA GHEORGHIU, CONSTANTIN BACIU and COSTICĂ BEJINARU

Abstract: : Reducing or even eliminating nickel contempt into the cast iron electrodes is still a major challenge for those who are interested on cast iron welding. The present work demonstrates that an important role plays the cuantity of fluxing elements into the electrode coat upon the qualities of .he weld. The fluxing element quantity is expressed by the mass ratio and its role is estimated through the adherence of the deposed material on the base material, a grey cast iron grade.

Keywords: base material, electrode wire, electrode coat, fluxing elements.

Weldability is defined as the capacity of a material to be welded under the imposed fabrication conditions into a specific designed structure (assembly) in order to perform satisfactory in the intended service.

For the materials with a poor weldability the imposed fabrication conditions are of ultimate interest and should take into account the quality of the consumables, the welding regime and other specific techniques (peening, preheat, etc.).

Cast irons are difficult to weld. Their weldability has been controlled especially through an adequate technology which includes substantial base material preheating.

Coinage the nickel consumables has revolutionized cast irons welding. The preheat temperature has decreased and the finite welds could be chipped. Many other problems remained the same; among them the discontinuities that encounter during welding at the interface add material and base material

But replacing or at least reducing nickel amount into the electrodes for cast iron welding is a concern all over the world /1/, /2/.

1. Theoretical considerations

For any weldment, the final quality is the result of the complex interaction between the molten filler wire, electrode coat and base material in the weld pool, phenomena that occur under a well established welding regime. So, the discontinuity amount should have a complex dependence. The purpose of the work is to establish some aspects regarding the coat influence, more precise the quantity of the protective coat fraction

In this study we emphasis on the effect of the flux quantity upon the weld quality. The quantity of flux coat formula is reported to the total quantity of materials that should be transferred through the arc, which are the wire and the alloying

elements included in the electrode paste, prime carbon, silicon and manganese. This is done by mass ratio k, as defined in relation (1):

$$k = \frac{m_{flux}}{m_{act}} \quad (1)$$

where: m_{flux} – total weight of the flux compounds as listed into Table 1;

m_{act} the active add filler material, that is usually the wire, in the present work it contains also the adequate alloying elements in the paste.

In the experiment k has three imposed values: 0,4 , 0,5 and 0,7.

2. Experimental conditions

As base material was used grade Fc250 grey cast iron. As electrodes core was used steel wire of S10 grade. The electrode coat included alloying elements (graphitizing role, including carbon in two forms) and protective elements are designed as fluxing elements. Among the main functions of an electrode coat should be remember those regarding the molten material protection from the atmosphere, refine of the weld pool and control in some degree the cooling rate. All those functions are accomplished though the fluxing elements contempt.

In the experiment were used fluxing materials for general purpose; the percentage of each and their main role to play in welding process are listed in table 1.

Table 1. Flux components into the designed electrodes

Compound	Formula	Function	Amount, %
Calcium carbonate	$CaCO_3$	Shield gas	35
Dolomite	$CaMg(CO_2)_2$	Shield gas	30
Rutile	TiO_2	Slag former	5
Silica	SiO_2	Slag former	5
Fluorspar	CaF_2	Arc stabilizer	10
Feldspar		Arc stabilizer	5
Sodium silicate		Binder	10

Powders of those components were mixed together; the sodium silicate, the only liquid compound, was added to the whole just before the electrode forming.

With this composition, the calculated index, B.I. for the specific case

$$B.I. = \frac{CaO + CaF_2 + MgO + K_2O + Na_2O + Li_2O + \frac{1}{2}(MnO + FeO)}{SiO_2 + \frac{1}{2}(Al_2O_3 + TiO_2 + ZrO_2)} \quad (2)$$

equals 2,2, that is a basic coat. Generally, higher the basicity index, cleaner is the weld, especially with respect to nonmetallic inclusions

3. Experimental work

The S10 wires were mechanical cleaned and air blasted, each of them just before the prepared coat be deposed on it.

Powders of carbon (graphite or carbon compound) ferrosilicon and ferromanganese in appropriate percentage for each experimental formula were mixed together with an appropriate amount of flux mixture, so the chosen experimental conditions – carbon equivalent and mass ratio value be accomplished.

Conditions of welding process: no preheat, welding current 100A, welding time 10 seconds, then a constant heat input.

Samples for each of the specified conditions (different carbon form, different carbon equivalent values and specified mass ratio values were welded. The influence of the mass ratio as well as the other influences were estimated through the adherence force of the deposited material at the base material.

4. Results

The average adherence force for at least three samples for each of the mentioned conditions is figured in the following charts.

Figure 1 describes the influence of the mass ratio on the adherence force for the mentioned different conditions.

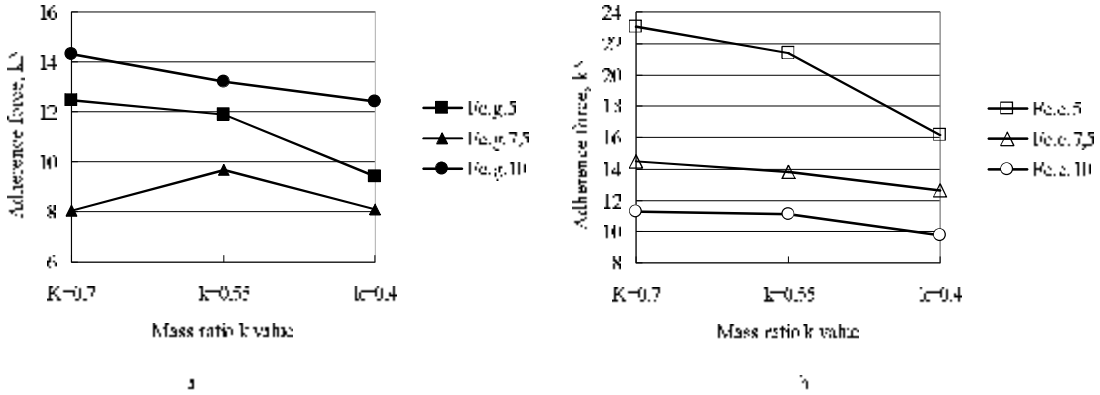

Fig. 1. Adherence force for: a. different mass ratio and carbon equivalent for carbon as graphite; b.different mass ratio and carbon equivalent for carbon as compound.

It is obviously that the increase of the mass ratio has a good effect on the adherence force of the deposed material. The influence varies for the different experimental conditions. So, in figure 2 one can compare the adherence force for the best coat formula for both carbon forms.

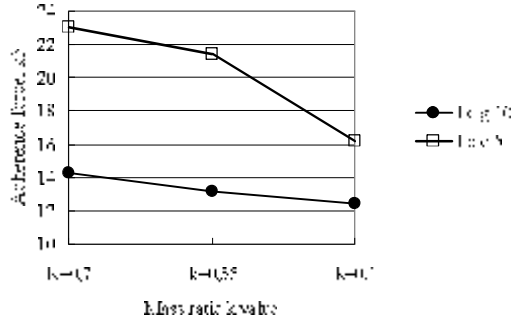

***Fig. 2.** Adherence force for the best coat formula for both carbon forms: Fe.g.10 – carbon graphite, carbon equivalent value equals 10; Fe.c.5 – carbon as compound, carbon equivalent value 5*

As can be seen, even the mass ratio value has less influence in case of the coat that contains graphite, an enhancement is obviously.

A global image regarding the interdependences that can be exhibited is presented in figure 3.

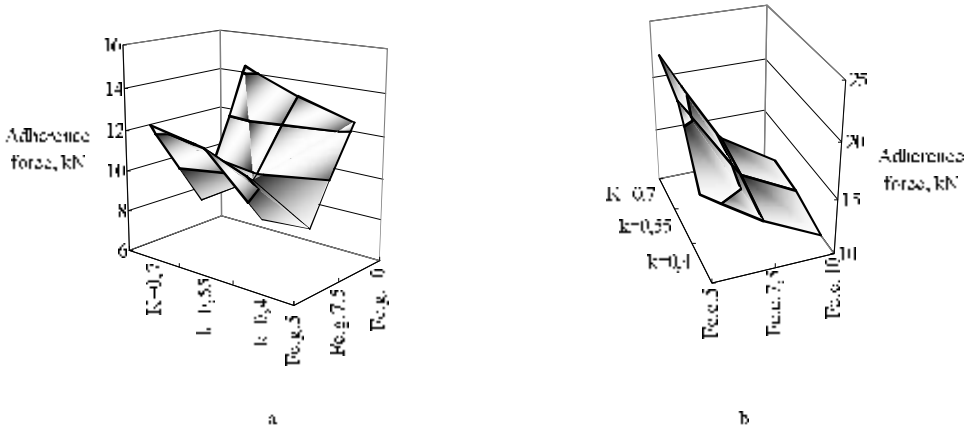

***Fig. 3.** The complete dependences in the experiment: a. adherence force for carbon as graphite; b.adherence force for carbon as compound.*

In case of carbon graphite the dependences are difficult to clarify. The important thing is that the highest adherence force occurs at the samples that exhibit the greater mass ratio. For the electrode paste with carbon as a compound, the trend is simplier: adherence force increase, with the mass ratio and decrease, with the increase of the carbon equivalent.

5. Conclusions

The flux quantity, expressed through mass ratio, as considered in this study has a major role into the weld quality estimated through adherence force. For the present is proved that a higher mass ratio is an essential parameter for increasing the adherence force, especially for carbon into compound form.

The electrode paste has a main influence on the weld quality both through fluxing elements quantity and alloying elements, carbon, form.

The adhesion force gives us a quantitative evaluation of the interface quality.

Received April 28, 2007 *The "Gh.Asachi" Technical University Iaşi*

REFERENCES

1. Zhou. Z. F., Sun. D. Q., Ren, Z. A. - *New advances for cast iron welding in China in the last decade*, IIW, Doc. II-1231-94, april 1994

2. Stauder, F., Fargues, J., Damagnez, P *Deux solutions innovantes pour le soudage a l'arc et electrodes enrobees des fontes GS*, Doc. IIS IX – 1855 - 96

CONSIDERAŢII PRIVIND REALIZAREA UNOR ELECTROZI PENTRU SUDAREA FONTELOR FĂRĂ NICHEL

Rezumat: Reducerea sau chiar eliminarea conţinutului de nichel în electrozii destinaţi sudării fontelor reprezintă însă o provocare pentru cei implicaţi în sudarea fontelor. Lucrarea demonstrează rolul cantităţii de elemente cu rol protector, de flux, din înveliş, asupra calităţii sudurii. Cantitatea de elemente protectoare este exprimată prin raportul maselor k, iar efectul ei este apreciat prin aderenţa materialului depus la materialul de bază, fontă cenuşie.

BULETINUL INSTITUTULUI POLITEHNIC DIN IAŞI
Tomul LIII (LVII), Fasc. 4, 2007
Secţia
ŞTIINŢA ŞI INGINERIA MATERIALELOR

CONVERSION OF FLY ASH TO ZEOLITES FOR WASTE WATER TREATMENT. I. ESTABLISH THE EXPERIMENTAL CONDITIONS

BY

MARIA HARJA, GABRIELA CIOBANU, LĂCRĂMIOARA ISTRATI and GABRIELA CĂRJĂ

Abstract: Coal combustion by-products are estimated in around 115 million tons per year. A large portion of this production is accounted for the coal fly ash (FA). From application of this coal fly ash zeolite obtaining is interesting product, with high environmental applications. Zeolites may be easily obtained from FA by direct alkaline conversion processes. In this paper we characterize fly ash obtained in Iasi and establish the experimental conditions to obtain high cation exchange capacity (CEC) zeolites. Also, we compare our fly ash composition and physical properties with fly ash utilize to obtained zeolites, in order to find optimal experimental conditions. From types of zeolites what may be obtained, in this study we presented different zeolitic products for waste water (with high CEC). In order to use the ash in the mentioned direction, we have proposed ourselves to characterise it chemically, mineralogically and technologically. For this characterisation we performed the chemical analysis for the oxidical compounds, the thermogravimetrical, and the FTIR analysis.

Keywords: coal fly ash; zeolite synthesis; cation exchange capacity; heavy metals uptake, environment.

1. Introduction

The fly ash produced from the burning of pulverized coal in a coal-fired boiler is a fine-grained, powdery particulate material that is carried off in the flue gas and usually collected from the flue gas by means of electrostatic precipitators, baghouses, or mechanical collection devices such as cyclones.

In 1996, approximately 16.2 million tons of fly ash was used. Of this total, 13.3 million tons (approximately 22% of the total quantity produced), were used in construction-related applications. Between 1985 and 1995, fly ash usage has fluctuated between 8.8 and 13.6 million tons per year, averaging 11.3 million tons per year [1, 2]. Approximately 70 to 75% of fly ash generated is still disposed or storage lagoons. In Iasi all quantities of coal ash is disposed of the landfills. Much of this ash, however, is capable of being recovered and used. Examples of these applications are [3, 4, 5]:

- Additives for immobilization of industrial and water treatment wastes
- Extraction of valuable metals, such as Al, Si, Fe, Ge, Ga, V, Ni, Zn.
- Land stabilization in mining areas.
- Sorbents for flue gas desulfurization.
- Fireproof materials.
- "Slash" (fly ash/sludge blend) production for soil amendment
- Filter material for the production of different products.
- Ceramic applications.

The compositional similarity of fly ash to some volcanic material, precursor of natural zeolites, was the main reason to experiment with the synthesis of zeolites from this coal by-product. Zeolites are crystalline aluminium silicates, with group I or II elements as counterions. Their structure is made up of a framework of $[SiO_4]^4$ and $[AlO_4]^5$ tetrahedra linked to each other at the corners by sharing their oxygen's. The tetrahedra make up a three-dimensional network, with lots of voids and open spaces. It is these voids that define the many special properties of zeolites, such as the adsorption of molecules in the huge internal channels (Fig. 1) [6]

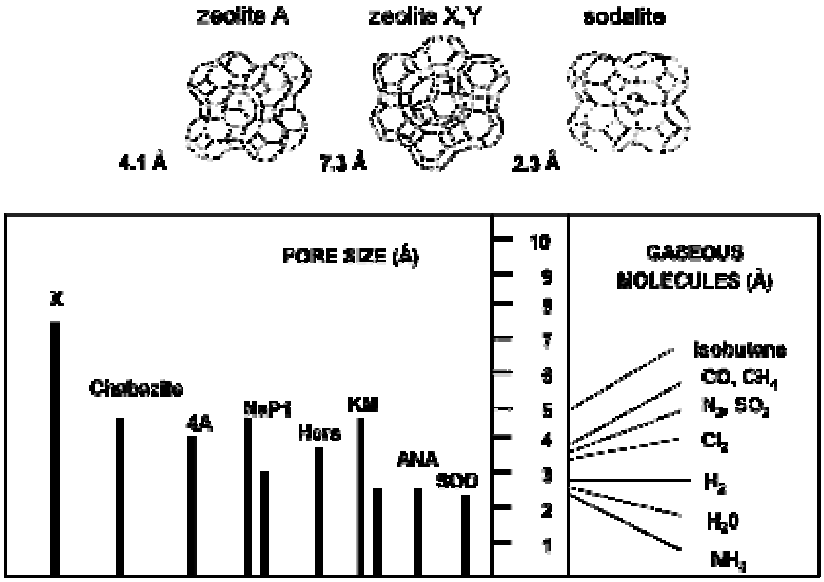

Fig. 1. Top: The channel diameter of zeolites is dependent on the structure. Bottom: Examples of channel size for selected zeolites which may be synthesized from fly ash compared with the diameter of some gaseous molecules.ANA- analcime; 4A - zeolite A, X - zeolite X, Hers - herschelite (Na-chabazite), SOD - sodalite; KM -phillipsite.

We see that zeolites with large pore size (7.3 A) have a wide range of industrial applications, mainly based on [6]:

Ion exchange: exchange inherent $Na^1/K^1/Ca^{21}$ for other cations on the basis of ion selectivity.

- Gas adsorption: selective absorption of specific gas molecules
- Water adsorption: reversible adsorption of water without any desorption chemical or physical change in the zeolite matrix.

Since the initial studies 1985, many patents and technical articles have proposed different hydrothermal activation methods to synthesize different zeolites from fly ash. All the methodologies developed [6, 7, 8, 9] are based on the dissolution of Al Si-bearing fly ash phases with alkaline solutions (mainly NaOH and KOH solutions) and the subsequent precipitation of zeolitic material.

In order to use the ash for synthesis of zeolites, we proposed characterise it chemically, mineralogically and technologically. For this we performed the chemical analysis for the oxidical compounds, the thermogravimetrical, and the FTIR analysis. Also, we have analysed to determine their density and their Blaine specific surface.

2. Experimental

In Iasi, where the main source of thermal power is the energetic huile, which contains over 18% ballast, it is necessary to find some proceedings to allow this waste's capitalisation. From application of this coal fly ash, zeolite obtaining is interesting product, with high environmental applications. Zeolites may be easily obtained from FA by direct alkaline conversion processes

The use possibilities of the ash are induced both by the chemical and mineralogical composition and by the technical proprieties. This is why we have designed experiments which allow a complete characterization of the ash, and the possible directions of capitalization.

Physical Properties. Fly ash consists of fine, powdery particles that are predominantly spherical in shape, either solid or hollow, and mostly glassy (amorphous) in nature. The carbonaceous material in fly ash is composed of angular particles. We have determined the granulometrical distribution for the samples taken by dry screening. The results we got are expressed by oversize, in accordance with the particles' average diameter. Samples have 83-91% particles smaller than 40 μm, this is why we performed granulometrical analysis for these samples, using the Andreasen dropper and the sedimentation scale. The experimental data is presented in figure 2.

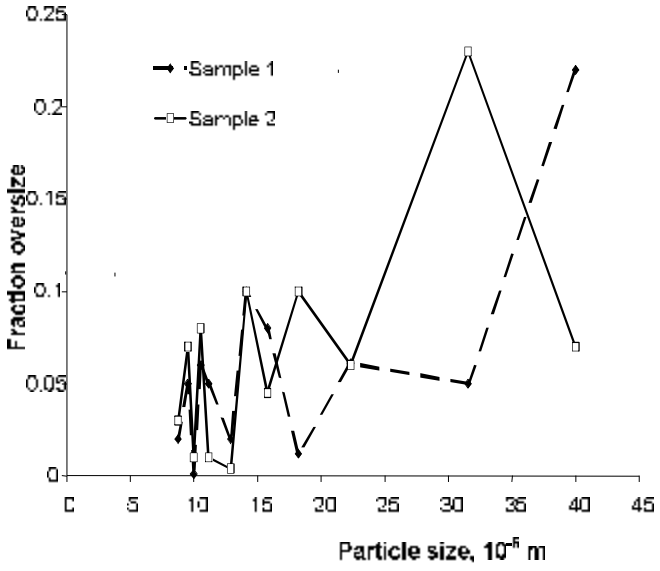

Figure 2 The granulometrical distribution, wet screening.

The specific gravity of fly ash usually ranges from 2.1 to 3.0, while its specific surface area (measured by the Blaine air permeability method) may range from 170 to 1000 m^2/kg. The color of fly ash can vary from tan to gray to black, depending on the amount of unburned carbon in the ash, the lighter the colour indicated the lower the carbon content

Chemical Properties. The chemical properties of fly ash are influenced to a great extent by those of the coal burned and the techniques used for handling and storage. The principal components of coal fly ash are silica, alumina, iron oxide, and calcium, with varying amounts of carbon, as measured by the loss on ignition (LOI).

Chemical composition is presented in table 1. Function of chemical composition our ashes are classified in Class F. The chief difference between Class F and Class C fly ash is in the amount of calcium and the silica, alumina, and iron content in the ash. In Class F fly ash, total calcium typically ranges from 1 to 12 percent [10], mostly in the form of calcium hydroxide, calcium sulfate, and glassy components in combination with silica and alumina. The loss on ignition, which is a measurement of the amount of unburned carbon remaining in the fly ash, is one of the most significant chemical properties of fly ash, especially as an indicator of suitability for use as a cement replacement in concrete.

Table 1. The characterisation of coal ash.

Composition, %	Sample 1	Sample 2
SiO_2	51.198	51.21
Al_2O_3	26.93	25.08
Fe_2O_3	6.98	6.28
CaO	8.31	5.21
MgO	1.075	0.7596
Ignition loss 1200°C – total loss, %	2.42	1.3
Density (kg m^{-3})	2340	2518
Ration SiO_2/Al_2O_3	1.9	2

Even though the results we got regarding the chemical oxidic composition correspond to the ones reported in the reference literature [11, 12]. For the assay we have performed the thermogravimetrical analysis using a MOM Budapest Q-1500 Thermogravimeter, the TG and DT curves beeing processed in fig.3.

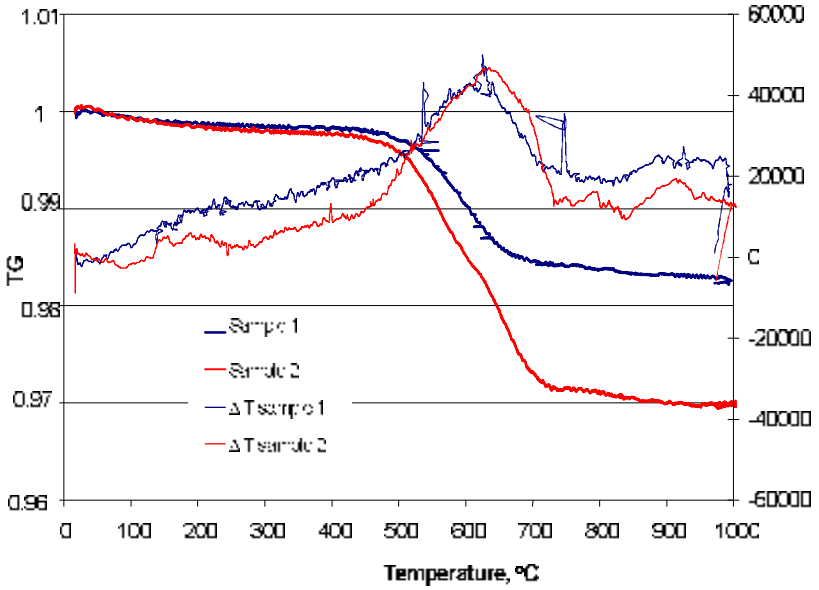

Figure 3. The thermogravimetrical analysis curves.

From figure 3 for samples 1 and 2 the losses are of 2.84%, respectively of 1.7% (including humidity), in according with ignition loss.

The destructive chemical analysis allows determining the oxidical compounds in the sample without offering any information about ash's „mineralogical" composition. To get some further information about the way the oxidical compounds bond we have performed the IR analysis using a DIGILAB FTS 2000 spectrometer. The obtained spectrums are presented in figure 4.

The analysis of IR spectrums proves that in the ash samples we can find compounds like: hematite, quartz, kaolin, illit, lime, montmorilonite, carbon. Moreover these are the compounds which can be found in the clayey material, respectively the fuel's ballast

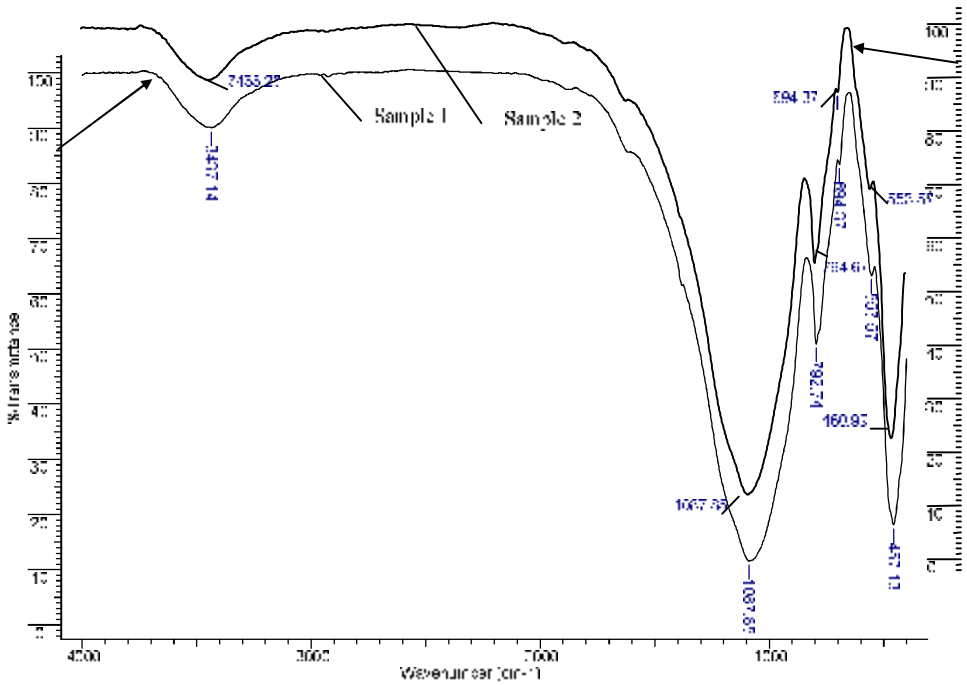

Figure 4. IR spectrum for ashes.

3. Results and discussion

Coal fly ashes resulted in Iasi has chemical proprieties as ashes from Spain. Querol et all. [9] utilize 11 types of ashes for synthesis of zeolites. Our fly ash have characteristics as sample 2 and samples 5 [13], with ration SiO_2/Al_2O_3 in range 1.9-2.

To avoid a synthesis process with the generation of waste water, Al(III)/Si(IV) high ratio of this type of zeolite accounts Park [8, 9] developed a synthesis strategy based on the use of salt mixtures instead of the aqueous solutions as the reaction medium. This interesting process has limitations since, up to now, only low CEC zeolites are obtained to the high temperature needed in the activation process. Hollman et al. [14] developed a two-stage synthesis procedure that enables the synthesis of >99% pure zeolite products from high-Si solutions obtained from a light alkaline attack of fly ash. Moreover, the solid residue from this attack could be converted into classic zeolitic products by using the conventional conversion method. This process has the advantage of producing pure zeolitic material, instead of the blend zeolite/residual fly ash particles obtained from other strategies. Moreover, high-pore volume zeolites, including zeolites X and A, may be obtained in this process [15]. All

these different processes resulted in the synthesis of low-silica sodium and potassium zeolitic - NaP1, A, X, KM, chabazite, faujasite) material.

The fly ash activation is usually carried out in digestion bombs or autoclaves, varying the activation agent (mainly KOH and NaOH), temperature (100-200°C), conversion time (3 – 48 h), solution concentration (0.5, 1, 2, 3 and 5 M), and solution/sample ratio (1–20 ml g^{-1}).

Most of the studies on the use of fly ash-derived zeolites in the field of water purification have shown that the zeolitic material obtained may reach CECs from 0.3 to 4.7 meq g^{-1} (Table 2), and that there is a competition between cations in a solution to occupy exchangeable places in zeolites.

Table 2. Cation exchange capacity (meq g^{-1}) obtained for zeolitic material synthesized from fly ash.

Zeolitic product	CEC
4A– X	4.7
NaP1	2.7
herschelite	2.1
KM and linde F	1.9
analcime	0.6
sodalite	0.3
fly ash	< 0.05

Because 4A-X, NaP_1, herschelite KM and linde F have high CEC further we selected from literature the experimental conditions for synthesis this zeolite, table 3.

Table 3 Zeolites synthesized from fly ash as a function of activation agent (NaOH or KOH), temperature, concentration and activation solution/fly ash ratio (ml g^{-1}) [13].

10–18 ml g1		
0.5–3.0 M NaOH	90–175 °C	NaP1
0.5–1.0 M KOH	150–200 °C	KM, tobermorite
3.0 M KOH	< 150 °C	linde F, tobermorite
1–3 ml g^{-1}		
1.0 M NaOH	200 °C	NaP1 and herschelite for 8 h activation
2.0–3.0 M NaOH	90 °C	A zeolite
	150 °C	NaP1 (herschelite traces), faujasite (if aging)
	200 °C	NaP1, herschelite
2.0 M KOH	150–200 °C	KM zeolite
5.0 M KOH	150 °C	KM, chabazite and linde F traces

The conversion efficiencies are dependent on the contents of non-reactive phases and resistant aluminium silicate phases, such as mullite and quartz, and the grain size distribution. For higher aluminium–silicate glass content, shorter activation periods and lower solution/ fly ash rates are needed to reach high zeolites synthesis yields.

Other important parameters for the zeolitization of fly ash are the activation time, the concentration of the activation agents and fly ash/solution ratio. The time

needed to obtain a high synthesis yield is inversely proportional to the glass content. High-glass fly ashes are zeolitized in short period (6–8 h), but longer reaction times (24 – 48 h) are required to obtain similar synthesis yields from high-mullite or quartz fly ashes.

The highest synthesis yields are obtained in 12–24 h using a high-activation solution/fly ash ratio (10 – 20 ml g^{-1}) due to the total dissolution of mullite, quartz, and the glassy matrix. Both temperature and concentration of the activation agent have also a very important influence on the zeolite types obtained. Low temperature and concentration (i.e. 0.5 – 3 M and < 150 °C) allows the synthesis of high-CEC zeolites such as NaP1, A, or chabazite.

The high Al (III)/Si (IV) ratio of these zeolites accounts for the high CEC of some of them such as NaP1, 4A, X, KM, F, chabazite, herschelite, and faujasite. Owing to this high CEC (up to 5 meq g^{-1} of some pure zeolites), these zeolites have a high potential for application in water decontamination [16, 17, 18].

The cation exchange decontamination may be advantageous in cases, such as extraction wells, where it can be performed with no solid waste (precipitates) in the bottom as it occurs when pH treatments are applied to precipitate heavy metals. From the results, a tentative order for the affinity of different ions to the zeolite exchange sites was obtained: $Fe^{3+} > Al^{3+} > Cu^{2+} > Pb^{2+} > Cd^{2+} \sim Tl^{+} > Zn^{2+} > Mn^{2+} > Ca^{2+} = Sr^{2+} > Mg^{2+}$ [6]. These results demonstrate that NaP1 and 4A zeolites have a higher affinity for metal ions than for Ca^{2+} and Mg^{2+}.

4. Conclusions

Based on the experimental results we got, the analyzed ash belongs in F class resulting after the combustion of a bituminous fuel. This type of ash can be used to obtain zeolitic materials for the uptake heavy metals

The potential industrial application of zeolitic materials is varied. Thus, zeolite X has a high CEC (5 meq g^{-1}), while hydroxy-sodalite (2.3 Å) accounts for the low potential application for both molecular sieving and ion exchange.

For zeolitization of fly ash the activation time is 12-24 h, the concentration of the activation agents 0.5-3.0 M and fly ash/solution ratio 10-20 ml g^{-1}. Temperature may be smaller that < 150 °C for synthesis zeolites with a high CEC.

Received March 20, 2007 *The "Gh.Asachi" Technical University Iaşi*

REFERENCES

1. European Association for Use of the By-Products of Coal-Fired Power-Stations (ECOBA) web site http://www.ecoba.com/.

2. American Coal Ash Association (ACAA), web site: http://www.acaa-usa.org/

3. Dirk, G., *Pulverised fuel ash products solve the sewage sludge problems of the wastewater industry* **Waste Manag. 16 (1–3)**, 1996, **51–58.**

4. Laperche, V. and Bighamb, J.M., *Quantitative, Chemical, and Mineralogical Characterization of Flue Gas Desulfurization By-Products*, **Journal of Environmental Quality, 31,** 2002. **979-988.**

5. Querol, X., Moreno, N., Umaña, J.C., Juan, R., Hernández, S., Fernández, C., Ayora, C., Janssen, M., García, J., Linares, A., Cazorla, D., *Application of zeolitic material synthesized from fly ash to the decontamination of waste water and flue gas*, **PROGRES Workshop on Novel Products from combustion residues**, Morella, Spain, 2001, **163– 172.**

6. Querol X., Moreno. N., Umana J.C., Alastuey A., Hernandez, E., Lopez-Soler A., Plana F., *Synthesis of zeolit from coal fly ash: an overview*, **Coal Geology, 50,** 2002. **413 – 423.**
7. Park, M., Choi, C.L., Lim, W.T., Kim, M.C., Choi, J., Heo, N.H., *Molten-salt method for the synthesis of zeolitic materials: I. Zeolite formation in alkaline molten-salt system*, **Microporous Mesoporous Mater. 37,** 2000, **81– 89.**
8. Park, M., Choi, C.L., Lim, W.T., Kim, M.C., Choi, J., Heo, N.H., *Molten-salt method for the synthesis of zeolitic materials. II. Characterization of zeolitic materials* **Microporous Mesoporous Mater. 37,** 2000, **91– 98.**
9. Querol, X., Umaña, J.C., Plana, F., Alastuey, A., Lo´pez-Soler, A., **Medinaceli**, A., Valero, A., Domingo, M.J., Garcia-Rojo, E., *Synthesis of Na zeolites from fly ash in a pilot plant scale. Examples of potential environmental applications* **Fuel, 80,** 2001, **857– 865.**
10. ASTM C 618 http://www.undeerc.org/carre
11. Querol, X., Plana, F., Alastuey, A., Lo´pez-Soler, A., *Synthesis of Na-zeolites from fly ash.* **Fuel, 76 (8).** 1997,**793– 799.**
12. Reynolds, K.A., Kruger, R.A., Rethman, N.F.G., *The manufacture and evaluation of an artificial soil (STASH) prepared from fly ash and sewage sludge.* **Fly Ash Utilization Symposium, Lexington, KY, USA,** 1999, **378– 385.**
13. Querol, X., Umaña, J.C., Plana, F., Alastuey, A., Lo´pez-Soler, A., Medinaceli, A., Valero, A., Domingo, M.J., Garcia-Rojo, E., *Synthesis of Na zeolites from fly ash in a pilot plant scale. Examples of potential environmental applications*, **International Ash Utilization Symposium, Centre for Applied Energy Research, University of Kentucky, paper 12,** http://www fly.ash.info, 1999.
14. Hollman, G.G., Steenbruggen, G., Janssen-Jurkovicova, M., *A two-step process for the synthesis of zeolites from coal fly ash*,. **Fuel, 78,** 1999, **1225– 1230.**
15. Amrhein, Ch., Haghnia, G.H., Kim, T.S., Mosher, P.A., Gagajena, R.C., Amanios, T., de la Torre, L., *Synthesis and properties of zeolites from coal fly ash.* **Environ. Sci. Technol. 30,** 1996.**735– 742.**
16. Singer, A., Berkgaut, V., *Cation exchange properties of hydrothermally treated coal fly ash.* **Environ. Sci. Technol. 29 (9),** 1995.**1748– 1753.**
17. Lin, C.F., His, H.C., *Resource recovery of waste fly ash: Synthesis of zeolite-like materials.* **Environ. Sci. Technol. 29(4),** 1997. **1109– 1117.**

CONVERSIA CENUŞII ÎN ZEOLIŢI PENTRU TRATAREA APELOR UZATE. I. STABILIREA CONDIŢIILOR EXPERIMENTALE

Rezumat: Produsele de ardere din termocentrale sunt estimate la 115 mil. tone pe an. O mare cantitate din aceste produse este deţinută de cenuşă (FA). Dintre direcţiile de utilizare ale cenuşii obţinerea de zeoliţi prezintă interes, în special în protecţia mediului. Zeoliţii pot fi uşor obţinuţi din cenuşă prin conversie directă. În această lucrare noi am caracterizat cenuşa obţinută în Iaşi şi am stabilit condiţiile experimentale în vederea obţinerii unui zeolit cu o capacitate de schimb ionică mare (CEC). De asemenea, am comparat proprietăţile fizice şi chimice al cenuşii cu alte tipuri de cenuşi utilizate deja la obţinerea zeoliţilor pentru a găsi condiţiile experimentale optime. Dintre tipurile de zeoliţi care se pot obţine în această lucrare am prezentat diferite produse zeolitice pentru tratarea apelor uzate (având capacitate de schimb ionic crescută). Pentru utilizarea cenuşii în direcţia menţionată am efectuat analiza chimică, mineralogică şi tehnologică. Pentru caracterizare am făcut analiza chimică a compuşilor oxidici, analiza termogravimetrică şi FTIR.

BULETINUL INSTITUTULUI POLITEHNIC DIN IAŞI
Tomul LIII (LVII), Fasc. 4, 2007
Secţia
ŞTIINŢA ŞI INGINERIA MATERIALELOR

EVALUATION OF METAL ALLOYS BIOCOMPATIBILITY BY MEANS OF CELL CULTURE

BY

E. IACOB[1]; I. RUSU[2]; OANA IACOB[3], O. CARP[4] and VERONICA SARMASANU[5]

Abstract: The aim of our study was to confirm biocompatibility of Nitinol (Ni-Ti alloy) and Titanium, and to clarify some aspects regarding cytotoxicity in cell cultures. We conclude that Nitinol and Titanium has good biocompatibility „in vitro" and induced no toxic effects, or decrease in cell proliferation, or inhibition of the growth of cells in contact with the metal surface..

Keywords: biocompatibility, nitinol, cell cultures, cytotoxicity

1. Introduction

In this report the surface properties of nickel-titanium alloy (nitinol), and titanium, was tested *in vitro* by means cell cultures. We try to clarify the primary cytotoxicity in human cell cultures.

Altough nitinol is one of most popular biomaterials but are still few confirmative biocompatibility data available.

2. Matherial and methods

We have used BSC – 1 (kidney monkey cells) line and osteoblast – like cells (SAOS-2).

Chips 2/2 cm of metalic alloys were incubated for 7 days with cell cultures at 37^0 C.

In parallel we used controls for every sample, with no metalic chips. The medium Eagle was tested too.

We have collected samples from every culture on days 3 and 5, and count the cells

The proliferation of cell culture BSC – 1 and SAOS 2 was identical like the controls both nitinol and titanium samples.

3. Results

The results of current study indicate that metal ions have no significant side effects on short term, in living tissues.

Both nitinol and titanium metals have a good biocompatibility and seems induced no toxic effect, or decrease the cell proliferation

4. Conclusions

These experiment demonstrate the utility of employing cell cultures to investigate biocompatibility of implant materials.

Certainly, further studies to more closely simulate *in vivo* conditions, are required.

Received April 3, 2007

[1] *Univ. de Medicină şi Farmacie "Gr. T. Popa" Iaşi*
[2] *Universitatea Tehnică „Gh. Asachi" Iaşi*
[3] *Institutul de Sănătate Publică Iaşi*
[4] *Spitalul Judeţean Constanţa*
[5] *Spitalul Clinic de Recuperare Iaşi*

REFERENCES

1.B.Thierry, M.Tabrizian, O. Savagado, L.H. *Fahlo, Efects of Sterilization Processes on NiTi Alloy: Surface Characterisation*, **J. Biomed. Mater. Res.**, 2000, 49, 88 – 98.
2. J.Ryhanen, E Niemi, W.Sarlo, E.Niemela, P Sandvik, T.Salo, *Biocompatibility of Shape Memory Metal and Its Corrosion Behavior In Human Cell Cultures*, **J.Biomed.Mater. Res.**, 1996, 35, 451 – 457.
Melissa Shettlemore, Kirk Bundy, *Toxicity Measurement of artopedic Implant Allay Degradation Products Using a Bioluminiscent Bacterial Assay*, **J. Biomed. Mater. Res.**, 1999, 45, 395 – 403.

EVALUAREA BIOCOMPATIBILITĂŢII ALIAJELOR METALICE PRIN INTERMEDIUL CULTURILOR CELULARE

Rezumat: Scopul acestui studiu a fost de a confirma biocompatibilitatea nitinolului (aliaj de Ni-Ti) precum şi a titanului şi de a elucida unele aspecte legate de eventuala citotoxicitate a acestor metale cu ajutorul culturilor celulare. Concluziile rezultate din acest studiu arată că atât nitinolul cât şi titanul prezintă o bună biocompatibilitate şi nu induc un efect citotoxic, nu scad rata de proliferare a celulelor şi nici nu produc o inhibiţie a creşterii celulare în contact cu suprafeţele metalice.

BULETINUL INSTITUTULUI POLITEHNIC DIN IAŞI
Tomul LIII (LVII), Fasc. 4, 2007
Secţia
ŞTIINŢA ŞI INGINERIA MATERIALELOR

BEHAVIOR OF VARIOUS METALS IN THE RED SEA CORAL-REEF ENVIRONMENT

BY

D. ITZHAK, R. VAGO, G. PASTERNAK and S. MOISA

Abstract: This study focuses on the behavior of various metal substrates, including Ti-2, Ti-7, Ti-12, hastelloy C-276, AISI 304, AISI 316 and Avesta 254 stainless steels, commercial copper, brass 70Cu/30Zn, mild steel ST-37, galvanized steel, silver 99.99% and aluminum alloy 6061, in a coral reef marine environment. The experimental setup was deployed at a depth of 6 m in the coral reef fringing the Red Sea at Eilat. After three months of exposure, the copper and brass 70Cu/30Zn plates were still free of biofilm. A non-adhesive film was found on the silver plate and early stages of sessile organisms such as algae, bryozoa, tunicates, tube worms, calcareous corals and hydrocorals could be seen on the surfaces of all the other metals. The titanium alloys and Hastelloy C-276, whose open circuit potential and potentiodynamic polarization curves indicated passive electrochemical behavior, showed negligible corrosion rates. Enhanced bio-adhesion and development of sessile organisms were observed on all the metal surfaces exhibiting passive electrochemical behavior. A corrosion rate of 9.5 mpy was measured for mild steel ST-37, which exhibited only insignificant fouling settlement. Corrosion rates of 3.3, 3.4, 0.2, 0.3 and 0.6 mpy were registered for commercial copper, brass 70Cu/30Zn, AISI 304, Al 6061 and galvanized steel, respectively. Corrosion was negligible on all the other metals. Despite the chemical calcification products found on the galvanized steel and aluminum alloy 6061, fouling settlement on these substrates was limited. It is suggested that alkaline conditions, followed by powerful electrochemically reduction of dissolved oxygen, leading to formation of small amounts of hydrogen peroxide at the metallic surface area. These localized biocidic conditions prevent early development of biofilm and fouling organisms on these metals.

Keywords: coral reef environment, Red Sea, corrosion, biofouling, passivity, biocide effect.

1. Introduction

Metals are extensively used in marine engineering applications. Mild steels such as ST-37 (1020) are the metals most commonly encountered in such settings, but some marine applications require specific types such as stainless steels, titanium alloys, nickel-based super alloys, or copper alloys[1]. Prolonged immersion in seawater exposes the metals to the action of high ionic concentrations and elevated electrical conductivity. The resulting corrosion is further aggravated by epibiota and the presence of various marine organisms representing different phyla, life strategies and morphologies, such as: microbes, algae, fungi, sessile and colonial invertebrates[2,3,4,5]. The upper most epibiota is constructing the framework into which other organisms and suspended solid particles are entrapped and eventually consist the biofouling[6,7,8,9,10]. Biofouling alter the electrochemical environment of the metal surface by creating crevice conditions that influence the oxidation-reduction potential, through a mechanism related to microbiological induced corrosion (MIC)[11,12,13]. The metal-biota interface affects the open circuit potential (OCP) and other electrochemical parameters, including passivation current density, breakdown potential, and pitting potential [14,15,16,17]. Calcareous deposition works synergistically with the epibiota to

favor localized attacks (under-deposit, crevice and pitting corrosion) and causes metals to shift from a passive to a metastable state[18,19,20].

It is well documented that films of microscopic organisms begin to form on structural metals and alloys within a few hours of their deployment in ambient waters[21]. Fouling settlement generally begins with the development of biofilm - a thin layer composed of microalgae and bacteria, which secrete mucus containing cellular constituents[22].

In tropical oceans, deposition of biofilm is followed by the settlement of reef building organisms such as algae, tunicates, corals, sponges and hydrozoa[23]. Such environments contain a rich diversity of micro and macro organisms, often acting in consort, that is, with one species creating environmental conditions in which another can flourish and grow.

In his review, Dexter[22] summarizes studies dealing with various metals and particularly carbon steel, stainless alloys and unspecified titanium alloy exposed to natural, filtered or synthetic seawater. He emphasizes the creation of anaerobic conditions beneath the biofilm, with the development of sulfate reducing bacteria (SRB), which are known to play a major role in the corrosion of steel. The changes in pH that take place under marine biofilm can be much greater than those occur in the ambient environment[22]. Values as low as 5, can be expected under aerobic biofilm containing acid producing bacteria[25], and even lower pH values in the range of 1-2 under discrete biodeposits[26].

Most published studies describe experiments carried out in the laboratory in seawater, filtered seawater, or synthetic seawater, i.e., under conditions that can not promote a natural fouling flux.

In the present study we focused on the behavior of various alloys under field condition. The study was carried out in the tropical environment of the coral reef in the Gulf of Eilat. In spite the great importance of the reefs as a diverse ecosystem which shelter a huge diversity of organisms and support fishing and tourism industry, there are very limited studies dealing with metallic engineering issues in this ecosystem.
The following metal groups were examined:
1. Electrochemically active metals with pronounced biocidic effects: commercial copper and brass 70Cu/30Zn.
2. Electrochemically active metals with no biocidic effect: mild steel ST-37, and galvanized steel.
3. Electrochemically metastable alloy: Al 6061.
4. ectrochemically passive alloys: Ti-2, Ti-7, Ti-12, Hastelloy C-276, AISI-304, AISI-316 and Avesta-254 stainless steel
5. Nobel metal with known biocidic effect: silver 99.99%,
The formation of biofouling on different metallic substrates and the effects of the biogenic settlement on the corrosion behavior of the metals were monitored

2. Experimental procedure

Field experiments were carried out in the shallow zone of the fringing reef situated in the northern tongue of the Red Sea, the Gulf of Eilat. Care was taken to assure that the field experiments would be carried out in the reef in the natural aquatic

environment. The experimental setup was deployed at a depth of 6 meters adjacent to the H. Steinitz Marine Biology Laboratory. Underwater setup, inspection and handling were carried out in the natural environment, using SCUBA

A set of plates made of different metals was attached to a PVC platform, which was secured to steel frames to avoid the effects of sediment load. For good reproducibility and easy handling[27], three samples (5cm * 5cm) of each metal were attached to the PVC platform (Fig. 1). Prior to exposure, the mild steel ST-37, commercial copper and brass 70Cu/30Zn samples were cleaned with hydrochloric acid to remove corrosion products. The entire set of samples, including the pre-treated mild steel ST-37, commercial copper and brass 70Cu/30Zn, was degreased with detergent, rinsed with de-ionized water, and then dried with acetone

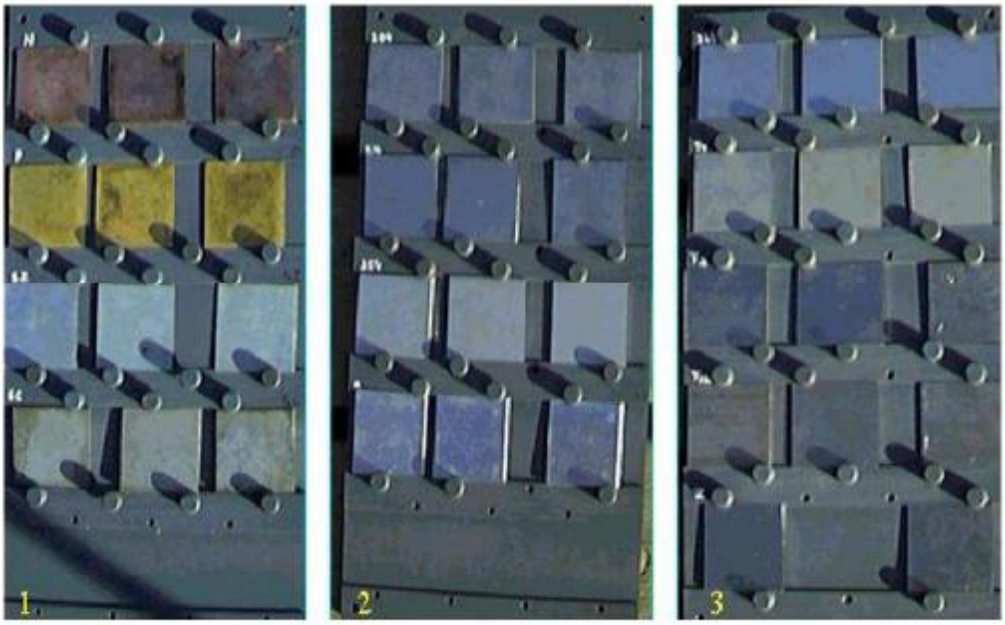

Fig. 1: A set of metal plates mounted on a PVC rack before exposure.

The following metals were studied: Ti-2, Ti-7, Ti-12, Hastelloy C-276, AISI-304, AISI-316 and Avesta-254 stainless steel, commercial copper, brass 70Cu/30Zn, mild steel ST-37, galvanized steel, silver 99.99%, and aluminum alloy 6061.

Cyclic potentiodynamic polarization measurements of the metal plates were carried out in Red Sea water (4.2wt%) at ambient temperature (77°F) using scanning rate of 2 mV/sec[28], from cathodic to anodic direction, starting 500mV to 1500mV, against an Ag/AgCl standard reference electrode. The measurements were made in separated half-cells, connected by sintered glass bridge. This was done to avoid chlorine influence on the tested samples, when working in a non-separated cell, due to chloride oxidation taking place on the platinum electrode at the initial stages of the scanning. The open circuit potential (OCP) of the metal plate was measured against an Ag/AgCl electrode at the same conditions[29].

The exposed metal plates were retrieved from the underwater experimental zone after three months and inspected in the laboratory for growth of biofouling. After fine brushing, to remove excess sediment, and rinsing with de-ionized water, the

samples were treated with acetone and examined by scanning electron microscopy (SEM). Corrosion rate was determined gravimetrically[30].

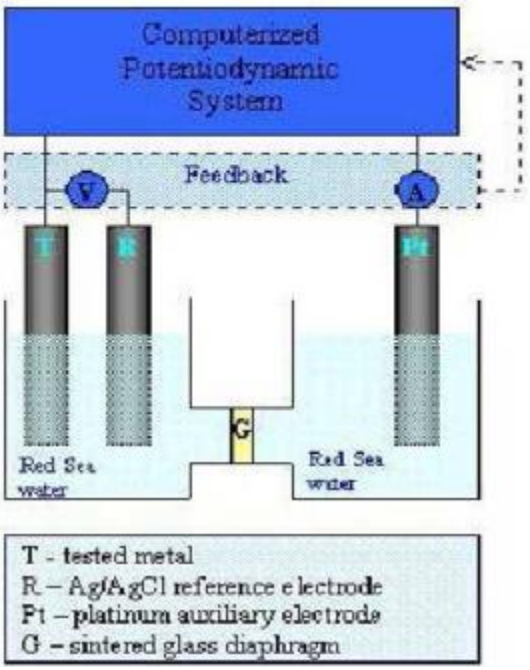

Fig. 2: Diagram of the cyclic potentiodynamic measurement system

3. Results and discussion

Macro observations of the metals after three months of exposure to the coral reef environment are presented in Fig. 3. The results revealed several distinct patterns of behavior:

1. A biocidic effect in the cases of commercial copper, brass 70Cu/30Zn and silver 99.99%.
2. A chemical calcification effect with mild fouling settlement for Al 6061, galvanized steel and mild steel ST-37
3. Heavy biofouling with no significant chemical calcification for the electrochemically passive metals: titanium alloys, stainless steels and Hastelloy C-276.

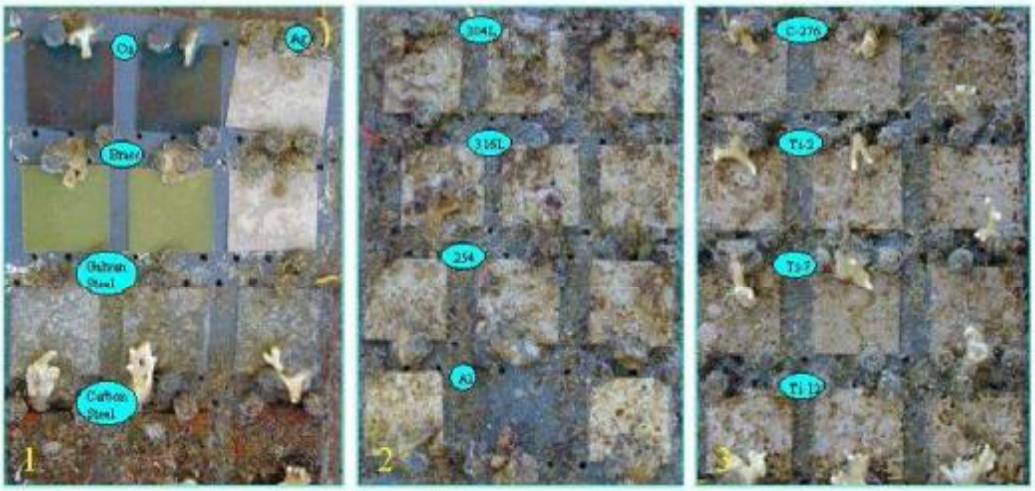

Fig. 3: Typical appearance of various metals after three months of exposure to the coral reef environment.

No biofouling was detected on the surface of the commercial copper or brass 70Cu/30Zn plates. A non-adhesive slim, thin film was found on the silver 99.99% plate with no significant biofouling. A thick layer of corrosion products and an adhesive biofilm were seen on the ST-37 mild steel. A black corrosion layer related to the formation of sulfide compounds produced by SRB under anaerobic conditions, were obtained beneath the upper reddish layer. The main sulfide crystalline phase identified was Marcasite, FeS_2. The literature usually reported the formation of FeS, as the main sulfide produced by the SRB[22]. Our results may indicate a formation of various polysulfide phases, under anaerobic conditions as a result of the SRB presence. The corrosion products combined with the crystalline phases of the biofouling were identified by XRD as: Marcasite – FeS_2, Siderite - $FeCO_3$, Hematite - Fe_2O_3, Feroxyhyte FeOOH, Lawencite - $FeCl_2$, $Fe(OH)_2$, $Fe(OH)_3$, Magnetite - $FeFe_2O_4$, and carbonate phases of calcium and magnesium. On the galvanized steel, pitting corrosion was observed and later transformed into a uniform attack. The corrosion process has been followed by a heavy chemical calcification, resulted in white precipitates identified by XRD as the following crystalline phases: Magnesite - $MgCO_3$, Dolomite - $CaMg(CO_3)_2$, Calcite - $Ca_xMg_{(x-1)}CO_3$, Aragonite - $CaCO_3$, Hydroxincite $Zn_5(CO_3)_2(OH)_6$, $Zn_1CO_3(OH)_6H_2O$ and Wuelfingite - ε-$Zn(OH)_2$. Although heavy chemical calcification process took place on the galvanized steel surface, only few patches of fouling settlement were observed on this substrate, within three months. Al alloy 6061 exhibited few fouling settlements combined with chemical calcification deposits. X-ray diffraction reveals the following crystalline phases: Brucite $Mg(OH)_2$, Magnesite $MgCO_3$, $CaCO_3$ in the forms of Calcite, Aragonite and Vaterite. It should be emphasized that only in this case, $Mg(OH)_2$ was identified. Similar findings were reported previously[31]. The authors found enhanced biomineralization combined with Mg accumulation on the metal-biomineral interface in the case of Al 6061 alloy. The electrochemically passive alloys: titanium alloys, stainless steels and Hastelloy C-276, exhibited heavy biofouling settlement and encrustation of the metal with Calcite and Aragonite $CaCO_3$, most probable of biogenic origin.

Scanning electron microscopic observations of the biofouling on the surfaces of the electrochemically passive alloys revealed both calcareous and non-calcareous organisms such as: algae, corals, hydrocorals, bryozoans, worms, diatoms, and coccolithophore and partially covered with filamentous algae. Coral at an early stage of settlement was found on Ti-12 and encrustation by colonies of the hydrocoral *Millepora dichotoma* were observed on AISI-304 and AISI-316.

Cyclic potentiodynamic polarization curves are presented in Fig. 4 and 5. Mild steel ST-37 exhibited the highest corrosion rate - about 9.5 mpy. Slimy biofilm with no significant fouling settlement was found on the mild steel ST-37 plates. It is suggested that sulfate-reducing bacteria (SRB) developed under the upper layer of the corrosion products (Fig. 3), causing enhanced anodic dissolution due to acidic corrosion attack[21]. As mentioned before, formation of the black sub-layer, composed of FeS_2 confirmed the idea that enhanced corrosion process of the mild steel is mainly caused by SRB although passivation behavior is demonstrated by the potentiodynamic polarization curves. Copper and brass 70Cu/30Zn showed similar corrosion rates - 3.3 mpy and 3.4 mpy, respectively. Potentiodynamic polarization curves indicate high cathodic activity

in the cases of silver 99.99% and commercial copper with no significant cathodic over-potential, due to the low activation energy for the hydrogen evolution on the cathodic surface. In the case of brass 70Cu/30Zn, sharp increase of the cathodic over-potential is observed at current densities between 10^{-5}-10^{-4}A/cm^2. This may be related to the formation of hydroxy-carbonated zinc compound such as $Zn_5(CO_3)_2(OH)_6$ on the cathodic surface, decreasing the electrical conductivity in the electrode-electrolyte boundary layer. In all the titanium alloys, a stable passivity is observed, with no breakdown potential and with no sensitivity to pitting corrosion in the potential tested range. This electrochemical passivity is demonstrated by the full immunity to the coral reef marine environment. Hastelloy C-276, Avesta 254, AISI-304 and AISI-316 stainless steels showed passive behavior, with passive transpassive transition. In the case of AISI-304 and AISI-316, high sensitivity to pitting and localizes corrosion attack is demonstrated by the cyclic potentiodynamic test. Highly improved passivation behavior is observed in the cases of Hastelloy C-276 and Avesta 254, with no sensitivity to pitting corrosion and with high breakdown potential of about 900mV. This behavior explains the negligible corrosion damage, recorded in these metals. Al-6061 showed a moderate corrosion rate of about 0.2 mpy. Potentiodynamic polarization measurement indicates metastable anodic passivation behavior followed by current oscillations between 10^{-4}-10^{-3}A/cm^2, and significant sensitivity to localized corrosion attack demonstrated by a clear hysteresis phenomenon. Cathodic polarization shows sharp over-potential due to concentration polarization and diffusion difficulties taking place in the interface electrode-electrolyte due to the formation of adhesive insolating layer of hydroxy/carbonate magnesium compounds, produced at the low cathodic potential.

Nobel values (–130 mV _ 120 mV) of OCP and $E_{CORROSION}$ were measured in the cases of Ti-2 and silver, as compared to active OCP values below –500 mV that were measured in the cases of Al-6061, galvanized steel, and mild steel ST-37. Based on pH-potential equilibrium Pourbaix diagram[32], the pH on the surface can be evaluated by using the measured OCP and the relevant diagram. Iso-potential extrapolation of the curves related to the hydrogen reduction reaction (line a in the diagram) leads to the theoretical pH which exist on the metal surface. OCP value of about –500mV vs. Ag/AgCl indicates local alkaline pH of about 12. This alkaline pH at the electrolyte-metal boundary layer reflects chemical calcification processes that take place on the exposed metal. Our evaluated pH values in the cases of Al-6061, galvanized steel, and mild steel ST-37 are in agreement with measured results described in the review by Hartt et al.[33].

As a result of anodic dissolution of Zn and Al, small amounts of hydrogen peroxide are produced through powerful reduction of dissolved oxygen in the interfacial boundary layer according to the following reaction: $O_2 + 2H^+ - 2e \rightarrow H_2O_2$. This process is typical of Al and Zn corroded in an oxygenated aqueous solution[30]. In addition to the high pH values, hydrogen peroxide acts as an effective oxidizing agent hampering the development of the fouling population. We suggest that this process took place both on the Al-6061 plate, which was moderately biofouled, and on the galvanized steel, which showed only slight biofouling.

The heavy fouling found on the passive metals Ti-2, T-7, T-12, Hastelloy C-276, AISI-304, AISI-316 and Avesta-254 is probably traceable to the electrochemically inert character of these surfaces, which precluded significant

changes in pH values. In coral reef ecosystems, where sessile organisms compete vigorously for settlement substrate[22], bio-colonists are quick to invade the empty surface presented by the passive metals.

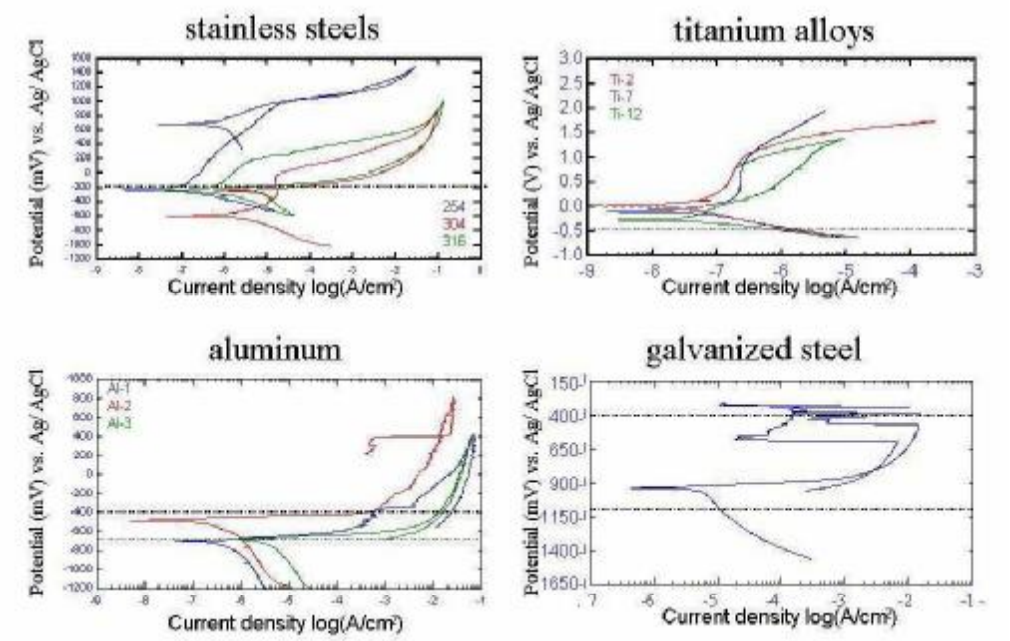

Fig. 4: Cyclic potentiodynamic polarization curves of examined metals. Scanning rate: 2mV/sec

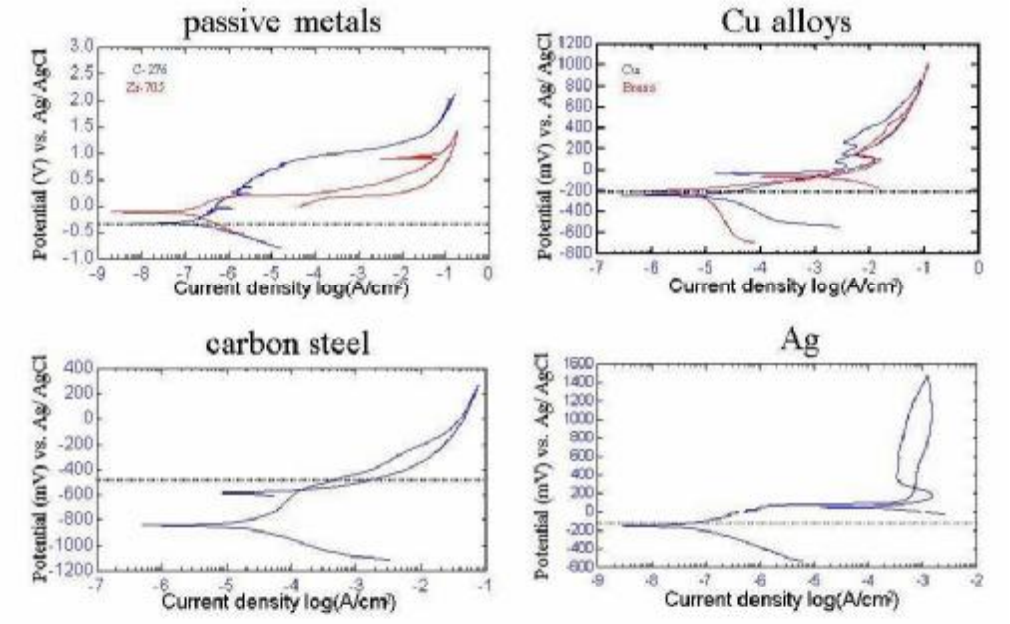

Fig. 5: Cyclic potentiodynamic polarization curves of examined metals. Scanning rate: 2mV/sec

4. Conclusions

1. Electrochemically passive metals in coral reef ecosystems are subjected to heavy settlement of marine bio-colonists, due to stable chemical and physical conditions.
2. Chemical calcification processes are accelerated by electrochemically active and metastable metals such as Al-6061 and galvanized steel, due to alkaline pH, developed on the metal-electrolyte boundary layer. This resulted in various hydroxy/carbonate compounds.
3. Hydrogen-peroxide formation on the surfaces of Al-6061 and galvanized steel inhibits the biofouling settlements, in the early stages of the exposure, when the active metal surface is exposed to the environment.

Acknowledgments

The authors wish to thank the staff of the H. Steinitz Marine Biology Laboratory, Eilat, for their field and technical support during this study. The research was partially supported by the Koret Foundation grant award, the Institute for Applied BioSciences, Ben-Gurion University of the Negev, Beer-Sheva, Israel; Dead Sea Bromine Group (DSBG), Beer-Sheva, Israel and The Israeli Federation for Underwater Activities.

Received April 20, 2007

Ben University of the Negev, Israel

REFERENCES

1. G.J. Brankovich, M.L.F. deMele, H.A. Videla, J. Mar. Tech. Soc. 24 (1991); p. 28-32.
2. J.P. Rilley, R. Chester, **Introduction to Marine Chemistry**, Academic Press, London, (1971).
3. F.L. LaQue, **Marine Corrosion; Causes and Prevention**, J. Willey & Sons, Inc., New York, (1975), p. 107.
4. W.H. Hilbertz, "*Electrodeposition of Minerals in Solution and its Enhancement by Biological Growth for Structural Applications*" **Sea Grant Report** No. 04-6-158-4111, University of Texas, (1976).
5. G.C. Cox, **Corrosion**, 6 (1950), p. 161-165.
6. G.I. Leob, R.A. Neihof, *In Applied Chemistry at Protein Interfaces*, **Advances in Chem.** Series 145, American Chem. Soc. Washington, DC, (1975); p. 319-335.
7. K.C. Marshall, **Interface in Microbial Ecology**, Harvard University Press, Cambridge, MA, (1976).
S.C. Dexter, **J. Coll. Interf. Sci.** 70 (1979); p. 346-354.

8. W.A. Corpe, *Microbial surface components involved in adsorption of microorganisms onto surfaces*. In Britton G, Marshall K.C. (eds) **Adsorption of Microorganisms to Surfaces**. John Willey, New York, (1980); p. 105-144.
9. M. Fletcher, M.J. Latham, J.M. Lynch, P.R. Rutter. "*The characteristics of interface and their role in microbial attachment*". In: Berkeley R, Lynch J, Rutter P, Vincent B (eds) **Microbial Adhesion to surfaces**. Ellis Horwood Ltd, Chichester, (1980); p. 67-78.
10. R.A. Buchananm A.L. Kovacs, C.D. Lundinm, K.K. Khan, J.C. Danko, P. Angell, S.C. Dexter, **Mater. Perform**. 36 (1997); p. 46-55.
11. D.H. Pope, D. Duquette, P. C. Wayner Jr., A. H. Johannes (eds) "**Microbially influenced corrosion: a state-of-the-art review**". 2nd edition, Nat. Assoc. Corr. Eng. (1984).
12. G. Salvago, G. Taccani, G. Fumagalli, "*Review of effects of biofilms on the probability of localized corrosion of stainless steels in seawater*". In: **Microbiologically Influenced Corrosion Testing** (eds. J.R. Kreans and B.J. Little), **American Society for Testing and Materials**, Philadelphia (1994); p. 70-95.
13. Al-Hashem, M. Salman, J. Carew, **Corrosion** 99 (1999); p. 25-30.
14. H.A. Videla, **Biodeterioration & biodegradation** 34 (1994). p. 254-257.
15. H.A. Videla, et. Al "*Corrosion and biofouling studies in brazilian offshore seawater injection systems*", **Corrosion** 89/191, NACE, Houston, TX.
16. I.R. Breger, J.A. Breger, **Applied and Environ. Microb.** 51 (1986); p. 1186-1198.
17. M.J. Franklin, D.C. White, H.S. Isaacs, **Corr. Sci.** 32 (1991). p. 945-952.
18. G. Subramanian, P. Chandrasekaran, M. Eashwar, S. Guruviah. **Bull. Electroch.** 6 (1990); p. 582-583.
19. B. Griffin, L.R. Cornwell, W. Seits, E. Estes. **Mater. Perform**. 28 (1989); p. 71-74.
20. M. Eashwar, G. Subramanian, P. Chandrasekaran, S.T. Manickam, S. Maruthamuthu, K. Balakrishnan, **Biofouling**, 8 (1995); p. 303-312.
21. S.C. Dexter. **Biofouling**, 7 (1993) p. 97-127.
22. P.A.Wagner, R.I. Ray,"*Surface analytical techniques for microbiologically influenced corrosion - a review*". In: **Microbiologically Influenced Corrosion Testing** (eds. J.R. Kreans and B.J. Little) American Society for testing and materials, Philadelphia. (1994): p. 153-169.
23. R.C. Fitzhardinge, J.H. Bailey-Brock, **Bull. Mar. Sci.** 44 (1989); p. 567-579.
24. D.H. Pope, T.P. Zintel, A.K. Kuruvilla and O.W. Siebert, "*Organic acid corrosion of carbon steel*". **Corrosion/88** (1988); p. 79.
25. D.H. Pope, T.P. Zintel, "**Methods for investigation of under-deposit microbiologically influenced corrosion**", **NACE paper** No 249, Presented at *CORROSION/88* St Louis, MO (1988).
26. S.C. Dexter, "*Laboratory solutions for studying corrosion of aluminum alloys in seawater*", In: **The use of synthetic environments for corrosion testing** (eds. P. Francis and T. Lee) (1988); p. 217-234.
27. J.E.G. Gonzalez, F.J.H. Santana, J.C. Mirza-Rosca, **Corr. Sci.** 40 (1998); p. 2141-2154.
28. **ASTM, G 5 –94** "Standard reference test method for making potentiostatic and potentiodynamic anodic polarization measurements", American Society for testing and materials, Philadelphia.
29. A. Neville, T. Hodgkiess, X. Destriau, **Corr. Science** 40 (1998); p. 715-730.
30. R. Vago, G. Pasternak, D. Itzhak, **Jornal Material Science Letters** 20 (2001); p. 1049.
31. M. Pourbaix, **Atlas of Elecerochemical Equilibria in Aqueous Solutions**. NACE International Cebelcor. Houston. (1974). p. 644.
32. W. H. Hartt, C. H. Culberson, S. W. Smith, **Corrosion**, 40 (1984); p. 609-618.

COMPORTAREA DIFERITELOR METALE ÎN MEDIUL DE CORALI DIN MAREA ROŞIE

Rezumat: Prezentul studiu se axează asupra comportamentului diferitelor metale în mediu marin de recif de corali. Au fost studiate 9 tipuri de eşantioane de metale şi aliaje: 3 tipuri de aliaje de titaniu (Ti-2, Ti-7, Ti-12), superaliajul Hastelloy tip C-276, 3 tipuri de oţel inoxidabil (AISI 304, AISI 316, Avesta 254), cupru comercial, alamă tip 70Cu/30Zn, oţel carbon obişnuit (DIN ST-37), oţel galvanizat, argint de puritate 99,99%, aliaj de duraluminiu tip 6061. Experimentele s-au desfăşurat într-o nişă special amenajată, la o adâncime de 6 m, în

recifful de corali existent la Eilat, Marea Rosie. Dupa 3 luni de expunere, pe esantioanele de cupru si alama nu s-a observat existenta unui biofilm superficial. Pe esantionul de argint s-a observat un strat neaderiv; pe celelalte esantioane a fost observat un stadiu incipient de organisme colonizate, precum alge, bryozoa, tunicate, viermi tubulari, corali calcarosi si hidrocorali. Pentru aliajele de titaniu si Hastelloy C-276, curbele de polarizare au indicat un comportament electrochimic de tip pasiv, prezentand rate neglijabile de coroziune. Odata cu intensificarea aderiunii biologice si dezvoltarea de colonii de organisme, pe suprafata tuturor esantioanelor metalice s-a constatat un comportament electrochimic de tip pasiv. Rata de coroziune inregistrata pentru otelul ST-37 a fost 0.5 mpy, prezentand o bio-depunere minima. Ratele de coroziune inregistrate au fost de 3.3, 3.4, 0.2, 0.3 si 0.6 mpy pentru cuprul comercial, alama 70Cu/30Zn, AISI 304, Al 6061 si respectiv otelul galvanizat. Pentru celelalte esantioane, coroziunea a fost neglijabila. Chiar daca pe otelul galvanizat si aliajul de duraluminiu 6061 au fost observate produse de coalifiere chimica, bio-depunerile au fost minime. Se pare ca aceasta se datoreaza conditiilor alcalinice, drept efect a reducerii electrochimice intensive a oxigenului dizolvat, care conduce la formarea de cantitati mici de peroxid de hidrogen pe suprafata metalica. Aceste conditii biocidice localizate, conduc la prevenirea dezvoltarii de bio-film si colonizari de organisme pe aceste metale.

BULETINUL INSTITUTULUI POLITEHNIC DIN IAŞI
Tomul LIII (LVII), Fasc. 4, 2007
Secţia
ŞTIINŢA ŞI INGINERIA MATERIALELOR

STUDY ON THE THERMAL EXPANSION AND ELASTIC PROPERTIES OF THE ELINVAR ALLOYS

BY

MIHAI LOZOVAN, VIOREL DOBREA, BACIU CONSTANTIN and MIHAIŢĂ PEPTĂNARIU

Abstract: The Elinvar-type alloy is very sensitive to the thermal treatments, but we observed that its thermal expansion coefficient is relatively constant in the temperature range 20-150°C, for all the thermal treatments that we subjected to it. The thermal treatmen. gives to investigate alloy a mechanical strength between 320 and 350 HV 0.5 and a value of the thermal expansion coefficient that makes it appropriate for complex metal-glass-ceramic seals. By combining the effects produced by the cold plastic deformation and temperature of thermal treatment, alloys with monitored thermal coefficient of the elastic modulus can be obtained. Some options for the application of the studied alloys are discussed.

Keywords: Elinvar, thermal expansion coefficient, thermal elastic coefficient.

1. Introduction

Guillaume found that the 32Ni12CrFe Invar alloy with Mn and Si additions present an elastic modulus that does not depend on the temperature [1]. He named this alloy Elinvar. Pilling and Talbot [2] discovered the alloy with constant elastic modulus that gets hardened by precipitation. This alloy has been named Elinvar with titanium and has a modified recipe, as compared to the classical Elinvar alloy, by Ti and Al additions. Studies on the phase structure, the influence of the thermal and mechanical treatment on magnetic and mechanical properties have already been reported [3-4].

2. Experimental procedure

The alloys are elaborated by melting and casting in an inductive furnace endowed with a crucible at a pressure of 0.133 N/m^2.

The ingots were forged as 12x12 mm^2 bars, which were annealed inside a furnace with hydrogen atmosphere for 10h at 1200°C and then cooled in water from this temperature.

This thermal treatment was meant to ensure the alloy homogenization, desulphuration and decarburation. We investigated the Elinvar alloy with Ti presenting the following composition: 42.05 %Ni; 5.61 %Cr; 2.5 % Ti; 1.12 %Mn; 0.71 %Si; 0.73 %Al and balance Fe [1].

The hardness was measured at the room temperature by means of the microhardness-testing machine MHT4 attached to an Olympus microscope.

2.1. Thermal expansion of Elinvar alloys

The influence of some thermal treatments on the thermal expansion of Elinvar alloy is studied.Prior to measurements the studied samples were subjected to the following thermal and mechanical treatments:

a) heat rolling;
b) heating at 1000°C for 1h + water quenching;
c) heating at 1000°C for 1h + water quenching + 5h at 500°C + air cooling;
d) heating at 1000°C for 1h + water quenching + 5h at 550°C+air cooling;
e) heating at 1000°C for 1h + water quenching + 5h at 600°C + air cooling;
f) heating at 1000°C for 1h water quenching + 4h at 675°C + air cooling.
The obtained results are presented in figures 1, 2 and 3

2.2 The thermal coefficient of the elastic modulus of Elinvar alloys

In order to restrict and control the errors introduced by the temperature variation of the elastic modulus, we conducted studies on an Elinvar alloy with titanium, concerning the influence of the cold plastic deformation and the temperature of the thermal treatment on the thermoelastic coefficient β. The material shaped as strips has been annealed at 1000°C and rapidly cooled within a furnace with argon atmosphere.

The thermal treatment ensures hardness smaller than 90-110 HV (hardness Vickers number), which enabled the cold rolling on a six-roller mill with the following degrees of section reductions: 15, 35, 51 and 73% respectively [5].

From the cold rolled strips, samples of 150x5mm have been taken. These have been subjected to annealing thermal treatment (4h) at different temperatures (200, 350, 450, 550, 650°C) in a furnace with argon atmosphere.

The obtained results are presented in figures 4 and 5

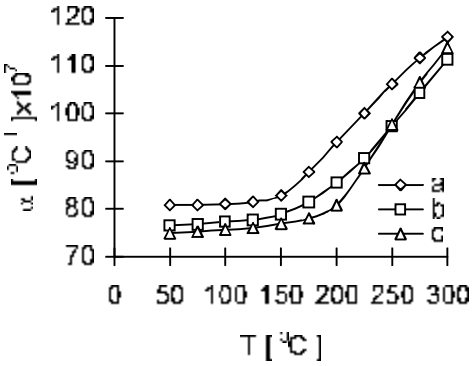

Fig. 1 The temperature dependence of thermal expansion of Elinvar alloy after a, b, c, thermal treatments.

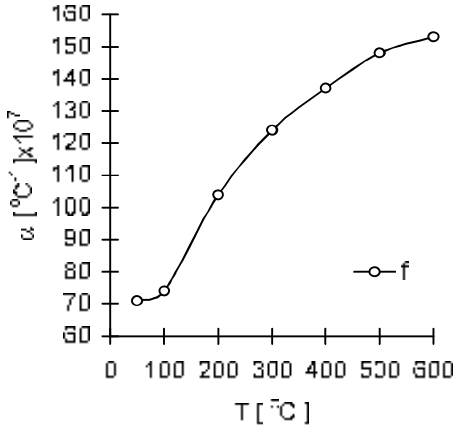

Fig. 2. The temperature dependence of thermal expansion of Elinvar alloy after f thermal treatment.

The elastic modulus has been measured using the method of sinusoidal oscillations of a sample suspended with two thin wires made of Ni-Cr alloy within a furnace with air heating. The dependence of the thermal coefficient of the elastic modulus of the Elinvar alloy with titanium, on the temperature of treatment and on the degree of cold plastic deformation is presented in Fig. 3 and Fig. 4 respectively.

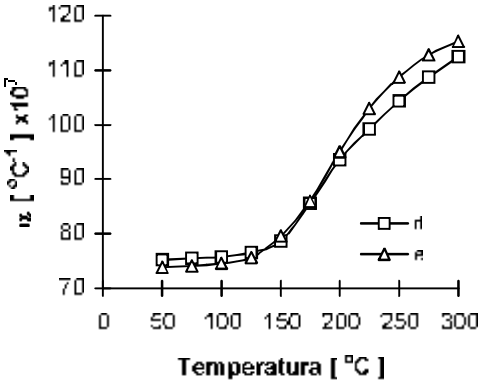

Fig. 3. The temperature dependence of thermal expansion of Elinvar alloy after d and e thermal treatments

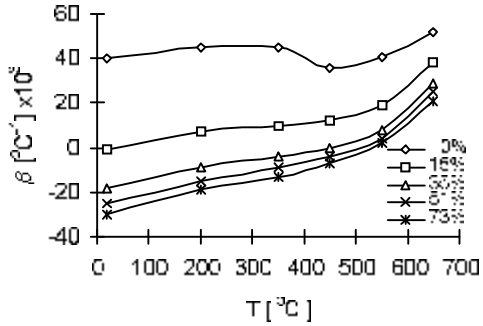

Fig. 4. The dependence of the thermal coefficient of the elastic modulus of the Elinvar alloy with titanium, on the temperature of treatment and the degree of cold plastic deformation.

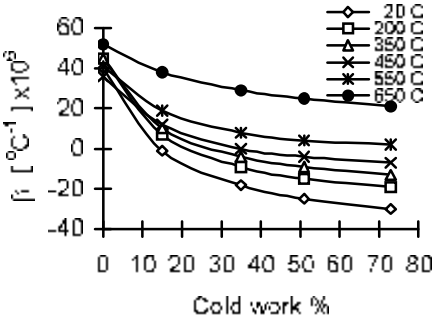

Fig.5. The dependence of the thermal coefficient of the elastic modulus of the Elinvar alloy with titanium, on the degree of cold plastic deformation and the temperature of treatment.

4. Conclusions

The analyses of the obtained results lead to the following conclusions:

The thermal treatment (f) gives to investigate alloy a mechanical strength between 320 and 350 HV 0.5 and a small value of the thermal expansion coefficient, which makes it appropriate for complex metal-glass-ceramic seals.

By combining the effects produced by the cold plastic deformation and the temperature of thermal treatment, alloys with monitored β can be obtained.

Received March 31, 2007 *National Institute of R & D for Technical Physics Iaşi*

REFERENCES

1. C. T. Guillaume, **Proc. Phys. Soc.** (London). **32,** 1920, **374**
2. A. M. Pilling, N. B. Talbot, *Age Hardening of Metals*, **Am. Soc. Metals, Cleveland**, 1940. **231**
3. T. J. Hayes, A. P. Miodownik, **Phys. Stat. Sol. (a), 10,** 1973, **K 43**

4. M. Lozovan, H. Chiriac, **Bul. Inst. Polit. Iasi, Tom XL (XLIV)**, 1994, **471**
5. C. Chiriac, M. Lozovan & al., **Bul. Inst. Polit. Iasi, Tom XLIII (XLVII), Fasc. 1-2, Sectia IX**, 1997, **115**

STUDIU ASUPRA DILATĂRII TERMICE ŞI A PROPRIETĂŢILOR ELASTICE ALE ALIAJELOR ELINVAR

Rezumat: Lucrarea prezintă unele rezultate privind influenţa tratamentelor termice asupra dilatarii termice si asupra coeficientului termic al modulului de elasticitate al aliajelor Elinvar cu titan. Tratamente termice adecvate conduc la aplicatii specifice acestor aliaje in treceri metal-sticlă-ceramică sau elemente elastice pentru traductoare de presiune.

BULETINUL INSTITUTULUI POLITEHNIC DIN IAŞI
Tomul LIII (LVII), Fasc. 4, 2007
Secţia
ŞTIINŢA ŞI INGINERIA MATERIALELOR

MODELS OF INFORMATION ASYMMETRIES

BY

MIHAELA LOZOVAN

Abstract: The subject of corporate dividend policy has captivated economists for a long time, resulting in intensive theoretical modeling and empirical examinations. A number of conflicting theoretical models lacking strong empirical support define current attempts to explain the puzzling reality of corporate dividend behavior. The purpose of this paper is to examine the academic efforts to model dividend policy analysing the he recent theories called models of information asymmetries..

Keywords: dividend policy, dividend theory, signaling model, agency cost, cash flow

1. Introduction

Corporate dividend policy has captured the interest of economists of this century and over the last five decades has been the subject of intensive theoretical modeling and empirical examination. Initial forays into theorizing corporate dividend policy are divided as to their prediction of the dividend payment's effect on share price. Over the last century, three schools of thought have emerged. One faction sees dividends as attractive and as a positive influence on stock price. A second bloc believes that stock prices are negatively correlated with dividend payout levels. The third group of theories maintains that firm dividend policy is irrelevant in stock price valuation.

2. Full information models - the tax factor

Tax-adjusted models surmise that investors require and secure higher expected returns on shares of dividend-paying stocks. The imposition of a tax liability on dividends causes the dividend payment to be grossed up to increase the shareholder's pre-tax return. Under capital asset pricing theory, investors offer a lower price for the shares because of the future tax liability of the dividend payment. One consequence of the tax-adjusted model is the division of investors into dividend tax clienteles, an argument first proposed in the seminal work of Miller and Modigliani (1961). In later research, Modigliani (1982) finds that the clientele effect is responsible for only nominal alterations in portfolio composition rather than the major differences predicted by Miller (1977).

Masulis and Trueman (1988) propose model cash dividend payments as products of deferred dividend costs. Their model predicts that investors with differing tax liabilities will not be uniform in their ideal firm investment/dividend policy. As the

tax liability on dividends increases (decreases), the dividend payment decreases (increases) while earnings reinvestment increases (decreases).

Differences are minimized by segregation of investors into clienteles. The model developed by Farrar and Selwyn (1967) assumes that investors maximize after-tax income. In a partial equilibrium framework, investors have two choices. Individuals choose the amount of personal and corporate leverage and also whether to receive corporate distributions as dividends or capital gains. This model contends that no dividends should be paid; rather, that share repurchase should be used to distribute corporate earnings.

The Farrar and Selwyn (1967) model is extended into a general equilibrium framework by Brennan (1970). In this setting, investors maximize their expected utility of wealth. Although the model is more robust, the predictions are similar to those of the Farrar and Selwyn model; an equilibrium with dividend-paying firms is not consistent with a zero required return per unit of dividend yield. Auerbach (1979a) develops a discrete-time, infinite-horizon model in which shareholders (as opposed to firm market value) maximize their wealth. If a capital gains/dividends tax differential exists, wealth maximization no longer implies firm market value maximization.

Subsequently, Auerbach (1979b) posits that dividend distributions occur because of the consistent, long-term undervaluation of corporate capital. The undervaluation is the result of a dynamic process encompassing multiple periods of total reinvestment of all firm profits followed by firm returns less than the returns expected by investors.

3. Signaling models

The market imperfection of asymmetric information is the basis for three distinct efforts to explain corporate dividend policy. The mitigation of the information asymmetries between managers and owners via unexpected changes in dividend policy is the cornerstone of dividend signaling models. Agency cost theory uses dividend policy to better align the interests of shareholders and corporate managers. The free cash flow hypothesis is an ad hoc combination of the signaling and agency costs paradigms; the payment of dividends can decrease the level of funds available for perquisite consumption by corporate managers.

Akerlof's (1970) model [1] of the used car market as a pooling equilibrium in the absence of signaling activities illuminates the costs of information asymmetries. The generalization of Akerlof's model by Spence (1973, 1974) became the prototype for all financial models of signaling. The model defines a unique and specific signaling equilibrium in which a job seeker signals his/her quality to a prospective employer. Although the scenario is developed using the employment market, Spence contends that extension to a limited number of other settings (admissions procedures, promotions, and credit applications) is possible.

Bhattacharya (1979, 1980), Talmor (1981), Hakansson (1982), John and Williams (1985), Miller and Rock (1985), Bar-Yosef and Huffman (1986), Makhija and Thompson (1986), Ambarish, John and Williams (1987), Ofer and Thakor (1987), Kumar (1988), Kale and Noe (1990), Rodriguez (1992), and many others offer signaling models of corporate dividend policy. The proponents of signaling theories

believe that a corporate dividend policy used as a means of putting the message of quality across has a lower cost than other alternatives. The use of dividends as signals implies that alternative methods of signaling are not perfect substitutes (Asquith and Mullins, 1986) [2].

4. Agency cost

The recognition of potential agency costs associated with the separation of management and ownership is not new; differences in managerial and shareholder priorities have been recognized for more than three centuries. Adam Smith (1937) adjudged the management of early joint stock companies to be negligent in many of their activities. These problems were especially prevalent in the British East Indies Company and attempts to monitor managers were largely unsuccessful because of inefficiencies and costs associated with shareholder monitoring (Kindleberger, 1984). Scott (1912) and Carlos (1992) question these assertions, while control and organization were less than ideal, the continued success and long life of the corporation imply generally sound managerial practices. Although some fraud no doubt existed, the majority of managerial activities coincided with shareholder desires

Modern agency theory seeks to explain corporate capital structure as the result of attempts to minimize the costs associated with the separation of corporate ownership and control. Agency costs are lower in firms with high managerial ownership stakes because of the better alignment of shareholder and manager goals (Jensen and Meckling, 1976) and in firms with large block shareholders that are better able to monitor managerial activities (Shleifer and Vishney, 1986). Agency problems result from information asymmetries, potential wealth transfers from bondholders to stockholders through the acceptance of high-risk and high-return projects by managers, and failure to accept positive net present value projects and perquisite consumption in excess of the level consumed by prudent corporate managers (Barnea, Haugen, and Senbet, 1981) [3].

Dividend policy influences these relations in two ways. Fama and Jensen (1983) [4] espouse that potential shareholder and bondholder conflicts can be mitigated by covenants governing claim priority. These orderings can be circumvented by large dividend payments to stockholders. Debt covenants to minimize dividend payments are necessary to prevent bondholder wealth transfers to shareholders (John and Kalay, 1982). Although potentially substantial in precipitation of agency costs, its dividend policy is not a major source of bondholder wealth expropriation. In firms where dividend payouts are limited by bondholder covenants, dividend payout levels are still below the maximum level allowed by the constraints (Kalay, 1982) [5].

The second way dividend policy affects agency costs is the reduction of these costs through increased monitoring by capital markets. Large dividend payments reduce funds available for perquisite consumption and investment opportunities and require managers to seek financing in capital markets. The efficient monitoring of capital markets reduces less than optimal investment activity and excess perquisite consumption and hence reduces the costs associated with ownership and control separation (Easterbrook, 1984).

5. The free cash flow hypothesis

Prudent managers working in the shareholders best interests should invest in all profitable opportunities. Management and owner separation affords corporate managers the temptation, however, to consume or otherwise waste surplus funds. The inefficient use of funds in excess of profitable investment opportunities by management was first recognized by Berle and Means (1932). Jensen's (1986) free cash flow hypothesis updated this assertion, combining market information asymmetries with agency theory. The funds remaining after financing all positive net present value projects cause conflicts of interest between managers and shareholders. Dividend and debt interest payments decrease the free cash flow available to managers to invest in marginal net present value projects and manager perquisite consumption.

6. Conclusions

The combination of agency and signaling theory should better explain dividend policy than either theory alone, but the free cash flow hypothesis does a better job of rationalizing the corporate takeover frenzy of the 1980's (Myers, 1987 and 1990) than it does of providing a comprehensive and observable dividend policy.

Received April 14 2007 *"Al. I. Cuza" University of Iassy*

REFERENCES

1. Akerlof George, 1970. *The Market for 'Lemons', Quality Uncertainty and the Market Mechanism,* **The Quarterly Journal of Economics, 84, 488-500**.

2. Asquith Paul and David W. Mullins, Jr., 1983. *The Impact of Initiating Dividend Payments on Shareholders' Wealth*, **The Journal of Business, 56, 77-96**.

3. Barnea Amir, Robert A. Haugen and Lemma W. Senbet, 1981, *Market Imperfections, Agency Problems, and Capital Structure: A Review*, **Financial Management, Vol. 10, no. 3, 7-22.**

4. Fama Eugene F., 1974. *The Empirical Relationships Between the Dividend and Investment Decisions of Firms,* **The American Economic Review, 64, 304-318.**

5. Kalay Avner, 1980, Signaling, *Information Content, and the Reluctance to Cut Dividends,* **Journal of Financial and Quantitative Analysis, 15, 855-869.**

MODELE ALE ASIMETRIEI INFORMAȚIONALE

Rezumat: Subiectul politicii de dividend a preocupat economiștii pentru foarte mult timp, drept urmare rezultând multe modele teoretice și experimente empirice. Un număr destul de mare de modele reprezentând teorii ale politicii de dividend, fără a avea un suport teoretic, au încercat să delineeze realitatea puzzle-ului referitor la comportamentul corporațiilor în ceea ce privește politica de dividend. Scopul acestei lucrări este acela de a examina noile modele ale politicii de dividend, analizând cele mai recente teorii denumite "modele ale asimetriei informaționale".

BULETINUL INSTITUTULUI POLITEHNIC DIN IAŞI
Tomul LIII (LVII), Fasc. 4, 2007
Secţia
ŞTIINŢA ŞI INGINERIA MATERIALELOR

FIRM'S OPTIMAL CAPITAL STRUCTURE DECISION

BY

MIHAELA LOZOVAN

Abstract: In this paper, I discuss factors that affect a firm's capital structure, and I look at the genesis of the concept of using debt to control managers and to reconcile this thinking with the need to survive in the competitive environments of today.

Keywords: capital structure, leverage, business risk, tax position, managerial attitude

1. Introduction

Firms can choose whatever mix of debt and equity they desire to finance their assets, subject to the willingness of investors to provide such funds. And, as we shall see, there exist many different mixes of debt and equity, or capital structures - in some firms, such as Chrysler Corporation in USA , debt accounts for more than 70 percent of the financing, while other firms, such as Microsoft, have little or no debt.

An optimal capital structure is a critical decision for any business organization. The decision is important not only because of the need to maximize returns to various organizational constituencies, but also because of the impact such a decision has on an organization's ability to deal with its competitive environment.

2. The Target of a Firm : Optimal Capital Structure

The prevailing argument, originally developed by *Modigliani and Miller* (1958) [1], is that an optimal capital structure exists which balances the risk of bankruptcy with the tax savings of debt. Once established, this capital structure should provide greater returns to stockholders than they would receive from an all-equity firm.

Despite its theoretical appeal, researchers in financial management have not found the optimal capital structure. The best that academics and practitioners have been able to achieve are prescriptions that satisfies short-term goals. For example, in a recent Harvard Business Review article, readers were left with the impression that the use of leverage was one way to improve the performance of an organization [2]. While this can be true in some circumstances, it fails to consider either the complexities of the competitive environment, or the long-term survival needs of the organization.

The use of leverage either to discipline managers or to achieve economic gain is the 'easy way out', and, in many instances, can lead to the demise of the organization. The fact that an optimal capital structure has not been found is an indication of some flaw in the logic. We believe that the original question was framed incorrectly. Rather than: What is an optimal mix of debt and equity that will maximize shareholder wealth;

it should have been: Under what circumstances should leverage be used to maximize shareholder wealth? Why? Because debt and equity have profound long-term implications for corporate governance that far exceed the exigencies of the moment.

Determining the exact optimal capital structure is not a science, so after analyzing a number of factors, a firm establishes a target capital structure it believes is optimal, which is then used as a guide for raising funds in the future. This target might change over time as conditions vary, but at any given moment the firm's management has a specific capital structure in mind, and individual financing decisions should be consistent with this target. If the actual proportion of debt is below the target level, new funds will probably be raised by issuing debt, whereas if the proportion of debt is above the target, stock will probably be sold to bring the firm back in line with the target debt/assets ratio.

Capital structure policy involves a trade-off between risk and return. Using more debt raises the riskiness of the firm's earnings stream, but a higher proportion of debt generally leads to a higher expected rate of return; and, we know that the higher risk associated with greater debt tends to lower the stock's price. At the same time, however, the higher expected rate of return makes the stock more attractive to investors, which, in turn, ultimately increases the stock's price. Therefore, the optimal capital structure is the one that strikes a balance between risk and return to achieve our ultimate goal of maximizing the price of the stock.

Four primary factors influence capital structure decisions:

1. *The first is the firm's business risk,* or the riskiness that would be inherent in the firm's operations if it used no debt. The greater the firm's business risk, the lower the amount of debt that is optimal.
2. *The second key factor is the firm's tax position.* A major reason for using debt is that interest is tax deductible, which lowers the effective cost of debt. However, if much of a firm's income is already sheltered from taxes by accelerated depreciation or tax loss carry forwards, its tax rate will be low, and debt will not be as advantageous as it would be to a firm with a higher effective tax rate.
3. *The third important consideration is financial flexibility, or the ability to raise capital on reasonable terms under adverse conditions.* Corporate treasurers know that a steady supply of capital is necessary for stable operations, which, in turn, are vital for long-run success. They also know that when money is tight in the economy, or when a firm is experiencing operating difficulties, a strong balance sheet is needed to obtain funds from suppliers of capital. Thus, it might be advantageous to issue equity to strengthen the firm's capital base and financial stability.
4. *The fourth debt-determining factor has to do with managerial attitude* (conservatism or aggressiveness) with regard to borrowing. Some managers are more aggressive than others; hence some firms are more inclined to use debt in an effort to boost profits. This factor does not affect the optimal, or value- maximizing, capital structure, but it does influence the target capital structure a firm actually establishes.

3. Agency Theory

One of the defining characteristics of business in the 1990s was the adoption of prescriptions from agency theory to address the managerial excesses of the 1970's and

1980's. The classic agency theory concept was developed by *Berle and Means* (1932) [3]. They observed that ownership and control had become separated in larger corporations as a result of the dilution in equity positions. This situation provided an opportunity for professional managers, as those in control, to act in their own best interest. Today, the central issue for agency theory is how to resolve the conflict between owners and managers over the control of corporate resources through the use of contracts which seek to allocate decision rights and incentives.

Managers have a number of incentives to pursue growth-oriented strategic options. The larger the organization, the greater the economic and political power of the top management teams, and the greater the ability of the organization to marshal resources necessary to deal effectively with its competitive and social environment. Also, larger organizations are seen as being able to maintain their freedom from the discipline of the capital markets. As a generalization, it can be said that growth does lead to increasing the wealth of shareholders. However, the concern is that too many of the activities associated with increasing the size of organizations are motivated not by a desire for maximizing shareholder wealth, but by opportunities for the self-aggrandizement of management.

The contractual device suggested by agency theory to accomplish the transfer of wealth from the organization to the investors is debt creation. Debt provides a means of bonding manager's promises to pay out future cash flows. It also provides the means for controlling opportunistic behavior by reducing the cash flow available for discretionary spending. Top managers` attention is then clearly focused on those activities necessary to ensure that debt payments are made. Companies failing to make interest and principal payments can be declared insolvent and can be dissolved. This use of debt as a disciplinary tool makes survival in the short-term the central issue for all concerned.

Agency theory also has important implications for the relationship between stockholders and debt-holders. Stockholders are interested in the return over and above that amount which is required to repay debt. Debt-holders are only interested in the debt payment specified in the contract. Stockholders are seen as sometimes being interested in pursuing riskier business activities than debt-holders would prefer. When this occurs debt-holders may charge higher prices for debt capital and institute greater control measures to prevent top managers from investing capital in riskier undertakings.

However, agency theory does not take into consideration competitive environments, nor does it consider the necessity for managers to make choices beyond a stockholder wealth-maximizing perspective. This would seem to be a serious omission for two reasons. First, debt and equity represent different constituencies with their own competing, and often mutually exclusive, goals. Second, as the level of debt increases, the corporate governance structure can change from one of internal control to one of external control.

For firms that adopt debt as a control mechanism, lenders become the key constituents in the corporate governance structure. This can have a significant impact on both managerial discretion, and on the ability of an organization to deal effectively with its competitive environment.

4. Conclusions

These four points largely determine the target: capital structure, but, as we shall see, operating conditions can cause the actual capital structure to vary from the target at any given time.

The results of this study should be seen as a serious challenge to the traditional capital structure literature. We discover that the first duty of managers is to ensure the long-term survival of the organization within its competitive environment. In a world devoted to quick fixes, and short-term thinking edited by sound bites, it is difficult to take time to think through serious challenges. As environments become more competitive, those who make the time to reach appropriate decisions will be the ones left standing.

Received April 14, 2007 *"Al. I. Cuza" University of Iassy*

REFERENCES

1. Modigliani, F. and M. H. Miller, *The cost of capital, corporate finance and the theory of investment*, **American Economic Review, Vol. 48,** 1958, **261-297;**
2. Champion, D, *Finance: The joy of leverage*. **Harvard Business Review,** Vol.77 No.4. 1999. 19-22;
3. Berle, A. A. Jr. and G. C. Means, **The Modern Corporation and Private Property.** William S. Hein & Co.. Buffalo. 1982. 396

DECIZIILE FIRMEI PENTRU REALIZAREA UNEI STRUCTURI FINANCIARE OPTIME

Rezumat: În această lucrare se prezintă factorii care afectează structura capitalului firmei şi se analizează geneza conceptului referitor la folosirea datoriilor pentru a controla managerii, ţinându-se cont şi de necesitatea supravieţuirii întreprinderii în turbulentul mediu competitiv actual.

BULETINUL INSTITUTULUI POLITEHNIC DIN IAŞI
Tomul L(III (LVII), Fasc. 4, 2007
Secţia
ŞTIINŢA ŞI INGINERIA MATERIALELOR

THE INCREASING DIESEL ENGINE CON ROD BEARINGS RELIABILITY BY USING PVD (PHYSICAL VAPOUR DEPOSITION) PROCESS

BY

FLORIN MARIAŞIU

Abstract: In the last years the development of Diesel engines injection equipment, especially in direction of inceasing injection pressure's and effective pressure's (to obtained better thermodynamic conditions in burn process to reduce the level of the noxes) has raised new problems in the desing of the Diesel engines components. The engine components must achieve a lightweigt construction, more compact design and an increasing reliability in use. However the goal to design and realise the Diesel engine's components using ecological materials it's an .he same level of importance (in compliance with present EU regulation). The experiments done with AlSn20Cu overlay con rod bearings (using the PVD process) achieve the proposed goals by a higher reliability in use trough increasing the specific load-bearing capacity of up to 100 MPa.

Keywords: Physical Vapour Deposition, con rod bearing, reliability, Diesel engine.

1. Technologically aspects

The PVD technology was developed and proposed to use in automotive industry in years of 1980 by KS Gleitlager GmbH, but the first effective apllication for mass production was realized in 1989 on Volkwagen Corrado [1]. In the present more and more important producers from automotive industry (Audi, Volkwagen, Daimler-Crysler, BMW etc.) using different components manufactured trough PVD technology. Because of the costs, the apllication of PVD technology to the comercial autovehicles was neglicted, but the new developments and researches in the this field of interest make possible to aplly this technology with relative lower costs

Generally the in the PVD technologically process the atoms are broken out of a specific coating material under ultra vaccumatic conditions with aid of accelerated argon ions, these subsequently depositing uniformly onto the bearing shell (figure1). A gain by using this process is that the deposited layer has a very fine an most important, a uniform distribution of tin [2]

In this experiment ware used the two tipes of con rod bearings: the "traditional" con rod bearings (three-metal plain bearing with PbSn10Cu2 layer); the new type of con rod bearings (plain bearings with AlSn20Cu layer).

The differences between those two type of bearing (thickness and composition of layers) are presented in figure 2 and figure 3.

2. Experimental results

The present paper show the obtained experimental results by using of physical vapour deposition con rod bearings cover an mounted in an Mercedes Benz OM501LA engine (235 kW) in corellation of the goal to increase the reability.

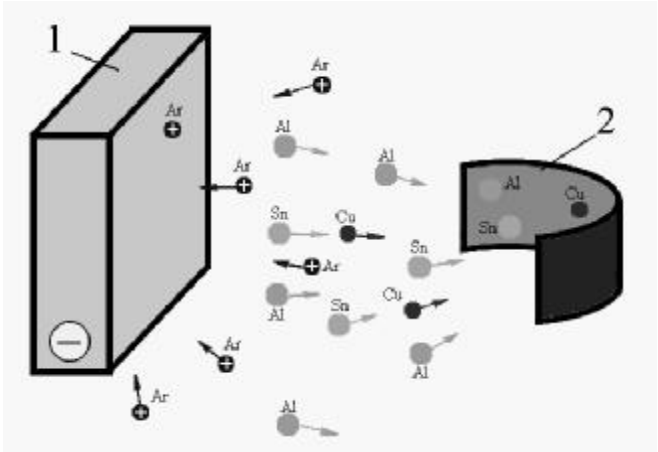

Fig.1. Physical Vapour Deposition process principle (1- target; 2- con rod bearing)

This experiment was possible by the Mantrans SRL firma involvment, which accepted the engine modification and the use of this engine in normal transport conditons

To realize of a better comparision between the "traditional" con rod bearings and those they are transformed trough the physical vapour deposition technology, the both types of con rod bearings was mounted in equal number (3+3) on the same engine (figure 4).

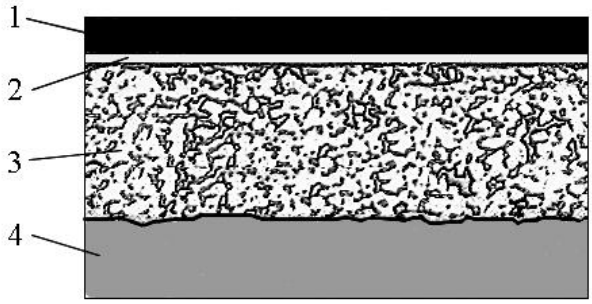

Fig.2. Thickness and composition of PbSn10Cu2 con rod bearing layer (1-running layer PbSn10Cu2; 2- adhesive layer; 3-sliding layer CuPb24Sn4; 4-steel back)

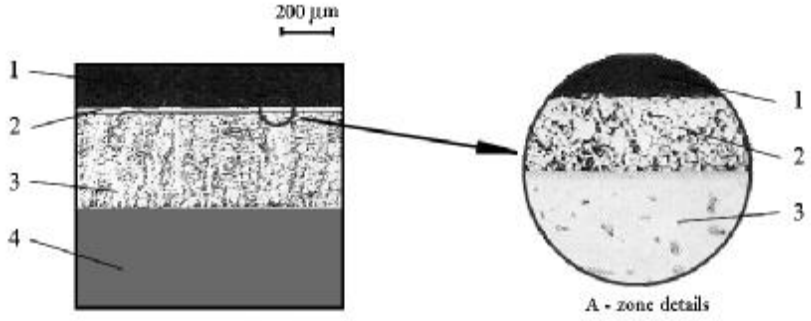

Fig 3. Thickness and composition of PVD con rod bearing layer (1-running layer AlSn20Cu; 2- adhesive layer Ni; 3-sliding layer CuPb24Sn4; 4-steel back)

The measurements was realisated along the way of 40.000 kilometers, without an exactly putting in order of measurement period (the vehicle was used every day in intern and international good transport).

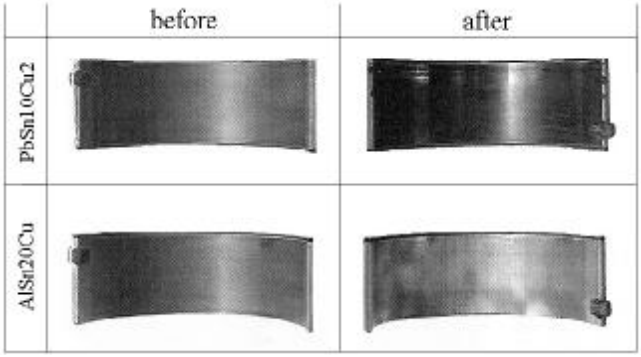

Fig.4. The conrod bearings used in experiment (foto)

The obtained datas that looking the wear speed of con rod bearings are presented in figure 5.

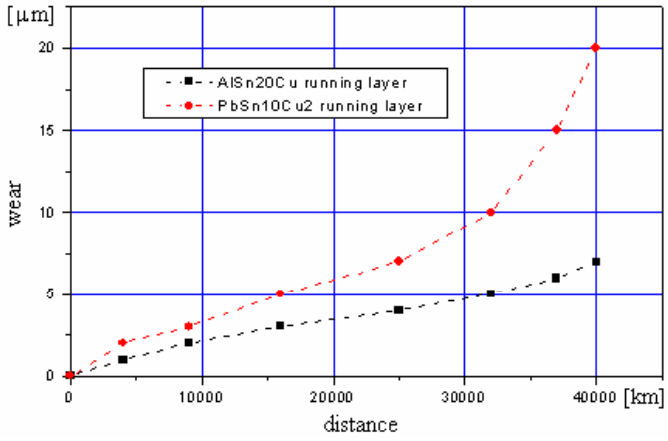

Fig.5. The wear speed of con rod bearings

3. Conclusions

By obtained data's interpretation along the way of the experiment it can note the folowing:

- the shape of wearing speed curve it is linear for PVD coating con rod bearings (that represented the fact that this type of con rod bearings support better a higher load capacity) and the wearing speed curve show that the reability of three-metal plain bearing with PbSn10Cu2 layer is going down in time (under the action of the same load capacity);
- the differencess between the wearing speed of the con rod bearing lead to increasing of corective and preventive maintenace period (approx. 60%, at 40.000km), with directly influences over the transport costs;
- the PVD technology can open new opportunities to study the use of different materials as running layer to be an ecological alternative at present lead-manufactured engine (and automotive) componets;

- the PVD technology can be succesfully applied even in the Diesel engine construction for heavy duty trucks (in mass production);
- on the future will be achieve new researces by influences of PVD technology apllications over the other engine components, injection pumps componets etc.

Received April 11, 2007 *Technical University of Cluj-Napoca*

REFERENCES

1. Müller, Manfred, **Moderne Motore benötigen Gleitlager aus modernen Werkstoffen" in "Werkstoffe im Automobilbau**, ISSN 0024-8525, Viewveg Publishing House , 1998.
2. ***, www.pvd-coating co.uk

CREŞTEREA FIABILITĂŢII CUZINEŢILOR UNUI MOTOR DIESEL PRIN APLICAREA TEHNOLOGIEI PVD

Rezumat: În ultimii ani dezvoltarea echipamentelor de injecţie ale motoarelor cu aprindere prin comprimare (Diesel) în direcţia creşterii presiunii de injecţie (pentru o se obţine mai bune condiţii termodinamice ale procesului de ardere în vederea reducerii nivelului de noxe emise) a ridicat probleme în proiectarea si construcţia componentelor motorului. Acestea trebuie sa aibă o construcţie uşoară, compactă şi o fiabilitate crescută. Pe lângă aceste deziderate nu sunt neglijate şi cerinţele europene referitoare la utilizarea materialelor ecologice în construcţia motoarelor. Lucrarea prezintă posibilitatea satisfacerii cerinţelor enumerate anterior prin utilizarea în construcţia motorului cu aprindere prin comprimare a cuzineţilor acoperiţi cu un strat de alaj AlSn20Cu prin procesul PVD.

BULETINUL INSTITUTULUI POLITEHNIC DIN IAŞI
Tomul LIII (LVII), Fasc. 4, 2007
Secţia
ŞTIINŢA ŞI INGINERIA MATERIALELOR

THEORETICAL STUDIES ON ELUTRIATION OF PARTICLES FROM FLUIDIZED BEDS

BY

ALINA ADRIANA MINEA

Abstract: When a fluid is pumped upward through a bed of fine solid particles a. a very low flow rate the fluid percolates through the void spaces without disturbing he bed. This is a fixed bed process. If the upward flow rate is very large the bed mobilizes pneumatically and may be swept out of the process vessel. At an intermediate flow rate the bed expands and is in what we call an expanded state. In the fixed bed the particles are in direct contact with each other, supporting each other's weight. In the expanded bed the particles have a mean free distance between particles and the particles are supported by the drag force of the fluid. The expanded bed has some of the properties of a fluid and is also called a fluidized bed. The uses for fluidized beds are limited to our imaginations. Typical uses include: reactors, heat exchange, drying operations, coating, solidification, growth of particles, adsorption, bio fluidization and many others. The performances improvement of heating equipment must be correlated with energy consumption which mainly is reflected in blank production price. Increasing of heat transfer and physical-mathematical simulation of heat process takes to the necessity of re-designing the work chamber by taking into account the constructive-functional particularities of the equipment. As it is stated, generally for heat treatment is recommended electric furnaces. The fluidized bed furnaces are still very few known and heat process is difficult to control.

Keywords: elutriation, fluidized bed, heat transfer

1. Introduction

Elutriation is the process in which fine particles are carried out of a fluidized bed due to the fluid flow rate passing through the bed. Typically, fine particles are elutriated out of a bed when the superficial velocity through the bed exceeds the terminal velocity of the fines in the bed. However, elutriation can also occur at slower velocities

Fine particles are present in fluidized beds from several sources:

- Feed streams
- Mechanical attrition or breakage of larger particles
- Temperature stress cracking
- Size reduction due to chemical reactions, shrinkage, etc.

When fines elutriation is a significant problem and modifications to the bed design cannot aid in reducing the problem, fines can often be recovered such as with cyclones or hydrocyclones.

Leva measured the rate of elutriation (total mass per time) from a bed of particles with a bimodal size distribution. He found that:

(1) When the column height above the bed is small, the elutriation rate is high. But if the height exceeds a certain minimum size then the rate is a constant minimum value (Figure 1).

This occurs because small particles that are expelled from the top of the bed have high

velocities and they require greater distance to slow down and turn around to return to the bed. (2) The elutriation process causes a decrease in particle concentration. The concentrations may be empirically modeled by an Arrhenius type expression as:

$$C = C_0 e^{-Mt} \quad (1)$$

where C = concentration at time, t; Co is the initial concentration; and M is an empirical constant.

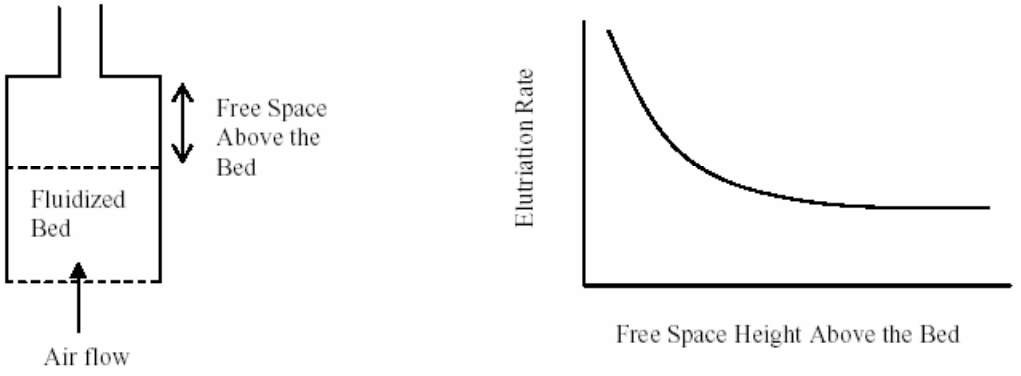

Figure 1. Elutriation Rate (total mass/time) vs the free space height above the bed. A fluidized bed behaves similar to a mixture of liquids with different volatilities. In the liquid-liquid mixture, the more volatile material leaves the mixture at the lower boiling temperature.

By analogy with boiling of liquid mixtures, finer particles have a lower boiling temperature than larger particles. The boiling temperature is analogous to the fluidization velocity. The higher the velocity, the greater the rate at which the low boilers will leave the bed. The free space height above the bed serves as a condenser, to cool and slow down the elutriated particles and return them to the mixture. The greater the boiling rate, the greater capacity that is needed of the condenser, hence the greater free space height.

Not all elutriation bad. Sometimes elutriation can be helpful. For example, elutriation may be used to remove dusts or very fine particles from coarser particles.

Definition of Terms

Lets define some terms that we can use to describe the elutriation process.

The flux of solids carried out of the top of the column is called entrainment, G_s.

The bulk density of the solids in the exiting gas stream is called the holdup, ρ^0.

We note that the entrainment is related to the holdup and the superficial velocity by

$$G_s = \rho^0 V_0 \quad (2)$$

Free Board Height, *Hf*, is defined to be the measure of the free space above the boundary between the dense phase and the lean phase (Figure 3).

For design, we need to know the rate of entrainment and the size distribution of the entrained particles in relation to the size of the particles in the bed. A fluidized bed usually has two regions or phases: dense bubbling phase and lean dispersed phase (Figure 2).

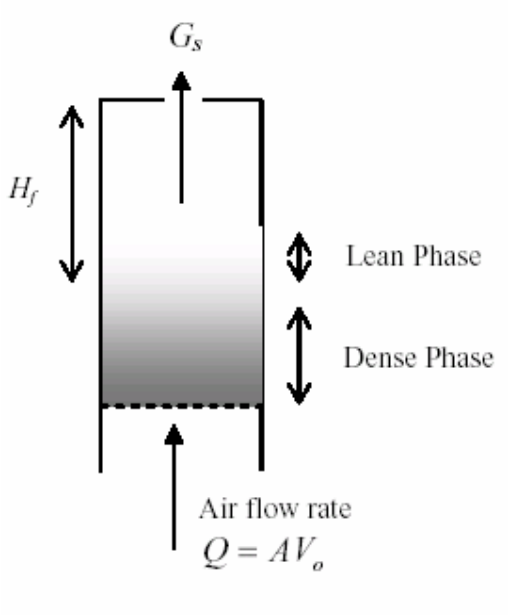

Figure 2. Fluidized bed with flux rate Gs.

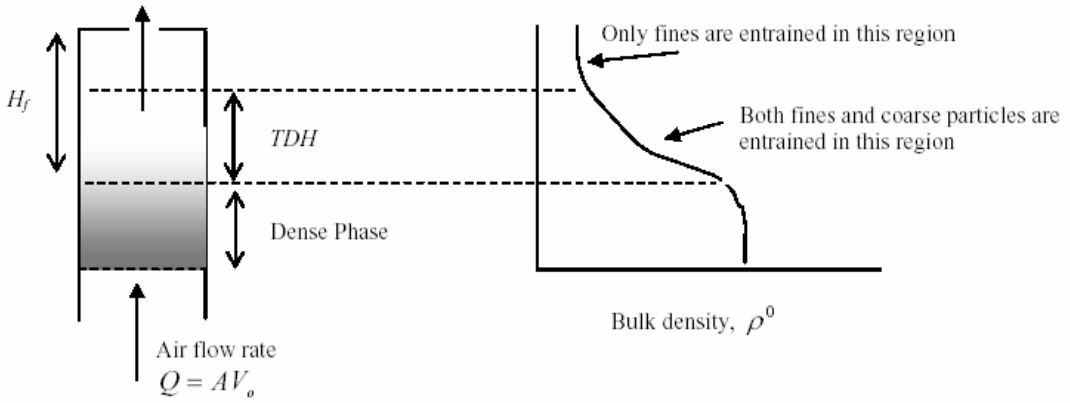

Figure 3. Both fines and coarse particle are entrained in the Transport Disengagement Height (TDH) region. Above the TDH only fines are entrained.

The Transport Disengagement Height (TDH) is the height above the dense-phase/leanphase boundary above which entrainment and bulk density do not change appreciably.

TDH depends upon the superficial velocity and the particle properties. The TDH is the height at which the kinetic energies of particles due to the collisions in the bed has been expended against gravity potential, and the coarse particles whose terminal velocities are greater than the superficial velocity are able to fall back down to the bed. The fine particles, whose terminal velocities are less than the superficial velocity, continue to be entrained out of the column

When H_f > TDH, then the holdup and entrainment rates are close to their minimums.

Usually H_f= TDH is the most economical design height for the fluidized bed. If H_f < TDH, then coarse particles will be carried out of the column.

2. Estimation of tdh for geldart a particles

For beds of fine particles there are several methods discussed in literature. Kunii and Levenspiel give a good review of this literature. In these notes you are only given a brief introduction.

METHOD 1. Zenz and Weil proposed a correlation between dimensionless TDH and the vessel diameter. For catalyst pellets in 20 to 150 micron size range, on a log-log plot, the relation between the dimensionless TDH and the vessel diameter are nearly linear as indicated in Figure 4.

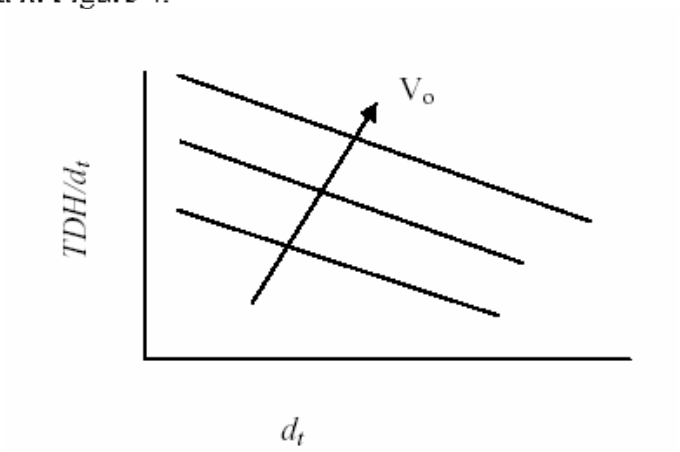

Figure 4. Dimensionless TDH/d_t vs vessel diameter, d_t

We can model the data on the chart in the form of

$$\text{Log}(TDH / d_t) = m \text{ Log}(d_t) - \text{Log}(b) \quad (3)$$

where d_t is the vessel diameter

Taking data points from the chart and plotting them we can curve fit to find the parameters m and b:

$$m = -0{,}115\ V_0 - 0{,}587 \quad (4)$$

$$b = 4{,}64\ V_0 \quad (5)$$

Finally, we take the above equations and try to compress the chart by plotting the dimensionless TDH/dt versus the Froude Number, to get the plot shown in Figure 5.

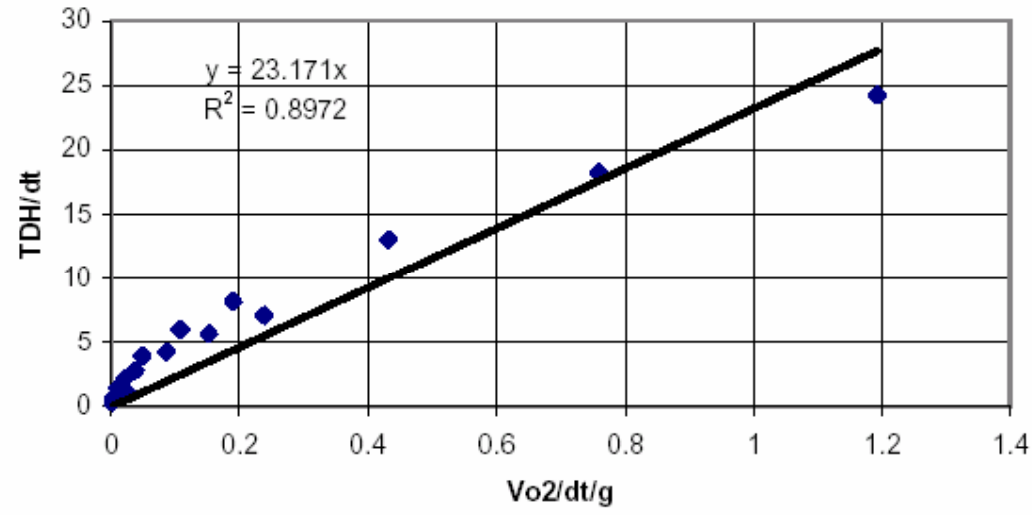

Figure 5. Dimensionless TDH/dt versus Froude Number.

If we take the linear fit in Figure 5 to represent the material behavior, then we can relate

$$\frac{TDH}{d_t} \quad 23{,}171\frac{V_c^2}{d_t g} \tag{6}$$

or, upon rearrangement, we get.

$$\frac{V_c^2}{TDH \cdot g} \quad \text{constant} \quad 0{,}0432 \tag{7}$$

The constant in Eq.(7) is likely to be material specific. Fournol independently determined, for a fluidized bed of fine catalyst particles, d_p=58 microns, the TDH for this material to be given by

$$\frac{V_c^2}{TDH \cdot g} \quad 0{,}001 \tag{8}$$

3. Entrainment rate from tall vessels

There are several methods for estimating entrainment rates. Following the work by Zenz we assume that the flux rate of solid size d_{pi} is proportional to its mass fraction, x_i,

$$G_{si} \quad x\, G_{si}^* \tag{9}$$

Where G_{si}^* is the flux rate from an imaginary bed of all particles of size d_{pi}. This approach extends the analogy between fluidized beds and boiling of a liquid mixture. Raoult's Law for an ideal fluid mixture equates the partial pressure of component *i* in the vapor phase to the mole fraction in the liquid phase times the pure fluid vapor pressure.

$$P_i \quad x_i P_i^* \tag{10}$$

hence, the flux rates are analogous to the vapor pressures.

The procedure to determine the flux rate from a bed with known particle size distribution is as follows:

1. Divide the size distribution into narrow intervals and find which intervals have terminal velocities greater than the superficial velocity (these are the particles that are entrained, because $H_f > TDH$).
2. Find G_{si}^* for each size range.
3. The total entrainment is given by:

$$G_s \quad \sum x_i G_{si}^* \tag{11}$$

In terms of a continuous size distribution, $P(d_p)$, the total entrainment rate is given by

$$G_s \quad \int G_{si}^* P(d_p) dd_p \quad \text{(integration over all particles entrained)} \tag{12}$$

To apply this procedure, a correlation such as shown in Figure 6 is required to find G_{si}^*.

From this plot the value of G*s may be determined for Geldart A particles and for fines removed from larger particle beds. For Geldart class B, C, or D particles (the larger particles) other predictive models are available

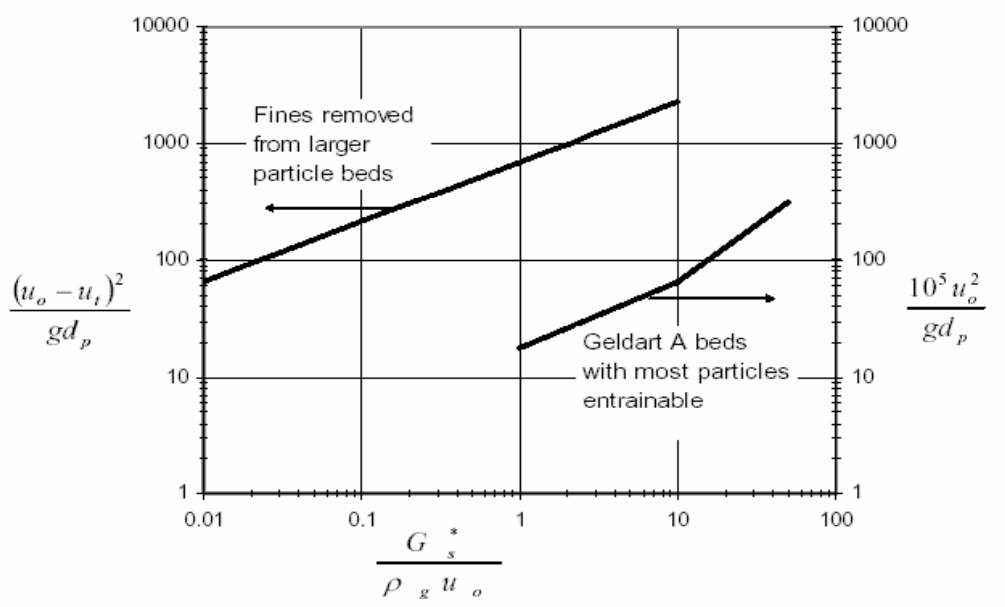

Figure 6. Data taken from Kunii & Levenspiel, Fluidization Engineering, 2ed, Butterworth, Boston, 1991

4. Conclusion

The main concern in a competitive and lasting economy is finished product price which is also affected of production costs. An important energetic economy can be obtained by re-dimensioning the work space that can be realized through transfer process intensification. There are studies in the domain which can be extended about industrial equipments. The trouble with these studies is that they have a restricted applicability in theoretic fits. During this theme it is intended to expand the theoretic researches concerning heat processes intensification and their use in industrial practice. In conclusion the fundamental research with concrete technical applications and the experimental verification of theoretic models represent a significant contribution to the development of knowledge in domain

Received April 17, 2007 *The "Gh.Asachi" Technical University Iaşi*

REFERENCES

1. Kunii and Levenspiel (*J. Chem. Eng. Japan*, **2**, 84, 1969)
2. Lewis *et. al.* (*Chem. Eng. Prog. Symposium Series*, **58** (38), 65, 1962)
3. Wen and Chen (*AICHE J.*, **28**, 117, 1982)
4. Kunii and Levenspiel (*Fluidization Engineering*, 2ed, Butterworth, Boston, 1991)
5. R.E. Balzhiser, M.R. Samuels, and J.D. Eliassen. (*Chemical Engineering* Thermodynamics, Prentice Hall, Englewood Cliffs, New Jersey, 1972)

CONTRIBUTII TEORETICE PRIVIND ELUTRIATIA PARTICULELOR DINTR-UN PAT FLUIDIZAT

Rezumat: Aceasta lucrare prezinta unele studii teoretice privind aplicatiile industriale ale instalatiilor cu pat fluidizat. Aceasta tehnica este relativ necunoscuta in tara, iar problemele fluidizarii coerente sunt inpartial rezolvate. In acest context, lucrarea isi propune elucidarea unor aspecte privind functionarea coreeta a unei astfel de instalatii de incalzire, in ideea protejarii resurselor energetice.

BULETINUL INSTITUTULUI POLITEHNIC DIN IAŞI
Tomul LIII (LVII), Fasc. 4, 2007
Secţia
ŞTIINŢA ŞI INGINERIA MATERIALELOR

DYNAMIC OF MECHANO-ELASTIC SYSTEMS FOR CHANGING OF SPOOL AT WAVING MACHINES

BY

VASILE VIOREL MOLDOVEANU, OVIDIU CALANCIA and LEONACHE DRĂGOI

Abstract: In this paper work it is analyzing changing mechanism dynamic of filling format, commencing from differential equation of operating movement of mechano-elastic system. It is analyzing changing system evolution of spool in connection with axial weaver's reed mechanism kinematics, resulting useful factors for machinery design.

Keywords: aluminium alloy.

1. Introduction

The concern of Weaving Machines designers, regarding automatisation of waving process, take place tenaciously for long time, with experiments and laborious study of reliability and maintenance on systems of changing filling format, with purpose of ensuring longer running life of weaving machines, without servicing. In this regard it is an evident evolution: from mechanic weaving machines, manual feeded with filling, designers and manufacturers developed automatic weaving machines, with mechanic and mechano-elastic changing systems of spool/shuttle, presently, the widest part of waving machine park, contain weaving machines with axial feeding of filling on large formats, from reels

Authors concentrate the study on a mechano-elastic system for changing of spool (SMESC), due the following reasons: in weaving machines park in Romania are machines equipped with this kind of changers, and knowing deeply of this are leading to a reasonable operation of waving machines and improving their reliability; have to gain textile equipment designers, because , in present paper are analyzed the dynamic of a mechano-elastic system which interfere in waving machine operation into a extremely short time interval without perturbing technological process-, in correlation with main mechanisms cyclograms of weaving machine.

2. Dynamics analysis

Are known cinematico- functioning structure of a mechano-elastic system for changing of spool (SMESC), at a cotton automatic weaving machine [1].

During changing process of spool, action angular level of spool is subdued to major stress as a consequence of forces and moments which are acting upon it into a very short time interval. In figure 1a are shown dynamic elements, as follow:

Q - is opposite resistance from previous spool when new one press upon it.;

R response in base plate "O " connection;
M_1 – is the moment of inertial forces applied to the hammer as a result of his descends lowered speed;
M_2 - is the moment applied upon mallet from spiral spring fitted on the shaft "O", which have the task to bring back in initial position after completion of changing process;
G - weight of mallet.

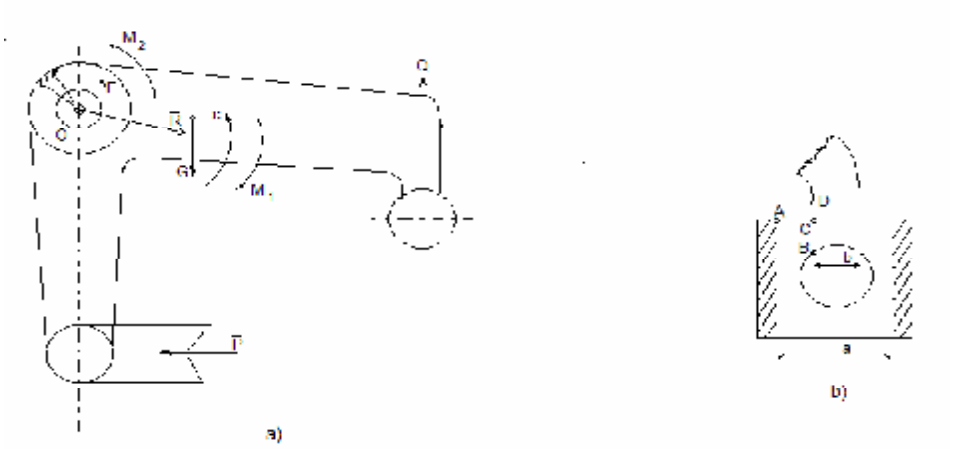

Q force subject of dimensions and elastic quality of fixing device of spool in shuttle, of ring dimensions on spool and surface finishing (polishing) of this metallic items. Q force could be determined in two ways; both of them based by experiment/test; establish directly Q force using a dynamometer; establish necessary mechanical work for extracting previous spool from shuttle and is obtaining using the following formula (1):

$$Q = W/S \tag{1}$$

Where: W is the mechanical work applied and S is the space travelled by spool up to the point of releasing by fixing device in shuttle. Following the experiments, medium value established of Q forces is 125 Newton's

Moment M_1 are establishing with the following formula (2):

$$M_1 = -J_0 \cdot \varepsilon \tag{2}$$

Where J_0 is dynamic inertia moment of mallet against his revolving axis, and ε represent his angular acceleration; both values can be determined according [1].

P force is unknown as modulus and is established from forces equation applied to mallet against his revolving axis. R force is a total unknown vector and is establishing from polygon forces applied to mallet.

M_2 moment is establishing with the formula (3):

$$M_2 = F \cdot r \tag{3}$$

Where F is tangential force given by spiral spring, and r is the radius of spring coil.

Spiral spring which give M_2 momentum, must be calculated, paying attention to certain condition. Thus, at completion of changing process, the mallet commence movement of return under spiral spring forces, and the shuttle are moving together with weaver's reed which are oscillating going away from extreme position of it. A point of shuttle are moving to right (fig. 1b), and b point of mallet is lifting. If internal edge A of shuttle arrive in C point earlier or in same time with B edge of mallet, then

happen damages to the shuttle by the mallet. To ovoid this occurrence must introduce in SMESC a spiral spring with a certain elastic constant, which ensure lifting B point of mallet up to D position, in period of time when shuttle are moving in transport movement from A to C. CD distance are safety distance.

A point an the shuttle will travel on distance AC = (a – b)/2

In case axial weaver's reel the movement rule is:

$$X_A = K\{\rho[1 - \cos(\omega)] + (\rho^2/2L)\sin^2(\omega)\} \quad (4)$$

where: ρ – is radius of mechanism crank; L – length of connecting rod; K – an number more than one which indicate the ratio between distance of A point of shuttle to oscillating axis of weavers reel and distance between weaver's reel pin and his axis; ω – angular argument of (4) formula.

With the experimental established value of items *a, b, ρ,* and L is possible to write AC = X_A, then establish ω ;which now will be noted ω_1.

Movement rule of SMESC mallet, during lifting under the force of spring action will result from moment equilibrium given by formula (5):

$$F \cdot r - J_0 \cdot \beta \quad (5)$$

Where: β is angle traveled by end of the spring together with the mallet, and β'' is angular acceleration. Tangential forces is in direct ratio with angle traveled by mallet and spring, in relation with initial position, before changing process.. result F = c*β, where *c* is elasticity constant of the spring., unknown of the problem. β angle is increasing during changing development up to his maximum value and decrease while reversing to initial position.

Is obtaining:

$$J_0 \cdot \beta + c \cdot r \cdot \beta = 0 \quad (6)$$

Noted $k^2 = c \cdot r/J_0$, and replacing in (6), obtain differential equation second degree (7):

$$\beta - k^2 \cdot \beta = 0 \quad (7)$$

General key of differential equation is:

$$\beta = M \cdot \sin(kt) - N \cdot \cos(kt) \quad (8)$$

Where M and N are constants established from initial conditions of movement

Derivating successively differential equation (7), resulting (9) and (10)

$$\beta = M \cdot k \cdot \cos(kt) - N \cdot k \sin(kt) \quad (9)$$

$$\beta = -M \cdot k^2 \cdot \sin(kt) - N \cdot k^2 \cdot \cos 9kt) \quad (10)$$

Obtaining equation:

$$\beta = \beta_0 \cos(kt) \quad (11)$$

Where: β_0 is torsion angle of spiral spring between ending stage of spool changing and initial stage of mallet reversing movement. This way will result equality $\beta_0 = \beta_{max}$. Distance traveled by B point of the mallet (figure 1b) is given by function:

$$S_B = h(\beta_0 - \beta) \quad (12)$$

Where: h is distance between oscillating axis of the mallet and his B edge, and β - actial angle of spring torsion. By replacing obtain:

$$S_B = h \cdot \beta_0[1 - \cos(kt)] \quad (13)$$

Knowing distance S_b = BD, (figure 1b), and time φ_1/ω, where φ_1 is turning angle of main shaft of unit during weaver's reel movement on distance AC, and ω - angular speed of main shaft.

3. Use, interpretation, conclusions

Commencing from geometric, kinematics and dynamics elements established in advance, establish afterward unknown k and spring elasticity constant, c.

In this way, for a = 31mm; b = 14 mm; $X_A = (31 - 14)/2 = 8,5$ mm; $S_B = 10$ mm; $\rho = 70$ mm; L = 280 mm; K = 1,08; r = 20 mm; h = 145 mm; $\omega = 20\ s^{-1}$; $J_0 = 0,013\ kg.m^2$; $\beta_0 = \pi$.

Replacing in formula (4), result:

$$8,5 = 1,08 \{ 70 [1-\cos(20t)] + (4900/560)\sin^2(20t)\} \qquad (4^*)$$

Solving trigonometrically equation (4*), obtain mallet lifting duration, on the distance BD, $t_1 = 0,0215$ s.

Replacing in formula (13), obtain:

$$10 = 145 \cdot \pi \cdot [1 - \cos(k \cdot 0.0215)] \qquad (13^*)$$

From formula (13*) obtain k = 9,8.

In the last, from formula $k^2 = c \cdot r / J_0$ rezult spring constant, c= 62N.

Concluding, a SMESC designer need to establish value of spring constant, and to choose suitable spring; a spring with higher elastic constant will induce shock and vibrations in system, with untimely wear in joints and disturbance in functioning. And a spring with lower elastic constant will bring damages of shuttle and blocking of the machine

Methodology from present work also can be used when designing also other mechano-elastic systems for machine equipment.

Received April 29, 2007 *The "Gh.Asachi" Technical University Iaşi*

REFERENCES

1. Dragoi, L., **Proiectarea utilajelor textile. Utilaje din ţesătorie**. Editura Dosoftei, Iaşi, 1995
2. Dragoi, L., **Elemente de proiectare a utilajelor din ţesătorie**. *Aplicaţii*. Editura BIT. Iaşi, 1997
3. Dragoi, L., **Tribotehnica**. Editura BIT, Iaşi, 1997
4. Dragoi, L., **Manualul Inginerului Textilist**. Editura AGIR. Bucureşti, 2004
5. Dragoi, L., **Acţionări hidraulice şi pneumatice la maşini din domeniul textile-pielărie** Editura Performantica. Iaşi, 2006

DINAMICA SISTEMELOR MECANO-ELASTICE DE SCHIMBARE A CANETELOR DE LA MAŞINILE DE ŢESUT

Rezumat: În lucrare se analizează dinamica mecanismului de schimbare a formatelor de bătătură, plecând de la ecuaţia diferenţială a mişcării de acţionare a sistemului mecano-elastic. Se analizează dinamica sistemului de schimbare a canetei în corelaţie cu cinetica mecanismului axial al vătălaşi, rezultând elemente utile în proiectarea utilajelor.

BULETINUL INSTITUTULUI POLITEHNIC DIN IAŞI
Tomul LIII (LVII), Fasc. 4, 2007
Secţia
ŞTIINŢA ŞI INGINERIA MATERIALELOR

CONSIDERATIONS REGARDING THE COMPOSITIONAL AND AESTHETIC ELEMENTS OF THE TEXTILE MACHINES

BY

OVIDIU CALANCIA, VASILE VIOREL MOLDOVEANU and PETRONELA DRAGOI

Abstract: The recent researches in design, construction and exploitation of textile machines show that work productivity is connected with the ergonomics and design of processing machines. The paper presents some aspects regarding the compositional theory and the ways of harmonization of forms in designing textile machines. Also there are presented more modalities of using colors for finishing machines, all these applied according to visual communication theory.

Keywords: harmonic decomposition, visual communications, immaculate colors, color contrast.

1. Compositional aspects in designing

Some aspects of the compositional theory regarding the harmony of the shapes are specific to the architecture. It is difficult to transfer the theoretical elements of the architecture into technical field; some specific particularities that make the difference between technical field and architecture require a substantial and scientific activity regarding the ways of designer to realize the compositional technique of the textile machines.

Initially, in the first phase of a project, the designer has a variety of alternatives; he will choose one. It is possible that the chosen alternative to be disputed later. Therefore, in the early phase, it is necessary to specify the compositional idea that will be developed in the future. Than, after the compositional scheme of the textile machine becomes clear, the next phase is to elaborate the technical structure regarding the space capacity organization.

The specific of the compositional proceedings, as compositional ways, consist of their synthesis at scale, proportions, rhythm and the nuance of shapes. The dimensional relationships of the shape' s elements constitutes the realization basis of the entire composition.

The proportion represents the aesthetic category that indicates the relations between the dimensions of the component parts of the machines and the human being and objects around. Establishing the proportions, the designer combines the functional, constructive, performance and material aspects with the aesthetic laws

The rhythmic structure of a geometrical assembly in plane or space is realized according to *harmonic decomposition* principle, a rectilinear segmentation establishing a continue proportion inversed constantly. This proportional segmentation is called "*the gold section*"; the expression can be used in correlation with the compositional structure.

The geometrical shape it is also very important. There exist certain regulator networks, defined by the practical adaptation to proportion.

2. The functional and aesthetic role of the color

The color is the constitutive part of the world we live, having an important influence to each individual. The color concept refers to a variety of sensations and ideas, depending of physical, emotional, historic and philosophic environment. The sensitivity at colors can be developed; the ability to communicate using colors can be learned.

The new work organization and the automatization of the production processes enforce the accuracy of spaces, lightness and a clear and logical distribution of the equipment, functional and well colored machines. Therefore, the designer will have to take account to functional-utilitarian, physical – psychological and aesthetic – artistic elements.

The effects of the colors to human body are different depending on age and tiredness. So, the red is well received in the morning, but in the afternoon becomes difficult to be distinguished. In change, the green is well received all day without any diminutions of the perceived power. The blue is always distinguished, the perception quality increases during the afternoon. The blue has a positive influence to the view, but the red influences negatively.

Used during the short time responsibilities, the yellow can determine an increasing of the work process; used in activities that involve a precise supervision of machine' s components, the yellow can have a negative influence to the operation' s execution. The yellow has an important role used in the signal system, warning the dangers.

An efficient method to increase the visibility of colors is the contrast. According to the recent studies, the most chromatic visible contrast is yellow on black, and the less one is red on green. The recommended colors for the textile machines are:

- dark and light grey;
- the bluish green in different nuances;
- blue;
- light green and dark green.

Recently, it has been used brown or orange.

The fundamental criterion to choose the colors for extended areas is to find the optimum visibility of the eye situated in the central zone of spectrum. The machine components that must be distinguished should have a color that enforces the eye to easy adaptation from a wavelength to other. These colors called focal must be chosen with wavelength bigger than the general shade of the machine wavelength. In this way, the differences between colors will not fatigue the eye.

3. The communication through color

Nowadays, there exists a generalization in the practicing of functional colors in the command board of the equipments. The colors are used to inform the worker through colored lights or to transmit information about the machines. One of the chromatic fundamental conditions of the command boards is the perfect distinguish of the colors: each color must depend by the general shade of the board and it is influenced by the other colors. The selection of the color on the command board depends also by the memorizing capacity of the code, in which each shade has an important significance. Because the chromatic memory isn't too good, it must be used basic elements of the code, at the most five shades, preferably selected from the pure colors of the spectrum:

- Red;
- Orange;
- Yellow;
- Green;
- Blue.

In the chromatic code of a command board it is recommended the application of the visual communication theory that says that the most frequent and important signals must be visible in a simple and obvious way in a single color. Also, the most significant elements of the board must be placed in a central visibility zone because the operator must distinguish the colors. A selection criterion of the colors is the necessary speed of a certain operation. Therefore, for those operations that involves a high response speed are indicated the signalizations with red, yellow or orange; meanwhile, for the other operations it can be used green of blue

Other important condition of command board function is the frequency of the colored signals appearance which if it is too often, can go to tiredness of the operator and total lost of the perception capacity. Because of this problem, the yellow being very visible can be used for very short signals and blue or red can be used for long signals.

- The yellow color unlike black is used as warning for unseen dangers.
- The orange unlike black warns the accidents dangers in the dangerous parts of the machines
- The red unlike white warns: Stop, Direct Danger and Forbidden Areas, so on.
- The green unlike white means the missing of any danger.
- The blue unlike white shows the security technical parts of the machines.

4. The aesthetic distinguish of the tissue

The latest improvements in the textile machine design determine the progress regarding the work productivity. But, the latest researches shows tat the work productivity in textile is depended by the high quality of equipment, their structure, their "friendly" surface and their design. Therefore, the designer must have an active role in realization of new equipment.

A specific characteristic of textile machines is their powerful relation with the human being. Solving the complex problem regarding the relation between human and machine, the engineers and specialists in ergonomic and design field release constantly the human by the necessity to accommodate with the machine. Therefore, they adopt the machine to anatomical particularities and spiritual needs of human being. So, the designer it is very important in realization of new textile equipment.

In the first phases of the designing of the tissue machines, the specialists decide the combination and the place in space of the main mechanisms of the machines. This idea becomes materialized comparing the place of the shedding mechanism of some tissue machines. So, at the P175M machine, the shedding mechanism is located in the center of the seating contributing at the reduction of the machine` s size. At the STB-216 tissue machine, the drive of the shedding mechanism is placed in a closed box outside of the seating; in this way is been reduced the assembling costs and the adjustments are easy to be done. Also, because the operating elements are placed in bay with liquid lubricant, the hardness of the noise decreases and the durability increase.

In the case of tissue machines with shuttle, the mechanisms are located in such a position so that their operation to be supported on the machine` s skeleton. The open mechanisms can create services dangers, they must be clean constantly and they need a supplementary oiling. Using aesthetic fenders, the work components can be protected by the dust; also, the fender facilitates the machine `s manipulation and increases the work safety. An example is the aesthetic fenders of Elitex K-58/1 textile machines

The ergonomic factors have an important role for workers Some of the conditions regarding this problem are:

- Good sanitary and hygienic characteristics that can assure the function at maximum capacity of work;
- Parameters, gauges, ergonomic sizes depending by the human body particularities and its possibilities to move;
- The accommodation of the human sight, hearing and touch particularities;
- High aesthetic qualities with a positive emotional influence to human being.

The application of the colors in the design process of the tissue machines involves:

- The buttons that indicates STOP or DAMAGE are colored in red;
- The signals and the buttons START / WORK are colored in green;
- The buttons and other operation elements with secondary importance are colored in grey shades.

The next principles must be followed:

- As bigger as an component is the color must be light;
- As small as a component is the color must be saturated;
- The support components must have dark colors and shades

The adequate colors are light green or light grey for seating and big components, combined with black color for small pieces. The steel components can be covered with plastic. Such a finishing operation of the areas can be distinguished using light green on the seating of the tissue machines.

Received April 20, 2007 *The "Gh.Asachi" Technical University Iaşi*

REFERENCES

1. Jones, C.I., **Design, metode si aplicatii**, Editura Tehnică, Bucuresti, 1975
2. Dragoi, L., **Proiectarea utilajelor textile** Editura Dosoftei, Iasi, 1995
3. Dragoi, L., **Proiectarea utilajelor textile** *Aplicatii*. Editura BIT, Iasi. 1997
4. Dragoi, L., **Tribotehnica**. Editura BIT, Iasi. 1998
5. Dragoi,L., **Mentenanţă si fiabilitate in industria textilă**. Editura Performantica. Iaşi, 2007

CONSIDERAŢII ASUPRA ELEMENTELOR COMPOZITIONALE SI ESTETICE ALE MAŞINILOR TEXTILE

Rezumat: Cercetările recente în design-ul, construcţia şi exploatarea maşinilor textile arată că productivitatea muncii este în legătură directă cu parametrii ergonomici ai acestora. Lucrarea prezintă câteva aspecte privind teoria compoziţională şi metodele de armonizare a formelor în proiectarea maşinilor textile. De asemenea, autorii au prezentat modalităţi de utilizare a culorilor în finisarea maşinilor textile aplicate conform teoriei comunicării vizuale.

BULETINUL INSTITUTULUI POLITEHNIC DIN IAŞI
Tomul LIII (LVII), Fasc. 4, 2007
Secţia
ŞTIINŢA ŞI INGINERIA MATERIALELOR

TAILORING OF PEROVSKITE OXIDE NANOPOWDERS AND SINTERING TO NANOCRYSTALLINE DENSE CERAMICS

BY

P.NANNI[1], M.T. BUSCAGLIA[2], R.V.CALDERONE[1], V.BUSCAGLIA[2], L.MITOŞERIU[1,3] and M.VIVIANI[2]

Abstract: Some ceramics with perovskite-like structure, such as $BaTiO_3$ (BT), are ferroelectric materials. Although they can be employed for underwater acoustic sensors, actuators, PTCR resistors, ferroelectric memories, and embedded capacitance in Printed Circuit Board, the main application is in the field of communication and microelectronics. The authors proved a new way to easy obtain well defined, no agglomerated, stoichiometric and equiaxed BT and ST nano-powders with a very narrow Particle Size Distribution.

Keywords: perovskite

Some ceramics with perovskite-like structure, such as $BaTiO_3$ (BT), are ferroelectric materials [1]. Due to their very high permittivity (normally ε =1500-4000 according to the grain size) and low losses, they are extensively used in the electronic industry where they find manifold applications. Although they can be employed for underwater acoustic sensors, actuators, PTCR (Positive Temperature Coefficient of Resistivity) resistors, ferroelectric memories, and embedded capacitance in Printed Circuit Board (PCB) [2], the main application is in the field of communication and microelectronics (Multilayer Ceramic Capacitors, MLCCs).

At present, continuous advances toward component miniaturisation lead the high-tech ceramics on the way of grain size reduction below a few hundred of nanometres to improve the performance of the devices and possible to reduce their costs. In the case of MLCCs, the current trend is to increase the number of dielectric layers above 500 and decrease their thickness below 1 μm. This objective can be achieved under two conditions: production of high quality nanopowders (≤ 100nm) with narrow particle size distribution and relatively low sintering temperature that prevents grain growth whilst leading to high densification

Recently, an increasing interest has been focused on soft chemistry methods. Ultra-fine, non-agglomerated BT and $SrTiO_3$ (ST) nanopowders with narrow particle size distribution were prepared by our group prepared according to the direct precipitation reaction (T<100°C; P=10^5 Pa; pH ≈14):

$$(Ba/Sr)Cl_2(aq) + TiCl_4(aq) + 4NaOH(aq) \rightarrow (Ba/Sr)TiO_3(s) + 4NaCl(aq) + 3H_2O(l) \quad (1)$$

where (aq) indicates the salts dissolved in aqueous solution [3, 4]. The thermodynamic conditions for hydrothermal synthesis of BT stated by Lenka and Riman [5].

The reaction (1) was carried out either in batch or mini tubolar reactors. For larger amounts a Segmented Flow Tubular Reactor (SFTR) was employed [6, 7]. An

excess of Ba over the $BaCl_2/TiCl_4$ stoichiometry ratio (R=1.11) was always used to compensate depletions due to the washing step.

STFR (Fig.1) essentially composes of a *micromixer*, where the reactants are efficiently mixed and a *segmenter* in which the supersaturated solution is separated by an organic immiscible fluid into micro-batch volumes (≈60 mL) in a continuous mode.

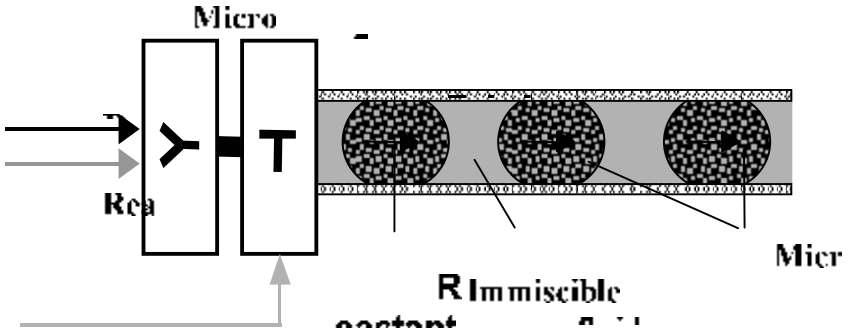

Fig. 1. Operating schema of SFTR showing the formation of segmented micro-batch volume.

Each micro-volume is fed into the tubular reactor (Ø 4mm, length 20m) kept in a thermostatic bath, and meets exactly the same residence time and the same reaction conditions all throughout the length of the tubular reactor. As a result, the formation of practically identical nano-particles is observed, as each micro-volume behaves like a microreactor. Eventually the powder dispersion, separated from the immiscible fluid by decantation, is collected, washed and finally dried

It is known, that to obtain high-quality powders, some critical points such as nuclei formation, crystallite growth and aggregation of crystallites must be controlled because the preparation of nanopowders is very sensible to all these synthesis parameters. In particular a strict control of supersaturation and temperature strongly reduces the heterogeneity conditions of the reactors, and in turn makes possible the control of cations concentration that determines the final particle size. In fact, when the concentration increases the particle size decreases We showed that these requirements are successfully achieved by employing SFTR technology and we succeeded in tailoring BT nanopowders in the range 15÷1,500 nm, with a satisfactory stoichiometry control (Fig. 2 a-c and 3)

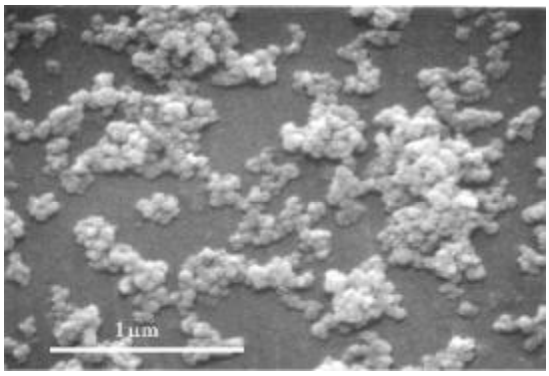

Fig 2a Example of $BaTiO_3$ nanopowders in the range 30-50 nm

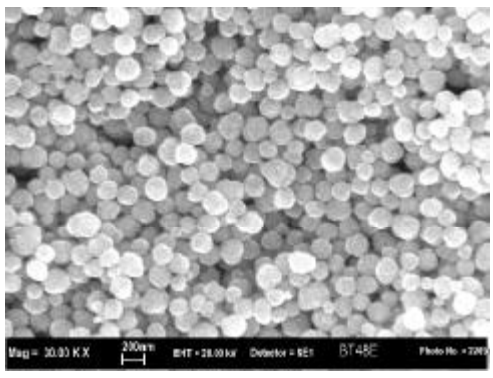

Fig 2b. Example of $BaTiO_3$ nanopowders in the range 150-200 nm

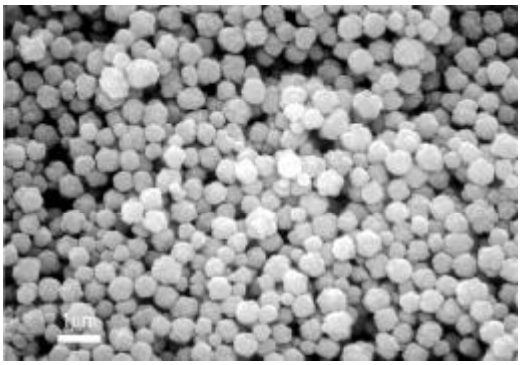

Fig 2c. Example of $BaTiO_3$ nanopowders in the range 500-700 nm

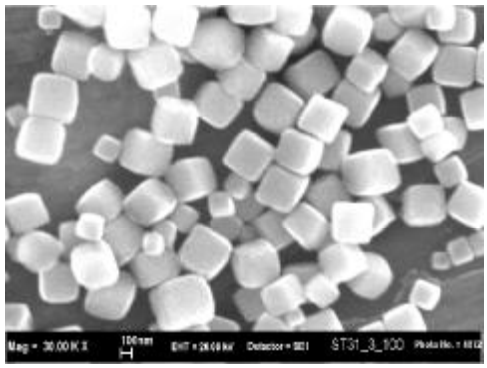

Fig 3. Example of $SrTiO_3$ nanopowders with an average size of 400 nm

The authors proved [3,4] that the reaction (1) represents an easy way to obtain well defined, no agglomerated, stoichiometric and equiaxed BT and ST nano-powders with a very narrow Particle Size Distribution as shown in Fig. 4, where the dimensional volume distribution is reported.

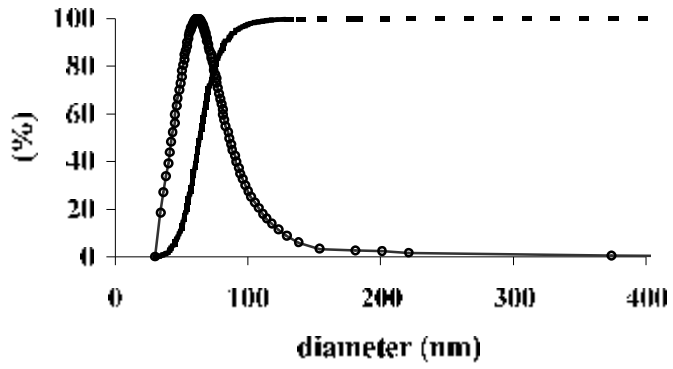

Fig. 4. Dimensional volume distribution (--- cumulative; o frequency)

The production of high-quality nano-powders is a necessary but not sufficient condition to obtain dense nanocrystalline ceramics unless innovative sintering procedures are applied to prevent grain growth below a few tenth of nm. Spark Plasma Sintering (SPS) allows a rapid densification of powders that we used [8,9] to prepare dense, bulk nanocrystalline BT ceramics in the range 30-100 nm (relative density: >97%) (Fig. 5a-d).

From these experimental results, a critical grain size for possible disappearance of ferroelectricity in BT was evaluated in the range 10-30nm

The dielectric constant of nanocrystalline ceramics (≤100nm) is shifted to lower temperatures and strongly depressed in comparison with coarse ceramics. It is also less sensitive to temperature.

In spite the macroscopic P(E) loops are indicating a frozen polarisation, the local AFM piezoresponse investigations show that even at the smallest grain size the material conserves its ferroelectricity [9]. The overall functional properties of the BT nanoceramics are the result of combined grain size and grain boundary phenomena.

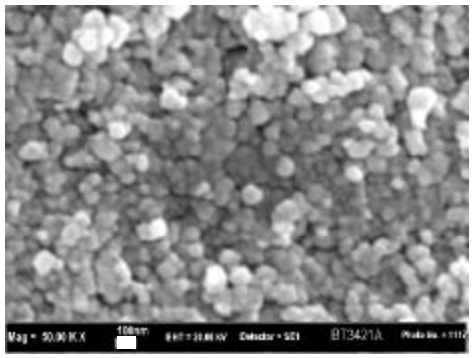

Fig. 5a. $BaTiO_3$ nanocrystalline ceramic (g.s. ≈100 nm; bar 100 nm)

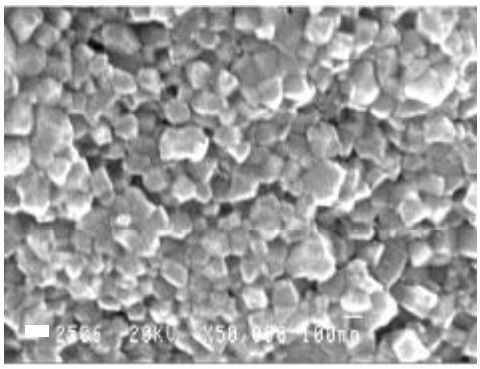

Fig. 5b. $BaTiO_3$ nanocrystalline ceramic (g.s. ≈ 50 nm; bar 100 nm)

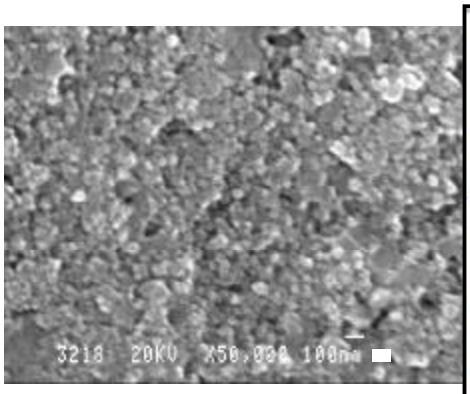

Fig. 5c. $BaTiO_3$ nanocrystalline ceramic (g.s. ≈ 30 nm; bar 100 nm)

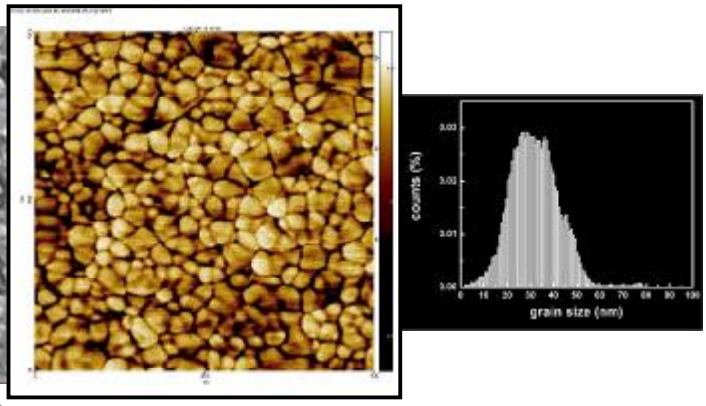

Fig. 5d. AFM image of 30 nm $BaTiO_3$ ceramic and g.s. distribution

A progressive reduction of the tetragonal distortion with decreasing grain size was observed together with a decrease of the tetragonal-cubic transition enthalpy (Fig.6)[10].

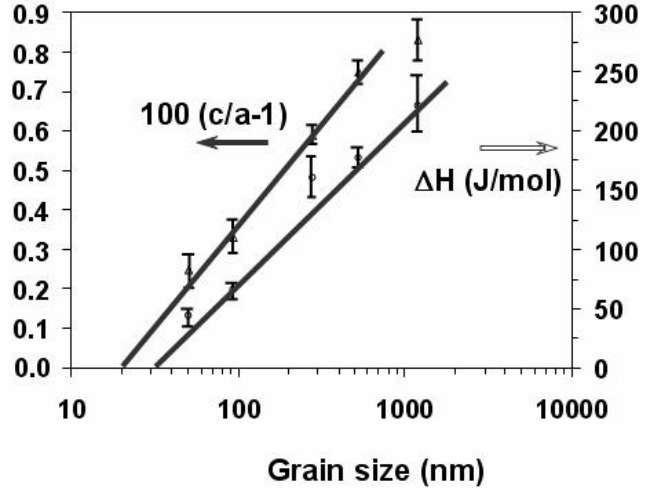

Fig. 6. Tetragonality [100(c/a-1)] and Tetragonal-cubic enthalpy (ΔH) versus grain size

Received April 24, 2007

[3] *DICheP, Faculty of Engineering, University of Genoa, Genoa, Italy*
[4] *IENI-CNR, Department of Genoa, Genoa, Italy*
[5] *"Al.I. Cuza" University, Iasi*

REFERENCES

1. A.J.Moulson and J.M.Herbert. "**Electroceramics**", Chapman and Hall, London UK 1990, pp 68-79.
2. A Rae et al, *Ceram.* Trans. 100 (1999) 1.
3. A.Testino, M.T.Buscaglia, M.Viviani, V.Buscaglia and P.Nanni, *J. Am. Ceram. Soc., 87 (2004) 79.*
A Testino, M.T.Buscaglia, M.Viviani, V Buscaglia, C.Bottino and P.Nanni, *Chem. Mater. 16 (2004) 1536.*
4. V R.Calderone, A.Testino, M.T.Buscaglia, M Bassoli, C Bottino, M.Viviani, V Buscaglia and P.Nanni, *Chem. Mater. 18 (2006) 1626,*
5. M.M. Lencka and R.E. Riman, *Chem. of Mater.*, 5 (1993) 61; M.M Lencka and R.E. Riman, *Ferroelectrics*. 151 (1994) 159. J.O. Eckert Jr., C.C. Hung-Houston, B.L. Gersten, M.M Lencka and R.E. Riman, *J Am Ceram. Soc , 79 (1996) 2929,*
6. J.Lemaitre, N.Jongen. R.Vacassy and P.Bowen. *"Production of Powders"*, Patent Nr. WO 98/02237. Jan. 22, 1998.
7. P.Bowen, M.Donnet, A.Testino, M.Viviani, M.T.Buscaglia, V.Buscaglia and P.Nanni,". *Key Eng. Mater., 216-213 (2002) 21.*
8 V.Buscaglia, M.Viviani, M T.Buscaglia, P Nanni, L.Mitoseriu, A Testino, T Stytsenko, M Daglish, Z.Zhao and M.Nygren, *Powder Technology*, **148**, 24 (2004).
9. M.T.Buscaglia, M.Viviani. V.Buscaglia, L.Mitoseriu, A.Testino, P.Nanni et al , *Phys. Rev. B. 73 (2006) 064114*
10. Z.Zhao, V Buscaglia, M.Viviani, M.T.Buscaglia, L.Mitoseriu, A Testino, M.Nygren, M.Johnsson, P.Nanni. *Phys. Rev. B, 70 (2004) 024107*

EVOLUŢIA COMPORTĂRII HISTERETICE A UNOR ALIAJE CU MEMORIA FORMEI ÎN FUNCŢIE DE SARCINA APLICATĂ

Rezumat: Unele ceramici cu structura pereskovite, cum ar fi $BaTiO_3$ (BT), sunt materiale feromagnetice. Deşi acestea pot fi folosite pentru senzori acustici submarine, actuatori, rezistori PTCR, memorii feroelectrice şi capacităţi PCE, principala utilizare a lor es.e în domeniul comunicaţiilor şi microelectronicii. Autorii prezintă o nouă cale de obţinere ieftină nano-pulberilor tip BT şi ST cu o distribuţie a mărimii particulelor foarte optimă.

BULETINUL INSTITUTULUI POLITEHNIC DIN IAŞI
Tomul LIII (LVII), Fasc. 4, 2007
Secţia
ŞTIINŢA ŞI INGINERIA MATERIALELOR

CONSIDERATION CONCERNING THE MANUFACTURING OF MARAGING 300 STEEL

BY

I. NEDELCU*, IRINA CARCEANU**, G. COSMELEATA***, I. ROCEANU**** and V. BOTAN*****

Abstract: The aims of the paper consists in the development of Maraging steels which are characterised by ultra-high strength due to the precipitate formed during ageing. Development of new maraging steels has drawn much attention from industry, targeting for specific applications. Maraging steels work well in electro-mechanical components where ultra-high strength is required, along with good dimensional stability during heat treatment. Several desirable properties of maraging steels are: ultra-high strength at room temperature; good weldability ; section size is an important factor in the hardening process; simple heat treatment, which results in minimum distortion;superior fracture toughness compared to quenched and tempered steel of similar strength level ;low carbon content, which precludes decarburization problems. The paper presents briefly some aspects regarding the present stage in production of maraging steels and the effect of thermal treatment on the mechanical characteristics and on the types of intermediate metallic compounds which result in the process of hardening by precipitation for Maraging steel.

Keywords: hardening by precipitation; maraging steels; thermal treatments.

1. Introduction

The recent rapid development of this type of steel is due to an assembly of higly important properties such as: high mechanical resistance, with remarkable ductility and tenacity; simple thermic treatments; good weldability; criogenic resistance; easily deformable and processable. [1, 2, 3]

In the case of usual hardenable steel utilized in the car construction industry, the process of hardening results in the formation of a hard and fragile martensite, which shall in turn be reannealed to obtain desired mechanical characteristics. In the case of MARAGING steel on the other hand, hardening results in the formation of a soft, ductile martensite, with a high content in nickel and very little carbon. The high mechanical characteristics are obtained through an ageing treatment due to the precipitation of some complex intermetallic phases.

Furthermore, the technology of fabrication of small pieces with high resistance, using conventional steel, is far more complicated and expensive than that of small pieces with high tenacity made out of maraging steel. Consequently, the advantages acquired by the usage of this type of steel are both technic and economic. [4]

Carbon is the main element which confers the high resistance but in the same time the fragile character of steel, which is why the actual tendency regarding the development of high-resistance alloys is to dramatically lower the contained carbon. On the other hand, a very low percent of carbon (< 0,03%) needs to be associated with

a martensitic, soft and massive structure, and with hardening by ageing. And this is actually how the name of „maraging" came into play.

The development of maraging steel emerged from the Fe – Ni binary alloy, with a percent of Ni ranging between 18 and 25. This results in a massive martensite if air-cooled. The equilibrium diagram for Fe – Ni is illustrated in Figure 1.

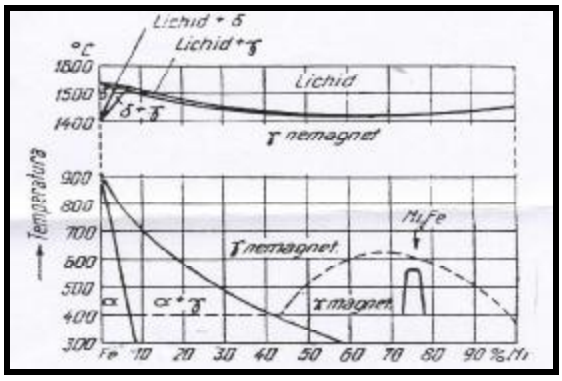

Fig. 1.The Fe-Ni equilibrium diagram

This martensite does not contain carbon as it is the case with usual Fe-C steel, it is not modified tetragonally, having a regulated cubic shape. It is called α_0 solid solution, having the same chemical composition like the austenite it resulted from

For practical necessities, a real metastable diagram of Fe-Ni alloys can be utilized (Figure 2), which presents thermic histeresis

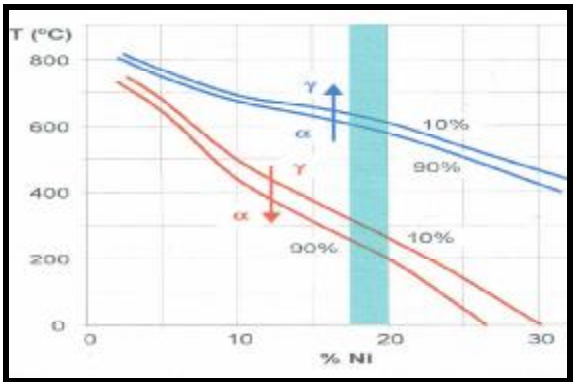

Fig. 2. Real metastable diagram of Fe-Ni alloys, the side of Fe.

The elements for alloying selected after Ni have been Mo ~ 5% and Ti ~ 1%. Applying an ageing treatment in the 450 – 500 ^{O}C interval has lead to the formation of the following precipitates: Ni_3Mo or $Ni_3(Mo,Ti)$ Ni_3Ti or Fe_7Mo_6. Excess titanium neutralizes carbon by forming carbon carbide. This alloying had a suplimentary effect: lowering the point of martensitic M_S and M_F transformation. The following element introduced in maraging steel was Co. Its effect is significant for the formation of a high-resistance and high-tenacity alloy by lowering the solubility of Mo in Fe (solid solution α), consequently leading to the formation of more precipitates, which in turn results in the increase of the martensitic M_S and M_F transformation temperatures. Other potential alloying elements are Al, Nb, Zr, Be, W, V, Cu, Ta. These are

substitution elements which produce the hardening. The normal thermic treatment cycle for MARAGING Co-Mo-Ni steel, laminated or forged, consists of a solubilization reannealing at 820^0 C with air-cooling followed by an ageing treatment for the martensite (maraging) at 480^0 C or 450^0 C with air-cooling.At the temperature of 820°C the phase transformation takes place ($\alpha \Rightarrow \gamma$), as well as the recrystallization of the austenite and the dissolution of the precipitates. After the cooling at 820^0 C, regardless of the speed, the $\gamma \rightarrow \alpha^1$ transformation takes place (austenite-martensite).

The hardening of Maraging steel is obtained by the thermic ageing treatment, a period in which the formation of the intermetallic precipitates in the martensitic mass takes place.perioadă în care are loc formarea precipitatelor intermetalice în masa martensitică.[5, 13, 16, 17, 18]. The highly reduced variation of dimensions during the thermic treatment is remarkable (0.06-0.08% when placing in solution and 0.04% when ageing). This reduced variation of the dimensions allows the processing of the pieces at finite quotas prior to the final ageing treatment. With the purpose of improving the features of warm-deformability another thermic treatment of partial austenitizing is conducted, at a temperature of about 650^0 C. There is poor reference in the specialized literature regarding the necessity of this thermic treatment. Air-cooling facilitates the technologic process of the thermic treatment, both when placing in solution and when ageing. This excellent complex of mechanical and technological features is due to hardening by precipitation of a series of intermetallic compounds in the special martensitic mass (lath martensite).

The specialty literature states different views concerning the hardening mechanism (precipitation) as well as the different phases of the intermetallic compounds. Therefore, for the process of germination (nucleation) in the ageing reaction, there are two accepted theories: – precipitation by classic germination [6]; - precipitation by spinodal decomposing [7].

There are two types of mechanisms responsible for the hardening of the precipitates, which are implied in the movement of the dislocations: - a looping mechanism [8,9]; - a shearing mechanism [10,11], and the reannealed austenite. There are numerous opinions of various researchers regarding the types of precipitates emerged at the thermic ageing treatment. Therefore, these determinations include precipitated phases such as [17]: γ – Ni_3Mo [6,10], η – Ni_3Ti [6,13,14], laves phases Fe_2Mo [6,10],σ – FeMo [6], μ – $Fe_7\ Mo_6$ [6,13], FeTi [6,15], Fe_2Ti [6] and the dispersed austenite[16]. In the hereby project we shall attempt to identify by means of electronic microscopy the types of precipitates which appear after the classical cycle of thermic treatment 820°C/1hour/air (placing in solution) and ageing at 480°C/3hours/air, and to analyze considering the shape, dimensions and the distance between precipitates, the main hardening mechanism.

2. Experimental work

For the experimentation, a charge of maraging 300 steel was ellaborated, by double vacuum remelting (which implies vacuum induction and arc in vacuum remelting). The ingot weighs 40 kg and has the diameter Ø 120 mm. The chemical composition of the obtained ingot is presented in Table 1

Table 1. Chemical composition of the obtained ingot

C	Si	Mn	P	S	Al	C	Ni	Mo	Ti
0,028	0,05	0.08	0,007	0,005	0,077	9,3	18,8	4.6	0,36

The utilized materials for the ellaboration were ARMCO steel, electrolytic nickel, molybdenum and pure titanium, Al 99,995%. The forging has been done on pneumatic forging hammer from Ø 120 to 40mm and then to 20mm

The performed thermic treatments have been as follows:

1. Placing in solution at 820°C, maintaining for 1 hour, air-cooling followed by water-cooling;

2. Ageing treatment at the following temperatures: 400°C, 420°C, 440°C, 480°C , 500°C, the ageing interval being 3 hours;

3. Ageing treatment at 480°C with maintaining durations of: 0,1h; 0,5h; 1h; 3h; 5h; 7h; 9h.

The samples for the traction test have been ellaborated in accordance with ASTM E9, having a calibrated area of 6,25 mm, and the resilience samples have been made with a V canal having dimensions of 10x10x55 mm. For the structural analysis thermally treated (at 820°C /1hour/air and 480°C /3 hours/air) samples have been used. Out of the 20mm bar, cylindric samples have been prelevated, with a size of 3 mm and a length of 50-70 mm. The final thinning has been accomplished by electrolytic polishing.

3. Obtained results and interpretation

3.1. The efect of the cooling method after austenitizing (air and water)

There have not been any significant effects noticed, regarding the influence of the cooling speed on the final mechanical features after conducting the thermal ageing treatment at 480°C/3hours/air. It is remarkable that when air cooling after the treatment for solubility, in the martensitic structure there remains an important amount of austenite of approximately 3%, which means the precipitation has not taken place. This austenite (γ) at the next ageing treatment shall transform in reannealed stable austenite (γ').

3.2. The influence of the ageing temperature on the mechanical characteristics

The initial thermal treatment of the bars has been: placing in solution at 820^0 C/1hour/air. The results of the mechanical trials that have been conducted are presented in Table 2.

Table 2. The results of the trials regarding the influence of the ageing temperature on the mechanical properties

No	Stamping	Ageing temperature	$R_{p0.2}$ DaN/mm^2	R_m DaN/mm^2	Z %	KCV J/cm^2
1	33;43	400	170.1	177.3	46	25
2	34;44	420	176.9	183.6	44	26
3	35;45	440	181.4	185.8	43	23
4	36;46	460	184.0	188.2	44	22
5	37;47	480	184,2	191,3	41	22
6	38;48	500	177,2	183,0	43	20

By analyzing the data shown in Table 2, the conclusion to be drawn is the increase of the mechanical characteristics along with the ageing temperature whilst maintaining a constant ageing interval (3 hours). The maximum of the resistance characteristics is obtained within the range of 480^0 C ± 10^0C. at lower temperatures of precipitation (400-440^0 C), the mechanical resistances, R_m and $R_{p0,2}$ are lower but associated with higher plasticity values (Z) and tenacity values (KCV) than in the case of the improvement at 480^0 C.The acquired results confirm that the mechanisms of precipiting at lower temperatures are slow, leading to fine precipitations of intermetallic compounds in the martensitic matrix, which are responsible for the lower resistance features and higher tenacity. The slight tenacity gain accomplished by ageing at 400-440^0C, with the price of an important loss in mechanical resistance compared to ageing at 480^0 C does not justify the ageing treatment al lower temperatures. The optimal association of resistance and tenacity properties is accomplished at temperatures of approximately 480^0 C with a maintaining duration of 3 hours.

3.3. The influence of the ageing maintaining duration (precipitation) on the resistance at cracking and on toughness

The results of the determinations are presented in Table 3

NOTE: The initial toughness of the samples after thermal treatment by placing in solution at 820^0C/1hour/air has varied between 29-32 HRC.By analyzing the results, one can easily observe the fast increase of the toughness proportional with the maintaining duration, subsequently demonstrating the high precipitation speed (the maraging reaction). Consequently, after maintaining at 480^0 C for 6 minutes, the toughness increased from approximately 32 HRC to 38.2 HRC.The precipitation processes combined with hardening are more intense during the initial periods of time, whilst for higher maintaining durations, the increases are minimal and have a tendency towards lowering.

Table 3. The experimental results regarding the influence of the ageing duration on toughness and resistance to cracking

No crt	Marcaj	Timp de imbatranire (ore)	Duritate HRC	Rezistenta la rupere R_m DaN/mm^2
1	53;63	0,1	38,2	146,3
2	54;64	0.5	45.4	170.4
3	55;65	1,0	50,5	186,2
4	56;66	3.0	53.0	195.3
5	57;67	5,0	52,0	191,4
6	68;68	7.0	53.2	190.5
7	59;69	9,0	53,0	194,0
8	61;71	11.0	53.0	189.5

3.4. The microstructural analysis

The investigations of the studied steel's microstructure after the treatments of placing in solution (820^0C/1hour/air) and of ageing (480°C/3hours/air) have been effectuated by scanning electronic microscopy (SEM) and transmission electronic microscopy (TEM).

The results of the micro structural analysis effectuated on Maraging 300 steel samples are shown in Figure 5. The structure of the material is constituted of martensite with fine granulation with finely contoured grain limits. These limits are identical to the limits of the former austenite grains.

In Figure 3, is presented the nickel and molybdenum compounds which have an uniform repartition within the field, within obviously greater nickel density.

The identification of the types of precipitates has been possible at more than 10000X magnifying. The samples thinned by electrolysis have been investigated by means of TEM. The microstructure of the Maraging steel which was studied is presented in Figure 4, in an image TEM magnified 10500:1 and in Figure 5 magnified 21000:1. One can observe the boundaries between the former austenitic grains and fine martensite needles with a diameter of 0,5-1 μm.

Fig.3. Secondary electrons image from the micro structure of the sample SEI 4020:1

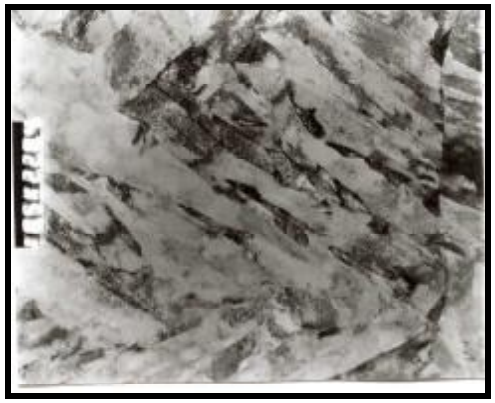

Fig.4. TEM image in luminescent field, 10500:1

The identification of the types of precipitates has been possible at more than 10000X magnifying. The samples thinned by electrolysis have been investigated by means of TEM. The microstructure of the Maraging steel which was studied is presented in Figure 4, in an image TEM magnified 10500:1 and in Figure 5 magnified 21000:1. One can observe the boundaries between the former austenitic grains and fine martensite needles with a diameter of 0,5-1 μm.

Also in Figure 6 magnified 13500:1, one can observe the existence of a cubic-shaped precipitate with a diameter of approximately 2 μm. The EDAX micro structural analysis has identified the existence of titanium nitride.

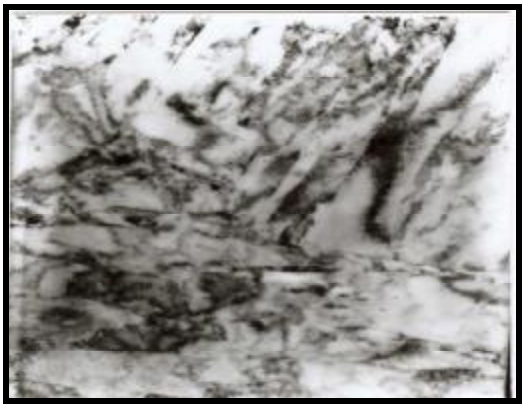

Fig.5. TEM image in luminescent field, 21000:1

Fig.6. TEM image in luminescent field, 13500:1

At over 100000:1 magnification, the substructure of individual martensite needles can be identified. For example in Figure 7 the TEM image in luminescent field, at magnification of 160000:1, indicates the fact that the substructure consists of very fine precipitates inside the matrix, with an interface between the martensite needles. The identification of the precipitates has been accomplished by TEM images in dark field. By using images in dark field on the same micro zone the Ni_3Mo phase is identified, with an orthorhombic network (spot 211). In Figure 8 there is the TEM image in dark field corresponding to the spot [211] of the Ni_3Mo phase. The SIGMA phase corresponds to the FeTi precipitate, according to specialists.

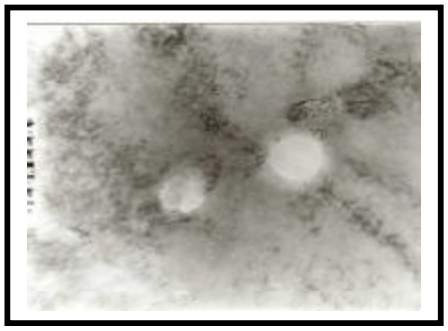

Fig.7 TEM image in luminescent field, 160000:1-The martensite and spherical precipitates

Fig 8. TEM image in dark field.160000:1 Orthorhombic phase Ni_3Mo, spot (211)

In Figure 9 the diffraction image is shown, with spots corresponding to both the matrix and to the precipitates. The precipitates have been identified as being an orthorhombic phase Ni_3Mo and a tetragonal SIGMA phase. The matrix's zone ax is [311], that of the Ni_3Mo compound is [120], and that of the SIGMA phase is [211].The image in Fig.10 realized in dark field, magnification 120000:1 shows the presence of the Ni3Mo precipitates, with orthorhombic structure (spot 211).

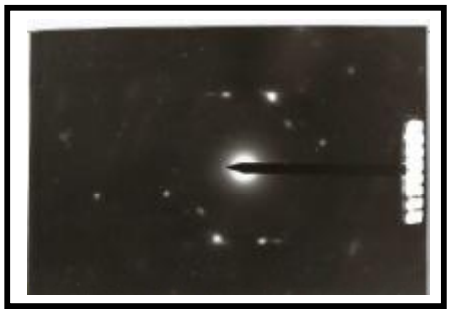

Fig.9. Diffraction electron image associated to the micro aria

Fig.10. TEM image in dark field 120000:1-Ni3Mo precipitates

4. Conclusions

The microstructure of the studied steel (Maraging 300) after conducting the thermal treatments (placing in solution and ageing) consists of lath martensite with a high density of dislocations.

Based on this martensitic structure, which lacks tetragonal structuring, with ageing, depending on temperature and maintaining duration, the precipitation of the

intermetallic phases takes place, and consequently the hardening according to an Orowan mechanism.

The spheric precipitates formed, with sizes between 2-4 nm, determine the moving dislocations to form loops (looping) or shears (shearing), which implies a significant increase of the mechanical resistance from the solution-included state to the precipitated state, with the preservation of high tenacity characteristics.

Our determinations showed two types of precipitated phases as follows: - an orthorhombic γ Ni_3Mo phase; - a tetragonal σ FeMo phase.

Received April 15, 2007

**SC Prelucrari Metalurgice PRODSRI.*
***Metallurgical Research Institute of Bucharest*
****University POLITEHNICA of Bucharest*
*****Defence University "CAROL I" of Bucharest*
******SC ZIROM SA*

REFERENCES

1. Decker, R.F., Bash, I.T., Goldman A.J. – **ASM Trans Quaterly**. 1964, nr. 55, pp.58-76.
2. Dennis, W.H. – **Maraging steels – Iron and steel, may** 1968
3. Decker, R.F., Bash, I.T., Goldman A.J. – *Maraging nikel-cobalt-molybdenum steels*, **Rev. ASM Trans Quaterly**, 1962:55.
4. Castagne, I.L., Cazin, Y. – *Development d'acier maraging a haute resistence* **Revue de Metallurgie**, ian. 1969.
5. Bourgeot, I – *Durcissement par revenue des martensites Fe-Ni-Mo et FeNiCoMo*, **Les Mem. La Metalurgie**, 2. 1973.
6. Floreen S. – **Metall. Rev.**, 1968, vol. 126(13), pp. 115-28.
7. Zhanli Guo. Wei Sha – **Materials Transaction, vol. 43, no. 6 (2002), pp. 1273-1282,**
8. ASuderman, V.K., Kim, S.J., Wayman, C.M **Metalls. Trans. A**, 1990, vol. 21A, pp. 2655-2668,
9. Sinha, P.P., Tharian, K.T. – **Mater. Sci. Technol.** 1998. vol.14, pp1-9.
10. Viswanathan, U.K., Dey, G.K., Asundi, M.K **Metall. Trans. A**, 1993, vol.24A, pp.2429-2442
11. Floreen S., Decker, R.F. – **ASM Trans. Q**., 1962, vol 55, pp.518-530
12. Pampillo, C.A., Paxton, H.W. – **Metall. Trans.**, 1972, vol 3, pp 2895-2903
13. Sha. W, Cerezo, A., Smith, G.D.W. – **Metall. Trans.A.** 1993, vol 24A, pp.1221-1232,
14. Tewari, R., Mazumdev, S., Batra, I.S., Dey, G.K., Banerjec, S **Acta Mater.**, 2000, vol. 48, pp. 1187-1200
15. Spitzing, W.A., Chilton, J.M., Barton, C.J. **ASM Trans.Q.** 1968, vol.61, pp.635-639.
16. Thomas, G., Cheng, L., Mihalisin, J.R **ASM Trans. Q.** 1969, vol.62, pp.852-857,
17. Yi-He, Ke Yang, Wei Sha **Metall. Trans. A**, vol.36A, september 2005. pp. 2273-2287.

CONSIDERATII PRIVIND REALIZAREA OTELURILOR MARAGING 300

Rezumat: Scopul lucrarii consta in realizarea si dezvoltarea otelurilor maraging 300 care prezinta caracteristici fizico-mecanice si structurale de exceptie si anume: rezistenta mecanica asociata cu o foarte buna tenacitate; rezistenta la oboseala remarcabila (de cca. 3 ori mai mare decat la otelurile clasice inalt aliate); sudabilitate ridicata; prelucrabilitate prin aschiere foarte buna ce poate fi facuta la dimensiuni finale. Lucrarea prezinta cateva aspecte legate de stadiul actual al producerii otelurilor de tip maraging precum si efectul tratamentului termic asupra caracteristicilor fizico-mecanice si structurale ale acestor oteluri.

BULETINUL INSTITUTULUI POLITEHNIC DIN IAŞI
Tomul L(III (LVII), Fasc. 4, 2007
Secţia
ŞTIINŢA ŞI INGINERIA MATERIALELOR

ASPECTS REGARDING THE MODERNIZATION OF THE AIR-STEAM DROP HAMMERS WITH DOUBLE EFFECT

BY

NEDELCU MARIA[1] and SUSAN MIHAI[2]

Abstract: This work presents the modernization possibilities of the double effect air-steam drop hammers, with distribution through four valves, which have as objective function the consumption of driving agent.

Keywords: drop hammer, modernization, distribution with valves, driving agent, logical diagram, optimization

1. Introduction

The modernization of the air-steam drop hammers (which use as working agent -medium- the compressed air or steam), often called also the pneumatic-steam hammer, is nowadays one of the possibilities of achieving the technical progress for this type of equipments [1].

2. The optimal calculus of the distribution mechanism at the double effect air-steam drop hammer

In this part of the paper we will present a calculation method (4) which shows the continuous variety of the energetic parameters reported to the movement of the hammer's ram

The calculus method takes into consideration the valve distribution system for a double effect air-steam drop hammer, as presented in figure 1 [4].

The movement equation is, for the distance x(m) routed by the ram:

$$m\ddot{x} = mg + p_{ec}s_s - p_{ex}s_i - F_F - p_{ec}s_t \qquad (1)$$

from which we get

$$\ddot{x} = \frac{mg + (p_{ec} - p_{ex})s_t - (p_{ex} - p_{ec})s_i - F_f}{m} \qquad (2)$$

where $S_t = S_s + S_i$ (3)

For the admission phase of the fluid, admitting a pressure drop of Δp per 1 m of the stroke:

$$P_{ex} = p_a - X\ \Delta p,\ \ p_{ex} = c_t \qquad (4)$$

and

$$x \in (0, H_s)$$

Taking in mind (4), the equation (2) will be written:

$$\ddot{x} = \frac{mg + (p_{ec} - p_a - x\Delta p)s_t - (p_{ec} - p_{ex})s_i - F_f}{m} \qquad (5)$$

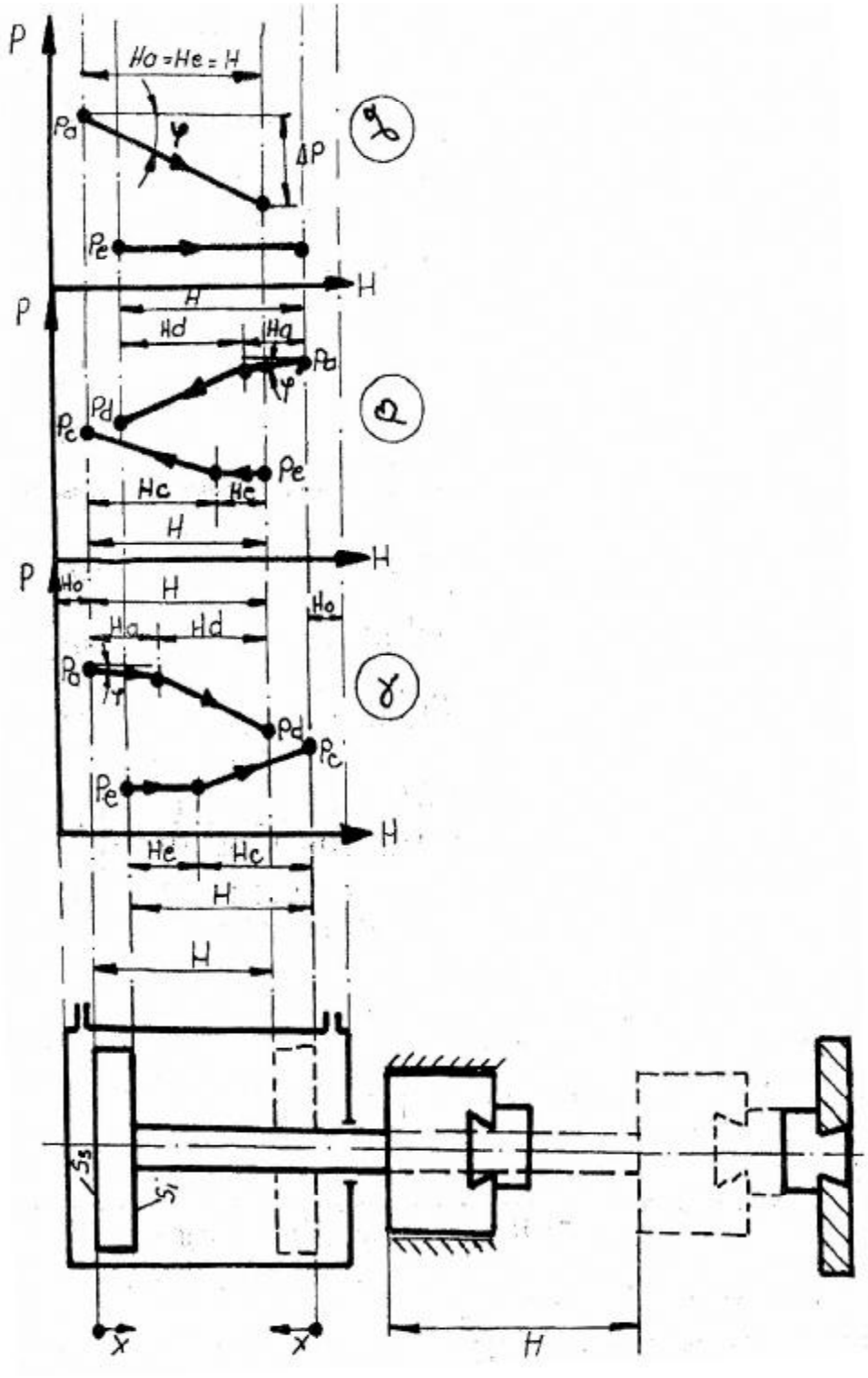

Fig. 1. Valve distribution system for double effect air-steam drop hammer
m - ram's weight ; H - maximum stroke of the ram ; a admission ; d slackening ; c compression ; e exhaustion ; p pressure ; S_s - upper piston surface ; S_i - inner piston surface ; F_f - friction force ; H_0 - dead space ; α - lowering with admission and slackening in the upper space and exhaustion ; β - abduction ; γ - lowering with permanent admission in the upper space and permanent exhaustion in the lower space.

which can be written also:

$$\ddot{x} + \omega x^2 = A_1 \tag{6}$$

where:

$$A_1 = \frac{mg + (p_r - p_{at})s_a - (p_r - p_{at})s_i - F_f}{m} \tag{7}$$

and

$$\omega = \sqrt{\frac{\Delta p \cdot S_a}{m}} \tag{8}$$

Solving equation (6) we get:

$$x = \frac{A_1}{\omega^2}(1 - \cos \omega t) \tag{9}$$

$$\dot{x} = \frac{A_1}{\omega} \sin \omega t \tag{10}$$

$$\dot{x} = A_1 \cos \omega t \tag{11}$$

For $x = H_a$ we can calculate the admission time:

$$t_a = \frac{1}{\omega} \arccos\left(1 - \frac{H_a \omega^2}{A_1}\right), \quad v_a = \frac{A_1}{\omega} \sin \omega t_a \tag{13}$$

and

$$a_a = A_1 \cos \omega t_a \tag{14}$$

For the slackening phase the motion equation is:

$$a_c = A_1 \cos \omega t_a \tag{15}$$

Considering as origin point for x the point where slackening begins and considering that this has a politropic character (parameter n), we can write:

$$p_{ic}(H_a + H_c + x)^n = (p_r - \Delta p H_a)(H_c - H_a)^n \tag{16}$$

or

$$p_{ic} = (p_a - \Delta p H_a)\left(\frac{H_c + H_a}{H_c + H_a + x}\right)^n \tag{17}$$

The same for the compression phase:

$$p_{ic} = p_r - \left(\frac{H_a + H - H_a}{H_c + H - H_a - x}\right)^n \tag{18}$$

Considering equations (17) and (18), we can conclude from (15):

$$\ddot{x} = -\frac{mg - F_f - p_{at}s_a + p_{at}s_i}{m} + \frac{(p_r - \Delta p H_a)(H_a + H_a)s_a}{m} \cdot \frac{1}{(H_a + H_a - x)} - \frac{p_a(H_a + H - H_a)}{m} \cdot \frac{s_i}{H_a + H - H_a - x} \tag{19}$$

Notations:

$$A_2 = \frac{mg - F_f - p_{at}s_a - p_{at}s_i}{m} \tag{20}$$

$$A_3 = \frac{(p_r - \Delta p H_a)(H_a - H'')s_a}{m} \tag{21}$$

$$A_1 = \frac{\rho_a (H_0 + H - H_a)^n}{m} s \qquad (22)$$

The equation (20) can also be written:

$$\ddot{x} = A_2 - A_3 \cdot \frac{1}{(H_0 + H_c + x)} - A_4 \cdot \frac{1}{(H_0 + H - H_a - x)^n} \qquad (23)$$

Notation: $\dot{x} \quad y(x) \quad \rightarrow \quad \ddot{x} \quad y\frac{dy}{dx}$.

We can apply in case of equation (23):

$$ydy = \left[A_2 + \frac{A_3}{H_0 + H_c + x} - \frac{A_4}{(H_0 + H - H_a - x)^n}\right] dx$$

Integrating the equation we obtain:

$$y^2 \quad 2A_2 x + \frac{1}{1 \quad n}\frac{2A_3}{(H_0 + H_c + x)^{n-1}} + \frac{2A_4}{(1 \quad n)(H_0 + H \quad H_a \quad x)^n} + 2C_1 \qquad (24)$$

The expression (24) becomes for the initial conditions:

$$t \quad t_0;\ x = 0;\ \dot{x} = \frac{A_1}{\omega}\sin\omega t_0$$

$$\frac{A_1^2}{\omega^2}\sin^2\omega t_0 = \frac{1}{1-n}\frac{2A_3}{(H_0 + H_c)^{n-1}} - \frac{2A_4}{(1-n)(H_0 + H - H_a)^{n-1}} - 2C_1$$

We get:

$$C_1 = \frac{A_1^2}{2\omega^2}\sin^2\omega t_0 - \frac{1}{1-n}\frac{A_3}{(H_0 + H_c)^{n-1}} - \frac{A_4}{(1-n)(H_0 - H - H_a)^{n-1}}$$

And the ram's velocity at the end of the slackening phase of the fluid:

$$v_d^2 = 2A_2 H_d + \frac{A_1}{\omega^2}\sin^2\omega t_0 + \frac{2A_3}{n \quad 1}\left[\frac{1}{(H_0 + H_c + H_d)^{n-1}} - \frac{1}{(H_0 \quad H_c)^{n-1}}\right] -$$

$$-\frac{2A_4}{n-1}\left[\frac{1}{(H_0 + H - H_a + H_d)^{n-1}} - \frac{1}{(H_0 - H - H_a)^{n-1}}\right] \qquad (25)$$

Noting $H_a - H_c = kH$ and $H_d - H_c = (1\text{-}k)H$, expression (25) becomes:

$$v_d^2 = 2A_2(1-k)H + \frac{A_1}{\omega^2}\sin^2\omega t_0 + \frac{2A_3}{n-1}\left[\frac{1}{(H_0 + H)^{n-1}} - \frac{1}{(H_0 - kH)^{n-1}}\right] -$$

$$-\frac{2A_4}{n-1}\left[\frac{1}{(H_0)^{n-1}} - \frac{1}{(H_0 - (1-k)H)^{n-1}}\right]$$

We know that: $v \quad \frac{dx}{dt} \quad \rightarrow \quad dt \quad \frac{dx}{v}$

And for the slackening phase:

$$t_d \quad \int_0^{t_d} \frac{dx}{v(x)} \quad \int_0^{H_d} f(x)dx \qquad (26)$$

In order to calculate the definite integration (26) we use the trapeze method which for the curve graduation $(0 \ldots H_d)$ in N equal intervals permits us to write expression (26) as:

$$t_d = \frac{h}{2}\sum_{i=1}^{H_d}\left[f(x_i) + f(x_i - 1)\right] \qquad (27)$$

Where:

$$h = \frac{H_{sl}}{N-1} \quad \text{şi} \quad x_i = x_{i-1} - h; \quad x_1 = 0$$

N = number of points in which we divide the interval

The lowering time will be:

$$t_c = t_a + t_d \tag{28}$$

The logic of this calculation is similar to the one used for lowering. The ram's movement equation is:

$$m\ddot{x}' = -mg + (p_{ex} + p_{at} - x'Ap)s_s - (p_c - p_{ex})s_s - F_f' \tag{29}$$

$$A_1' = \frac{-mg - (p_c - p_{ex})s_s - (p_{at} - p_{ex})s_s - F_f'}{m} \text{ and } \omega' = \sqrt{Aps_s / m}$$

thus we obtain the ram's movement equation for abduction:

$$\ddot{x}' + \omega'^2 x' = A_1' \tag{30}$$

$$\dot{x}' = \frac{A_1'}{\omega'^2}(1 - \cos\omega' t) \tag{31}$$

$$\dot{x}' = \frac{A_1'}{\omega'^2}\sin\omega' t \tag{32}$$

$$\dot{x}' = A_1' \cos\omega' t \tag{33}$$

Which for $x' = H_s'$ becomes:

$$ta' = \frac{1}{\omega'}\arccos\left(1 - \frac{H_s\omega'^2}{A_1'}\right) \tag{34}$$

$$v_c' = \frac{A_1'}{\omega'^2}\sin\omega' t_c' \tag{35}$$

$$a_c' = A_1' \cos\omega' t_c' \tag{36}$$

For the slackening phase, the calculation is made in the same way as for the abduction and the constants become:

$$A_3' = \frac{mg - F_f' + p_{at}s_s - p_{ex}s_s}{m} \tag{37}$$

$$A_2' = \frac{(p_c - Ap_aH_1)(H_2 - H_1)^n}{m}s_s \tag{38}$$

$$A_4' = \frac{p_c(H_0 + H - H_c)^n}{m}s_s \tag{39}$$

and in a similar way for lowering:

$$v_d' = 2A_3'(1-k)H + \frac{A_1'}{\omega'^2}\sin\omega' t_c' - \frac{2A_4'}{n-1}\left[\frac{1}{(H_c + H)^{n-1}} - \frac{1}{(H_0 - kH)^{n-1}}\right] - \frac{2A_4'}{n-1}\left[\frac{1}{(H_2)^{n-1}} - \frac{1}{(H_0 + (1-k)H)^{n-1}}\right] \tag{40}$$

and

$$t_c' = \frac{h'}{2}\sum_{i=2}^{n_0}\left[\Gamma'(x_i) - \Gamma'(x_{i-1})\right] \tag{41}$$

Where:

$$h' \quad \frac{H'_c}{N-1} \qquad , \qquad x_i - x_{i-1} - h'$$

and

$$C_1 - \frac{A_1'^2}{2\omega'^2}\sin^2\omega' t_1 - \frac{1}{1-n}\frac{A'_1}{(H_c+kH)^{n-1}} - \frac{A'_1}{(1-n)(H_c+(1-k)H)^{n-1}} \quad (42)$$

The abducting time $t_r - t'_R + t'_d$ (43)

Number of strokes per minute $n_c - \frac{60}{t_c + t_c + t_g}$

Where t_s is the heating time at the end of a stroke.

The hitting power for the stroke H (without semi-product on the hammer)

$$E \quad \frac{mv_c^2}{2} \text{ and } E_{ef} = \eta E \quad (44)$$

where :

E_{ef} – effective energy

η rated capacity of the hammer

In case we consider the height h of the semi-product, this will be considered when calculation the height at lowering and also abduction (H1 = H + h).

3. Optimisation elements for the ditribution of the drop hammer of 12.5 kN.

The diagram is presented in figure 2 [4].

As objective function we chose minimum consumption of fluid. This can be calculated for a strike, using the expression:

$$\varphi - H_{as}S_s + H_{ai}S_i, m^3/\text{beat} \quad (45)$$

Where H_{as} and H_{ai} are respectively the admission strokes of fluid during the lowering and abduction of the ram. Evidently, for total admission (k = 1), H_{as} H_{ai} – H

Calculation data:

Ram's stroke …	H = 0,5 ….0,7	m
Dead space …	H_0 = 0,1 H	m
Piston's diameter. .	D = 0,5	m
Cane`s diameter…	d_t = 0,35	m
Ram's weight…	m = 1250	kg
Hitting power…	E = 36	kJ
Number of hits .	n_c – 120..150	lov/min
Pressure when inputting the liquid …	p_a – 6 x 10^5	Pa (absolute value)
Pressure when exhausting the liquid .	p_e = 1,2 x 10^5	Pa
Pressure drop...	Δp_a – 2 x 10^5	Pa/m
Fiction force	F_f = 0,1 mg	N
Polytrophic coefficient	n = 1,25	
Number of divisions	N – 25	
Efficiency	η = 0,69	

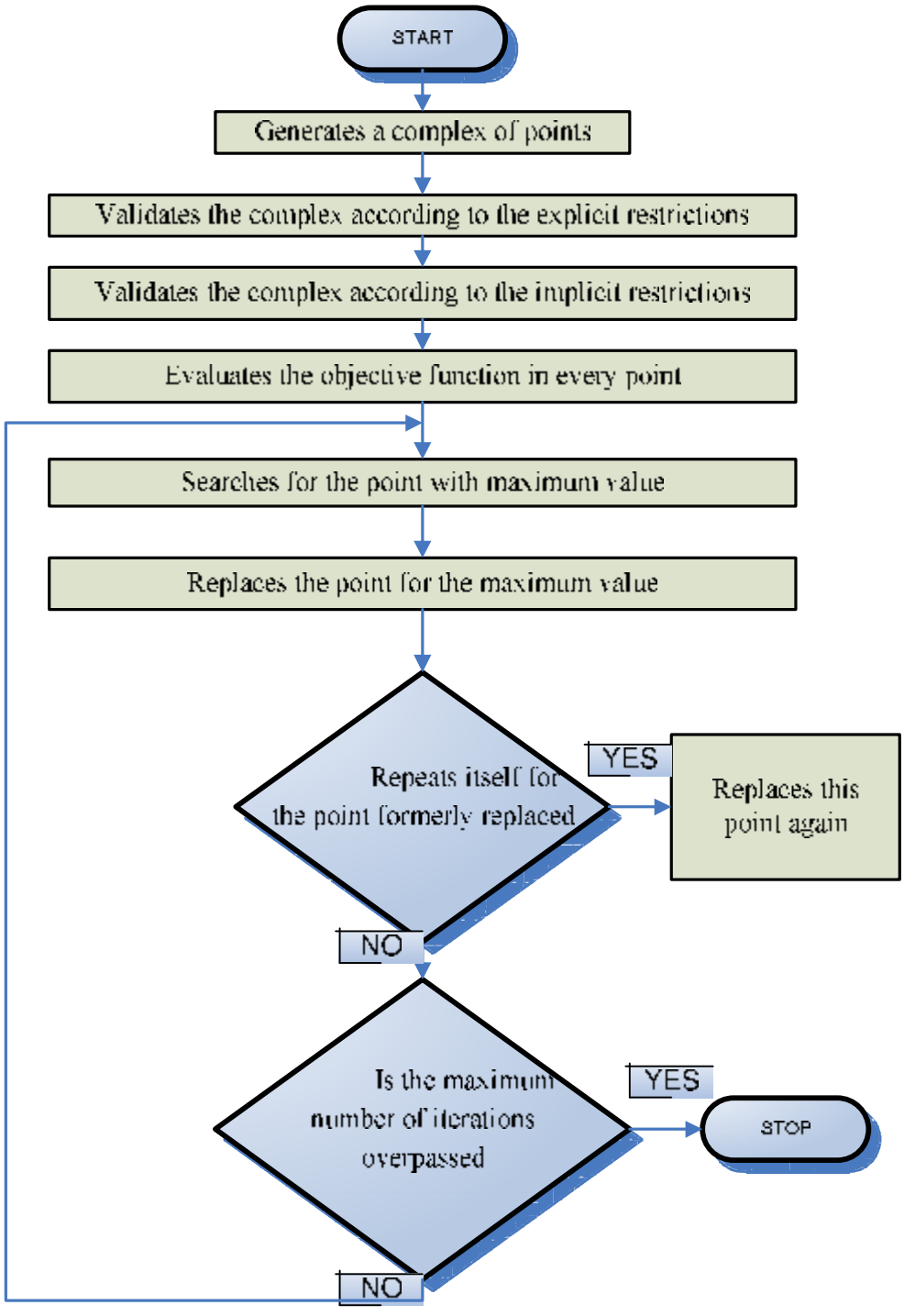

Fig. 2 [4] Diagram modernization of the drop hammer

As implicit variables we chose the hitting power and the number of hits per minute and as independent explicit variables of the projection II, D, d_t and m. Optimal obtained results: m = 620 kg; D = 0,3982 m; d_t = 0,2042 m; H = 0,4086 m

4. Conclusions

This paper presents ways of modernization of the drop hammers with fixed bed plate existing in Romania, with distribution through four valves, and which function according to the diagram shown in figure 1.

As objective function it was considered the minimum consumption of working agent, according to equation (45).

The calculation example takes studies the double effect drop hammer, with fixed bed plate, with the weight of the mobile part 12,5 kN.

Received April 26, 2007

[1] Scoala de Arte si Meserii "N.Stolenu" Baia, Jud. Suceava
[2] *The "Gh.Asachi" Technical University Iaşi*

REFERENCES

1. Moldovanu V., Maniu A., **Utilaje pentru deformari plastice**, E.D.P. Bucuresti, 1982
2. Moldovanu V., Chirita V., **Exploatarea rationala a masinilor de forjat**, E.T. Bucuresti 1979
3. Susan M., **Deformarea metalelor prin forjare**, Ed. Tehnopress Iasi 2002
4. Moldovanu. V., Dimitriu S., **Modernizari in sectiile de forjare**, Ed. Transilvania Press, Cluj-Napoca 1993

CONSIDERATII PRIVIND MODERNIZAREA CIOCANELOR MATRITOARE ABUR-AER CU DUBLU EFECT

Rezumat: In lucrare se prezintă posibilităţi de modernizare a ciocanelor matriţoare abur-aer cu dublu efect, cu distribuţia prin patru supape, având ca funcţie obiectiv agentul motor.

BULETINUL INSTITUTULUI POLITEHNIC DIN IAŞI
Tomul L(III (LVII), Fasc. 4, 2007
Secţia
ŞTIINŢA ŞI INGINERIA MATERIALELOR

THE THERMODYNAMICAL ANALYSIS OF THE ECONOMICAL-ECOLOGICAL EVENTS MUST BE COMPLETED WITH ESTIMATIONS BASED ON THE SYSTEM THEORY AND PROCESS KINETICS

BY

AVRAM NICOLAE, MIRELA SOHACIU, IRINA VÎLCIU and BRÂNDUŞA NETTY MILEA

Abstract: Today, it becomes really necessary to define and bring in operation new models, which characterize the relationships between the economy, ecology and environment. The thermodynamical analysis of the economical-ecological events, which is already used, is placed within such a framework. In order to develop the environmental engineering as a scientific branch it is necessary to complete such an activity with new analyses based on information theory applied to the systems and kinetics of chemical-metallurgical processes.

Keywords: economy, ecology, environment, models, thermodynamical analysis

1. Introduction

The dynamics of resources utilization, which are considered *productive components of natural medium*, has a great significance for the metallurgical engineer in the analyses performed to characterize the *economical – ecological - environmental relationships*. The role of the natural resources in the optimization of the economical-ecological models is justified by reasons as:

- the natural resources have the *stock-support* function for the economical inputs;
- the resource provides directly streams useful for the economical agents;
- the natural capital, under certain conditions, can be substituted with the other forms of capital;
- while they are not exhausted, the natural resources can compensate the negative effect of the waste emission in the environment; they contribute in such a way to maintain *the capacity of auto-sustainability* (including *the auto-recirculation)* of the environment

The conversion of the above findings into real instruments of bringing in operation the environmental resources as dynamic factor of sustainable development imposses laborious analyses, which will be presented below

2. The thermodynamical analysis of the economy – ecology - environment (resources) system

One starts from the following hypotheses:

a) The I^{st} and II^{nd} principles of thermodynamics can be used to evaluate the relationships between different economical-ecological parameters (indicators);

b) Concrete evaluations can be made by using as working tools *the thermodynamical potential, enthropy, negaenthropy (antienthropy), respectively.*

In the literature on economical theory there is used the thermodynamic isochore potential or the free energy Helmholtz, F. In metallurgy, where the quasitotality of the processes runs at constant pressure, it is necessary to use the isobar potential or the free enthalpy Gibbs, G.

Function of the enthalpy II, the temperature T and enthropy S, the variation of G potential between two levels of the process or two its qualitative stages is:

$$\Delta G = \Delta II - T\,\Delta S \qquad (1)$$

In the nature, a process can be self-developing (spontaneous), without energy consumption, only when the thermodynamic potential decreases and reaches the zero in the equilibrium state.

The characterization of these processes is given by the inequality:

$$G_{final} - G_{initial} = \Delta G = (\Delta II - t\,\Delta S) < 0. \qquad (2)$$

Inverse conversions, where G increases, are impossible under no circumstances

The enthropy S is a measure of the disorder degree (chaos) of matter organization. The S increase (according to the G decrease) characterizes the spontaneous tendency of the systems to chaos. The isolate physical systems are permanently subjected to the tendency of enthropic degradation, chaos, which reaches the maximum in the final stage of the natural equilibrium. Because of the permanent changes of matter, energy and substance, the open systems, like the production ones are, can organize the activity to an antienthropic direction, to minimal levels of the enthropy value. In such circumstances, the level of ordinate organization can be evaluated using parameters as negaenthropy or antienthropy (aS). One can state that at a given moment of the transformation (development), the system becomes a depositary of antienthropy.

The thermodynamical analysis of economy-environment systems can generate results as those presented furtherly:

- Metallurgical processes cannot perform spontaneously from theirself. They need a special condition to run, which is characterized by enthalpy consumption, thus $G_{final} > G_{initial}$. G_{final} corresponds to the product delivery state for consumption.
- The increasing variation through enthalpy consumption, $\Delta G > 0$, can be a measure of energy for the *added value* during the transformation process of resources into consumption products. It can be stated, for example, that during the transformation of usual plate into an enamelled one, new added value can be evaluated using the difference between thermodynamic potentials of both states ($G_{\text{enamelled plate}} - G_{\text{usual plate}}$).
- $G_{initial}$ must contain also the energy quantum requested by *autophagy (selfconsumption) processes* for capitalization of resources having inferior quality.
- Complying with the Ist principle, there are no processes running without losses (material and energetic ones) from the own boundary to the environment. Under such circumstances, *one propose to analyse pollution (transfer of materials and energy to environment) as process loss to the environment.*
- Pollution considered as being a loss to the environment, is an enthropical phenomenon increasing the degree of disorder (e.g. the dust released into the

atmosphere). Natural resources are ordinated materia. One can state that through technological processing of raw materials *negaenthropy stocks of the natural environment* are used. Technology itself is a source of negaenthropy by increasing the degree of natural order.

- Materials and energy released into the environment as pollutants increase their own degree of disorder directly proportional to the increase of distance from sources
- The enthropy of resources stock decreases function of the increase of their diversity and specialization.
- Based on the above mentioned, one can take following measures:
  - more recyclings mean a lower degree of ordinate materials and energy; it is recommended to *reduce the number of recyclings in a stream.*
  - the recycling within an aggregate (*internal recycling)* is superior to *external recyclings;*
  - due to the fact that the degree of disorder increases directly proportional to the distance from the metallurgical aggregate, one recommends that recovery has to be performed *as near as possible to the source.*
- The environmental downgrading by pollutant emissions (high enthropy), can and must be compensated by creating ecological goods and services (antienthropic stock increase). One can conclude that recycling of wastes must be combined with natural raw material additions

3. Using the systems theory in order to perform the analysis of economical-ecological events

The simpliest (primary) systemic structure of a production stream is:

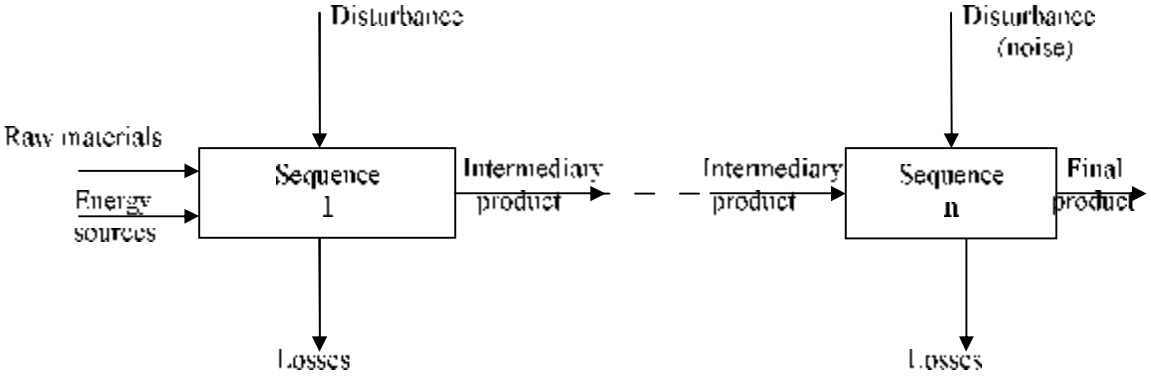

Based on the systems theory, one can retain following:

- that pollution has to be considered as a disturbance (noise) of the process system running. According to the systems theory, *a certain amount of noise must exist* for order keeping, which has to provide information on the systems condition.
- complying with the above mentioned, a certain amount of disturbance has to be provided in order *"to keep alive"* the system. Thus, *one sustains that "null - pollution" has not only to be reached, but also a minimal pollution amount has to be provided.*
- as a proposal, *feed-back routes* must be considered a support for recirculated secondary materials.

- if recirculated secondary materials (wastes) are subjected to feed-back, they can perform two tasks, namely:
  - transport of materials (secondary materials resources - RMS) and energy (secondary energy resources - RES);
  - information transport mainly referring to technological deviations which produced wastes; by reintroducing them into primary stream sequences, such information become *instruments for system (self)control*;
- the amount of recirculated wastes with feed-back support depends upon the value of entries, which can be diminished by *minimizing* raw materials, fuel and energy *specific consumptions*. In this manner, one contributes to fulfilling an old dream of industrial producers: *dematerialization and decarbonization - denitration of production streams.*

4. Analysis based on the kinetic theory of processes

The above defined analyses can provide information concerning the spontaneous running direction of a process or the costs required for sustaining the process running in reverse direction.

As concern production processes, *the unfolding rate of a certain event* is also very important. In such a context, it is interesting to mention that for development strategies modelling not only the *propagation direction of phenomena, but the evolution rate of history too.*

In the case of metallurgy, one could observe that the utilization of enthalpy is demanded for the reversal of G. A similar measure has to be taken for economic-productive projects and processes which show the trend to spontaneous running in the desired direction, but which naturally *are very slow* and are not economically efficient.

Information concerning the rate of processes are provided by *the kinetic theory of processes.* That means in the case of analysing some indicators such as *productivity, resources exploitation* etc., one must use analyses based on process kinetics.

Received March 6, 2007 *Polytechnic University Bucharest*

REFERENCES

1. Nicolae, A., ş.a., **Operaţionalizarea conceptului DD în siderurgie**. Ed. Printech, Bucureşti. 2006;
2. Negrei, C., **Economia şi politica mediului**, www.asc.ro;
3. Grădinaru, I., **Protecţia mediului**. Editura Economică, Bucureşti, 2000.

ANALIZA TERMODINAMICĂ A EVENIMENTELOR ECONOMICO-ECOLOGICE, COMPLETATE CU ESTIMĂRI BAZATE PE TEORIA SISTEMELOR ŞI CINETICA PROCESELOR

Rezumat: A devenit astăzi necesară definirea şi aplicarea a noi modele, ce trebuie să caracterizeze relaţiile dintre economie, ecologie şi mediu. Analiza termodinamică a evenimentelor economico-ecologice este o modalitate care se aplică deja în acest domeniu. Pentru dezvoltarea ingineriei de mediu, ca ramură ştiinţifică, vor trebui realizate asemenea modelări, cu folosirea teoriei informaţiei aplicate acestor sisteme şi a cineticii proceselor chimice şi metalurgice.

BULETINUL INSTITUTULUI POLITEHNIC DIN IAŞI
Tomul LIII (LVII), Fasc. 4, 2007
Secţia
ŞTIINŢA ŞI INGINERIA MATERIALELOR

STUDY ABOUT BRAZING TECHNOLOGY

BY

IONEL OLARU

Abstract: Brazing can be described as the joining of two components by a coalescence of the surfaces in contact with each other. Brazing is the more modern solid phase techniques are typified by friction welding, being also an ancient process, is one that involves a braze metal which melts at a temperature above 450 °C but below the melting temperature of the components to be joined so that there is no melting of the parent metals. Torch brazing is commonly used on copper, brass, and other copper alloys, as well as steel, stainless steel, aluminum, carbides, and various heat-resistant materials.

Keywords: aluminum, brazing, brazed joint.

1. Introduction

Aluminum is available in both wrought and cast forms. The wrought forms comprise hot and cold rolled sheet, plate, rod, wire and foil. The ductility and workability of aluminum mean that extrusion is a simple method of producing complex shapes, particularly for long, structural members such as I and II beams, angles, channels, T-sections, pipes and tubes. Forging, both hot and cold, is used extensively as a fast, economical method of producing simple shapes. Precision forging is particularly suitable for aluminum alloys, giving advantages of good surface finish, close tolerances, optimum grain flow and the elimination of machining.

Aluminum is compound by the atoms, in the metal atoms are arranged and each grain is a crystal with a regular array of atoms but at the boundaries between the grains there is a mismatch, a loss of order, in the orientation of these arrays.

Grain size is not generally used to control strength in the aluminum alloys, although it is used extensively in reducing the risk of hot cracking and in controlling both strength and notch toughness in C/Mn and low-alloy steels.

In general terms, as grain size increases, the yield and ultimate tensile strengths of a metal are reduced. The yield strength σ_y, is related to the grain size by the Hall–Petch equation:

$$\sigma_y = \sigma_1 + k_y d^{-1/2} \qquad (1)$$

where d is the average grain diameter, and σ_1 and k_y are constants for the metal Typical results of this relationship are illustrated in Fig. 1.

If consider an ideally brazing this is meant the complete joint comprising the brazed metal, heat affected zones and the adjacent parent metal, should have the same properties as the parent metal. There are, however, a number of problems associated with the brazing of aluminum and its alloys that make it difficult to achieve this ideal The features and defects that may contribute to the loss of properties comprise the

following: oxide inclusions and oxide filming, solidification (hot) cracking or hot tearing, reduced strength in the weld and heat affected zones, lack of fusion, reduced corrosion resistance

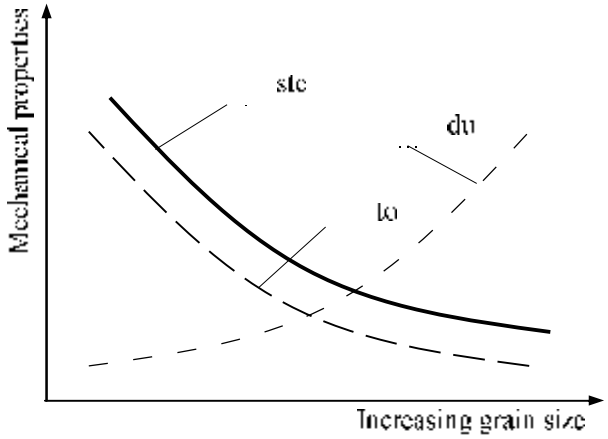

Fig. 1. General relationship of grain size with strength, ductility and toughness

Few mechanical properties for aluminum alloys are shown in Table 1

Table 1. Mechanical properties for aluminum alloys

Alloy	Condition	Proof (Nmm^2)	Ultimate tensile strength (Nmm^2)	Elongation (%)
1060	O	28	68	43
1060	H18	121	130	6
5083	O	155	260	14
5083	H34	255	325	5
6063	O	48	89	32
6063	TB(T4)	100	155	15
6063	TF(T6)	180	200	8
2024	O	75	186	20
2024	TB(T4)	323	468	20

2. Brazing preparations

Components for brazing may be flat, preformed, sheared, sawn or milled to give the desired shape or to provide the weld preparation. Lubricants used during these processes must be removed if weld quality is to be maintained.

Degreasing may be accomplished by wiping, brushing, spraying or vapors degreasing with commercially available solvents. This is best done before any mechanical cleaning takes place. Mechanically cut edges may carry burrs along the cut edge that will trap dirt and grease. These burrs should therefore be removed from weld preparations by scraping with a draw tool do not wires brush only as this may fail to remove them completely.

Scraping is also an excellent method for removing the oxide film. Stainless steel wire brushes, stainless steel wire wool or files may also be used to remove the oxide.

There are few more important decisions that affect the success of brazing than that of correct brazed joint design. Problems with weld quality or performance can

often be attributed to the wrong design of edge preparation. Brazed joint design is determined by the strength requirements, the alloy, and the thickness of the material, the type and location of the joint, the access for brazing and the brazing process to be used.

There are three fundamental forms of weld, the butt, the fillet and the edge weld, (Fig. 2), from which can be developed six ore more basic joint types, these are the butt, T-joint, corner, cruciform, edge and lap joint and more.

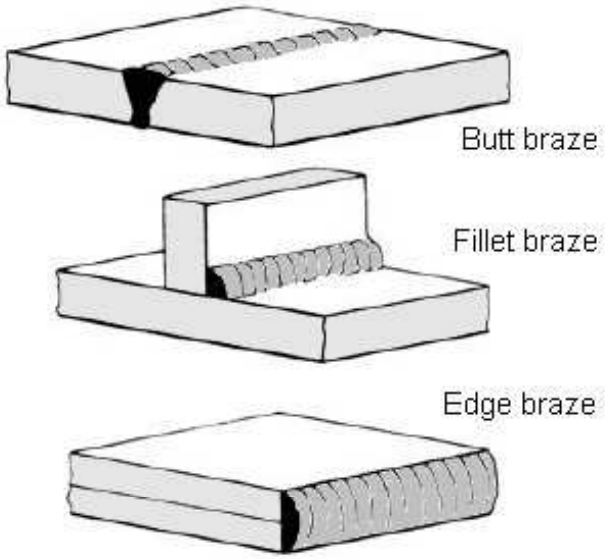

Fig. 3 Butt, filler and edge brazes

3. Brazing operation

Torch brazing utilizes a fuel gas flame as the heat source for the brazing process. The fuel gas is mixed with either air or oxygen to produce a flame, which is applied to the workpiece until the assembly reaches the proper brazing temperature. Then, preplaced filler metal will be melted or hand-fed wire can be introduced (Fig. 4).

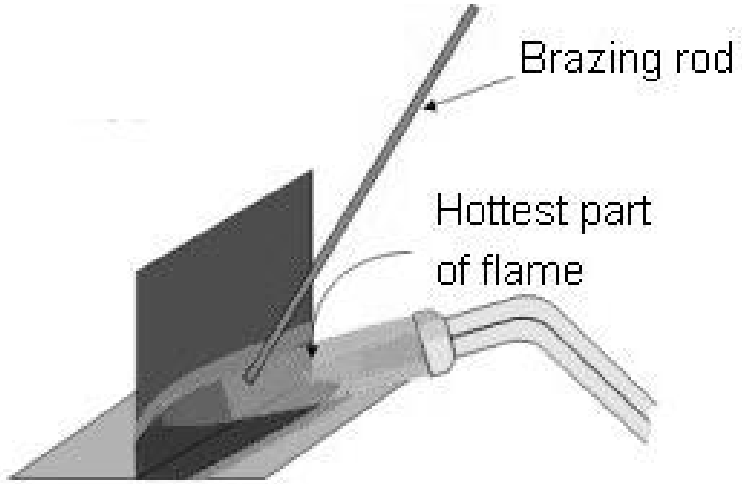

Fig. 4. Torch brazing

Torch brazing is commonly used on copper, brass, and other copper alloys, as well as steel, stainless steel, aluminum, carbides, and various heat-resistant materials. Most combinations of these materials can also be torch brazed. It is necessary to use flux with these materials, except when a phosphorus brazing alloy is used to braze pure copper parts. In this case, the phosphorus acts as the flux. The low-temperature silver-base and silver/copper/phosphorus filler metals are commonly used with torch brazing. Various other copper-base and gold-base filler metals can also be used with this process.

Torch brazing is often used to join copper and Bundy steel tube assemblies for the heating, air conditioning, and refrigeration industries. The process is also commonly used when brazing heat exchangers, bicycles, furniture, carbide tools, plumbing components, automotive subassemblies, medical instruments, and many other workpiece types. A wide range of components can be torch brazed, including small joints for jewelry parts, large-diameter (75 mm, or 5 in.) tubes, and fitting joints. The process provides strong, leak-tight joints on a wide variety of base materials.

The equipment for torch brazing has several components (Fig. 5). Single torches are typically used for hand brazing, whereas multiple torches can be used in an automated system. The gas-oxygen is mixed in the torch body and is adjusted using the needle valves on the torch. Gas-air combinations can be mixed at the torch or, alternatively, a central mixing system can be used to supply many torches, particularly in automated applications.

Fig. 5. Automated torch brazing system

Torch brazing gases are normally supplied from bulk sources. An individual gas cylinder may supply one torch, whereas large bulk tanks are used to supply many torches or an automated system utilizing many burners. In all torch brazing systems, regulators are used to safely control the gas distribution. Individual regulators are used on the gas and oxygen lines. Standard safety precautions should be utilized when handling the equipment, and operators should be thoroughly trained in safety practices related to the use of compressed and combustible gases.

Received March 15, 2007 *University of Bacau*

REFERENCES

1. ***, **Brazing handbook**, 4th ed., American welding society, 1991
2. ***, **The brazing book**, Handy & Harman/Lucas-Milhaupt, inc., 1991
3. Gene Mathers, **The welding of aluminium and its alloys**, Woodhead Publishing Ltd. Cambridge England, 2002

STUDII PRIVIND TEHNOLOGIA BRAZĂRII

Rezumat: Brazarea poate fi descrisă ca: fiind îmbinarea a două elemente componente prin: fuziunea suprafeţelor în contact cu o alta printr-un material de adaos. Brazarea este cea mai modernă tehnică în fază solidă care este caracterizată printr-o sudură prin frecare, de asemenea un foarte vechi proces, este acela de amestecare a metalului de brazare care se topeşte la o temperatură de aproximativ 450°C dar mai mică decât temperatura de topire a componentelor ce urmează a fi lipite, deci aceasta nu se realizează prin amestecarea metalelor principale. Brazarea cu flacără este mai mult utilizată cu cupru, alamă, şi alte aliaje pe bază de cupru, la fel de bine ca oţelul, oţelul inoxidabil, aluminiul, şi multe alte materiale rezistente termic.

BULETINUL INSTITUTULUI POLITEHNIC DIN IAŞI
Tomul LIII (LVII), Fasc. 4, 2007
Secţia
ŞTIINŢA ŞI INGINERIA MATERIALELOR

OVERVIEW ON WELD AND BRAZE DEFECTS AND NON DESTRUCTIVE TESTING METHODS

BY

IONEL OLARU and CODRIN COBREA

Abstract: Brazing is the more modern solid phase techniques that are typified by friction welding, being also an ancient process, is one that involves a braze metal which melts at a temperature above 150 °C, but below the melting temperature of the components to be joined so that there is no melting of the parent metals. The braze defects are described as defects of geometry, their causes and the non-destructive testing techniques that may be used to detect them. Many of these defects are caused by the welder, because of either a lack of care or a lack of skill, and emphasis the need for adequate training.

Keywords: aluminum, brazing, braze defects

1. Introduction

Non destructive testing methods may be used to reveal defects that would be difficult or impossible to detect by visual examination. The techniques are used during manufacture as a quality control tool to determine the quality of the work. The extent of non destructive testing methods depends upon the application and the criticality of the joint and is generally specified in the relevant application standards or contract specification.

It is important for non destructive testing methods to be included in the planning of the fabrication process as it can require substantial time and resources. Full account of this must be taken if disruption of production and delays to the program are to be avoided

The requirement to perform non destructive testing methods must also be taken into account during the design phase. As with brazing, access for non destructive testing methods must be planned into the component. The implication of this is that both welding engineers and designers must be conversant with the techniques and their limitations if the processes are to be used effectively.

2. Penetrate examination

This is a technique that is capable of detecting surface breaking defects only. It relies upon a colored or fluorescent dye, sprayed upon the surface, penetrating these defects. After cleaning the excess from the surface, the dye within the defect is drawn to the surface by spraying on a developer in the case of the color contrast dye or by exposing the surface to ultra-violet light. The defect is revealed by the dye staining the developer or by fluorescing (Fig. 1).

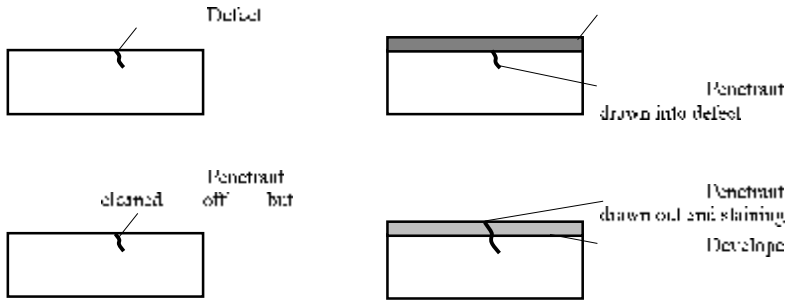

Fig. 1. Penetrant examination principles.

Figure 2 is a typical penetrant examination indication. The fluorescent dye gives greater sensitivity than the color contrast dye and does not require the use of a color contrast developer but does require the use of a ultra-violet light and preferably a darkened room. The cleaners, penetrant dyes and developers can all be obtained in aerosol cans, making the process extremely portable and ideal for site use

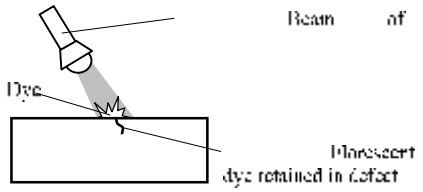

Fig. 2 Fluorescent light penetrant examination principles

Advantages: it can be used on both ferrous and non-ferrous metals, it is very portable, large areas can be examined very quickly, it can be used on small parts with complex geometry, it is simple, cheap and easy to use and interpret.

Disadvantages: it will only detect defects open to the surface, careful surface preparation and cleanliness are required, it is not possible to retest a component indefinitely, there may be health and safety problems with some of the chemicals, there are health and safety problems with fumes in confined spaces.

3. Eddy current examination

Eddy current examination is a process that may be used on any material that will pass an electric current. A coil carrying an alternating current is placed close to the item to be examined, inducing an eddy current in the specimen.

Defects in the specimen will interrupt this eddy current flow and these perturbations can be detected by a second, search coil. The coils can be placed either side of a thin plate-like sample or can be wound to give side-by-side coils in a single probe. These may be shaped to fit in the bore or around the outside of pipes and tubes and in these applications the process lends itself to automation. The equipment is calibrated using a defect-free specimen.

The accuracy can be affected by metallurgical condition, standoff and coil dimensions. For these reasons eddy current testing is used only rarely on welded components, although it is excellent in examining continuously welded tube from pipe mills. The process has been developed over recent years to make it more portable and simpler to use.

Microprocessor based control and recording units, improved and more tolerant probes and light-weight electronics have enabled the technique to be used on-site for the examination of structures in service, where it is an effective tool for the detection of cracking and corrosion problems. It is also possible for the depth of surface cracks to be determined

4. Ultrasonic examination

The ultrasonic examination of welds uses the same principles as when sonar is used for the detection of submarines. A 'sound' wave emitted from a transmitter is bounced off an object and this reflection captured by a receiver.

The direction and distance of the object can be determined by measuring the elapsed time between transmission and detection of the 'echo'. In welded components this is usually done by moving a small probe, containing both transmitter and receiver, over the item to be examined and displaying the echo on an oscilloscope screen.

The probe transmits a beam of ultrasound that passes through the metal and is reflected back from any defects, much like shining a torch at a mirror, in principle with the same rules applying to the reflection of the beam

Deeply buried defects such as lack of fusion, lack of penetration and cracks in addition to volumetric defects such as slag entrapment and porosity are all easily detected.

The frequency of the ultrasonic waves is generally in the range of 2–5MHz, the lower frequencies being used for the examination of coarse grained material and on rough surfaces. The higher-frequency probes are used for the detection of fine defects such as cracks, non-metallic inclusions, lack of fusion and voids. The beams are transmitted as either compression waves or shear waves and, ideally, a defect should be oriented normal to the wave to give the maximum reflection. Projecting the beam at a glancing angle at a planar defect can result in the beam being reflected away from the receiver and lost – remember the analogy of the torch and the mirror.

The probe angle should be selected to optimize the reflection of the sound beam. Probes that project the beam into the test piece at an angle normal to the plate surface are ideally suited to the detection of laminar defects, i.e. those lying parallel to the plate surface and for determining the plate thickness (Fig. 3).

Advantages: it is very good for the detection of planar defects and cracks, it can easily determine defect depth. it is readily portable, access is required to one side only, there are none of the health and safety problems associated with the radiographic technique.

Disadvantages: very skilled operators are required, surface breaking defects are difficult to detect, accurate sizing of small (<3 mm) defects is difficult or impossible, the geometry of the joint can restrict the scanning pattern and prevent accurate

interpretation, no permanent objective record is available, the process can be slow and laborious.

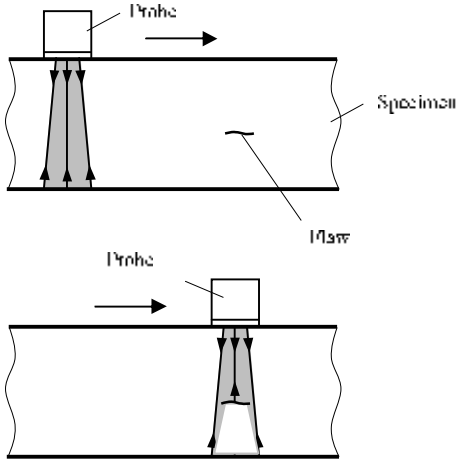

Fig. 3. Compression wave examination.

4. Radiographic examination

Electromagnetic radiation has properties that are useful for industrial radiography purposes. The rays travel in straight lines and cannot be deflected or reflected by mirrors or lenses; they have wavelengths that enable the radiation to penetrate many materials, including most metals. They will, however, damage living tissue and therefore present some health and safety problems.

The radiation, either X-rays from a suitable source or gamma rays from a radioactive isotope, is absorbed as it passes through the material. This absorption increases as the density of the material increases so that if a photographic film is placed on the side opposite the radiation source, any less dense areas will appear as darker areas on the film (Fig. 4), to give a shadow picture of the internal features of the test sample once the film has been processed.

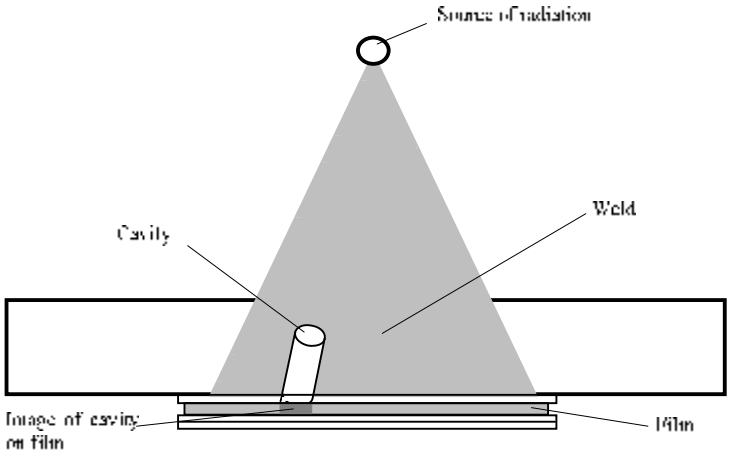

Fig. 4 Principles of radiographic examination of a weld.

Advantages: a permanent record is available, both buried and surface defects can be detected and the technique is particularly good for finding volumetric defects such as slag and porosity, the equipment is portable, particularly the gamma ray sources, all materials can be examined.

Disadvantages: the capital cost of equipment, which will need to include the processing and viewing facilities, access is required to both sides of the component, the source on one side, the film on the other, there are problems in detecting planar defects and fine cracks if these are normal to the beam, there is a limitation on the thickness that can be radiographed and defects easily detected, skilled and experienced radiographers are required, the depth and through thickness dimension of a defect is very difficult to determine.

Received March 15, 2007 *University of Bacau*

REFERENCES

1. ***, **Brazing handbook**, 4th ed., American welding society, 1991;
2. ***, **The brazing book**, Handy & Harman/Lucas-Milhaupt, inc., 1991.
3. Gene Mathers, **The welding of aluminium and its alloys**, Woodhead Publishing Ltd, Cambridge England, 2002.

STUDIU ASUPRA DEFECTELOR DE SUDURĂ/BRAZARE ŞI METODE NONDESTRUCTIVE DE ANALIZĂ A ACESTORA

Rezumat: Brazarea este cea mai modernă tehnică în fază solidă care este caracterizată printr-o sudură prin frecare, de asemenea un foarte vechi proces, este acela de amestecare a metalului de brazare care se topeşte la o temperatură de aproximativ 450°C dar mai mică decât temperatura de topire a componentelor ce urmează a fi lipite, deci aceasta nu se realizează prin amestecarea metalelor principale. Defectele brazării (lipirii) sunt descrise cu defecte de geometrie, pentru detectarea lor utilizându-se tehnici nondistructive. Multe din aceste defecte sunt cauzate de sudor, din cauza neatenţiei sau a lipsei îndemânării, necesitând o instruire specifică.

BULETINUL INSTITUTULUI POLITEHNIC DIN IAŞI
Tomul LIII (LVII), Fasc. 4, 2007
Secţia
ŞTIINŢA ŞI INGINERIA MATERIALELOR

MEMS USE IN HEALTH MONITORING OF COMPOSITE AERONAUTICAL REPAIR STRUCTURES

BY

S. OPRISAN*, A. BUZAIANU, I.FULOREA, N.CONSTANTIN, C. BANU, B.SPINEANU and I.R.MARIN

Abstract: : The MEMS systems (Micro-Electro-Mechanical Systems) are revolutionising the advanced studies and research in microelectronics, mechanical engineering and material sciences. The application of MEMS for the health monitoring of bonded composite patches used to repair or reinforce is now recognised as a very effective and versatile procedure to monitor and report damage. With the instant report on the status of composite aeronautical structures it is possible to prevent failure and develop health-monitoring techniques for the safety of critical bonded composite repairs. This work attempts to introduce some details on the use of MEMS and present a possible solution for measuring the health of epoxy bonded composite structure repairs of aeronautical panels.

Keywords: MEMS, repair structure, composites, finite element analysis, design SHM.

1. Introduction

The increased uses of composite materials and the systematic optimisation of structural components involve a precise knowledge of the load situation. When it comes to the safety warranty of aeronautical structural repairs, it is becoming more and more important to have a MEMS sensor technology specifically adapted to the properties of these composites. Such a technology could be used for load analysis and component monitoring during aeronautical structure exploitation. The application in this case consists in integrating a sensor in the composites to meet the demand for control protection and structural monitoring, damage analysis and control signal. The MEMS technique has developed a strain gage that may be embedded in the structure during in the intervention-repair process. It creates a "smart patch" system, which is based on self-monitoring and the ability to automatically detect disbanding in the composite patches. The role of the "smart patch" approach is to provide a real-time continuous monitoring of the patch performance so as to ensure the load transfers are maintained. The basic form of this concept will incorporate an "in situ" sensor to monitor the structural condition of the patch system in service and the status of the remaining damage in the basic structure [1]. Is create a subsystem as a Structural Health Monitoring (SHM).

2. Basic concepts

The use of composite materials in aircraft composite structures has increased in the past few decades as a result of the many advantages they offer compared to metals.

Repair composite panel structures, unlike traditional metal structures, have high strength and / to stiffness ratios, a good fatigue resistance and are less sensitive to deterioration caused by corrosion and creaking. Nevertheless they are more sensitive to other types of damage, mainly damage that can cause disbanding and internal crushing. Therefore, in order to improve their performance, one has to ensure that repaired structures are durable and maintainable.

This work presents the first step in a research on smart composite patches in repair methodology, using an embedded MEMS sensor, specially tailored to monitor the repair integrity during service. The same embedded MEMS are also used to evaluate stress in cure cycles. Cure cycle monitoring by MEMS involves the measuring of the strain inside the patch at many locations. It is thus possible to estimate the residual strain caused by the thermal expansion coefficient mismatch between the composite material and the aluminium substrate panels. The use of embedded MEMS may also replace the conventional electrical thermocouples that are placed around the patch during curing in the classical technological process.

A schematic description of a smart repaired composite patch on an aluminium panel is presented. By adapting, varying and selecting the locations of the MEMS sensor to the specific patch design, we obtained strain at the patch most critical areas [2]. The technological process and the experimental set-up to demonstrate the MEMS technique is illustrated in Figure 1.

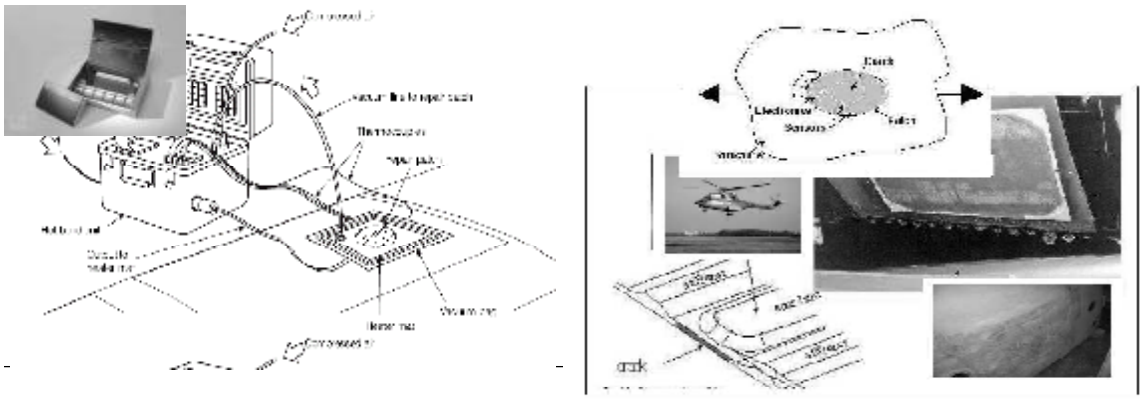

Fig.1 Typical Equipment for repair (Hexcel composites-left). The experimental set-up to demonstrate the MEMS technique (right). Includes the tapering-repair effect.

2.1 Smart patch specimen including MEMS

The common MEMS for structurally integrated measurements consist of vertically attached contact pins, for contacting the strain gage embedded in the composite material. The measuring leads are only connected to the gold-plated pins after manufacture, outside the structure, which makes all the handling easier. The strain gage is symmetrical in design, with structural strain being applied equally to the measuring grid from both sides.

The measuring grid sits is in a specimen, suitable for detecting a local strain state. They MEMS are to be recommended for determining the maximum point of notch stresses and similar stresses. It makes possible to register and evaluate the failure

criteria for their applicability to composite repair and to determine the feasibility of for validation with the test data.

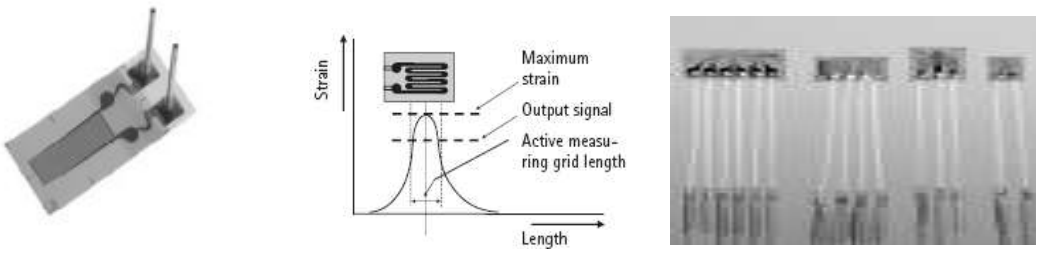

Fig.2. MEMS specimen tip structurally integrated measurement technology.

2.2 Finite element discretization

The combination of epoxy composite materials used in the experiment were evaluated as contoured in multilayered skins function of laminas constituents. The process may vary depending on bagging materials, closure methods, bleeder materials, mould materials, silicone rubber vacuum bags, etc. The criteria were determined for establishing the methodology that could be applied through software systems. The systems included particular products (programs) that can use standardized methods for the electronic feeding of data needed for modelling and simulation. The existing procedures may de changed to suit the system integration into the software environment architecture. The CAD and ANSYS programs were used to support the data feeding and the automated parameters modelling. This was performed through finite element modelling, for a large variety of composite patches, task simulations, ranges of destructive forces as well as for establishing detailed criteria for damage repair.

One of our primary objectives in constructing a numerical model isn't was to enable the optimisation of the device design and the operating conditions for a variety of experiments with different composite type patches placed in panel structures.

INPUT DATA Analytical Approach

- Material properties for laminate structure and patch, E_{xx} , E_{yy} , G_{xy} and υ_{xy} ,
- Thickness of laminate and patch. Dimension of patch and damage, including major and minor axis and depth of grind out. Stress around elliptic opening.
- Boundary condition in far – field stresses
- Epoxy adhesive properties (failure adhesive analysis)

The elliptical beams were tested in order to evaluate the effect of externally bonded component- material reinforcement on variation of epoxy glass-carbon pre-preg composites.

Analysis stages are evaluated according to TANAKA-MURA method [3].

The finite-element analysis to modelling of repair composite pre-preg materials may be performed as well as of the resulted response by using MEMS sensors in repair interventions.

The finite-element method of analysis is unrestricted by the types of composites or patch size of pre-preg because the device systems are embedded in repair structures. A finite-element formulation is presented for modelling the composite architecture. The numerical results are in good agreement with the available experimental data

based on epoxy pre-preg composites. The numerical approach presented may be used in approximate models for micro sensors but it is possible to make more realistic modelling of transient response of embedded MEMS. Unfortunately, the models are in general very simplified in order to maintain the required computational effort at a reasonable level [4]. This modelling, in most cases is complicate and, in consequence, there is a severe loss in accuracy. In the application under discussion we used shell-type elements for which coupling was made through a coupled matrix formulation between the two mechanical domains. It is important to mention that meshing of a true scale 3D model using traditional solid elements (bricks or tetrahedral) would result in an unreasonable number of elements

$$\sigma_\theta = \frac{p a^2}{\ell^2}\sin^2\theta - \frac{p b}{\ell^2} R_e\left\{\frac{e^{-i\theta}}{(a\sin\theta-\lambda_1 b\cos\theta)(a\sin\theta-\lambda_2 b\cos\theta)}\right.$$
$$\left.\left[(\lambda_1+\lambda_2)b^2\sin^3\theta+(2-\lambda_1\lambda_2)a^2 b\sin^2\theta\cos\theta+b^2\cos^3\theta\right]\right\}$$

$$\sigma_\theta = \frac{-\tau a b}{\ell^2}\sin 2\theta + \frac{\tau}{\ell^2} R_e\left\{\frac{i e^{-i\theta}}{(a\sin\theta-\lambda_1 b\cos\theta)(a\sin\theta-\lambda_2 b\cos\theta)}\right.$$
$$\left.\left[(\lambda_1 a+\lambda_2 a-i\lambda_1\lambda_2 b)b^2\sin^3\theta+(2-\lambda_1\lambda_2)a^2 b\sin^2\theta\cos\theta+i(1-2\lambda_1\lambda_2)\right.\right.$$
$$\left.\left.ab^2\sin\theta\cos^2\theta+(a-i\lambda_1 b-i\lambda_2 b)b^2\cos^2\theta\right]\right\}$$

$$\sigma_\theta = \frac{q b^2}{\ell^2}\sin^2\theta + \frac{q a}{\ell^2} R_e\left\{\frac{e^{-i\theta}}{(b\sin\theta-\lambda_1 a\cos\theta)(b\sin\theta-\lambda_2 a\cos\theta)}\right.$$
$$\left.\left[(\lambda_1+\lambda_2)b^2\sin^3\theta-(2-\lambda_1\lambda_2)b^2 a\sin^2\theta\cos\theta+a^2\cos^3\theta\right]\right\}$$

$$\ell^2 = a^2\sin^2\theta + b^2\cos^2\theta$$

$$\lambda^4 + \left(\frac{E_x}{G} - 2\upsilon\right)\lambda^2 + \frac{E_x}{E_y} = 0$$

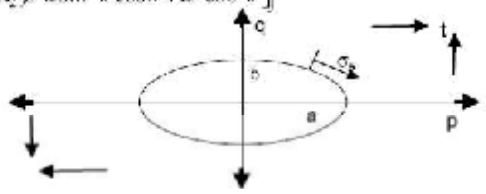

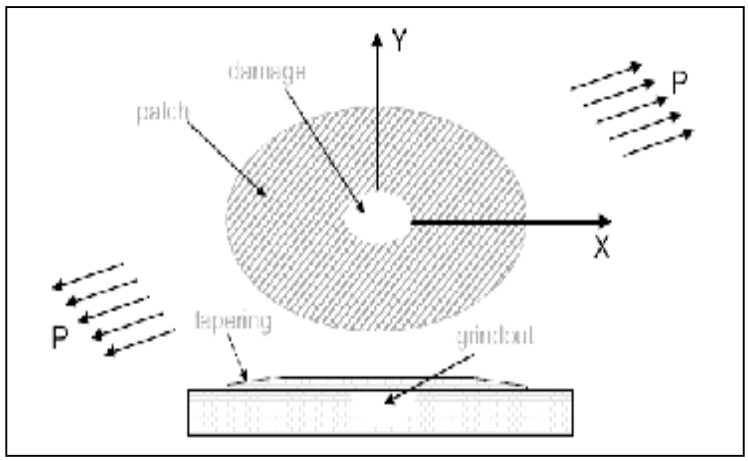

Fig.3. Development of a method for determining stress/strain algorithm at the edge of a damage area under arbitrary far-field loading (stress around elliptic opening-Boeing solution).

In the first state of simulation, we considered only a singular type of composites: epoxy pre-preg glass fibres or epoxy pre-preg carbon fibres. The numerical results were obtained by considering:

1. Aluminium: $E_{Al} = 73.1$ GPa; $\nu_{Al} = 0.33$

2. Lamina composite stratification in 8 layers $[0°/90°/0°/90°]_s$. Lamina properties are:

$E_1 = 98$ GPa; $E_2 = 7.8$ GPa; $E_3 = 7.8$ GPa; $G_{12} = 4.7$ GPa; $G_{23} = 3.2$ GPa; $G_{13} = 4.7$ GPa; $\nu_{12} = 0.34$ GPa; $\nu_{23} = 0.44$ GPa; $\nu_{13} = 0.34$ GPa;

3. Adhesive: $E_{Ad} = 1.25$ GPa; $\nu_{Ad} = 0.38$

Each composite lamina of the plate is assumed to behave as an orthotropic material, with its material axes oriented arbitrarily with respect to the laminate coordinates. The "smart" material layer can be orthotropic, but taken to be isotropic in actual calculations

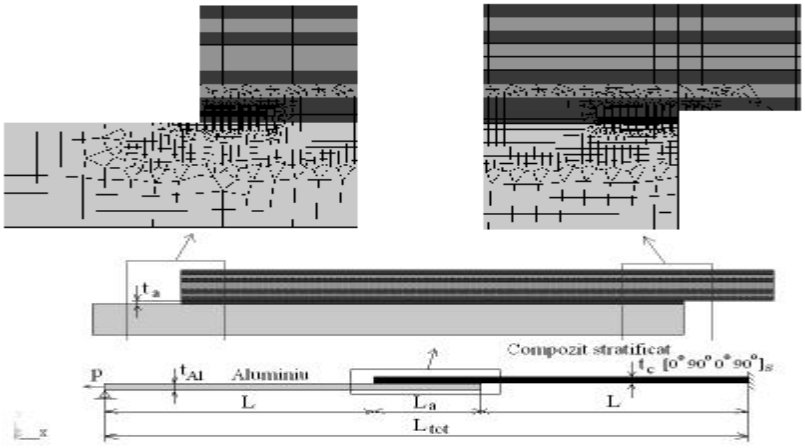

Fig.4. Evaluation of laminate failure criteria for their applicability to composite repair. Finite element discretization, geometry and boundary condition.

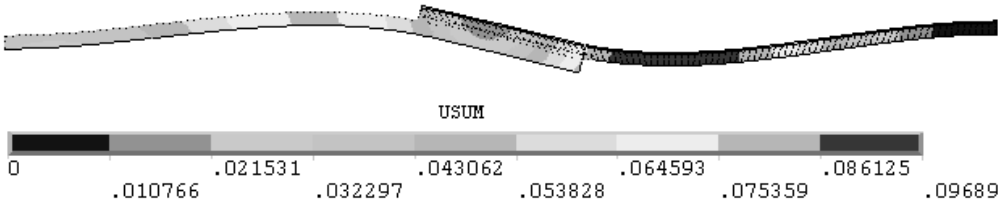

Fig. 5. FEM model showing step development equivalent plastic strain (package ANSYS)

3. Design solution and results

The choice of pre-preg composite and lamina combinations depends upon several factors: cost, stiffness and failure mode consideration being the most important. The ultimate strength and ultimate strength to density are all sufficiently high so that there is little effective difference. The fatigue strain capability (the critical parameter) is about the same for glass, Kevlar and carbon. Glass composites have the lowest cost which is currently one-tenth to one-third of the price of high modulus materials. Glass composites also present the favourable slow failure mode which is required to achieve improved safety and reliability. Kevlar, while not so good as glass, still retains this characteristic failure mode. Carbon fibber composites tend to fail in a manner similar to brittle metals. However, when combined with glass in suitable proportions, the favourable failure modes can be achieved. The high modulus materials offer greater stiffness to density. Thus they give the designer the ability to tailor his stiffness to meet specific and optimum composite combinations in

applications. Epoxy resign is the matrix material for structural composites, such as epoxy glass or carbon fibber composites. The superior mechanical and chemical properties of epoxy are due to the three-dimensional network structure that results from the curing process. A low molecular weight resin is transformed into a high molecular weight polymer. As a result, the surface structure affects numerous properties, such as the inter-lamina sheer strength and the impact resistance. Figure 6, shows variations in the repair of a structural aeronautical panel, to make thick composite patches using pre-pregs laminas to IAR 316 Puma

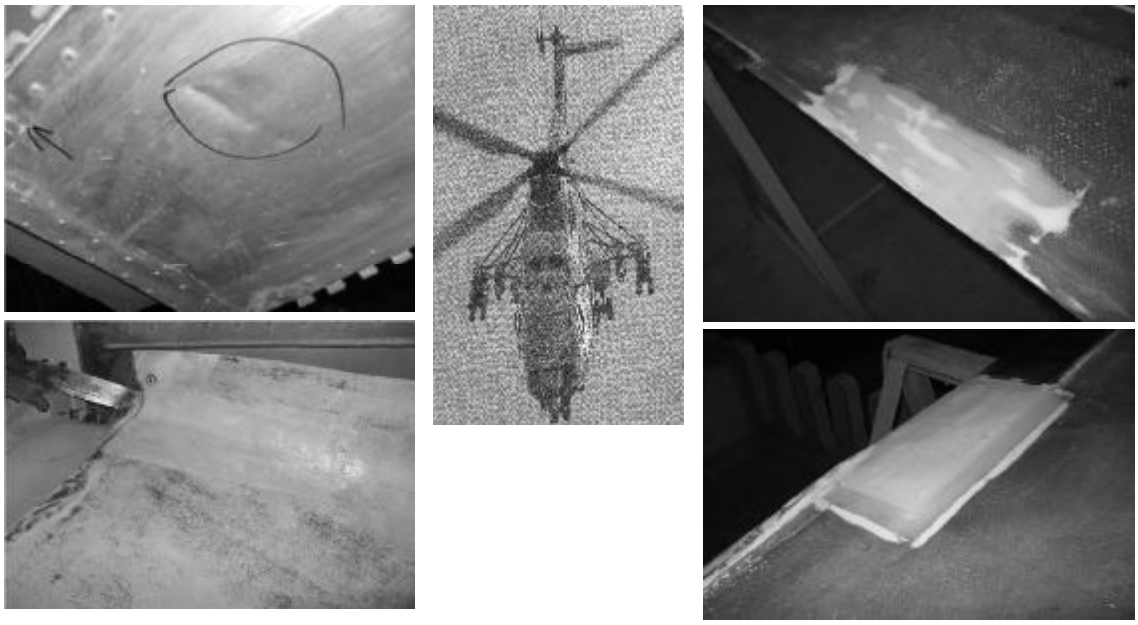

Fig. 6. Examples of damage experimented during service of IAR 360 helicopters (Define damage of panels)

The temperature was controlled during the process with the PR-500 epoxy resin system. The temperature of the composites for filling the reticulation in the resin was 140^{0}C. The temperature of superficies of laminas for curing was 170^{0}C.

3.1 Details of the repair and Design

In order that a finite element solution be reliable, efficient and accurate for engineering design problems, it must be based on reliable formulations and use effective elements that have been proven to be optimal. The design problems refer to contact conditions, for which reliable testes should be used.

- Bonded carbon or glass/ epoxy patch repair was designed to lower stress. It's necessary to determinate Intensity factor K in the crack tip below threshold value K_{th} to stop crack growth.
- Crack tip was stop-drilled and the hole was cold-worked before patching.
- In surface aluminium treatment panels, oxide layer was removed from wing skin by blasting.
- Exposed panel surface was treated with silane solution to develop chemical bond between aluminium surface and epoxy adhesive.

- Patch bonding:1mm thick patch manufactured from carbon-glass/epoxy pre-preg is bonded with adhesive film at 90^0 C temperature.

A bag moulding process has been developed, featuring a reusable vacuum bag. These bags, which are made from high strength silicone rubber, are used for curing and bonding the panels with composite pre-pregs, to assure structures rability. Damage tolerance of the tested composite blades was evaluated by crack propagation measurements on a full scale blade test section. Criteria for the selection of composite materials for repair structures are:

- Susceptibility to defects that can pass on non destructive test
- Defect should not extend to a crack and a potentially catastrophic failure.
- The crack should not progress rapidly at normal stress levels

The final design obtained from the laminate computer optimization program required a series of layer contours with a larger number of layers in areas of higher stresses. The maximum number of layers in each skin is a variable. The direction of these layers is 0^0 , +/- 45^0 and 90^0 . A simplified layer outline is shown in Figure 4. The evaluation of laminate failure was based on analytical criteria applied to test samples; experiments lead to the development of a solution for determining the breaking limits of damaged panels under repair. A design methodology needs to be formulated that can be incorporated into the software and used to determine the patch design for given skin material properties and damage [4]. This should evaluate:stress in the inclusion under general loading, stress around the elliptic opening, analysis of adhesives for tapered adherents patch.

3.2 Results

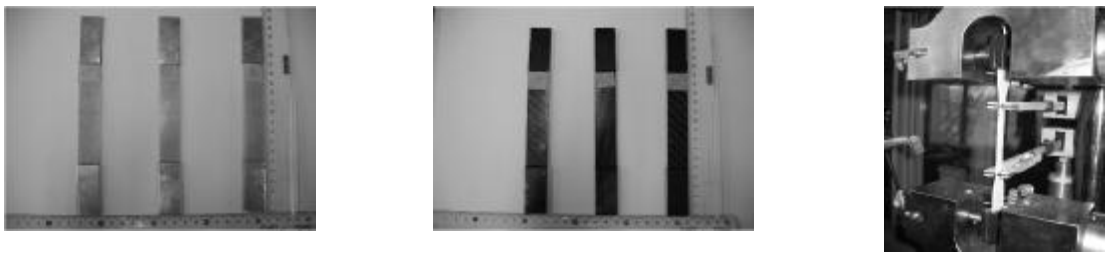

Fig.7 Tension test specimens and the test machine, (longitudinal and transverse direction, epoxy glass-carbon pre-preg composite).

Table nr.1. Tensile strength and tensile modulus of test specimens composites

Material Tip	Configuration	Medium Stress [MPa]	Modulus E [MPa]	Poisson's Ratio
Carbon fibre reinforced epoxy (4-layer)	0^0	354.70	41 700	0.3
	90^0	230,76	13 061	0,3
	45^0	102 23	15 242	0,2
E-glass fibre reinforced epoxy (3-layer)	0^0	238,20	8 995	0,3
	90^0	259.90	6 291	0.2
	45^0	120 90	5 027	0,2

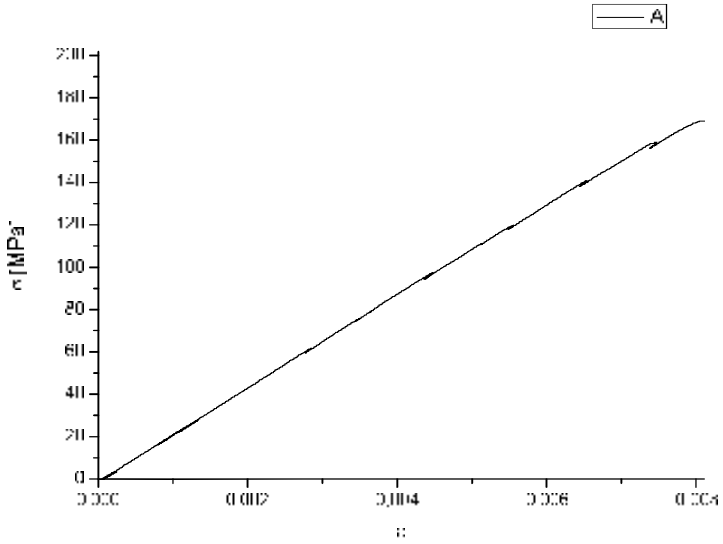

Fig.8. Typical stress curves for carbon pre-preg reinforced epoxy.

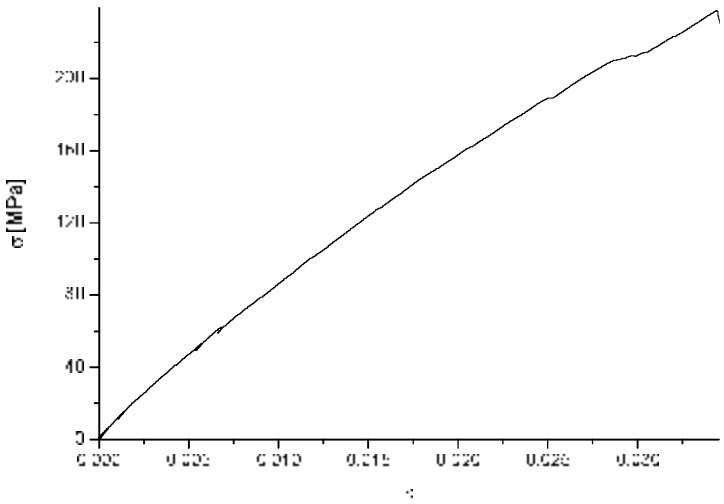

Fig. 9: Typical stress curves for E-glass pre-preg reinforce epoxy

4. Conclusion

This paper described the composite structure technology applied in the design and manufacture of the aeronautical structural repair components. Recent developments of MEMS technology can readily optimize the repair panel structures with tailored and tips of composite structures.

1. This technology is best in its abilities to provide an excellent surface finish, rapid repair cycling and is typically suitable for MEMS monitoring.

2. Tensile and compressive properties from repair structures were evaluated using a finite element model including reactionary ship whiz with micro-electromechanical systems (MEMS).

3. The final repair configuration of aeronautical structures cannot be obtained directly from bonding epoxy adhesives only. Composite repairs based on mixed pre-preg materials does not need a patch pre-forming process, irrespective of the configuration of the panels on which they are applied.

Acknowledgements

The authors thank the Romanian Ministry of Education and Research for having financially supported this research project within the National CEEX Programme.

Received April 11, 2007

**S.C. STRAERO S.A. Bucharest*
S.C. MTTAV S.A. Bucharest

REFERENCES

1. A.A. Baker, F. Rose, R. Jons. **Advances in the Bonded Composite Repair of Metallic Aircraft Structure**, Elsevir 2003,Vol 1,
2. D. Gorinevsky, G Gordon, S.Beard, A. Kumar, *Design of Integrated SHM System for commercial Aircraft Applications*, in 5 th International Workshop on Structural Health Monitoring, Stanford, CA, September 2005.
3. T. Telkc, *Application of model-based diagnostic technology on the Boeing 777 airplane*, Proceedings of 13th DASC, AIAA/IEEE Digital Avionics System Conference, page 1-5.
4. J.J. Wang, C.N. Duong, *Analytical Approach for Analysis of Bonded Composite Repair on Composite Structures*. Structures Technology Phantom Works The Boeing Company, September 2002, Aircraft Conference NASA.
5. D. Gorinevsky, S. Body and G. Stein, *Optimization-based tuning of low-bandwidth control in spatially distributed system*, American Control Conference, Vol 3, pp 2658-2663, Denver, CO, June 2003.

MONITORIZAREA STRUCTURILOR COMPOZITE UTILIZATE IN REPARATIILE AERONAUTICE PRIN INTERMEDIUL MEMS

Rezumat: Sistemele Micro-Electro Mecanice sau pe scurt **MEMS**-urile au revolutionat diverse'e activitati ingineresti din domeniul microelectronicii, ingineriei mecanice sau a stiintei materialelor. Lucrarea se doreste a fi o introducere intr-un domeniul particular de utilizare a acestor microdispozitive si prezinta posibilitatea de monitorizare a starii componentelor structurilor aeronautice la care s-au efectuat reparatii prin utilizarea compozitelor cu matrice epoxidica si elemente de ranforsare pe baza de pre-preguri din fibre de sticla, fibre de carbon, fibre aramidice, etc.

BULETINUL INSTITUTULUI POLITEHNIC DIN IAŞI
Tomul LIII (LVII), Fasc. 4, 2007
Secţia
ŞTIINŢA ŞI INGINERIA MATERIALELOR

THE SORTING INSTALLATION BASED ON ULTRASONIC WAVES

BY

M. PEPTANARIU[1], M. SUSAN[2], M. LOZOVAN[1] and P. DUMITRAŞ[3]

Abstract: The separating process of different types of powder with very small granulation is difficult due to the sieve clogging, particles getting caught in the meshes. Ultrasonic vibrations of low frequencies are applied to the sieves in order to separate particles; however this can't stop sieve clogging. Ultrasonic waves are used for powders of tens of microns. Ultrasonic waves are applied directly to the sieves or to the sieve holders when multiples sieves are used. Ultrasonic vibrations are applied perpendicularly to the sieves or to the side of the sieve. Using ultrasonic vibrations we get some advantages like: a lower sorting time, a longer sieve life and reduced mesh blindness. This article presents a method of ultrasonic wave use with multiple sieves and with specific size of meshes. Thus, a selective and continue sorting is achieved. The ultrasonic system presented is activated by an ultrasonic generator which emits a frequency equal to the resonance frequency of the ultrasonic system.

Keywords: ultrasonic waves, particles, resonance frequency

1. Introduction

The granulometric selection of powders is done by using a number of sieves with meshe sizes in descending order. Different sieve standards are made for this purpose, according to the mesh size [1]. Because fine sieves have tiny meshes, they are prone to blindness and malfunction. The application of ultrasounds to the sieves prevents sieves from clogging, and increase sieves' life span. This kind of sieving using ultrasound technology is world wide used with success

In most cases ultrasonic vibrations are applied directly to the sieves and this can be done to the side with vibrations transverse to the flow [2], [3], or on the center, perpendicular to sieve [4]. When a sieve assembly is being used, ultrasounds are applied to the sieve holder.

Usually, this is the case of industrial powder separation processes where high quantity of probe is used and the separation process is done continually. Such applications need large installations with great ultrasonic power. In this paper is presented an ultrasonic system for thin powders with step separation which uses a sieve assembly with progressive decreasing meshes. In this case ultrasounds are applied to sieve directly to the sieve in the flow direction. The particularity of this system is the sieve placement between sonotrodes.

2. Experimental

The ultrasonic system for thin powder separation consists of an ultrasonic transductor 1, sonotrode 2, filters (sieve like) 3, powder recover cases 4, fixings 5, collar 6. The system schema is presented in Fig.1.

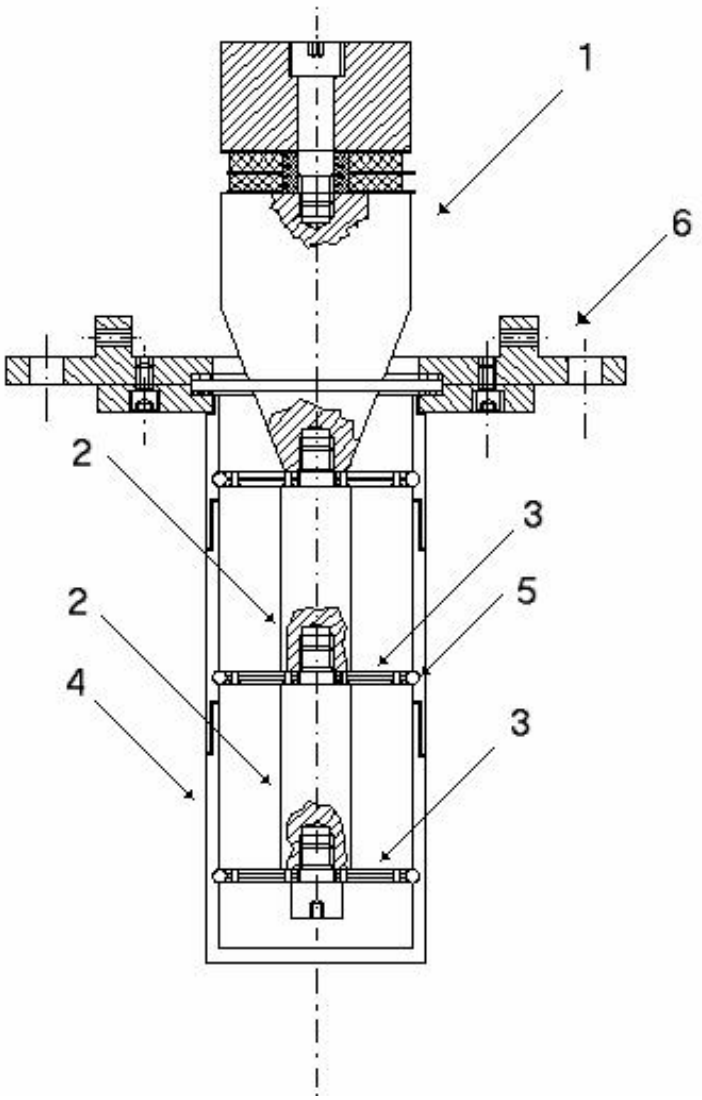

Fig. 1. The ultrasonic system.

The acoustic transformer used is conic like, made of duralumin. The transductor is piezoceramic, made with two piezoceramic rings and duralumin ends for emitter and steel for reflector [7-9]. It is powered with high frequency electric current from a specific ultrasonic generator.

The ultrasonic transductor, the acoustic amplifier and sonotrodes are made in $\lambda/2$, where λ is the wave length of ultrasounds and the resonance of transductor [10-11]. The powder recovering housings are cylinders concentric with the sonotrodes and they are made of metal or other materials (PVC, polyamide, etc.).

Each sieve is fitted together with the ultrasonic assembly and sonotrodes by screw-cutting and is positioned for maximum vibration. In Fig.2 is presented the vibration amplitude for the system. Filters are two identical discs with a sieve between These discs have cuttings for powder and the sieve is fitted by gripping them. Each holding has over his outer circumference a channel where a rubber fixing can move (5) and which prevents the powder passing between filters and cylinder walls. Fig.2

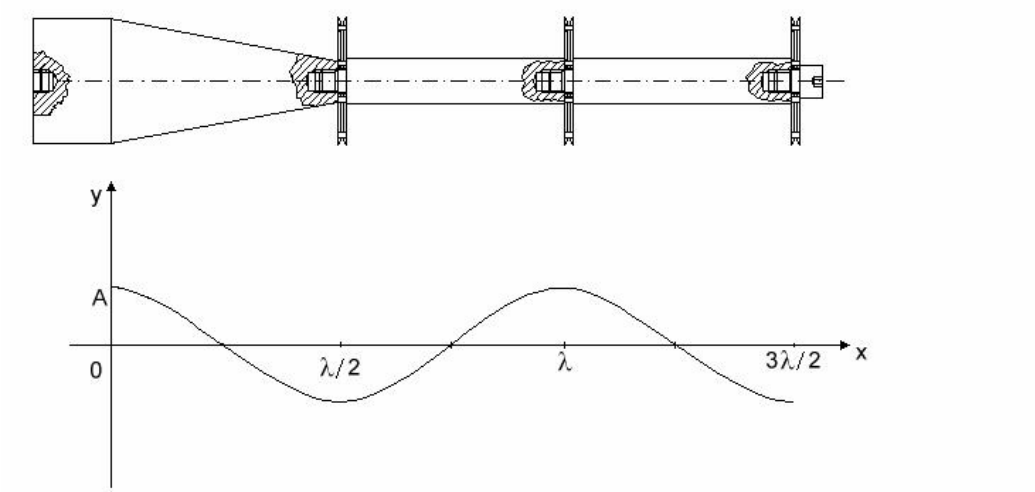

Figure 2.

The unfiltered powder is loaded in a compartment near the acoustic transformer. The entire system position is vertical related to the ultrasonic transductor in his upper part.

Thus, during the ultrasound action over the system, by free falling, the grains up to a certain size pass through the first sieve, and then smaller ones pass through the next sieve and so on, and the last compartment will store the smallest grains.

Because the entire system is closed, when the ultrasounds are applied the air column from each tube will oscillate and improve the throughput of sieving.

3. Results and discussion

The granulometric selection of powders using ultrasonic waves has made possible to get powders with granules of microns in size, which is not possible by granulometric sorting with sieves only exposed to low frequency mechanical vibrations. Different powder sizes can be achieved with this system.

The outturn of this system is very high, ultrasonic vibrations increasing the powder speed and sieve blindness is reduced. This system can also separate magnetic powders by using a demagnetization tool.

For magnetic powders magnetization occurs because friction during sieving. Another advantage is the fact that sieves which are small and detachable can easily be cleaned together with the frame in an ultrasound bath, increasing their lifespan.

Received April 25, 2007

[1] *National Institute of R&D for Technical Physics Iasi*
[2] *The "Gh.Asachi" Technical University Iasi*
[3] *I.F.A. Chişinău, Republica Moldova*

REFERENCES

1 http://www.clevelandvibrator.com/ultrasonic_laboratory.htm
2 http://www.hielscher.com/ultrasonics/sieve_04.htm
3 http://www.endecotts.com/otherproducts/sieve_cleaner.htm

4 http://www.mpi-ultrasonics.com/ultrasonic_sieving.html
5 http://www.telsonicusa.com/screening.htm
6 http://www.coleparmer.com/catalog/vcatalog_page.asp?p=1753
7. O. Dragan, C.Ianeu, D.Drimer, s.a. **Ultrasunete de mari energii**,Ed. Academiei, Bucuresti (1983
8 Edmons P.D , **Ultrasonics**. Academic Press, New York (1981)
9. Foster F.S., Hundt J.W., **Ultrasonics**, vol 16, nr.3 (1978)
10. Peptanariu M , Hristoforou E , Neagu Maria, Chiriac H., *Ultrasonic Equipment Used to Weld Cylindrical Plastic Components* Proceeding of 3rd International Symposium on Advanced Electromechanical Motion Systems, B20, 215-216 (1999)
11. Chiriac H , Peptanariu M., Lozovan M , Neagu Maria, Buzea Cristina, *On the Casting of Fe-Ni-Invar Alloy in Ultrasonic Field*, Ultrasonics Symposium 1998 vol I, 751-753,

INSTALATIE DE SORTARE BAZATA PE OSCILATII ULTRASONICE

Rezumat: Sortarea pulberilor cu dimensiuni foarte mici, este dificila din cauza infundarii sitelor, blocand trecerea particulelor prin ochiurile acestora. In vederea separarii acestor pulberi, se aplica sitelor vibratii mecanice de joasa frecventa, dar acestea nu reusesc sa impiedice infundarea sitelor. Pentru pulberi cu dimensiuni de ordinul zecilor de microni, se utilizeaza vibratiile ultrasonice. Acestea se aplica direct sitelor sau suporturilor de site, in cazul in care sunt mai multe. Vibratiile ultrasonice pot fi aplicate transversal sau pe directia de curgere a pulberilor. Actiunea undelor ultrasonice prezinta o serie de avantaje: impiedica infundarea sitelor, micsoreaza timpul de sortare si mareste durata de utilizare a sitelor. Lucrarea de fata, prezinta un mod de utilizare a vibratiilor ultrasonice cu mai multe site cu anumite dimensiuni ale ochiurilor de retea. Astfel se face o sortare selectiva si continua a pulberilor. Sistemul ultrasonic prezentat este activat de un generator ultrasonic ce trebuie sa emita o frecventa de lucru egala cu frecventa de rezonanta a sistemului ultrasonic

BULETINUL INSTITUTULUI POLITEHNIC DIN IAŞI
Tomul L(III (LVII), Fasc. 4, 2007
Secţia
ŞTIINŢA ŞI INGINERIA MATERIALELOR

ULTRASONIC ENSEMBLE USED TO DRAW METALLIC PIPES AND WIRES IN ULTRASONIC FIELD

BY

M.PEPTANARIU[1], M.SUSAN[2] and P. DUMITRAŞ[3]

Abstract: During the pipe drawing in ultrasonic field, as the result of metal passage through the surfaces of the die subjected to ultrasonic vibrations, the ultrasonic pressing effect appears. This effect leads to the modification of the friction coefficient and the friction vector position. The manner used to apply the ultrasounds also depends on the type of materials meant to be drawn through the threading die. In the case when the ultrasounds are used for pipe drawing, these can be applied in the deformation focus through the plug or die. A combination can be also used. In case of wire drawing, the ultrasounds are applied directly in the deformation focus. This work presents a type of ultrasonic ensemble which can be used both for wires and pipes whose outer diameters are smaller than 5mm, with ultrasounds application right in the deformation focus.

Keywords: ultrasonic field, pipes, deformation

1. Introduction

By using the ultrasounds in the pipe cold drawing on the plug, one can notice that the pipes eccentricity if 40% lower than that of the pipes drawn without using the ultrasounds [1-3]

The pipe drawing in ultrasonic field can be carried out with or without a plug, namely in the cavity. By the application of the ultrasonic oscillations on the die in the drawing direction, a considerable diminution of the force necessary for deformation is obtained. The diminution of the drawing force is explained by the decrease of the external friction, is of the surface effect.

Figure 1 presents a manner to apply the ultrasonic vibrations for metallic pipes drawing in ultrasonic field. In this case, plug drawing is used.

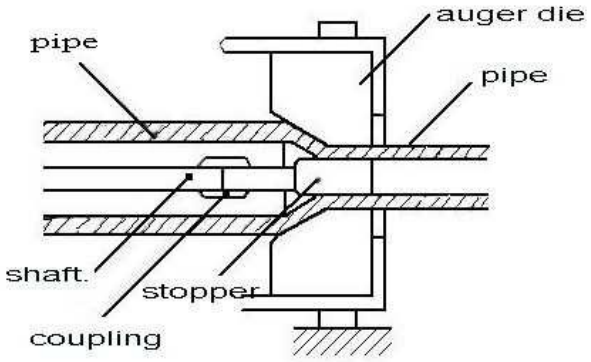

Fig.1

One can notice the arrangement of the plug and the die, the ultrasounds acting on the pipe by means of the metallic rod and parallel with the pipes drawing direction.

In the following, we shall present a method to use the ultrasounds in the case of drawing without plug, by means of a die installed straight on the acoustic transformer. The die is fastened at the end of the acoustic transformer, through friction, being located in a vibration maximum of the ultrasonic system

The ultrasonic transducer can be magnetostrictive or piezoceramic. In this case, a piezoceramic transducer is used, accomplished by means of a pair of piezoceramic rings [4-5].

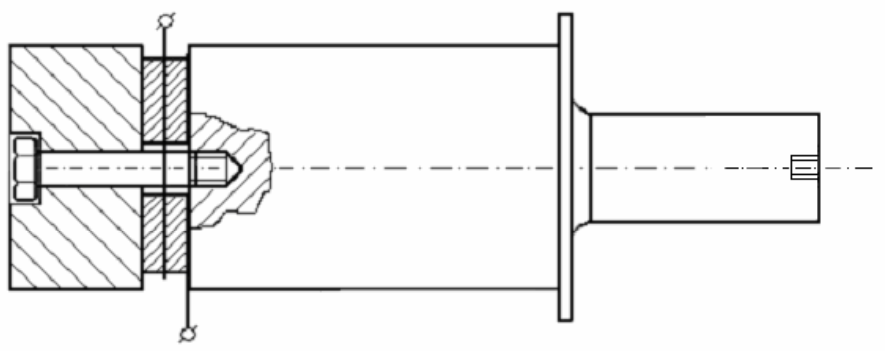

Fig.2

The acoustic transducer (the amplifier) is made of titanium or steel; it can be conical or with steps. Figure 2 presents an ensemble of stepped ultrasonic transducer which can be connected with a probe or another acoustic transformer attached to the die

2. Experimental

Figure 3 presents an ultrasonic transducer ensemble which permits pipes drawing in ultrasonic field.

In this case, the metallic pipe or wire to be drawn is introduced within a channel executed inside the acoustic transducer, with the side inlet bore and the outlet centred on the die. The ultrasounds act in the drawing direction and the ultrasonic field acts right in the focus.

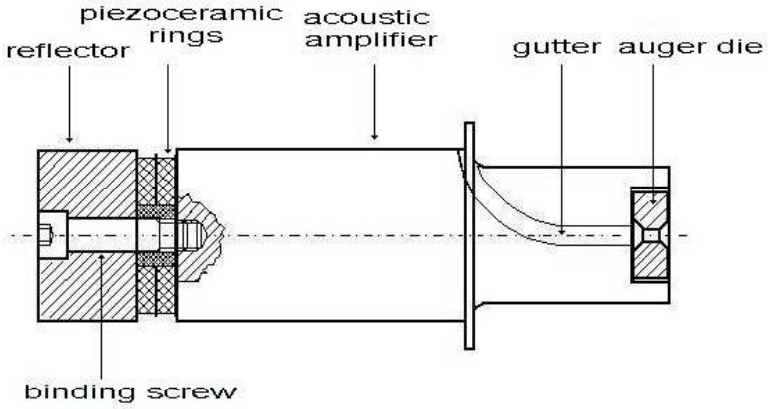

Fig.3

Starting from this example, another ultrasonic system was conceived for drawing the wires and pipes with the outer diameters smaller than 5mm (Fig. 4).

The main elements of the system are indicated in the figure. The material used to execute the ultrasonic transducer and acoustic transformer is the steel.

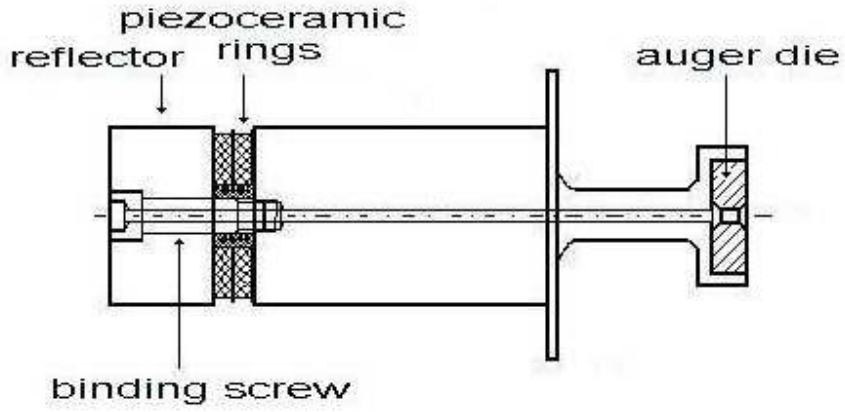

Fig. 4

This presents a good transmission of the ultrasonic waves, as well as an increased mechanical resistance (as compared to aluminium). The most indicated material will be titanium, but it is hard to procure

3. Results and discussions

The entire system has an axial symmetry and it can be introduced directly in the flow sheet without stressing the material to be drawn. As the channel is axial, the acoustic transducer can be built with a bigger difference between the diameters of the two steps, which permits a higher amplification of the oscillations amplitude.

The channel being axial, it can be executed with a higher precision, without material deformations or cross-section non-uniformities. It is well known that any asperity or non-uniformity results in a concentration of the ultrasound energy in the zone, which make the system yield decrease.

In all these cases, in order to apply the ultrasonic field a high frequency installation is necessary which should deliver the ultrasonic energy necessary for the ultrasonic system. This installation includes a high frequency generator which must deliver an electric signal with a frequency equal to the resonance frequency of the ultrasonic ensemble.

Received April 25, 2007

[1] *National Institute of R&D for Technical Physics Iasi*
[2] *The "Gh.Asachi" Technical University Iaşi*
[3] *I.F.A. Chişinău, Republica Moldova*

REFERENCES

1. O. Dragan, C.Iancu, D.Drimer, s.a. **Ultrasunete de mari energii**,Ed. Academiei, Bucuresti (1983

2. Edmons P.D., **Ultrasonocs**, Academic Press, New York (1981)
3. Foster F.S., Hundt J.W., **Ultrasonics**, vol 16, nr.3 (1978)
4. Peptanariu M., Hristoforou T., Neagu Maria, Chiriac H., *Ultrasonic Equipment Used to Weld Cylindrical Plastic Components Proceeding of 3rd International Symposium on Advanced Electromechanical Motion Systems*. B20, 215-216 (1999).
5. Chiriac H., Peptanariu M., Lozovan M., Neagu Maria, Buzea Cristina, *On the Casting of Fe-Ni-Invar Alloy in Ultrasonic Field*, Ultrasonics Symposium 1998, vol 1, 751-753.

ANSAMBLU ULTRASONIC UTILIZAT PENTRU TREFILAREA TEVILOR METALICE SI SARMELOR IN CAMP ULTRASONIC

Rezumat: La tragerea tevilor in camp ultrasonic, ca urmare a trecerii metalului prin suprafetele matritei supusa vibratiilor ultrasonice, apare efectul de matritare ultrasonica. Acest efect duce la schimbarea coeficientului de frecare si a pozitiei vectorului frecare. Modul de aplicare a ultrasunetelor este functie si de tipul materialului ce urmeaza a fi tras prin filiera. In cazul utilizarii ultrasunetelor la tragerea tevilor metalice, acestea se pot aplica in focarul de deformare prin dop sau matrita. Se pot aplica si combinat. Pentru cazul tragerii firelor, ultrasunetele se aplica direct in focarul de deformare. Lucrarea de fata prezinta un tip de ansamblu ultrasonic ce poate fi utilizat atat pentru fire cat si pentru tevi a caror diametre exterioare sunt sub 5mm, cu aplicarea ultrasunetelor direct in focarul de deformare.

BULETINUL INSTITUTULUI POLITEHNIC DIN IAŞI
Tomul LIII (LVII), Fasc. 4, 2007
Secţia
ŞTIINŢA ŞI INGINERIA MATERIALELOR

STUDY CONCERNING THE MILLING PARAMETERS ON THE STRUCTURES AND PROPERTIES OF NI-TI ALLOYS

BY

ANGELA POPA*, IRINA CÂRCEANU*, C. MACOVEI* and V.CÂNDEA**

Abstract: The Ni-Ti alloys are more and more used in top fields like aerospace and biomedical industry due to the characteristics of them, especially the shape memory effect. The homogeneous structures of Ni-Ti alloys are directly influencing the shape memory effect. In order to realize a good homogeneity of the Ni-Ti alloys it was used for fabrication a series of powder metallurgy techniques. The paper presents briefly some aspects regarding the present stage in production of homogeneous mixtures of Ni-Ti alloys.

Keywords: Ni-Ti alloys, powder metallurgy

1. Introduction

The alloys from Ni-Ti system are known because of their termo-mechanical properties such as superplasticity and shape memory effect.These alloys are characterized also by some other properties like: high mechanical properties, great corrosion resistance in range of transformation temperatures, biocompatibility and an long cycle of life versus the imagery of magnetic resonance, that which recommendthe alloy for use in cardiology, orthopedy, stomatology.

The achievement of Ni-Ti 50:50 alloy through classical metallurgy presents maNY drawbacks such as: absence of some integrad tehnological flow; the special equipment is a great consumer of energy; necessity of remelting to obtain some high purity and to achieve a one structure with high ductility, etc. This is the reason why during the last years it is used more and more specific powder metallurgy techniques to acieve the Ni-Ti 50:50 alloy that eliminate the above mentioned drawbacks Moreover utilization of specific powder metallurgy techniques presents a lot of advantages respectively: achievement of some products with complex geometries, elimination of chemical and structural segregations, etc. However at the utilization of specific powder metallurgy techniques appear some aspects that need a special e attention duration the processing of Ni-Ti 50:50 alloys, like:

- necessity to obtained one homogeneous phase type NiTi, through inter-diffusion and to avoid to appear other inter- metallic stable phases type NiTi 2 and Ni3 Ti;
- necessity to eliminate the porosity in order to improve the mechanical properties of parts which increase with compaction pressure.

A procedure used in the last year for Ni-Ti alloys achievement is mechanical alloying in mill type Attritor, planetar mill with ball, rotary mill with ball, etc.

In this paper are presented some results obtained for achievement of the Ni-Ti 50:50 alloy through milling into Attritor mill in weat medium.The scope of this paper was to esatblished the milling parameters especially the best duration milling of the Ni-Ti alloy on the initiation of reciprocal diffusion between the constitutive elements of alloy.

2. Experiments

The elementary Ni and Ti powders used for achievement of Ni-Ti50:50 alloy afterbeing characterized from the point of view of chemical compositions, of physical characteristics and of morphological aspects was gravimetrically measured .The wrong performance of measurement operation lead to a chemical composition out side of concentration limits indication and lead to physics and mechanical properties unsuitable for the scope.

The gravimetric measure was performed by a balance with accuracy of + 0,01. The mechanical alloying respectively maximum impact force (between ball, materials and the wall of mill), maximum deformation of ball, number of particles caught in the knocking moment, radius of materials caught in the knocking moment were calculated in conformity with Hertz's general theoriy of mechanical alloying[1], after the formulas:

* Maximum impact force F_{max}:

$$F_{max} \quad \frac{\sqrt{2}}{3}\left(\frac{5\sqrt{2}}{3}\pi\right)^{0,6}\left(\frac{E_b}{1 \quad \nu_b^2}\right)^{0,4} \quad \rho_b^{0,6} R_b^2 V_b^{1,2} \tag{1}$$

E_b = elasticity module of ball; ρ_b = ball density;
ν_b = Poisson's coefficient of ball;
R_b = ball radius; V_b = speed of ball before knocking.
From formula (1) it resulted: $(F_{max})_{steel} \approx 33.000$ N

* Maximum deformation of ball, δ_{max}:

$$\delta_{max} \quad \left(\frac{5\sqrt{2}}{4}11 \bullet \rho_b \frac{1-\nu_b^2}{} \bullet v_b\right)^{0,4} \bullet R_b \tag{2}$$

From formula (2) resulted: $(\delta_{max})_{steel} = 1,22 \times 10^{-4}$ m

* Radius of materials caught in the knocking moment,

$$r_h; r_h - R_b 1,4750 \bullet v_p^{0,4} \left(\frac{\rho_b}{E_p}\right)^{0,2} \left(\frac{\beta}{\beta \quad 1}\right)^{0,4} \tag{3}$$

where:

$$\beta = R/R_b \tag{4}$$

R= radius of curvature of precincts
From formula (3), it resulted $r_{h\,steel} = 0,0024$ m.
Other parameters of milling were:
- milling speed: 200 rot/min;
- milling time: 15h ,30 h;
- grade of filling of precincts: 25%;
- report of weight ball/materials: 1/1;
- type of milling: wet - alchool;
- medium of milling: argon.

After milling of the alloy which was obtained it was dried in drying stove to 200 °C, for 5 h. After drying the Ni-Ti 50:50 alloy was characterized from the point of view of chemical composition of physics characteristics and morphological aspects. The morphological aspects it was investigated with electronic microscope type IIITACIII S-2600 N equipped with analyse dispersive in energy system (EDS).

3. Results and disscusion

In Table 1 is presented chemical composition of elementary powders, respectively Ni and Ti. The physics characteristics of elementary powders it was established in conformity with SR EN ISO 4490:2003[1]; SR EN 23923-1:1998[2] and SR EN 23923-2:1999 [3].The results are presented in table 2 were it can seen that the both powders do not flow, the Ti powders has a FSSS lesser than Ni powders and the apparent density is much higher than Ni powders. The analyses of morphological aspects of the Ni powders , Figure 1 a to size (x3000) emphasize a conglomerate of micron and under-micron like chain; the image from Figure 1b, to size(x 6000) emphasize the booklet form of the 0,1-3 μm dimensions with a frequency small however and for the polygonal form of the particles. The particles of the Ti powders have an aspects like little breaches, are heterogeneous like form and dimensions, Figure 2a; with a small frequency appears the big particles which exceed 100μm (x 1000), Figure 2 b .

Table 1. Chemical composition of elementary powders.

Powder type	Element contents, % wt.					
	Ni	Ti	Al	Si	Mg	Fe
Titanium	-	rest	0,010	0,001	0,050	0,050
Nickel	99,9	Co 0,01	Cu 0,01	C 0,01	S 0,02	< 0,01

Table 2. Physical characteristics of elementary powder

Powder type	Average diameter FSSS (μm)	Flowing rate (s/50 g)	Apparent density (g/cm^3)
Titanium	4.74 ± 0.01	not flow	2,01 ± 0,01
Nickel	2.52 ± 0.01	not flow	3,78 ± 0,01

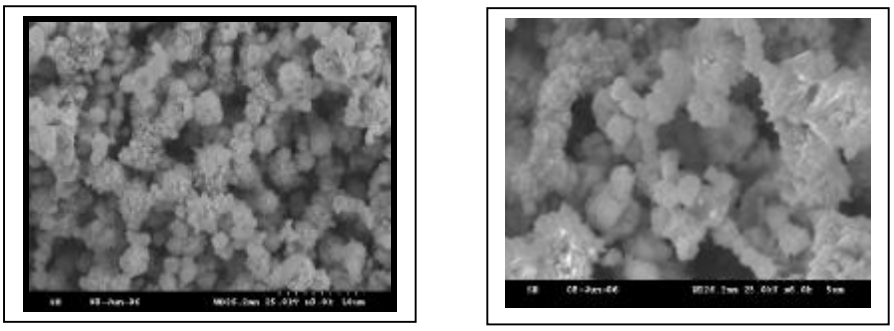

a) *b)*

Fig. 1. Morfological aspects of Ni powders :
a) – conglomerate of particles, x 3000, b) – booklet form of particles, x 6000

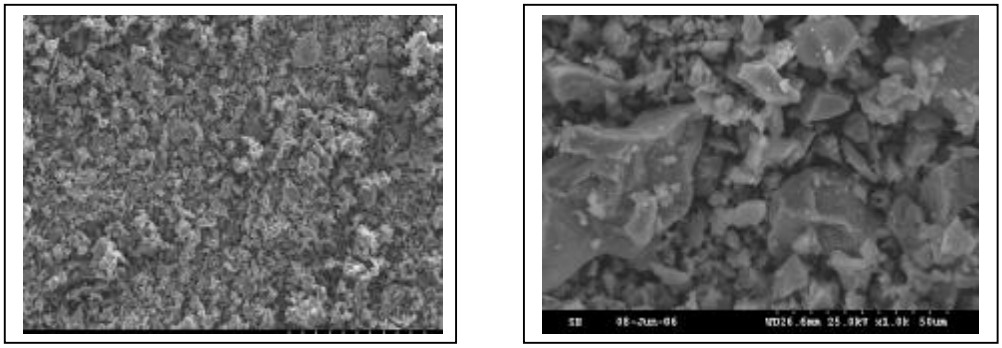

a) *b)*

Fig. 2. Morhological aspects of Ti powders:
a) general aspect , x 200; b) big particles of Ti powder, x 1000

The chemical composition of Ni-Ti alloy achieved through mechanical milling is presents in Tabel 3, and it results that the gravimetric measurement was accurately performed thus obtaining the chemical composition which was projected. In Table 4 are presented the physical characteristics of alloy obtained from which it can established that the increase of mechanical milling duration of the elementary powders from 15 h to 30 h leads to a growing of apparent density simultaneous with diminution of size particles.The diminution apparent density after 30 h milling can be explained by modification of the form factor of particles in milling duration (the particles form alters so that upon a time with growth time of milling the sharpened edge of particles to get round). That meanses because of growing of the milling duration they were obtained patricles with rounded forms, therefore the packing grade of particles increase once with diminution of distance between particles.

Tabel 3. Chemical composition of Ni-Ti 50;50 alloy

Sample nr./milling time	Content element , % wt.						
	Ni	Ti	Fe	Al	Si	Mg	C
1 / 15 h	49,56	49,40	0,50	0,25	0,11	0,09	0,09
2 / 30 h	50,10	49,08	0,36	0,22	0,12	0,06	0,06

Tabel 4. Physical characteristics of Ni-Ti 50;50 alloy

Sample nr./ milling time	Average diameter FSSS (μm)	Flowing rate (s/50 g)	Apparent density (g/cm^3)
1 / 15 h	0,50 – 0,01	not flow	3,30 = 0,01
2 / 30 h	0,30 + 0,01	not flow	3,48 0,01

In Figure 3a and 3b we can see the repartition Ti and Ni in Ni-Ti mixture. From Figure 4 we can see the presence of some conglomerate with irregular shape, formed through welding of much more particles, obtained after 15 h of milling; after 30 h of mechanical milling it can be to remarked under-micron composite particles which presents spheroidization tendency, Figure 5.

In order to put into evidence the influence of mechanical alloying process on the beginning of reciprocal diffusion from materials obtained it was performed o lot of analyses with electronic microscope, obtained electron images secondary on the samples analyses, like as the repartition characteristics radiation force X for Ti (L_α) and Ni(K_α).

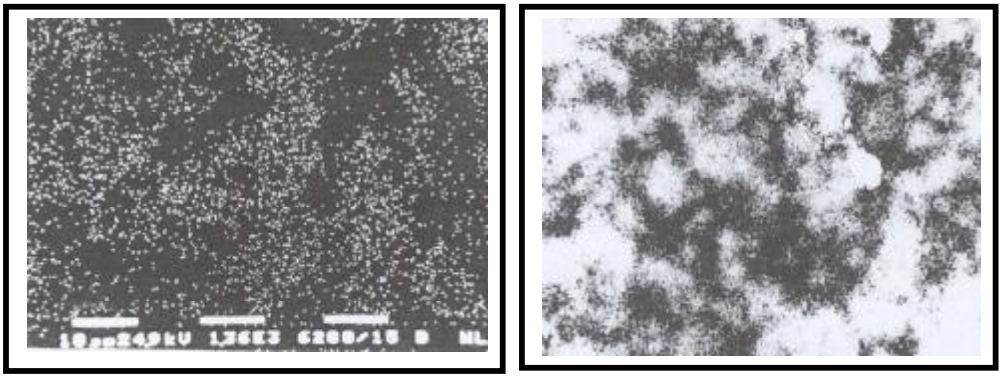

a) b)

Fig.3. Repartition of: a) Ti; b) Ni, in Ni-Ti mixture. X 2840

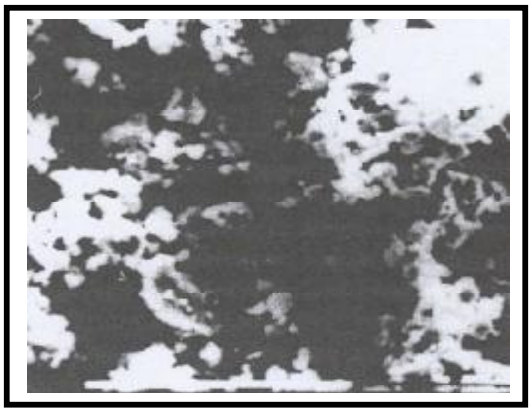

Fig.4. Particles ensemble NiTi, X 4780

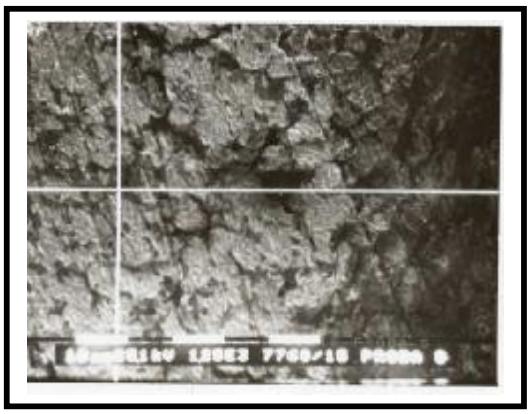

Fig.5. Mixture mechanical alloying NiTi, X 4780

4. Conclusions

The experimental works lead to following conclusions :

■ With increase of the milling duration growth apparent density of the materials simultaneous with diminution size of particles.

■ With increase of the milling duration it was obtianed particles with rounded forms, therefore the packing grade of particles increase once with diminution distance between particles.

■ Of the duration much more of 15 h of milling apears the conglomerate phenomena of irregulare form process through welding much more particles.

Received April 9, 2007

**Metallurgical Research Institute of Bucharest*
***Technical University of Cluj-Napoca*

REFERENCES

1. Hertz F, Giffet E, *Kmematic Approach of the Mechanical Alloying Physics in the Planetary Ball and Attritor Mill*, **Pm World Congress**, Paris, vol.2, june 1991, 212-221
2. Koch C.C & others, *Mechanical Milling and Alloying*, **Materials Science and Tyechnology** – 15, New York, 1991, 193-247.
3. Irina Cârceanu, **Master's Degree** Alloying by Non-Conventional Proceeding Some New Type of Materials Use in Powder Metallurgy, Bucharest 2005.
4. Angela Popa, Irina Cârceanu, **Studies ICEM** CEEX National Programs 2005-2007.

STUDIU PRIVIND INFLUENȚA PARAMETRILOR DE MĂCINARE ASUPRA STRUCTURII ȘI PROPRIETĂȚILOR ALIAJELOR Ni-Ti

Rezumat: Aliajele NiTi sunt din ce in ce mai mult folosite in industrii de vârf ca industria aerospatiala și biomedicală datorita caracteristicilor lor, in special cele de efect a memoriei. Omogenitatea structurală a aliajelor Ni-Ti influențează direct efectul de memorie a formei. Pentru a realiza o bună omogenitate structurală a aliajelor Ni-Ti acestea sunt fabricate prin utilizarea tehnologiilor specifice ale metalurgiei pulberilor. Lucrarea prezintă câteva aspecte privind stadiul prezent in producerea unor amestecuri omogene din aliaje Ni-Ti.

BULETINUL INSTITUTULUI POLITEHNIC DIN IAŞI
Tomul LIII (LVII), Fasc. 4, 2007
Secţia
ŞTIINŢA ŞI INGINERIA MATERIALELOR

SOME RESULTS OF RESEARCHES REGARD SOLUBLE SALT REMOVING FROM SECONDARY ALUMINIUM DROSS / SALTS SLAG

BY

MARIA ROMAN*, ROMANIŢA TEODORESCU*, VIOREL BĂDILIŢĂ*, LUCIA FIRESCU* and MARIA GHEORGHE**

Abstract: Soluble salts removing from secondary aluminium dross is important because on the one hand there is possibility to bring in the economic circuit of soluble salts and on the other hand to obtain clean secondary aluminium dross, without soluble salts, which is possible to be processed for aluminium recovery like coagulants. The paper presents some results of experiments, which have had the objective to study the leaching process in water of the soluble compound from secondary aluminium dross / salts slag.

Keywords: secondary aluminium dross, leaching process, soluble salts de-pollution, coagulant

1. Introduction

Aluminium dross, scrap, skims or salt slag is the residual waste material, which are produced from any process in which aluminium is melted. By their high aluminum and soluble salt content, these technological residues can be an important source of environmental pollution but they can be an important source of row materials for other industrial useful products. For that there are many preoccupations of aluminum specialists, from all over the world, to establish efficient possibilities to recover aluminum from these technological residues and reduce landfilling for environmental protection.

One method to recover aluminum is to obtain products which can be utilized like coagulants. But, that require previous process for remove soluble salts which accompany aluminum.

One of the technologies, which are practise to remove of soluble salts, like NaCl and KCl, are based on physical proceedings of leaching in water, final products beings the solid salts or their solutions, [1,2,3,4] and clean secondary aluminium dross.

To establish optimum work parameters and the flow sheet for an efficient technology for recovery of the soluble salts from fine fraction of secondary aluminum black dross/salt slag, there sampled technological residues from three platforms with similar profile: SC ALMET SA from Năvodari, SC GEORGE IMPEX SRL from Potcoava, SC SILNEF SA from Braşov

The first company is *SC ALMET SA* Năvodari, which process scrap and spills to obtain casting alloys and wrought alloys for extrusion. For scrap melting they use revolving cylindrical furnace or crucible melting furnace. They work in quality system in conformity with SR EN ISO 9001:2001, SR EN ISO 14001:2005 and OHSAS 18001:2004 standards. To increase performance rating they use scrap sorting, melting

deoxidizing, refining and filtering operations. The skimming from the first melt is in part reuse in their foundry circle. Technological residues are kept on the authorize slag dump till they are delivery to aluminum dross specialize processors.

The second company is *SC FABRIMIXT SA* Câmpina, which process scrap, spills and dross to obtain ingot casting alloys Technological residues are kept on their the authorize slag dump. For scrap melting they use revolving cylindrical furnace or crucible melting furnace. To increase performance rating they use melting deoxidizing, refining and filtering operations. The skimming from the first melt is in part reuse in their foundry circle.

The third company is *SC GEORGE IMPEX SRL* Potcoava which process only aluminum dross from primary and secondary aluminum companies. For dross melting they use revolving cylindrical furnace or crucible melting furnace. The dross is crushed and the metal particles are sort from nonmetals components by shaking sieve. In the coarse faze there is more aluminum metallic thereby this part is melt to recover aluminum. The fine faze is technological residues and they are kept on the authorize slag dump.Those three secondary aluminum processors use the same furnace for melting but thy use the different starting material and they use different technological methods. One of the first analyses of process metallurgical methods influence can be observed from preliminary solid material balance for each company. These results show that technological residues percent depends on quality of started materials, which are processed. If for SC ALMET SA company the residues percent is ~18 % and ~ 24% for SC FABRIMIXT SA Câmpina company, for company SC GEORGE IMPEX SRL this percentage is more high ~57%.

2. Experimental procedure

The samples were characterization by chemical analysis, particle size distribution analysis and phase analysis.

Chemical analysis were performed conform specific metallurgical nonferrous Rumanian standards on each particle size distribution. The results show that the elemental compositions are distinct for each company. Technological residues of ALMET have uniform composition of metals Al, Cu, Mg, Mn, Ni, Cr, Ca, Ti, Fe; on particle size; the content of Si is more in fine fraction which is under 0,5 mm; the content of K is bigger than content Na. Technological residues of GEORGE IMPEX have more Cu in bigger particle fraction; the content in Zn and Ca is more in fine fraction; - the content of silicon is more in bigger particle fraction; content of Na is bigger than content of K. FABRIMIXTS` technological residues has a variable content of aluminum about ~10% between fine and bigger particle fraction; Zn and Ca are more in fine fraction; content of Na is bigger than content K; content of - SO_4^{2-} and NO_3 are more in fine fraction >0,5mm; - content of Fe is bigger then the others dross. All samples have P but have not F. Elemental chemical analysis gives not enough sufficient data about characteristics of technological residues

Particle size distribution show that technological residues from GEORGE IMPEX have fine particle size, those from FABRIMIXT have medium *particle size*, those from ALMET have the bigger granulation.

Phase analysis was made by diffractions analysis, which was made by X ray (DRX) and Bragg-Brentano method, couple $\Theta - 2^*\Theta$, on polycrystalline plane samples.

Diffractions studies were made by DRON 2.0 apparatus with characteristic ray CuKα1&2. Experimental data were digital collected by systematic scanning method in angular space 2*Θ: 4 ÷ 84 grad. Phase qualitative analyses were made by methods of Hanawalt, in conformity with standards of A.S.T.M. *Phase analysis* was made on two separate started samples to demonstrate that the material has major differences characteristics between samples. The samples were washed in distillate water at room temperature, keeping starting granulation. Washing solution was filtered and crystallization. The obtained material was analyzed for determined soluble phases. The washed phase was analyzed too. There didn't identify certainly the phases ε $SiAl_2O_2N_7$ or ε $7AlN*SiO_2$ because overlap of their diffractions peak with peak of other phases presents, exception of the main peak. The phase β – Al_2O_3 is a transition alumina those structure can be stabilization of lower content of Na_2O, K_2O, CaO, MgO or $(NO)_2O$. Sometime this phase can contain crystallization water.The phases Spinely / Spinelyde are cubic structures similar with Spineli: $MgO*Al_2O_3$, in which the bivalent metal is total or partial substitute by Fe^{+2}, Cu^{+2}, Zn, Ca, or tetravalent metal can be substitute by Fe^{+3}, Cr^{+3}, etc. Similar there are known aluminum oxnitride with Spinely structure: $Al_{2.7\ 0.33x}O_{4-x}N_x$, Al_3NO_3, Al_3N_1. Technological residues of ALMET have content of metallic aluminium under 1% in the non washed fraction and ~ 4% in washed fraction, but there are aluminium in form of alumina ~26÷29% in the non washed fraction and ~17 % in washed fraction and in form of AlN ~32÷40% in the non washed fraction and ~ 34% in the washed fraction and in the Spinely / Spinelide structure, which are present in percent ~15÷19% in non washed fraction and 15% in washed fraction.The content of metallic silicon is under 1% but there is silicon in form silicon dioxide ~4÷10% in the non washed fraction and ~23 % in the washed fraction. There is any magnesium oxide. The content of soluble phase in washing phase, after crystallization, is ~ 89 %. Technological residues of GEORGE IMPEX have content of metallic aluminium ~14-17% in the non washed fraction and ~ 43% in washed fraction, but alumina content is more lower ~5÷7% in the non washed fraction and ~6 % washed material and in AlN form ~23÷24% in the non washed fraction and ~15% in the washed fraction and it is possible in the Spinely/ Spinelide structure, which are present ~ 12÷19% in the non washed fraction and ~ 10% in the non washed material; The content of metallic silicon is ~ 2-3% in the washed fraction and ~ 6% in the washed fraction but there is silicon in form silicon dioxide ~9÷14% in the non washed fraction and ~10 % in the washed fraction. The content of magnesium oxide is ~3-4% in the washed fraction and 2% in the washed fraction.The content of soluble phase in washing phase, after crystallization, is ~ 94 % in the technological residues of FABRIMIXT have high content of metallic aluminium ~37÷38% in the non washed fraction and ~ 51% in washed fraction, but alumina content is more lower ~9÷12% % in the non washed fraction and ~6 % in the washed material and in AlN form ~19÷20% in the non washed fraction and ~6% in the washed fraction and it is possible in the Spinely/ Spinelide structure, which are present ~ 5÷11% in the non washed fraction and ~ 3% in the non washed material. The content of metallic silicon is ~ 5-7% in the washed fraction and ~ 7% in the washed fraction but there is silicon in form silicon dioxide ~17÷18% in the non washed fraction and ~23 % in the washed fraction. The content of magnesium oxide is ~3% in the washed fraction and it isn't in the washed fraction. So, results show important differences between those three analyzed materials. That data are important for choose the right parameters of any process of aluminium black dross/salt slag.

There was studied the washing of the salt slag under many aspects to determine influence of different condition of salt solubilization like, work conditions, number of counter current washing step (one, two, three or four), with or without grinding.
The salts slag were sifted, washed with/without simultaneous grinding, dry and disintegration to remove the soluble salts from the salt slag for a good processing to obtain coagulants.

Experiments were made with ordinary laboratory equipment, which was composed by washing vessel with electric agitator, gas bulb, ball mill, aspirator bottle, Buchner funnel, drying cabinet.

3. Results and discutions

To determine influence of work conditions the samples were washed with channel or distilled water, by continuous stirring of solid and liquid phases, 60 minutes/steps time of mixing at normal or high temperature (20 or 40^{0}C), with solid - liquid ratio equal to 1:1. Washing solutions and solid materials were chemical analyzed. Figure 1 shows Na&K content in solid washing phases function by working conditions

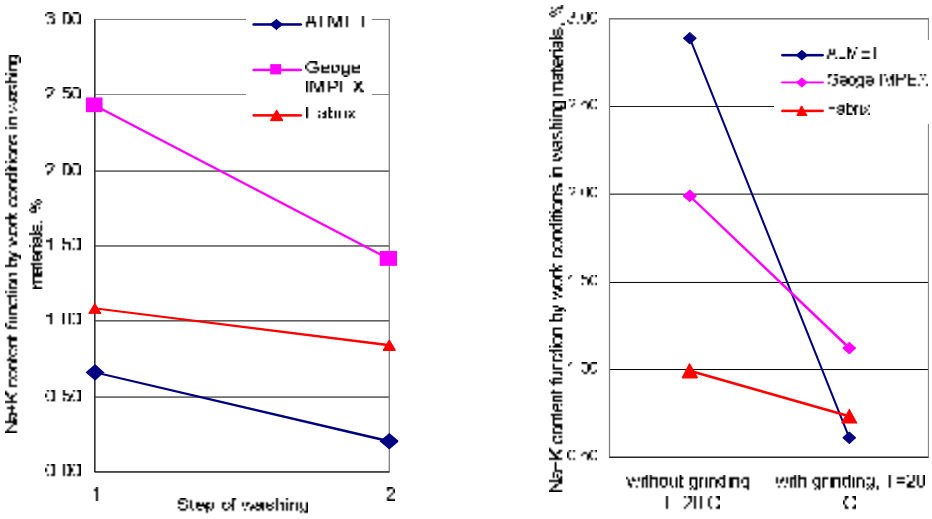

Figure 1. Na&K content function by work conditions in solid washing phases

The results show that washing of salt slag at 20^{0}C removing of the NaCl and KCl isn't enough quantitative but washing salt slag at 40^{0}C is much better; the solutions are more concentrated in Na and K. Washing with grinding at 20^{0}C lead to similar results like washing at 40^{0}C, and in the mean time assure an optimum particle size. Washing of samples in two steps, at the same temperature, lead to a high efficiency of washing.

To determine number of washing stages, experiments were carried out in a laboratory installation under the following conditions: one and a lot number of the washing steps, by re-pulping fresh water on every steps 40^{0}C temperature 1 hour time of stirring. Finally, the distribution of Na and K ions in washing waters resulted in every stage and in solid washed phase was determinate, figure 2 and 3.

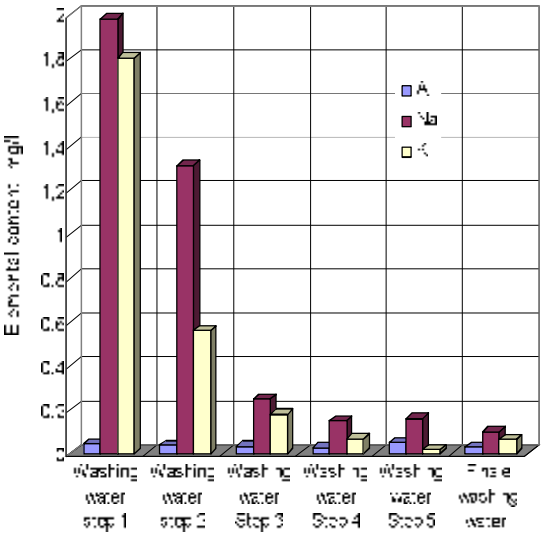

Figure 2. Determination of the number of washing steps for ALMET salt slag

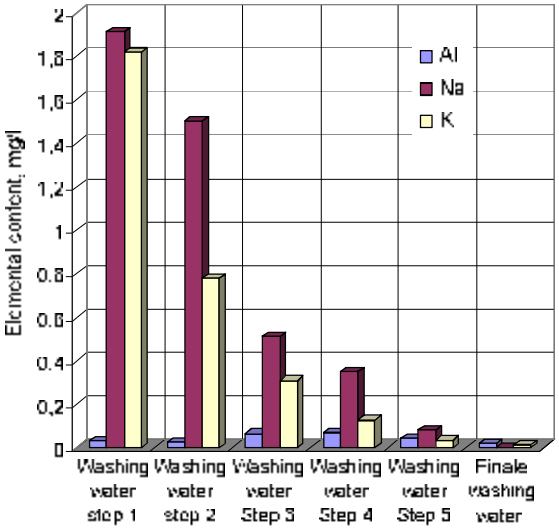

Figure 3. Determination of the number of washing steps for George IMPEX salt slag

The results show that:

- For a good washing of the salt slag it is necessary many washing steps;
- The quantitative elimination of the Na and K soluble ions take place in the first three washing steps;
- The washing waters from the first and the second steps have the high content in Na, K ions;
- The concentration of Na, K ions in washing waters regresses gradually from first step to last step;
- Finally, in washed slag there are insoluble Na, K ions lied in stable structures

The remained K ions in the washed slag is less then 0,05 % but the quantities of Na ions are more then 1,65 respectively 1,77 %. Therefore, for advanced washing of the slag, there are necessary 5 washing steps.

Starting with the variation of the NaCl and KCl solubility with temperature it was studying the variation of the concentration of the both salts in washing waters and in the washed salt slag/unwashed salt slag. Finally it was calculated the washing efficiency. The solubility of NaCl in water at 20^0C is 26,39 g/l very appropriately of KCl 25,5 g/l. The solubility of NaCl in water at 40^0C is 26,68 g/l. The solubility of KCl in water at 40^0C is 28,7 g/l. Successfully washing of the salt slag was made: in the first step by water re-circulation at 4 fresh salt slag samples and in the second step by washing of the same salt slag in 4 steps with fresh water. Practically: some salt slag was washed in 4 steps with equal fresh water quantities; some water was successfully contacted with 4 quantities of fresh salt slag in 4 steps. In the some time it was realize the washing of the salt slag in counter-flow, in 4 steps, at ratio S:L = 1:1, with grinding in 4^{th} step for simultaneously decreasing of the particle size. The experiments were made with a mixture in equal parts of the 3 kind of the salt slag: ALMET, George IMPEX, FABRIX.

The experiments show that:

- The washing efficiency of NaCl and KCl in every step at 20^0C are very low 8 16%, the final washing efficiency after 4 re-pulping being aprox.70% for KCl and 65% for NaCl;
- It is necessary the re-circulation of the NaCl and KCl solutions to increase their concentration. In that situation the washing efficiency is 70% for KCl and 75% for NaCl;
- The washing with grinding in 4^{th} step offer in the mean time a high fineness of the salt slag and high concentration of the solutions in NaCl and KCl, figure 4.

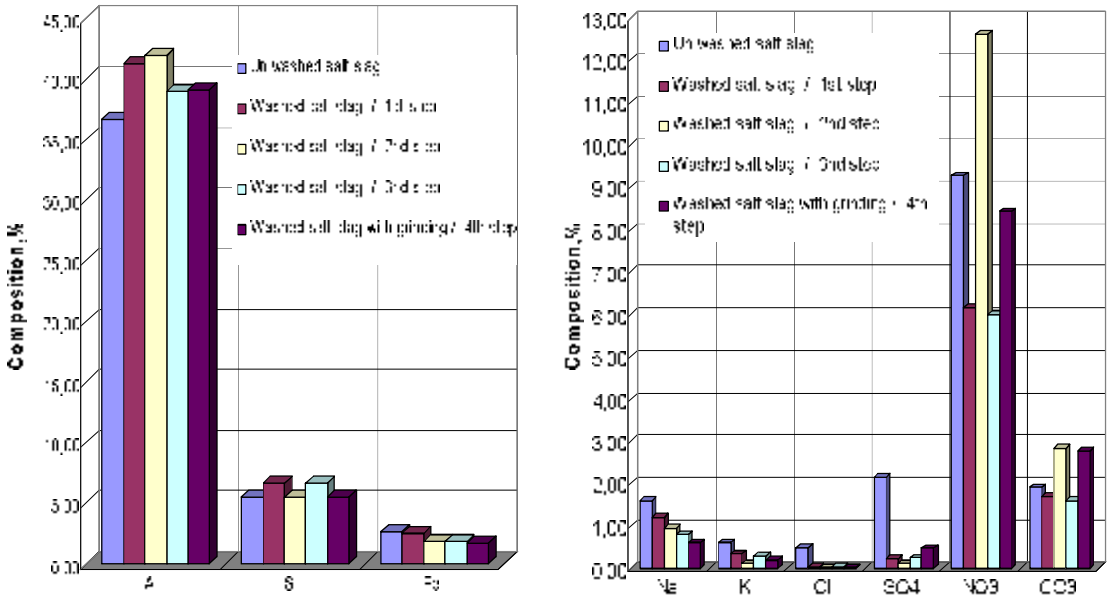

Figure 4. The composition of the salt slag washed in counter current in 4 steps with grinding in 4^{th} step

There were selected the following conditions to next work:
- The counter-flow washing, in 4 steps, with grinding in 4^{th} washing step;
- The counter-flow washing, at ratio S:L=1:1, which offer good washing conditions, salt slag without soluble salts like NaCl and KCl (Cl content in washed slag is <0,02%); the concentrated washing waters in salts;
- The washing waters resulted in first steps will be re-circulating in the washing process till crystallization concentration of the solutions will be realized;
- The washing lids to Cl contents under 0,03% in salt slag;
- Na and K content in washed salt slag indicate other combinations of these elements then like NaCl and KCl;
- Washing efficiency can be obtained by applying researches technology in report with soluble salts NaCl and KCl from salt slag is over 98%.

Finally was proposed the flow sheet for the counter current washing of the slag salts. For obtaining of NaCl and KCl salts from the solution, their separation, from the solutions, were realized by their concentration at high temperature, evaporation and then separation of the crystals. Known that the variation of NaCl and KCl solubility with temperature are inverse, in the first stage it was made crystallization of NaCl and, in the second stage, it was made crystallization of KCl at low temperature. NaCl it

was made in the first step at 80÷90^{0}C evaporate temperature and 35^{0}C crystallization temperature. Separation of KCl it was made in the second step at 20^{0}C crystallization temperature. There was introduced 1000 ml solution of NaCl and KCl in the evaporation reactor at 80÷90^{0}C. The temperature was maintained constantly till crystallization concentration of NaCl was assured. In that moment it was stopped solution heating and begin slowly down the temperature to 35^{0}C which is crystallization temperature for NaCl. There were separated from the solutions 17g crystals of NaCl, which were filtered, washed with NaCl saturated solutions, dried and analyzed. The solution was heating again to 80÷90^{0}C where it was maintained constantly till necessary crystallization concentration was assured. The solution was slowly refrigerated to 20^{0}C. There were separated from the solutions 23,6 g crystals of KCl, which were filtered, washed with KCl saturated solutions, dried and analyzed. After that there were remain 45 ml mother lye with the composition which is show in table no.1

Table 1. The results obtain at evaporation and crystallization phase

INTRODUCED / RESULTED MATERIAL.		Al	Na	Cl	NaCl	K	Cl	KCl	Cl
1000 ml / Washing water conc.	g/l	0,037	15,00	23,12	38,12	9,00	8,18	17,20	32,50
	g	**0,037**	**15,00**	**23,12**	**38,12**	**9,00**	**8,18**	**17,20**	**32,50**
118 ml / solution	g/l	0,130	84,75	129,30	215,29	74,42	68,57	142,78	201,70
	g	**0,015**	**10,00**	**15,41**	**25,4**	**8,90**	**8,10**	**17,44**	**23,81**
NaCl Crystals / 17,0 g	%	0,130	30,00	46,25	76,25	0,22	0,20	0,42	48,00
	g	**0,022**	**5,10**	**7,86**	**12,96**	**0,04**	**0,03**	**0,07**	**8,16**
Mother lye / 56 ml	g/l	0,170	107,14	165,17	272,14	32,50	29,46	62,50	194,60
	g	**0,010**	**6,00**	**9,25**	**15,24**	**1,82**	**1,65**	**3,50**	**10,90**
KCl Crystals / 23,6 g	%	0,016	17,00	26,20	43,20	30,00	27,27	57,28	54,66
	g	**0,004**	**4,012**	**6,18**	**10,20**	**7,08**	**6,43**	**13,52**	**12,90**
TOTAL	g	0,036	15,11	23,29	38,39	8,94	8,11	17,08	31,96

4. Conclusions

To establish optimum work parameters and the flow sheet, which are necessary to establish an efficient technology for removing of the soluble salts from fine fraction of secondary aluminum salt slag there were sampled salt slag resulted on three platforms with similar profile: SC ALMET SA from Năvodari, SC GEORGE IMPEX SRL from Potcoava, SC SILNEF SA from Braşov.

The samples were sifted, washed with/without simultaneous grinding, dry and disintegration. There was studied the washing of the salt slag under many aspects to determine influence of different condition of salt solubilization like, work conditions, number of counter current washing step (one, two, three or four), with or without grinding.

The experiments show there are possible to obtain solutions with high content in Na and K in the following conditions:

- the washing in countercurrent with grinding in 4th step at 40^{0}C and S:L ratio = 1:1;

- the washing with grinding in 4th step offer in the mean time a high fineness of the slag and high concentration of the solutions in NaCl and KCl;
- the washing efficiency of NaCl and KCl on every step at 20^0C are between 8 : 16%, the final washing efficiency after 4 re-pulping being aprox.70% for KCl and 75% for NaCl;
- the removal of NaCl and KCl from solutions resulted in aluminum slag washing with water, was realized by their concentration by evaporation at the temperature and then the separation of the crystals in two cooling steps at 35^0C for NaCl and 20^0C for KCl

Finally there was proposed a proper flow sheet for the counter current washing of the slag salts and conditions to obtain NaCl and KCl salts from the washing solution

Acknowledgements

We thank those three companies for their support in our researches.

Received March 15, 2007

**National R&D Institute for Nonferrous and Rare Metals IMNR, Pantelimon, Jud. Ilfov*
***Technical Bilding University, Bucharest*

REFERENCES

1. B.I. US nr. 5,102,453 , Cl C22B 21/00, 7 apr. 1992
2. B.I. US nr. 6.238,633 , Cl C01F 1/00, 29 mai 2001
3. Engitec Technologies S.p.A Milano. Italia
4. ***, **Manualul chimistului vol.**1
5. Hazardous Waste Section Department of the Environment and Heritage http://www.deh.gov.au/industry/chemicals/hazardous-waste
6. Waste management www.sims-group.com/au/divisions/aluminium

CÂTEVA REZULTATE A CERCETĂRILOR PRIVIND ÎNDEPĂRTAREA SĂRURILOR SOLUBILE DIN ZGURILE DE ALUMINIU SECUNDAR

Rezumat: Lucrarea prezintă câteva rezultate ale cercetărilor pentru îndepărtarea sărurilor solubile din zgurile negre de aluminiu secundar ca primă etapă a unei tehnologi ecologice de obținere a unui coagulant pe bază de aluminiu. Experimentările au avut ca obiectiv studiul procesului de solubilizare în apă a compușilor solubili prezenți în zgurile negre de aluminiu rezultate la trei procesatori români de deșeuri de aluminiu cu profil similar: ALMET Năvodari, GEORGE IMPEX Potcoava, SILNEF Brașov.

BULETINUL INSTITUTULUI POLITEHNIC DIN IAŞI
Tomul L(III (LVII), Fasc. 4, 2007
Secţia
ŞTIINŢA ŞI INGINERIA MATERIALELOR

METHODS OF MODELLING FOR PREDICTING RELIABILITY AND RISK

BY

IOAN RUSU, CONSTANTIN BACIU, MARIA BACIU, NICOLAU BOGDAN and MITICĂ BULAI

Abstract: Because the combination of reliability and maintainability will dictates the proportion of time that any item is available for use the authors present some methods of modeling the risk and reliability in industrial branches. The key parameters are failure rate and down time, both of which determine the failure costs. As a result, techniques for optimizing maintenance intervals and spares holdings have become popular since they lead to major cost savings.

Keywords: reliability, maintainability, risk, modeling

1. Block diagram

The block diagrams define what constitutes a system failure since this will determine which failure modes at the component level actually cause a system to fail. There may well be more than one type of system failure, in which case a number of predictions giving different reliabilities will be required. This step is absolutely essential if the predictions are to have any significance

In this method it is necessary to describe the system as a number of functional blocks which are interconnected according to the effect of each block failure on the overall system reliability. In figure 1 it is presented a series diagram representing a system of two blocks such that the failure of either block prevents operation of the system. Figure 2 shows the situation where both blocks must fail in order for the system to fail. This is known as a parallel, or redundancy, case. Figure 8.3, shows a combination of series and parallel reliability. It represents a system which will fail if block A fails or if both block B and block C fail The failure of B or C alone is insufficient to cause system failure.

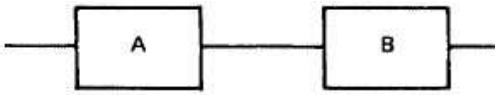

Figure 1.

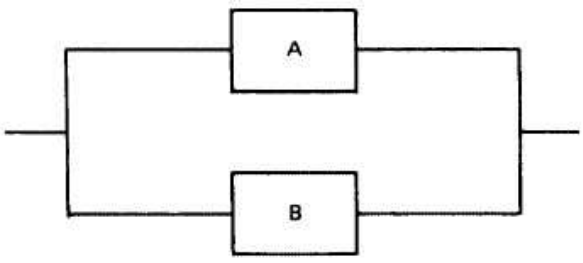

Figure 2.

A number of general rules should be borne in mind when defining the blocks:

1. each block should represent the maximum number of components in order to simplify the diagram;

2. the function of each block should be easily identified;

3. blocks should be mutually independent in that failure in one should not affect the probability of failure in another;

4. blocks should not contain any significant redundancy otherwise the addition of failure rates, within the block, would not be valid;

5. each replaceable unit should be a whole number of blocks;

6. each block should contain one technology, that is, electronic or electro-mechanical;

7. there should be only one environment within a block

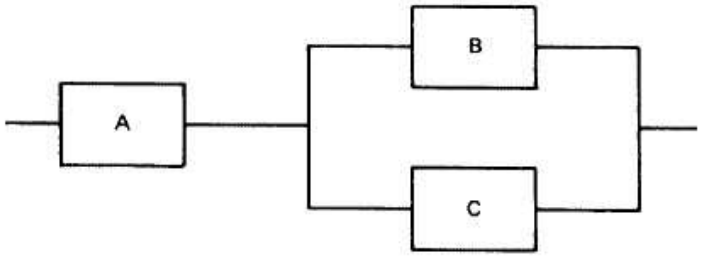

Figure 3.

2. Common cause (dependent) failure

Common cause failures (CCF) often dominate the unreliability of redundant systems by virtue of defeating the random coincident failure feature of redundant protection. Whereas simple models of redundancy assume that failures are both random and independent, common cause failure (CCF) modelling takes account of failures which are linked, due to some dependency, and therefore occur simultaneously or, at least, within a sufficiently short interval as to be perceived as simultaneous.

Typically, causes arise from:

- requirements (incomplete or conflicting);
- design (common power supplies, software, noise etc.);
- manufacturing (batch related component deficiencies);
- maintenance/operations (human induced or test equipment problems);
- environment (temperature cycling, electrical interference, etc.).

There are developed the following types of CCF model:

- the SIMPLE BETA (β) model, which assumes that a fixed proportion (β) of the failures arise from a common cause. The estimation of (β) is assessed according to the system;
- the PARTIAL BETA model, also assumes that a fixed proportion of the failures arise from a common cause. It is more sophisticated than the simple BETA model in that the contributions to BETA are split into groups of design and operating features which are believed to influence the degree of CCF. In traditional PARTIAL BETA models can be found the following groups of factors, which represent defences against CCF:
  - similarity (diversity between redundant units reduces CCF);
  - separation (physical distance and barriers reduce CCF);
  - complexity (simpler equipment is less prone to CCF);

- analysis (previous data analysis will have reduced CCF);
- procedures (control of modifications and of maintenance activities can reduce CCF);
- training (designers and maintainers can help to reduce CCF by understanding root causes);
- control (environmental controls can reduce susceptibility to CCF, e.g. weather proofing of duplicated instruments);
- tests (environmental tests can remove CCF prone features of the design);

- the SYSTEM CUT-OFF model offers a single failure rate for all failures (independent and dependent both combined). It argues that the dependent failure rate dominates the coincident failures. Again, the choice is affected by system features such as diversity and separation. It is the least sophisticated of the models in that it does not base the estimate of system failure rate on the failure rate of the redundant units
- the BOUNDARY MODEL uses two limits of failure rate. Namely, limit A which assumes all failures are common cause and limit B which assumes all failures are random. This method is a mathematical device, having no foundation in empirical data, which relies on a subjective assessment
- the MULTIPLE GREEK LETTER model is similar to the BETA model but assumes that the BETA ratio varies according to the number of coincident failures. Thus two coincident failures and three coincident failures would have different BETA's. However, in view of the inaccuracy inherent in the approximate nature of these models it is considered to be too sophisticated and cannot therefore be supported by field data until more detailed information is available.

All the models are, in their nature, approximate but, because CCF failure rates which are much greater than the coincident independent failures, then greater precision in estimating CCF is needed than for the redundant coincident models

3. Fault tree analysis

A FAULT TREE is a graphical method of describing the combinations of events leading to a defined system failure. In fault tree terminology the system failure mode is known as the top event. The fault tree involves essentially three logical possibilities and hence two main symbols. These involve gates such that the inputs below gates represent failures. Outputs (at the top) of gates represent a propagation of failure depending on the nature of the gate. There are three types og gates:

- the OR gate whereby any input causes the output to occur;
- the AND gate whereby all inputs need to occur for the output to occur;
- the voted gate, similar to the *AND* gate, whereby two or more inputs are needed for the output to occur.

Figure 4 shows the symbols for the *AND* and *OR* gates and also draws attention to their equivalence to reliability block diagrams. The *AND* gate models the redundant case and is thus equivalent to the parallel block diagram. The *OR* gate models the series case whereby any failure causes the top event

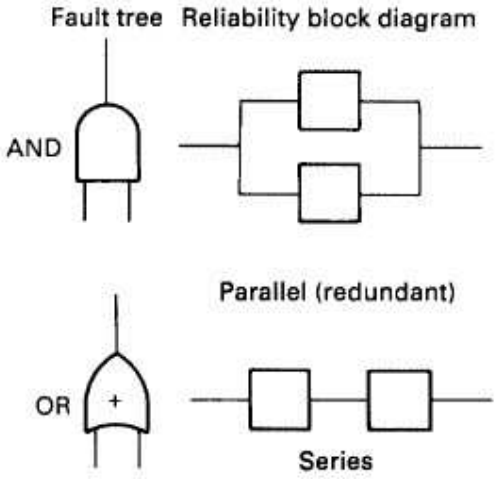

Figure 4.

An example of a fault tree is constructed as shown in figure 5 in which two additional symbols can be seen. The rectangular box serves as a place for the description of the gate below it. Circles, always at the furthest point down any route, represent the basic events which serve as the enabling inputs to the tree.

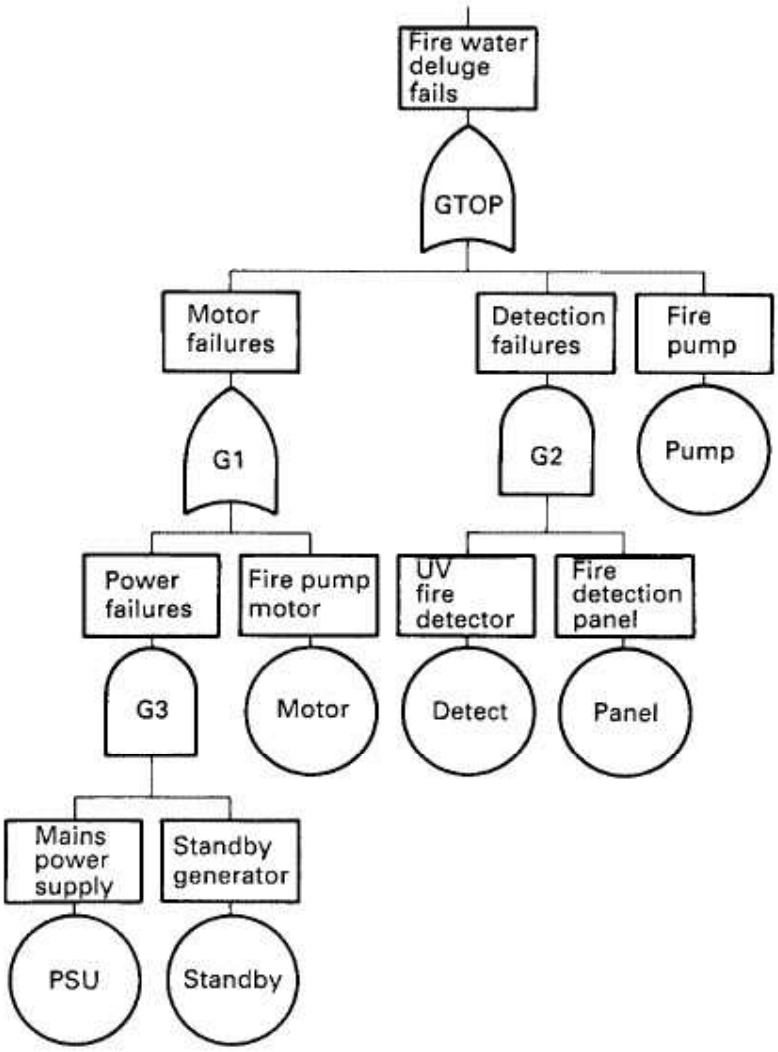

4. Event tree diagrams

Whereas FAULT TREE analysis is probably the most widely used technique for quantitative analysis, it is limited to AND/OR logical combinations of events which contribute to a single defined failure (the top event). Systems where the same component failures occurring in different sequences can result in different outcomes cannot so easily be modelled by fault trees. The fault tree approach is likely to be pessimistic since a fault tree acknowledges the occurrence of both combinations of the inputs to an AND gate whereas an EVENT TREE or CAUSE CONSEQUENCE model can, if appropriate, permit only one sequence of the inputs.

The Event Trees or Cause Consequence Diagrams (CCDs) resemble decision trees which show the likely train of events between an initiating event and any number of outcomes. The main element in a CCD is the decision box which contains a question/condition with YES/NO outcomes. The options are connected by paths, either to other decision boxes or to outcomes. Comment boxes can be added at any stage in order to enhance the clarity of the model.

The main difference between the two models (fault tree and event tree) is that the event tree models the order in which the elements fail. For systems involving sequential operation it may well be easier to model the failure possibilities by event tree rather than to attempt a fault tree.

Table 1 summarizes the main differences between Event Tree and Fault Tree models

Table 1

Cause Consequence	Fault Tree
Easier to follow for non-specialist	Less obvious logic
Permits several outcomes	Permits one top event
Permits sequential events	Static logic (implies sequence is irrelevant)
Permits intuitive exploration of outcomes	Top-down model requires inference
Permits feedback (e.g. waiting states)	No feedback
Fixed probabilities	Fixed probabilities and rates and times

Received April 20, 2007 *The "Gh.Asachi" Technical University Iaşi*

REFERENCES

1. Badiru B. A., **Expert Systems Applications in Engineering and Manufacturing**, Prentice Hall, Inc., Englewood Cliffs, New Jersey, 1992;
2. Dornbusch, R., Fischer. S., **Macroeconomic**. Editura Sedona. Timişoara, 1998;
3. Dumitru Zait. Panaite Nica, **Introducere in modelarea econometrica**, Editura Universităţii „Al. I. Cuza" Iaşi. 1999;
4. Ilies Liviu , **Managementul firmei**, Editura : Dacia, 2001;
5. Ioan Ciobanu, Ruxandra Ciulu, **Strategiile competitive ale firmei**, Ed Polirom. 2005;
6. Ionescu Gh. Gh., **Modelarea si optimizarea deciziilor manageriale**, Editura : Dacia. 1999;
7. Stoica, M. **- Proiectarea sistemelor tehnico economice**. Editura Economica, Bucureşti, 2000.

8. Ştefan Pece, **Evaluarea riscurilor in sistemul om – maşină.** Editura: Atlas Press, Bucureşti, 2003;
9. Alexandru Darabont ş.a., **Evaluarea calităţii de securitate a echipamentelor tehnice**, Editura: AGIR Bucureşti, 2001.

METODE DE MODELARE UTILIZATE LA ANALIZA FIABILITĂŢII ŞI RISCULUI

Rezumat: Deoarece combinaţia dintre fiabilitate şi mentenanţă va dicta timpul de utilizare a unui obiect, autorii prezintă câteva metode de modelare a fiabilităţii şi riscului în ramurile industriale. Parametrii cheie ai ratei de distrugere şi timpului în care are loc aceasta determină costurile procesului respectiv. Ca urmare, tehnicile de optimizare a intervalelor de întreţinere devin din ce în ce mai populare, ele determinând economii substanţiale.

BULETINUL INSTITUTULUI POLITEHNIC DIN IAŞI
Tomul LIII (LVII), Fasc. 4, 2007
Secţia
ŞTIINŢA ŞI INGINERIA MATERIALELOR

REINFORCEMENT OF RECYCLED ALUMINUM ALLOY SCRAP WITH SAFFIL CERAMIC FIBERS

BY

M. SAMUEL

Abstract: The development of the automotive industry requires materials to fulfill the following properties; low density, low coefficient of thermal expansion, high wear resistance, high modulus of elasticity, and high strength at ambient and elevated temperatures. Aluminum scrap composite alloys reinforced by ceramic fiber, may fulfill most of the above requirements. In the present work, production of composites by direct conversion of granulated 2014 Al scrap alloy with Al_2O_3 SAFFIL fiber into final products by hot extrusion will be introduced. Three different reduction ratios of extrusion will be investigated. The mechanical properties at ambient and elevated temperatures, the microstructure, and fiber length are evaluated. Experimental results show that the relative strengthening of the composites at ambient and elevated temperature up to 360°C is significantly higher compared to that of the Al-2014 conventional alloy. With added 10 vol. % Al_2O_3 Saffil fibers, ultimate tensile strength (**UTS**) and yield strength (**YS**) at 270°C are increased by 77%, 86% respectively. The Vickers hardening increased by 43% and the elastic modulus increased by 27 % at ambient temperature. This is due to the fact that the resulted composites contain fibers up to 10 vol. % have a very good internal cohesion.

Keywords: 2014 Al scrap alloy, SAFFIL ceramic fibers, Composites, hot extrusion.

1. Introduction

Development of the modern technologies, mainly in the automotive industry, impose new regulations for environmental protection, create demands for new structures of materials with improved mechanical properties such as high wear and creep resistance at ambient and elevated temperature [1-3]. Particular-reinforced metal-matrix composites (MMC's) comprise a class of new generation of materials whose properties can be tailored to suit a particular applications [4-8]. The most common methods of producing particulate reinforced MMC's may be classified as: liquid metallurgy (LM) or powder metallurgy (PM) techniques.

In the LM techniques of squeeze casting, fibers are infiltrated with liquid metal, producing nearly fully dense composites with pseudo –3D random fiber orientation. Reasonable properties were achieved with this method [9]. Extrusion is subsequently applied to the reinforced fiber cast billets to obtain a finer microstructure and alignment of fibers. This is performed in order to improve the affectivity of the fiber reinforcement [10]. The high shear stresses inherent in solid state processing have led to extensive fiber breakage [10-12]. Extensive fiber breakage has also been found as a major problem during composite production by conventional powder processing method [13]. In addition, the above mentioned methods require sophisticated technology as well as high fabrication costs [14, 15].

The direct conversion of aluminum scrap alloy admixed with reinforced fibers into compact metal by hot extrusion requires simple technology, low production cost and results in a very low air pollution emission [15].

Silicon carbide, aluminum oxide and boron carbide are the most commonly used particulate or fiber reinforcements. It is suggested to consider aluminum oxide because of its high modulus, availability, and low cost.

The present study is to elucidate the evaluation of the mechanical properties and microstructure of Al-2014 scrap alloy with Al_2O_3 Saffil fibers produced by the direct conversion and hot extrusion method. Since, the extrusion reduction ratio (λ) is considered as an important factor that affect the fiber length and matrix microstructure, then, it is taken into consideration during the present study.

2. Experimental procedure

2.1 Materials

In this study, the following materials are used. Al-2014 granulated scrap alloy produced by comminution mechanically with special machine [15]. This scrap is classified into two groups. The first is consisted of scrap length 0.5 – 2.0 mm, and the 2nd is consisted of length less than 0.5 mm (see Fig. 1). The chemical analysis of the base alloy is tabulated in Table 1. The above mentioned scrap alloy is reinforced with Al_2O_3 Saffil fibers. This fiber was produced by Imperical Chemical Industries, United Kingdom (see Fig. 2). The saffil fiber Al_2O_3 diameter was approximately 3 μm. The chemical analysis and physical properties of the fiber are tabulated in Table 2 [16].

Table 1. The chemical analysis for the 2014 Al scrap alloy

Cu%	Mg%	Mn%	Si%	Ni%	Fe%	Zn%	Ti%	Al	Density (g/cm^3)
4,30	0,85	0,78	0 70	0,10	0,70	0,30	0 20	Rem	2,68

Table 2. The chemical analysis and physical properties of Al_2O_3 SAFFIL fiber (type RF590) [16]

Chemical analysis		Physical properties	
Al_2O_3 - δ	96-97%	Melting temperature (Tm)	>2000 °C
SiO	3-4%	Applied temperature (Tp)	1600 °C
Fe,Cr,Ni,Mg,Na,Ca,chloride	Trace amount	Tensile stress (UT) Modulus of elasticity (T_y)	2000 MPa 300 GPa
		Density (ρ_f)	3,3 g/cm^3
		Mohs hardness	9

2.2 Composite fabrication

The composite were prepared by dry mixing the granulated 2014 Al scrap alloy and saffil fibers with an organic additive which acts as a process control agent in a high – power ball mill for 3 hours with a horizontal axis rotating at 300 r.p.m.. The ball mill was made of hardened chromium steel with 20 mm diameter. The weight ratio of the grinding balls to the composite is 10:1 (mixture capacity of 350 g). The loading of the composite takes place in air atmosphere. The granulated aluminum scrap alloy reinforced with 2,5,10 and 20 vol. % Al_2O_3 saffil fibers mixed with 1 5 vol.% lithium stearate ($CH_3(CH_2)_{16}COOLi$). Using hydraulic press, the milled powder was cold compacted up to 70% of green density by uniaxial pressing at 208 MPa in a

floating die (see Fig. 3). The pressure applied during this cold compaction was deliberately kept as low as possible to restrict fiber breakage at this stage [17,18]. Before the cold compaction takes place, a lithium streate (dissolved in methanol) was used as a lubricant to the die wall and punch faces.

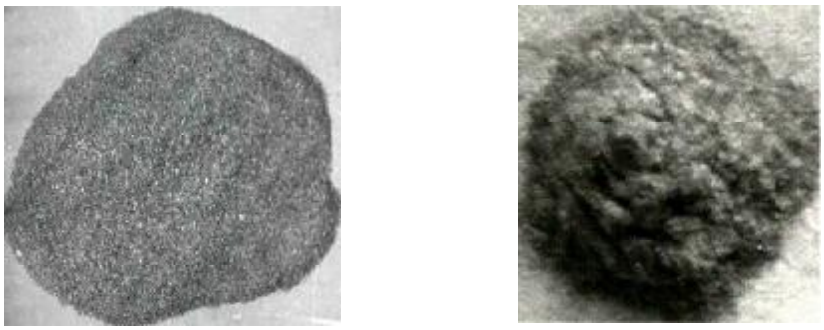

Fig. 1. Al - 2014 granulated scrap alloy size.

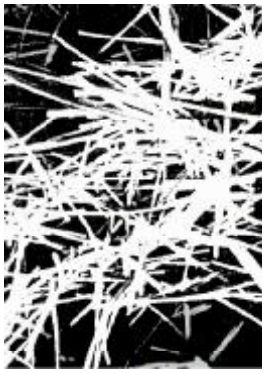

Fig. 2. Al_2O_3 fibers SAFFIL produced by Imperical Chemical Industries, UK.

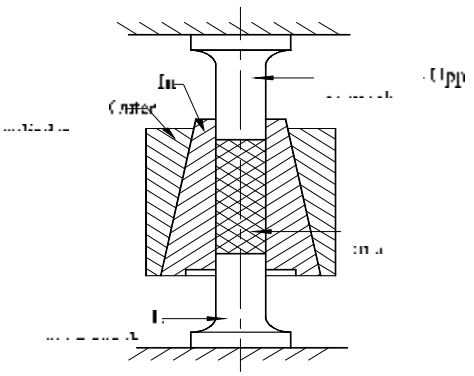

Fig. 3. Floating die of cold compaction.

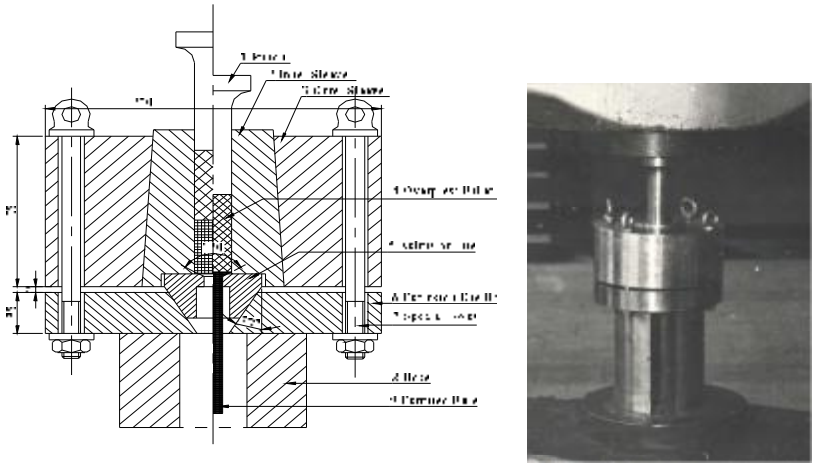

Fig. 4 The extrusion device.

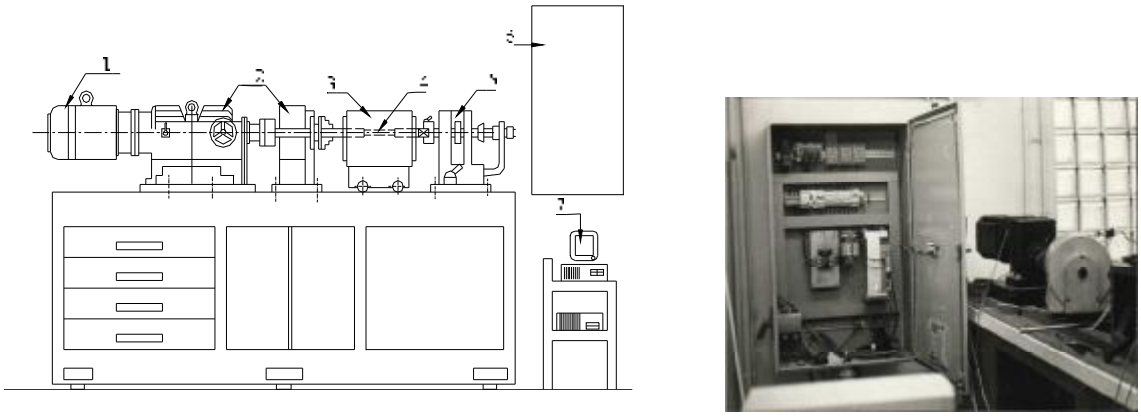

Fig. 5 The computer controlled torsion test screw plastometer. 1- electrical motor. 2- driving set 3- dual cylindrical reheating split furnace 4- test sample 5- measurements set 6- control key panel 7- computer.

After the cold compaction has been completed, sintering process takes place. In this process temperature and sintering time are very critical parameters. This is due to the fact that low temperature and time lead to incomplete sintering whereas high temperature and time produce chemical reaction between the matrix and the reinforced fiber, which in turn results in a weak interface bond. Therefore, the sintering temperature and time of the billet were optimized experimentally to provide the best results. The optimum parameters were found as: sintering temperature 520°C, sintering time 2 hours in pure argon (99.998% purity) at atmospheric pressure. At the end of the sintering process the billets were left to be cooled in air

The resulted billets composite and the extrusion device will be heated up to 490°C for 2 hours before soaking is performed which takes a time of 0.3 hour.

Following the above processes, extrusion takes place in a device as shown in Fig. 4 with the following parameters. Extrusion container has a bore diameter of 41mm, lubricated with mixed of graphite and lithium stearate (dissolved in stearic acide) prior to each experiment. The extrusion die was chosen conical in shape, with an apex angle of 120°, and an extrusion reduction ratios (λ) of 4:1, 16:1 and 38:1. The die was lubricated each time before a billet was extruded. The internal surface of the extrusion die, billet, and extrusion container were kept at 490°C temperature throughout the extrusion operations. Maximum extrusion pressure was chosen to be 850 MPa and the extrusion rate of 10^{-2} m/s for all materials. The low extrusion rate chosen makes possible formation of good diffusion bonds between granulated aluminum scrap alloy and aluminum oxide fibers, and enables the plastic flow material matrix into pores and holes [19-21]. The resulted extrudates were round bars of diameter 20, 10 and 6.5 mm for λ= 4:1, 16:1 and 38:1, respectively.

A series of tensile test were performed at ambient and elevated temperatures using computer controlled torsion test screw plastometer shown in Fig. 5, at a strain rate of 2.5×10^{-4} s^{-1}. The 2% offset yield strength and ultimate tensile strength were obtained as an average over a minimum of three samples. Ambient temperature tensile test were conducted in accordance with ASTM standard E8 [22]. For all samples, tensile test were performed after thermal exposure of 500°C for up to 5 hours, and

precipitation hardening of 150°C for up to 16 hours (T6). The relative long thermal exposure used results in the diffusional transport of matter to the precipitation particles and improve bonding. However, short precipitation time accelerates the precipitation hardening process [23, 24] which results in a stress fields around saffil ceramic fibers.
Elevated temperature tensile tests were conducted at 200, 270 and 360°C in accordance with ASTM standard E21 [25]. Samples were heated in a dual cylindrical reflecting split furnace with a chromel alumel thermocouple fixed to the sample gauge section to monitor the test temperature within − 2°C. For the above elevated temperature tensile tests, each sample was kept at the used temperature for five minutes prior to testing operation.

The Vickers hardness test was performed at ambient and elevated temperature for five samples of the composite material produced. For each sample, the extrusion ratios (λ) 4:1, 16:1 and 38:1 were considered.

Two more tests were conducted after the tensile test to asses the microstructure of the produced composites. These are:
(1)optical metallography test to reveal the microstructures, fracture contours and profiles.
(2)scanning test using electron microscope to observe and monitor the fracture surface.

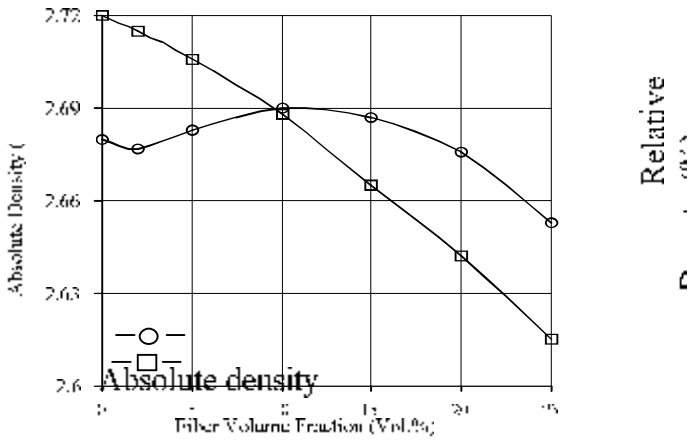

Fig. 6 The absolute and relative densities versus fiber volume fraction, V_f, (vol.%).

3. Results and discussions

For convenience of presentation, the experimental results are documented in such a way to illustrate the effect of temperature and volume fraction, V_f ,of fibers upon the density, microstructure, and mechanical properties of the produced composite materials

3.1. Effect of V_f upon density

The absolute density of the extruded materials was measured by a method based on Archimdes principle. The results obtained for absolute densities of the composite materials are given in Table3. It can be noticed from the table that the densities of the composites are marginally higher than those of the base alloy suggesting that the

change in densities are less sensitive to the change in fiber volume fraction. However, highest density of 2.69 g/cm^3 was found for the composite of 10 vol. % volume fraction extruded at λ= 16:1 in which case the applied extrusion provide a significant density change. For the same composite, using fiber density of 3.3 g/cm^3, with different values of mass fraction (M_f), the relative densities obtained are tabulated in Table 4. From these results, it can be seen that all composites at V_f = 10 vol.% fiber are fully dense.The results in Tables3and4 are drawn in Fig.6 versus fiber volume fraction. It can be seen from this figure that the relative and absolute densities are identical at V_f = 10vol. %.

3.2. Effect of V_f upon microstructure

To minimize the number of photographs, this investigation has been conducted at only one value of extrusion ratio λ = 16:1. The results of optical micrograph for the composite materials with 2, 5, 10 and 20 vol. % Saffil ceramic fibers are illustrated in Fig. 7. It is seen that the distribution of fibers in transverse cross-section is most uniform for ceramic fiber loadings for all volume fraction values used. In longitudinal sections of composites with V_f 5 and 10 vol. % ceramic fibers, a banding of fiber enriched and depleted layers are very pronounced. It can also be seen that the pores are healed and Saffil ceramic fibers have more uniform and homogeneous distribution after extrusion process. This is because extrusion produces extensive shear deformation of the matrix, causing break-up of the prior Al_2O_3 rich cement network in the billet, resulting in a more uniformity in microstructure which in turn improves the mechanical properties of the composites.

Table 3. Absolute densities of composite materials as determined by weight measurement using Archimedes principle. (experimental error + 1%)

Volume Fraction of Al_2O_3 fiber, V_f (vol.%)	Absolute density (g/cm^3)		
	Extrusion ratios (λ)		
	4:1	16:1	38:1
0	2.660	2.680	2.670
2	2.663	2.667	2.679
5	2.670	2.683	2.691
10	2.675	2.690	2.681
20	2.641	2.674	2.661

Table 4. Relative densities of composite materials derived from fiber mass fraction, M_f at a fiber density of 3.3 g/cm^3 *($\rho_c = V_{fm}\rho_m + V_{ff}\rho_f$)

Volume fraction of Al_2O_3 fiber, V_f (Vol.%)	Fiber mass fraction, M_f	Theoretical density ρ_c^* (g/cm^3)	Relative density %(±1%)		
			Extrusion ratios (λ)		
			4:1	16:1	38:1
0	0.000	2.680	99.3	100.0	99.6
2	0.020	2.690	99.0	99.5	99.6
5	0.051	2.710	98.4	99.0	99.3
10	0.100	2.730	98.0	98.5	98.2
20	0.201	2.780	95.0	96.2	95.7

3.3. Effects of V_f and temperature upon mechanical properties

Fig. 8 shows the effect of change in volume fractions of saffil ceramic fibers upon the Vickers hardness test conducted at ambient and different values of elevated temperatures. From this figure, it can be seen that the hardness increases as the vol.% of ceramic fiber increases. This probably occurs because the homogenous distribution of the reinforcement and fine intermetallics were still present in the matrix after solution heat treatment and age hardening (precipitation hardening) of composite materials. On the other hand, it can also be noticed that the hardness decreases as the test temperature increases. This is because the elevated temperature over 270°C causes

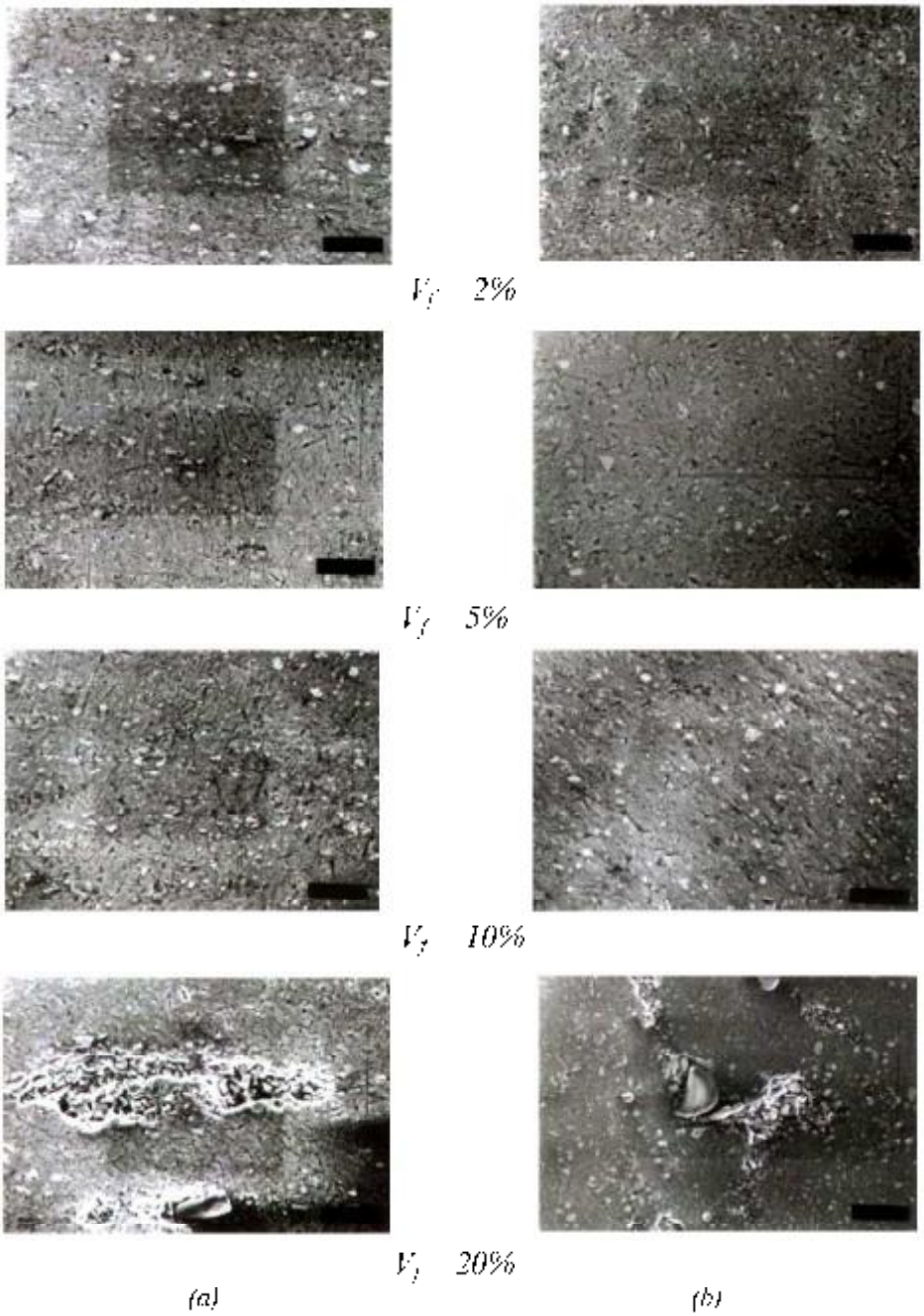

Fig. 7 Optical micrographs of different of V_f at FR = 16:1 composite in (a) longitudinal section and (b) transverse section. (500X).

the coagulation in ligature bonds between the intermetallic phases in the matrix composite. In other words, the hardness of reinforced composite materials at ambient and elevated temperature is always higher than the hardness of the conventional 2014 Al alloy.

Fig. 9 shows the Young's modulus of extruded composite materials as a function of volume fractions of ceramic fiber. Note that the theoretical results obtained from the mixtures rule are also shown in the same figure. From this figure, it is observed that the strengthen fiber elements caused an augmentation to the elastic modulus, E_c, of 2014 Al structure. It can also be seen that the maximum modulus of elasticity for the composite with V_f = 10 vol.% is higher by about 27% than that for the conventional alloy. Moreover, it is observed that the elastic modulus for the composite, E_c with15 vol.% of ceramic fiber is marginally decreased, whereas it decreases rapidly after that. The latter effect is most probably due to debilitation of bonds between inter phases boundaries and the reduction in the relative density of the composites [23] (see Fig.6).

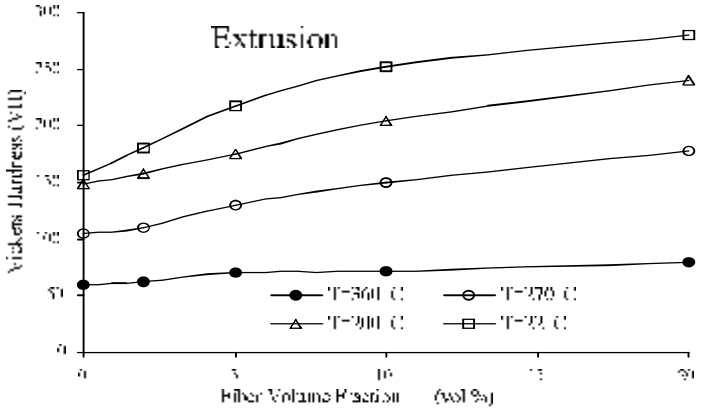

Fig. 8 Vickers hardness of composite materials at ambient and elevated temperatures

The experimental results are also compared with the theoretical results obtained using the mixtures rule in Fig. 9. From this figure, it can be seen that the calculated elastic modulus is exactly the same as the measured modulus up to 10vol.% fibers. As the V_f increases after that, the elastic modulus of the composite start to fall below that predicted by the mixtures rule. This is due to the fact that the composite contains ceramic fiber enriched layers which exhibit bad internal coherence [27 - 30] Therefore, it is suggested that the upper limit of V_f must not exceed 10 vol.% Al_2O_3 fiber to obtain sufficient ability to surround the fibers with the matrix material

Fig. 10, shows the modulus of elasticity for both 2014 Al alloy and composite material at elevated temperatures. It can bee seen that the reinforced composite have a better stiffness than 2014 Al alloy at all temperature tests. This result agrees well with the fact that the good bonding boundaries of fibers with the matrix material play a major role in the stiffness. Based on this result, one can say that the 2014 Al scrap with 10 vol.% ceramic fiber produced by hot extrusion (developed in the present work) can be considered as a good candidate for high-stiffness applications.

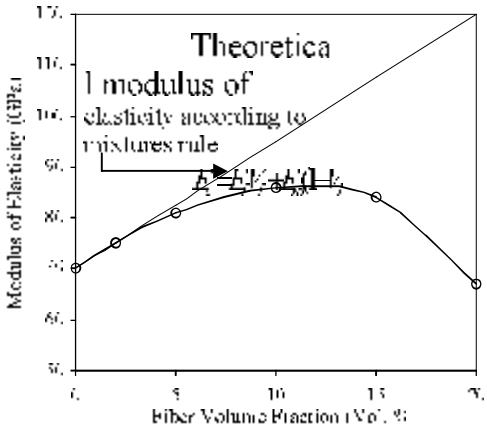

Fig. 9 The Young's modulus of extruded composite materials at ambient temperature.

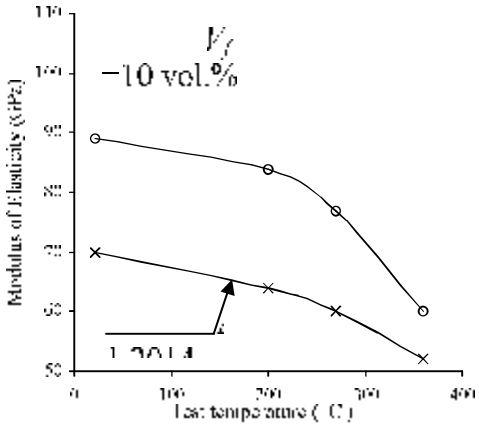

Fig. 10 The Young's modulus of extruded composite materials at elevated temperatures

3.4 Effect of V_f and temperature upon tensile strength

The effect of extrusion ratio variations and fiber volume fraction (vol.%) on the ultimate tensile strength (UTS) at ambient temperature using small and large scrap size are plotted in Figs. 11 and 12, respectively. From these figures, it is seen that the composite material offer excellent strength with 10 vol.% fiber extruded at **λ**=16:1. At this ratio and small scrap size more than 590MPa for UTS was obtained at ambient temperature. Composites with volume fraction of 10 vol.% extruded at **λ**=4:1 and 38:1, show less UTS than the case with **λ**=16:1. In all cases, the UTS for the composite materials is better than that of the conventional aluminum alloy. Moreover, from Fig. 11 and Fig. 12, it is seen that as the scrap size increases, the UTS decreases.

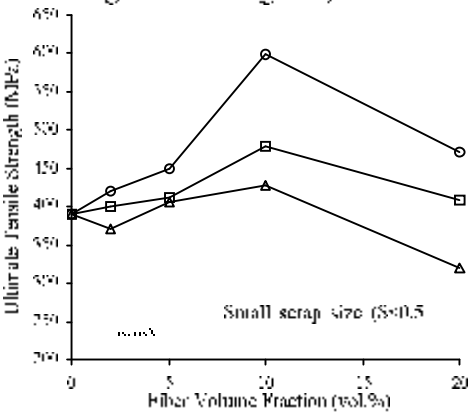

Fig. 11 Ultimate tensile strength of the materials at ambient temperature for small scrap size (S).

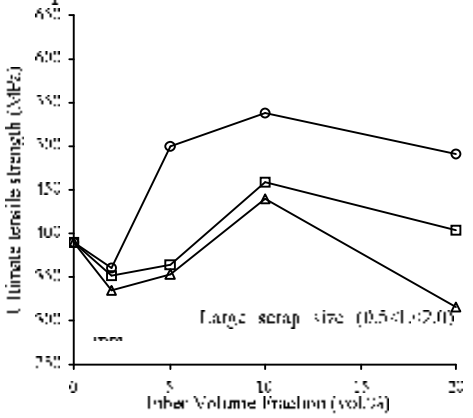

Fig. 12 Ultimate tensile strength of the materials at ambient temperature for large scrap size (L).

(▲) **λ**= 4:1 (■) **λ**= 16:1 (●) **λ**= 38:1

The observed dependence of yield strength (YS) on the volume fraction of saffil ceramic fiber at ambient temperature for small and large scrap alloy sizes is illustrated in Fig. 13. It can bee seen that, for each composite, the yield strength increases as the volume fraction of fiber increases. Moreover, Fig. 13 also shows that the YS values ranged from 224MPa to 418.6 MPa and 220.5 MPa to 376,4 MPa for small and large sizes, respectively. These results are consistent with those obtained for the UTS case given above.

Fig. 14, shows the ductility data obtained during the tensile tests experiments. From this figure, it is noticed that no significant variation in the ductility as the extrusion reduction changes. However, a remarkably higher elongation values were found for both the matrix composite extruded at λ=16:1 using small scrap size (see Fig. 14-a). Moreover, Figs. 13 and 14 reveals that, YS and ductility values for composites with 20 vol.% fall behind those obtained for 10 vol.% fiber.

Note that, generally the UTS,YS and ductility are directly proportional to the reduction ratio. However, it is found in the present study that the highest values for the above parameters are obtained at λ=16:1.Whereas, at λ=38:1,the elastic modulus and absolute density are decreased most probably due to the decohesion of ceramic fibers in the composite matrix. In addition, at λ=4:1 the above parameter values are decreased due to the residual porosity in the composite matrix. Moreover, at high fiber volume fraction (20 vol.%), agglomeration for the fibers in the composite matrix at all values of λ causes a decrease in the parameter values. This is more pronounced in the case of large scrap alloy size.

Figs. 15 and 16 show the behavior of the composites at an elevated temperature of 360°C. It is noticed that, under this condition, all composites are significantly stronger than the conventional 2014 Al alloy. In each composite, the ultimate tensile strength and yield strength are decreased as the temperature increased. There is a decrease of about 38% in strength at 270°C as compared with that of ambient temperature. Above 270°C, the variation in the dispersoid volume fraction has little effect on the ultimate tensile strength and yield strength. The most regular increase in strength parameters with increasing fiber volume fraction was observed for materials extruded at λ=16:1. Fig. 16 shows the plastic elongation strain (ε) of the materials. It can be concluded from this figure that high elongations are obtained at high volume fraction and λ=16:1.

The influence of scrap size at elevated temperature upon ultimate and yield strength of the alloy containing a volume fraction of 10vol.% Al_2O_3 fiber at similar conditions is illustrated in Fig. 16. In absolute values, an increase in scrap size from 0.5 mm to 2.0 mm results in a 20% decrease in tensile and yield strength at 270°C. At higher temperatures, however, the decrease is much lower and the variation in scrap size have no significant effect on strength.

From the above results, many explicit observations must be discussed. Firstly, at ambient temperature, the 0.2% yield strength (YS) increase with increasing volume fraction of fiber up to 10 vol.% Al_2O_3 fiber which is consistent with expectations. There are several possible explanations for this result: (i) the Orowan strengthening in which case, an increase in volume fraction of fiber for constant particle size due to dynamic recovery, results in a smaller interparticle spacing. Hence, during hot extrusion, which hinder the bypass of fibers by dislocations, higher yield strength occurs [31]; (ii) strengthening based on the increase in dislocation density due to the difference in the coefficient of thermal expansion between the aluminum alloy matrix and the fibers [32]; (iii) Friend strengthening [33], of a discontinuous fiber reinforced composite predicted by a simple shear lag model. In which a composite matrix exhibiting a large differences between failure stress and yield stress (i.e. a high work hardening material), would have less strengthening potential at low fiber volume fractions than a composite matrix with a low work hardening. However, Friend's result

was based on the assumption that fibers were long enough for breakage at the fiber failure stress through transfer of load by shear. The critical fiber length above which this occurs is given by [33],

$$l_c = \sigma_{uf}\, d_f / \tau \qquad (1)$$

where σ_{uf} is the fiber fracture strength, d_f is the fiber diameter and τ is the shear stress at the interface between matrix and fiber. Applying $\tau=(1/2)\,\sigma_y$ and σ_y of the 2014 Al = 278 MPa [26]into eqn. (1) yields a critical fiber length of $l_c = 21.6\mu m$. This result shows that during deformation, L_c might decrease due to an increase in τ caused by matrix hardening. In the present work, in which l_c remains in the order of 21.6 μm, the shear load transfer up to the fiber fracture stress is likely to occur at ambient temperature in all of the composites specially at V_f=10 vol.% Al_2O_3 saffil fiber and λ=16:1

The ultimate tensile stress (UTS) increases initially with the addition of Al_2O_3 fiber. For higher volume fractions of fibers, however, the UTS decreases (over 10 vol.%). The decrease in UTS at the higher volume fraction of ceramic fibers occurs because the composites fail before they achieve the expected maximum strength. This is due to the present porosity and extrusion cracks.

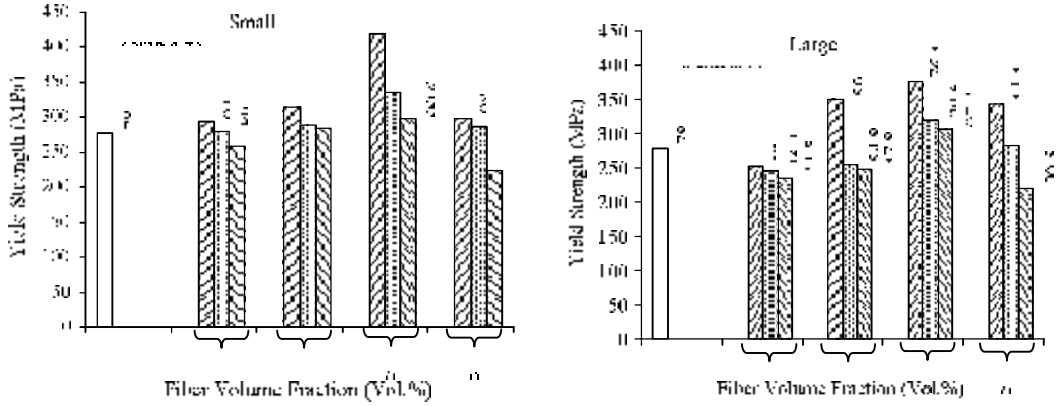

Fig. 13 Yield strength as a function of fiber volume fraction (vol.%) and Al-2014 scrap size at ambient temperature, (a) small scrap size, (b) large scrap size.
Al-2014 conventional alloy [26], λ 4:1, λ 16:1, λ 38:1.

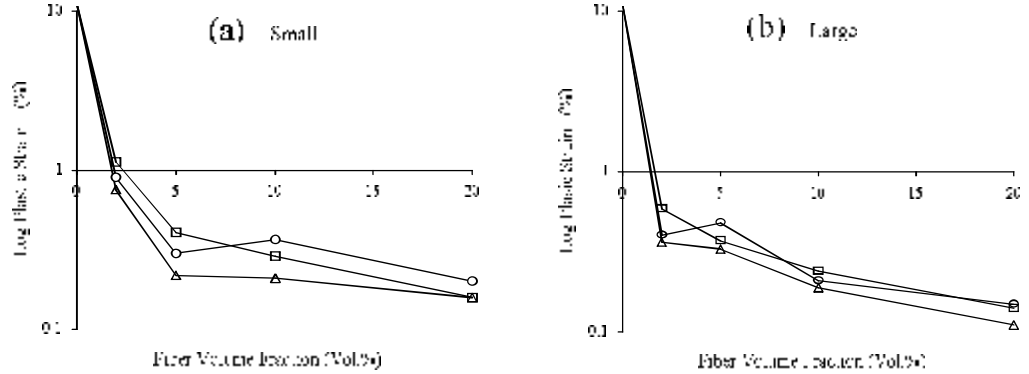

Fig. 14 Ambient temperature ductility of composite materials as a function of fiber volume fraction (vol.%) and size of 2014Al.

(△) λ= 4:1 (○) λ= 16:1 (□) λ= 38:1

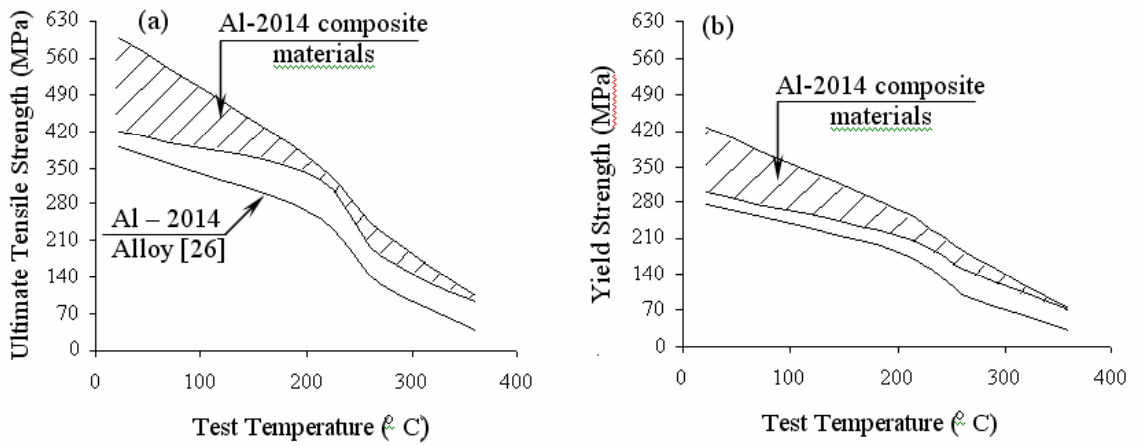

Fig. 15 The UTS and YS of the composite materials at elevated temperatures, λ 16:1.

Fracture at ambient temperature in the 2014 Al scrap composite system occurs by micro void coalescence. Voids are initiated at the dispersoids and subsequently crack propagation occurs by coalescence of these voids. Thus, the size of the fractures or dimples observed on the fracture surface correspond to the interparticle spacing or the grain size as shown in Fig. 18-a. With increasing volume fraction of Al_2O_3 fibers, the interparticle spacing decreases thus reducing the total strain after void initiation. This in turn results in decreased ductility, as given in Fig.14.

Secondly, at elevated temperature, thermally assisted deformation mechanisms become operative at these temperatures, and therefore, the effectiveness of the fine dispersoid stabilized grain structure to resist the dislocation motion is reduced. As the temperature increases above 250°C, the difference in yield strength of the composites is getting small. This reduction in YS is due to the size of intermetallic phases is not a significant controlling factor of strength at these higher temperatures. (Note that the intermetallic phases produced during the solution and precipitation heat treatments are $CuAl_2$, $(FeMn)_3SiAl_{12}$, $Cu_2Mg_5Si_6Al_5$ and $CuMgAl_2$). Moreover, although the average intermetallic phase sizes have increased via coarsening, its influence on strength is only effective up to 250°C. At temperatures higher than 250°C, the large differences in precipitation size do not have significant effects on the YS and UTS.

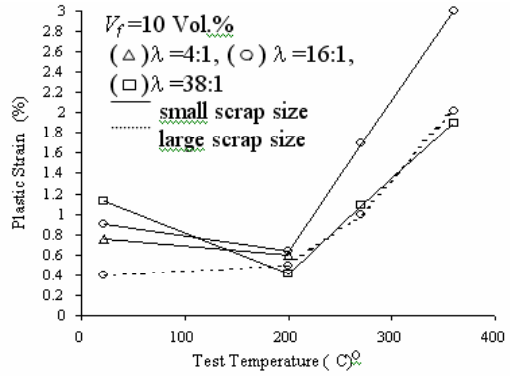

Fig. 16 Elevated temperatures ductility of the composite material as a function of λ and scrap size.

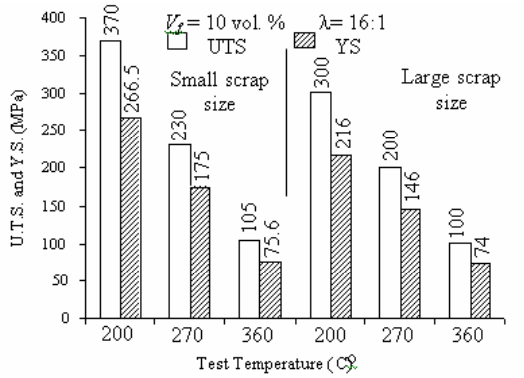

Fig. 17 UTS and YS versus test temperatures for small and large scrap size.

LE Burn, et al. [34] studied the elevated temperature behavior of an Al-Fe-Mn alloy and found that the drop in elevated temperature strength could not be explained by intermetallic coarsening alone, but also to a loss in strength of the intermetallic phases.

The observations in our experimental study suggest that the microstructural features which are impediments to dislocation motion (e.g. grain boundaries) are playing a major role in strengthening at the lower temperatures. Thus, volume and size of intermetallic phases have an effect on the strength of the composite materials before 250°C. At 250°C and above, the decreasing in strength can be attributed to a decreasing in friction stress (σ_0). At higher temperatures thermally activated processes, such as climb, become more prominent and the deformation behavior will be similar to that of a precipitation particles-free matrix.

Although, the effect of the grain boundaries is much more complicated phenomenon to explain its influence on the strength of the composite materials at elevated temperature, nevertheless, N. Hasen [35] reported that the strengthening effect of the grain boundaries is small at 400°C in dispersion strengthened Al-oxide products. However, in the present study, the presence of the intermetallic does strengthen the composite significantly. For example, 2014 Al conventional alloy has an ultimate tensile strength of 40 MPa at 360°C [26] and the UTS of 2014 Al composite with V_f = 10 vol.% Al_2O_3 fiber was found 105MPa at 360°C (see Fig. 15-a).

Based on the above discussion, a possible explanation for the observed UTS and YS behavior of the 2014 Al scrap reinforced with saffil ceramic fibers is as follows: up to 250°C, the strength of the composite materials is primarily determined by the grain boundaries and the volume fraction of intermetallic precipitation particles in the matrix. Above 250°C, the composite behave as if the dispersoids does not exist. The absolute magnitude of the strength, however, is higher than that of the conventional alloy. This is postulated to be due to the intermetallic phases on the boundaries that interact with the grain boundary dislocations, which in turn provide some resistance to the thermally activated movement of dislocations from one grain to the other. Whereas, in conventional alloy, this thermally activated dislocation movement across the boundaries would not be hindered by any dispersoids.

In Fig. 16 it was observed that the plastic strain exhibited a ductility dip at 200°C for small scrap size composites deformed at low strain rate. This result was also reported by other investigators [36, 37]. In their studies, they attributed the observed ductility dip at high temperature to dynamic strain ageing (DSA) associated with the diffusion of some atoms of alloying elements in solid solution. However, from the author point of view, the origin of the ductility dip is due rather to the temperature dependence of both the work hardening exponent, n, and the strain rate sensitivity, m. This explanation takes into account the necking theory of tensile bars [38], which states that the uniform strain is an increasing function of both n and m coefficients. This is very clear in Fig. 16, where it was observed that the strain rate sensitivity in all cases is quite small. Therefore, one can say that the work hardening exponent, n, is the more effective coefficient. This is confirmed in Fig. 16, where the plastic strain of small scrap size composite is higher than that of the composite with large scrap size at the same conditions, since $n_{\text{small size}} > n_{\text{large size}}$.

4. Fractograph

The fracture surface of samples are tested at ambient and elevated temperatures by scanning electron microscopy (SEM). In both test conditions, cell-like depression (dimples) were highly prominent (see Fig. 18-a). These dimple structures are representative of ductile void formation in the matrix. They are often related to the presence of fractured irregular particles. The dimple boundaries may also be centered around fibers, whose circular contours are often hardly distinguishable. From Fig. 18-a, it can be noticed that the fibers at minor places of the structure are protruded slightly of the fracture surface and is coated with a matrix phase which appearing brittle. This is because some fibers had lost its circular cross-section, therefore, it is believed that decohesion had occurred along this cladding phase.

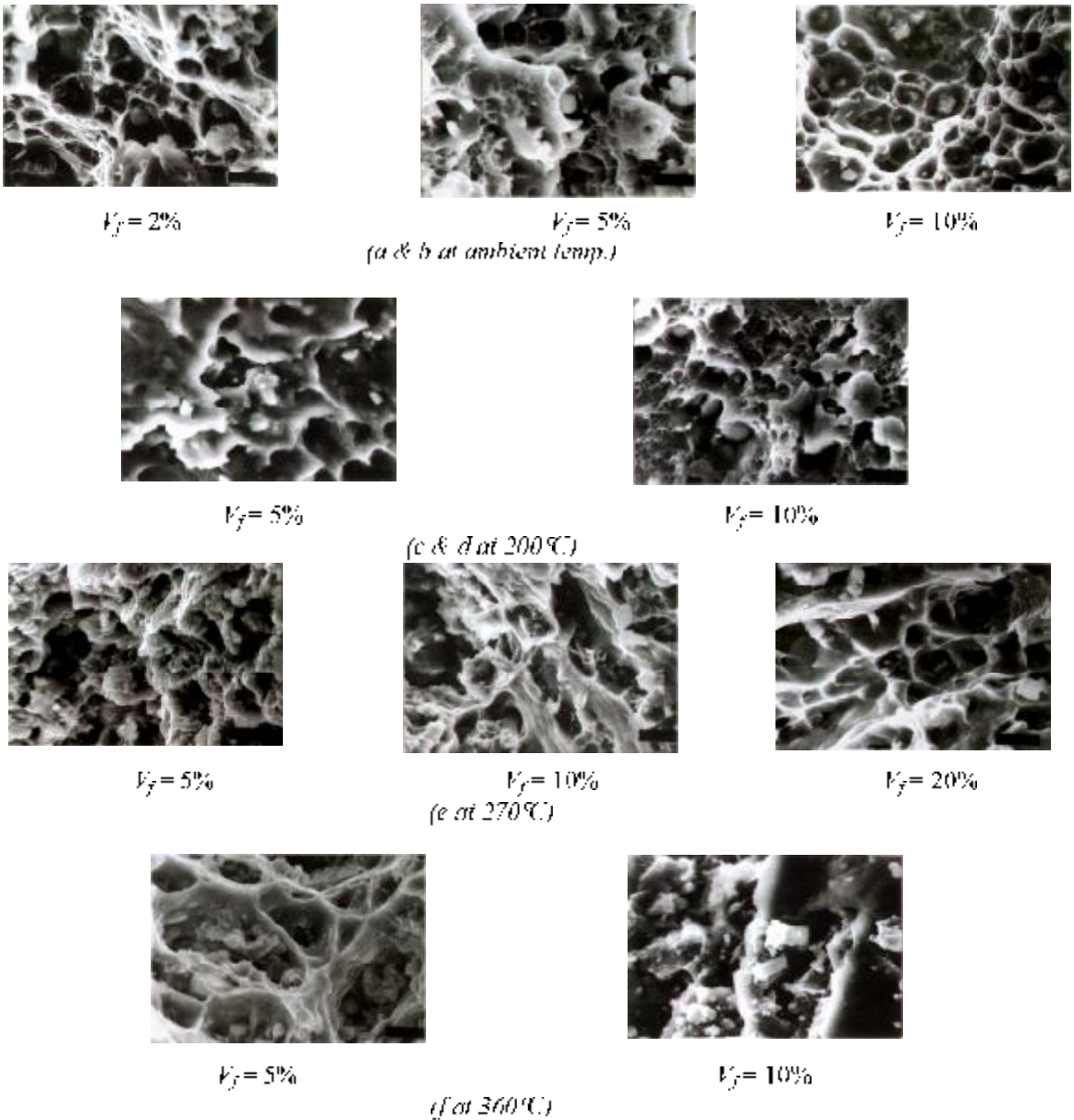

Fig. 18 Tensile fracture surfaces of composite materials 2014 Al /Saffil ceramics fibers, (2000X).

It is shown that [39], the brittle intermetallic phases on the surface of ceramic fiber are capable of influencing the fracture morphology of fibers in a composite material. Hence, when fibers are gathered in an aggregate, decohesion at limited places of the fiber-matrix interface is occurred (see Fig. 18-b). Since the protruded fibers are not widely spreaded at the fracture surface, good bonds between the matrix and the fibers are exist. At 200°C, the fracture surface morphology exhibited similar results as given above with more clearly evident dimples (see Figs. 18- c and d).

At 270°C, the fracture surface morphology exhibits new features. Saffil ceramic fibers in the vicinity of the fracture surface can be seen to have nucleated voids only at their terminations, although mostly a fraction of the fiber ends remain covered with metal. This feature, again emphasizing the good bond between the matrix and ceramic fibers. This is clear in the microfractograph shown in Fig. 18-e.

At 360°C, the overall fracture surface is seen to be very irregular and devoid of dimples, Fig. 18-f.

5. Conclusions

Production of composites by direct conversion of 2014 Al granulated scrap with Saffil ceramics fibers into final products by hot extrusion results in materials characterized by very low porosity. From the experimental work and results mentioned above it can be concluded that:

1- Saffil short ceramic fiber-reinforced 2014 Al granulated scrap composites prepared by direct conversion route were, (from a view point of the mechanical properties in the longitudinal direction), best extruded at the intermediate extrusion reduction ratio (λ = 16:1) of all investigations.

2- A higher reduction ratio (λ = 38:1) decreased the elastic modulus, most likely due to decohesion of intermetallic particles in the matrix. For the same λ, when the volume fraction of fibers exceeds 10 vol.%, the relative strengthening is reduced. On the other hand, a lower reduction ratio (λ = 4:1)causes residual porosity at volume fraction of fiber exceeds 10 vol.%.

3- The extruded composite materials display excellent tensile strength and stiffness both at ambient and elevated temperatures. The improvements in strength and stiffness are due to the presence of a high content of intermetallics and inert dispersoids. Intermetallic phases play an important role in the strengthening of aluminum scrap alloys and inert dispersoids effectively stabilize the structure at the elevated temperature.

4- The best combination of strength and stiffness was obtained for small 2014 Al granulated scrap size with 10 vol.% saffil ceramic fiber.

5- For composite extruded at 16:1 the increased improvements in UTS were found 53%, 40%, 77% and 90% at 22°C, 200°C, 270°C, and 360°C, respectively. Moreover, additional improvement of 27% in elastic modulus and 61% in hardness at ambient temperature are also obtained.

6- Although, the composite material with more than 10 vol.% ceramic fiber exhibited low strength, stiffness and ductility, it could be suitable for applications where other properties such as dimensional stability and low thermal expansions are the primary requirements.

7- The ductility variation of the composite materials is due to the following behaviours: low strain rate sensitivity, dependence of the strain hardening exponent on grain size, and the limitation of plastic deformation by the presence of a high content of intermetallic phases. The formation of cracks or microvoids at the interface between the particle and the matrix as well as fracture of the intermetallic precipitation particles are also the main reasons for the reduced ductility.

Due to the importance of wear resistance, fatigue strength, bending strength, and thermal conductivity of 2014 Al scrap material reinforced with Saffil ceramic fiber, a further study is being conducted, and the results will be published later.

Acknowledgements

The author is grateful to Prof. J. Gronostajski (D.Sc.) for valuable guidance during the work reported in this paper. Thanks are due to Dr. A. Niechajowicz and Prof. A. Matuszak (D.Sc.) for many discussions, and to the stuff of workshop and laboratories of the Metal Forming Department, Institute of Machine Building Technology, Technical University of Wroctaw, Poland.

Received April 24 2007 *Faculty of Engineering, Mansoura University, Egypt*

REFERENCES

1. Y. Kurihara, **J. Metals**, 45. (1993) 32.
2. T. Takasuga, **Int. Symp. on Aluminum in Transportation**, (1989).
3. Z. Tanabe,et al.,**Technical Bulletin of Sumitomo Light Metal Industries Ltd.**,27, (1986) 1.
4. I. A. Ibrahim, et al.: *Particular reinforced metal matrix composites a review*, **J. of Mater. Sci.**, Vol. 26. (1981) 1137.
5. S. V. Nair, et al.: *Silicon carbide reinforced aluminum metal matrix composites*, **Int. Met. Rev**., Vol. 30, (1985) 275.
6. D. L. Mcdanels: *Analysis of stress-strain fracture and ductility behavior of aluminum matrix composites discontinuous silicon carbide reinforcement* **Metall. Trans**. A, Vol. 16A, (1985) 1105.
7. J F. Dolowy: *Increasing focus on SiC reinforced aluminum composites*, **Light Metals Age**, Vol. 44.(1986).
8. J. White, et al.: *Metal matrix composites based on aluminum lithium and silicon carbide*, **J. Physique**, Vol. 48, (1987) 3.
9. T. W. Clyne and F. Mason, **Metall. Trans.**, Vol. 18A, (1987) 1519.
10. A. Sakamoto, et al., **Proc. of ICCM V**. San Diego. California. July (1985).
11. K. Suganuma, et al., **J. Mater. Sci. Lett**, Vol. 6, (1987) 1347.
12. C. A. Stanford and T W. Clyne, **Comp. Sci Technol**., Vol. 35. (1989) 121.
13. M. Maclean and R. Dower: *Aluminum alloy short fiber MMC using the PM route*, **Proc. of Int. Powder Metal. Conf.** London. U.K.. (1990) 252.
14. K. Kitora: *Recent technical development in the Japanese aluminum industry*, **Aluminum**, 66, Jahrgang, 718. (1990) 755.
15. M. Samuel: *A new technique for recycling aluminum scrap*, under publication.
16. Prospect of Imperial Chemical Industries "*SAFFIL-Alumina Fiber*", Runcorn, Cheshier, U.K., (1994).

17. J. H. Terhaar and J. Duszczyk. *Mechanical properties and microstructure of a P/M aluminum matrix composites with δ-alumina fibers and their relation to extrusion*, **J. of Mater. Sci.**, Vol. 29, (1994) 1011.
18. J. Z. Gronostajski and M. Samuel, **Int. conf., IMC 16**, Dublin, Ireland, Vol. II, (1999) 1327.
19. J. Z. Gronostajski, et al.: *Production of composites on the base of AlCu₄ alloy chips*, **J. of Mater. Proc. Tech.**, Vol. 60, (1996) 719.
20. M. Wojtaszek, et al.: *Structure of hot extruded aluminum powder based composites with 1.5% by mass additive of Al_2O_3 fibers*, **Int. Con. Of Material Sci. AMT'98**, Karkow, Poland, Vol. 4, (1998) 758.
21. J. Gronostajski and M. Samuel. *Aluminum base composites for high temperature application*, **XV^th Int. Con. Of Advanced Matel. and Tech.**, Krakow-Krynica, Poland, (1998) 750.
22. **ASTM, Standard E 8-90a**. Annual Book of ASTM Standards. Vol. 3.01 American Society for Testing and Materials, Philadelphia, PA, (1991) 130.
23. Jacek. W. Kaczmar **Scientific papers of the Inst. of Mech. Eng. And Automatic, Wroctaw**, Poland, No. 65, (1997).
24. M. Samuel, et al.: *Mechanical properties and industrial applications of aluminum base composites*. **2^nd Int. Sem. of advanced Tech. of Sheet Metal Forming**, Wroctaw, Poland, (1996) 107.
25. ASTM, Standard E21-79. **Annual Book of ASTM Standards**, Vol. 3.01, American Society for Testing and Materials. Philadelphia, PA, (1991) 190.
26. **Metal Handbook**, Properties and Selection: Nonferrous alloys and special-purose materials, 10^th ed., Vol. 2. (1990) 77.
27. M.R.Krishnadev. et al.: *Characterization of the microstructure, fracture morphology and toughness of particulate and short-fiber reinforced aluminum matrix composites*, **Microstructure Sci.**, Vol. 16, (1988) 125.
28. P. Yih and D. Cung: *Powder metallorgy fabrication of metal matrix composites using coated fillers*, **Int. J. of Powder Metallorgy and Powder Tech.**, Vol. 31, (1995) 333.
29. X. P. Niu, et al.: *High-strength and high-stiffness Al-ceramics alloy fabricated by double mechanical alloying*, **pmi**, Vol. 25, No. 3, (1993) 118.
30. Jae C. Lee, et al. *Control of the interface in SiC/Al composites*, **Scripta Materialia**, Vol. 41, No. 8, (1999) 77.
31. P. M. Kelly: *The quantitative relationship between microstructure and properties in two phase alloys*, **Int. Met. Rev.**, Vol. 18, (1973) 3.
32. R. J. Arsenault and R. M. Fisher: *Microstructure of fiber and particulate SiC in 6061 Al Composites*. **Scr. Metall.**, Vol. 17, (1983) 67.
33. C. M. Friend: *The effect of matrix properties on reinforcement in short alumia fiber-aluminum metal matrix composites*, **J. of Materials Sci.**, 22, (1987) 3005.
34. LE Brun, et al.:, **Advanced Materials and Processing**, 1, (1990) 231.
35. N. Hansen: *Effect of grain size on the mechanical properties of dispersion strengthened Al-oxide products*, **Trans. Of Metallurgical Society of the AIME**, 245, (1969) 1305.
36. N. J. Lindsay and V. D. Scott. *High temperature joining of fiber reinforced metals*, **Proc. of the 7^th Int. conf. On composite Materials**, Guangzhou, Chiny, 1, (1989) 417.
37. J. Moerman, et al.. *The recycling of metals*, **Proc. of 1^st Int. Conf., ASM Euroean**, Dusseldorf, (1992) 127.
38. E.W. Hart, **Acta Metall.**, 15, (1967) 351.
39. S. Ochiai and k. Osamura: *Influences of interface on fracture behaviour and strength of unnotched unidirectional metal matrix composites*, **J. Mater. Sci.**, 27, (1992) 4667.

RANFORSAREA DEŞEURILOR RECICLATE DIN ALUMINIU CU FIBRE CERAMICE TIP SAFFIL

Rezumat: Dezvoltarea industriei de automobile necesită materiale care să prezinte următoarele proprietăţi: densitate scăzută, coeficient de dilatare termică mic, rezistenţă mare la uzură, modul de elasticitate ridicat şi

rezistență ridicată la temperaturi ridicate sau cele ale mediului ambiant. Aliajele compozite pe bază de deșeuri din aluminiu ranforsate cu fibre ceramice îndeplinesc toate cerințele de mai sus. În lucrarea este prezentată realizarea de produse compozite prin conversia directă a deșeurilor din aliaj 2014 Al sub formă de granule și fibre din Al_2O_3 SAFFIL, folosind extruziunea la cald. Sunt analizate proprietățile mecanice la temperatura ambiantă și la temperaturi mai mari, microstructura și lungimea fibrelor.

BULETINUL INSTITUTULUI POLITEHNIC DIN IAŞI
Tomul LIII (LVII), Fasc. 4, 2007
Secţia
ŞTIINŢA ŞI INGINERIA MATERIALELOR

THE EFFECTS ON STRUCTURE AND HARDNESS OF BEARING STEELS TREATED CRYOGENICALY

BY

SORIN IACOB STRUGARU, CORNELIU MUNTEANU, ADRIAN ALEXANDRU, RACLARIU GICU CATALIN, CHIHAI STELIAN and TANASUCA SORINEL

Abstract: The paper presents the influence of cryogenic treatments on phasic composition and hardness of bearings steels100Cr6 and 100CrMnSi6-4 SRUN ISO 683-17: 2002, the equivalents of steels RUL 1 and RUL 2 – STAS 1456-89. After application of these thermal treatments, the quantity of residual austenite decreases, the submicronics dimensional carbides density increases and the hardness increases with positive influences above durability of bearings.

Keywords: bearings steel, cryogenic, residual austenite

1. Introduction

The construction of bearings is confronting at this moment with new demands concerning the dimensional stability, noise level and durability. All of these are ensured by the presence of a small quantity of residual austenite, of a very fin carbides and a fine martensite in important quantity. The structure which presents such conditions it may be obtained only by application of some unconventional processing: quenching below 0^0C, quenching in ultrasonic or magnetic field, thermo-mechanical treatments etc

These qualities of final structure cannot be obtained only if the initial structure obtained after the thermal treatment of normalising and annealing (800^0C/3h, cooling and maintaining at 700-720^0C/4h; slow cooling in oven) is formed by fine and homogeneous globular perlite.

The parameters of classic quenching and tempering and the quantity of residual austenite depending on initial structure of 100Cr6 and CrMnSi6-4 bearing steel are presented in table 1.

We can say that by classic thermal treatments the smallest quantities of residual austenite (11.3 ÷ 13.6%) are obtained after the application of some variants of thermal treatments V or VI which ensures in structure the fine and homogene globular pearlite.

Continuously cooling in oil at -30^0C or -60^0C results a phasic constitution optime for the properties of exploitation of bearings.

The bearings treated below 0^0C it sale with attractive prices thanks to the destination of devices or machines which contains rotating organs. Such destinations may be the device and machines which must ensure the security of humans in trains, plains, spaceships; devices which works in polar zones etc

Technical literature in this domain appreciate that the implementation of thermal treatment below 0^0C processing will increase the cost price with 13%, but this increase is covered by the demands of the market.

Table 1

Steel	Initial state		Lamellar pearlite (I)	Fine globular pearlite (II)	Partial unglobulizate pearlite (III)	Inhomogeneous globular pearlite (IV)	Homogene globular pearlite (V)	Fine globular pearlite normalized (VI)
100Cr6	Quenching	Admited interval (^{0}C)	820-830	810-860	810-830	810-850	810-835	810-840
		Optim interval (^{0}C)	-	810-840	-	-	820-830	820-830
		Maintaining time (min)	15	15-30	15-30	15-30	15-30	15-30
	2h(^{0}C)Tempering		180-200	180-200	180-200	180-200	180-200	180-200
	Corresponding AR (2h at 180^{0}C after tempering) (%)		16.6-17	11.6-15.2	13-14.2	11.5-14.4	11.3-13	12-15.5
CrMnSi6-4	Quenching	Admited interval (^{0}C)	800-830	800-850	-	-	810-840	800-830
		Optim interval (^{0}C)	-	820-830	-	-	-	-
		Maintaining time (min)	15-20	15-20	-	-	15-20	15-20
	2h(^{0}C)Tempering		180-200	180-200	-	-	180-200	180-200
	Corresponding AR (2h at 180^{0}C after tempering) (%)		18.8-20	17-20	-	-	15.6-19.2	13.2-17

2. Experimental programme

The researches were made on rings of bearings by two alloyed steels for bearings with chemical composition determinate which is presented in table 2.

Table 2

Chemical composition (%)								
Steel (SR EN ISO 683-17)	C	Si	Mn	P	S	Cr	Mo	Others
100Cr6	0.93-1,05	0,15-0,35	0.25-0,45	0,025	0,015	1,35-1,6	Max,0.1	Al Max,0,05
determination	0,98	0,30	0,36	0,018	0,014	1,45	-	
100CrMnSi6-4	0.93-1,05	0,45-0,75	1,00-1,20	0,025	0,015	1,40-1,65	Max,0.1	-
determination	1.00	0.51	1.15	0.015	0.010	1.48	-	

The bearings elements were thermally treated by the variants given in table 3.

Table 3

Thermal treatments variants	Technological parameters
A	Quenching at 840°C in oil at 60°C, tempering at 190°C/3h
B	Quenching at 840°C in oil at 60°C, cooling at -30°C, tempering at 170°C 1.5 h
C	Quenching at 840°C in oil at 60°C, cooling at -60°C, tempering at 170°C 1.5 h

The samples thermal treated by these variants were investigated by optical microscopy X rays diffraction and Rockwell hardness determination

3. Experimental results

Microscopically researches were made on an optical microscope Neophote 21 at 500:1 magnification after the attack with natal 3% reactive.

The structure of the researched bearings steels after the primar thermal treatment of normalizing and globulization annealing is presented in figure 1, a,b were can be observed the globular pearlite which is fine and homogene in the two steel.

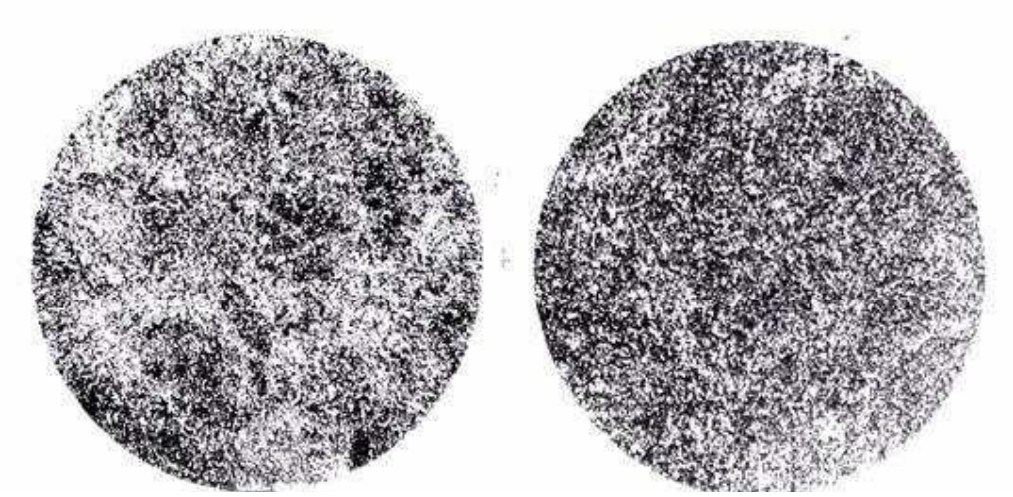

a. *b.*

Fig. 1. The structure of 100Cr6(a) and 100CrMnSi6-4 (b) after the globulization annealing (500:1)

The bearings steels structures after classic quenching and tempering (A variant) is formed by martensite very fine, residual austenite and carbides, as is presented in figure 2, a, b.

The structures of bearings steels after cooling at -30°C and -60°C and tempered at 170°C are formed by very fine martensite, small quantities of residual austenite and carbides with small dimensions as is presented in fig. 3 a, b and 4 a,b.

The value of hardness and quantities of residual austenite (AR) difractographic determinated on the bearings steels are presented in table 4.

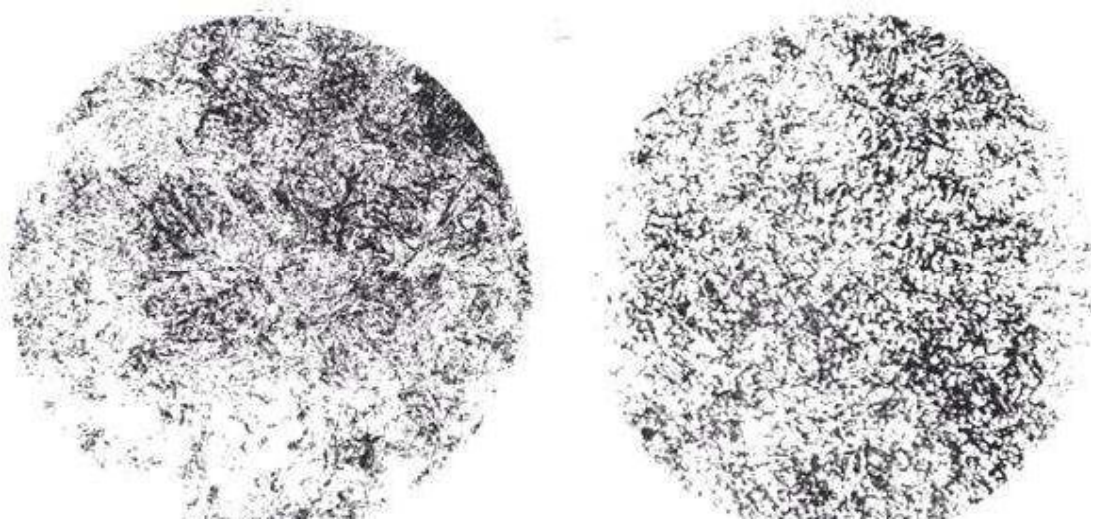

a. *b.*

Fig. 2. The structure of 100Cr6(a) and 100CrMnSi6-4 (b) after quenching in oil and tempering 500:1

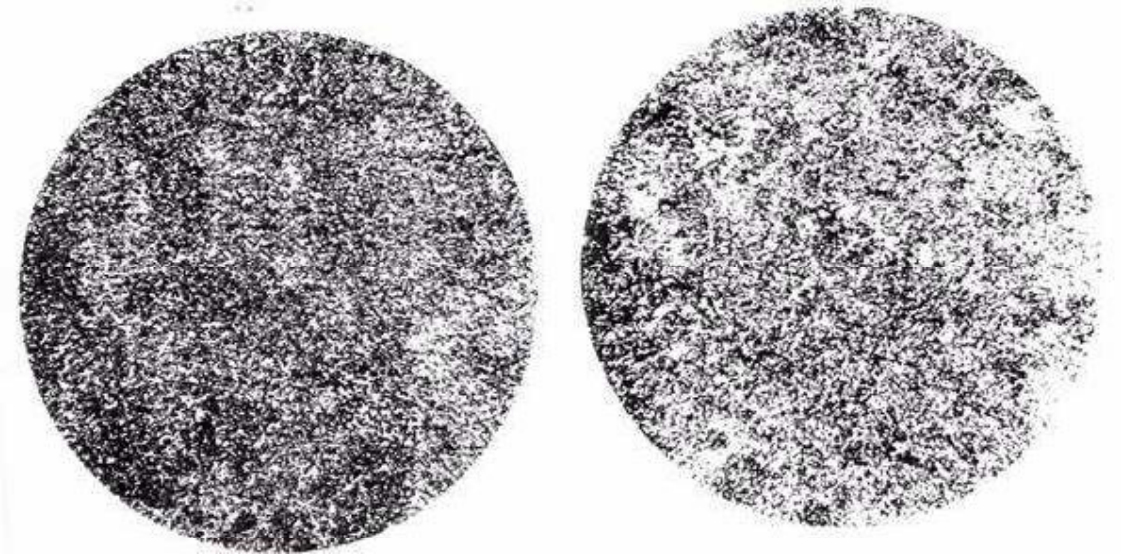

a. *b.*

Fig. 3. The structure of 100Cr6(a) and 100CrMnSi6-4 (b) after cooling at -30°C and tempering 500:1

Table 4

Steel	Quenching					Tempering			
	Heat temp (°C)	Time (min)	Cooling Temp./ Maintain temp. (°C)	HRC	AR(%)	Heat temp (°C)	Maintain Time (min)	HRC	AR (%)
100 Cr 6 (RUL 1)									
	840	30'	oil 60°	63	16.5	190	3 h	61	9.85
	840	30'	-30°/30'	64	7.38	170	1.5 h	63.5	6,28
	840	30'	-60°/30'	66	6.13	170	1.5 h	64	4,08
100CrMnSi6-4 (RUL 2)	840	30'	oil 60°	63	20,98	180	3 h	62	17,80
	840	30'	-30°/30'	65	12.8	170	1.5 h	64	7.13
	840	30'	-60°/30'	66	10,18	170	1.5 h	64	6,74

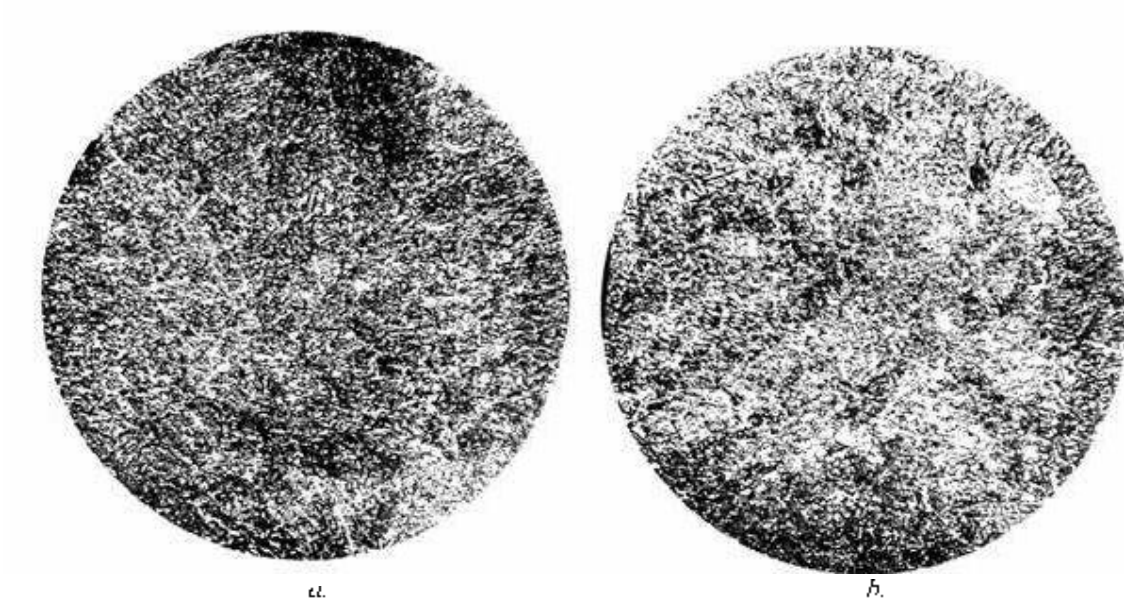

a. b.

fig. 4. The structure of 100Cr6(a) and 100CrMnSi6-4 (b) after cooling at -60^{0}and tempering 500:1

It see that with the increasing of cooling temperature at -30^{0}C and -60^{0}C the quantity of residual austenite decrease from 9.85%, at 6.38%, respective 4.08% for the 100Cr6 steel and from 17.8% at 7.13% respective 6.74 for 100CrMnSi6-4 steel and the hardness increase from 61 HRC at 64 HRC

4. Conclusions

By application of thermal treatments at temperatures below 0^{0}C in the bearings steels takes place important phasic modifications - decrease the quantity of residual austenite, increase the density and uniformity of the small dimensional carbides (0.001 mm).

These structural modifications determine the increase of hardness and in the end the increase of bearings fiability.

Received April 21, 2007 *The "Gh.Asachi" Technical University Iaşi*

REFERENCES

1. Gary Jeff **Cryogenic Treatment of Steel** University of Texas of Austin, Department of Mechanical Engineering, Spring, 1999

2. Carlson Earl – **Cold Treating and Cryogenic Treatment of Steel**, ASM Handbook, vol. 4, Heat Treating, 1991.

3. Alexandru Ioan, Bulancea Vasile. Effect *of Cryogenic Cooling on Residual Stresses, Substructure*, cap 26, **Handbook of Residual Stresses and Distortion of Steel**, U.S.A., 2002.

EFECTUL TRATARII CRIOGENICE ASUPRA STRUCTURII SI DURITATII OTELURILOR PENTRU RULMENTI

Rezumat: Lucrarea prezinta influenta tratamentelor termice criogenice asupra compozitiei fazice si duritatii otelurilor de rulmenti 100Cr6 si 100CrMnSi6-4 SR EN ISO 683-17 :2003 echivalentul otelurilor RUL 1 si RUL 2 – STAS 1456-89. In urma aplicarii acestor tratamente termice cantitatea de austenita reziduala scade, densitatea carburilor cu dimensiuni submicronice creste si duritatea se mareste cu efecte pozitive asupra durabilitatii rulmentilor.

BULETINUL INSTITUTULUI POLITEHNIC DIN IAŞI
Tomul L(III (LVII), Fasc. 4, 2007
Secţia
ŞTIINŢA ŞI INGINERIA MATERIALELOR

VARIATION OF MECHANICHAL CARACTERISTICS OF HIGH STRENGTH WIRES DRAWN IN ULTRASONIC FIELD

BY

M. SUSAN[1], M. PEPTANARIU[2], D.C. ACHITEI[1], R.G. CARABET[1] and M. CHIRIAC[3]

Abstract: The changes of the mechanical characteristics of some high resistance wires, drawn in ultrasonic field while the die is located into the oscillation maximum of the waves and actuated parallel to drawing direction, have been mainly determined by the work – hardening decrease caused by "the surface effect of the ultrasonic" as a consequence of the fractional regime of the plastic deformation.

Keywords: damping effect of ultrasonic, ultrasonic wire drawing, mechanical characteristics, work – hardening decrease.

1. Introduction

The drawing of high resistance wires in ultrasonic field represents one of the modern technologies of plastic working of metals, besides other techniques that use directional flows of magnetic, light, electric and so an energies.

Ultrasonic or ultra-acoustic waves represent a variety of elastic waves with the frequency ranging between 16000 and 10^{10} Hz [1]. The area of the elastic medium in vibrating state which lodges the ultrasonic waves is denominated as ultrasonic field

As in the case of other plastic working technologies of metals, at wire drawing in ultrasonic field high energy ultrasonic are used. These ultrasonic, when propagating through an elastic medium such as a metal, undergo a damping effect which depends upon time (see domain II of figure 1). Domain I are specific for passive applications, for determining some physical properties, for flow detector and so on while in domain III, among some softening processes, ultra-acoustic hardening processes may occur.

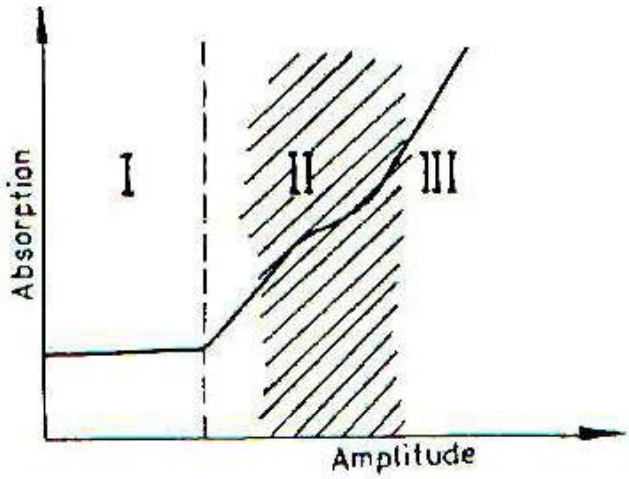

Figure 1. The damping effect of ultrasonic in metals, as a function of time [1]

For high resistance wire drawing, it is recommended that the deformation focus is located in the oscillation maximum of the waves while the tool is actuated parallel to the drawing direction [3]. Under these conditions, as compared to classic wire drawing, a sensible reduction of the drawing force is obtained due to the "surface effect of ultrasonic". This effect is explained by means of the "mechanism of frictional force reversion", illustrated in figure 2 [2].

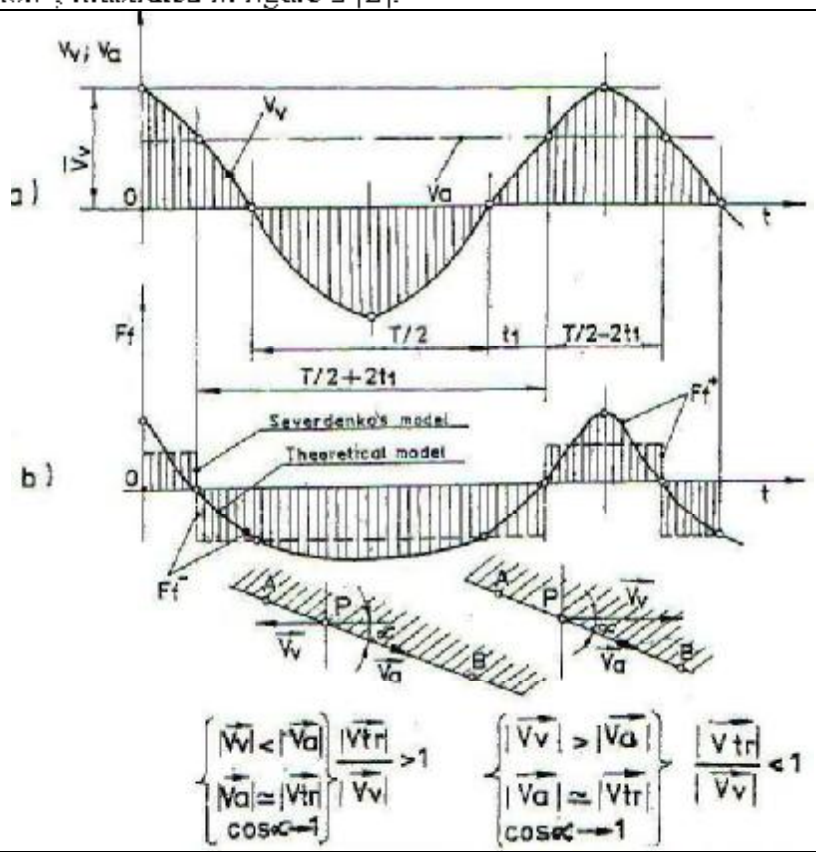

Figure 2. Frictional force reversion drawing a complete oscillation period of the tool :
a) oscillation and drawing rates (v_o and v_{tr}, respectively ; v_o v_{tr}) ;
b) frictional force (F_f) reversion [2]

Actually, during a complete oscillation period, plastic deformation occurs fractionally (by impulses). Thus, the deformation is produced only during $T/2+2t_1$ since during $T/2$ $2t_1$ the reversion of the frictional force vector is caused by to the "surface effect of ultrasonic" (the separation of the metal-tool surfaces is contact) the Coulomb friction being taken in to consideration.

2. Experimental tests and results

The experiments have been carried out at a laboratory level a wires made of RUL 1V / STAS 11250-89 steel-grade with the chemical composition given in Table 1.

Table 1.Chemical composition of RUL 1V steel-grade in wt.%, according to STAS 11250-89.

C	Mn	Si	Cr	S	P	Mo	Ni, Cu
1.10	0.40	0.30	1.50	0.02	0.02	0.08	0.2

The wire drawing installation, with hydraulic control, is equipped with a UZG 2-4M ultrasonic generators, that functions in conjunction with magnetostrictive transducers at the resonance frequency of 17500 Hz, and includes standard force concentrators of the type PMS 15A-18.

The oscillating system is of the "closed" type being designated according to "$n \cdot \lambda/2$". The die is located in the oscillation maximum of the waves and actuated parallels to the drawing direction, as shown in figure 3

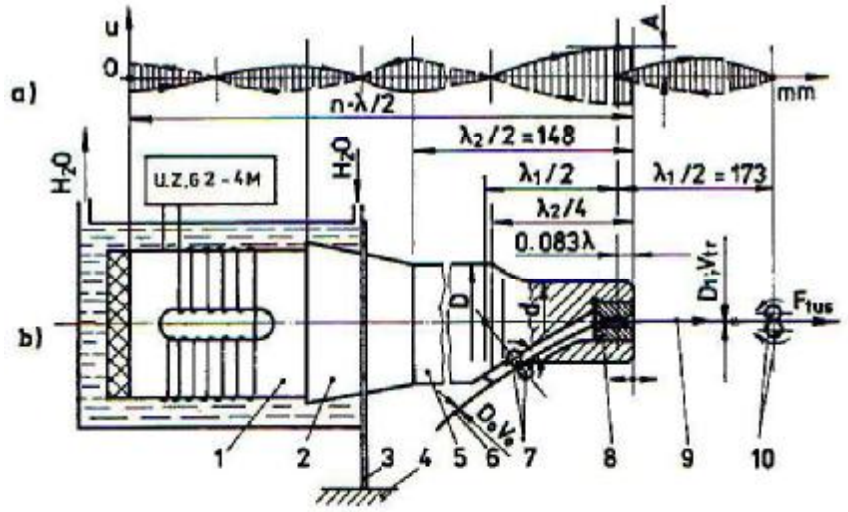

Figure 3. Schematic structure of the oscillating system [3] :
1) magnetostrictive transducer ; 2)conical concentrator , 3) nodal flange ; 4) resistance structure of the drawing equipment ; 5) cylindrical step concentrator ; 6) raw wire ;
7) ultra-acoustic energy reflector , 8) die ; 9) draw wire , 10) ultra-acoustic energy reflector ;
a) oscillation of the work concentrator ; b) oscillation of the wire.

The wavelength is determinate as:

$$\lambda = c/f, \tag{1}$$

where:

c is the propagation rate of ultrasonic within the given medium ;

f – is the resonance frequency.

Closing the oscillation system is accomplished by means of the reflectors of ultra-acoustic energy, located at certain well-defined distances [3] in order to obtain a stable system of stationary waves within the wire.

The work concentrator is made from a titanium – based alloys, BT3 (90%Ti, 6%Al and 4%V with $\rho = 4.42 kg/dm^3$), resisting at ultrasonic fatigue.

For drawing the RUL 1V wires, both with and without ultrasonic, WC – Co metallic carbides dies are used. These dies have the opening semi-angle $\alpha = 8°$ and a total 41% cross-section reduction (determinate between two applied heat treatments for structure restoring) of soap powder is used as a lubricant. The degrees of cross-section reduction are determinate for a pass with:

$$\delta_i = 1 - (D_i/D_{i-1})^2, \tag{2}$$

and for the whole operation (the total degree of system reduction) with:

$$\delta_{tot} = 1 - (D_i/D_0)^2. \tag{3}$$

The raw wires, with an initial diameter D_0 = 3.85 mm, are in annealed condition, being properly prepared for drawing. The effiency of ultrasonic drawing is emphasized by:

$$\Delta F \quad 100 \cdot \left[F_0 - \left(F_{us} / F_0 \right) \right], [\%] \tag{4}$$

where:

F_0 – is the drawing force for classic wire drawing;

F_{us} – is the force used at ultrasonic field wire drawing.

The experimental determination of the force, either with and without ultrasonic was accomplished by means of a tensiometric bridge, type N 2314.

In order to better emphasize force fluctuations they were recorded as a function of time by means of plotter, type Recorder XY Endim 620.02

Thus, the stability of the checked out by means of the force constancy at ultrasonic field wire drawing.

The technologic, ultrasonic and force parameters used within the experiments, are listed in Table 2

Table 2. Ultra-acoustic, technologic and force parameters used for experiments

Symbol of the drawing series	Drawing course	Ultra-acoustic parameters			Technologic parameters					Force parameters		
1	$D_i \rightarrow D_f$ [mm]	f [Hz]	A [μm]	v_v [μm]	δ_t [%]	δ_{tot} [%]	α [°]	v_c [m/s]	v_c / v_v -	F_0 [N]	F_{us} [N]	ΔF [%]
1 / 1	3.85 →3.60	17500	28	3,0	14	14	8	0,03	0,01	1280	866	32.34
1 / 2	3 60→3,45	17500	28	3,0	10	21	8	0 03	0,01	1350	1053	22 00
1 / 3	3 45→3,50	17500	28	3,0	10	28	8	0,03	0 01	1225	812	33,71
1 / 4	3 50→3,20	17500	28	3,0	8	32	8	0 03	0,01	982	708	27 90
1 / 5	3 20→3,10	17500	28	3,0	8	36	8	0,03	0 01	950	613	35,47
1 / 6	3 10→3,00	17500	28	3,0	8	41	8	0 03	0,01	882	530	40 00

The mechanical resistance parameters have been determined a long specimen, according to STAS 6951-80. From each of the wires, drawn either with or without ultrasonic, three samples have been taken.

The tensile mechanical characteristics, normally: ultimate strength (R_m), technical flow strength ($R_{p0.2}$) and ultimate strain (A_{100}), have been determined from the recorded stress-strain curves. For a more accurate determination, the tensile curves have been plotted by using an extensometer. The values listed in Table 3 have been obtained as an average of three tests.

The tensile tests have been carried out on a EU-40-type machine, with a drawing speed of 20 mm/min, according to the prescriptions found in STAS 6951-80. The mechanical characteristics have been calculated according to STAS 200-87. Besides the three above mentioned tensile mechanical characteristics, Table 3 also contains the average values of $HV_{0.1}$ Vickers micro-hardness, determined according to STAS 7057-78, by means of a PMT-3 micro-hardness tester

Table 3. Values of tensile mechanical characteristics, obtained as an average of three tests

Symbol of the drawing series	Drawing course	Wire drawing stresses		Mechanical characteristics							
				Classic wire drawing				Ultrasonic wire drawing			
1	$D_0 \rightarrow D_1$ [mm]	σ_{tr} [MPa]	σ_{tus} [MPa]	R_{m} [MPa]	R_{ef} [MPa]	A_{100} [%]	$HV_{0.1}$ -	R_{m} [MPa]	R_{ef} [MPa]	A_{100} [%]	$HV_{0.1}$ -
0	3.85	-	-	630	475	18.0	179	630	475	18.0	179
T/1	3.85→3.60	127	83	935	855	14.2	230	905	811	15.0	215
T/2	3.60→3.45	146	113	1025	998	12.2	250	1003	939	13.0	234
T/3	3.45→3.30	44	95	110	1080	10.4	275	1090	1045	11.8	249
T/4	3.30→3.20	123	88	170	1145	9.5	288	1152	1117	11.0	268
T/5	3.20→3.10	126	81	245	1225	9.0	298	1230	1201	10.0	284
T/6	3.10→3.00	125	75	335	1319	8.5	304	1323	1302	9.0	292

The maximum value of the oscillation (vibration) rate of tool is determined with the relationship:

$$v_e = 2\pi \cdot f \cdot A \qquad (5)$$

where:

f – is resonance frequency ;

A is the oscillation amplitude of the tool.

The wire drawing stresses are determined during the drawing processes carried out, both with and without ultrasonic, as the ratio between the force values and drawn wires cross-sections.

3. Conclusions

The changes of the mechanical characteristics, during the drawing of RUL 1V wires in ultrasonic field with the die located in the oscillation maximum of the waves and actuated parallel to the drawing direction, have been mainly determined by the "surface effect of ultrasonic" that is by the diminution of the "friction force at the metal-tool contact".

During a complete oscillation period of the tool, the plastic deformation of the metal occurs only for the duration of $T/2 + 2t_1$ (when a certain amount of ultra-acoustic energy is introduced within the wire) since on the $T/2 - 2t_1$ time interval the metal-tool contact surfaces are separated.

Actually, under such circumstances, plastic deformation is produced by impulses (fractionally) causing a decrease of the wire drawing force on the drawing series, a stabilization of the plastic deformation process, a work-hardening decrease and a diminution of the cold working non-uniformity.

All these effects induce changes of the mechanical characteristics, generally illustrating an increase of plasticity, at the wives drawn in ultrasonic field

Thus, the possibility to increase both the deformation degree and the safety level of plastic deformation may be foreseen.

Received April 25, 2007

[1]*The "Gh.Asachi" Technical University Iaşi*
[2]*Institutul de Fizica Tehnica Iasi / IFT Iasi*
[3]*S.C. Rezistoterm S.R.L. Iaşi*

REFERENCES

1. Susan,M .s.a , **Trefilarea si tragerea metalelor. Prelucrari cu ultrasunete**, Editura Sedcom Libris. Iasi. 1997.
2. Susan,M , s.a , *The metal-tool contact friction at the ultrasonic vibration drawing of ball-bearing steel wires*, Rev Metal Madrid 35(1999), pp 379,..383
3. Susan.M., **Cercetari privind influenta campului ultrasonor in procesele de trefilare a sarmelor din oteluri de rulmenti**, Teza de doctorat. Universitatea tehnica "Gh.Asachi" Iasi

VARIATIA CARACTERISTICILOR MECANICE LA TREFILAREA SARMELOR DE INALTA REZISTENTA IN CAMP ULTRASONIC

Rezumat: : Modificarea caracteristicilor mecanice pentru sarmele de inalta rezistenta mecanica trefilate in camp ultrasonor, cu filiera situata in maximul oscilatiei undelor si actionata paralel cu directia tragerii, sunt determinate in special de reducerea eruisarii - cauzata de efectul de suprafata al ultrasunetelor, respectiv , deregimul fractional al deformarii plastice.

BULETINUL INSTITUTULUI POLITEHNIC DIN IAŞI
Tomul L(III (LVII), Fasc. 4, 2007
Secţia
ŞTIINŢA ŞI INGINERIA MATERIALELOR

SUBSTRUCTURAL CHANGES IN WIRES DRAWN IN ULTRASONIC FIELD. THE SONODRAW SYSTEM

BY

M. SUSAN[1], V. ILIESCU[2], M. PEPTANARIU[3], P. DUMITRAS[4] and ŞT. TOMA[1]

Abstract: In the paper, one analyses by diffractographic, study the reduction of stresses state for drawn made from RUL 1V in super- sounds filed with "closed", oscillating systems, dimensioned $n \cdot \lambda/2$,with the die placed in the maximum of oscillation, operated parallel to the drawing direction – system Sonodraw.

Keywords: wires, drawing, ultrasonic field/ Sonodraw system, residual stresses, diffractographic research

1. Introduction

The principle scheme in the drawing of the wires with high mechanical resistance in ultrasonic field/ Sonodraw system, with closed oscillatory systems (the use of ultrasonic energy reflectors) is presented in figure 1 [1].

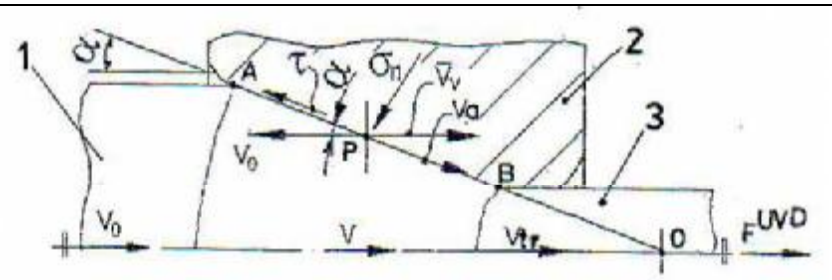

Figure 1. The principle scheme in wires drawing in ultrasonic field Sonodraw system: 1 blank wire, 2 auger die, 3 drawn wire.

In wires drawing in Sonodraw system, with the auger die activated parallel with the drawing direction, produces the surface effect "of the ultrasounds" meaning the reduction of metal-tool contact friction. Practically, the plastic deformation produces in impulses, with influences on the stress state for drawn wires because the cold hardening is much diminished with respect to classical drawing.

The subject we intend to treat in this paper the diffractographic research concerning the ultrasounds influence on the second degree (σ_{II}) remanent tensions and respectively on the crystalline network micro-deformation (ε), by making a röentgenographic comparative study, for the wires from RUL1V/STAS11250-89 wire drawing with and without ultrasounds, aving as comparing element the tensional state and the micro-deformations for the semi-manufactured, the annealed state.

The chemical composition determined for the RUL1V wires used for experiments considered in percentages [%]: C = 1.10; Mn = 0.40; Si = 0.30; Cr = 1.50; S = P = 0.02; Mo =0.08; Ni = 0.20 and Cu = 0.20, enters within the bounds specified in the product standard.

The semi-manufactured wires proceed from the same rolled wire lot, subjected then to the processing by classic wire drawing up to the D_0=3.85 mm diameter and annealed in protective atmosphere conditions (T *s* 800°C; CO=4%; CO_2=max.0.5%; H2=5%; CH_4=U5 %; with H_2O at 35°C - dew point) and hardness between 170-207 IIB (for the experiments there were sorted the wires semi-manufactured with a hardness at the superior limit of the technology interval admitted).

The wire drawing was made by only one passing from D_0 = 3.85 mm to D_1 = 3.60 mm, for which the degree of section reduction 8 - 14% $\left(\delta = 1 \quad (D_1/D_0)^2 \cdot 100\right)$,[%], with the wiring speed (v_{tr}) of 0.03 m/s using metallic carbides die (WCr), with a opening angle of conicity of $\alpha = 8°$ and as lubricant soap dust.

For a classic wire drawing , it was utilized the same technological ensemble as for the wire drawing in ultrasounds field, of course, without having the die activated with ultrasounds when wire drawing in ultrasounds field the die is situated in the maximum of the waves oscillations and activated in parallel with the direction of wiring, with various oscillating amplitudes of the die A = 8; 18 and 28 μm for which we have the variation speeds of the tool v_v = 0.9 ; 2.0 and 3.0 m/s $(v_v = 2\pi fA)$ using cylindrical concentrators in treads made of titanium based alloys.

The wire drawing installation in ultrasounds field is made up from the wire drawing tool, with hydraulic actioning, the ultrasounds generator U.Z.G.2-4M, made of concentrators PMS15A-18 type. The technological conditions for wire drawing with and without ultrasounds are presented in table 1 (1 semi-manufactured wires, annealed state; 2,3,4 - wire drawing in ultrasounds field, 5 - classic wire drawing).

2. Experimental researches and results

The roentgenographic study was done on the DRON 3 diffractometer with molibden cathode ($MoK_{\alpha 1}$, with λ = 0.7107 A), in the second conditions: the measuring field 15-40°; potential difference U = 25 KV; cathodic intensity I = 10 mA; the spinning speed of the sample 4 grad/min; paper speed 1800 mm/h; emergence 1 mm; entrance 0.25 mm.

Table 1

Symbol sample	Ultra-acoustic parameters			Technologic parameters				
I	f [KHz]	A [μm]	v_v [m/s]	D_0 [mm]	D_1 [mm]	α [°]	v_{tr} [m/s]	ö, [%]
1	-	-	-	3.85	-	-	-	-
2	17.5	8	0.9	3,85	3.60	8	0,03	14
3	17,5	18	2,0	3.85	3.60	8	0,03	14
4	17.5	28	3.0	3.85	3.60	8	0.03	14
5	-	-	-	3.85	3.60	8	0,03	14

In Bragg model of diffraction, the family of planes (hkl), defined by the interplanar distance d_{hkl} will produce the maximum value of diffraction only if the length radiation λ, will fall on this family under an angle θ, in condition [1]:

$$2d_{hkl} \cdot \sin\theta = n \cdot \lambda \quad (1)$$

For poly-crystals, Bragg condition is defined by the relation:

$$2d_{nh\,nk\,nl} \cdot \sin\theta = \lambda \quad (2)$$

where:

nh, nk, nl represents a family of parallels planes with (hkl), but which is situated at a interplaner distance:

$$2d_{nh\,nk\,nl} = d_{hkl}/n \quad (3)$$

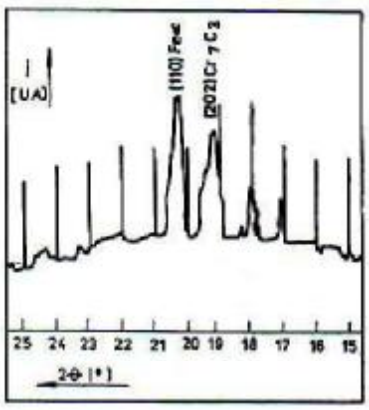

Figure 2. Section of the wires diffractogram RUL IV in annealed state.

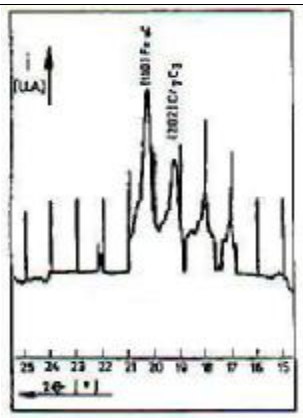

Figure 3. Section of the wires diffractogram RUL IV wire drowing in classic conditions

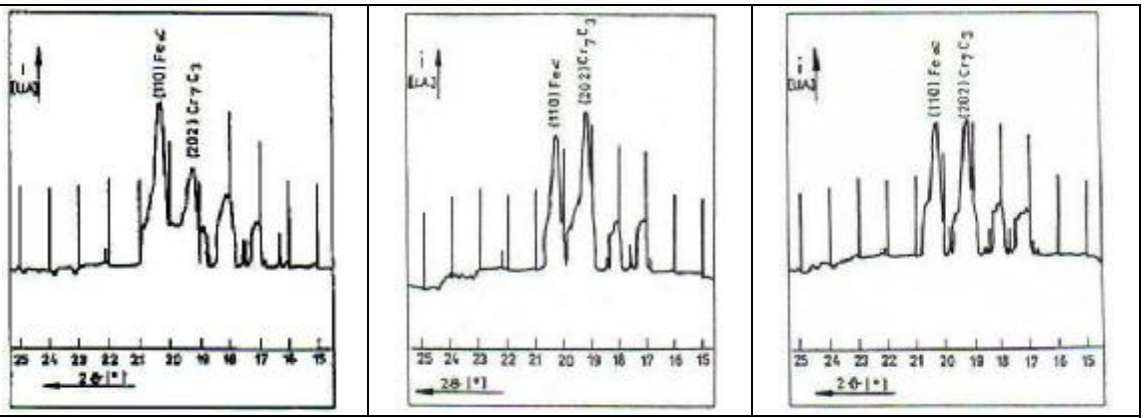

Figure 4. Section of the diffractograms RUL IV, wire drowing in ultrasonuds field: a)A = 8 μm; A = 18 um, c)A = 28 μm.

For the tensional state analysis, when wire drawing from RUL IV (after specific checking and correcting), reflex (110) Fe_α was taken into account, figures 2, 3 and 4

For determining interplanar distances (taking into account the corresponding angular positions), we used the following expression:

$$d_i = \frac{\lambda \cdot (MoK_{\alpha 1})}{2 \cdot \sin\theta_i} \quad (4)$$

The micro-deformation (ε), or deformation of second degree for the polycrystals can be obtained using the relation [2]:

$$\varepsilon = \frac{d_i - d'}{d_{ij}} = \frac{\Delta d}{d_i} \tag{5}$$

in which: d' - in the interplanar distance of a family of planes from the wire drawn sample, with or without ultrasounds; d_0 - refers to the same family of planes for the RUL 1V wires in annealed state. Taking into account Hooke's law, the second degree tensions (σ_{II}) can be determinate with the relation [3]:

$$\sigma_{II} = \varepsilon \cdot E = \frac{\Delta d}{d_{ij}} \cdot E \tag{6}$$

in which: E represents the modules of longitudinal elasticity ($E = 21 \cdot 10^4$ MPa, we didn't noticed any modifications of the modules of longitudinal elasticity when wire drawing RUL 1V wires in. ultrasounds field). The experimental results for the studied samples are presented in table 2.

Table 2

Symbol sample	Parameters defining tensional state			
	$2\theta_i$ [°]	d. $\frac{\lambda \cdot (MoK_{\alpha 1})}{2 \cdot \sin\theta_i}$ [Å]	ε (x 10^{-3})	σ_{II} [MPa]
1	20,22	2,24762	-	-
2	20,27	2,24495	2,52	53
3	20,25	2,24407	1,57	33
4	20,23	2,24620	0,63	13
5	20,30	2,23842	4,09	86

3. Conclusions

The analysis of experimental results obtained, by comparative roentgenographical study at RUL 1V wire drawing in ultrasounds field / system Sonodraw ; evidences the tensional state reduction, respectively, the fact that micro-deformation of the crystalline network is much more diminished in the same time with the oscillation amplitude growth of the die in comparison with the classical wire drawing.

Received April 25, 2007

[1]*The "Gh Asachi" Technical University Iaşi*
[2]*S.C. CABLERO S.R.L. Iasi*
[3]*Institutul de Fizica Tehnica Iasi / IFT Iasi*
[4]*Academia de Stiinte a Moldovei, Chisinau.*

REFERENCES

1. Susan,M., s.a , *The metal-tool contact friction at the ultrasonic vibration drawing of ball-bearing steel wires*, **Rev. Metal.Madrid** 35(1999), pp. 379...383.
2. Gheorghies,C., **Controlul structurii fine a metalelor cu radiatii X**, Editura Tehnica, Bucuresti, 1990.
3. Purnica,C., s.a., **Tehnici speciale de analiza fizico-chimica a materialelor metalice**, Ed. Tehnica, Bucuresti, 1988.

SCHIMBARI DE SUBSTRUCTURA IN SARMELE TREFILATE IN CAMP ULTRASONIC – SISTEM SONODRAW

Rezumat: In lucrare, prin studiu difractografic, se analizeaza reducerea starii tensionale pentru sarmele din RUL 1V trefilate in camp ultrasonor cu sisteme oscilante „inchise", dimensionate in nλ/2, cu filiera situata in maximul oscilatiei undelor si activata paralel cu directia de tragere – sistem Sonodraw.

BULETINUL INSTITUTULUI POLITEHNIC DIN IAŞI
Tomul LIII (LVII), Fasc. 4, 2007
Secţia
ŞTIINŢA ŞI INGINERIA MATERIALELOR

CONTRIBUTIONS REGARDING THE MODERN TECHNOLOGY OPERATIONALIZATION, WITH EQUPMENTS MADE IN ROMANIA FOR THE INTRODUCTION OF THE UNDERGROUND PIPES, WITHOUT DIGGING

BY

CLAUDIA TĂNASE, C. ŞTEFĂNESCU and V. NECULĂIASA

Abstract: The direct introduction, into soil, of the underground, without open ditch pipes, in the modern technology, becomes possible in Romania too, in that an air rocket (FORE type, 80 mm diameter) with direct advancement, through percussion has been created and produced, for the first time in the country. Our proposal is to develop the equipment and the specific work technology. The equipment is made of the air rocket and the accessory set. With their help, the application of the new, ecological, extremely efficient technology for the introduction of the underground, witheu, digging pipes becomes operational.

Keywords: pneumatic rocket, auger bit, pneumatic hammer

In the town infrastructure construction, the necessity of introducing water, sewage, natural gas, energy, telecommunications underground pipes, without open ditches at surface, is currently considered. The new, ecological, high performance in the field technology is currently applied in the developed countries. This one became operative in Romania also, through the production of the pneumatic rocket and the specific accessory set.

1. Theoretical grounds

The pneumatic rocket and the specific accessory set for the introduction of the underground pipes without ditch made the object of the research contract no. 43/1996 of SC MITECO SA Iasi. The operating system was presented at TIB 2000 (Bucuresti International Fair) and was awarded the excellence in research medal and degree. The contract included only the technical study phase. The design and execution of the pneumatic rocket was done by internal order, from personal sources (MITECO), strictly limited for a reduced functional model (short form) designed for soft soils which also included the specific accessory set.

The pneumatic rocket is the basic component of the underground, without ditch pipe introduction system. This one may generate a micro tunnel and may simultaneously or in separate order pull the pipe inside the formed hollow
The description and operation of the pneumatic rocket, including the modern technology of introducing and installing the underground, without ditch pipes was presented at the Scientific Communication Session of the "Gheorghe Asachi" Technical University, Iasi, in July 2006 [1].

Innovative technical solutions for doubling or tripling the weigh of the main piston generating percussions in order to increase the energetic percussion parameters of the pneumatic rocket were proposed at the Scientific Communication Session of the Bacau University, in August 2006. The increase was done under restrictive conditions in order to stick to the initial configuration of the steel piece. In order to increase the soil penetration force of the rocket and reach the energetic parameters similar to those met in the reference models produced in USA and Germany, material choice is essential

The duty cycle of the pneumatic rocket as a self maintained percussion generator, without classical (compressed air) distributor, with mobile pieces in motion was minutely detailed at the Scientific Communication Session of the Bacau Technical University, in October 2006 [3].

Hereinafter, we shall detail the technology and full work equipment made of the pneumatic rocket and the accessory set for the introduction of the underground wires and pipes without ditch.

2. Constructive solution description

2.1 Work equipment

The work equipment is made of:

- the air rocket
- the accessory set

The pneumatic rocket is a lineal pneumatic engine with an oscillatory and a self maintained movement of the main piston in the rocket's body. The pneumatic, self-propulsive engine may be compared with a self maintained percussion-generator. The rocket (percussion motor generator) presents an automatic duty cycle and it is supplied with compressed air.

The accessory set includes: the power source (motor air-compressor), launcher, shooter, expander, a device for coupling and warping the underground wires and pipes into the micro-tunnel

2.2 The technology of introducing the underground, without digging pipes.

The modern technology of introducing the underground, without digging pipes presents two operational stages:

- micro-tunnel generation
- underground cable and pipe drawing into the micro-tunnel

The two stages can take place simultaneously or in separate sequences, according to the case. The technological work scheme is illustrated in figure 1.

The underground, without digging pipes introduction technology can start only after the launching pit where the work equipment is placed, respectively the exit pit at the end of the route that may be situated at max. 150m away from the starting point, is arranged.

Both pits (launching and exit) will be worked out by excavation, at the required depth, pre-established at start for introducing the underground pipe or cable.

The launching pit is adjusted so as to be able to take over the length of the pneumatic rocket, the accessories (launcher-shooter), the used pipe (rigid or flexible) and the

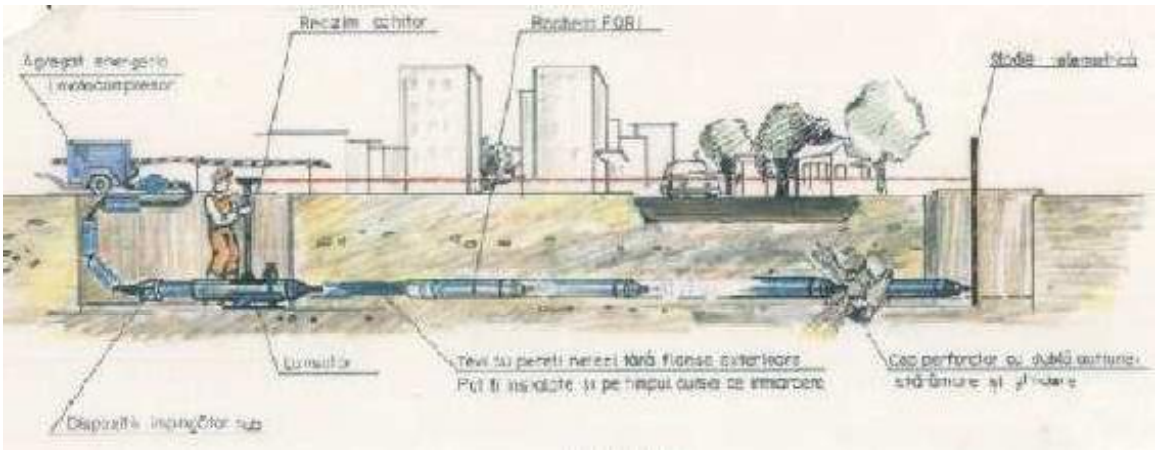

Figure 1 The technological work scheme

human operator. Inside the pit the launcher, fastened into the soil with four metallic rods is placed. The pneumatic rocket is placed on the launcher, this one being secured with the adjustable fixing strap with roller.

The launcher has an adjusting device for the angle of adjustment, with two bolts which allow the launch of the pneumatic rocket into the soil at the wished angle (always a negative one 0 max.-90°, with 0° at horizontal advance and respectively 90° at the vertical, downwards advance).

The pneumatic rocket (figure 2) is coupled at the air source (motor air-compressor) through flexible pipes for compressed air capable of standing a nominal pressure of 8-10 bars.

Figure 2 The FORI 80 pneumatic rocket, along with the accessory set.

Into the exit pit (terminus) the telemetric stadium for the work depth control is placed.

Usually, when the two main operations (micro-tunnel generation and underground pipe introduction into the micro-tunnel) take place simultaneously in one pass, the flexible pipes which connect the rocket with the air source are previously passed through the pipe to be installed and then are coupled to the motor air-

compressor. Obviously, their length must be correlated (5-6 cm larger than the length of the pipes to be installed).

Behind the rocket the haulage device for rigid pipe sections is coupled or the flexible pipe specific coupling device with ring of wires unrolling.

In this way, two distinct operating systems meet, according to the nature of the pipe to be introduced into the micro-tunnel:

- The introduction technology of the underground rigid, without digging pipes;
- The introduction technology of the underground flexible, without digging pipes;
- a) The introduction technology of the underground rigid, without digging pipes is schematically illustrated in figure 1;

Behind the rocket the haulage device for rigid pipe sections is coupled, according to the detail in figure 3.

Figure3 The coupling and haulage device of the rigid pipes sections.

The described sequences are operational work stages which were carried out with the help of the FORI 80 pneumatic rocket and its accessories; this equipment was physically made for the first time in the country and experimented under real work conditions on the field.

In order to extend the practical application range when introducing the new pipes with diameters superior to the ones tested so far (80 mm), an improved cable warping technique of the pneumatic rocket with the help of a cable hoist is presented.

The pneumatic rocket generates during the first stage a micro-tunnel in which the warping cable is introduced. In the second stage, the opening of the micro-tunnel is drifted with the help of the expander. The head of the rocket with the expander passed over the body of the rocket is pulled with a cable with the help of the cable hoist at the surface (over the exit pit). The rigid pipe section with increased diameter is coupled behind the rocket. In this way, results a more effective advance and work system, overlapping the self-propulsion of the pneumatic rocket with the cable warping force of the cable hoist

Obviously, the technology can become operational by replacing the old, degraded or destroyed underground pipes, in which case the first stage (micro-tunnel generation) is eliminated. Thus, on the same route of the existing underground network a new pipe may be introduced inside the existing one subject to spraying. On the top of the rocket a casing splitter for breaking, tearing and breaking into fragments the old pipe is fixed in an articulate way. The expander pushes the destroyed fragments into the walls of the micro-tunnel. The division into fragments of the old pipe is simultaneously followed by the introduction of the new, replacement pipe. In the

figure 4 the functional work scheme for the replacement of underground, rigid, without digging pipes is illustrated.

Figure 4. The introduction technology of the underground rigid, without digging pipes.

The breaking up of the old pipe is illustrated in figure 5 (detail).

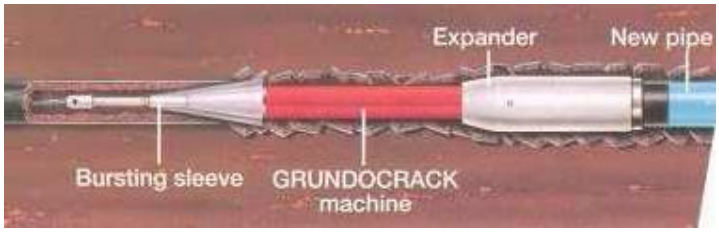

Figure 5. Detail - old pipe spraying.

In order to optimize the work technology, an installation for the preparation of the paste used for the cementation of the old pipe fragments in the wall of the micro-tunnel is required in order to lubricate, protect and reduce the rubbing when passing the new pipe through the micro-tunnel. An installation for the homogenization of the additive cement concrete mixture provided with pomp sends the lubricating mixture through the hose pipe to the interested area.

A detail of the lubrication and protection installation of the new pipe inside the micro-tunnel is illustrated in figure 6.

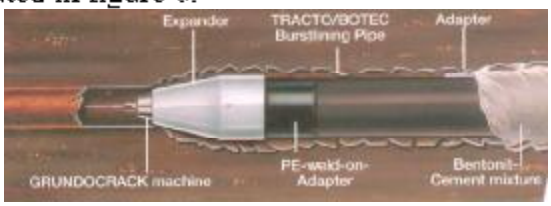

Figure 6. Lubrication and protection of the new pipe in the micro-tunnel detail

b) The technology used for the introduction of the *flexible underground pipes* without digging is schematicatically illustrated in figure 7

Behind the rocket the specific haulage device for flexible pipes is coupled with rings of wire unrolling.

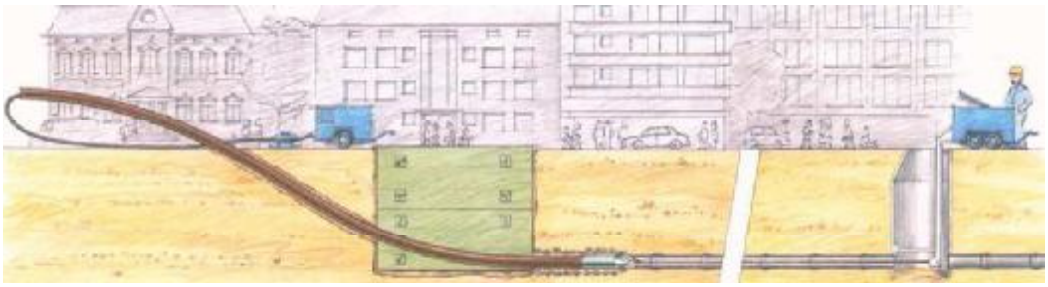

Figure 7. The introduction technology of the flexible underground pipes without digging.

The whole operational process takes place strictly at the underground mounting quota of the pipe without open digging at the surface under perfectly ecological conditions without affecting the current activities carried out at surface: passenger, road, and railway surface traffic, without degrading or destroying the vegetation in the parks, cultivated gardens or disturbing the ecologic balance represented by the flora and fauna of the sub crossed areas.

2.3 Conclusions after the operational testing of the equipment (the pneumatic rocket short functional model with the full accessory set)

- The pneumatic rocket functioned well for oblique to vertical trajectories, into slightly cohesive soils and fillings.
- The rocket was not efficient for hard soils with roots and stone inclusions etc, *soils were the short model employment is not allowed.*
- Continuing the research for the creating a long type performant model- meant for hard soils with root and stone inclusions (max 30%) is considered necessary.

3. The advantages of the proposed solution

- The extremely compact internal structure of the pneumatic rocket, allowed the elimination of the classical distributor described in the technical literature schemes
- The main piston has multiple functions that also incorporate the compressed air distribution function, by the internal, personal wiring with a special configuration.
- The installation technology of the underground, without ditch pipes, by way of the proposed pneumatic rocket ensures advantages highly superior to the classical technologies with open ditch currently applied in Romania, in that expensive operations such as: digging, banks propping up, filling after installing the pipe, filling compaction, transporting the excess earth, pumping out the ground waters are eliminated.
- The new technology is ecological, effective and does not disturb the normal course of the passenger, road, and railway surface traffic in the sub crossed area.
- It ensures the observance of most severe European and international norms regarding environment protection and environment ecological equilibriums maintenance.

For the time being, there is no alternative in order to reach the presented advantages without the pneumatic rockets being produced in the country if the necessity of their realization is understood or they will be compulsory imported [9-12] in 2007, when the restrictive ecological norms of the U.E in the field will be applied in Romania too.

Received April 29, 2007 *The "Gh.Asachi" Technical University Iaşi*

REFERENCES

1. Claudia Tănase, Ing. V. Neculăiasa, *Contributions regarding the promotion of new ecological technologies for introducing underground without ditch pipes*, Scientific paper Gh. Asachi Technical University, Iaşi, July 2006.
2. Claudia Tănase, V. Neculăiasa. **Ph D** *New super-heavy materials used in the construction machinery structure with major power impact on the firing pin piston at the pneumatic rocket for introducing underground without ditch pipes* Scientific paper Bacău University, August 2006.
3. Claudia Tănase, V. Neculăiasa. **Ph D** *Contributions regarding the creation of the pneumatic rockets for introducing underground without ditch pipes* Scientific paper Bacău Technical University, January 2007
4. St. Mihăilescu ş.a. . *Construction machinery*, 3 vol. Poligrafică Publishing House 1984
5. C. Drăghici , *Design Guide for Machines Constructions*, Technical Publishing House 1989
6. ***, Prospects of the companies: Vermeer S.A (USA), Tracto-Technik (Germany), Injectoforaj (Romania).
7. ***, Hydraulic - Hydraulics-Mecatronics and Pneumatics Magazine, ISSN/1453-7303.
8. ***, Contract CNCSIS no. 43/1996
9. ***, www.tracto-technik.de
10. ***, www.radiodetection.co.uk
11. ***, www.finneg.ro
12. ***, www.vermeer.usa

CONTRIBUŢII PRIVIND TEHNOLOGIA MODERNĂ DE OPERARE CU ECHIPAMENTE ROMÂNEŞTI DE POZIŢIONARE A ŢEVILOR SUBTERANE FĂRĂ SĂPĂTURI

Rezumat: Introducerea directă în sol fără realizarea de săpături prin noua tehnologie propusă, a devenit posibilă şi în România, prin concepterea şi realizarea unei rachete de tip FORI de 80 mm diametru. Studiul nostru se referă la dezvoltarea echipamentului respectiv şi a tehnologiei de lucru.

BULETINUL INSTITUTULUI POLITEHNIC DIN IAŞI
Tomul LIII (LVII), Fasc. 4, 2007
Secţia
ŞTIINŢA ŞI INGINERIA MATERIALELOR

LAYERS WITH HIGH ABRASIVE WEAR RESISTANCE DEPOSED ON ALLOYED STEELS WITH DUPLEX TREATMENTS

BY

SORINEL TANASUCA, ADRIAN ALEXANDRU, RACLARIU GICU CATALIN, MIHAILESCU NECTAR and SORIN IACOB STRUGARU

Abstract: In this paper work, the authors wants to present which is the influence of the thermal treatments before and after deposition and alloying by electrical spark on the abrasive wear resistance

Keywords: electric spark, electrode, layer, hardening

1. Introduction

The surface engineering, as technical interdisciplinary science is a new concept who appeared in high developed industrial countries as a result of spectacular development of the surface treatments.

A deffinition of this concept was given by David Melford, prime vicepresident of The Institute of Metals (UK) and by Tom Bell from The University of Birmingham (UK): The surface engineering is in the esence a designed method for surface and sublayers of metals which are designed together as a system which confer good performances for metallic materials and which are non specific for any of them token separately.

The demanded properties for the superficial layer are different of those of basic metals and almost in contradiction with them. The technologies of superficial treatments or thin layers deposition have each at them some disadvantages so in current practices the use of the combination of two or more methods for increasing the performances is a trend today. The duplex technologies permit to obtain metallic parts with variable properties in a large range which respond for the most exigently requirements

The electrical deposition by the electric spark method is verry efficient.

The process of alloying and deposition by electric spark or inverse electroerosion has some advantages as: high adherence of the deposed layers, simple and cheap machines and technology, and some disadvantages as: large roughness of the alloyed surface, the appearance in superficial layers of the parts of the residual stress which decrease the wear resistance

The efficient combination of alloying and deposition by electric spark with a superficial thermic treatment can make disappear many of these disadvantages may disapear.

2. Method of work

The experimental researchers of the alloying and deposition by electric spark and determination of the influence of the thermic treatments before and after, upon the

structural changes were made on the following steels:39MoAlCr15, 115MoVCr115, which are described in table 1.

Table 1

Table	Steel type	CHEMICAL COMPOSITION, %										
		C	Mn	Si	P	S	Cr	Mo	Ni	V	Al	Cu
1	39MoAlCr15	0,41	0,52	0,34	0,025	0,020	1,57	0,21	0,18	0,03	0,98	0,2
2	155MoVCr115	1,58	0,41	0,22	0,021	0,025	11,7	0,72	0,16	1,05	0,03	0,23

Table 2

Steel	Variant	Electrode	HV_{30} daN/mm²	Δm_1 g after time, in minutes						Δm_2 g	Vm. g/h	I_u g/h·m²
				10	20	30	40	50	60			
39MoAlCr15	C-CIF-DAES	WCo8	1332	0,001	0,004	0,008	0,010	0,028	0,051	0,051	0,051	0,1869
		TiC5Co6	1079	0,001	0,005	0,01	0,012	0,036	0,064	0,064	0,064	0,2345
	E-DAES-CIF	WCo8	1097	0,002	0,006	0,018	0,024	0,032	0,082	0,082	0,082	0,3005
		TiC5Co6	949	0,002	0,011	0,020	0,039	0,055	0,121	0,121	0,124	0,1545
155MoVCr115	C-CIF DAES	WCo8	2007	0,0008	0,001	0,004	0,006	0,0082	0,02	0,020	0,020	0,0733
		TiC5Co6	1686	0,001	0,002	0,008	0,01	0,013	0,034	0,034	0,034	0,1246
	E-DAES CIF	WCo8	2690	0,0006	0,001	0,002	0,003	0,0054	0,012	0,012	0,012	0,04398
		TiC5Co6	2202	0,001	0,002	0,005	0,006	0,009	0,023	0,023	0,023	0,0845

Alloying and deposition by electric spark uses the inverse polarity the part which is processed is the cathode and the electrode is the anode in this case the deposition takes place in air or other gas, with or without a rotation movement

By comparing with other methods, the alloying and deposition by electric spark presents a series of advantages: the deposed metallic layer present a resistant connection with the basis material; the method makes possible the deposition of pure metals (Ni, Cr, Mo, W, Ti) or metallic alloys; it is not necessary a preliminary preparation of the deposition surface etc.

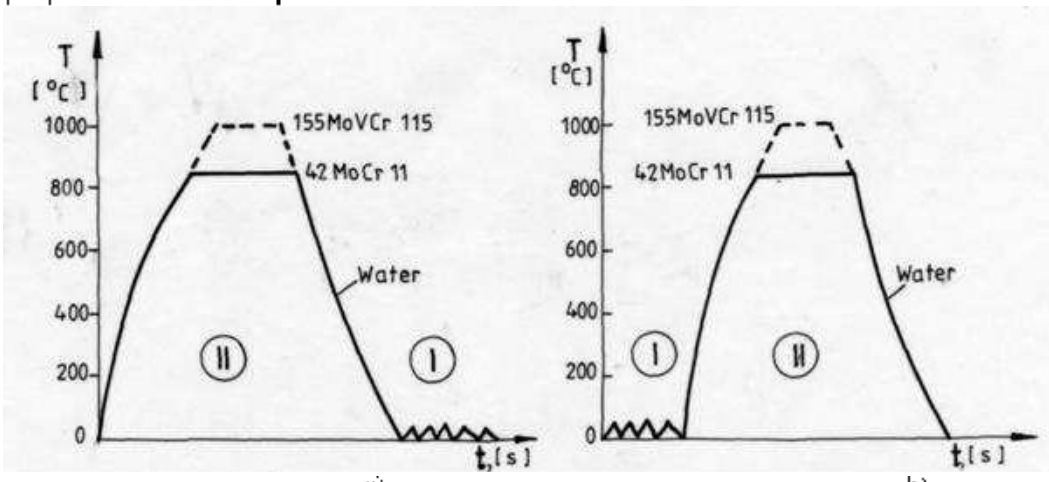

Fig 1. The duplex variants of treatment depositing and alloying by electrical spark superficial hardening by induction

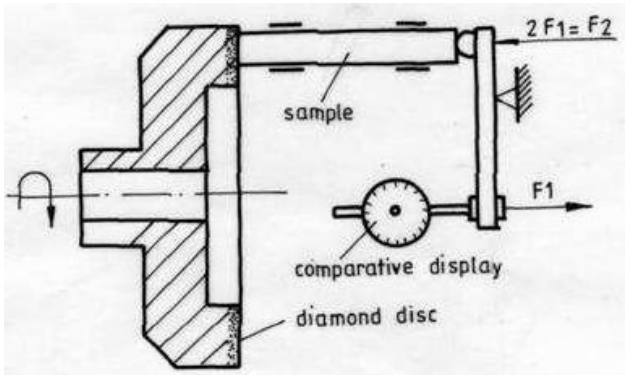

Fig.2. The device for abrasive wear testing

The samples from the two alloy steels were processed in two variants of duplex treatments:

a) superficial hardening – deposition and alloying by electric spark;

b) deposition and alloying by electric spark – superficial hardening (fig.1).

At the processing by deposition and alloying by electric spark there were used sinterizated electrodes from metallic carbides (WCo8, Ti15Co6). The samples from the two steels with sizes ϕ 8x60 mm, processed after duplex treatments were tested at abrasive wear. The device for abrasive wear test is presented in fig.2.

3. Experimental results

The wear resistance was determinated by the masic wear (V_m) defined by STAS 8069-87.

$$V_m = \frac{\Delta m_e}{t}, \text{ g/h}$$

The intensity of masic wear is calculated with the relation:

$$I_m = \frac{\Delta m_e}{A_f \cdot L_f}, \text{ g/h·m}^3$$

A_f, L_f – the surface and the length of friction.

The hardness, the masic loses Δm and Im for pressing the samples with a 20 N force by a total friction length of 5428 m of the two studied steels, processed by C and E variants with WCo8 and Ti15Co6 electrodes are presented in table 2 and figure 3.

The variation of masic loses during friction for the steels 39MoAlCr15 and 155MoVCr115 are shown in fig.4.

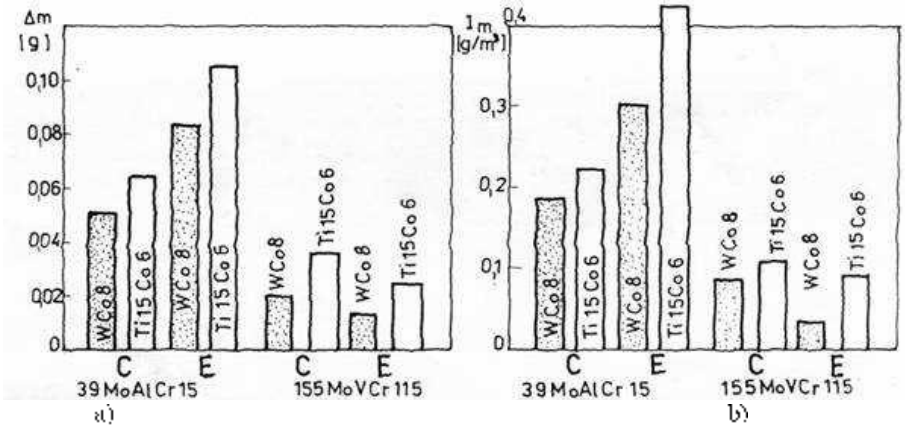

Fig.3.a) Δm; b) Im

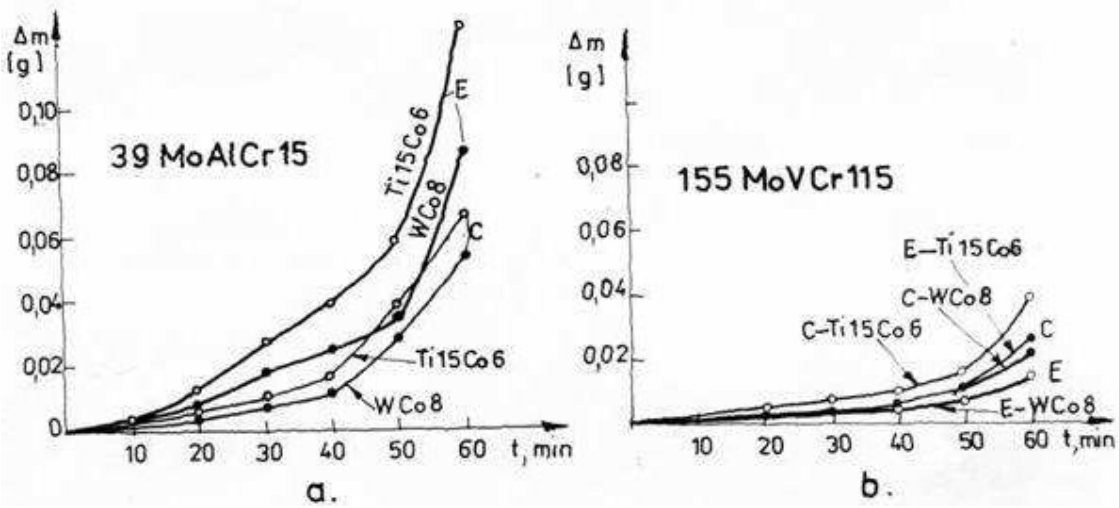

Fig. 1. The variation of mass loses as time at friction for the steels 39MoAlCr15 and 155MoVCr115

4. Conclusions

1) The high alloyed tools steel 155MoVCr115 which has in the deposed layers a very large hardness (1686÷2690 $HV_{0.05}$) present a very good abrasive wear resistance by comparing with the 39MoAlCr15 steel which has the microhardeness in the deposed layers only (949÷1332 $HV_{0.05}$);
2) The deposed layers with WCo8 electrode ensures a higher wear resistance as those deposed with Ti15Co6 electrode;
3) The duplex treatments variants which were applied at 39 MoAlCr15 steel at which the last operation was the deposition and alloying by electric spark (C variant induces higher wear resistance);
4) At the high alloyed tools, steel 155MoVCr115 higher wear resistances are obtained by the duplex treatment variants at which the last operation is superficial hardening.

Received April 17, 2007 *The "Gh.Asachi" Technical University Iaşi*

REFERENCES

1. Alexandru, A. **Doctorate Thesis**, January 2002.
2. Alexandru, A., Pop, F. **Metallic materials with hardened deposit created by electric arc with vibrating electrode**. Proceedings EUROMAT-JUNIOR, Lausanne, 1994.
3. Pop, D., Pop, F., Alexandru, A. **Hardened deposition with tungsten carbides on steel specimens.** Proceeding, vol. II, EUROMAT, Lisabona, 1998.

STRATURI CU INALTA REZISTENTA LA UZURA DEPUSE PE OTELURI ALIATE CU TRATAMENTE DUPLEX

Rezumat: In aceasta lucrarea autorii prezinta care este influenta tratamentelor termice inainte si dupa depunere si aliere prin scanteie electrica asupra rezistentei la uzura.

BULETINUL INSTITUTULUI POLITEHNIC DIN IAŞI
Tomul LIII (LVII), Fasc. 4, 2007
Secţia
ŞTIINŢA ŞI INGINERIA MATERIALELOR

THE INFLUENCE OF EXTERNAL FACTORS UPON THE TRANSFORMATIONS AT TEMPERING IN HIGH-SPEED STEELS

BY

N. TORODOC and I. GIACOMELLI

Abstract: The major influence of the final structure upon the behavior in use of the tools being known, the transformation kinetics at tempering and upon applying of external magnetic fields has been studied. Thus, upon different quenched samples, several tempering temperatures have been tried out, and also a vibratory field has been applied to the usual temperature of 560 °C.

Keywords: energy field, high-speed steel, tempering

1. Theoretical considerations

After quenching, in the structure of the high-speed steels, beyond martensite and carbides also significant amounts of residual austenite are kept, that can reach 30% or even more. This is not useful due to two reasons: a smaller hardness results, and the residual austenite being unstable in time, can lead to the modification of the properties and the dimensions. Also, at eventual later thermochemical treatments, the diffusion is considerably slowed down. At the tempering temperature, the transformation of residual austenite into martensite takes place by the decrease of the stability and of carbon content.

An acceptable theory considers that while keeping at tempering temperature from the martensite, carbides of the alloying elements precipitate. Thus, also the carbon content of martensite is decreasing, a difference of chemical potential between it and residual austenite is being created. In consequence, a net transport of carbon atoms by diffusion from austenite to martensite takes place.

This process sensitizes the austenite, and its transformation into martensite takes place during the exposure to room temperature. In fig. 1 this process is shown quantitatively, and also the simulation of the transformation by keeping for a longer time at 560 °C.

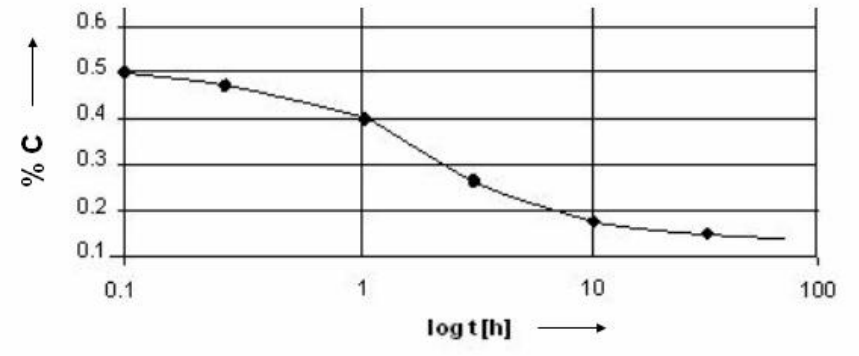

Fig. 1 Carbon content vs. time

It must be mentioned that the austenite has to undergo transformation in a short time after quenching in order to prevent the stabilization phenomenon.

2. Experimental studies

According to those shown above, the transformation of residual austenite has at its basis the diffusion of carbon, and the diffusion being a process which is thermally activated, tempering temperatures of quenched samples, between 560and 640 ° C have been applied, as shown in tables 1-3.

Table 1

Nr	Type of steel	Quenching				% residual austenite after 2 subsequent temperings at 560°C, with the durations			
		[t]°C	medium	Hardness [HRC]	A rez [%]	15 min	30 min	45 min	60 min
1	Rp3	1270	oil	60,5	28.5	14,5	9 2	5,5	4,75
2	Rp5	1190	oil	61	27	18 6	11,4	7,6	5,9

Table 2

Nr	Type of steel	% residual austenite after 2 subsequent temperings with the following temperatures and durations							
		580°C				600°C			
		15 min	30 min	45 min	60 min	10 min	20 min	30 min	40 min
1	Rp3	13,2	8 8	4 7	4 25	13	8,1	5 2	4,8
2	Rp5	15.5	904	7.0	5.1	14.9	9.2	6.8	5.0

Table 3

Nr	Type of steel	% residual austenite after 2 subsequent temperings with the following temperatures and durations							
		620°C				640°C			
		5 min	10 min	15 min	20 min	5 min	10 min	15 min	20 min
1	Rp3	14.2	8.0	5.3	4.4	12.9	6.3	4.1	2.1
2	Rp5	15,3	69 6	6 2	4,9	11 6	6,8	3,8	2,6

Also in these tables, as well as in the diagrams from the next figures the modification of the quantity of residual austenite is shown

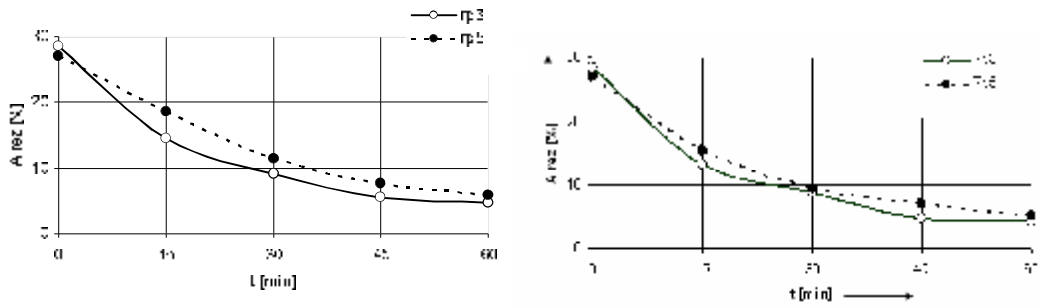

Fig. 2a. Tempering at 560 and 580°C

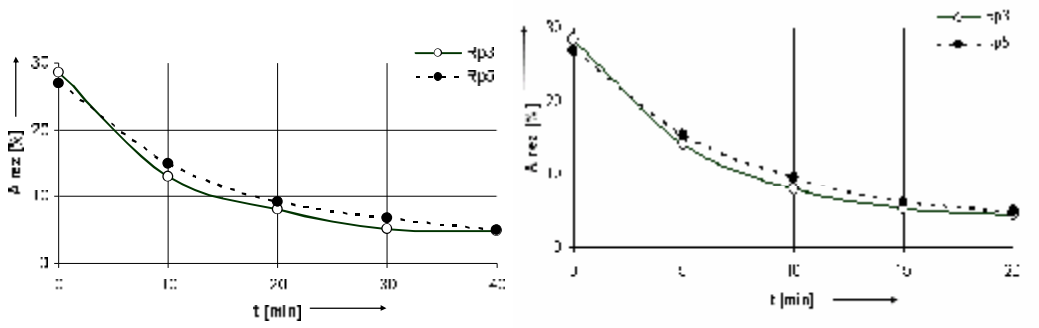

Fig. 2b Tempering at 600 °C and 620 °C

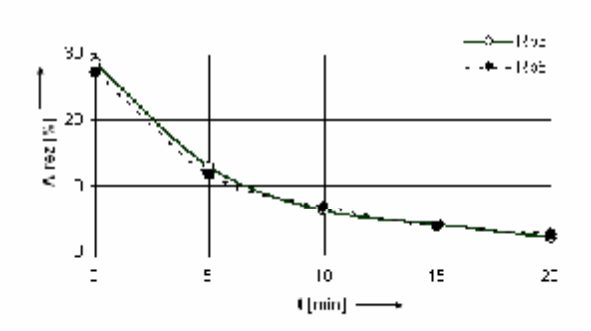

Fig. 2c. Tempering at 640 °C

Fig. 2: Residual austenite content at tempering at different temperatures

The major influence of the temperature at heating upon the kinetics of the transformation of the residual austenite can be observed. Thus after keeping for 20 min at 620 °C, the same transformation rate than after 60 min at 560 ° C. At higher temperatures, like for example 640 ° C, the transformation is even faster and more complete.

In the same time it is mentioned that alongside with the increase of the tempering temperature, there is the risk of the decrease of hardness to values below 60 HRC, which is not indicated for cutting tools. In table 4 this aspect is exemplified.

Table 4

Nr	Type of steel	HV hardness after 2 subsequent temperings at 640 degrees C with the following durations			
		15 min	30 min	45 min	20 min
1	Rp3	870	741	641	593
2	Rp5	831	665	569	515

Another series of experiments has searched to show the influence upon the kinetics of the transformation of residual austenite of the mechanical vibrations, applied to the liquid medium in which the tempering has been carried out (at 560 ° C). The quenched samples have been tempered in molten salt baths, without vibrations and respectively with the tempering vessel undergoing mechanical vibrations with a frequency of 50 Hz. The result obtained are presented in table 5 and the diagrams in fig. 3 a and b.

Table 5

Nr	Type of steel	HV hardness after 2 subsequent temperings at 640 degrees C with the following durations							
		15 min	30 min	45 min	60 min	10 min	15 min	20 min	25 min
1	Rp3	7.4	5.2	4,7	4,25	4,9	4.6	4	3,8
2	Rp5	10,2	8,4	8	7,8	8,8	6,5	5.1	4,8

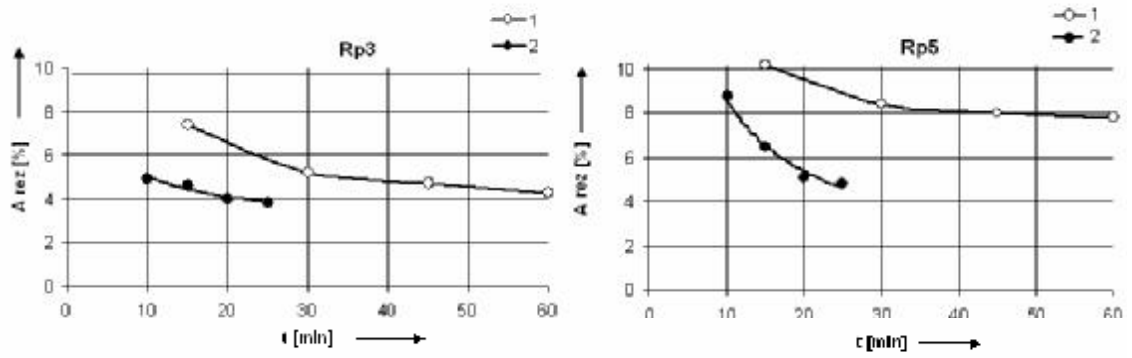

Fig. 3 The kinetics of the decomposition of residual austenite in the absence (1) of and in the presence of (2) the vibratory field: a) Rp3 steel b) Rp5 steel

3. Conclusions

The residual austenite is being transformed into martensite by tempering processes, the kinetics of transformation being influenced by its temperature in the following way:

- increase of the temperature from 560 to 580 ° C leads to a non-significant increase of the transformation rate
- increase of the temperature to 600 ° C leads to an increase of the transformation rate with ca. 30%
- increase to 620 ° C reduces the duration of the equivalent transformation three times
- The tempering temperature of 640 ° C has a major influence, the duration of keeping of 10-12 min has the same effect upon the transformation of austenite like 60 min at 560 ° C

Higher tempering temperatures also affect the structure en ensemble. Thus the martensite can gradually transform itself into other structures, and the carbides can coagulate. In consequence, the hardness and also possibly the resistance to heat are decreasing.

For the increase of the productivity at the tempering operation, the increase of the temperature has to be precisely correlated with the duration of keeping in the tempering process. This duration can be thus reduced from 3 x 1 hours to 2 x 10 minutes

The vibratory field that is superimposed to the thermal field of 560 °C has also spectacular effects on the transformation. But in the same time the vibratory field does not affect the martensitic mass, the hardness being determined only by the temperature of the temperings.

Received April 7, 2007 *The Transilvania University of Braşov*

REFERENCES

1. Giacomelli et al: **Nonconventional tehnologies with phase transformations** (in romanian). Lux Libris press.
2. O.M Bataineh, 2002, **Pulsed magnetic treatment of cutting tools**, Master Thesis, Department of Mechanical Engineering, University of Minnesota, Minneapolis, MN
3. Omar Bataineh, Barley Klamecki, Barry G. Koepke , *Effect of pulsed magnetic treatment of drill wear* **Journal of Materials Processing Technology** 2003
4. Popescu N. et al: **High Speed Steels**-Editura Tehnica Bucuresti 2002
5. A.J.Liu, F.Tang, X.J. Luo, J.F. Mei, H.Z. Fang, *Research on residual stress reduction by strong pulsed magnetic treatment* **J. Mater. Process. Technol** 74.
6. J.Morales, I. Sandoval. **AISE Steel Technolog** 76
7. S. Wei, J. Zhu **Trans Mater. Sci. Eng.** A 254.

INFLUENŢA FACTORILOR EXTERNI ASUPRA TRANSFORMĂRILOR LA CĂLIRE ÎN OŢELURILE RAPIDE

Rezumat: Ştiind influenţa structurii asupra proprietăţilor sculelor s-a studiat cinetica transformării la călirea în câmp magnetic. S-au studiat de asemenea influenţele a diferite temperatura de revenire, precum şi aplicarea vibraţiilor la 560°C.

BULETINUL INSTITUTULUI POLITEHNIC DIN IAŞI
Tomul L(III (LVII), Fasc. 4, 2007
Secţia
ŞTIINŢA ŞI INGINERIA MATERIALELOR

PHYSICALLY MODIFIED POLYURETHANE FOAMS AS EFFICIENT SORBENT MATERIALS IN LIFE QUALITY ASSURANCE

BY

L. TOFAN, C. PADURARU and D. BILBA

Abstract: In last decades the flexible polyurethane foams of polyether type with open cells became accessible and efficient sorbents for a wide range of ionic and non-ionic species from liquid and gaseous media by batch and dynamic techniques. In this context the behavior of "Spumalim" flexible polycheric polyurethane foam (Romania) modified by physical adsorption of dimethylglioxime (chelating reagent) and tri-n-buthyl phosphate (organic extractant) in retention process of some metallic ions in traces has been studied. The experimental results are very promising for polyurethane foams utilization in development of separation concentration and determination of high application interest.

Keywords: sorption, polyurethane foam, chelating reagen, open- cells.

1. Introduction

Polyurethane foams can be defined as polymers containing bonds of urethane type in which a proportion of the solid phase is replaced by gas in the form of numerous small cells. The gas may be in continuous phase to give an open cell material or it may be discontinuous in the form of discrete, non-communicating cells [1]. According to their chemical structure, the polyurethane foams can be of polyether and polyester type.

To obtain the flexible polyurethane foams of polyether type is most widely used a polyether with molecular weight of 3000 and more than 90% secondary hydroxyl terminal groups which is obtained by cationic polymerization or polycondensation of the propylene oxide (Scheme 1). This polymer reacts with isocyanates (80/20 and 65/35 mixtures of the toluene diisocyanate 2.4–and 2.6-isomers) forming a prepolymer which is finally treated with water. The bubbles of carbon dioxide emitting from reaction expand the mixture to foam, due to the high viscosity of the mass reaction(Schemes 2–3)[2]:

In order to reaction rate increase and establish and optimum ratio between the chain extension and the foaming reaction are used tertiary amines and organometallic compounds as catalysts.

The physico – chemical properties of the polyurethane foams (Table 1) depend on structural factors (crystalinity, degree of cross linking, chain rigidity).

The polyurethane foams can be considered as solide membranes. If the gas bubbles occupy a volume smaller than 76%, the membranes may be spherical; if they occupy a larger volume, the spheres will be distorted into polyhedra (pentagonal dodecahedra on average) [1].

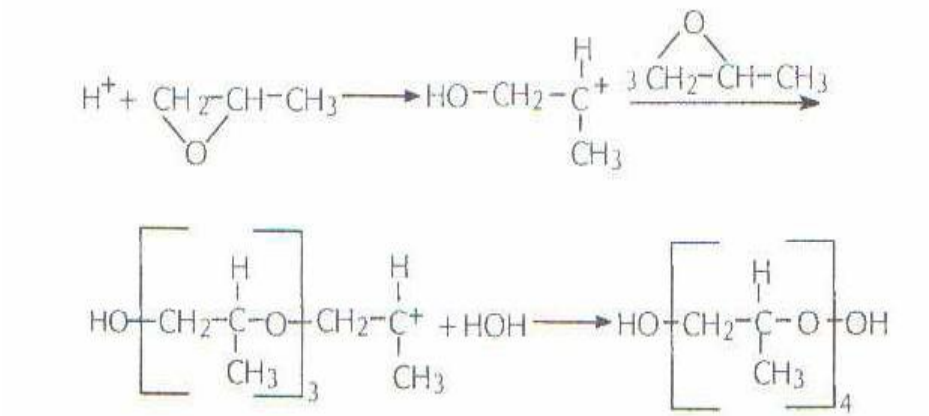

(1)

(2)

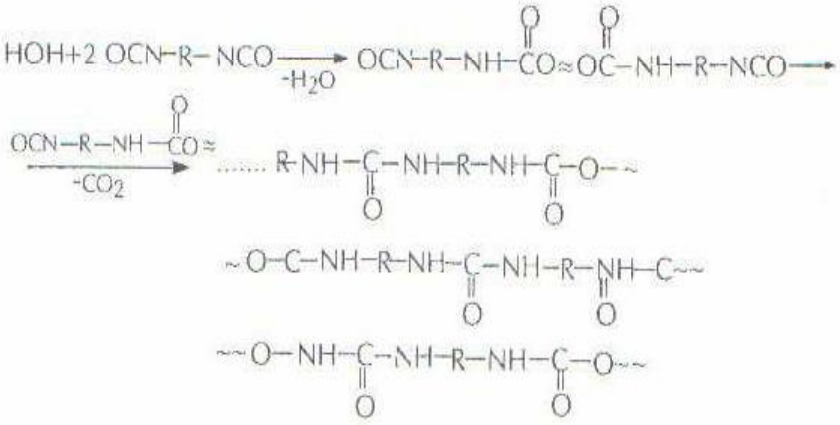

(3)

Table 1. Physico – chemical features of the polyurethane foams

Character	Hydrophobic
Porosity	Large
Reversible swelling in	Water. HCl until 8M, H_2SO_4 until 4M , HNO_3 until 2M, glacial CH_3COOH. NH_2OH 2M, NaOH 2M, organic solvents (benzene, carbon tetrachloride, chloroform, acetone, alcohols)
Dissolution in	Concentrated H_2SO_4, concentrated HNO_3
Degradation by	Heating to 180 – 220°C UV exposure
Anionic exchange capacity	Low
Surface area m^2/kg	7.6-32.5
Bulk density, kg/m^3	15- 35
Sorption rate of chemical species	Relative fast

Polyurethane foams have a wide range of applications in batch or dynamic separation and preconcentration of inorganic and organic species, gas and liquid chromatography and cells immunosorption [3,4].They can be efficiently used both in

unloaded form [5-9] and after a physical or chemical treatment [10-16]. The remarkable properties (Table1) make the flexible open–cell polyurethane of polyether type an ideal support for immobilizing by physical adsorption of various selective reagents and extractants.

The experimental results presented in this study point out the excellent sorption properties of the "SPUMATIM" flexible open cell polyurethane foam of polyether type impregnated with dimethylglyoxime(DMG – chelating reagent) and tri–n–butyl phosphate (TBP organic extractant) in batch retention of Ni(II), Pd(II) and Fe(III), Ga(III) ions, respectively.

2. Experimental

Foam Purification

The "SPUMATIM" flexible open – cell polyurethane foam of polyether type was purified according to the procedure described in Figure 1.

PRETREATMENT for several hours with HCl solution of 1 mol / L

↓

RINSING with bidistilled water (until the washings are free from Cl^- ions)

↓

WASHING with acetone (for entire removal of organic impurities)

↓

DRYING at 70 – 80^{0}C

Fig. 1. Scheme of polyurethane foam purification

Table 2. Systematization of the studies concerning the sorption of some cation on "SPUMATIM" flexible open-cell polyurethane foam impregnated with dimethylglioxime (DMG) and tri-n-butylphosphate (TBP) results

	Polyurethane foam - DMG		Polyurethane foam - TBP	
	Ni(II)	Pd(II)	Fe(III)	Ga(III)
Foam content in modifier agent	6,3866 mg DMG/g foam		5.1714 g TBP/g foam	
Optimum conditions of cations sorption medium acidity time to equilibrium reaching	pH= 8,5 45 min	pH= 0,9 45 min	HCl 4M 90 min	HCl 6M 360 min
Retained cations elution from foam	1:1 mixture of HCl 1M and C_2H_5OH		HCl 10^{-1}M	
The instrumental method used to determination of cations	Atomic absorption spectrometry	Atomic absorption spectrometry	Spectrophotometry	Spectrophotometry
The quantitative description of the retention process on the basis of Langmuir isotherm: - q_0 (mmole/g pretreated foam) (mg/g pretreated foam) - sorption constant, K_L	0,0322 1.8933 4.769	0,02272 2.4174 5,365	0,769 42.948 4.420	0,526 36.672 2,484

The thermodynamic characterization of the sorption process. -Gibbs free energy variation, ΔG, kJ/mol - sorption enthalpy, ΔH, kJ/mol - sorption entropy, ΔS, kJ/mol	-3,838	-4,127	-3,639	-2,235 17,960 0,066

Foam Impregnation

In order to impregnation with DMG or TBP, the purified (cut into cubes of about 5 mm edge) was equilibrated with the modifier agent. To ensure complete saturation, the cubes of foam were remained overnight in contact with DMG solution or the extractant agent(TBP). Then, to remove the excess of the modifier agent, the impregnated foam was washed. Finally, the DMG or TBP polyurethane sorbent was dried and kept in a dessicator.

General Sorption Procedure for Metallic Ions

To point out the major role of the modifier agent in the selective retention of microelements on polyurethane sorbents the following systems: polyurethane foam – DMG – Ni (II), polyurethane foam – DMG – Pd (II), polyurethane foam – TBP – Fe(III), polyurethane foam – TBP – Ga(III) have been studied. Weighed samples of about 0.1g of impregnated foam were equilibrated with volumes of 25mL aqueous solution containing known and variable amounts of metallic ions under study. (Ni(II), Pd(II), Fe(III) and Ga(III)). After a determined time of contact, at constant temperature, the phases were separated by filtration. The cation content in filtrate was determined by methods listed in Table 2.

3. Results and discussion

- "SPUMATIM" flexible open–cell polyurethane foam of polyether type impregnated with dimethylglyoxime was investigated as sorbent for Ni(II) and Pd(II) cations[17]. In order to establish the optimum conditions of Ni(II) and Pd(II) ions concentration and separation by forming chelates with dimethylglyoxime loaded polyurethane foam the influences of solution pH, contact time, cations concentration and foreign ions presence on batch sorption process have been studied (Table 2).
- The dependence between the concentration at equilibrium of the retained cations in the foam phase and metallic ions concentration at equilibrium in solution has been expressed by isotherms of Langmuir type.
- It is considered that sorption of Ni(II) and Pd(II) ions take place on large surface area of polyurethane foam modified with dimethylglyoxime by solid – liquid interactions.
- The presence of some cations such as Cu(II), Cd(II), Zn(II), Co(II) (Ni(II)/Pd(II):foreign ion ratio of 2:1) did not affect significantly Ni(II) and Pd(II) retention
- In good agreement with the stability domains of corresponding dimethylglyoximates in aqueous solutions, the obtained values for retention percentages of Ni(II) and Pd(II) on polyurethane sorbent are comparable.

- The characterization of the sorption process on the basis of distribution coefficients values indicate the high selectivity of dimethylglyoxime – polyurethane foam for Ni(II) in ammoniacal solutions and Pd(II) from strong acidic solutions.
- The obtained results point out the fact that by the sensible choice of the experimental conditions, concentrations of the Ni(II) and Pd(II) cations from diluted aqueous solutions, as well as their separations each other and from Cu(II), Cd(II), Zn(II), Co(II) by selective sorption on "SPUMATIM" flexible open–cell polyurethane foam of polyether type modified with dimethylglyoxime may be carried out.

➢ Although the Fe(III) and Ga(III) ions are well retained on untreated foam, the analytical performances of the cellular material in sorption of Fe(III) and Ga(III) traces were significantly improved by its impregnation with tri–n–butyl–phosphate [18-19].

- The effect of medium acidity, contact time, concentration of cations in external solutions and temperature has been studied in the batch sorption systems polyurethane foam–TBP–Fe(III) and polyurethane foam– TBP–Ga(III) (Table 2).
- The Fe(III) and Ga(III) distribution coefficients dependences on medium acidity(solutions of HCl until 8M concentrations) point out the existence of a good agreement between the behaviour of tri n butyl phosphate as stationary phase in liquid liquid chromatography on polyurethane foam solid support and the literature data concerning the liquid–liquid extraction of Fe(III) and Ga(III) with tri–n–butyl–phosphate.
- The proposed mechanism of oxonium type for extraction of Fe(III) and Ga (III) from solutions 4 6 Min HCl on polyurethane foam pretreated with tri n butyl phosphate was results obtained after the partial replacement of HCl with 4M NaCl.
- The quantitative characterization of the retention proces son the basis of Langmuir isotherm model indicated that the flexible polyether polyurethane foam loaded with tri–n–butyl–phosphate has a higher tendency to sorb Fe(III) than Ga (III) ions.
- For a thermodynamic description in polyurethane foam TBP Ga(III) HCl sorption systems, the ΔG, ΔH and ΔS values have been calculated [19]. The negative values of Gibbs free energy changes for three working temperatures (5^0C, 25^0C and 40^0C) show a reasonable affinity of TBP – polyurethane foam against Ga(III) (spontaneous process of sorption). The positive value of ΔH (variation of enthalpy accompanying the Ga(III) sorption indicates an endothermic process, facilitated by the temperature rising. The positive entropy changes (ΔS) characterize an increase in the disorder of the system on Ga(III) sorption by the polyurethane foam (probably due to the release of hydration water molecules surrounding the gallium ions).
- In dynamic conditions, the retention of Fe(III) on a column filled with polyurethane foam loaded with tri n butyl phosphate is quantitatively(99.3 99.9%) from hydrochloric solutions (4M) with an initial concentration 5.6 39.2 mg Fe(III) [18].
- The properties of an column packed with tri n butyl phosphate loaded polyurethane foam do not change significantly with time, the sorption capacity of Fe(III) being almost constant over 10 cycles of sorption desorption.
- The proposed method can be used for separation and concentration of trace amounts of iron, purification of some salts like: $AlCl_3$, $ZnCl_2$, $CuCl_2$, $MgCl_2$, $CaCl_2$, as well as hydrochloric acid.

Received April 24, 2007 *The "Gh.Asachi" Technical University Iaşi*

REFERENCES

1. T. Braun, A.B.Farag, *Anal.Chim.Acta*, 99,1-36, (1978)
2. C.Simionescu, C.Vasiliu-Oprea, V Bulacovschi, C.Negulianu, **„Chimie macromoleculara"**, Editura Didactica si Pedagogica, Bucuresti,1985
3. T Braun, J.D Navratil, A B.Farag, **Polyurethane Foam Sorbents in Separation Science**, CRC Press, Inc., Boca Raton, Florida, 1985
4. S.G.Dmitrienko, Y.A. Zolotov, *Russ. Chem. Rev. (U.S.S.R.)* 71(2) 159, (2002)
5. L.Tofan, D Bilba, A.Nacu, *Mat. Plast (Bucharest)* 31 (1994) 245
6. S G. Dmitrienko, L.N Pyatkova, Y.A. Zolotov, *J Anal. Chem.* 57(10) 875, (2002)
7. M.N.Abbas, N.B.El-Assy, S.Abdel Moniem, *Anal. Lett.* 22 ,1555, (1989)
8 S.G.Dmitrienko,E.N Shapovalova,M.V Kochetova,O.A Shpigun, Y A.Zolotov, *J. Anal. Chem.* 57(11) ,1009, (2002)
9. G.Dmitrienko, L.V.Goncharova, V.K.Runov, V.N. Zakharov, L.A.Aslanov, *Russ. J. Phys. Chem.*, 71(12) ,2014,(1997)
10. S Palagyi,T.Braun, **Elements and Inorganic Species on Solid Polyurethane Foam Sorbents in Preconcentration Techniques for Trace Elements**, CRC Press, Boca Raton Ann Arbor London, p 364, 1993
11. L.Tofan, D.Bilba, A.Nacu, C.Paduraru, *Mat. Plast. (Bucharest)*, 32,210, (1995)
12. A M.Elhosseiu, M.A Zaid, M.F.El-Shahat, *International Journal of Environmental and Analytical Chemistry*, 12(15) ,935, (2004)
13. M.M. Saeed, R. Ahmad, *Radiochim. Acta*, 93(6) ,333, (2005)
14. G.D.Matos, C.R T Tarley, S L C.Ferreira, M A.Z.Arruda, *Ecletica Quimica* 30(1) ,65, (2005)
15. T. A. Moawed, M.A A. Zaid, M F El-Shahat, *Acta Chromatographica* 15 220, (2005)
16. E.A. Moawed, *Acta Chromatographica*, 14 ,198, (2004)
17. L Tofan, C. Paduraru, D Bilba, A. Nacu, *Bull Polyt. Inst. (Jassy)*, tomul 36 ,31, (1996)
18. D.Bilba, L.Tofan, C. Paduraru, A.Nacu, *Rev. Roum Chim.* 43 ,493, (1998)
19. L.Tofan,. C.Paduraru, D.Bilba, O Toma, *Chemistry Journal of Moldova*, in press

SPUMĂ POLIURETANICĂ MODIFICATĂ FOLOSITĂ CA MATERIAL DE ABSORBȚIE ÎN ECOLOGIA

Rezumat: În ultimii ani spumele flexibile poliuretanice cu celule deschise au devenit solvenți din ce în ce mai accesibili și mai eficienți pentru un spectru larg de substanțe ionice și non-ionice lichide și gazoase. În acest context s-a studiat comportarea spumei poliuretanice flexibile "Spumatin" modificată prin adsorbția fizică de dimethylglioxim și tri-n-butlyl fosfat.

BULETINUL INSTITUTULUI POLITEHNIC DIN IAŞI
Tomul L(III (LVII), Fasc. 4, 2007
Secţia
ŞTIINŢA ŞI INGINERIA MATERIALELOR

THE INFLUENCE OF DIFUSSION ON THE ALLUMINIUM LAYERS ADERENCE DEPOSED BY THERMAL SPRAUING

BY

ST. L. TOMA, D.G. GĂLUŞCĂ, C. BEJINARIU and N. TIMOFTE

Abstract: In the succession of the formation phases of metallization layer we meet the next types of adherence: mechanical, metallurgical, spreading, superficial and physical. Each of these types action by a mechanism very precise. The way that these mechanisms are in contact, and the percent of each of them interfere in the formation process of the layer, con is influenced by: the metallisation way; the substrate material; the layer material; the proceedings after the metallization process. The paper has a purpose the influence determination of thermal treatment on the aluminum layers laid down using the thermal spray as a thermal processing after metallization.

Keywords: thermal spraying, adherence, and aluminum layer deposition.

1. Introduction

The deposition of aluminum by thermal spraying on different metal or nonmetal surfaces is a technologic method used to obtained new surfaces with high resistance on the corrosion and wear

The physical and mechanical proprieties of the coatings of aluminum lay down by thermal spraying, depend of the adherence of the laying material (named addition material) to the base materials (named substratum).

In the succession of the forming the stratum between the particles of the base and the addition materials we are meeting many types of adherences: mechanical, metallurgical, spreading, superficial and physical.

2. The technologic parameters of the metallization process. Thermal treatment.

The weight of them, you can find in system, influences the characteristics of the deposition start. Going on these reasons we suppose that the provocation of diffusions on the level stratum – substratum may go to the increasing of the weight of the adherence. That is why it will be a variation of the mechanic proprieties.

For the realization of the researching we choose as a support a low allied steel OLC 15 (STAS 880 – 88). We can find its composition in the table nr1. From this material we made cylinder tests Ø 32 x 70 mm.

Table 1

The substrate	Chemical composition [%]								
	C	Mn	Si	S	P	Cr	Ni	Mo	Cu
OLC 15	0,12 ÷ 0,18	0,3 ÷ 0,65	0,15 ÷ 0,37	0,002 ÷ 0,004	0,04	-	-	-	-

As a share material I choose wire aluminum of metallization like ST 99,5 having the chemical composition 99% Al and 0,5% Cu.

The laying was realized using the metallic by spraying with electric arc using a manual pistol metallization with two wires, type PME, realized by IOR – Bucharest.

The metallization installation has a drive a and rewind disposition of the wire, a rectifying welding RSC 400 and steam roller with needles filter.

The protection system made, fig. 1, was:

- One layer (realized in on pass);
- Many layers realized in two or three succeeded passes.

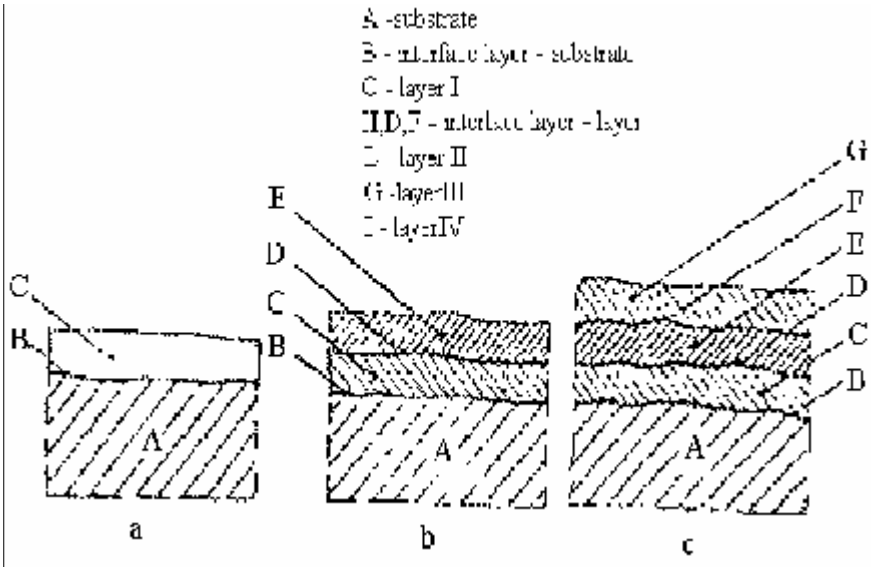

Fig. 1 The protection system: a) one layer; b,c) many layers

For the execution of these researches I realized about 48 cylinder tests.

Their surface under the metallization were cleaned mechanic in the purpose of eliminating the oxides, the dust, fats or other change tings by sandblasting with a sand jet silica. The work parameters used are:

- the work pressure:	3 atm.
- sand granulation:	1 5 mm
- the incidental angle of the sand between the normal on the surface:	50^0-70^0

Then the surface substratum was wormed up at 120^0 C, in an electric furnace of the thermal treatment having a thermocouple determining the temperature.

The work condition of the metallization by thermal spraying in electric arc were are were table 2.

The metallising tests by thermal spraying where subdued to a very attentive control macroscopic with a lentil having a power 10 x, to eliminate during the researching the tests with surface faults like a exfoliation

The thickness of the layer obtained was determined by measurement using the accuracy micrometer in three different points on the same axe

In the table no.3 you will find the values of the thickness of the layers attained.

Table 2.

Parameters	Cylindrical tests	
	Layer 1	Layer 2,3,4
The distance layer – substratum [mm]	80	120
The rotation speed of the universal [rot./min]	105	63
The mooring speed of the pistol [m/min]	1,9	1.6
The diameter of the wire of Al [mm]	1,2	1.2
The pressure of the compressed air [at]	5,5	6.5
The force of the meting current [A]	180	190
The preheating temperature of the substratum [°C]	120	120
Inclination angle of the spraying jet given the perpendicular line on the surfaces [grad]	15	0
The advancement speed of the wires [m/min]	2	2,5

Table 3.

No. of passes	Type of proof	g [mm]
I	cylindrical	0,25
	cylindrical	0,28
II	cylindrical	1,47
	cylindrical	1,56
III	cylindrical	2,26
	cylindrical	2,71
IV	cylindrical	3,36
	cylindrical	3,97

After metallisation a number of 24 cylinder tests having different thickness were subdued to a thermal treatment the diffusion – diagram fig.2, in a electrical furnace with induction heating.

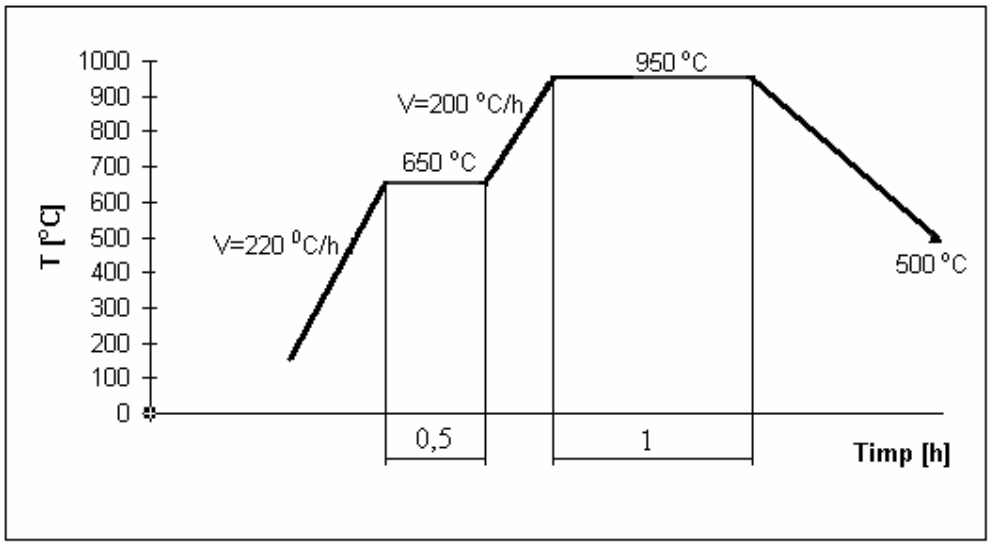

Fig.2 Thermal treatment diagram

The aluminum layer on the proof was covered with a $Na_2SiO_2x9H_2O$ solution to be protected of the atmosphere from the furnace.

Figure 3 presents microstructures of the structure metal sprayed diffused sample.

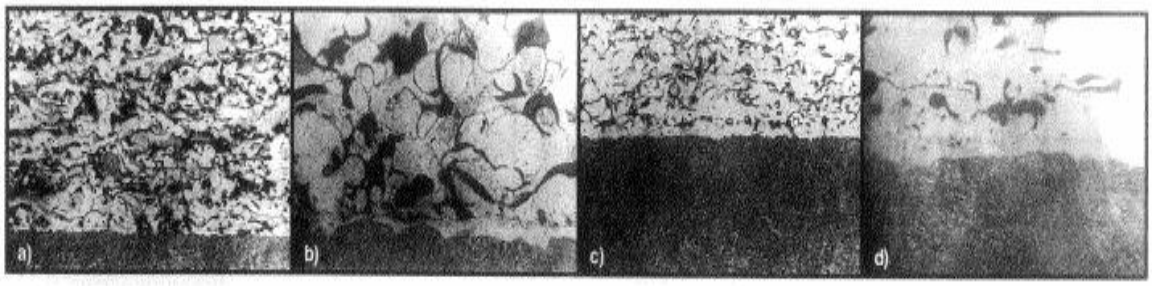

Fig.3 Microstructure, metal sprayed diffused sample: base OLC15, deposed layer Al (ST 99,5); multiplication 100x (a,c) and 400x (b,d); 5% attack nital

3. The experimental determination of the shear strength of the aluminum layers thermal treatment or non-treatment.

To research the influence of the spreading thermal treatment on the adherence of aluminum layers attained by thermal spraying I considered eloquent, the comparison of adherence layers value moralized and non thermal treatment, with the adherence layers having the some thickness but treatment

For the cylinder tests the adherence was determinate by shear strength like in STAS 11684/$_1$ – 83. The specimen types used are presented in the fig.4

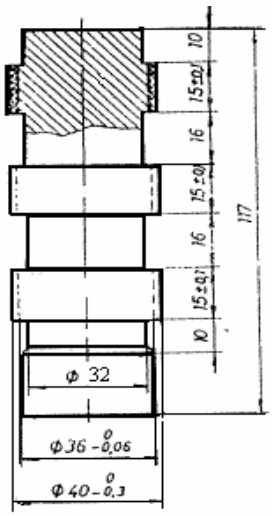

Fig.4 Sample for the determination of the adherence by shear strength

Figure 5 presents macrostructure oh the metal-sprayed samples with diffusion.

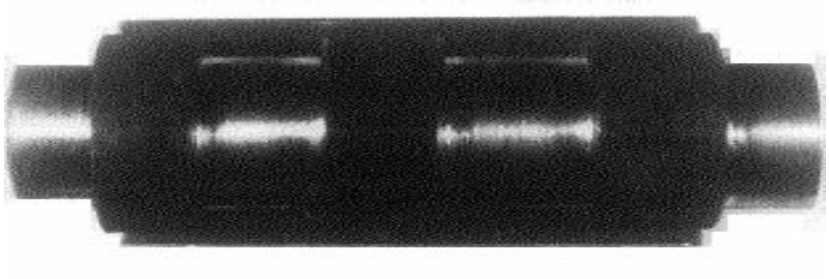

Fig.5 Sample for the adherence testing of the deposited layer before shear strength testing.

The adherence by shear strength can be determinated with:

$$\tau_{cf} \quad \frac{F_{max}}{S} \ [N/mm^2]$$

where: F_{max} - the maximum compression force appliqued to the test [N];

S - the cross section of the ring [mm^2].

I excludes from these researching those tests where the breaking was between deposes layers.

Figure 6 presents the sample for the adherence testing of the deposited layer.

Fig.6 Sample for the adherence testing of the deposited layer after shear strength testing.

The results obtained are in the table no.4

Table 4.

Number of othe layer	Non treatment layer				Treat treatment layer			
	g [mm]	S [mm^2]	F [N]	τ_{rd} [N/mm^2]	g [mm]	D [mm^2]	F [N]	τ_{rd} [N/mm^2]
I	0,25	25,31	932	36,82	0,25	25,31	989	39,07
	0,28	28,38	962	33,89	0,28	28,38	1017	35,83
II	1,47	154,49	1655	10,71	1,47	154,49	1835	12,52
	1,56	164,39	1842	11,20	1,56	164,39	1987	12,08
III	2,26	243,12	2150	8,84	2,26	243,12	2442	10,04
	2,71	295,36	2749	9,306	2,71	295,36	2915	9,86
IV	3,36	373,06	3227	8,65	3,36	373,06	3310	8,87
	3,97	448,39	3617	8,06	3,97	448,39	3695	8,24

In the figure 7 presented the shear strength, depending on the layer thickness, determined both for the treat sample and no treats one

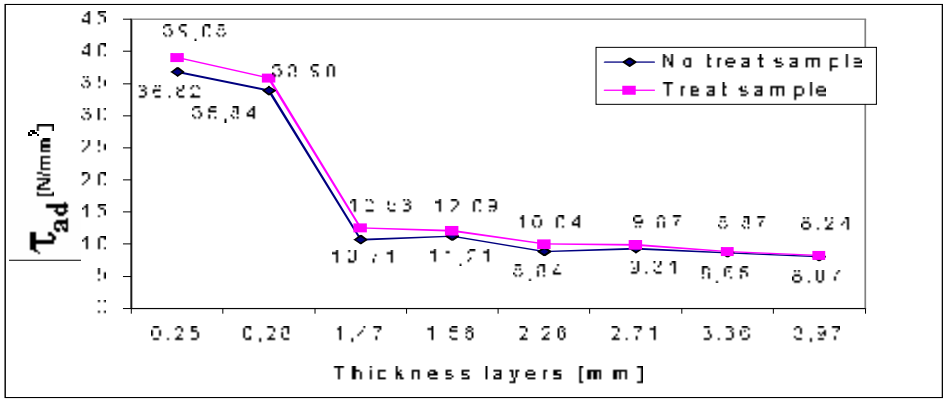

Fig.7 The shear strength

3. Conclusions:

After this thermal treatment we noticed:

- Some of cylinder tests whose thickness was bigger then 2,5 mm have zonal exfoliation in the aluminum layers and the level layer – substratum. I excluded from my researching those tests, which present exfoliation at the level layer substratum.
- Proof whose thickness was less than 1 mm, after the spread thermal treatment had the surfaces very exfoliation by removing the metallic layer the substratum remained powerful allied.
- For little thickness of the depose layer we observe a meaningful growth of the adherence obtained after thermal metallisation. This aspect demonstrated that in layers with little thickness prevails the spreading adherence
- The tests with the thickness between 1 – 2,5 mm had a very good behaved at this spread thermal treatment. They haven't on their surface traces of exfoliation. Also in their composition we observe a less porosity.

The main element to realize equilibrium is the spreading of aluminum in iron, but il also appear the spreading of iron in aluminum. To the tests with the thickness less than 2,5 mm after the microscope analyses, I establish the disappearance of the delimitation between.

Received April 23, 2007 *The "Gh.Asachi" Technical University Iaşi*

REFERENCES

1. Alexandru I., Popovici R. ş.a. - **Alegerea şi utilizarea materialelor metalice**. Editura Didactică şi Pedagocică - R.A Bucureşti 1997
2. *** - **The thermal spray technology leader** - Tafa, 2002
3. *** - *Thermol Spray Buyes Guide* - **National Thermal Spray Conferens** - In Advansed Materials & Preocesses ASM - International Nr 5, Vol. 145, mai 2004.

INFLUENŢA DIFUZIEI ASUPRA ADERENŢEI STRATURILOR DE ALUMINIU DEPUSE PRIN PULVERIZARE TERMICĂ

Rezumat: În succesiunea de formare a unui strat metalizat se întâlnesc următoarele tipuri de aderenţă: mecanică, metalurgică, difuzivă, superficială şi fizică. Fiecare din aceste tipuri acţionează după un mecanism bine precizat. Modul în care acţionează aceste mecanisme, precum şi ponderea cu care ele intervin în procesul de formare a stratului pot fi influenţate de procedeul de metalizare, materialul substratului, materialul stratului, prelucrările ulterioare procesului de metalizare. Lucrarea are ca scop determinarea influenţei tratamentului termic de difuzie asupra aderenţei difuzive a straturilor de aluminiu obţinute prin pulverizare termică.

BULETINUL INSTITUTULUI POLITEHNIC DIN IAŞI
Tomul LIII (LVII), Fasc. 4, 2007
Secţia
ŞTIINŢA ŞI INGINERIA MATERIALELOR

THE DETERMINATION OF THE SPECIFIC EQUATION AT THE IMPACT BETWEEN A TRUNCATED SPHERICAL LIQUID DROPLET AND A FLAT SURFACE

BY

ST. L. TOMA, D.G. GĂLUŞCĂ, C. BACIU and M. SUSAN

Abstract: The impact between a metallic liquid droplet and a flat surface is influenced by several factors, such as: the superficial tension which exists on the droplet - substrate interface, the superficial tension on the droplet - air interface, the velocity and droplet viscosity. The paper propose is to determinate of specifically equation at the impact between a melting droplet (at truncated sphere) and a flat surface at metallization by thermal spraying. The mathematical model exposed allows to calculate the droplet height in a time unit; ar; the contact radius between the drop and substrate.

Keywords: droplet, velocity, kinetic energy, potential energy, mechanical works.

1. Introduction

Liquid drop impact with a solid surface has been a topic of interest in many different engineering applications. The impact analyses between a liquid droplet and the substrate can be approached using mathematical models based on the mechanical fluids theory, the law of energy conservation, of impulse and mass conservation. I would like to obtain this analyze using the analyses models based on the Langrage equations, with the correct assumptions regarding the droplet deformation, assuming that the droplet has a spherical shape, and during the impact its geometrical shape is a sphere calotte fig.1-a and its height (λ_1) is modified in a proportional reverse with the impact period.

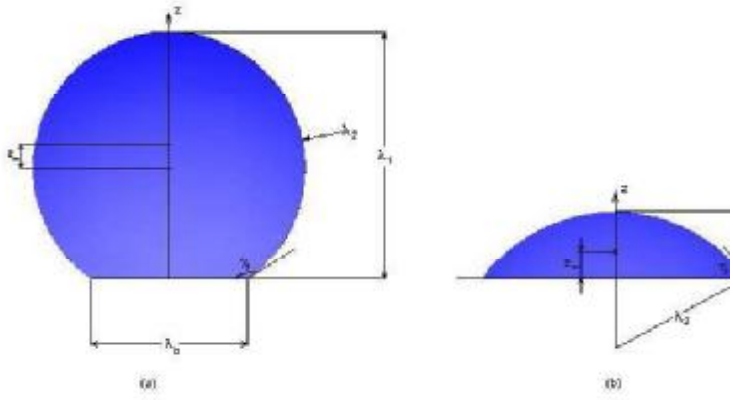

Fig.1 The particle deformation: a) During the impact (the impact), b) After the impact

I consider that after the impact the particle is spreading on the substrate surfaces taking its disk geometrical shape, fig. 1- b, known in the specialty literature as the pancake. In function of the particle velocity at the impact moment and with the superficial tension and viscosity, the drop can remain stuck on surface, can rebound or it can divide itself in smaller particles.

Watcher and Westerling have experimentally demonstrated that in the case of a liquid droplet which hit the surface of substrate, if the Weber number –relation 2.1, is We>80 then the droplets are spreading on the substrate surface. Similar observations were made by Styricovich and Pederson.

$$W_e = \frac{\rho_p \cdot d_p \cdot v^2}{\sigma_p} \qquad (1)$$

where: ρ_p – the density of the fluid particle; [g/mm^3]
d_p the initial diameter of the particle; [mm]
v – the particle velocity; [m/s]
σ_p the superficial tension of the particle. [N/mm^2]

To analyze the impact between the particle and surface substrate I shall consider that its target surface is flat, rigid, and impenetrable, and I shall try to define the particle height as a function of time under some differential equations means, depending on the: Weber number, superficial tension and viscosity. The solutions of these equations solving allow the determination of height (λ_1) in every moment of impact. The variation of the impact pressure, regarding the time, can be calculated using the energy conservation law In the energetic calculation I shall include different values for superficial tension which exists at the interface level droplet substrate, the existed superficial tension at the separation surface particle droplet and particle viscosity.

2. Problem formulation

Initial I assume that the spherical particle of initial diameter d_p- and surface superficial tension „σ_a" (in air), impacts free substrate surface with the velocity v_p. I neglect the interaction between the particle and the air (the compressed air) and I assume that during the impact the particle volume is constant, and at the interface particle exists the superficial tension σ_i. We choose a system of cylindrical axis zOr with the origin in the first contact point of the particle with the substrate surface, fig.2.1.a. We adopt the next notations regarding the geometrical dimensions of particle during the impact:

- λ_1-the particle height during the λ impact (mm);
- λ_2-the radius of truncated particle (mm);
- z_m the location of the mass centre (mm);
- λb- the contact circle radius between the particle and the substrate (mm);
- d_p – the initial diameter of the particle

The geometry of the sphere calotte is determinate by:

The height λ_1, which represents the maximum distance between the surface substrate and furthest point from the particles surface;

The parameter z_m gives information about the location of the mass centre
The value of z_m allows us to determine very precisely the geometrical shape of the particle during the impact. This value $z_m=\lambda_2$ demonstrates that the particle has no contact with the substrate surface. In these conditions we define the dimensionless factor:

$$x=\frac{\lambda_1}{d_p} \tag{2}$$

Using the geometrical elements of the sphere calotte (fig. 1), we can suppose the next relations:

$$\frac{\lambda_2}{d_p}=\frac{x\cdot(2+x^3)}{6}=N(x) \tag{3}$$

In these conditions the coordinates of the mass center are: $x_m=0$, $y_m=0$, $z_m=\frac{2\cdot x+x^4}{6}\cdot d_p$.

We note the report:

$$M(x)\quad\frac{z_m}{d_p}\quad\frac{2\cdot x+x^4}{6} \tag{4}$$

The relationship between the geometric parameters λ_1 and z_m represents a measure of the drop deformation. The drop volume V free surface area A during the deformation and the contact area A_b are given by the relations:

$$V\quad\frac{\pi\cdot d_p^3}{6} \tag{5}$$

$$A\quad 2\cdot\pi\cdot\lambda_1\cdot\lambda_2 \tag{6}$$

$$A_b\quad\pi\cdot(2\cdot\lambda_1\cdot\lambda_2\quad\lambda_1^2) \tag{7}$$

Initially, when the spherical drop first touches the target surface, the paremeters defined above have the values: $\lambda_1^0\quad d_p;\lambda_2^0\quad d_p/2;\lambda_b^0\quad 0;z_m^0\quad d_p/2;A^0\quad\pi\cdot d_p^2;A_b^0\quad 0$ and represents the boundary conditions.
The potential energy (Ep) of the drop can be expressed as a function of superficial tension which exists on the free surface (σ_p) and the superficial tension which appear at the interface drop substrate (σ_{ls}):

$$E_p=\sigma_p\cdot A+\sigma_b\cdot A_b \tag{8}$$

We substitute 2 - 7 in the relation 8 and after the simpification we shall obtain the relation:

$$E_p=\frac{\sigma_p\cdot d_p^2\cdot\pi}{3}\cdot\left(2\cdot x^2+x^{-1}+\frac{\sigma_b}{\sigma_p}\left(x^{-1}\quad x^2\right)\right)=\sigma_p\cdot d_p^2\cdot L(x) \tag{9}$$

where: $$L(x) \quad \frac{\pi}{3}\cdot\left(2\cdot x^2 + x^{-1} + \frac{\sigma_s}{\sigma_p}\left(x^{-1} \quad x^2\right)\right) \tag{10}$$

The kinetic energy of the droplet is expressed as a function of radious flow velocity (v_r) and the flow velocity along the O_z direction and density by the relation:

$$E_c = \frac{1}{2}\cdot m_p \cdot v^2 \quad \frac{1}{2}\cdot\rho\cdot\int_V \left(v_r^2 + v_z^2\right)dV -$$
$$\frac{1}{2}\cdot\rho_p\cdot\left[\frac{M'(x)}{M(x)}\cdot\frac{dx}{dt}\right]^2\cdot\int_V (z^2 + r^2/4)\cdot dV \quad \rho_p\cdot V\cdot d_p^2\cdot A(x)\cdot\left(\frac{dx}{dt}\right)^2 \tag{11}$$

Where: $$A(x) \quad \left[\frac{M'(x)}{M(x)}\right]^2\left(\frac{13x^5}{180} + \frac{11x^2}{144} + \frac{x^{-1}}{72}\right)$$

In the above relation I assume that for z = 0, r = 0 the elementary particles are ideal stationary and irrotationaly having an axisymetric distribution:

$$v_r \quad \frac{1}{2}\cdot\frac{M'(x)}{M(x)}\cdot\frac{dx}{dt}\cdot r \tag{12}$$

$$v_z \quad \frac{dz_m}{dt} + \frac{M'(x)}{M(x)}\cdot\frac{dx}{dt}\cdot(z \quad z_m) \tag{13}$$

This axisymetric velocity field clearly satisfies the condition:

$$\frac{1}{r}\frac{\partial(r\cdot v_r)}{\partial r} + \frac{\partial v_z}{\partial z} - 0 \tag{14}$$

$$\frac{\partial v_r}{\partial z} - \frac{\partial v_z}{\partial r} \quad 0 \tag{15}$$

The velocity field has also a stagnation point at the origin which satisfies the inviscid boundary condition at z =0. From the equations 12, 13 14 and 15 we shall obtain:

$$v_r(0,0,t) \quad 0; \qquad v_z(0,0,t) \quad 0 \qquad v_z(r,0,t) \quad 0. \tag{16}$$

In these conditions the velocity fields is a physics measure specific for the drop deformation, realizing the coupling between the flow field and mass centre.

It is found experimentally that drop splatter occurs for W_e>80, so our analyze was restricted to Weber numbers below this value We<80.

$$F_p - \sigma_p\cdot A + \sigma_s\cdot A_s \tag{17}$$

During the impact, we consider an element with a unitary volume which is deformed in a very short time, for which we can affirm that the difference between the variation of kinetic energy and potential energy is transformed in a mechanical works (L_u), necessary to defeat the friction force which exists on the interface droplet – substrate

$$\Delta E_c - \Delta E_p \quad L_u \tag{18}$$

The mechanical work (Lu) can be expressed in function of the tension that exists on the interface droplet substrate (τ), the radial displacement on the contact surface of the drop, of a volume element, Δd_1, and the elementary area of the drop which is at the contact with the substrate surface

$$L_u \quad \tau \cdot \Delta d_r \cdot dA \tag{19}$$

For an interval of time between t_1 and t_2 we can write that:

$$\int_{t_1}^{t_2}\left[\Delta(E_c \quad E_p) \quad \int_{A}\tau \cdot \Delta d_r \cdot dA\right]dt \quad 0 \tag{20}$$

Because the existent velocity field it doesn't determine the friction forces we can consider that for z = 0 the shear stress is proportional with v_r and with the viscosityof liqued drop and with the constant ξ and inverse proportional with the height drop.

$$\tau \quad \xi \cdot \mu \cdot v_r \tag{21}$$

The radial displacement Δd_r associated with radial component of velocity v_r has the expression;

$$\Delta d_r \quad \frac{1}{2}\ln[M(x)] \cdot r \tag{22}$$

By substituting the:

$$2 \cdot A(x) \cdot \frac{d^2x}{dt^2} + A'(x)\left(\frac{dx}{dt}\right)^2 + \frac{\mu \cdot c}{12 \cdot \rho_p \cdot d_p} B(x)\frac{dx}{dt} + \frac{\sigma_p}{\rho_p \cdot V} L'(x) \quad 0 \tag{23}$$

Which has the initial conditions:

$$x(0) \quad 1. \quad \left.\frac{dx}{dt}\right|_{t=0} \quad \frac{v}{d_p} \tag{24}$$

In which equation 23, A(x) it describes the kinetic energy expression, L'(x) describes the derivative of the potential energy, M(x) gives us information about the drop height, and the B(x) function derives from the dissipation equation of energy –relation nr. 20. And has the expression:

$$B(x) = \left|\frac{M'(x)}{M(x)}\right|^2 \cdot \left(x^4 \quad 2x \quad x^2\right) \tag{23}$$

3. Conclusions

The expression no 23 represents the differential equation wich caracterize the impact between a truncated liquid sferical droplet and the substrate surface.
We obtain the equation 23 in the next condition:
- the droplet is spherical and the initially diameter„d_p", the density „ρ_p" and the superficial tension „σ_a" (in air);
- during the impact droplet is as truncated sphere;
- the droplet volume is constant;
- the droplet is bounding free the substrate surface with the velocity „v_p";
- the interaction between the troplet and the air is negleted;
- at the interaction between the droplet and the substrate there is a superficial tension

The resolution the equation 23 allows us to determinate the height variation of the droplet in time, in function of superficial tension (σ_a and σ_h) viscosity and velocity.

Received April 27, 2007 *The "Gh.Asachi" Technical University Iaşi*

REFERENCES

1. Hunges, L.S. and Yaro, S.C., "*Experimental investigation of the impaction of water droplets on cylindrical objects*," **Int. J. of Multiphase Flow**, **25**, 1545-1559, 2001.
2. Stephen Wolfram - **The Mathematica book** – 5thed – 2005
3. Mourougou-Candoni, N., Prunet-Foch, B., Legay, F., Vignes-Adler, M. and Wong, K., *Influence of dynamic surface tension on the spreading of surfactant solution droplets impacting onto a low-surface-energy solid substrate*, **J. Coll. Int. Sci.**, 192:129, 1997.

DETERMINAREA ECUAȚIILOR SPECIFICE LA IMPACTUL DINTRE O PARTICULĂ SFERICĂ, LICHIDĂ ȘI O SUPRAFAȚĂ PLANĂ

Rezumat: Impactul dintre o particulă de metal topit şi o suprafaţă plană este influenţat de o serie de factori cum ar fi tensiunea superficială existentă la interfaţa particulă – substrat, tensiunea superficială existentă la interfaţa particulă – aer, viteza şi vâscozitatea particulei. Lucrarea are ca scop determinarea ecuaţiilor specifice existente la impactul dintre o particulă topită (sub formă de calotă sferică) şi suprafaţa plană a substratului. Ecuaţiile matematice determinate permit calcularea variaţiei înălţimii particulei în unitate de timp, a razei de contact dintre particulă şi substrat în funcţie de vâscozitatea, tensiunea superficială şi viteza particulei în momentul impactului.

BULETINUL INSTITUTULUI POLITEHNIC DIN IAŞI
Tomul L(III (LVII), Fasc. 4, 2007
Secţia
ŞTIINŢA ŞI INGINERIA MATERIALELOR

THEORETICAL CONSIDERATIONS REGARDING TO THE SUPERFICIAL TENSION INFLUENCE ON THE CONTACT BETWEEN A MELTING DROPLET AND A FLAT SURFACE

BY

ST. L. TOMA, D.G. GĂLUŞCĂ, C. BACIU, M. SUSAN and C. BEJINARIU

Abstract: The impact between a metallic liquid droplet and a flat surface is influenced by several factors, such as: the superficial tension which exists on the droplet - substrate interface, the superficial tension on the droplet - air interface, the velocity and droplet viscosity. The purpose of this paper is to a present a mathematical model to illustrate the superficial tension influence on droplet behavior after the impact (the droplet is thermal sprayed on a flat surface). The mathematical model exposed allows to calculate the droplet height in a time unit, an the contact radius between the drop and substrate. The contact radius value is compared with the experimentally results from the technical literature.

Keywords: superficial tension, impact, melting droplet, and thermal spraying.

1. Introduction

The impact between a metallic liquid droplet and a flat surface is influenced by several factors, such as: the superficial tension which exists on the droplet - substrate interface, the superficial tension on the droplet - air interface, the velocity and droplet viscosity.

During the impact, a droplet is characterized by kinetic and potential energy and I consider an element with a unitary volume which is deforming in a very short time, for which we can affirm that the difference between the variation of kinetic energy and potential energy is transforming in a mechanical works (L_m), necessary to defeat the friction force which exists on the interface droplet – substrate. By using the variation energy law I obtain:

$$\Delta E_c \quad \Delta E_p \quad L_u \tag{1}$$

Where: ΔE_c –kinetic energy variation

ΔE_p – potential energy variation

L_u – mechanical works necessary to defeat the friction force which exists on the interface droplet – substrate

Initially, when the spherical drop first touches the target surface, the parameters defined above have the values: $\lambda_1^0 - d_p; \lambda_2^0 - d_p/2; \lambda_3^0 - 0; z_m^0 - d_p/2; A^0 - \pi \cdot d_p^2; A_s^0 - 0$

(λ_1-the particle height during the λ impact, λ_2-the radius of truncated particle, λ_3- the contact circle radius between the particle and the substrate).

The potential energy (Ep) of the drop can be expressed as a function of superficial tension which exists on the free surface (σ_p) and the superficial tension which appear at the interface drop substrate (σ_{ls}):

$$F_p = \sigma_p \cdot A + \sigma_b \cdot A_b \tag{2}$$

We substitute in the relation 8 and after the simpification we shall obtain the relation:

$$L_p = \frac{\sigma_p \cdot d_p^2 \cdot \pi}{3} \cdot \left[2 \cdot x^2 + x^{-1} + \frac{\sigma_b}{\sigma_p} \left(x^{-1} - x^2 \right) \right] = \sigma_p \cdot d_p^2 \cdot L(x) \tag{3}$$

where:

$$L(x) = \frac{\pi}{3} \cdot \left[2 \cdot x^2 + x^{-1} + \frac{\sigma_b}{\sigma_p} \left(x^{-1} - x^2 \right) \right] \tag{4}$$

The kinetic energy of the droplet is expressed as a function of radious flow velocity (v_r) and the flow velocity along the O_z direction and density by the relation:

$$E_c = \frac{1}{2} \cdot m_p \cdot v^2 = \frac{1}{2} \cdot \rho \cdot \int_V \left(v_r^2 + v_z^2 \right) dV$$

$$E_c = \frac{1}{2} \cdot \rho_p \cdot \left[\frac{M'(x)}{M(x)} \cdot \frac{dx}{dt} \right]^2 \cdot \int_V (z^2 + r^2/4) \cdot dV = \rho_p \cdot V \cdot d_p^2 \cdot A(x) \cdot \left(\frac{dx}{dt} \right)^2 \tag{5}$$

Where: $A(x) = \left[\frac{M'(x)}{M(x)} \right]^2 \left(\frac{13x^2}{180} + \frac{11x^2}{144} + \frac{x^{-1}}{72} \right)$;

x - the dimensionless factor, $x = \frac{\lambda_1}{d_p}$;

z_m - the location of the mass centre, $z_m = \frac{2 \cdot x + x^4}{6} \cdot d_p$;

d_p - the initial diameter of the particle

In the above relation I assume that for z = 0, r = 0 the elementary particles are ideal stationary and irrotationaly having an axisymetric distribution.

In these conditions the velocity fields is a physics measure specific for the drop deformation, realizing the coupling between the flow field and mass center.

It is found experimentally that drop splatter occurs for W_e>80, so our analyze was restricted to Weber numbers below this value We<80.

The mechanical work (Lu) can be expressed in function of the tension that exists on the interface droplet – substrate (τ), the radial displacement on the contact surface of the drop, of a volume element, Δd_1, and the elementary area of the drop which is at the contact with the substrate surface (dA).

$$L_u = \tau \cdot \Delta d_r \cdot dA \tag{6}$$

2. Solving the specific equation of the impact

For an interval of time between t_1 andt_2 we can write that:

$$\int_{t_1}^{t_2} \left[\Delta (E_c - E_p) - \int_A \tau \cdot \Delta d_r \cdot dA \right] dt = 0 \tag{7}$$

Because the existent velocity field it doesn't determine the friction forces we can consider that for z = 0 the shear stress is proportional with v_r and with the viscosityof liqued drop and with the constant ξ and inverse proportional with the height drop.

$$\tau = \xi \cdot \mu \cdot v_r \tag{8}$$

The radial displacement Δd_r associated with radial component of velocity v_r has the expression:

$$\Delta d_r = -\frac{1}{2}\ln[M(x)] \cdot r \tag{9}$$

By substituting the:

$$2 \cdot A(x) \cdot \frac{d^2x}{dt^2} + A'(x)\left(\frac{dx}{dt}\right)^2 + \frac{\mu \cdot c}{12 \cdot \rho_p \cdot d_p} B(x)\frac{dx}{dt} + \frac{\sigma_p}{\rho_p \cdot V} L'(x) = 0 \tag{10}$$

Which has the initial conditions:

$$x(0) = 1, \quad \left.\frac{dx}{dt}\right|_{t=0} = -\frac{v}{d_p} \tag{11}$$

In which equation 12, A(x) it describes the kinetic energy expression, L'(x) describes the derivative of the potential energy, M(x) gives us information about the drop height, and the B(x) function derives from the dissipation equation of energy –relation nr. 10. And has the expression:

$$B(x) = \left[\frac{M'(x)}{M(x)}\right]^2 \cdot \left(x^4 - 2x + x^{-2}\right) \tag{12}$$

We shall introduce in our calcule dimensionless time t^* and surface tension and viscosity parameters TS and VIS respectively throught:

$$t^* = \frac{t}{\left(\frac{\rho_p \cdot d_p^3}{\sigma_p}\right)^{\frac{1}{2}}} \tag{13}$$

$$TS = \frac{\sigma_r}{\sigma_p} \tag{14}$$

$$VIS = \frac{d_p \cdot \xi}{12} \cdot \frac{W^{\frac{1}{2}}}{R_e} \tag{15}$$

Where: R_e is a Reynolds number defined by:

$$R_e = \frac{\rho_p \cdot d_p \cdot v}{\mu} \tag{16}$$

And ξ is constant element which has to create boundary layer effect so $\xi = 0$-1. ($\xi = 0$ in the fluid and $\xi = 1$ at the interface drop – substrate).

We shall try to reduce the second order differential equation to a first order system of differential equations:

$$\begin{cases} \dot{x} = y \\ \dot{y} = \dfrac{-[C(x)y^2 + D(x) \cdot y + E(x)]}{2 \cdot A(x)} \end{cases} \tag{17}$$

Where: $\dot{x}$ - represents the x differential obtained by intrioducing t^*;
C(x), D(x) and E(x) are given by the expressions 28, 29 and 30

$$C(x)=\left(\frac{13x^{-1}}{36}+\frac{11x}{72}+\frac{x^{-2}}{72}\right)\cdot\left(\frac{1}{3}-\frac{2x^{3}}{3}\right)\cdot\left(\frac{x}{3}+\frac{x^{-1}}{6}\right)+\left(\frac{13x^{2}}{90}-\frac{11x^{2}}{72}-\frac{x^{-1}}{36}\right)\cdot\left(\frac{1}{3}+\frac{2x^{3}}{3}\right)-2x^{2}\left(\frac{x}{3}+\frac{x^{-1}}{6}\right)\cdot\left(\frac{1}{3}+\frac{2x^{3}}{3}\right)^{2}-\left(\frac{x}{3}+\frac{x^{-1}}{6}\right)^{3} \tag{18}$$

$$D(x)=VIS\cdot(x^{-4}-2x+x^{-2})\cdot\left(\frac{1}{3}+\frac{2x^{3}}{3}\right)\left(\frac{x}{3}+\frac{x^{-1}}{6}\right)^{2} \tag{19}$$

$$E(x)=2\left[4x-x^{-2}-TS\cdot(2x+x^{-2})\right] \tag{20}$$

The boundary conditions for the system no 17 is:

$$x(0)=1, \qquad y(0)=-W^{1/2} \tag{21}$$

The differential system (17)-(21) was solved numerically by use of a Runge-Kutta method for several values of the parameters *W*, *TS*, and VIS. The parameter *We* – Weber number, is a measure of the impact velocity. The parameter *TS* is the ratio of the surface tensions on the contact surface and free surface. The equilibrium shape of the drop, if it remains on the surface, is expressible in terms of this parameter, since from (4) the equilibrium drop height, $\bar{x}$, is given by:

$$L'(x)=0, \tag{25}$$

which implies

$$\bar{x}=\left[\frac{(1+TS)}{2(2-TS)}\right]^{-\frac{1}{3}} \tag{26}$$

This drop height is in agreement with that given by a truncated sphere with a static meniscus contact angle γ_s (see Fig. 1) related to TS by

$$\cos\gamma_s=-TS \tag{27}$$

The parameter VIS is defined in (15) in terms of W, R, and an unknown constant C that introduces an effect similar to a boundary layer. We have not tried to determine a value for this constant. The inviscid case is represented by C = 0. In the numerical computations we merely chose values of VIS to observe the effect of viscosity.

Going from the relations no. 13, 14,15, and using the Weber number (We) Reynolds number we shall obtain:

$$VIS=\frac{\sqrt{\pi}}{12}\left(\frac{W_e^{1}}{R_e}\right)^{\frac{1}{2}}=\frac{\sqrt{\pi}}{12}\left(\frac{\mu^{2}}{\rho_l\cdot d_s\cdot\sigma_s}\right)^{\frac{1}{4}} \tag{28}$$

For impact specific applications between a metal liquid drop with a flat heated surface the maximum value of VIS parameter is VIS = 0,1. This constant represents a value enough height of the energy amortization in the numerical results already showed.

In the numerical calculations made to obtained height drop variation during the impact x-function of time t* we gave values to VIS parameter and Weber number (VIS =0, W_e =1) and we obtained, for different TS values in the range 1-1.5,the variation curves which are presentated in fig. 2.

The curves indicated in fig. 3 express the dependencebetween the height drop-x, and the time during contact-t* and they are obtained for VIS = 0, three different values of TS (0.5; -0.5; -0.866), and for four different values for Weber number W_e (1; 2; 4; 9)corresponding to each considerate values for TS.

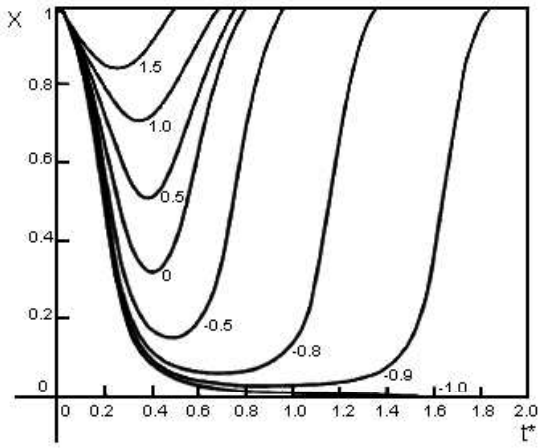

Fig. 2 The drop spreading height (x) in function of time during contact (expressed by the temporal term t) for various TS with W_e 1 and VIS 0.*

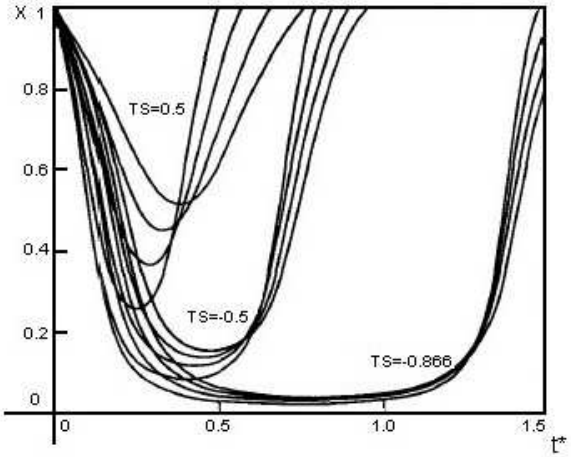

Fig. 3 The drop height (x) in function of time during contact (expressed by temporal term t) for VIS 0 and W_e 1, 2, 4, 9, various TS.*

The varition range of the temporal parameter **t*** is:
-t*∈ [0, 2] for the fig.2
-t*← [0, 1.5] –for fig. 3

3. Conclusions

In the static conditions the contact angle defined with the relation 34 can be: $\gamma_s - 180^0$ for TS = 1; $\gamma_s - 90^0$ for TS = 0; $\gamma_s - 0^0$ for TS = -1. For $|TS| > 1$ there is no interpretation in terms witch correspond to the static contact angle.

The figure 2 indicate that after impact the drop height decreases to minimum, and then it can return to the initial sphere shape (x = 1).The rebounding effect can be also obtained for TS > -1. for which the static contact angle is 0,the liquid particle continue to spread itself and it doesn`t rebound. From fig.2 you can observe that the minimum height of the drop depends to parameter value TS.

Figure 3 shows that the dependence between the drop height and the impact time is strongly influenced by the dimensinless parameter of superficial tension TS than the dimensinless parameter of viscosity VIS.

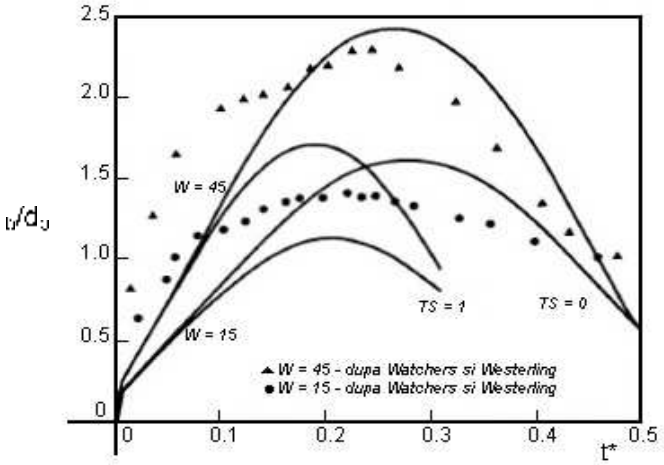

Fig. 4 The contact circle radius between the particle and the substrate - λ_s, definite in λ_s/d_0, in function of time during contact (expressed by temporal term t) - for WS 0, TS 0, 1, W – 15, 45' - curves continue is theoretical results; curves interrupted is experimental results obtains of Watchers and Westerling*

Also shown on Fig. 4 are the experimental results of Wachters and Westerling [3]. It is clear from these results that the $TS = 0$ curves correspond more closely to experiment than do the $TS = 1$ curves. It is expected that the surface tension next to the 400°C surface would be less than the value in air, so that TS would be less than unity. We also observe that the experimental curves for contact radius increase faster and approach zero slower than do the theoretical results. The latter discrepancy is understandable if we observe that upon rebound the experimental drops become quite elongated rather than retaining the shape of a truncated sphere.

Received April 27, 2007 *The "Gh.Asachi" Technical University Iaşi*

REFERENCES

1. Rheins, M., *"Phenomena of liquid drop impact on solid and liquid surfaces,"* ***FluidDynamics Research***, **12**, 61-93, 2003.
2. Stephen Wolfram - **The Mathematica book** – 5thed – 2005
3. *** - **The thermal spray technology leader** - Tafa. 2002
4. *** - **Thermal Spray Buyes Guide** - National Thermal Spray Conferens - In Advansed Materials & Preocesses ASM - International Nr. 5, Vol. 145, mai 2001.

CONSIDERAŢII TEORETICE CU PRIVIRE LA INFLUENŢA TENSIUNII SUPERFICIALE ASUPRA IMPACTULUI DINTRE O PARTICULĂ TOPITĂ ŞI O SUPRAFAŢĂ PLANĂ, LA METALIZARE PRIN PULVERIZARE TERMICĂ

Rezumat: Impactul dintre o particulă de metal topit şi o suprafaţă plană este influenţat de o serie de factori cum ar fi: tensiunea superficială existentă la interfaţa particulă – substrat, tensiunea superficială existentă la interfaţa particulă – aer viteza şi vâscozitatea particulei. Scopul lucrării îl constituie prezentarea unui model matematic care să ilustreze influenţa tensiunii superficiale asupra comportării – în faza de post impact – a unei particule pulverizate termic pe o suprafaţă plană. Modelul matematic expus permite calcularea variaţiei înălţimii particulei în unitate de timp, precum şi a razei de contact dintre particulă şi substrat în timpul impactului. Valorile razei de contact obţinute sunt comparate cu rezultate experimentale existente în literatura de specialitate.

BULETINUL INSTITUTULUI POLITEHNIC DIN IAŞI
Tomul LIII (LVII), Fasc. 4, 2007
Secţia
ŞTIINŢA ŞI INGINERIA MATERIALELOR

GENERAL INVESTIGATION OF COMPLEX CO-W ALLOYS TO SPINAL IMPLANTS

BY

E. VASILE[1], A. BUZAIANU[1], DOINA RADUCANU[2], ELVIRA ALEXANDRESCU[1], V.D. COJOCARU[2], I. RUSU[3], C. MUNTEANU[3], M. LOZNEANU[3] AND O. CARP[4]

Abstract: The continuous diversification of manufacturing technologies used for obtaining metallic implants, requires additional testing: the identification of chemical components in very small samples as well as the imaging and analysis of micro-areas obtained from implants. In order to evaluate and characterize the structure of complex Co-W alloys implants two questions need to be answered: what are the tip phases in the alloy and what the peculiarities of such elements are: homogeneity, distribution, size, conten, elements and other parameters.

Keywords: cobalt alloy, biomedical application, spinal implant, SEM investigation.

1. Introduction

In principle, a spinal fixation implant system for the correction and fixation of human spine has to facilitate an anatomically correct fusion. The spinal fixation system may include a connector, a spinal rod and a spinal fixation component. The spinal fixation component includes a fixation device such as a hook or screw for securing the spinal rod to the vertebrae of lumbar spine. Co-Cr-Mo alloys are used on a large scale in implants and prosthetics. Historically, many of the commercial cobalt-base alloys are derived from cobalt-chromium tungsten and cobalt-chromium-molybdenum systems. The first investigation has been conducted by Elwood Haynes at the beginning of the 20th century. When he discovered the cobalt-chromium system of alloys, Haynes named them the "Stellite alloys" after the Latin Stella ("star", because of their star-like lustre).Exigencies related to the quality of cobalt multiphase alloys requirements were met: all system components were found to be biocompatible, non-ferromagnetic and producing little magnetic resonance artefact. Compression and torque results were found to be compatible to standard metallic pedicle screw and rod fixation systems. In 1935, the cobalt based alloy "Vitallium" Co30Cr5Mo, basically used in the aircraft industry, was introduced in medicine. In 1936, Venable and Stuk discovered the battery effects of metals in the body through the testing of the electrolytic effects of various metals on surrounding tissue and bone. These tests demonstrated the low level of corrosion of cobalt-superalloys. All system Co superalloys from implants must be biocompatible, according to ASTM F75, non-ferromagnetic, and produce little magnetic resonance.

2. Materials and methods

The majority of investment casting cobalt superalloys are cast in the open atmosphere as opposed to vacuum casting. The addition of nitrogen as an intentional

alloying element has allowed and achieves high levels of strength with good ductility and without sacrificing resistance and bio-compatibility.–Addition is easily and economically performed, within the argon-oxygen-decarburization (patented AOD) process, through direct injection of nitrogen gas.The high-strength cobalt-nickel-chromium alloy, originally developed by Smith [1], possessed a good combination of mechanical properties and excellent corrosion resistance. Initially, it was well qualified for aerospace application. Later Co-Cr-Ni-W alloys offered a great application value in surgical implants.

In the current cobalt alloys, carbon and tungsten contents are of utmost importance (the amount and type of carbide formation in the microstructure during solidification). Carbon content influences hardness, ductility and resistance to abrasive wear. Tungsten also plays an important role in these properties. As a result of their homogeneous microstructure and lower carbon contents, the cobalt-base super alloys (which typically contain tungsten rather than molybdenum) are even more resistant to aqueous corrosion, but still fall well short of the nickel-chromium-molybdenum alloys in corrosion performance. Corrosion resistance is important in selecting metals for spinal implants and arthroplasty. These alloys (Table1) are shielded against progressive corrosion by the formation of a protective surface oxidative film, which represents a benefit of this alloy type.

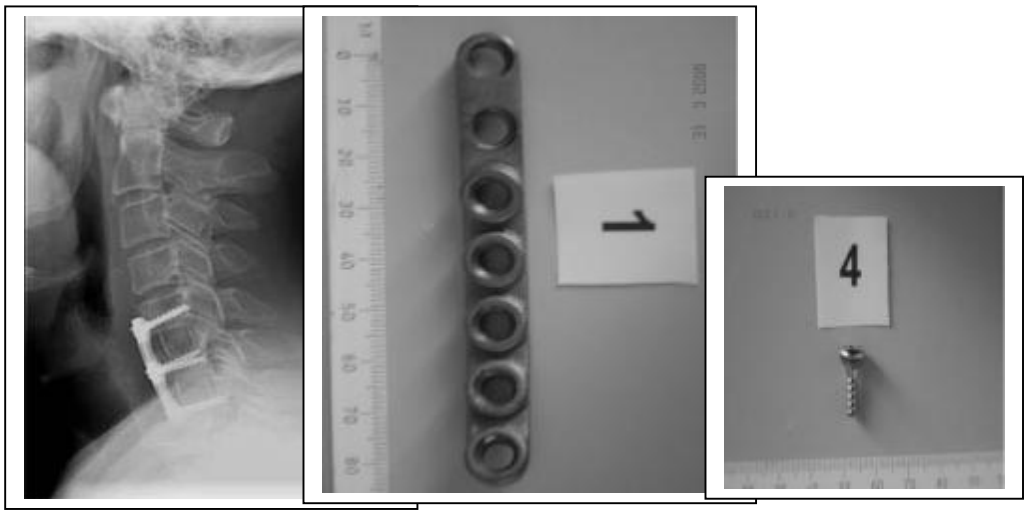

Fig.1: Radiograph of spinal implant fixation and components implant of tip Haynes Alloy 25 (HS 25).

Tungsten and molybdenum act as powerful strengthening agents within Co-superalloys, and the abrasion resistance generally increases as a volume fraction of the hard phase. The SEM (Scanning Electron Microscopy) investigation provided detailed information about the morphology and the structural modification of implants. However, it is difficult to confine structural studies to one single method. Therefore, it is necessary to obtain quantitative parameters as well

Table 1. Nominal composition of cobalt-based surgical implant alloys-(ASTM F75/ASTM F799).

Element (Max % wt)	Co (base)	Cr	Ni	W	Fe	Mo

Haynes Alloy (HS 25)	51	20	10	15	3	-
CoCrWNi (DIN ISO 5832-V)	50	21	11	16	3	-
Conicro 5010W	50	21	11	16	3	-

The toxicology and biological performance of Co-superalloys have been the object of numerous studies [2].The toxicity level of the various metallic elements was tested by investigating the reaction of the salts of these elements with cells. The CCR_{50} value, defined as the concentration of the studied substance that generates a 50% reduction in the survival of renal cells was measured.(Frazier and Andrews,Table 2).

Table 2. Limit of toxicity CCR 50 of different metal salts (Frazier and Andrews3).

Element ($\mu g\ ml^{-1}$)	**Fe**	**Mn**	**Co**	**Ni**	**Cr**	**V**
CCR_{50}	59	15	3.5	1.1	6×10^{-2}	3×10^{-2}

There is evidence that light levels of Co ions in tissues are the cause of genotoxic and mutagenic activity [3].This article intends to suggest a method for the study and diagnosis of the quality and durability of integral maintenance surgical implants using electron microscopy techniques. The spinal implant was received as an investment cast part in the production solution treated condition. Upon metallographic examination, 1mm was ground off the implant surface. This was done in order to remove any decarburized or deformed material, since the sectioning of the implant would possibly have induced an allotropic transformation within the metastable f.c.c. cobalt matrix alloy. An electrolytic etch in 5% nitric acid in methanol at 1.5 volts, was performed.

3. Results

Scanning electron microscope energy dispersive X-ray analysis (EDX spectrometer) was available for the qualitative chemical analysis of the implant.

Table 3. EDAX compositional analyzes of Co-Cr-Ni-W- Mo matrix alloy.

Element (wt %)	**Co base**	**Cr**	**Ni**	**W**	**Fe**	**Mo**
	50,14	21,41	13.46	11,19	3,58	0,22

These alloys are well suited for the production of implants that are designed for an extended period of use, if not permanent [4]. X-ray dispersive microanalysis does not detect carbon or nitrogen due to absorption of the characteristic X-ray of these elements by the detector. EDX microanalysis of this phase showed it to be high in tungsten, and contain smaller amounts of cobalt, chromium and molybdenum. This phase could be easily distinguished from the previously established M23C6 carbide (the basis of which is chromium in association with different cobalt ratios, where M = Cr,W,Mo).

The Vickers micro hardness was measured on the cross section of samples using a micro hardness analyzer. Micro hardness tests were invalid due to the presence of a thin work-hardened layer on the surface. The harnesses recorded 259-260HV (500gf) has resulted from the dispersion of carbide along the stacking faults. (Fig.3).

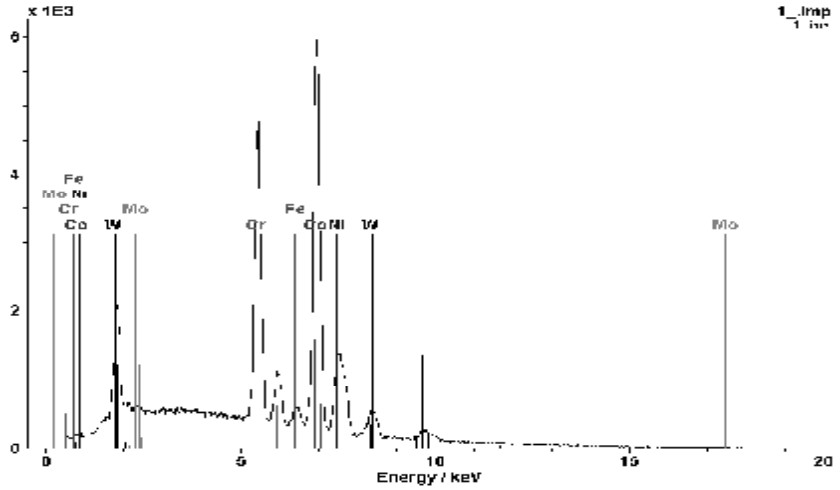

Fig. 2: EDX spectrum analysis of Co-Cr-Ni-W-Mo matrix alloy

The interrelation - in a discussion of mechanical properties, of the type of mechanical loading is indicated in Fig.3.

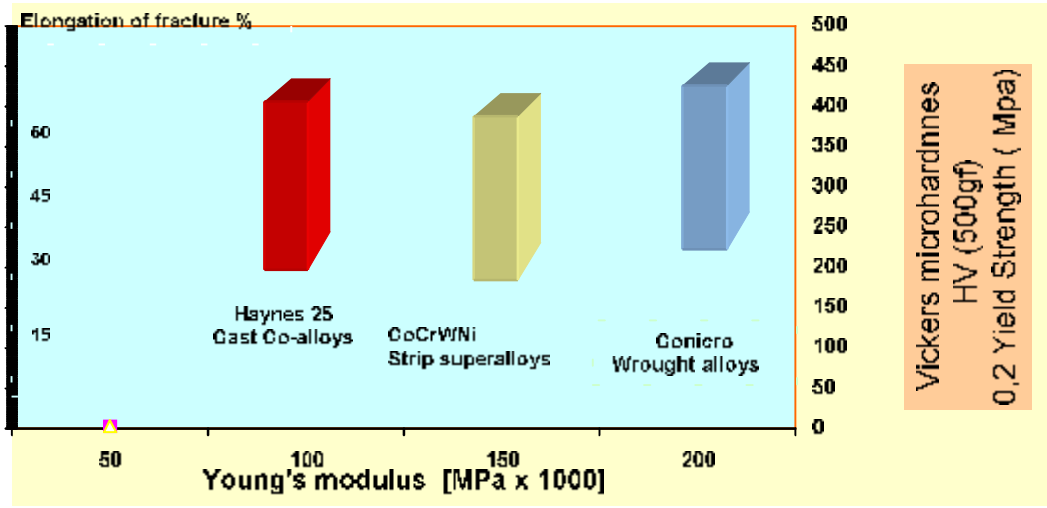

Fig.3. The interrelation of mechanical characteristics in Co-base alloys.

Measurement of sharp decreases in ductility [5] associated with commercial SEM type imaging microscopy constitute a rapid and easy method for the preliminary analysis of alloy samples that could be used in the design and fabrication of implants. SEM made possible to observe and analyse the homogeneity and chemical micro-structural aspect of Co-superaloys.

Micro and sub-micrometer defects were visualized in detail, providing information on aspects subjacent to the quality of implants, and the critical state for the optimum performance of these alloys (Fig 4-6). Figures 7 to 11 show the X-ray maps of the alloying elements; implicitly, the structural homogeny of the implant is also evident

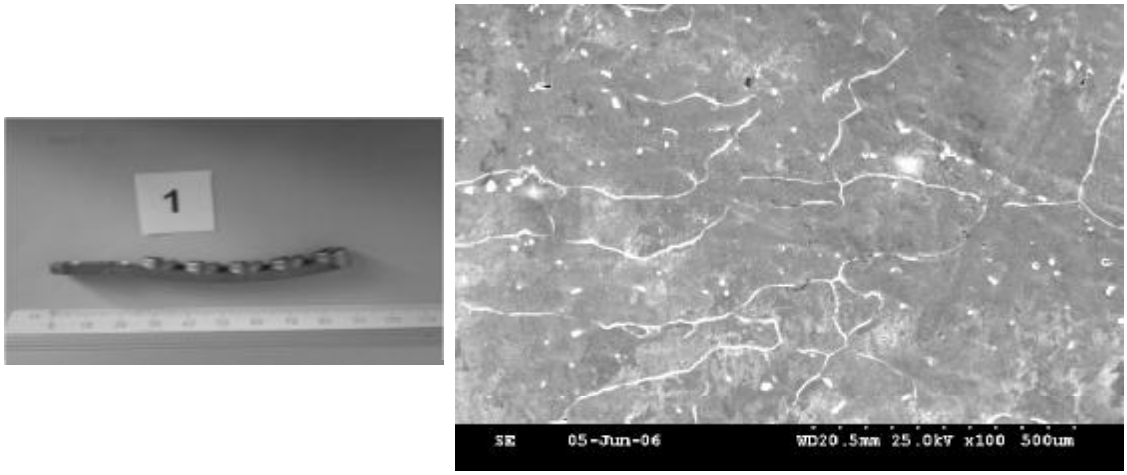

Fig.4: SEM analysis of Co-Cr-Ni-W-Mo implant. Residual carbide with feathery interdendritic precipitate.

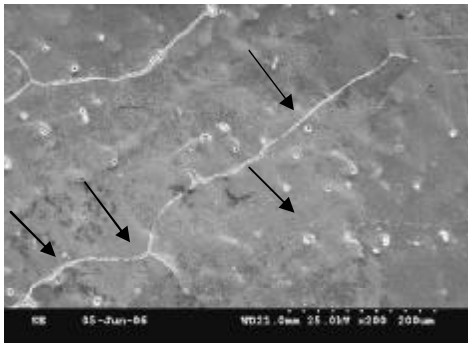

Fig.5. SEM analysis of Co-Cr-Ni-W-Mo implant. Residual carbide with feathery interdendritic precipitate.

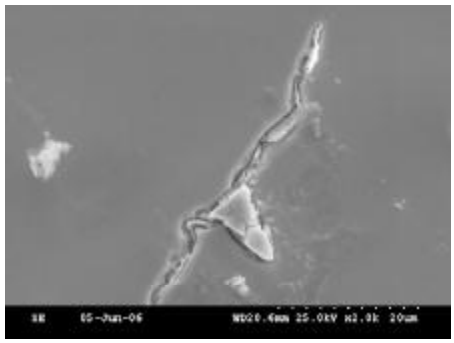

Fig.6: SEM analysis - the picture shows residual $M_{23}C_6$ carbide particles (the basis is W).

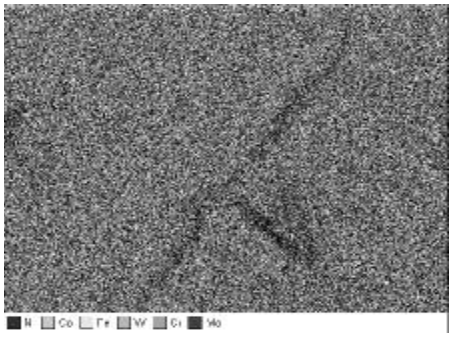

Fig.7: X-ray maps of the alloying elements.

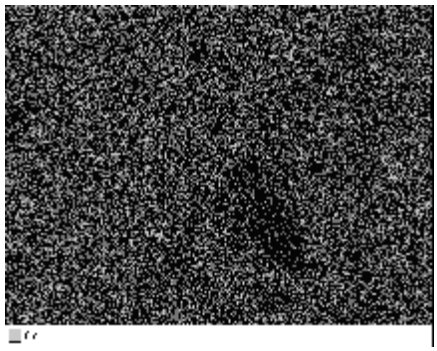

Fig.8: X-ray maps of the Co elements illustrating the residual carbide particle.

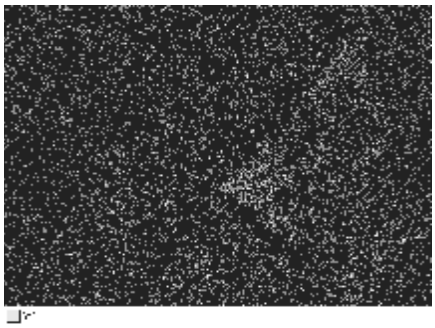

Fig.9: X-ray maps of the W element illustrating the residual carbide particle.

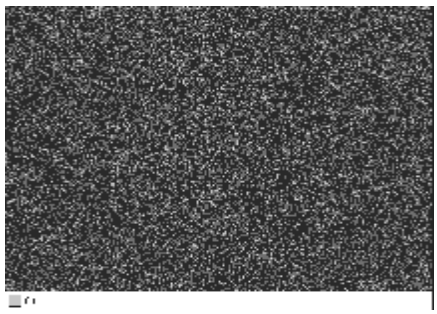

Fig.10: X-ray maps of the Cr elements illustrating the residual carbide particle.

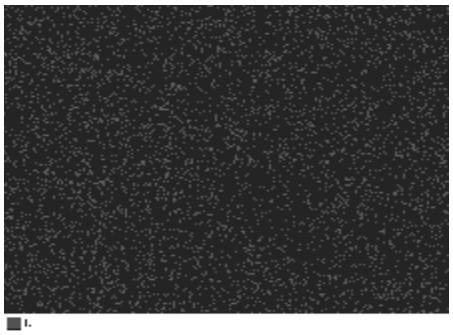

Fig.11: X-ray maps of the Ni elements illustrating the residual carbide particle.

4. Discussion and conclusions

SEM investigation has been recognized as the main suitable analytical method to describe the microstructure and suggest ways to maintain and increase its life improving properties over the duration of use of Co-W alloy implants. In order to evaluate and characterize the structure of implant or prosthetic materials it is necessary to establish: what are the tip phases the prosthetic material consists of and how these elements are distributed in phases. The SEM investigation provided detailed information about morphological modifications of spinal implants. The poor workability and high deformation resistance of Co-Cr-Ni-W alloy in the cast structure can be attributed to the non-uniform grain structures, shrinkages and impurity segregation after the initial melting practice. The addition of nitrogen as an intentional alloying element has allowed Co-Cr-Mo to achieve high levels of strength with good ductility and without sacrificing corrosion resistance and bio-compatibility [6].This addition is easily and economically accomplished in the AOD through the direct injection of nitrogen gas but also through nitrogen additions, using nitrogenated chromium. Iron, nickel and trace elements are kept to low levels through AOD refining and through careful selection of raw materials.The reduced chromium content and the absence of molybdenum would reduce the tendency to form hcp cobalt and network of intrinsic stacking fault [7].

The work intends to contribute to the development of structural approach methods and tools for the evaluation and improvement of integral maintenance spinal Co- alloys implants.

The information about different types of Co-alloys can lead to an imprecise evaluation of histopathological findings in respect to alloying constituents.

The importance of Co-superalloy will probably not diminish in the near future, because the adverse reaction to nickel is more frequent in comparison to cobalt or chromium particles.

Acknowledgements

The authors thank the Romanian Ministry of Education and Research for having financially supported this research project within the National CEEX Programme.

Received April 14, 2007

[1] *S.C. METAV-R&D S.A Bucharest*
[2] *University Politechnic of Bucharest*
[3] *Technical University "Gh. Asachi", Iasi*
[4] *Departament of Neurological Surgery - Emergency Hospital, Constanta.*

REFERENCES

1. G.D Smith, 1976),U.S Pat.3356542.
2. R.N.J.Taylor, R.B Waterhouse (1983), *A study of the ageing behaviour of a cobalt based implant alloy* in **J. Materials Science** 18: pp3265-3280.
3. Frazier,M.E. and Andrews,T.K. (1979) *In vitro clonal growth assay for evaluating toxicity of metal salts*, in **Trace Metals in Health and Disease** (ed N.Karash),RavenPress N.Y p71
4. R.J.Oskouian, M.D Richard (2004), *The future of spinal arthroplasty: a biomaterial perspective* in **Neurosurgery Focus** 17(3).
5. J.Teague, F.Cerreta, M. Stout (2004) *Tensile Properties and Microstructure of Haynes 25 Alloy after Aging at Elevated Temperatures for Extended Times* in **Metallurgical and materials Transaction** a, Volume35, Nr.9, pp.2767-2781(15).
6. T.Kilner, A.J.Dempsey, R.M.Pilliar, G.C.Weatherly, (1987) *The effects of nitrogen additions to a cobalt-chromium surgical implant alloy* in **J. Materials Science** 22: 565-574.
7. U.Holzwarth, P.Thomas, W Kachler, J Goske, A.Schuh, *Metallurgical differentiation of cobalt-chromium alloys for implants in orthopaedic*, 2005 (10)-1046-1049-51

INVESTIGATII GENERALE PE ALIAJE COMPLEXE Co-W UTILIZATE LA IMPLANTURILE SPINALE

Rezumat: Diversificarea continua a tehnologiilor utilizate pentru obtinerea implanturilor chirurgicale metalice, impun anumite tipuri de teste de material: identificarea compozitiilor chimice pe esantioane distincte, analiza microscopica pe microarii ale protezelor ce urmeaza a fi utilizate etc. In lucrare, sunt prezentate cateva din testele de omogenitate, distributie, marime de graunte, distributia chimica a elementelor si alte cateva proprietati de baza ale protezelor chirurgicale pe baza de cobal, ce au ca principale elemente de aliere wolframul, cromul si nichelul.

BULETINUL INSTITUTULUI POLITEHNIC DIN IAŞI
Tomul LIII (LVII), Fasc. 4, 2007
Secţia
ŞTIINŢA ŞI INGINERIA MATERIALELOR

PREPARATION OF MICROMETRE-SIZE COPPER POWDERS, BY REDUCTION IN LIQUID POLYOLS

BY

LIANA MARIA VLĂDUŢIU*, D. TALOI*, I. CONSTANTIN*, D. ŞOTCĂ** and FLORENTINA PERETEANU*

Abstract: The synthesis of copper powders in liquid polyols is a simple method for producing highly pure, regular forme and non-agglomerated monodisperse particles. Copper powders of micrometre-size have been produced by reducing CuO in a mixture of ethylene glycol and D-sorbitol, in the temperature range of 150-197°C. Addition of D-sorbitol prevents particle sintering. The obtained copper powder has been investigated by SEM and XRD analysis.

Keywords: cooper powders of micrometre-size, reduction, polyols.

1. Introduction

Crystalline metallic powders with micrometer size, which don't need post treatement at high temperatures, can be obtained by reduction of metallic salts through solvothermal process. The most frequently used are the polyols which are both reaction medium and reducing agent [1]. The chemical reaction can be schematized as follows [2]:

$$2CH_2OH-CH_2OH \xrightarrow{-2H_2O} 2CH_3CHO \xrightarrow{Me^{2+}} CH_3CO-COCH_3 + Me^0 + H_2O$$

The reduction of copper oxide by polyol process leads to the obtaining of the copper powder with micrometer size and regular form of the particles [3]. The copper powder having these characteristics is more and more used to obtaining electroconductive and antibacterian textile fibers [4].

2. Experimental procedure

Our researches intended to show the obtaining of the pure copper powder, with particles in the micrometer and submicrometer size range and of regular form, by reduction of copper oxide in ethylene glycol. It has been used a simple plant as shown in fig.1.

We have watched the influence of the reaction parameters: temperature, time and the rate of stirring, upon the conversion grade of copper oxide into metallic copper and of the properties of the obtained powder.We have used pure products (copper oxide produced by Fluka and ethylene glycol with b.p. 195^0 C), at a temperature ranging from 175-195^{0}C and the reaction time from 1-3 hours. The stirring rate of the suspension varied between 300-900 r.p.m. For preventing particles sintering different organic dispersal agents have been used.

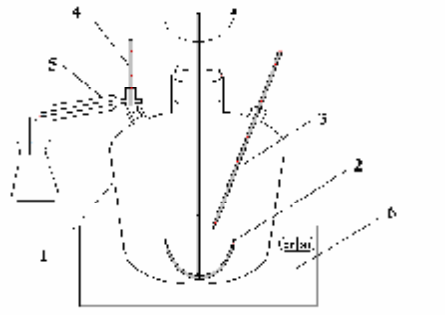

Fig.1. Laboratory plant

3. Results and discussions

Copper powder obtained as shown before, was examined by X-ray diffraction (XRD) using a Bruker AXS tipe 8 ADVANCE with Cu k RADIATION. The lattice parameter coincides with that of the copper metal which was calculated. No other impurities were detected. (fig.2)

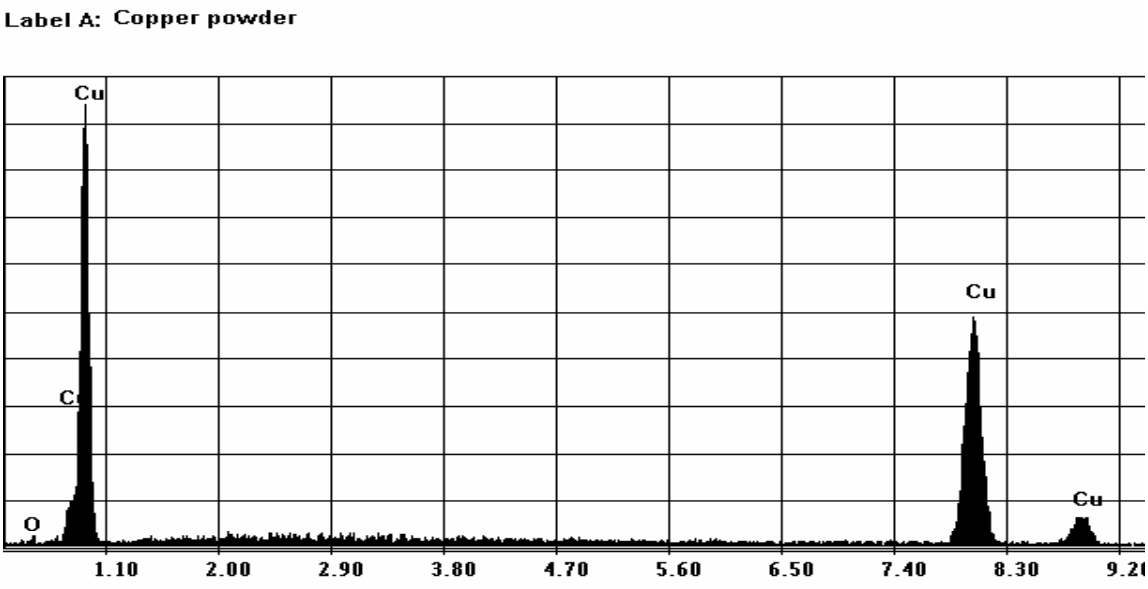

Fig. 2. Cooper powder X- ray difraction

The morphology of copper powders was assessed through SEM (fig. 3), which were carried on a FEI PHILIPS ESEM XL 30 TMP.

Figure 3a shows SEM image of the copper oxide precursor; fig. 3b SEM image of the copper powder resulted in the presence of the dispersal agents. As it can be seen the particles are individualised by regular geometrical forms; fig. 3c SEM image of the copper sintered in the absence of the dispersal agents.

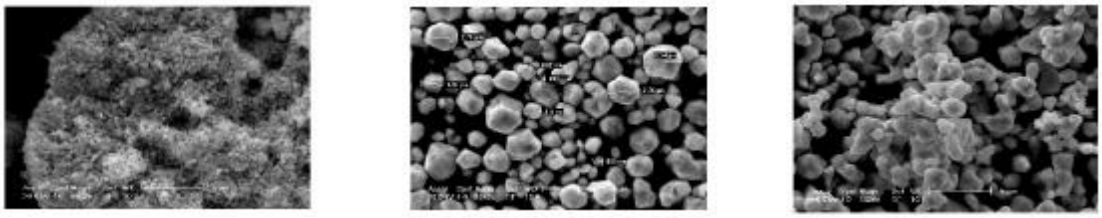

a *b* *c*

Fig. 3

Usually the purity of copper powders obtained in the way described varied between 98,66-100% metallic copper. By EDAX analysis the purity of copper powder is confirmed (fig.4).

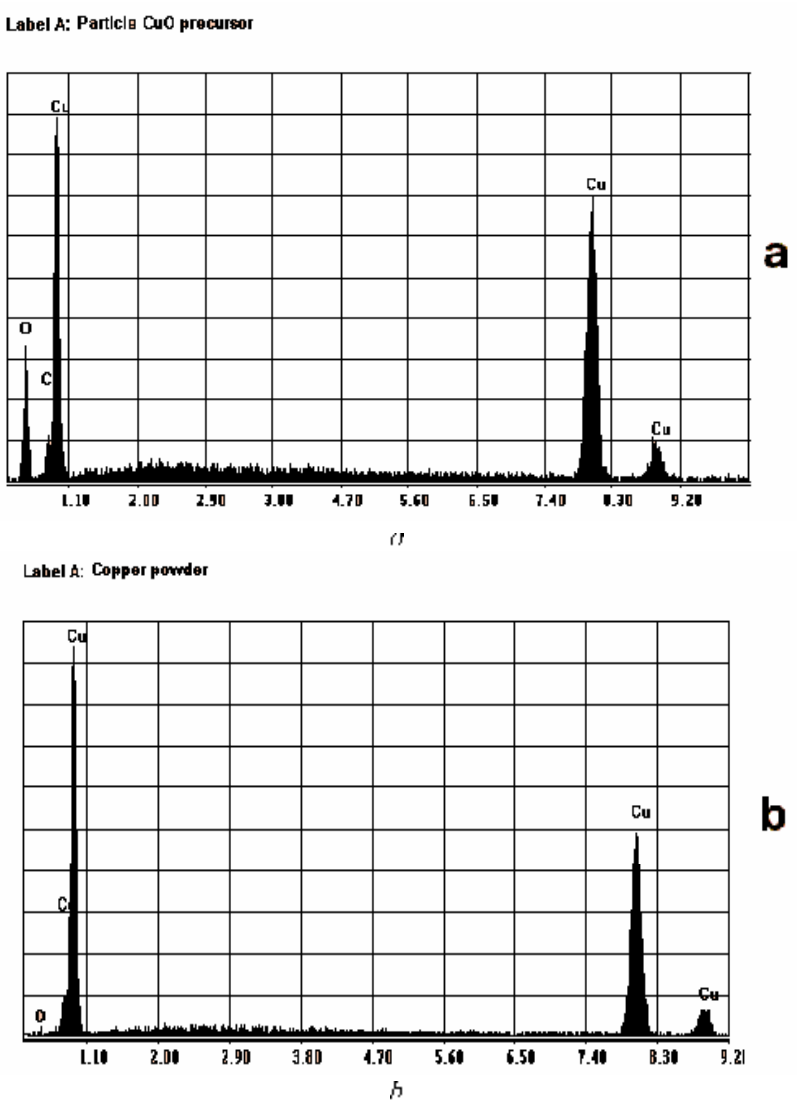

Fig. 4 EDAX analysis of a - precursor copper oxide, b - final copper powder

The mean size of the particles determined by Dynamic Light Scattering with Zetasizer Nano ZS instrument, is between 1480-1990 nm. (major fraction -1720 nm which represents 54%)

4. Conclusions

The solvothermal process described is simple to realise taking into consideration the plant and the reaction conditions; it allows the obtaining of a copper powder of advanced purity with micron and sub-micron sizes and regular form of the particles.The copper powders obtained in this process are successfully used in the synthesis of the electroconductive textile fiber

Received April 3, 2007

**University POLITEHNICA Bucharest*
***National Institute of Chemicals Research - ICECHIM - Bucharest*

REFERENCES

1. Yitai Qian, **Adv. Mater**. (1999) 11, no.13, p.1101
2. Fernand Fievet. Francois Fievet-Vincent. Jean Pierre Lagier, Bernard Dumont, J. Mater Chem, (1993), 396. p.627-632
3. Qing Li and. colab. **Journal of Crystal Growth** 243 (2002), p. 327-330
4. Emmanuel Gusana. Philippe Westbroek, Jean Hakuzimana, Paul Kiekens. Ghent University. Deparment of Textiles, Technologiepark 907, B-9052, Gent, Belgium

PREPARAREA PULBERII DE CUPRU DE DIMENSIUNI MICROMETRICE, PRIN REDUCERE IN POLIOLI

Rezumat: Obtinerea pulberii de cupru prin reducere in polioli, este o metoda relativ simpla pentru producerea unor particole monodisperse neaglomerate, de inalta puritate si forme regulate.Pulberea de cupru de dimensiuni micrometrice se obtine prin reducerea CuO in amestec de etilen glicol si D-sorbitol, la temperaturi de 150-197°C. Adaosul de D-sorbitol previne sinterizarea particolelor. Pulberea de cupru astfel obtinuta a fost analizata prin difractie de raze X si microscopie electronica de baleiaj (SEM).

BULETINUL INSTITUTULUI POLITEHNIC DIN IAŞI
Tomul L(III (LVII), Fasc. 4, 2007
Secţia
ŞTIINŢA ŞI INGINERIA MATERIALELOR

HIP JOINT- IMPLANTS

BY

E.WUSINCZKY*, D.I. WUSINCZKY and R.M.POPESCU*****

Abstract: If initially the progress in the hip replacement area were owed to using new materials that were better tolerated by the body and with a better behavior to the cyclical mechanical strains in a hostile environment in time the better results were the outcome of a better connectin bone/implant, meaning a better transfer of the tension, better stability between the two surfaces. If initially the progress in the hip replacement area were owed to using new materials that were better tolerated by the body and with a better behavior to the cyclical mechanical strains in a hostile environment in time the better results were the outcome of a better connectin bone/implant, meaning a better transfer of the tension, better stability between the two surfaces.

Keywords: human implant

1. The strains to which the hip joint is submitted

The hip joint has as primary physiological functions the dispatching of mechanical functions between the pelvis and the thighbone, but also the relative moving between the two parts of the bone structure. The hip joint is one of spherical type, with three degrees of movement freedom:

- flections – extensions
- abducent – adduction
- external relation – internal relation

This joint is lubricated by sinovial fluid. The combination between cartilage and sinovial fluid built up an extremely low friction factor

The hipbone is the toughest and longest bone in the human body and the most important long bone. It is composed by spongy bone and tough bone tissue.
The spongy bone tissue is present, generally, in the long bone epiphyses, while the tough bone tissue is present in their epiphyses (Figure1).

The mechanical strains, to which the superior extremities of the thighbone are submitted, are static during physical rest, and dynamic during the walking movement of the body.

During physical rest, standing on both feet the head of the thighbone is submitted to compression, the pressing pressure is almost 1/3 of the body`s weigh, divided equally on both thighbone heads. While standing on one foot, the pressing pressure rises up to a value three times higher than the body weigh.

During walking, the movements involve the oscillations of the gravity point in the body in three plans of the space. The acceleration of the body triggers the action of the ineptness forces. During standing on one foot the pushing rate rises rapidly to its highest value, which is almost four times higher than the body weigh, than it drops towards zero when the foot loses touch with the standing surface.

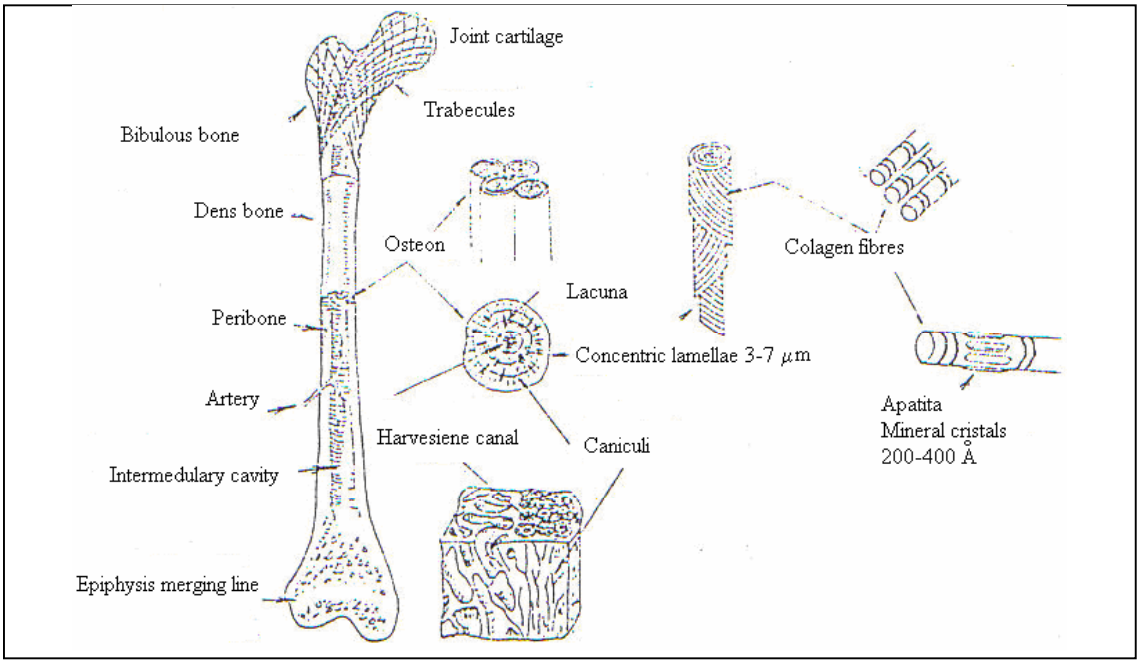

Fig. 1. The structural build of the thighbone

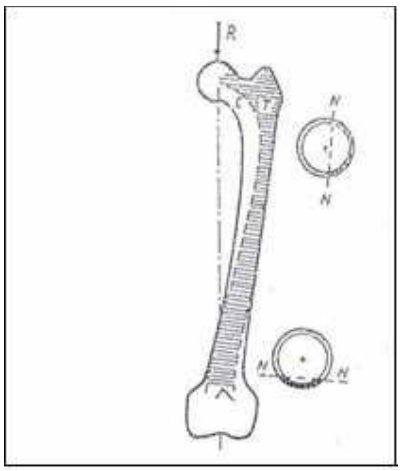

Fig. 2. Variation of the neutral axes thighbone

The "R" resultant which acts on the joints of the thighbone head (Figure 2) is divided in two components:

- a normal component "N" along the axes of the thighbone canal, which trigger compression pressure on the thighbone canal.
- a perpendicular component "S" on the "R" resultant, which strains the thighbone canal to a bending and sharing action.

The thighbone, in its whole, is submitted to a combined strain by compression and bending.

For the external extremities of the thighbone the strain area for compression is situated internally, and the one submitted to stretching externally. (Figure 3)

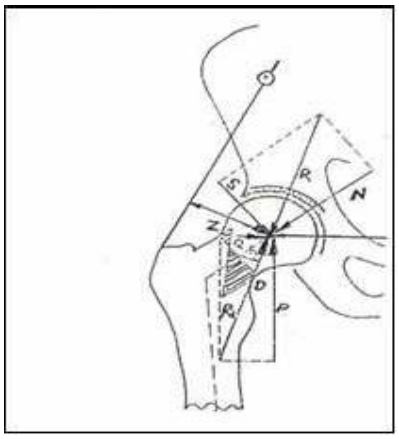

Fig. 3. Shearing strain for the thighbone canal

2. Hip replacement objectives

The different diseases of the hip joint change the bio mechanics of the hip, which on its turn influences the structural changes of the joint. If the condition is serious, with severe joint movement impairment, the only therapeutically possible solution remains the total hip joint replacement.

There are four main indicators for the hip joint replacement: pain, immobility, rigidity, and shape changing.

While the *clinical objectives* of the hip joint replacement are to reduce the intensity of pain and rising the degree of joint mobility, the *technical objective* is to ensure keeping the normal mechanical physiological needs of the bone tissue kept un-replaced through keeping the integrity and functionality of the implant / host tissue for a long period of use. (>10 years).

An analysis of total hip joint replacement is extremely complex and interdisciplinary involving knowledge from the following domains: materials science, mechanics, chemistry, biology, environmental, surface science, which have to be integrated into an unitary system (Figure 4).

3. Management implantable systems

The total hip joint implant is a mechanical ensemble with the function of overtaking the biomechanical function of the natural hip joint, in the conditions of the existence of a severe condition, and its effect of severely imparting the physiological function.

Generally, the hip joint implant components are fixed in the bone tissue either by cementing, when the implant is stabilized through a tying material (cement), or by direct contact of the bone tissue and the implant surface

If initially the progress in the hip replacement area were owed to using new materials that were better tolerated by the body and with a better behavior to the cyclical mechanical strains in a hostile environment, in time the better results were the outcome of a better connection bone/implant, meaning a better transfer of the tension, better stability between the two surfaces, respecting the imposed conditions, both into choosing the materials and the constructive shape of the prosthesis components.

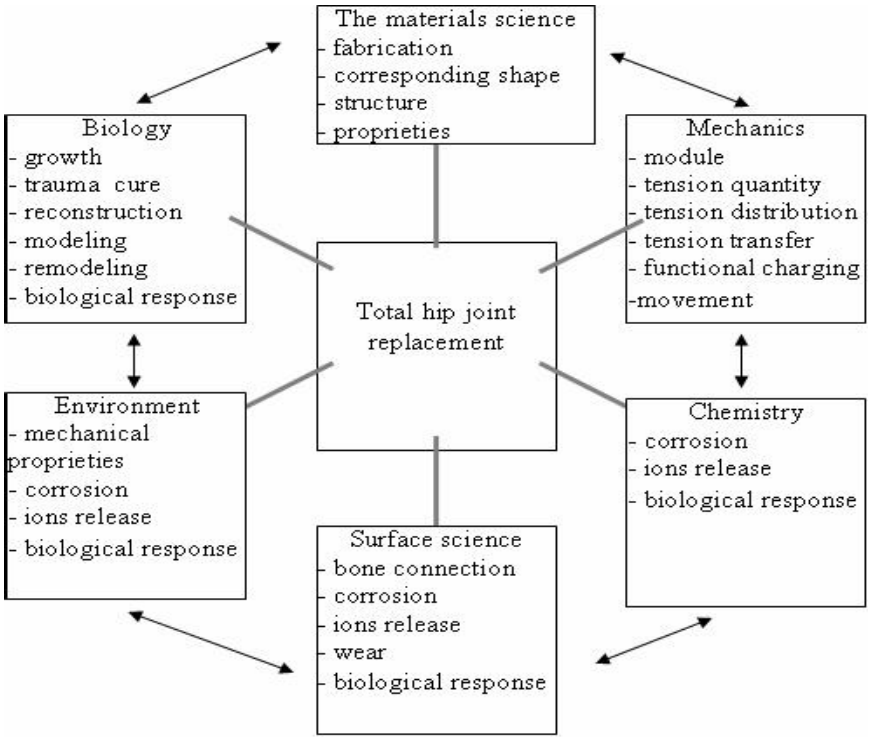

Fig.4. Factors which affect the joint implants

The hip prostheses, used currently are build by two sub-ensembles:

a) the acetabulary component, which can be:

- metal, with direct bone fixing
- metal, with cement fixation
- from high density polyethylene fixed in cement
- ceramic, fixed without cement
- acetabulary cup from plastic fixed on a metallic base anchored in the bone with cement

b) the thighbone component, which has a head, a femoral canal and a rod. The thighbone piece can be a single piece or it can be made up by two parts: the thighbone head constructed from different materials and the thighbone rod which contains the horse, on which the thighbone head is fixed rigidly or mobile.

Replacing the hip joint by cementing consists of a system that can be implanted whose components are fixed in the bone tissue with polymeric cement. The transfer of the strain from the pelvis to the inferior limb is made, as opposed from the natural joint, through artificial materials placed in between the two bones (the coxis bone and the thighbone) and the interface of the diverse materials of the thighbone components. (Figure5).

Fixing the bone by cementing is an active mechanical one, which creates two interfaces: bone/cement, and cement/ implant.

Loosing fixation and the destruction of the prosthesis implant system that have been cemented can be the result of the destruction of the material, of the prostheses, or of the cement, of the bone restructuring, and/or due to wear and tear, and the formation of abrasive particles through different mechanisms during use.

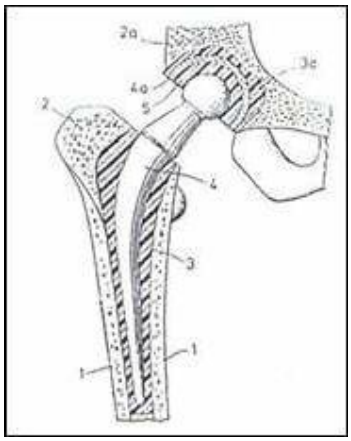

Fig. 5. *Total replacement scheme for a cemented joint: 1 - bone tissue, 2,.2a - trabecular bone tissue, 3,3a - cementing material, 4 - thighbone component, 4a - acetabular cup support, 5 - acetabular cup*

The attempts to avoid this kind of destruction had as a purpose the improvement of fixation through concentrating the attention on: the material for cementing, the materials and constitutive shapes of the components for the prosthesis, the properties of the interfaces.

Improving fixation through proprieties changing of the interfaces bone/ implant have been made by giving up fixing through cementing and using bone tissue capacity to build up a stabile connection with the implant, which can be kept for long periods of time.

Replacing the hip joint without cementing consists of an implantable system very similar to the one presented above, but he fixation is done by determining an adequate insertion of the implant into the bone tissue.(Figure 6)

Fixing without cementing can be made in the following three ways:

- through the use of superficially textured components
- through the use of porous covered components with different materials
- through the use of superficially bioactive materials

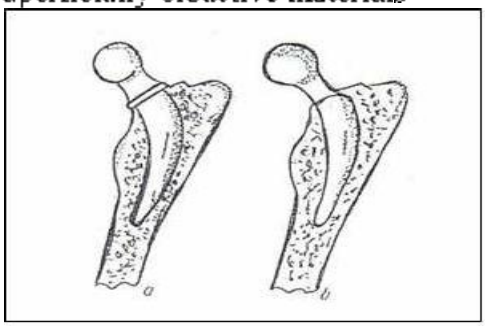

Fig.6. Thighbone component in the total hip joint replacement without cementing; a) thighbone rod with a collar b) thighbone rod without collar.

In the first case the fixation can be made through the growth of the bone tissue on the textured surface of the implant, resulting in a *morphological fixation.* In the second case through penetrating and developing of the bone tissue in the covering pores, obtaining a *biological fixation.* In the last case the fixation is due to chemical factors through which on the surface of the implant a layer of hidroxiapatitis is formed which is biologically active, resulting a *bioactive fixation.*

An improvement of the fixation can be obtained through combining these ways, respectively by using a ceramic bioactive covering over a porous surface, with the purpose of making a direct bound between the bone tissue inside the pores and the surface of the porous material.

Developing the interface bone tissue/implant is dependent on different factors: the volume properties and of surface of the implant material, the geometrical shape of the implant, the topography of the surface of the implant, relative interface movement, and the tissue response.

The process through which the implant is integrated in the bone tissue is known by the name of *osteo-integration*, which means that there is a direct contact between the living bone tissue and the implant surface. By "direct contact" is to be understood that between the living bone tissues and the implant surface there is no fibrous cell layer, the bone cells being anchored directly in the surface of the implant.

Other two concepts of materials which bear great importance in what the implant fixation is concerned are:

- Using *isoelastic materials*, which have mechanical proprieties similar to those of the replaced bone tissue, diminishing the tendencies of losing fixation by reabsorbing the neighboring tissue due to the process of bone reconstruction
- Using *analogous materials*, which have mechanical and biological proprieties similar to those of the replaced bone tissue as though, the differences between the behavior of the bone tissue, the interface and the implant to be minimal

Received April 9, 2007

**CJAS, Teritorial Insurance House of Health of Braşov*
***„Mircea Cristea" Tehnical College of Braşov*
****Transilvania University of Braşov*

REFERENCES

1. Iordachel, C., Petrescu, M. *Suporturi structurale ale functiilor biomecanice*. In: **Biomecanica**, Editura Academiei Romane, Bucuresti, 1989, p.30-88.
2. Antonescu, D., Constantinescu, I., Buga, M., Iliescu, N.: **Metode de calcul si tehnici experimentale de analiza tensiunilor in biomecanica**, In: Editura Tehnica, Bucuresti, 1986, pg.113-180.
3. Mendrea, O., Buga, M., Antonescu, D., Popescu, M., Marin, I.Gh., Iliescu, N., Constantinescu, I.: *Metode de calcul şi cercetări experimentale în analiza stărilor de tensiune din extremitatea superioară a femurului*. In. **Biomecanica**, Editura Academiei Romane, Bucureşti, 1989, p 169-190
4. Kokubo, T.: *Apatite formation on surfaces of ceramics, metals andpolymer in body environmen*. In: **Acta Materialia**, vol 46, nr.7, p. 2519-2527.
5. Hazan, R., Oran, V.: *Differential rate of bone growth to titan alloy and stainless steel implants:* In: **Interfaces in Medicine and Mechanics**, 1989, pg 318-321.

IMPLANTURI PNETRU ARTICULAŢIA UMĂRULUI

Rezumat: Dacă iniţial progresul în domeniul implanturilor de umăr se realiza doar în utilizarea de noi materiale mai bine tolerate de organism şi cu o mai bună comportare la tensiunile mecanice ciclice dintr-un mediu osilil, în ultimul timp atenţia cercetătorilor s-a îndreptat către realizarea unei mai bune legături os/implant, ce determină un mai bun transfer al tensiunii şi o mai bună stabilitate între cele două suprafeţe.

BULETINUL INSTITUTULUI POLITEHNIC DIN IAŞI
Tomul L(III (LVII), Fasc. 4, 2007
Secţia
ŞTIINŢA ŞI INGINERIA MATERIALELOR

TITAN BASED BIOMATERIALS BEHAVIOR USED IN JOINT REPLACEMENTS

BY

D.I. WUSINCZKY*, E.WUSINCZKY and R.M.POPESCU*****

Abstract: The titan base biomaterials have as advantages: osteointegration promotion (direct contact between the bone tissue and the implant without interposing a fibrous cellular layer), due to these biochemical proprieties of the superficial oxides, good resistance to corrosion (due to the oxide superficial layer), use and fatigue, but also a realitively low flexibility module. The propriets for the oxide layer influence both and response of the body and implant behavior manufactured from these materials during use period. The superficial oxide are formed, spontaneously, in air and have a layer thickness of 5-10 nm. The composition of the oxide from the external atomic layers is similar to that of TiO_2, being changed on the interface metal/oxide layer in an oxide combination (eg. TiO_1, TiO_2, TiO_3). Although TiO_2 is an isolator, in thin layers the electrons can pierce establishing structural changes of the absorbed proteins. Thicknesses bigger than 50 nm, obtained generally after mechanical processing, are sufficient to prevent this phenomenon.

Keywords: biomaterials, implant.

1. Introduction

There are three reasons for the apparent success of implants produced from titan based biomaterials:

- relatively good corrosion resistance, due to the oxide superficial layer
- the relatively low flexibility
- the tendency of osteo-integration promotion (direct contact bone tissue / implant without the intrusion of a fibrous cell layer), due to the biochemical properties of superficial oxides.

The properties for the oxide layer are considered one of the important factors which influence both the response of the body and implant behavior manufactured from these materials during use period.

The superficial oxides are formed, spontaneously, in air (1nm gauge in less than 1ms) and have a layer thickness of 5 10nm. The composition of the oxide from the external atomic layers is similar to that of TiO_2, being changed on the interface metal/oxide layer in an oxide combination (e.g. TiO_1, TiO_2, TiO_3).

Although TiO_2 is an isolator, in thin layers the electrons can pierce establishing structural changes of the absorbed proteins. Thicknesses bigger than 50 nm, obtained generally after mechanical processing, are sufficient to prevent this phenomenon.

It has been determined that the oxide layer that covers titanium based materials is capable of tying polyvalent cautions, both cautions and anions. One of the most important cautions absorbed on titan implant surface, when in contact with bodily fluids, is the calcium ion, which can generate a further absorption of the tied macro elements from that caution

2. Titan based biomaterials behaviour in fatigue in the high duration area

Due to a long use period of joint prosthesis, the critical mechanical propriety is its resistance to fatigue in the high duration area.

Tear by mechanical fatigue has two stages:

- tear initiation by fatigue
- tear continuation by fatigue

Both of these stages are characterized by mechanisms, velocities, and specific building conditions.

The durability, in mechanical fatigue situations, is determined by the following factors: tension accumulation, piece dimension, surface quality (roughness, physical-chemical proprieties of the superficial layer), medium tension, residual tensions, mechanical solicitation frequency, microstructure, use, etc.

3. Titan based biomaterials behaviour to wear

It is known that titan proprieties and those of its alloys are unsatisfactory, due to the low resistance to traction and its high affinity towards oxygen.

It is admitted, generally, that there are four fundamental mechanisms of use for metals: adhesive wear, abrasive wear, wear by fatigue and corrosive wear

In what joint prosthesis and hip join replacements, without cementing, the areas exposed to an intense wearing process are the areas in direct contact and in relative movement of the thighbone head and of the acetabulary cup, which make up the artificial joint.

Wear behavior of a material must be considered keeping in mind the mutual influence of the materials that are in direct contact. The materials used to manufacture the two components of the artificial hip joint are: of metal or ceramic for the thighbone head; polymers or ceramic for the acetabular cup. Adapting one of the two possible combination is made by bearing in mind two objectives: friction coefficient lowering, and wear reduction of the joint components. To fulfill these objectives two coupling strategies have been used:

- rough material / soft material
- rough material / rough material

A special interest has been shown towards promoting certain combinations metal / metal, which have extremely low wear rate.

Remarkable results have been obtained by using the combination alumina / alumina, obtaining a wear rate of 1-5μm/ year.

Certain solutions have started to be investigated, such as using a low density layer (polyurethane or hydro gel) on a high density layer, permitting the result of a moist friction and friction coefficient values of about 0.02;0.03 or0.05.

4. Titan based biomaterials corrosion behaviour

Corrosive environment. Corrosion is one of the major processes that happen when a metal is in intimate contact, by implantation, with at least one tissue of the

human body, having as a result their continuous damage and allowing different reaction compounds to form. Also, through this process metal ions are created which can have local or systemic noxious effects.

The physiological neutral environment of the human body is moist, which contains water, dissolved oxygen, salts, proteins, fat, and carbohydrates. The metal from the implant is continuously in contact with certain electrolytic bio fluids like the blood, extra cell fluid, and the sinovial fluid.

The extra cell fluid, which is most often in contact with the implants, contains great quantities of ions such as: Na^+, Cl^-, HCO_3^-, OH^-, as well as low quantities of other ions which have the Ph around the value of 7.2 – 7.4, maintained at a constant temperature of 34° C. As a result, the physiological environment is very aggressive, and as follows, the resistance to corrosion of the implanted metals is an important aspect of bio compatibility of these.

There are two aspects that control the corrosion of this environment:

- the saline solution is a great electrolyte, facilitating electro chemical mechanisms for corrosion
- there are more molecular and cellular species in the tissues that have the capacity to catalyze certain chemical reactions or to destroy certain components identified as foreign for the body.

hematomas (Figure1). The presence of certain cellular species or molecules can modify the Ph value, the environment becomes highly acid (Ph=3-4).

Titan based biomaterials corrosion. Metal corrosion in physiological human body environment is developing, generally, through conventional mechanisms and is to a great extent predictable. Because the

The normal value of the Ph is immediately modified after the implantation in the area affected by surgery, varying in the recovery period. At the time of the implant, the value of the Ph is changing towards acidic values of about 5.2 in the immediate tissues and becomes normal in a few days. The Ph value also depends on the existence of an infection or hematomas (Figure 1). The presence of certain cellular species or molecules can modify the Ph value, the environment becomes highly acid (Ph=3-4).

Titan based biomaterials corrosion. Metal corrosion in physiological human body environment is developing, generally, through conventional mechanisms and is to a great extent predictable. Because the physiological environment is moist, the corrosion percentage is of electrolytic kind; its harshness is modified by the presence of different ions (especially the chlorine kind), as well as by the presence of different molecular and cell species such as: proteins, phagocytes, osteoblastele, and so the physiological environment of the corrosion is difficult to establish

The modern treatment of electrolytic corrosion uses the concept of mixed potential. In this case the metal is considered a macro electrode on which there are simultaneously reactions of oxidation, or reduction, to which active components are part of the electrolytic solution. These processes are unrolling at a irreversible electrode potential, called mixed potential.

The concept of mixed potential, called corrosion potential, together with the overlapping partial curves tension – current develops the kinetic *base of the electrolytic corrosion.* The potential Ph diagrams, called *Pourbaix* diagrams make the *thermo dynamic base* of the same process.

The metals for implants which best resists to sea water, because most of the fluids in the human body have a high degree of chlorine and a similar Ph to that of sea water, are:

- 8 noble metals (Ag, Pt, Ir, Rh, Ru, Pd, Os) with a real metallic surface
- 5 passive metals (Ti, Ta, Nb, Zr, Cr) which are not covered with a protective, adherent, compact layer.

For most alloys used in implants the speed of corrosion is dependent on the properties and the stability of the passive film that is formed. The quality of the protective film is dependent on the ionic, molecular and cellular species present and also on their capacity of re-passive quick enough to avoid the attack on the metallic sub-layer.

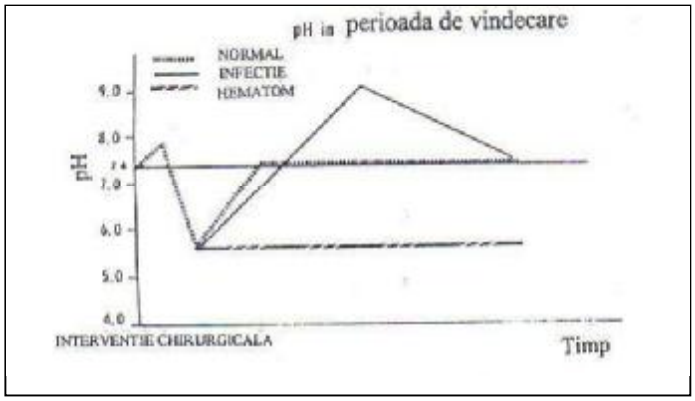

Fig. 1. Ph variations in the recovery period

The best known types of corrosion for the used bi-materials are: punctual corrosion (pitting), crevasse corrosion, corrosion under tension, fatigue corrosion, corrosion under corrosion, inter-gramelar corrosion.

Although titan is a metal that should corrode heavily, due to the oxide layer, it remains passive in the body, like shown in (Figure 2).

After the implantation in the human body the oxide layer suffers some changes in what the width and its constitution is concerned. if its integrity is altered the oxide layer, in the nearby tissue to the prosthesis, and also in some organs, titanium ions, and ions of the alloy elements have been discovered.

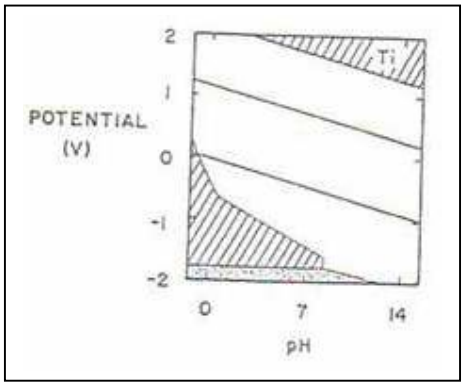

Fig. 2. Diagram Pourbaix for titan: the dotted area immunity, checked area corrosion, unmarked region passiveness

It is considered that metal ions release is happening through the chemical degradation of the oxide layer as well as through the corrosion of the metal surface.

Titan based metal passivity is influenced by the presence of alloy materials, as well as impurities, in the original material, as it can be seen from figure 3, an figure 4.

The presence of Nb and in a lesser extent of Zr determines a growth of resistance to corrosion, unlike Mo, V or Al.

Pure technical Titanium has the greatest resistance to corrosion compared to the bio-physic alloys, due to the monophasic structure and to its chemical composition.

The passive film on the surface of the titan based materials is chemically stabile, but recent research shows that the passive state is not stabile. In the presence of chlorine ions, the destruction at sub-microscopic level undergoes of the passive layer, although this phenomena does not lead to the localized corrosion.

The superficial change by bioactive ceramic covering or by superficial oxide transformation TiO_2, determines a growth in resistance to corrosion of titan based materials.

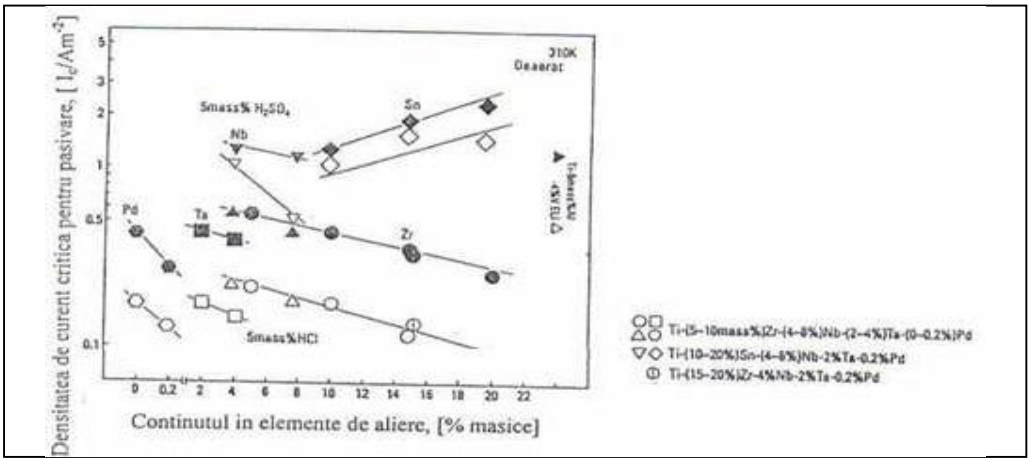

Fig. 3. The effect of: Zr, Nb, Ta, Pd, Sn on the density of the passive current

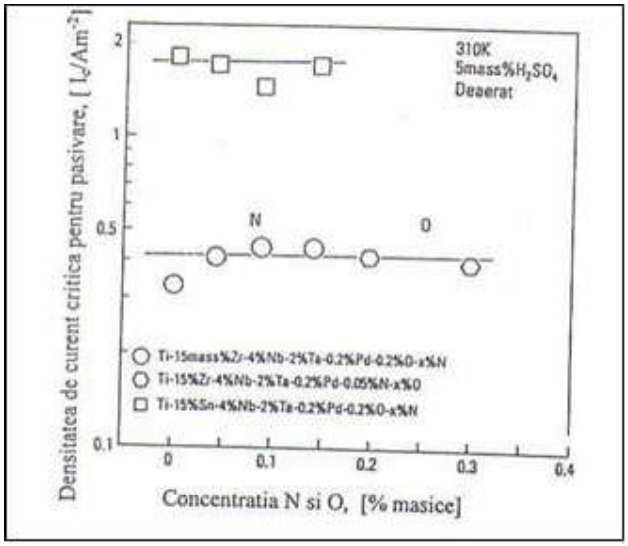

Fig. 4. The effects of : N and O on the density of the passive current.

Received April 9, 2007

*„Mircea Cristea" Telnical College of Braşov
**CJAS, Teritorial Insurance House of Health of Braşov
***Transilvania University of Braşov

REFERENCES

1. Ban, S., Hasegawa, J., *Electrochemical corrosion behaviour of hydroxiapatite-glass-titanium composite*. In: **Biomaterials**, vol 12, March, 1991, p. 205-209
2. Nakayama, Y., Yamamuro, T., Katoura, Y., Oka, M., *In vivo measurement of anodic polarization of orthopaedic implsant alloys: comparative study of in vivo and in vitro experiments*. In: **Biomaterials**, vol.10, August, 1989. p. 420-424.
3. Bundy, K.J., Kelly, R.G., Brown, E.L., Delahundy, C.M., *Ph shifts and precipitation associated with metal ions in tissue culture*, **Biomaterials**. vol.6. March. 1985. pg. 86-96.
4. Onciu, L., Ivascan, S., Apostolescu, Maria, Schmidt, Eugenia, **Coroziunea metalelor-Aspecte fundamentale si protectie anticoroziva**. Editura Stiintifica si Enciclopedica, Bucuresti, 1986.
5. Radoi, I., **Introducere in coroziunea si protectia metalelor si aliajelor**, Editura Facla, Timosoara, 1982.

BIOMATERIALE PE BAZĂ DE TITAN FOLOSITE LA ÎNLOCUIREA ARTICULAŢIILOR

Rezumat: Implanturile fabricate din biomateriale cu baza titan prezinta ca avantaje: promovarea osteointegrarii (contact direct tesut osos implant, fara interpunerea unui strat celular fibros), datorita proprietatilor biochimice ale oxizilor superficiali, rezistenta buna la coroziune, uzare si oboseala, cat si un modul de elasticitate relativ scazut. Proprietatile stratului oxidic se considera unul din factorii importanti ce influenteaza atat raspunsul organismului cat si comportarea implantului fabricat din astfel de materiale in timpul perioadei de utilizare. Oxizii superficiali se formeaza, in mod spontan, in aer si are o grosime a stratului de 5-10 nm. Compozitia oxidului din straturile atomice exterioare este similara cu cea a TiO_2, modificandu-se la interfata metal/ strat oxidic intr-un amestec de oxizi (de exemplu: TiO_2, TiO, TiO_3). Desi TiO_2 este un izolator, in cazul straturilor subtiri, electronii il pot strapunge determinand modificari structurale ale proteinelor adsorbite. Grosimi mai mari de 50 nm, obtinute in general prin prelucrari mecanice, sunt suficiente pentru a preveni acest fenomen.